

NONLINEAR EQUIVALENT LINEAR DESIGN METHOD TO DETERMINE UNBOUND  
AGGREGATE BASE LAYER MODULUS

By

ADITYA AYITHI

A DISSERTATION PRESENTED TO THE GRADUATE SCHOOL  
OF THE UNIVERSITY OF FLORIDA IN PARTIAL FULFILLMENT  
OF THE REQUIREMENTS FOR THE DEGREE OF  
DOCTOR OF PHILOSOPHY

UNIVERSITY OF FLORIDA

2011

© 2011 Aditya Ayithi

To my parents

## ACKNOWLEDGMENTS

First of all, I would like to express my sincere gratitude to my advisor, Dr. Dennis R. Hiltunen, whose valuable guidance, support and encouragement during my doctoral research made this possible. I have benefited tremendously from his experience and research methodology. He has provided me not only his knowledge but also emotional support as a great human being. I would like to thank my co-advisor Dr. Reynaldo Roque, for his guidance and encouragement in my research and emotional support during my stay at University of Florida. I would like to thank my other committee members Dr. Mang Tia and Dr. Bhavani V Sankar for their valuable comments and suggestions.

Special acknowledgements are extended to Florida Department of Transportation, project panel Dr. David Harahota, John shoucair and FDOT State Materials Office staff members Daniel Pitocchi, Dwayne Kirkland, Melissa Barrs, Mike Davis, Gregg Sapp and Timothy Blanton for their technical support and encouragement. I would like to thank our lab engineer George A. Lopp , whose technical support made my lab testing possible.

I would like to thank my parents for encouraging my studies. I would like to thank my brothers, sister-in-laws, niece and nephews for their encouragement to achieve my goals I would like to thank my mentor and friend Dr. Raman G.V. for his encouragement and support in pursuing doctoral studies. I would like to thank my college friends Ravi Chandra (banda) , Madhukar, Raghu, Ravi Tanniru, Hari (jandu) and CSS for their support. Last but not least, I would like to thank my graduate friends CS Koh, Weiato Li, Tran and Patrick for their help and support.

## TABLE OF CONTENTS

	<u>page</u>
ACKNOWLEDGMENTS .....	4
LIST OF TABLES .....	9
LIST OF FIGURES .....	12
ABSTRACT .....	29
CHAPTER	
1 INTRODUCTION .....	31
1.1 Problem Statement .....	31
1.2 Hypothesis.....	33
1.3 Objectives .....	34
1.4 Scope of Research.....	34
1.5 Organization of Dissertation.....	36
2 LITERATURE REVIEW .....	39
2.1 Modulus of Particulate Material .....	39
2.2 Resilient Modulus .....	40
2.3 Modulus Characterization for Complete Range of Strains.....	41
2.3.1 Small-Strain Modulus ( $G_{\max}$ or $E_{\max}$ ) .....	42
2.3.2 Shear Modulus (G) at Different Strain Levels: .....	44
2.3.3 Analytical Models to Estimate Shear Modulus at Different Strain Levels .....	46
2.4 Influence of Suction on Soil Modulus .....	47
2.5 Importance of Small-Strain Modulus Nonlinearity for Design and Analysis.....	51
2.6 Pavement Response Models .....	52
2.6.1 MEPDG Nonlinear Response Model .....	52
2.6.2 Single Effective Moduli Determination Based on Nonlinear Versus Linear Analysis Responses Comparison .....	53
2.6.3 PLAXIS-HSsmall Model.....	54
2.7 Closing Remarks .....	55
3 EXPERIMENTS .....	68
3.1 Fixed-Free Resonant Column Testing .....	68
3.1.1 Background and Testing Mechanism .....	68
3.1.2 Shear Modulus (G) .....	69
3.1.3 Shear Strain ( $\gamma$ ) .....	70
3.1.4 Equipment Setup.....	71
3.1.5 Calibration of the Drive System: .....	71
3.1.6 Limitations (We Experienced) of This Testing Equipment: .....	73
3.1.7 Equipment Credibility Verification .....	73

3.2	Free-Free Resonant Column Testing (Free-Free RC).....	74
3.2.1	Back Ground and Mechanism .....	74
3.2.2	Equipment Setup: .....	76
4	MATERIALS AND SPECIMEN PREPARATION .....	85
4.1	Materials .....	85
4.1.1	Sources.....	85
4.1.2	Characterization.....	85
4.2	Specimen Preparation and Installation.....	86
4.2.1	Dry Specimens.....	86
4.2.1.1	Dry specimen preparation.....	86
4.2.1.2	Dry specimen installation .....	87
4.2.2	Wet (Partially Saturated) Specimens .....	87
4.2.2.1	Wet specimen preparation .....	87
4.2.2.2	Wet specimen installation .....	88
5	EXPERIMENTAL RESULTS AND ANALYSIS .....	93
5.1	Fixed-Free Resonant Column Torsional Shear Testing.....	93
5.1.1	Dry Specimen Testing Results .....	93
5.1.2	Unsaturated (Wet) Specimen Testing Results .....	96
5.1.2.1	Equipment limitations.....	97
5.1.2.2	Confinement effect on unsaturated specimens .....	98
5.1.2.3	Results and analysis.....	98
5.1.2.4	Additional effective stress or additional confinement pressure provided due to suction, at $10^{-5}$ % strain magnitude.....	102
5.2	Free-Free Resonant Column Testing .....	103
5.2.1	Results and Discussion .....	103
5.2.2	A Method to Estimate Approximate Modulus at Given Conditions of Water Content, Confining Pressure and Strain Magnitude: .....	104
5.3	Laboratory Testing Results Closing Remarks .....	105
6	NONLINEAR FINITE ELEMENT MODELING OF BASE LAYER.....	118
6.1	PLAXIS: Hardening Soil-Small Model (Plaxis-HSsmall Model) .....	118
6.1.1	Parameters of HSsmall Model.....	119
6.1.2	Compatibility of Plaxis-HSsmall Model Modulus Reduction Model to Our Laboratory Determined Base Soils Modulus Reduction Behavior.....	120
6.2	Flexible Pavement Nonlinear Response Model.....	121
6.2.1	Axisymmetric Model.....	121
6.2.2	Pavement Cross Sections.....	122
6.2.3	Loading Conditions .....	122
6.2.4	Input Parameters for Surface and Subgrade Layers of Flexible Pavement ....	122
6.3	Initial Plaxis-HSsmall Pavement Model Runs and Recalibration .....	122
6.3.1	Footing Model Analysis and Verification .....	123
6.3.2	Model Recalibration .....	123

6.4	Recalibrated Nonlinear Input Parameters of Base Soils for Plaxis.....	124
6.4.1	Recalibrated Parameters of Newberry Limerock and Georgia Granite.....	124
6.4.2	Input Parameters for Miami Limerock .....	125
6.5	Demonstration of Response Model Nonlinear Behavior .....	125
6.5.1	Demonstration of Input Parameters' Nonlinearity .....	126
6.5.2	Demonstration of Pavement Model's Nonlinearity.....	126
7	BASE LAYER NONLINEAR MODELING ANALYSIS AND RESULTS .....	139
7.1	Nonlinear Equivalent Single Effective Base Modulus Determination .....	139
7.1.1	Methodology.....	139
7.1.2	An Example of Surface Deflection Basin Matching Between Nonlinear Modulus Base Case and Single Effective Elastic Modulus Base Case .....	140
7.1.3	Demonstration of Nonlinear Reduction of Single Effective Modulus with Increase in Load.....	141
7.2	Single Effective Moduli Data for Base Layer.....	142
7.2.1	Nonlinear Equivalent Single Effective Design Moduli Values for Base Layer ..	142
7.2.1.1	Influence of moisture content on base layer single effective design modulus.....	142
7.2.1.2	Influence of subgrade modulus on single effective base design modulus.....	143
7.2.1.3	Influence of structure type on single effective base design modulus .....	144
7.2.1.4	Comparison of single effective design moduli for different materials ....	144
7.2.1.5	Comparison of equivalent single effective design moduli with mepdg moisture effect model design moduli.....	146
7.3	Evaluation of Applicability of Single Effective Modulus in place of Nonlinear Modulus .....	147
7.3.1	Comparison of Nonlinear and Equivalent Linear Analysis Responses .....	147
7.3.2	Analysis of Nonlinear and Linear Responses in the Perspective of Rutting Performance Criteria.....	151
8	SUBGRADE LAYER NONLINEAR MODELING ANALYSIS AND RESULTS .....	174
8.1	Nonlinear Equivalent Single Effective Modulus Determination for Base and Subgrade Layers.....	175
8.1.1	Methodology.....	175
8.1.2	Material Parameters and Structural Inputs .....	176
8.1.3	An Example of Surface Deflection Basin Matching Between Nonlinear Base and Subgrade Case and Equivalent Linear Base and Subgrade Case ....	176
8.2	Comparison of Nonlinear and Equivalent Linear Analysis Results .....	177
8.2.1	Nonlinear Equivalent Single Effective Design Moduli Values for Base and Subgrade .....	177
8.2.2	Comparison of Nonlinear and Equivalent Linear Analyses Pavement Responses .....	178
8.2.3	Analysis of Nonlinear and Linear responses in the Perspective of Cracking and Rutting Performance Criteria .....	180

9	CLOSURE .....	190
9.1	Summary of Findings .....	190
9.1.1	Laboratory Testing on Unbound Aggregate Base Soils .....	191
9.1.2	Development of Nonlinear Response Model and Base Layer Nonlinear Modeling and Analysis .....	193
9.1.3	Nonlinear Modeling and Analysis of Base and Subgrade Layers .....	196
9.2	Conclusions .....	198
9.3	Recommendations .....	199
APPENDIX		
A	FIXED-FREE RESONANT COLUMN TESTING DATA FOR DIFFERENT BASE SOILS .....	201
B	NONLINEAR EQUIVALENT LINEAR EFFECTIVE BASE MODULI DATA FOR DIFFERENT TYPES OF BASE SOILS .....	205
C	COMPARISON OF NONLINEAR AND EQUIVALENT LINEAR RESPONSES OBTAINED FROM NONLINEAR BASE ANALYSIS .....	212
D	COMPARISON OF NONLINEAR AND EQUIVALENT LINEAR RESPONSES OBTAINED FOR NONLINEAR BASE AND NONLINEAR SUBGRADE ANALYSIS .....	280
	LIST OF REFERENCES .....	308
	BIOGRAPHICAL SKETCH .....	310

## LIST OF TABLES

<u>Table</u>	<u>page</u>
4-1 List of materials used for testing and their sources.....	89
4-2 Basic material parameters.....	89
4-3 Selected void ratios for dry specimen testing.....	89
5-1 $n_G$ and $A_G$ values for dry Newberry lime rock and Georgia granite.....	107
5-2 List of unsaturated specimen tested water contents.....	107
6-1 Input parameters of Plaxis-HSsmall model.....	127
6-2 Different types of pavement structures considered for analysis.....	127
6-3 Material input parameters for surface asphalt concrete and subgrade layers.....	128
6-4 Input parameters used in HSsmall model for footing settlement predictions (Lehane et al. 2008).....	128
6-5 Comparison of Actual and Modified calibration parameters.....	129
6-6 Recalibrated HSsmall input parameters for Newberry limerock.....	129
6-7 Recalibrated HSsmall input parameters for Georgia granite.....	130
6-8 Recalibrated HSsmall input parameters for Miami limerock.....	130
7-1 Equivalent elastic moduli values obtained for different pavement structures, with different subgrade moduli for Newberry limerock base.....	154
7-2 Effective equivalent elastic moduli values obtained for different pavement structures, with different subgrade moduli for Georgia granite base.....	155
7-3 Effective equivalent elastic moduli values obtained for different pavement structures and with different subgrade moduli for Miami limerock base.....	156
7-4 List of structures analyzed for pavement's various responses comparison.....	156
7-5 Asphalt Institute's rutting criteria analysis for structure-1 (200mm AC surface, 450 mm base).....	157
7-6 Asphalt Institute's rutting criteria analysis for structure-4 (100 mm AC surface, 300 mm base).....	158
8-1 Different material properties used for nonlinear base and nonlinear subgrade analysis.....	182

8-2	HS Small model nonlinear material inputs for Ottawa sand subgrade layer .....	182
8-3	Equivalent elastic moduli values obtained for structure-1 with Newberry limerock base and Ottawa sand subgrade .....	183
8-4	Equivalent elastic moduli values obtained for structure-4 with Newberry limerock base and Ottawa sand subgrade .....	183
8-5	Equivalent elastic moduli values obtained for structure-1 with Georgia granite base and Ottawa sand subgrade .....	184
8-6	Equivalent elastic moduli values obtained for structure-4 with Georgia Granite base and Ottawa sand subgrade .....	184
8-7	List of structures analyzed for pavement's various responses comparison .....	184
8-8	Asphalt Institute's rutting criteria analysis for structure-1 with nonlinear base and nonlinear subgrade .....	185
B-1	For structure-1, nonlinear equivalent linear effective moduli data for Newberry limerock base layer. ....	205
B-2	For structure-2, nonlinear equivalent linear effective moduli data for Newberry limerock base layer. ....	206
B-3	For structure-3, nonlinear equivalent linear effective moduli data for Newberry limerock base layer. ....	206
B-4	For structure-4, nonlinear equivalent linear effective moduli data for Newberry limerock base layer. ....	207
B-5	For structure-5, nonlinear equivalent linear effective moduli data for Newberry limerock base layer. ....	207
B-6	For structure-6, nonlinear equivalent linear effective moduli data for Newberry limerock base layer. ....	208
B-7	For structure-1, nonlinear equivalent linear effective moduli data for Georgia granite base layer. ....	209
B-8	For structure-2, nonlinear equivalent linear effective moduli data for Georgia granite base layer. ....	209
B-9	For structure-3, nonlinear equivalent linear effective moduli data for Georgia granite base layer. ....	210
B-10	For structure-4, nonlinear equivalent linear effective moduli data for Georgia granite base layer. ....	210

B-11 For structure-1, nonlinear equivalent linear effective moduli data for Miami limerock base layer. ....211

B-12 For structure-4, nonlinear equivalent linear effective moduli data for Miami limerock base layer. ....211

## LIST OF FIGURES

<u>Figure</u>	<u>page</u>
2-1 Characteristic modulus-strain behavior of soils with typical strain ranges for laboratory tests and structures .....	56
2-2 $G/G_{max}$ versus $\log \gamma$ curves of gravelly sandy soils .....	56
2-3 $G/G_{max}$ versus $\log \gamma$ curves of undisturbed and reconstituted riverbed gravel (a) for $\sigma_c=0.29$ MPa and (b) $\sigma_c=0.59$ .....	57
2-4 Effect of $\sigma_3$ on the $G-\gamma$ relationship ( $d_{max} = 1.27$ cm) .....	58
2-5 Variation of normalized shear modulus with shear strain .....	58
2-6 $G-\gamma$ relationship.....	59
2-7 Variation of $G_{max}$ of the field deposit with $\sigma_3$ .....	59
2-8 $G/G_{max} - \log \gamma$ relationship for gravelly soils .....	60
2-9 Comparison of calculated and measured values of normalized shear modulus.....	60
2-10 Data points defining $G/G_{max}$ versus $\gamma$ relationship for gravelly soils .....	61
2-11 $G$ versus $\gamma$ curves and $G/G_{max}$ versus $\gamma$ curves determined for test specimens containing 0, 20, 40 and 60% gravel size particles.....	62
2-12 Mean curves defining $G/G_{max}$ versus $\gamma$ relationships for gravelly soils at various confining pressures along with standard deviation boundaries for reduced data set.....	63
2-13 Shear modulus degradation curve proposed by Santos and Correia.....	63
2-14 Shear –wave velocity versus degree of saturation for different materials .....	64
2-15 FFRC test results of specimen exposed to constant moisture.....	65
2-16 The FFRC test results of specimens exposed to laboratory ambient .....	65
2-17 The FFRC test results of each material during first cycle of oven drying.....	66
2-18 The FFRC test results of each material during first cycle of wetting .....	66
2-19 Load-displacement curves at Bothkennar footing test, fitted using the proposed model.....	67
2-20 Comparison of measured foundation load settlement response at Shenton Park to prediction using Plaxis-HSsmall model.....	67

3-1	Fixed-Free RC testing specimen idealized testing specimen and Differential soil element.....	77
3-2	Shear Strain in soil specimen.....	77
3-3	Fixed-Free RC equipment used for our testing.....	78
3-4	Sectional view of Fixed-Free RC testing equipment.....	79
3-5	Controlling units of Fixed-Free RC equipment.....	80
3-6	Real time test execution window, showing resonant frequency reaching loop.....	81
3-7	Calibration specimen with added mass.....	82
3-8	Shear modulus versus % shear strain curves at different confining pressures for Ottawa sand.....	83
3-9	$G_{max}$ versus $\log \sigma_c$ relationship curve for Ottawa sand.....	83
3-10	Free-Free Resonant Column test equipment setup.....	84
3-11	Free-Free resonant column testing specimen.....	84
4-1	Representative samples.....	90
4-2	Grain size distribution.....	90
4-3	Dry specimen compaction and installation.....	91
4-4	Wet specimen compaction.....	92
5-1	Shear Modulus (G) versus % Shear strain ( $\gamma$ ) curves for dry Newberry limerock at $e_{OMC}$ .....	108
5-2	Shear Modulus (G) versus % Shear strain ( $\gamma$ ) curves for dry Georgia granite at $e_{OMC}$ ...	108
5-3	$G/G_{max}$ versus % shear strain ( $\gamma$ ) curves at $e = e_{OMC}$ for Newberry limerock.....	109
5-4	$G/G_{max}$ versus % shear strain ( $\gamma$ ) curves at $e = e_{OMC}$ for Georgia granite.....	109
5-5	Comparison of $G/G_{max}$ vs % shear strain ( $\gamma$ ) data of Newberry limerock and Georgia granite with Seed and Idriss maximum and minimum limits.....	110
5-6	$G_{max}$ versus confining pressure curve Newberry limerock at different void ratios.....	110
5-7	$G_{max}$ versus confining pressure curve Georgia granite at different void ratios.....	111
5-8	$G_{max}$ empirical equations for Newberry limerock and Georgia granite.....	111

5-9	Shear moduli (G) versus % shear strain ( $\gamma$ ) curves for Newberry limerock at different water contents .....	112
5-10	Shear modulus (G) versus %shear strain ( $\gamma$ ) curves for Georgia granite at different water contents .....	112
5-11	$G/G_{\max}$ versus shear strain curves for Newberry limerock for both dry & wet specimens .....	113
5-12	$G/G_{\max}$ versus % shear strain curves for Georgia granite, for both dry and wet specimens .....	113
5-13	$G/G_{\text{OMC}}$ versus water content (%) at different strain levels for Newberry limerock .....	114
5-14	$G/G_{\text{OMC}}$ versus water content (%) at different strain levels for Georgia granite .....	114
5-15	Additional confinement provided due to suction at $10^{-5}\%$ strain magnitude, at different water contents.....	115
5-16	Additional confinement provided due to suction at $10^{-5}\%$ strain magnitude at different degree of saturation .....	115
5-17	Young's Modulus versus % water content results obtained from Free-Free RC test on Newberry limerock .....	116
5-18	Young's Modulus versus % water content results obtained from Free-Free RC test on Georgia Granite.....	116
5-19	Comparison of Newberry limerock Free-Free RC test data with Fixed-Free RC very small-strain data and Toros (2008) data.....	117
5-20	Comparison of Georgia granite Free-Free RC test data with Fixed-Free RC very small-strain data and Toros (2008) data.....	117
6-1	Characteristic modulus–strain behavior of soil with typical strain ranges for laboratory tests and structures.....	131
6-2	Results from modified Hardin-Drnevich relationship compared to test data by Santos and Correia.....	131
6-3	Comparison of Newbery limerock and Georgia granite actual testing data with HSsmall model's Santos and Correia modified hyperbolic curve .....	132
6-4	Typical Plaxis-HSsmall model cross section model used for nonlinear analysis. ....	133
6-5	Typical HSsmall model finite element mesh of a pavement cross section.....	134
6-6	Cross sections considered for nonlinear base pavement analysis .....	135

6-7	Finite element mesh used for model recalibration analysis .....	136
6-8	Comparison of actual settlements with settlements predicted using regular parameters via Plaxis-HSsmall footing model.....	136
6-9	Comparison of actual settlements with settlements predicted using regular parameters and calibrated settlements via Plaxis-HSsmall footing model. ....	137
6-10	Approximate Miami limerock $G_{max}$ versus water content plot.....	137
6-11	Load versus settlement curve to demonstrate material input parameters nonlinearity....	138
6-12	Pavement surface deflection basin for different load demonstrating pavement model nonlinearity. ....	138
7-1	Critical locations for pavement response analysis .....	159
7-2	Surface deflection basin comparison for nonlinear and linear cases, for structure-1 with 10% w.c. base layer. ....	159
7-3	Nonlinear variation of single effective modulus with increase in load, for Newberry limerock base at 13% and 10% moisture contents.....	160
7-4	Nonlinear variation of effective modulus with increase in load, for Georgia granite base at 5.5% and 3.5% moisture contents.....	160
7-5	Newberry limerock effective base modulus versus subgrade elastic modulus relationship with decrease in moisture content, for different structures.....	161
7-6	Georgia granite effective base modulus versus subgrade elastic modulus relationship with decrease in moisture content, for different structures.....	162
7-7	Miami limerock effective base modulus versus subgrade elastic modulus relationship with decrease in moisture content, for different structures.....	163
7-8	Newberry limerock effective base modulus versus subgrade elastic modulus relationship for different structures, at constant moisture content.....	164
7-9	Georgia granite effective base modulus versus subgrade elastic modulus relationship for different structures, at constant moisture content.....	165
7-10	Miami limerock effective base modulus versus subgrade elastic modulus relationship for different structures, at constant moisture content.....	166
7-11	Comparison of effective moduli of all three materials at different base water contents and with subgrade modulus of 50 MPa and 125 MPa .....	167
7-12	Comparison of normalized effective moduli of all three materials obtained with subgrade modulus of 50 MPa and 125 MPa .....	168

7-13	Comparison of Newberry limerock effective base moduli values with MEPDG moisture model.....	169
7-14	Comparison of Georgia granite effective base moduli values with MEPDG modulus moisture model.....	170
7-15	Comparison of Miami limerock effective base moduli values with MEPDG moisture model.....	171
7-16	Comparison of horizontal tensile strain at bottom of AC layer ( $\% \epsilon_{xx}$ ) obtained for structure-1 and structure-4 with different base water contents .....	172
7-17	Comparison of vertical compressive strain at top of subgrade layer ( $\% \epsilon_{yy}$ ) obtained for structure-1 and structure-4 with different base water contents .....	173
8-1	FWD analysis of structure-4 .....	186
8-2	Comparison of nonlinear and linear surface deflections for structure-1 with 10% w.c. base and Ottawa sand subgrade. ....	187
8-3	Comparison of horizontal tensile strain at bottom of AC layer ( $\% \epsilon_{xx}$ ) obtained for structure-1 with Ottawa sand subgrade and different base water contents .....	188
8-4	Comparison of vertical compressive strain at top of subgrade layer ( $\% \epsilon_{yy}$ ) obtained for structure-1 with Ottawa sand subgrade and different base water contents .....	189
A-1	Shear Modulus (G) versus % Shear strain ( $\gamma$ ) curves for dry Newberry limerock at $e=0.5$ .....	201
A-2	Shear Modulus (G) versus % Shear strain ( $\gamma$ ) curves for dry Newberry limerock at $e=0.55$ .....	201
A-3	$G/G_{max}$ versus % shear strain( $\gamma$ ) curves at $e=0.5$ for Newberry limerock .....	202
A-4	$G/G_{max}$ versus % shear strain ( $\gamma$ ) curves at $e=0.55$ for Newberry limerock .....	202
A-5	Shear Modulus (G) versus % Shear strain ( $\gamma$ ) curves for dry Georgia granite at $e=0.25$ .....	203
A-6	Shear Modulus (G) versus % Shear strain ( $\gamma$ ) curves for dry Georgia granite at $e=0.29$ .....	203
A-7	$G/G_{max}$ versus % shear strain( $\gamma$ ) curves at $e=0.25$ for Georgia granite.....	204
A-8	$G/G_{max}$ versus % shear strain( $\gamma$ ) curves at $e=0.29$ for Georgia granite.....	204
C-1	Surface deflection comparison for nonlinear and linear cases, for structure-1 with 13% w.c. base layer. ....	212

C-2	Surface deflection comparison for nonlinear and linear cases, for structure-1 with 10% w.c. base layer. ....	213
C-3	Surface deflection comparison for nonlinear and linear cases, for structure-1 with 8% w.c. base layer. ....	213
C-4	Surface deflection comparison for nonlinear and linear cases, for structure-1 with 5.5% w.c. base layer. ....	214
C-5	Surface deflection comparison for nonlinear and linear cases, for structure-4 with 13% w.c. base layer. ....	214
C-6	Surface deflection comparison for nonlinear and linear cases, for structure-4 with 10% w.c. base layer. ....	215
C-7	Surface deflection comparison for nonlinear and linear cases, for structure-4 with 8% w.c. base layer. ....	215
C-8	Surface deflection comparison for nonlinear and linear cases, for structure-4 with 5.5% w.c. base layer. ....	216
C-9	$\sigma_{xx}$ at top of AC layer comparison for nonlinear and linear cases, for structure-1 with 13% w.c. base layer. ....	217
C-10	$\sigma_{xx}$ at top of AC layer comparison for nonlinear and linear cases, for structure-1 with 10% w.c. base layer. ....	217
C-11	$\sigma_{xx}$ at top of AC layer comparison for nonlinear and linear cases, for structure-1 with 8% w.c. base layer. ....	218
C-12	$\sigma_{xx}$ at top of AC layer comparison for nonlinear and linear cases, for structure-1 with 5.5% w.c. base layer. ....	218
C-13	$\sigma_{xx}$ at top of AC layer comparison for nonlinear and linear cases, for structure-4 with 13% w.c. base layer. ....	219
C-14	$\sigma_{xx}$ at top of AC layer comparison for nonlinear and linear cases, for structure-4 with 10% w.c. base layer. ....	219
C-15	$\sigma_{xx}$ at top of AC layer comparison for nonlinear and linear cases, for structure-4 with 8% w.c. base layer. ....	220
C-16	$\sigma_{xx}$ at top of AC layer comparison for nonlinear and linear cases, for structure-4 with 5.5% w.c. base layer. ....	220
C-17	$\epsilon_{xx}$ at top of AC layer comparison for nonlinear and linear cases, for structure-1 with 13% w.c. base layer. ....	221

C-18	$\epsilon_{xx}$ at top of AC layer comparison for nonlinear and linear cases, for structure-1 with 10% w.c. base layer. ....	221
C-19	$\epsilon_{xx}$ at top of AC layer comparison for nonlinear and linear cases, for structure-1 with 8% w.c. base layer. ....	222
C-20	$\epsilon_{xx}$ at top of AC layer comparison for nonlinear and linear cases, for structure-1 with 5.5% w.c. base layer. ....	222
C-21	$\epsilon_{xx}$ at top of AC layer comparison for nonlinear and linear cases, for structure-4 with 13% w.c. base layer. ....	223
C-22	$\epsilon_{xx}$ at top of AC layer comparison for nonlinear and linear cases, for structure-4 with 10% w.c. base layer. ....	223
C-23	$\epsilon_{xx}$ at top of AC layer comparison for nonlinear and linear cases, for structure-4 with 8% w.c. base layer. ....	224
C-24	$\epsilon_{xx}$ at top of AC layer comparison for nonlinear and linear cases, for structure-4 with 5.5% w.c. base layer. ....	224
C-25	$\sigma_{xx}$ at bottom of AC layer comparison for nonlinear and linear cases, for structure-1 with 13% w.c. base layer. ....	225
C-26	$\sigma_{xx}$ at bottom of AC layer comparison for nonlinear and linear cases, for structure-1 with 10% w.c. base layer. ....	225
C-27	$\sigma_{xx}$ at bottom of AC layer comparison for nonlinear and linear cases, for structure-1 with 8% w.c. base layer. ....	226
C-28	$\sigma_{xx}$ at bottom of AC layer comparison for nonlinear and linear cases, for structure-1 with 5.5% w.c. base layer. ....	226
C-29	$\sigma_{xx}$ at bottom of AC layer comparison for nonlinear and linear cases, for structure-4 with 13% w.c. base layer. ....	227
C-30	$\sigma_{xx}$ at bottom of AC layer comparison for nonlinear and linear cases, for structure-4 with 10% w.c. base layer. ....	227
C-31	$\sigma_{xx}$ at bottom of AC layer comparison for nonlinear and linear cases, for structure-4 with 8% w.c. base layer. ....	228
C-32	$\sigma_{xx}$ at bottom of AC layer comparison for nonlinear and linear cases, for structure-4 with 5.5% w.c. base layer. ....	228
C-33	$\epsilon_{xx}$ at bottom of AC layer comparison for nonlinear and linear cases, for structure-1 with 13% w.c. base layer. ....	229

C-34	$\epsilon_{xx}$ at bottom of AC layer comparison for nonlinear and linear cases, for structure-1 with 10% w.c. base layer. ....	229
C-35	$\epsilon_{xx}$ at bottom of AC layer comparison for nonlinear and linear cases, for structure-1 with 8% w.c. base layer. ....	230
C-36	$\epsilon_{xx}$ at bottom of AC layer comparison for nonlinear and linear cases, for structure-1 with 5.5% w.c. base layer. ....	230
C-37	$\epsilon_{xx}$ at bottom of AC layer comparison for nonlinear and linear cases, for structure-4 with 13% w.c. base layer. ....	231
C-38	$\epsilon_{xx}$ at bottom of AC layer comparison for nonlinear and linear cases, for structure-4 with 10% w.c. base layer. ....	231
C-39	$\epsilon_{xx}$ at bottom of AC layer comparison for nonlinear and linear cases, for structure-4 with 8% w.c. base layer. ....	232
C-40	$\epsilon_{xx}$ at bottom of AC layer comparison for nonlinear and linear cases, for structure-4 with 5.5% w.c. base layer. ....	232
C-41	$\sigma_{yy}$ vertical stress at top of base layer comparison for nonlinear and linear cases, for structure-1 with 13% w.c. base layer. ....	233
C-42	$\sigma_{yy}$ vertical stress at top of base layer comparison for nonlinear and linear cases, for structure-1 with 10% w.c. base layer. ....	233
C-43	$\sigma_{yy}$ vertical stress at top of base layer comparison for nonlinear and linear cases, for structure-1 with 8% w.c. base layer. ....	234
C-44	$\sigma_{yy}$ vertical stress at top of base layer comparison for nonlinear and linear cases, for structure-1 with 5.5% w.c. base layer. ....	234
C-45	$\sigma_{yy}$ at top of base layer comparison for nonlinear and linear cases, for structure-4 with 13% w.c. base layer. ....	235
C-46	$\sigma_{yy}$ vertical stress at top of base layer comparison for nonlinear and linear cases, for structure-4 with 10% w.c. base layer. ....	235
C-47	$\sigma_{yy}$ vertical stress at top of base layer comparison for nonlinear and linear cases, for structure-4 with 8% w.c. base layer. ....	236
C-48	$\sigma_{yy}$ vertical stress at top of base layer comparison for nonlinear and linear cases, for structure-4 with 5.5% w.c. base layer. ....	236
C-49	$\epsilon_{yy}$ at top of base layer comparison for nonlinear and linear cases, for structure-1 with 13% w.c. base layer. ....	237

C-50	$\epsilon_{yy}$ at top of base layer comparison for nonlinear and linear cases, for structure-1 with 10% w.c. base layer. ....	237
C-51	$\epsilon_{yy}$ at top of base layer comparison for nonlinear and linear cases, for structure-1 with 8% w.c. base layer. ....	238
C-52	$\epsilon_{yy}$ at top of base layer comparison for nonlinear and linear cases, for structure-1 with 5.5% w.c. base layer. ....	238
C-53	$\epsilon_{yy}$ at top of base layer comparison for nonlinear and linear cases, for structure-4 with 13% w.c. base layer. ....	239
C-54	$\epsilon_{yy}$ at top of base layer comparison for nonlinear and linear cases, for structure-4 with 10% w.c. base layer. ....	239
C-55	$\epsilon_{yy}$ at top of base layer comparison for nonlinear and linear cases, for structure-4 with 8% w.c. base layer. ....	240
C-56	$\epsilon_{yy}$ at top of base layer comparison for nonlinear and linear cases, for structure-4 with 5.5% w.c. base layer. ....	240
C-57	$\sigma_{yy}$ at bottom of base layer comparison for nonlinear and linear cases, for structure-1 with 13% w.c. base layer. ....	241
C-58	$\sigma_{yy}$ at bottom of base layer comparison for nonlinear and linear cases, for structure-1 with 10% w.c. base layer. ....	241
C-59	$\sigma_{yy}$ at bottom of base layer comparison for nonlinear and linear cases, for structure-1 with 8% w.c. base layer. ....	242
C-60	$\sigma_{yy}$ at bottom of base layer comparison for nonlinear and linear cases, for structure-1 with 5.5% w.c. base layer. ....	242
C-61	$\sigma_{yy}$ at bottom of base layer comparison for nonlinear and linear cases, for structure-4 with 13% w.c. base layer. ....	243
C-62	$\sigma_{yy}$ at bottom of base layer comparison for nonlinear and linear cases, for structure-4 with 10% w.c. base layer. ....	244
C-63	$\sigma_{yy}$ at bottom of base layer comparison for nonlinear and linear cases, for structure-4 with 8% w.c. base layer. ....	244
C-64	$\sigma_{yy}$ at bottom of base layer comparison for nonlinear and linear cases, for structure-4 with 5.5% w.c. base layer. ....	244
C-65	$\epsilon_{yy}$ at bottom of base layer comparison for nonlinear and linear cases, for structure-1 with 13% w.c. base layer. ....	245

C-66	$\epsilon_{yy}$ at bottom of base layer comparison for nonlinear and linear cases, for structure-1 with 10% w.c. base layer .....	246
C-67	$\epsilon_{yy}$ at bottom of base layer comparison for nonlinear and linear cases, for structure-1 with 8% w.c. base layer. ....	246
C-68	$\epsilon_{yy}$ at bottom of base layer comparison for nonlinear and linear cases, for structure-1 with 5.5% w.c. base layer. ....	247
C-69	$\epsilon_{yy}$ at bottom of base layer comparison for nonlinear and linear cases, for structure-4 with 13% w.c. base layer. ....	247
C-70	$\epsilon_{yy}$ at bottom of base layer comparison for nonlinear and linear cases, for structure-4 with 10% w.c. base layer. ....	248
C-71	$\epsilon_{yy}$ at bottom of base layer comparison for nonlinear and linear cases, for structure-4 with 8% w.c. base layer. ....	248
C-72	$\epsilon_{yy}$ at bottom of base layer comparison for nonlinear and linear cases, for structure-4 with 5.5% w.c. base layer .....	248
C-73	$\sigma_{yy}$ at top of subgrade comparison for nonlinear and linear cases, for structure-1 with 13% w.c. base layer. ....	249
C-74	$\sigma_{yy}$ at top of subgrade comparison for nonlinear and linear cases, for structure-1 with 10% w.c. base layer .....	250
C-75	$\sigma_{yy}$ at top of subgrade comparison for nonlinear and linear cases, for structure-1 with 8% w.c. base layer. ....	250
C-76	$\sigma_{yy}$ at top of subgrade comparison for nonlinear and linear cases, for structure-1 with 5.5% w.c. base layer. ....	251
C-77	$\sigma_{yy}$ at top of subgrade comparison for nonlinear and linear cases, for structure-4 with 13% w.c. base layer. ....	251
C-78	$\sigma_{yy}$ at top of subgrade comparison for nonlinear and linear cases, for structure-4 with 10% w.c. base layer. ....	252
C-79	$\sigma_{yy}$ at top of subgrade comparison for nonlinear and linear cases, for structure-4 with 8% w.c. base layer. ....	252
C-80	$\sigma_{yy}$ at top of subgrade comparison for nonlinear and linear cases, for structure-4 with 5.5% w.c. base layer. ....	252
C-81	$\epsilon_{yy}$ at top of subgrade layer comparison for nonlinear and linear cases for structure-1 with 13% w.c. base layer. ....	253

C-82	$\epsilon_{yy}$ at top of subgrade layer comparison for nonlinear and linear cases for structure-1 with 10% w.c. base layer. ....	254
C-83	$\epsilon_{yy}$ at top of subgrade layer comparison for nonlinear and linear cases for structure-1 with 8% w.c. base layer. ....	254
C-84	$\epsilon_{yy}$ at top of subgrade layer comparison for nonlinear and linear cases for structure-1 with 5.5% w.c. base layer. ....	255
C-85	$\epsilon_{yy}$ at top of subgrade layer comparison for nonlinear and linear cases for structure-4 with 13% w.c. base layer. ....	255
C-86	$\epsilon_{yy}$ at top of subgrade layer comparison for nonlinear and linear cases for structure-4 with 10% w.c. base layer. ....	256
C-87	$\epsilon_{yy}$ at top of subgrade layer comparison for nonlinear and linear cases for structure-4 with 8% w.c. base layer. ....	256
C-88	$\epsilon_{yy}$ at top of subgrade layer comparison for nonlinear and linear cases for structure-4 with 5.5% w.c. base layer. ....	257
C-89	Surface deflection comparison for nonlinear and linear cases, for structure-1 with 5.5% w.c. base layer. ....	258
C-90	Surface deflection comparison for nonlinear and linear cases, for structure-1 with 3.5% w.c. base layer. ....	258
C-91	Surface deflection comparison for nonlinear and linear cases, for structure-4 with 5.5% w.c. base layer. ....	259
C-92	Surface deflection comparison for nonlinear and linear cases, for structure-4 with 3.5% w.c. base layer. ....	259
C-93	$\sigma_{xx}$ at top of AC layer comparison for nonlinear and linear cases, for structure-1 with 5.5% w.c. base layer. ....	260
C-94	$\sigma_{xx}$ at top of AC layer comparison for nonlinear and linear cases, for structure-1 with 3.5% w.c. base layer. ....	260
C-95	$\sigma_{xx}$ at top of AC layer comparison for nonlinear and linear cases, for structure-4 with 5.5% w.c. base layer. ....	261
C-96	$\sigma_{xx}$ at top of AC layer comparison for nonlinear and linear cases, for structure-4 with 3.5% w.c. base layer. ....	261
C-97	$\epsilon_{xx}$ at top of AC layer comparison for nonlinear and linear cases, for structure-1 with 5.5% w.c. base layer. ....	262

C-98	$\epsilon_{xx}$ at top of AC layer comparison for nonlinear and linear cases, for structure-1 with 3.5% w.c. base layer. ....	262
C-99	$\epsilon_{xx}$ at top of AC layer comparison for nonlinear and linear cases, for structure-4 with 5.5% w.c. base layer. ....	263
C-100	$\epsilon_{xx}$ at top of AC layer comparison for nonlinear and linear cases, for structure-4 with 3.5% w.c. base layer. ....	263
C-101	$\sigma_{xx}$ at bottom of AC layer comparison for nonlinear and linear cases, for structure-1 with 5.5% w.c. base layer. ....	264
C-102	$\sigma_{xx}$ at bottom of AC layer comparison for nonlinear and linear cases, for structure-1 with 3.5% w.c. base layer. ....	264
C-103	$\sigma_{xx}$ at bottom of AC layer comparison for nonlinear and linear cases, for structure-4 with 5.5% w.c. base layer. ....	265
C-104	$\sigma_{xx}$ at bottom of AC layer comparison for nonlinear and linear cases, for structure-4 with 3.5% w.c. base layer. ....	265
C-105	$\epsilon_{xx}$ at bottom of AC layer comparison for nonlinear and linear cases, for structure-1 with 5.5% w.c. base layer. ....	266
C-106	$\epsilon_{xx}$ at bottom of AC layer comparison for nonlinear and linear cases, for structure-1 with 3.5% w.c. base layer. ....	266
C-107	$\epsilon_{xx}$ at bottom of AC layer comparison for nonlinear and linear cases, for structure-4 with 5.5% w.c. base layer. ....	267
C-108	$\epsilon_{xx}$ at bottom of AC layer comparison for nonlinear and linear cases, for structure-4 with 3.5% w.c. base layer. ....	267
C-109	$\sigma_{yy}$ vertical stress at top of base layer comparison for nonlinear and linear cases, for structure-1 with 5.5% w.c. base layer. ....	268
C-110	$\sigma_{yy}$ vertical stress at top of base layer comparison for nonlinear and linear cases, for structure-1 with 3.5% w.c. base layer. ....	268
C-111	$\sigma_{yy}$ vertical stress at top of base layer comparison for nonlinear and linear cases, for structure-4 with 5.5% w.c. base layer. ....	269
C-112	$\sigma_{yy}$ vertical stress at top of base layer comparison for nonlinear and linear cases, for structure-4 with 3.5% w.c. base layer. ....	269
C-113	$\epsilon_{yy}$ at top of base layer comparison for nonlinear and linear cases, for structure-1 with 5.5% w.c. base layer. ....	270

C-114	$\epsilon_{yy}$ at top of base layer comparison for nonlinear and linear cases, for structure-1 with 3.5% w.c. base layer. ....	270
C-115	$\epsilon_{yy}$ at top of base layer comparison for nonlinear and linear cases, for structure-4 with 5.5% w.c. base layer. ....	271
C-116	$\epsilon_{yy}$ at top of base layer comparison for nonlinear and linear cases, for structure-4 with 3.5% w.c. base layer. ....	271
C-117	$\sigma_{yy}$ at bottom of base layer comparison for nonlinear and linear cases, for structure-1 with 5.5% w.c. base layer. ....	272
C-118	$\sigma_{yy}$ at bottom of base layer comparison for nonlinear and linear cases, for structure-1 with 3.5% w.c. base layer. ....	272
C-119	$\sigma_{yy}$ at bottom of base layer comparison for nonlinear and linear cases, for structure-4 with 5.5% w.c. base layer. ....	273
C-120	$\sigma_{yy}$ at bottom of base layer comparison for nonlinear and linear cases, for structure-4 with 3.5% w.c. base layer. ....	273
C-121	$\epsilon_{yy}$ at bottom of base layer comparison for nonlinear and linear cases, for structure-1 with 5.5% w.c. base layer. ....	274
C-122	$\epsilon_{yy}$ at bottom of base layer comparison for nonlinear and linear cases, for structure-1 with 3.5% w.c. base layer. ....	274
C-123	$\epsilon_{yy}$ at bottom of base layer comparison for nonlinear and linear cases, for structure-4 with 5.5% w.c. base layer. ....	275
C-124	$\epsilon_{yy}$ at bottom of base layer comparison for nonlinear and linear cases, for structure-4 with 3.5% w.c. base layer. ....	275
C-125	$\sigma_{yy}$ at top of subgrade comparison for nonlinear and linear cases, for structure-1 with 5.5% w.c. base layer. ....	276
C-126	$\sigma_{yy}$ at top of subgrade layer comparison for nonlinear and linear cases for structure-1 with 3.5% w.c. base layer. ....	276
C-127	$\sigma_{yy}$ at top of subgrade layer comparison for nonlinear and linear cases, for structure-4 with 5.5% w.c. base layer. ....	277
C-128	$\sigma_{yy}$ at top of subgrade layer comparison for nonlinear and linear cases for structure-4 with 3.5% w.c. base layer. ....	277
C-129	$\epsilon_{yy}$ at top of subgrade layer comparison for nonlinear and linear cases for structure-1 with 5.5% w.c. base layer. ....	278

C-130	$\epsilon_{yy}$ at top of subgrade layer comparison for nonlinear and linear cases for structure-1 with 3.5% w.c. base layer. ....	278
C-131	$\epsilon_{yy}$ at top of subgrade layer comparison for nonlinear and linear cases for structure-4 with 5.5% w.c. base layer. ....	279
C-132	$\epsilon_{yy}$ at top of subgrade layer comparison for nonlinear and linear cases for structure-4 with 3.5% w.c. base layer. ....	279
D-1	Surface deflection comparison for nonlinear and linear cases, for structure-1 with 13% w.c. base layer and nonlinear Ottawa sand subgrade .....	280
D-2	Surface deflection comparison for nonlinear and linear cases, for structure-1 with 10% w.c. base layer and nonlinear Ottawa sand subgrade. ....	281
D-3	Surface deflection comparison for nonlinear and linear cases, for structure-4 with 10% w.c. base layer and nonlinear Ottawa sand subgrade. ....	281
D-4	$\sigma_{xx}$ at top of AC layer comparison for nonlinear and linear cases, for structure-1 with 13% w.c. base layer and nonlinear Ottawa sand subgrade. ....	282
D-5	$\sigma_{xx}$ at top of AC layer comparison for nonlinear and linear cases, for structure-1 with 10% w.c. base layer and nonlinear Ottawa sand subgrade. ....	282
D-6	$\sigma_{xx}$ at top of AC layer comparison for nonlinear and linear cases, for structure-4 with 10% w.c. base layer and nonlinear Ottawa sand subgrade. ....	283
D-7	$\epsilon_{xx}$ at top of AC layer comparison for nonlinear and linear cases, for structure-1 with 13% w.c. base layer and nonlinear Ottawa sand subgrade. ....	283
D-8	$\epsilon_{xx}$ at top of AC layer comparison for nonlinear and linear cases, for structure-1 with 10% w.c. base layer and nonlinear Ottawa sand subgrade. ....	284
D-9	$\epsilon_{xx}$ at top of AC layer comparison for nonlinear and linear cases, for structure-4 with 10% w.c. base layer and nonlinear Ottawa sand subgrade. ....	284
D-10	$\sigma_{xx}$ at bottom of AC layer comparison for nonlinear and linear cases, for structure-1 with 13% w.c. base layer and nonlinear Ottawa sand subgrade. ....	285
D-11	$\sigma_{xx}$ at bottom of AC layer comparison for nonlinear and linear cases, for structure-1 with 10% w.c. base layer and nonlinear Ottawa sand subgrade. ....	285
D-12	$\sigma_{xx}$ at bottom of AC layer comparison for nonlinear and linear cases, for structure-4 with 10% w.c. base layer and nonlinear Ottawa sand subgrade. ....	286
D-13	$\epsilon_{xx}$ at bottom of AC layer comparison for nonlinear and linear cases, for structure-1 with 13% w.c. base layer and nonlinear Ottawa sand subgrade. ....	286

D-14	$\epsilon_{xx}$ at bottom of AC layer comparison for nonlinear and linear cases, for structure-1 with 10% w.c. base layer and nonlinear Ottawa sand subgrade. ....	287
D-15	$\epsilon_{xx}$ at bottom of AC layer comparison for nonlinear and linear cases, for structure-4 with 10% w.c. base layer and nonlinear Ottawa sand subgrade. ....	287
D-16	$\sigma_{yy}$ vertical stress at top of base layer comparison for nonlinear and linear cases, for structure-1 with 13% w.c. base layer and nonlinear Ottawa sand subgrade. ....	288
D-17	$\sigma_{yy}$ vertical stress at top of base layer comparison for nonlinear and linear cases, for structure-1 with 10% w.c. base layer and nonlinear Ottawa sand subgrade. ....	288
D-18	$\sigma_{yy}$ vertical stress at top of base layer comparison for nonlinear and linear cases, for structure-4 with 10% w.c. base layer and nonlinear Ottawa sand subgrade. ....	289
D-19	$\epsilon_{yy}$ at top of base layer comparison for nonlinear and linear cases, for structure-1 with 13% w.c. base layer and nonlinear Ottawa sand subgrade. ....	289
D-20	$\epsilon_{yy}$ at top of base layer comparison for nonlinear and linear cases, for structure-1 with 10% w.c. base layer and nonlinear Ottawa sand subgrade. ....	290
D-21	$\epsilon_{yy}$ at top of base layer comparison for nonlinear and linear cases, for structure-4 with 10% w.c. base layer and nonlinear Ottawa sand subgrade. ....	290
D-22	$\sigma_{yy}$ at bottom of base layer comparison for nonlinear and linear cases, for structure-1 with 13% w.c. base layer and nonlinear Ottawa sand subgrade. ....	291
D-23	$\sigma_{yy}$ at bottom of base layer comparison for nonlinear and linear cases, for structure-1 with 10% w.c. base layer and nonlinear Ottawa sand subgrade. ....	291
D-24	$\sigma_{yy}$ at bottom of base layer comparison for nonlinear and linear cases, for structure-4 with 10% w.c. base layer and nonlinear Ottawa sand subgrade. ....	292
D-25	$\epsilon_{yy}$ at bottom of base layer comparison for nonlinear and linear cases, for structure-1 with 13% w.c. base layer and nonlinear Ottawa sand subgrade. ....	292
D-26	$\epsilon_{yy}$ at bottom of base layer comparison for nonlinear and linear cases, for structure-1 with 10% w.c. base layer and nonlinear Ottawa sand subgrade. ....	293
D-27	$\epsilon_{yy}$ at bottom of base layer comparison for nonlinear and linear cases, for structure-4 with 10% w.c. base layer and nonlinear Ottawa sand subgrade. ....	293
D-28	$\sigma_{yy}$ at top of subgrade comparison for nonlinear and linear cases, for structure-1 with 13% w.c. base layer and nonlinear Ottawa sand subgrade. ....	294
D-29	$\sigma_{yy}$ at top of subgrade comparison for nonlinear and linear cases, for structure-1 with 10% w.c. base layer and nonlinear Ottawa sand subgrade. ....	294

D-30	$\sigma_{yy}$ at top of subgrade comparison for nonlinear and linear cases, for structure-4 with 10% w.c. base layer and nonlinear Ottawa sand subgrade. ....	295
D-31	$\epsilon_{yy}$ at top of subgrade layer comparison for nonlinear and linear cases for structure-1 with 13% w.c. base layer and nonlinear Ottawa sand subgrade .....	295
D-32	$\epsilon_{yy}$ at top of subgrade layer comparison for nonlinear and linear cases for structure-1 with 10% w.c. base layer and nonlinear Ottawa sand subgrade .....	296
D-33	$\epsilon_{yy}$ at top of subgrade layer comparison for nonlinear and linear cases for structure-4 with 10% w.c. base layer and nonlinear Ottawa sand subgrade .....	296
D-34	Surface deflection comparison for nonlinear and linear cases, for structure-1 with 5.5% w.c. base layer and nonlinear Ottawa sand subgrade. ....	297
D-35	Surface deflection comparison for nonlinear and linear cases, for structure-1 with 3.5% w.c. base layer and nonlinear Ottawa sand subgrade. ....	297
D-36	$\sigma_{xx}$ at top of AC layer comparison for nonlinear and linear cases, for structure-1 with 5.5% w.c. base layer and nonlinear Ottawa sand subgrade. ....	298
D-37	$\sigma_{xx}$ at top of AC layer comparison for nonlinear and linear cases, for structure-1 with 3.5% w.c. base layer and nonlinear Ottawa sand subgrade. ....	298
D-38	$\epsilon_{xx}$ at top of AC layer comparison for nonlinear and linear cases, for structure-1 with 5.5% w.c. base layer and nonlinear Ottawa sand subgrade. ....	299
D-39	$\epsilon_{xx}$ at top of AC layer comparison for nonlinear and linear cases, for structure-1 with 3.5% w.c. base layer and nonlinear Ottawa sand subgrade. ....	299
D-40	$\sigma_{xx}$ at bottom of AC layer comparison for nonlinear and linear cases, for structure-1 with 5.5% w.c. base layer and nonlinear Ottawa sand subgrade. ....	300
D-41	$\sigma_{xx}$ at bottom of AC layer comparison for nonlinear and linear cases, for structure-1 with 3.5% w.c. base layer and nonlinear Ottawa sand subgrade. ....	300
D-42	$\epsilon_{xx}$ at bottom of AC layer comparison for nonlinear and linear cases, for structure-1 with 5.5% w.c. base layer and nonlinear Ottawa sand subgrade. ....	301
D-43	$\epsilon_{xx}$ at bottom of AC layer comparison for nonlinear and linear cases, for structure-1 with 3.5% w.c. base layer and nonlinear Ottawa sand subgrade. ....	301
D-44	$\sigma_{yy}$ vertical stress at top of base layer comparison for nonlinear and linear cases, for structure-1 with 5.5% w.c. base layer and nonlinear Ottawa sand subgrade. ....	302
D-45	$\sigma_{yy}$ vertical stress at top of base layer comparison for nonlinear and linear cases, for structure-1 with 3.5% w.c. base layer and nonlinear Ottawa sand subgrade. ....	302

D-46	$\epsilon_{yy}$ at top of base layer comparison for nonlinear and linear cases, for structure-1 with 5.5% w.c. base layer and nonlinear Ottawa sand subgrade. ....	303
D-47	$\epsilon_{yy}$ at top of base layer comparison for nonlinear and linear cases, for structure-1 with 3.5% w.c. base layer and nonlinear Ottawa sand subgrade. ....	304
D-48	$\sigma_{yy}$ at bottom of base layer comparison for nonlinear and linear cases, for structure-1 with 5.5% w.c. base layer and nonlinear Ottawa sand subgrade. ....	304
D-49	$\sigma_{yy}$ at bottom of base layer comparison for nonlinear and linear cases, for structure-1 with 3.5% w.c. base layer and nonlinear Ottawa sand subgrade. ....	304
D-50	$\epsilon_{yy}$ at bottom of base layer comparison for nonlinear and linear cases, for structure-1 with 5.5% w.c. base layer and nonlinear Ottawa sand subgrade. ....	305
D-51	$\epsilon_{yy}$ at bottom of base layer comparison for nonlinear and linear cases, for structure-1 with 3.5% w.c. base layer and nonlinear Ottawa sand subgrade. ....	305
D-52	$\sigma_{yy}$ at top of subgrade comparison for nonlinear and linear cases, for structure-1 with 5.5% w.c. base layer and nonlinear Ottawa sand subgrade. ....	306
D-53	$\sigma_{yy}$ at top of subgrade comparison for nonlinear and linear cases, for structure-1 with 3.5% w.c. base layer and nonlinear Ottawa sand subgrade. ....	306
D-54	$\epsilon_{yy}$ at top of subgrade layer comparison for nonlinear and linear cases for structure-1 with 5.5% w.c. base layer and nonlinear Ottawa sand subgrade. ....	307
D-55	$\epsilon_{yy}$ at top of subgrade layer comparison for nonlinear and linear cases for structure-1 with 3.5% w.c. base layer and nonlinear Ottawa sand subgrade. ....	307

Abstract of Dissertation Presented to the Graduate School  
of the University of Florida in Partial Fulfillment of the  
Requirements for the Degree of Doctor of Philosophy

NONLINEAR EQUIVALENT LINEAR DESIGN METHOD TO DETERMINE UNBOUND  
AGGREGATE BASE LAYER MODULUS

By  
Aditya Ayithi  
August 2011

Chair: Dennis R Hiltunen  
Co-Chair: Reynaldo Roque  
Major: Civil Engineering

Mechanistic-Empirical Pavement Design Guidelines (MEPDG) recommends use of material modulus in lieu of structural number for pavement base layer thickness design. Soil modulus is nonlinear with respect to effective confinement stress, loading strain and moisture (suction); and modulus nonlinearity need to be considered for an efficient base layer design and analysis. For practical design purposes, single effective modulus value of base layer need to be known and this modulus value should be able to approximately account for nonlinearities of the whole base layer. However, MEPDG does not describe a standard procedure for determining this single modulus value. This research study focuses on laboratory characterization of base soil modulus nonlinearity, developing a nonlinear response model for nonlinear pavement analysis and developing a practical linear design methodology to determine nonlinear equivalent single effective design modulus value for whole base layer.

First, Fixed-Free and Free-Free resonant column tests are conducted on two gravelly base soils used in the State of Florida, to characterize shear modulus (G) nonlinearity in the strain range of  $10^{-5}\%$  to  $10^{-1}\%$ , including small-level strains, under different loading confinements and moisture contents. Moisture suction effect on nonlinear modulus is evaluated. It is found that unsaturated gravelly soils modulus is linear at strains lower than  $10^{-5}\%$  and nonlinear thereafter.

Compared to dry soils, presence of moisture in unsaturated soils makes it more nonlinear with respect to strain. Suction effect can increase  $G$  in the strain range of  $10^{-5}\%$  to  $10^{-1}\%$ , but very significantly at strain levels less than  $10^{-3}\%$ . At any given moisture content, additional confinement due to suction does not decrease with increase in strain. Empirical equations are developed to calculate very small-strain modulus ( $G_{\max}$ ) of dry soils. A procedure to calculate approximate  $G$  value at given water content, confinement and strain magnitude is developed.

Second, using laboratory nonlinear modulus characterization data as material parameter inputs, a stress and strain dependent nonlinear response model for base layer analysis is developed via Plaxis-HSsmall model. Nonlinearity of the response model is verified with respect to stress and strain variation. Considering maximum surface deflection of nonlinear analysis as matching factor between nonlinear and linear design methods, a practical design methodology to determine equivalent single effective elastic modulus for base layer is proposed. Effect of moisture, subgrade modulus and layer thickness on base single effective modulus is analyzed. Stress and strain responses for both nonlinear and equivalent linear analysis are compared at critical locations. Influence of base nonlinearity on pavement performance is evaluated. It is found that use of single effective modulus in place of nonlinear modulus over estimates rutting performance, when structure thickness and base water content decreases together. Last, effect of subgrade modulus nonlinearity on pavement performance is also analyzed for limited cases. Equivalent single effective modulus for all layers is back calculated via Falling Weight Deflectometer (FWD) analysis of nonlinear analysis surface deflection. It is found that, subgrade nonlinearity may significantly influence rutting performance and elastic based rutting performance criterion overestimates rutting performance.

## CHAPTER 1 INTRODUCTION

### 1.1 Problem Statement

Mechanistic-Empirical Pavement Design Guidelines (MEPDG (2004)) for flexible pavement structures recommend use of modulus in place of layer coefficient, for unbound aggregate base layer thickness design. Resilient Modulus ( $M_R$ ) and Poisson's ratio ( $\nu$ ) are the two primary input parameters required for thickness design.  $M_R$  represents modulus of a material subjected to repeated traffic loading and can be determined in lab via a standard testing protocol (AASHTO T307).

Soil is a nonlinear material and its modulus nonlinearity is dependent primarily on effective confinement stress, loading strain, moisture content (suction) and some other parameters. MEPDG proposes three different levels of  $M_R$  input for pavement design analysis response model. Level-1  $M_R$  input takes material modulus nonlinearity into account, whereas level-2 and level-3  $M_R$  inputs assume material is elastic and assigns a single effective elastic modulus value for the whole layer. However; nonlinear design analysis response model based on level-1 nonlinear  $M_R$  input has not been calibrated for practical applications yet, because of various complicated nonlinear modeling issues involved in it. Thus, it seems that single effective elastic modulus approach using either level-2 or level-3  $M_R$  input would be most commonly used analysis in near future. Therefore determining single elastic modulus value is very critical for pavement response model analysis.

However, since soil is a nonlinear material, single elastic modulus approach should not discard the importance of modulus nonlinearity. Hence, the single elastic modulus value should be able to reflect the nonlinear behavior of base layer up to certain extent under real loading conditions. In parallel, if we can built a database of either nonlinear modulus parameters or

single effective elastic moduli values that can also reflect nonlinear behavior approximately, for different types of base materials, it may not be required to conduct expensive  $M_R$  laboratory testing at initial design stage and the whole design process would become more economical.

MEPDG is primarily based on  $M_R$  and its determination via AASHTO protocol. By following AASHTO T307 testing procedure, material modulus can be characterized only from intermediate ( $10^{-3}\%$ ) to larger strains ( $10^{-1}\%$ ), due to high deviatoric stresses applied in this test procedure and external measurement of loads and deformations. Recent research studies in geotechnical engineering revealed that it is necessary to consider modulus nonlinearity at small level strains ( $\leq 10^{-3}\%$ ) along with nonlinearity at intermediate to larger strains, to predetermine accurate pavement responses. Since moduli values at small level strains cannot be determined via AASHTO protocol due to procedural limitations, small-strain modulus nonlinearity cannot be characterized. Hence, accurate pavement responses cannot be calculated using moduli values obtained via AASHTO testing protocol. Therefore there is a requirement to seek for a different testing procedure, which can characterize material modulus nonlinearity at small level strains also along with intermediate to larger strains.

Moreover, AASHTO T307 gives us a set of  $M_R$  values corresponding to different stress levels and strain magnitudes, but not a single elastic modulus value which is required for MEPDG level-2 and level-3 material parameter inputs. Till now, no proper methodology is defined either in MEPDG or in literature about “how to determine the single elastic modulus value, required for level-2 and level-3  $M_R$  input for response model?” Therefore, there is a requirement to develop a proper methodology “to determine single effective design modulus value, which can also approximately reflect the modulus nonlinearity of whole base layer”.

Suction in partially saturated soils provides additional confinement, which in turn increases soil modulus. Research studies related to suction effect on soil modulus at different strain levels have revealed that suction effect can increase modulus at small level strains very significantly compared to intermediate and large strains. Since it is important to consider modulus nonlinearity at small-level strains, it is important to consider suction effect on modulus at small level strains too. MEPDG incorporates moisture effect (which includes suction effect also) on modulus via Integrated Enhanced Climatic Model (ECIM). ECIM is developed based on  $M_R$  testing data base for different types of soils. Since, these  $M_R$  values are determined via AASHTO protocol, which can measure modulus at intermediate to large strains only; ECIM does not consider suction effect at small level strains. Therefore it is necessary to develop a pavement response model which can consider suction effect at different strain levels including small-level strains also.

In view of above discussed issues regarding testing protocol adequacies, moisture (suction effect) model inabilities and no properly defined methodology to calculate single effective design modulus for base layer, there is a necessity to develop i) A lab testing method for modulus determination, which can accurately characterize modulus nonlinearity at different strain levels including small level strains ii) A design methodology to determine single effective modulus value for MEPDG level-2 and level-3 modulus inputs, which can also reflect modulus nonlinearity approximately and iii) Response model that can incorporate suction effect on modulus at small level strains, along with intermediate and larger strains.

## **1.2 Hypothesis**

A design methodology to determine single effective elastic design modulus of unbound aggregate base soils, that can be used as MEPDG level-2 and level-3 base material parameter input needs to be developed. Single effective elastic modulus can be determined such that it can

approximate base soil modulus nonlinearity with respect to effective stress confinement, loading strain including small level strains and moisture content.

### **1.3 Objectives**

The primary objective of this research work is to develop a design methodology for characterizing base layer design modulus for use in MEPDG that can address the issues discussed above.

Detailed objectives would be:

- Conduct a laboratory testing program on selected base materials, following a suitable testing methodology that can effectively account for the effects of confinement, strain magnitude and moisture on nonlinear modulus, including small-strain nonlinear modulus; and can characterize its nonlinear behavior
- To evaluate and quantify suction effect on nonlinear small-strain modulus
- To develop an appropriate pavement response model that can utilize the laboratory testing results and account for the above discussed modulus nonlinearity, under performance conditions.
- Based on deflections, stress and strain responses obtained from pavement response model analysis develop a practical design methodology to calculate single effective modulus for whole base layer that can approximate known nonlinearities, for use as MEPDG level-2 and level-3 material inputs.
- Demonstrate by various techniques that the overall approach, as well as the laboratory test results and pavement response model results are credible and appear to agree with other known properties and behavior.

### **1.4 Scope of Research**

In the State of Florida, limerock type aggregates are commonly used for base layer construction. It is proposed to select one limerock material and one non-limerock material for our testing. The two materials selected for our testing are i) Newberry limerock and ii) Georgia granite. Material collection and test specimen preparation are performed following standard procedures.

Fixed-Free Resonant Column (Fixed-Free RC) test method and Free-Free Resonant Column (Free-Free RC) test method are selected for material testing program. Fixed-Free RC tests can determine shear modulus ( $G$ ) of gravel type soils at different strain magnitudes including small level strains. In Fixed-Free RC testing, compacted specimens can be subjected to required stress confinement. Suction effect can be evaluated by conducting tests on specimens dried to different water contents. Therefore, via Fixed-Free RC testing, modulus nonlinearity of gravelly base soils can be characterized with respect to i) effective stress confinement, ii) loading strain magnitude including small level strains and iii) moisture or suction effect. These tests are conducted on standard size modified proctor compacted specimens. Free-Free RC test can determine shear modulus at very small level strain ( $G_{\max}$ ) at different water contents under no confinement, to evaluate suction effect on  $G_{\max}$ . Credibility of these testing results is established by comparing them with literature data.

A nonlinear pavement response model is developed via PLAXIS-HSsmall; a nonlinear finite element model based system that can utilize laboratory testing results. Using laboratory test results as material parameter inputs, above response model can characterize material modulus nonlinearity properly with respect to stress confinement, strain magnitude including small level strains and moisture or suction effect. Flexible pavement structures with different layer thicknesses or cross sections are analyzed under performance loading conditions, using the nonlinear response model.

A methodology to determine single effective elastic design modulus value for whole base layer that can be utilized as MEPDG level-2 and level-3 material parameter input is developed. Single effective base modulus determination methodology is developed such that various pavement responses such as surface deflections, stresses and strains obtained by nonlinear base

modulus analysis and equivalent linear single elastic base modulus analysis are approximately same. Effect of base layer nonlinearity on pavement performance is evaluated by comparing the responses obtained from nonlinear base modulus analysis and equivalent linear single base modulus analysis. Out of professional interest, effect of subgrade nonlinearity on pavement performance is also briefly evaluated for limited cases.

## **1.5 Organization of Dissertation**

An over view of remaining chapters of this dissertation is presented here. Chapter 2 gives an over view of Resilient Modulus ( $M_R$ ),  $M_R$  testing method and its adequacies, importance of modulus characterization including small-strain modulus nonlinearity in soils and possible laboratory testing methods, modulus nonlinearity influencing factors and its importance in geotechnical structural designs. Different models proposed by various researchers to calculate very small-strain modulus and modulus at different strain levels are discussed. Suction effect on small-strain modulus and importance of considering suction effect in determining design modulus is also discussed. Recent research efforts about importance of considering small-strain modulus nonlinearity for geotechnical structural analysis and design are also discussed.

Different types of materials selected for testing and their properties are presented in Chapter 3. A detailed explanation about specimen preparation methods, for both wet and dry materials, is also given in chapter three.

In Chapter 4, Fixed-Free RC and Free-Free RC test methods used in this research work are presented. Detailed explanations about equipment development background and types of parameters that can be measured with these equipments are discussed. Equipment setup, calibration, verification and limitations are also explained.

Chapter 5 mainly analyze and discuss various testing results obtained from both Fixed-Free RC and Free-Free RC tests. Specimen testing conditions like different moisture contents

tested, void ratios and pressure confinements are mentioned. Empirical equations are proposed to calculate very small-strain modulus of dry soils. Suction effect on small-strain modulus is evaluated and an indirect approach to calculate additional confinement due to suction is explained. Based on these testing results, a method to determine approximate modulus at any given water content, confinement and strain magnitude is explained.

Chapter 6 talks about PLAXIS- HSsmall model and required model material input parameters. Development of a nonlinear response model for base layer analysis via HSsmall model is discussed and how to obtain input parameters from lab testing results is explained.

Chapter 7 mainly talks about base layer nonlinear analysis. It presents a methodology to determine single effective design modulus for base layer thickness design. Different pavement cross sections are analyzed using HSsmall nonlinear response model. Single effective elastic base moduli values for different pavement structures at different base water contents and subgrade moduli are reported and analyzed. Effect of base nonlinearity on pavement performance is evaluated.

Importance of subgrade nonlinearity in pavement design and analysis is discussed in Chapter 8. A methodology to determine equivalent single elastic modulus for both base and subgrade layers is explained and effect of subgrade nonlinearity on pavement performance is analyzed briefly for limited number of structures.

Based on the results presented in Chapters 5,6,7 and 8, total findings are summarized in Chapter 9. Based on this entire research work information discussed in Chapters 2 through 8, conclusions and recommendations are presented.

Further test results details are presented in the appendices. Fixed-Free RC test results on dry specimens at different void ratios are given in Appendix A. Nonlinear equivalent single

effective base moduli database is given in Appendix B. Comparison plots of surface deflection, stress and strain responses obtained from nonlinear base analysis and equivalent linear base analysis, for different pavement structures is presented in Appendix C. Comparison plots of pavement responses obtained from base and subgrade nonlinearity analysis and equivalent linear analysis are presented in Appendix D.

## CHAPTER 2 LITERATURE REVIEW

The center point of proposed research work is determining effective base modulus for practical design purposes, while considering modulus nonlinearity. It is proposed to achieve this through laboratory testing and nonlinear modeling. Hence this literature review mainly talks about soil modulus and its influencing factors including suction, modulus at different strain levels including small level strains and its determination in laboratory, various analytical models developed to determine modulus at different strain levels, importance of modulus nonlinearity in geotechnical design calculations and pavement response models.

### 2.1 Modulus of Particulate Material

Material modulus represents its resistance to deformation under loading. Modulus or stiffness is the relationship between change of stress and change of strain, and is defined by ratio of stress over strain. Being a particulate material, soil modulus is nonlinear and primarily dependent on effective confining stress ( $\sigma_c'$ ), strain magnitude ( $\epsilon$ ) and void ratio ( $e$ ) (Seed & Idriss (1970), Hardin and Drnevich (1972), Yasuda and Mastumoto (1993)). In unsaturated soils, modulus is dependent on moisture content and its suction effect also (Wu et al. (1984), Quin et al. (1993), Cho and Santamarina (2001)).

In a pavement base layer, strain magnitudes are not constant throughout the layer. They are highest near or under the wheel load and diminishes to zero as moving away from wheel load, in a nonlinear manner. Soil modulus is maximum ( $G_{\max}$  or  $E_{\max}$ ) at strain levels lower than  $10^{-4}\%$  and decreases nonlinearly with increase in strain (Figure 2-1), generally in an S-shaped pattern. As shown in Figure 2-1, Atkinson and Sallfors (1981) presented a typical modulus reduction curve with increase in strain for soils, along with different strain levels involved in various types of geotechnical structures. Modulus nonlinearity for different strain levels that can be observed

under real loading conditions should be considered for accurate geotechnical design calculations (Atkinson (1991)), Elhakim and Mayne (2008), Lehane et al. (2008)).

## 2.2 Resilient Modulus

According to MEPDG (2004), resilient modulus ( $M_R$ ) and Poisson's ratio ( $\nu$ ) are the two basic material parameter inputs required for pavement layer thickness design. Behavior of a soil subjected to repeated traffic loading in a pavement layer is characterized by  $M_R$ .  $M_R$  is an elastic modulus based on recoverable strain under repeated loads and is defined as:

$$M_R = \frac{\sigma_d}{\epsilon_r} \quad (2-1)$$

where  $\sigma_d$ =deviatoric stress and  $\epsilon_r$ =recoverable axial strain.

Since its inception in AASHTO 1986 guidelines, lot of research has been done and well documented regarding  $M_R$ .  $M_R$  of soils can be determined in lab via standard testing procedure (AASHTO T307). For design calculations,  $M_R$  of a soil for any given stress condition ( $\theta$ ) is calculated using the basic constitutive equation:

$$M_R = k_1 * \theta^{k_2} \quad (2-2)$$

in which  $\theta$  is sum of three principal stresses, parameters  $k_1$  and  $k_2$  are material dependent and their values are determined from lab testing data. In standard  $M_R$  testing procedure, testing specimen is subjected to different predetermined combinations of confinement stress and deviatoric stress and resulting strain magnitudes are measured using strain gauges placed outside the triaxial testing chamber. Strain magnitudes that can be measured in AASHTO T307 testing are typically in the range of  $10^{-3}\%$  and higher. Hence the moduli values obtained from lab testing are good enough for the limited strain range that can be measured in lab.

MEPDG level-2 and level-3 design procedures for unbound aggregate base layer thickness design use single modulus value for the whole layer, which should be obtained from  $M_R$  lab

testing.  $M_R$  lab testing produces a set of moduli data corresponding to specific stress and strain levels, but not a single modulus value. MEPDG does not define a procedure about “how to determine single modulus value required for design, from laboratory data?”

To consider modulus nonlinearity with respect to stress and strain in pavement design procedures; first of all we should be able to measure modulus for a wide range of strain levels at any given confinement stress. One of the main challenges in measuring the modulus of soil at small level strains is choosing the right equipment and testing method for accurate strain measurements. A good testing method should be reliable, simple and quicker. Conventional lab testing equipments can measure modulus at strains as small as  $10^{-3}\%$ , with reasonable accuracy, where the strain gauges are placed outside the testing chamber. Moduli corresponding to strain range  $10^{-5}\%$  -  $10^{-3}\%$  can be measured only by using local strain gauges attached directly to the sample (Jardine et al. (1984), Atkinson (1991)). But these local strain gauges must operate satisfactorily in water or oil for a long time and also can not measure very small strains (i.e.  $\leq 10^{-5}\%$ ), which correspond to fundamental material property  $G_{max}$ . AASHTO T307 testing protocol requires to attach the strain gauges outside of the testing chamber. Thus standard  $M_R$  test cannot measure small level strains and accuracy of strain measurements less than  $10^{-3}\%$  becomes questionable. Also,  $M_R$  lab testing procedure is very tedious, time taking and skill required one, which makes the testing very expensive.

### **2.3 Modulus Characterization for Complete Range of Strains**

Past research efforts have proved that nonlinearity of soils for a wide range of strains including small level strains need to be considered for accurate settlements/deformations predictions in soils (Jardine et al. (1982), Atkinson (1991), Elhakim and Mayne (2008), Lehane et al. (2008)). It is now well acknowledged that strain/deformation predictions for geotechnical structures (e.g.: footings, retaining walls and braced excavations etc.) are not at acceptable level

of accuracy and one of the primary reasons for this inaccuracy is choosing a single linear elastic modulus value which corresponds to high level strain, to represent the soil behavior.

Quite a few numbers of analytical models were developed to calculate G at different strain levels, using  $G_{\max}$  as the benchmark. Determination of accurate  $G_{\max}$  representing in-situ soil condition is very critical. Research studies conducted about determination of G at different strain levels including Gmax, for different soil types and analytical models are developed to calculate G under known conditions are discussed in following sections.

### 2.3.1 Small-Strain Modulus ( $G_{\max}$ or $E_{\max}$ )

Since 1960, lot of research investigations were conducted and documented on  $G_{\max}$  of sands, silts and clay type soils and its influencing factors. Hardin and Richart (1963) measured longitudinal and shear wave velocities of Ottawa sand, crushed quartz sand and crushed quartz silt at small-strain level ( $10^{-3}$  rad) using free-free and fixed-free resonant column methods. They found that  $V_s$  for sands varied with approximately  $1/4$  power of confining pressure. At very small-strain,  $V_s$  of sands is function of mean effective confining pressure ( $\sigma_e$ ) and void ratio (e); and  $V_s$  of Ottawa sand can be expressed as:

$$V_s = (170 - 78.2 \times e)\sigma_e^{1/4}, \text{ for } \sigma_e < 2000 \text{ psf} \quad (2-3)$$

$$V_s = (119 - 56.0 \times e)\sigma_e^{3/10}, \text{ for } \sigma_e > 2000 \text{ psf} \quad (2-4)$$

where the unit of  $V_s$  is fps.

Hardin and Drnevich (1972) conducted resonant column tests on different types of soils to analyze the effects of confining pressure, strain amplitude, void ratio, number of loading cycles, degree of saturation and thixotropy. They found that shear modulus decreases and damping ratio increases very rapidly with increase in strain amplitude. The rate of decrease or increase in  $G_{\max}$  depends on many parameters and a single relationship between modulus or damping and strain

amplitude is not sufficient. At small strain amplitudes, modulus varies with 0.5 power of effective mean principal stress, but at larger strains modulus depends primarily on strength of soil and the variation is more nearly with 1.0 power. Modulus and damping ratio decreases with increase in void ratio and the effect is accounted by:

$$F(e) = \frac{(2.973 - e)^2}{(1 + e)}, \quad (2-5)$$

where e-is void ratio.

Shear modulus decreases for cohesive soils and increases for cohesionless soils with increase in number of loading cycles. Degree of saturation has no effect on modulus of cohesionless soils. In cohesive soils, modulus increases rapidly with decrease in degree of saturation.

Hardin and Drnevich (1972), Krizek (1974) and Kuribayashi (1974) have clearly shown that moduli values for sands are strongly influenced by three main factors: Confining pressure, strain magnitude and void ratio.

Seed et al. (1986) investigated shear moduli and damping characteristics of soils via cyclic undrained triaxial tests and derived an empirical equation to determine  $G_{max}$  as:

$$G_{max} = 1000 (K_2)_{max} (\sigma'_c)^{n_G} \quad (2-6)$$

They found that values of  $(K_2)_{max}$  for relatively dense well-graded gravels are likely to range from 80-180, compared with the range of about 55-80 for sands and gradation does not have much influence on shear moduli of gravels. They developed a normalized shear modulus versus shear strain curve for gravels similar to the curve for sands, and curve for gravels is little bit flatter compared to sand's curve (Figure 2-2). Based on in-situ shear wave velocity measurements, shear moduli of gravelly soils are between 1.25 and 2.5 times greater than that of sands.

Hardin and Richart (1963) proposed following empirical equation to calculate  $G_{max}$ , for known void ratio ( $e$ ) and effective confinement ( $\sigma_c'$ ):

$$G_{max} = A_G F(e) (\sigma_c')^{n_G} \quad (2-7)$$

where  $A_G$  and  $n_G$  are material constants,  $F(e)$  is function of void ratio and  $\sigma_c'$  is effective mean principal stress. Kokusho (1987), pointed out that as the grain size increase from clays to sands to gravels; rate of reduction in strain-dependent modulus becomes high at a smaller strain level.

Different formulations were developed between 1960 and 2000, to calculate  $G_{max}$  and most of them generally use a power law to describe the effect of confining pressure on  $G_{max}$ . Power law exponent  $n=0.5$  tends to fit for sands and  $n=0.5-0.75$  tends to fit for gravels. According to Pestana and Salavati (2006) the best formulation to calculate  $G_{max}$  is:

$$\frac{G_{max}}{P_{at}} = G_b \cdot e^{-1.3} \cdot \left[ \frac{P}{P_{at}} \right]^n \quad (2-8)$$

Where  $G_b$ - material constant and can be in the range of 400-800.

### 2.3.2 Shear Modulus (G) at Different Strain Levels:

Yasuda and Matsumoto (1993) conducted cyclic torsional simple shear tests and cyclic triaxial tests to investigate dynamic deformation characteristics of sand and rock fill materials. They found that  $G$  can be expressed as a function of shear strain, void ratio and confining stress. They also found that the absolute value of  $G$  for the rock fill materials is substantially higher than sand under the same relative density. The alteration of  $G$  of rock fill material occurred at smaller strains than for sands.

Yasuda et al. (1996) conducted large scale cyclic triaxial tests on undisturbed and reconstituted specimens obtained from river bed gravel foundation of an embankment dam, to determine  $G$  in the strain range of  $10^{-6}$  to  $10^{-3}$ . Undisturbed specimens of size 300 mm diameter

and 550 mm height were sampled by using freezing sampling method. From their testing investigation, they found that  $G_{\max}$  of undisturbed specimens was 1.5 to 2 times greater than reconstituted specimens. They reported that this difference is due to cementation and fabric produced by the effects of the geological time of sedimentation in undisturbed specimens.  $G/G_{\max}$  versus  $\gamma$  relationship was marked by almost identical declining tendencies in both undisturbed and reconstituted specimens (Figure 2-3), thus  $G$  versus  $\gamma$  relationship for undisturbed specimens can be determined from in-situ  $G_{\max}$ .

Lin et al. (2000) investigated characteristics of shear modulus ( $G$ ) and damping ratio ( $D$ ) of gravelly cobble deposits. They conducted both resonant column and cyclic triaxial tests to obtain  $G$  for a strain range of  $10^{-4}\%$  to  $1\%$ . They observed decrease of  $G$  with increase in  $\gamma$ , until  $\gamma \leq 0.1\%$  and increase in  $G$  thereafter (Figure 2-4 and 2-5) and attributed this behavior to gap gradation of the soils tested. Gravel cobble deposits contain 80% gravel and remaining is filling material. When they artificially increased the proportion of filling material,  $G$  decreased with increase in  $\gamma$  as mentioned in literature.  $G$  increases as the max particle size ( $D_{\max}$ ) increase and also with increase in confining pressure (Figure 2-6). There is no significant effect of either  $D_{\max}$  or  $\sigma_c$  on  $G/G_{\max}$  versus  $\gamma$  relationship. Based on their testing data, they developed an empirical equation to calculate  $G_{\max}$  of deposit at different confining pressures as shown in Figure (2-7).

Menq (2003) conducted free-free resonant column tests on sandy and gravelly soils and measured  $G$  in the strain range of  $10^{-5}\%$  to  $10^{-1}\%$ . He observed  $G_{\max}$  at strains  $\leq 10^{-4}\%$  for gravels and at strains  $\leq 10^{-3}\%$  for sands. Normalized modulus versus strain curves for gravels are more flatter than for sand and follow the same trend as reported by Seed et al. (1986) (Figure 2-8)

Gravelly soils are commonly used in base layer construction. Many researchers investigated small-strain modulus of sands, silts and clays; but little efforts were made to

determine moduli of gravel type soils. Being a large size aggregate, testing on gravel requires 4” to 6” diameter specimens and large size equipment, which makes testing complicated and also one of the reason for scarce literature of moduli of gravels.

### 2.3.3 Analytical Models to Estimate Shear Modulus at Different Strain Levels

General hyperbolic form of stress-strain relation to estimate G at shear strain  $\gamma$ , can be written as

$$\frac{G}{G_{max}} = \frac{1}{1 + \frac{\gamma}{\gamma_r}}, \quad (2-9)$$

where  $\gamma_r$  – reference strain =  $\frac{\tau_{max}}{G_{max}}$ .

Hardin and Drnevich (1972), based on their testing data base for different types of soils, modified above hyperbolic expression as:

$$\frac{G}{G_{max}} = \frac{1}{1 + \gamma_h} \quad (2-10)$$

where  $\gamma_h = \frac{\gamma}{\gamma_r} \left[ 1 + a e^{-b \left( \frac{\gamma}{\gamma_r} \right)} \right]$ , a & b are soil constants.

They proposed a = -0.5 and b = -0.16 for clean dry sands. They compared measured values with calculated values and shown in Figure 2-9.

Hardin and Kalinski (2005), based on their testing data, found that  $G/G_{max}$  versus strain ( $\gamma$ ) relationship vary with confinement stress level, whereas  $G/G_{max}$  versus  $\gamma/\gamma_r$  (normalized strain) relationship is independent of stress level. Thus, it is more convenient to use  $\gamma/\gamma_r$  instead of  $\gamma$  for modulus reduction relationship for gravels similar to sands as proposed by Hardin and Drnevich (1972).

Rollins et al. (1998) conducted an experimental program on gravels and reviewed results of fifteen testing programs (including their results) from literature and concluded that normalized

shear modulus curve is dependent on confining pressure and independent of sample disturbance, relative density and gradation. Based on 15 different testing results data, they proposed a best-fit hyperbolic curve model as given below and shown in Figure 2-10.

$$\frac{G}{G_{\max}} = \frac{1}{[1.2 + 16\gamma(1 + 10^{(-20\gamma)})]} \quad (2-11)$$

From their testing results, they observed an increase in  $G$  with increase in gravel content (Figure 2-11). They also observed that  $G/G_{\max}$  versus  $\gamma$  curves move from low end to high end with increase in confining pressure (Figure 2-12). According to their review, for gravels, at shear strains lower than  $10^{-4}\%$ , shear modulus and damping remain constant and shear modulus is at its maximum, i.e.  $G_{\max}$ .

Santos and Correia (2001) proposed a modified Hardin-Drnevich hyperbolic relationship to calculate shear modulus for different strain levels. The unique strain-dependent shear modulus degradation curve for soils is:

$$\frac{G}{G_{\max}} = \frac{1}{1 + a \left| \frac{\gamma}{\gamma_{0.7}} \right|} \quad (2-12)$$

where  $G_{\max}$  – maximum shear modulus

$a = 0.385$ ,  $\gamma_{0.7}$ –shear strain at  $G=0.7 \times G_{\max}$

They recommended that normalization of shear strain ( $\gamma$ ) with reference to threshold shear strain ( $\gamma_{0.7}$ ) makes it possible to define almost a unique strain-dependent stiffness degradation curve for sand and clays. Their proposed stiffness degradation curve with higher and lower limits is shown in Figure 2-13.

## 2.4 Influence of Suction on Soil Modulus

Wu et al. (1983), conducted resonant column tests on fine grained cohesionless soils to investigate capillary effects on  $G_{\max}$ . For their testing, they used 3.6 cm diameter and 8 cm height specimens compacted at required different water contents and void ratios. Specimens were tested

at 24.8, 49 and 98 kPa confinement pressure. For a given void ratio, starting from dry,  $G_{\max}$  increases with increase in degree of saturation and reaches a peak value and start decreasing thereafter with further increase in water content. Degree of saturation, where  $G_{\max}$  is at its peak is called as optimum degree of saturation. Capillary effects were greatest for soils with smallest effective grain diameter ( $D_{10}$ ) and at lowest confining pressure ( $\sigma_c'$ ). Additional confinement provided due to capillary suction is almost equal to 1.6 m of overburden of completely saturated soils. They found that the maximum capillary suction occurs between 5% and 20% water content.

Qian et al. (1993) conducted an experimental investigation of capillary effects on low-strain shear modulus (at strains lower than  $10^{-3}\%$ ) of partially saturated sands. They ran Hall type resonant column tests on fourteen sands with different gradations (four natural sands and remaining man-made from these four natural sands) to study the effect of void ratio ( $e$ ), confining pressure ( $\sigma_c'$ ), grain shape and grain size distribution. Specimens were prepared at different water contents and void ratios, same as procedure followed by Wu et al. (1983). They found that capillary effects increase small-strain shear modulus significantly and more pronounced for soils with low void ratio. Optimum degree of saturation increases with increase in void ratio and is not affected by confinement. Capillary influence decreases with confinement. The content of 400 minus sieve size fraction can affect both modulus and optimum degree of saturation.

Picornell and Nazarian (1998) conducted bender element tests on specimens of coarse sand, fine sand, silt and clay, prepared by separating a local soil into size fractions, to investigate the effect of soil suction on low-strain shear modulus ( $G_{\max}$ ) of soils. Predetermined soil suction was applied on specimens at different water contents, using pressure-plate apparatus. They

observed that as the soil particle size decreases, there is a progressive increase of saturated and residual water contents. As the water content decreases from saturated water content to residual water content,  $G_{\max}$  increase for all soils, for sands by a factor of 1.8 and for silts by a factor of 2.5 and for clays by a factor of 10. Much larger effect in clay specimens was attributed to presence of flatly particles that deform under forces imposed by the menisci resulting in increase in number of contact points where menisci can develop and act.

Cho and Santamarina (2001) conducted microscale particle level studies to investigate capillary effects on low-strain stiffness at different water contents. They conducted bender element tests on 1) glass beads, 2) mixture of Kaolinite and glass beads , 3) Granite powder and 4) sandboil sand. They also conducted microscale experimental study on menisci failure and recovery. Shear wave velocities ( $V_s$ ), measured from bender element tests for the above four materials at different degrees of saturation, are shown in Figure 2-14.

Some of the conclusions of their study are:

- Contribution of capillarity to inter particle forces involves both matric suction and surface tension.
- Equivalent effective stress due to capillary forces increase with decreasing water content, decreasing particle size and increasing coordination.
- Remolding is not an appropriate specimen preparation method (as followed by Wu et al. (1983) and Quin et al. (1992)) to study the behavior of low water content soils, since drying influences particle contact forces.
- Observed strains for menisci failure are in the range of  $\varepsilon = 0.01$  to 1 and higher than threshold strain for sands, so partial saturation is a stabilizing force for the soils skeleton. This strain at menisci failure decreases with decrease in water content.
- On the other hand, small menisci may fail before reaching the strain at peak strength of soils. Thus, capillary forces at low water contents cause an increase in low strain stiffness of soils, but may not contribute to the peak strength.

Toros (2008) investigated suction effects on small-strain Young's modulus ( $E_{\max}$ ) of Florida base course gravelly soils. He conducted Free-Free Resonant Column (FFRC) tests on 6

inch ×12 inch cylindrical specimens of Miami limerock, Newberry limerock, Ocala limerock, Loxahatchee Shell rock and Georgia Granite; which are typically used base layer materials in the State of Florida. Samples were compacted at optimum moisture content and exposed to four different ambiances 1) laboratory 2) outside 3) constant moisture 4) wetting and drying. For drying, specimens were placed in a oven and for wetting, oven dried specimens were soaked in a partially water filled tank. He investigated the time effect on  $E_{max}$  at constant moisture, water content effect on  $E_{max}$  at laboratory ambience, outside ambience and oven drying and water soaked wetting ambience.

Under constant moisture condition,  $E_{max}$  increases with time initially and remain more or less same, after that (Figure 2-15). He hypothesized that the behavior observed could also be due to increased suction or negative pore water pressure that occurs as the water in the material redistributes following compaction into more preferential positions within the inter-particle void spaces. This increased suction effectively adds confining stress to the particulate material and thereby increases the resistance to deformation (stiffness).

In both laboratory and oven drying methods,  $E_{max}$  increased significantly with decrease in water content (Figure 2-16 and 2-17). This stiffening with drying was explained by increase in suction, which effectively increase confinement and hence modulus. Regardless of the drying method, the Miami limerock changed the most and this behavior is partially explained by the fact that this material is coarsest, well graded, and at low void ratio.

Drying and wetting responses do not follow the same relationship and there is a hysteretic phenomenon whereby a different modulus is measured while drying to certain moisture content compared to while wetting to the same moisture content (Figure 2-18). This hysteretic

phenomenon is well known in unsaturated soil mechanics where the suction values reached at common moisture content are different between drying and wetting.

MEPDG incorporates suction effect on  $M_R$  of unbound aggregate via Enhanced Integrated Climatic Model (ECIM). ECIM is based on  $M_R$  lab testing database, and incorporates suction effect at  $M_R$  lab testing strain levels only (i.e. higher than  $10^{-3}\%$ ) and does not consider suction effect for complete range of strains including very small level strains. Moreover this model is developed based on testing data obtained from limited selected base soils only.

## **2.5 Importance of Small-Strain Modulus Nonlinearity for Design and Analysis**

Recent research studies in geotechnical engineering have helped in increasing the awareness of considering modulus nonlinearity for a complete range of strain levels in realistic prediction of ground deformations and surface settlements in geotechnical structures such as footings, braced excavations etc. (Jardine et al. (1986), Atkinson (1991), Elhakim and Mayne (2008), Lehane et al. (2008))

Jardine et al. (1986) studied the influence of nonlinear stress-strain characteristics on soil-structure interaction. They used laboratory measured nonlinear stress-strain properties for finite element analysis of footings, piles excavations and pressure meter tests, to assess the influence of small-strain nonlinearity in comparison with linear elastic behavior. From their study they concluded that although linear elasticity remains a convenient tool for expressing measurements of soil stiffness, unless the nonlinear nature of soil is taken account, interpretation of field measurements can be misleading. Also, small-strain nonlinearity has a significant influence on interpretation of equivalent elastic moduli of in-situ deformation tests.

Elhakim and Mayne (2008) developed a logarithmic modulus reduction algorithm to model and calculate soil modulus at different strain levels, using  $G_{max}$  as the benchmark. By incorporating these nonlinear moduli at different strain levels in settlement analysis calculations,

they were able to predict load-displacement response of footing on soft clay, very close to actual field measured load-displacement curve (Figure 2-19).

Lehane et al. (2008) conducted load tests on four different size footings on Perth sand. For their settlement predictions, they incorporated modulus nonlinearity for different strain levels including small level strains via Plaxis: HS-small model. They found that, foundation settlements predicted with Plaxis: HS-small model are much better than existing standard linear design methods and in some cases, close to actual measured load test settlements. (Figure 2-20)

In their analysis they observed that settlement predictions performed with in-situ measured parameters are more accurate than predictions performed with lab tested parameters. Settlements predicted with lab tested parameters are larger than settlements predicted using measured parameters, and in some cases 4 times larger. They explained that age and structure have a strong influence on  $G_{\max}$ , but the reference strain for in-situ and reconstituted sand are similar. Because of this difference in  $G_{\max}$ , settlement predictions with in-situ parameter are better than lab tested parameters. Based on their experience with Plaxis: HS-Small model, some limitations of the model were reported and they are:

1. Reference strain ( $\gamma_{0.7}$ ) is constant at all stress levels
2.  $G_{\max}$  varies with  $\sigma_3'$  only and is not dependent on the major principal effective stress.

## **2.6 Pavement Response Models**

### **2.6.1 MEPDG Nonlinear Response Model**

MEPDG recommends considering modulus nonlinearity of base soils for level-1 material parameter inputs. Nonlinear finite element response model for base layer analysis developed in MEPDG calculates nonlinear resilient modulus using the following equation:

$$M_R = k_1 p_a \left( \frac{\theta - 3k_6}{p_a} \right)^{k_2} \left( \frac{\tau_{oct}}{p_a} + k_7 \right)^{k_3} \quad (2-13)$$

$\theta$ - bulk stress at the peak of loading

$\tau_{oct}$  – octahedral shear stress at the peak of loading

$p_a$ - atmospheric pressure

$k_1$ - $k_7$  – material parameters

material parameters  $k_1$ ,  $k_2$  and  $k_3$  should be determined from  $M_R$  laboratory data.

Equation 2-13 calculates different  $M_R$  values for different stress levels based on corresponding stress state. These  $M_R$  values are calculated via constitutive equation, in which material parameters  $k_1$ ,  $k_2$  and  $k_3$  are determined from  $M_R$  laboratory data that is corresponding to limited strain range. Therefore these moduli values generated from nonlinear response model are appropriate for the limited strain range that can be measured in lab testing, but not a complete range of strains including small level strains required for accurate material nonlinear modeling.

MEPDG nonlinear response model for level-1 material nonlinear parameter inputs is not calibrated yet for complete designs analysis, and is not much useful for practical design purposes where a single effective moduli value is needed for initial design calculations.

## **2.6.2 Single Effective Moduli Determination Based on Nonlinear Versus Linear Analysis Responses Comparison**

Roque et al. (1992) performed a comprehensive analysis to determine whether linear elastic layer analysis can be used to accurately predict the nonlinear response of pavements. They performed nonlinear analysis using finite element computer program ILLIPAVE to predict nonlinear response of pavement structure. Surface deflections obtained from nonlinear analysis were used as matching factors to back calculate equivalent elastic moduli, using BISAR. 40 kN was used as design load for the analysis.

For nonlinear analysis, asphalt surface layer was considered elastic and both base and subgrade were considered nonlinear. ILLIPAVE uses stress dependent nonlinear moduli for nonlinear analysis. For better predictions and comparison, the upper 0.30 m of the subgrade was modeled as a separate layer. Comparison of surface deflections, stresses and strains between nonlinear analysis and back calculated linear analysis was made. But, these stresses and strains comparisons were made for surface layer only.

They found that, within the surface layer, fairly accurate predictions of deflections, stress and strain equal to nonlinear analysis can be made, when a single effective layer modulus was used to represent the surface and base layers. Nonlinear response of subgrade can be represented by two elastic layers and corresponding effective layer moduli. It may be very difficult to accurately represent the nonlinear response of weak pavement structures or silty-sand subgrade. This effective moduli determined at design wheel load can be applied to predict nonlinear pavement response at load levels of  $\pm 25\%$  of design load.

### **2.6.3 PLAXIS-HSsmall Model**

Plaxis-HSsmall model is the only commercially available and readily usable software, which can implement modulus nonlinearity in soils, with respect to both stress confinement and strain magnitude. HSsmall model considers nonlinear modulus at different strain levels (as high as  $10^1$ ) including very small level strain (i.e.  $\leq 10^{-6}$ ). Lehane et al. (2008) used for nonlinear modeling of soil under footing for settlement predictions and obtained fairly accurate results. Required input parameters for nonlinear modulus modeling can be obtained from resonant column testing and it is proposed to use Plaxis-HSsmall for development of nonlinear pavement response model. HSsmall model characteristics, back ground and required input parameters are explained in detail in Chapter 6.

## 2.7 Closing Remarks

Conclusions of this literature review are 1)  $G_{\max}$  of dry soils is primarily dependent on effective confining pressure ( $\sigma_c'$ ), and void ratio ( $e$ ), whereas  $G$  depends on strain( $\epsilon$ ) also. Gradation and max aggregate size are some of other various secondary influencing parameters. 2) Different empirical relationships were developed to calculate  $G_{\max}$  and hyperbolic models were developed to calculate  $G$  at different strain levels. Normalization of  $G$  with  $G_{\max}$  nullifies the effect of confinement. 3) Increase in suction due to drying of aggregate can increase modulus significantly. 4) Consideration of nonlinear small-strain modulus in geotechnical design and analysis improves soil deformation/settlements predictions.  $G_{\max}$  can be considered as benchmark for soil modulus nonlinearity. 5) Nonlinear small-strain stiffness of soils can have significant influence on determination of equivalent elastic modulus used for linear design and analysis. 6) It may be possible to determine single effective modulus which can approximate base layer nonlinearities, for a range of pavement structures and loads.

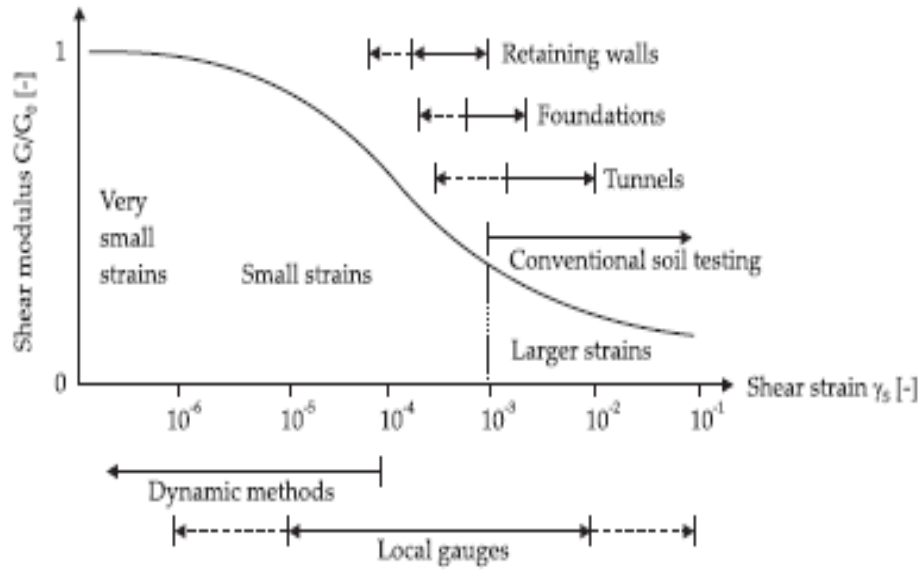


Figure 2-1. Characteristic modulus-strain behavior of soils with typical strain ranges for laboratory tests and structures (Reprinted by permission from Atkinson and Salfors (1991)).

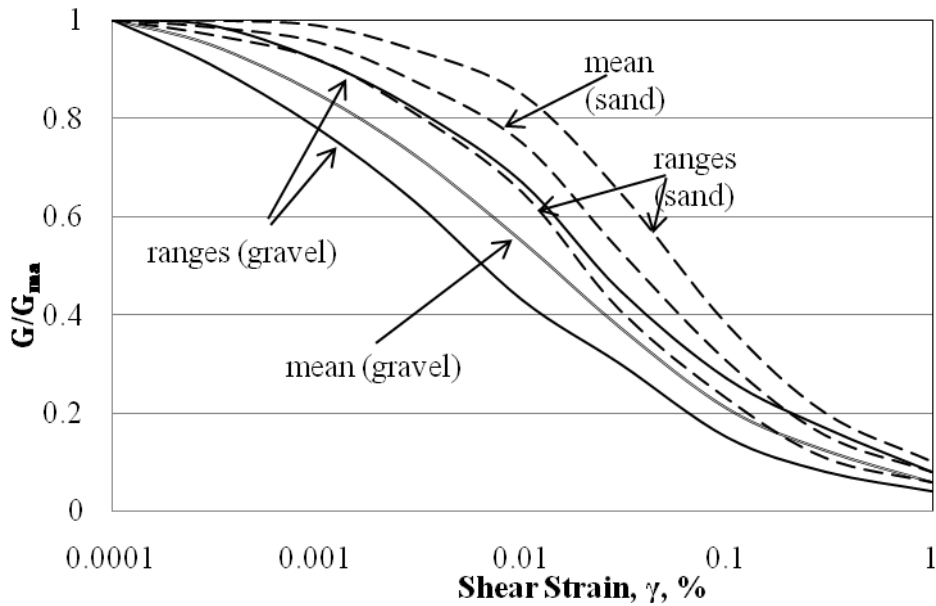


Figure 2-2.  $G/G_{max}$  versus  $\log \gamma$  curves of gravelly sandy soils (Reprinted by permission from Seed et al. (1986))

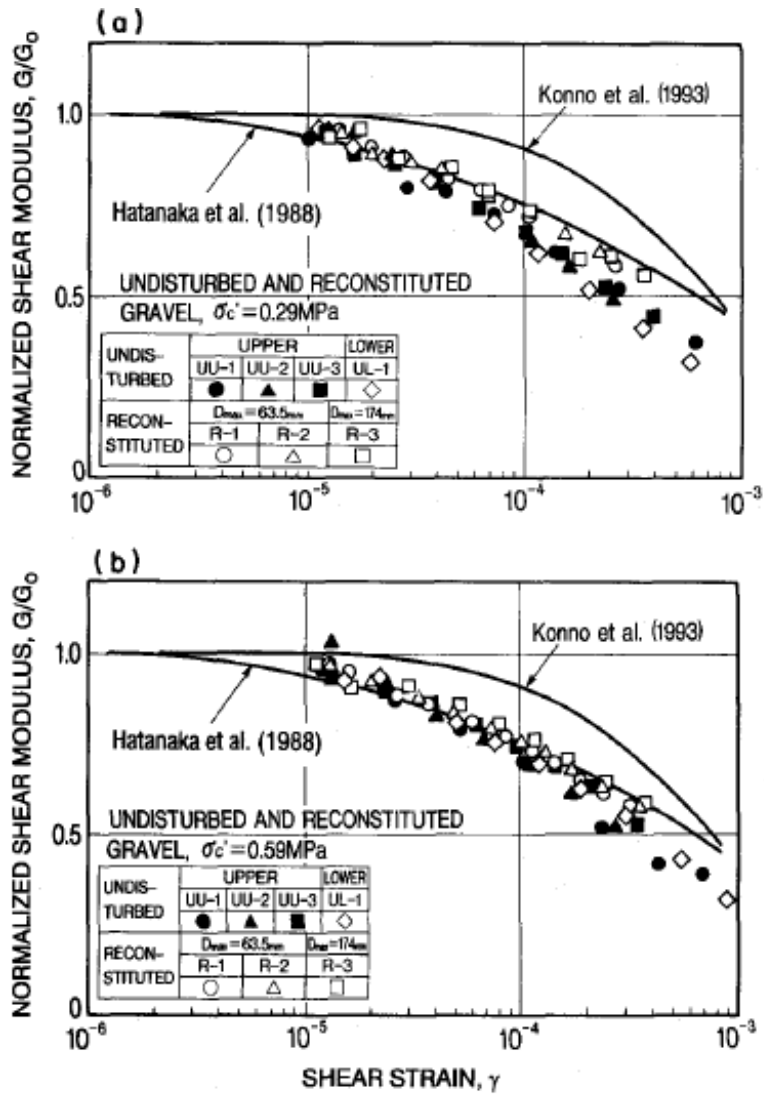


Figure 2-3.  $G/G_{\max}$  versus  $\log \gamma$  curves of undisturbed and reconstituted riverbed gravel (a) for  $\sigma_c = 0.29 \text{ MPa}$  and (b)  $\sigma_c = 0.59$  (Reprinted by permission from Yasuda et al. (1996))

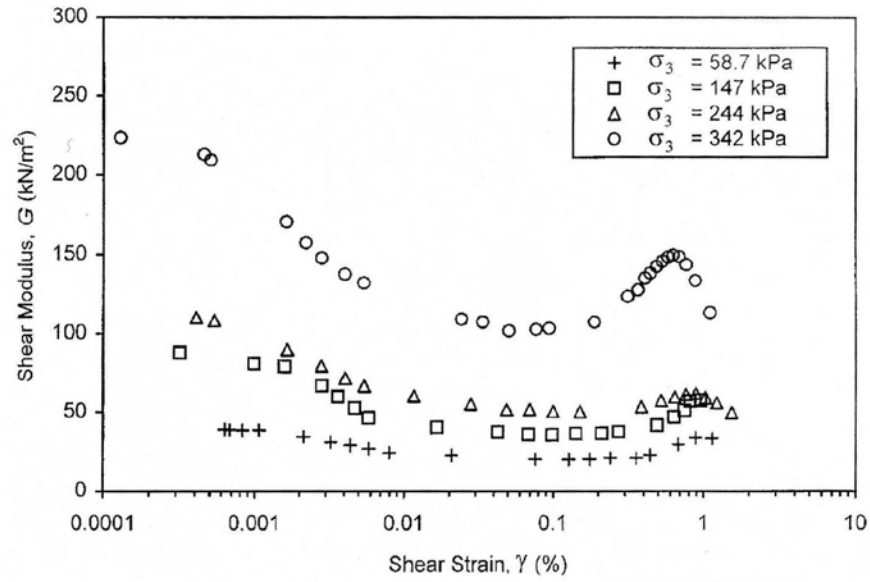


Figure 2-4. Effect of  $\sigma_3$  on the  $G$ - $\gamma$  relationship ( $d_{\max} = 1.27$  cm) (Reprinted by permission from Lin et al. (2000))

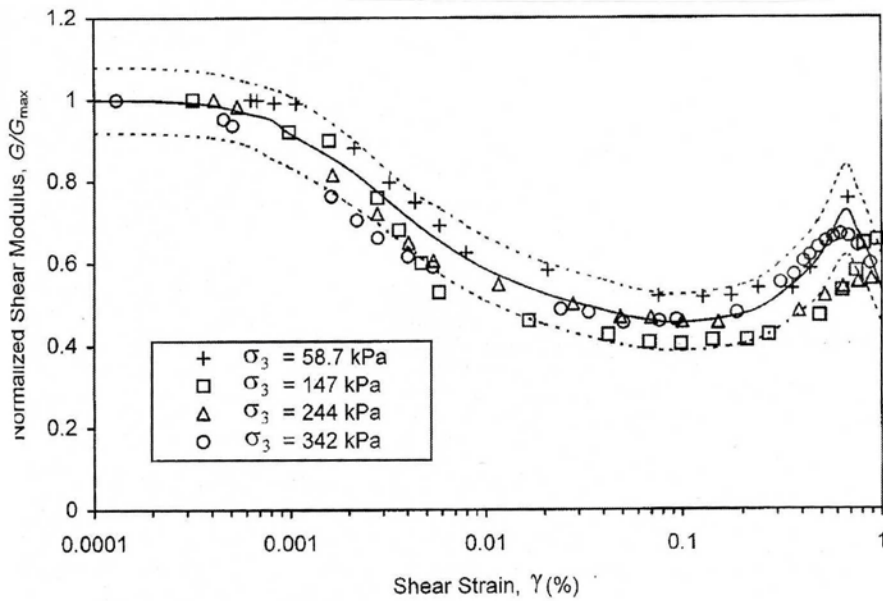


Figure 2-5. Variation of normalized shear modulus with shear strain ( $d_{\max} = 1.27$  cm) (Reprinted by permission from Lin et al. (2000))

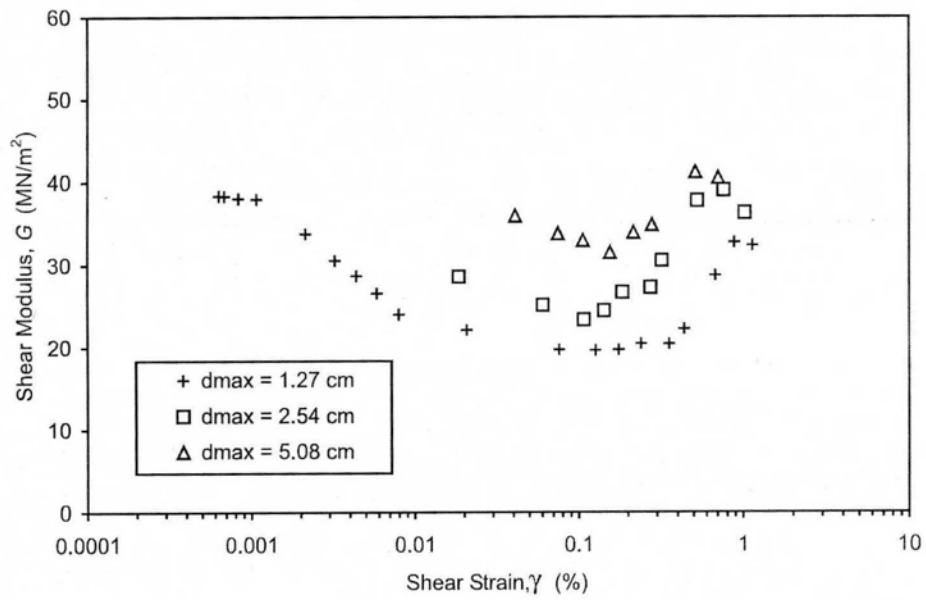


Figure 2-6.  $G$ - $\gamma$  relationship ( $\sigma_3 = 58.7 \text{ kN/m}^2$ ) (Reprinted by permission from Lin et al. (2000))

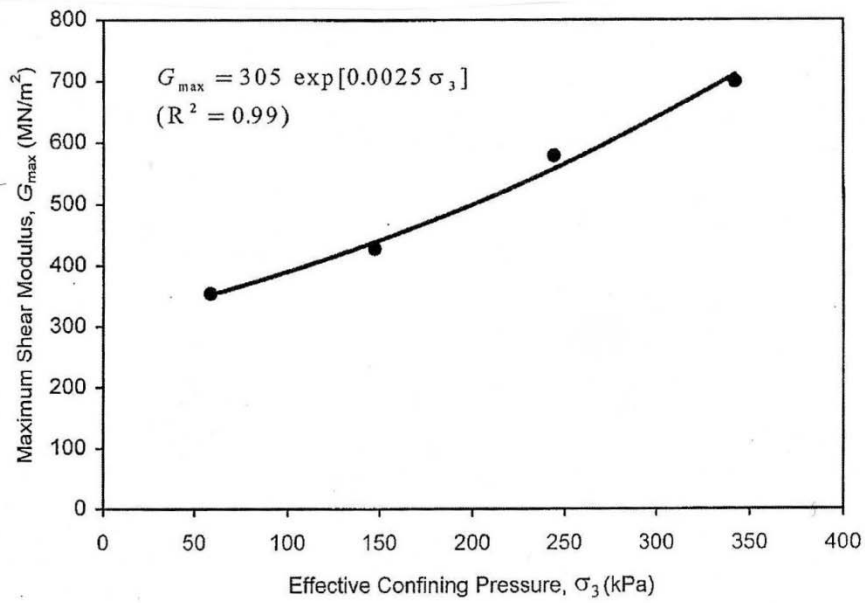


Figure 2-7. Variation of  $G_{max}$  of the field deposit with  $\sigma_3$  (Reprinted by permission from Lin et al. (2000))

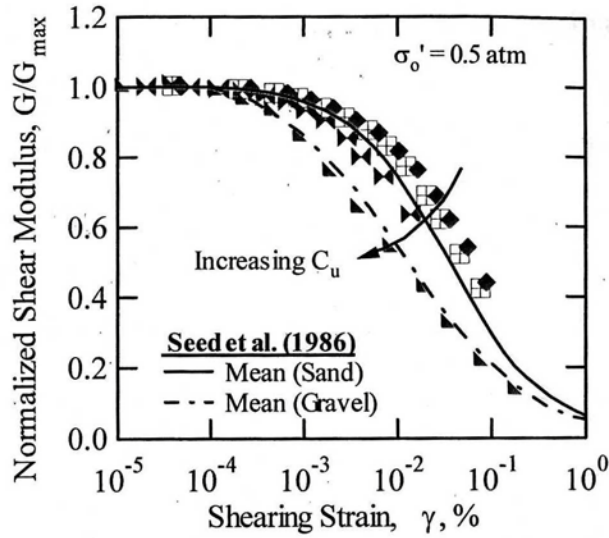


Figure 2-8.  $G/G_{\max}$  –  $\log \gamma$  relationship for gravelly soils (Reprinted by permission from Menq (2003))

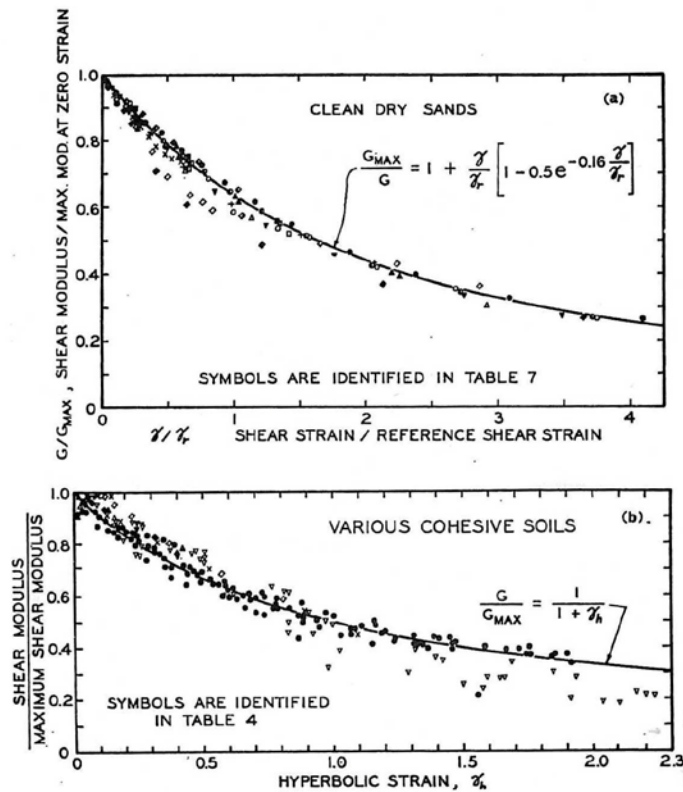


Figure 2-9. Comparison of calculated and measured values of normalized shear modulus (Reprinted by permission from Hardin and Drnevich (1972))

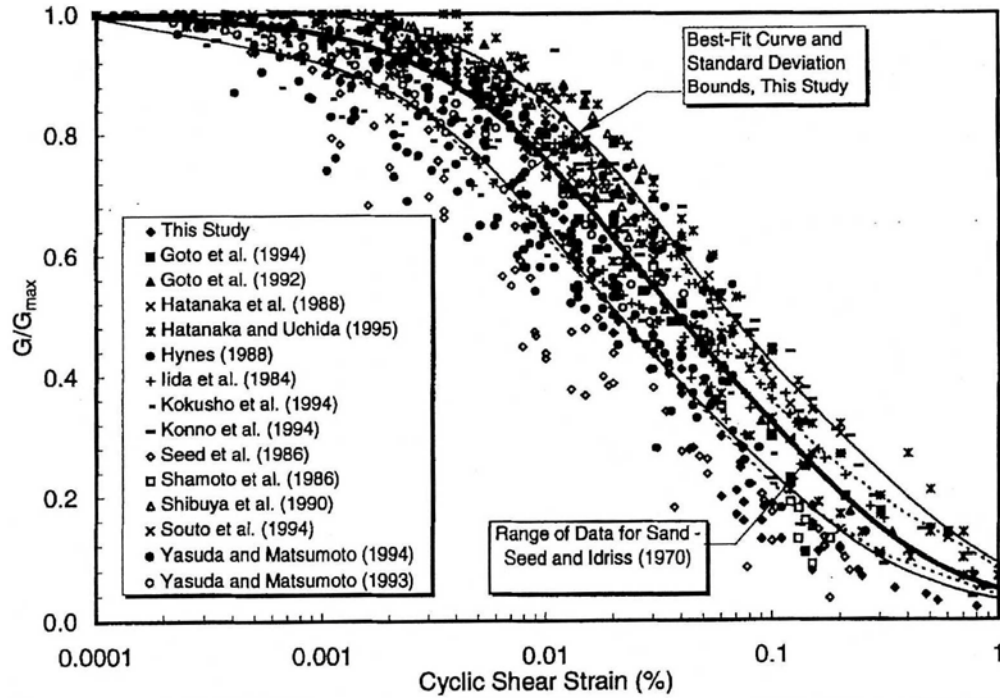
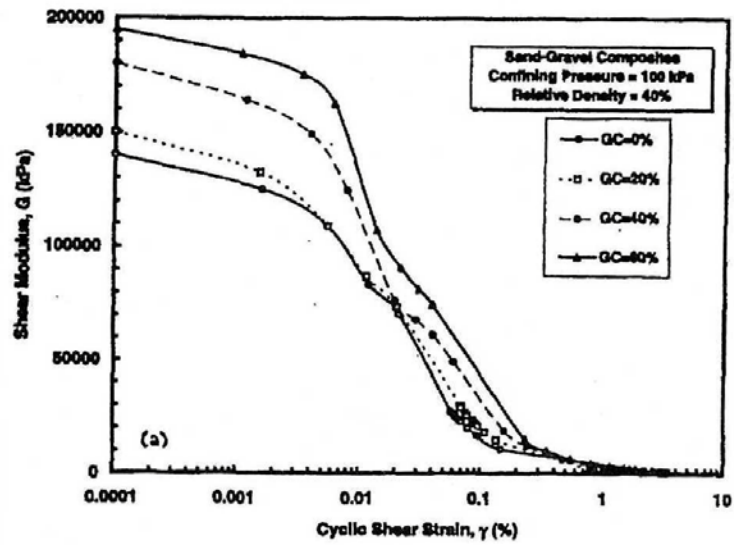
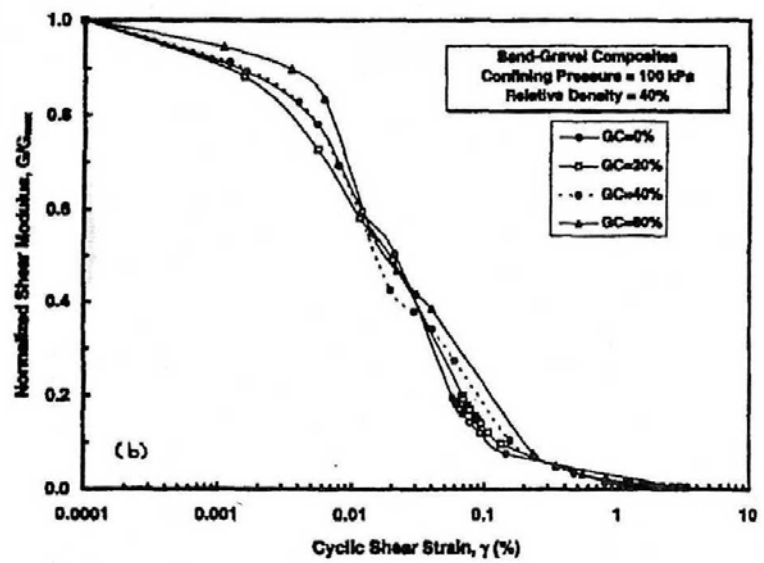


Figure 2-10. Data points defining  $G/G_{max}$  versus  $\gamma$  relationship for gravelly soils based on testing by all 15 investigators along with best-fit curve and  $\pm$  one standard deviation bounds for entire data set (Reprinted by permission from Rollins et al. (1998))



a



b

Figure 2-11. a)  $G$  versus  $\gamma$  curves and b)  $G/G_{max}$  versus  $\gamma$  curves determined for test specimens containing 0, 20, 40 and 60% gravel size particles (Reprinted by permission from Rollins et al. (1998)).

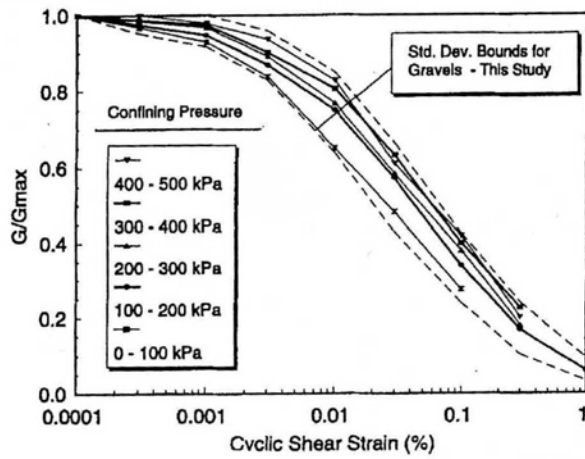


Figure 2-12. Mean curves defining  $G/G_{\max}$  versus  $\gamma$  relationships for gravelly soils at various confining pressures along with standard deviation boundaries for reduced data set (Reprinted by permission from Rollins et al. (1998)).

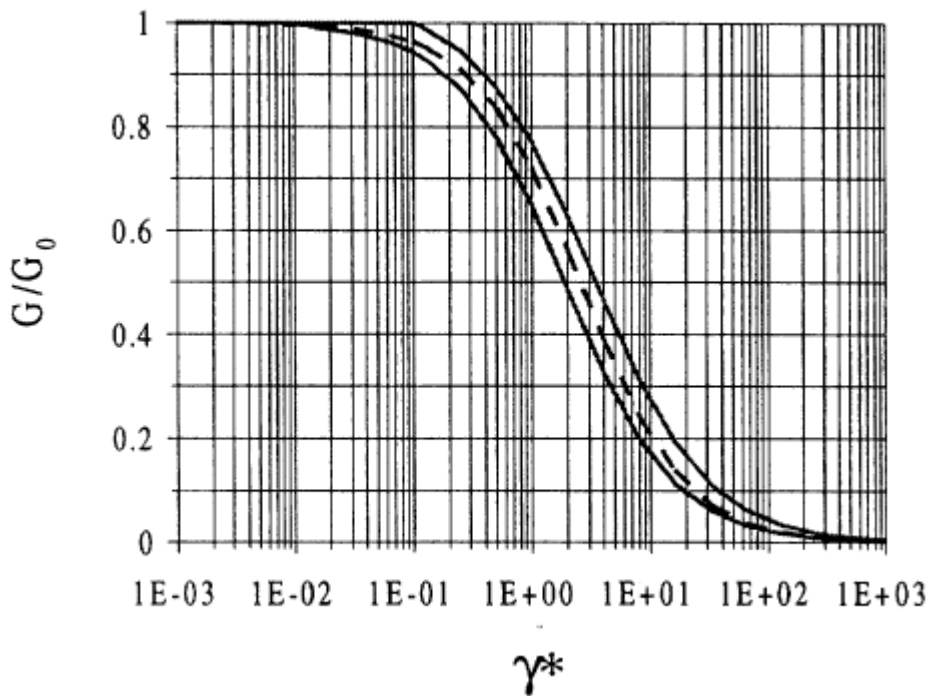


Figure 2-13. Shear modulus degradation curve proposed by Santos and Correia (2001) (Reprinted by permission from Santos and Correia (2001))

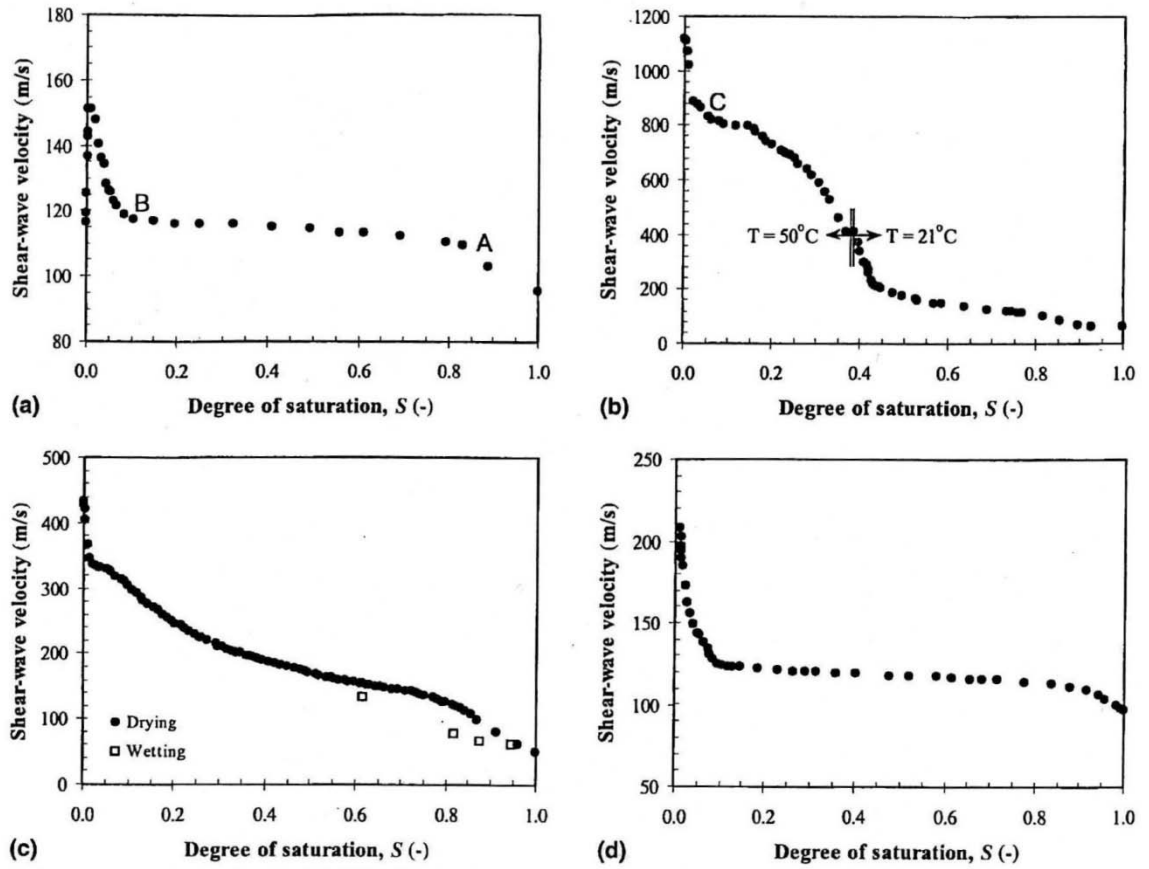


Figure 2-14. Shear –wave velocity versus degree of saturation for different materials : a) Clean glass beads ; b) Mixture of Kaolinite and glass beads; c) Granite powder; d) Sandboil sand. (Reprinted by permission from Cho and Santamarina (2001))

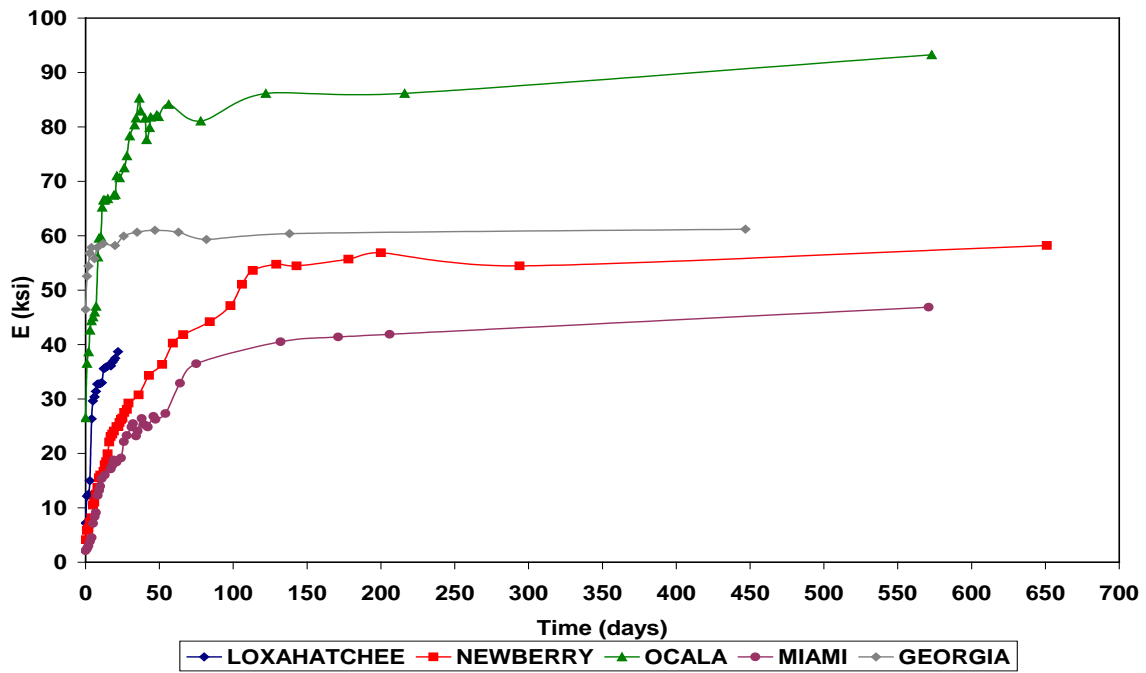


Figure 2-15. FFRC test results of specimen exposed to constant moisture (Reprinted by permission from Toros (2008))

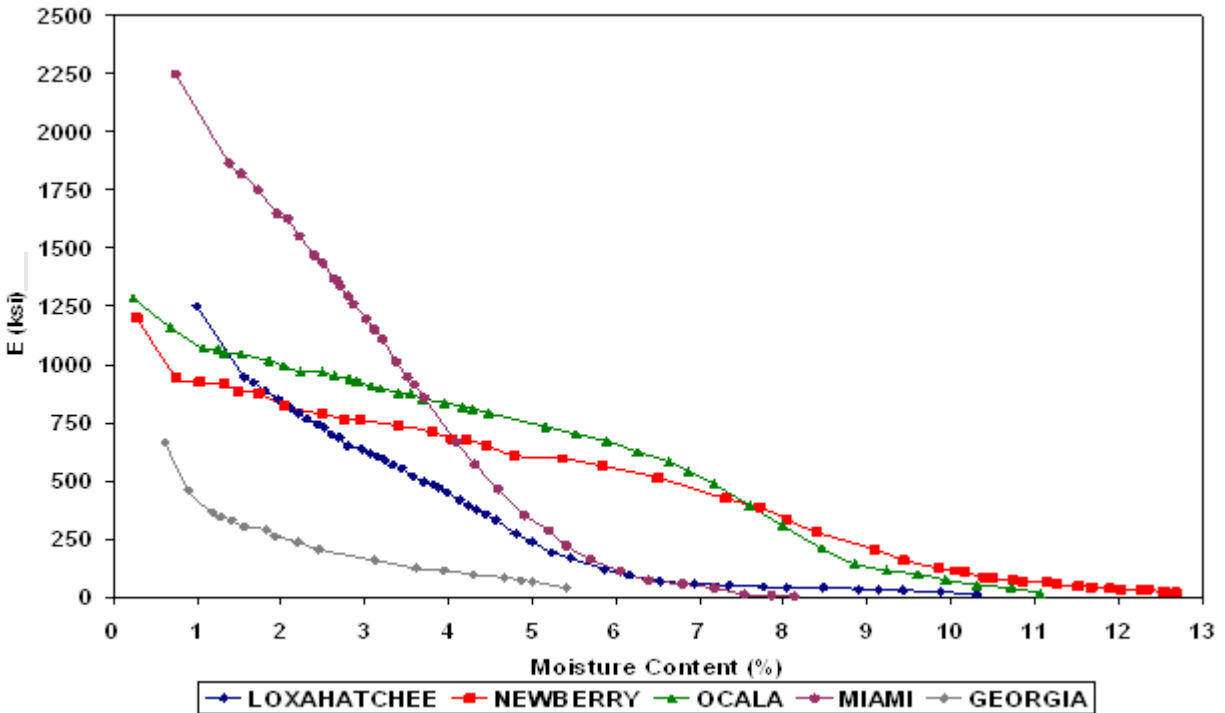


Figure 2-16. The FFRC test results of specimens exposed to laboratory ambient (Reprinted by permission from Toros (2008))

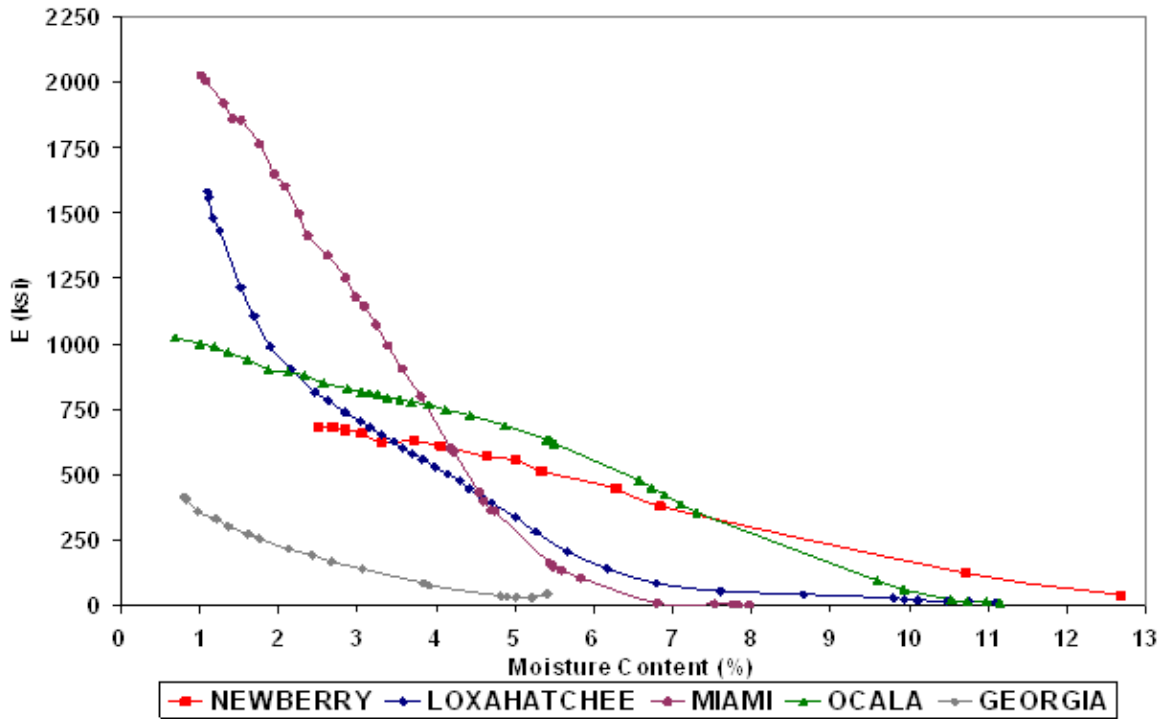


Figure 2-17. The FFRC test results of each material during first cycle of oven drying (Reprinted by permission from Toros (2008))

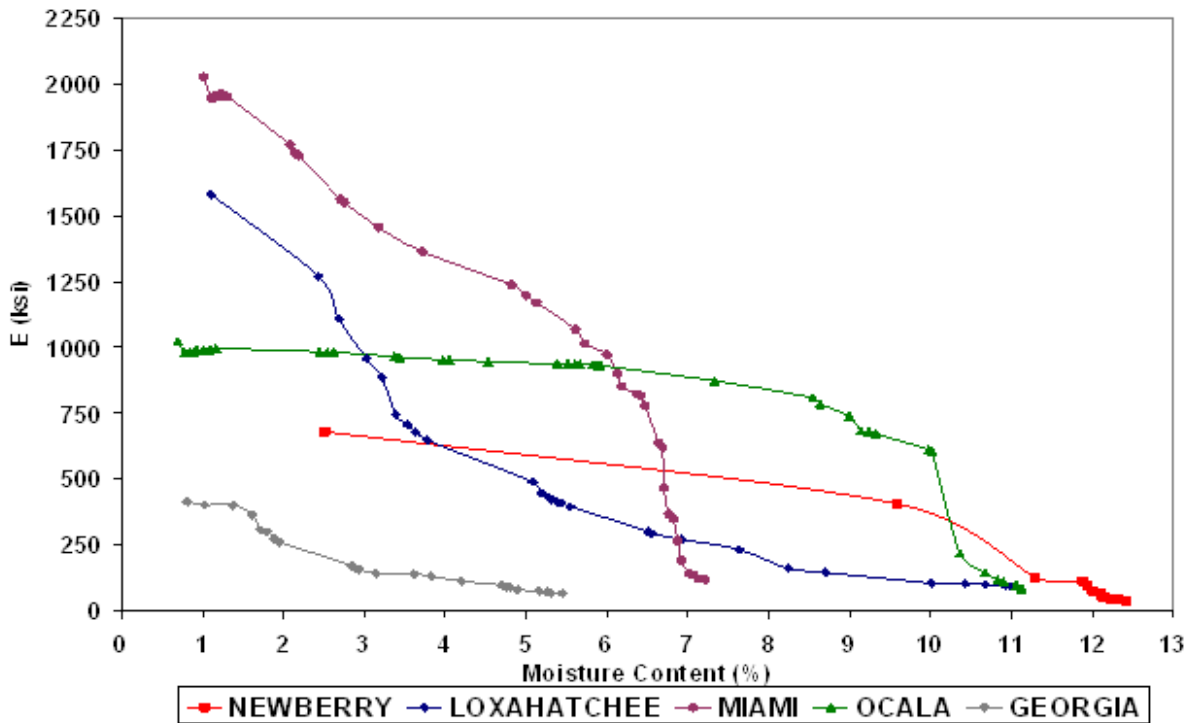


Figure 2-18. The FFRC test results of each material during first cycle of wetting (Reprinted by permission from Toros (2008)).

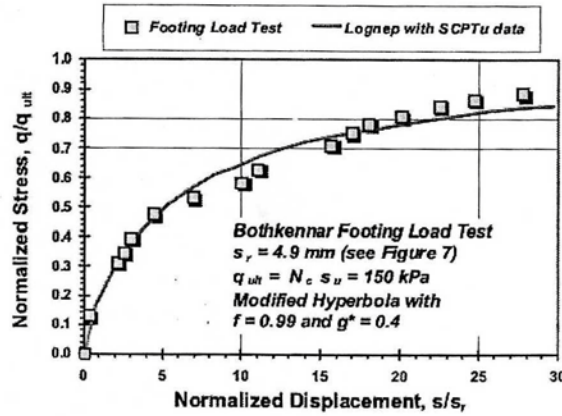


Figure 2-19. Load-displacement curves at Bothkennar footing test, fitted using the proposed model (footing performance data after High et al. (1997), Jardine et al.(1995)) (Reprinted by permission from Elhakim and Mayne (2008))

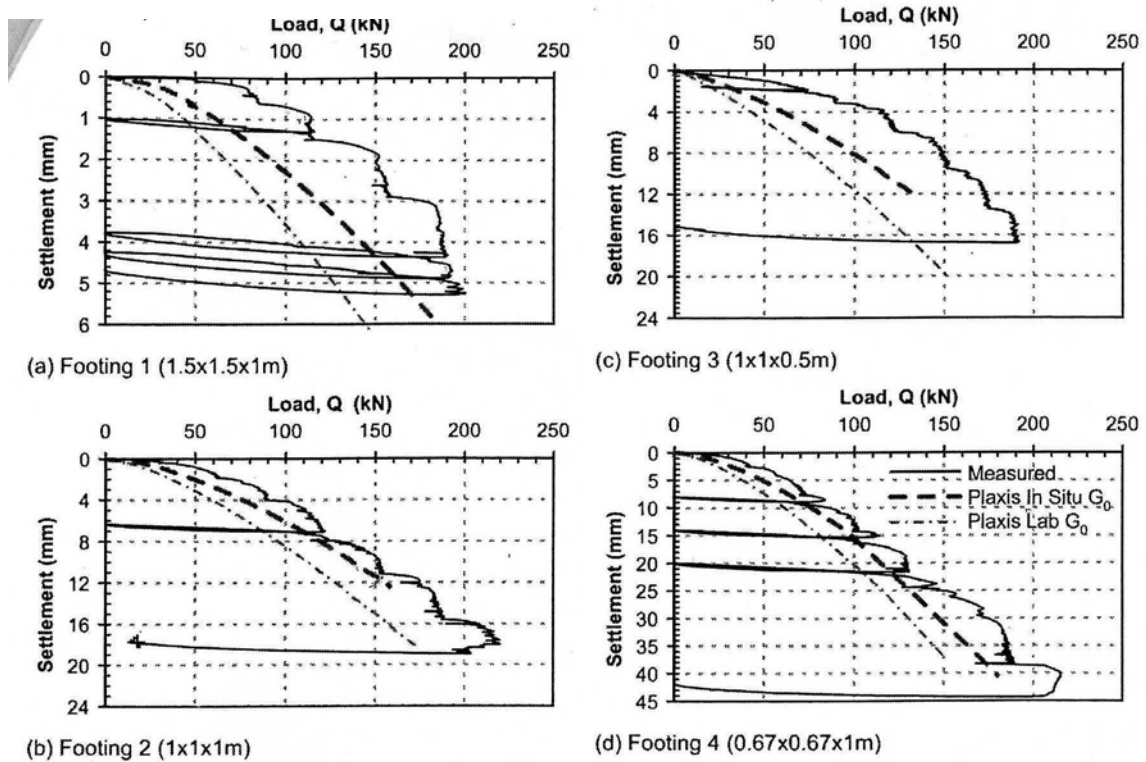


Figure 2-20. Comparison of measured foundation load settlement response at Shenton Park to prediction using Plaxis-HS Small model (Reprinted by permission from Lehane et al. (2008))

## CHAPTER 3 EXPERIMENTS

The first objective of this research study is to characterize modulus nonlinearity of selected base soils via a suitable laboratory testing program. Laboratory testing methodology should be selected such that it can effectively account for confinement stress, loading strain magnitude and moisture content effects on nonlinear modulus, including small-strain nonlinear modulus.

In literature review of Chapter 2, various research studies conducted to determine nonlinear small-strain shear modulus of sands and gravelly soils, via resonant column testing are discussed. Based on literature review and testing goals. Fixed-Free Resonant Column test and Free-Free Resonant Column test are selected for our laboratory testing, for nonlinear modulus characterization. Background, mechanism and limitations of these testing methods are discussed in this chapter.

### **3.1 Fixed-Free Resonant Column Testing**

Fixed-Free Resonant Column test (Fixed-Free RC) is a dynamic testing method, which can determine material nonlinear shear modulus ( $G$ ) under different confinement pressures and at very small to medium level strains.

#### **3.1.1 Background and Testing Mechanism**

Resonant Column method is based on one-dimensional wave equation derived from the theory of linear-elastic vibration. For our testing, Fixed-Free Resonant Column Torsional Shear (Fixed-Free RCTS) testing device is used. Using this equipment, both resonant column and torsional shear tests can be preformed. For our testing Fixed-Free Resonant Column (Fixed-Free RC) mechanics only is utilized. In Fixed-Free RC device, the soil column is fixed at the base and free to rotate at top. With this apparatus, an external cyclic torsional load is applied to top of the specimen. The loading frequency is gradually changed until maximum response (strain

amplitude) is found. The lowest frequency at which maximum strain amplitude obtained is the fundamental frequency ( $\omega_n$ ) of the soil specimen and driving system, for that specific applied torsional load. This fundamental frequency is function of soil modulus, specimen geometry and characteristics of resonant column device.

### 3.1.2 Shear Modulus (G)

The governing equation for motion for the Fixed-Free RC test as idealized in Figure 3-1a, for torsional vibration with a Kelvin-Voigt soil model is derived as follows. For a torque (T), applied to an elastic soil cylinder which generates angle of twist ( $d\theta$ ), along an incremental length of specimen (dz), can be expressed as:

$$T = GJ \frac{\partial \theta}{\partial z} \quad (3-1)$$

where  $T$ = torque,  $G$  = shear modulus of the soil and  $J$ = polar moment of inertia of the cross sectional area

From Figure 3-1b, the torque on two faces of the soil element are  $T$  and  $T + \frac{dT}{dz}$ . Using the torque (T), from Equation 3-1, we obtain:

$$\frac{\partial T}{\partial z} dz = GJ \frac{\partial^2 \theta}{\partial z^2} \quad (3-2)$$

Applying Newton's second law to the motion of the soil column and equating this net torque to the product of the mass polar moment of inertia and the angular acceleration:

$$\frac{\partial T}{\partial z} dz = I \frac{\partial^2 \theta}{\partial t^2} = \rho J dz \frac{\partial^2 \theta}{\partial t^2} \quad (3-3)$$

where  $I$  = mass moment of inertia =  $\rho J dz$ ,  $\rho$  = soil mass density

From soil mass density ( $\rho$ ), and shear wave velocity ( $V_s$ ), Shear modulus (G) can be calculated as:

$$G = \rho V_s^2 \quad (3-4)$$

Substituting  $\frac{\partial T}{\partial z}$  from Equation 3-3 and using Equation 3-4, we obtain the wave equation in torsion for an elastic rod:

$$\frac{\partial^2 \theta}{\partial z^2} = \frac{1}{V_s^2} \frac{\partial^2 \theta}{\partial t^2} \quad (3-5)$$

The general solution to Equation 3-5, is found using separation of variables as:

$$\theta(z,t) = \left[ A \sin\left(\frac{w}{V_s} z\right) + B \cos\left(\frac{w}{V_s} z\right) \right] * e^{i\omega_n t} \quad (3-6)$$

where  $\omega_n$ =natural circular frequency and

A and B=constants dependent on the boundary conditions of the soil column.

The boundary conditions in this Fixed-Free RC system are:

1. The angular displacement at the bottom (fixed end ) is zero
2. The torque at the top of the soil specimen (free end) is equal to the inertia torque of the drive system but opposite.

By solving the Equation 3-1, by substituting these known boundary equations, final resulting expression is:

$$\frac{I}{I_0} = \frac{\omega_n h}{V_s} \tan\left(\frac{\omega_n h}{V_s}\right) \quad (3-7)$$

where I-mass moment of inertia,  $I_0$ - mass moment of inertia of drive system, h-height of specimen.

Once the shear wave velocity ( $V_s$ ) is determined, shear modulus ( $G$ ) can be calculated from Equation 3-4.

### 3.1.3 Shear Strain ( $\gamma$ )

The shear strain in a cylindrical resonant column loaded in torsion varies from zero at the center line of specimen to a maximum value at its outer edge as shown in Figure 3-2. Since a single or unique value of shear strain amplitude with the measured shear modulus ( $G$ ), is required, conventionally  $r_{equ}$  is assumed as  $2/3(r_0)$  for solid specimens with radius  $r_0$ .

Shear Strain ( $\gamma_r$ ) is calculated as follows:

$$\gamma_{(r)} = \frac{r_{equ} \theta_{max}}{h} \quad (3-8)$$

Where  $r_{equ}$  -equivalent radius of specimen= $\frac{2}{3} r_0$

$$r_0 \text{ -Radius of solid specimen, } \theta_{\max} \text{ -maximum angle of twist} = \frac{x}{r_{\text{sensor}}}$$

$r_{\text{sensor}}$  -distance of target center (or fiber optic sensor) from specimen's central axis

$x$ —radial displacement of target.

The radial displacement of target is measured by fiber optic sensor system, which can measure strains in the range of  $10^{-5}\%$  to  $10^{-1}\%$ .

### 3.1.4 Equipment Setup

Fixed-Free RC equipment consists of a perspex glass cylindrical chamber with leak proof top and bottom covering plates at both ends of the chamber (Figure 3-3 and Figure 3-4). Bottom cap of the specimen is attached firmly to the chamber's bottom plate, and top end of the specimen is left free to rotate, thus bottom end becomes fixed end and top end becomes free end. Torsional loading motor is attached to specimen's top cap with proper supporting system. A fiber optic sensor target to measure radial displacements is attached to specimen's top cap. This target extends out from the top cap, in specimen's radial direction. Fiber optic sensor cable is attached to one of chamber supporting rods and positioned facing the target. This sensor system measures the radial displacements of target caused due to torsional loading. Entire testing chamber unit is fixed firmly to a loading frame for stability. Tests can be run and controlled through a software program, which sends control signals to resonant column interface and servo amp unit (Figure 3-5a), controlling torsional loading motor and amount of load to be applied. The fiber optics sensor system (Figure 3-5c) sends target displacement information back to the controlling software, which eventually calculates the resonant frequency ( $\omega_n$ ) internally using software (Figure 3-6). Air confinement can be applied via pressure control panel (Figure 3-5b).

### 3.1.5 Calibration of the Drive System:

When torsional load is applied during testing, torsional motor rotates top specimen cap along with the testing specimen. Weight of the cap and motor, along with specimen's weight,

becomes part of total weight of the testing system. To nullify the effects of top specimen cap and motor weight and to determine the properties of specimen alone, calibration of driving system is required.

Calibration of driving system is performed using a metallic specimen instead of real soil specimen (Figure 3-7). The metallic specimen is assumed to have zero or close to zero damping and a constant torsional stiffness (k). Then from Newton's second law, the mass moment of inertia is related to the natural or resonant frequency ( $\omega_n$ ) as follows:

$$I = \frac{k}{\omega_n^2} \quad (3-9)$$

Recommended procedure to find the mass moment of inertia of the driving system ( $I_0$ ) is to perform two resonant column tests with the metal calibration specimen, one by itself and the other with an added mass. After performing frequency sweep with constant force amplitude, the solutions will be:

$$\text{without added mass: } I_0 + I_{cal} = \frac{k}{\omega_1^2} \quad (3-10)$$

$$\text{with added mass : } I_0 + I_{cal} + I_{mass} = \frac{k}{\omega_2^2} \quad (3-11)$$

where  $I_0$ =mass moment of inertia of the drive system and any other fixture that will be used during actual soil testing

$I_{cal}$  = mass moment of inertia of the calibration specimen

$I_{mass}$  = mass moment of inertia of the added mass

$\omega_1$  = resonant frequency of calibration specimen without the added mass

$\omega_2$  = resonant frequency of calibration specimen with the added mass

By combining equations 3-10 and 3-11, we get:

$$I_0 = \frac{(I_{cal} + I_{mass})\omega_2^2 - I_{cal}\omega_1^2}{\omega_1^2 - \omega_2^2} \quad (3-12)$$

### **3.1.6 Limitations (We Experienced) of This Testing Equipment:**

The maximum frequency that can be applied using the torsional loading motor of our Fixed-Free RC equipment is 300 Hz. In other words, specimens with resonant frequency less than 300 Hz only can be tested with this equipment. Part of our testing program (explained in detail in Chapter 5) is to run tests on specimens compacted at optimum moisture content and then dried to different water contents, thus the modulus of material can be determined at different water contents and at different strain levels. But, after drying the specimen to below certain water content (as explained in later chapters), its resonant frequency is reaching beyond 300 Hz due to increase in its modulus. As a result, we are able to determine material modulus up to certain water content below OMC, but not all the way dried to zero water content.

### **3.1.7 Equipment Credibility Verification**

After installation, equipment is subjected to verification to make sure that the testing measurements are correct and credible. This verification is performed by conducting tests on Ottawa sand. For Ottawa sand, experimental results determined for shear modulus are available in literature, and thus our testing results can be compared with literature data for verification.

Verification test is conducted on 4 inch diameter and 8 inch height Ottawa sand specimen compacted to minimum void ratio ( $e_{\min}$ ) of 0.435. This compacted specimen is subjected to six different confining pressures ( $\sigma_c$ ) 50, 100, 150, 200, 250 and 300 KPa. Shear modulus ( $G$ ) at different strain levels in the strain range of  $10^{-4}\%$  to  $10^{-1}\%$  are measured at each confinement. These testing results are shown in Figures 3-8 and 3-9.

With the very small-strain modulus ( $G_{\max}$ ) (i.e.  $G$  at  $\gamma = 10^{-4}\%$ ) data at different confining pressures,  $G_{\max}$  versus  $\text{Log}(\sigma_c)$  plot is developed and shown in Figure 3-9. From this plot, an empirical relationship to calculate  $G_{\max}$  is developed in the form of (proposed by Hardin and Richart (1963))

$$G_{max} = A_G F(e) (\sigma_c^1)^{n_G} \quad (2-5)$$

where  $A_G$  and  $n_G$  are material constants and  $F(e) = (2.17-e)^2 / (1+e)$ ,

$G_{max}$  and  $\sigma_c^1$  are in kPa.

From our testing data, obtained value for

$n_G=0.5165$  and

$e=0.435$ ,  $F(e)=2.098$

By substituting values of  $F(e)$  and  $n_G$  in Equation 2-5, and solving it with the testing data, empirical equation obtained to calculate  $G_{max}$  is:

$$G_{max} = (5350) (2.098) (\sigma_c^1)^{0.5165} \quad (3-13)$$

$n_G = 0.5165$  obtained from our testing matches well with the literature data for Ottawa sand (Hardin and Richart (1963), Menq (2003)). Also, value of  $A_G=5350$  fall in the range of 3300 to 9000 for sands (Menq(2003)).

Thus, by comparing our Ottawa sand testing results with literature data, the credibility of Fixed-Free RC equipment data is successfully verified.

### 3.2 Free-Free Resonant Column Testing (Free-Free RC)

Free-Free RC testing method (Kim and Stokoe (1992), Menq (2003), Toros(2008)) is used to determine very small-strain modulus ( $G_{max}$  or  $E_{max}$ ) (i.e.  $\leq 10^{-5}\%$ ) of Florida base materials at different water contents. This test can be conducted very quickly on laboratory compacted specimens. Further, Free-Free RC test is nondestructive, and thus can be conducted on the same specimen at different water contents by drying it as required.

#### 3.2.1 Back Ground and Mechanism

Two different types of stress wave measurements can be conducted on a solid rod with Free-Free RC testing: 1) resonance measurements and 2) direct-arrival measurement. With

known specimen dimensions and measured resonance frequency ( $\omega_n$ ), unconstrained modulus or Young's modulus (E) can be determined using equations 3-14 and 3-15.

$$\text{Unconstrained compression wave velocity } V_c = 2 \omega_n l \quad (3-14)$$

where  $l$  – length of specimen,

$$\text{Young's modulus } E = \rho V_c^2 = \rho (2 \omega_n l)^2 \quad (3-15)$$

travel time ( $\Delta t$ ) of constrained compression wave is determined via direct-arrival measurement, from which constrained compression wave velocity ( $V_p$ ) is calculated as

$$V_p = \frac{l}{\Delta t} \quad (3-16)$$

where:  $l$ =length of the specimen,

$\Delta t$  = measured travel time of constrained compression wave

With known constrained compression wave velocity ( $V_p$ ) and unit mass of the specimen ( $\rho$ ), constrained modulus (M) can be calculated as

$$M = \rho V_p^2 = \rho \left( \frac{l}{\Delta t} \right)^2 \quad (3-17)$$

With known constrained and unconstrained wave velocities, Poisson's ratio ( $\nu$ ), can be calculated as:

$$\nu_{ME} = \frac{1 - \left( \frac{V_p}{V_c} \right)^2 + \sqrt{\left( \left( \frac{V_p}{V_c} \right)^2 - 1 \right)^2 + 8 \times \left( \frac{V_p}{V_c} \right)^2 \left( \left( \frac{V_p}{V_c} \right)^2 - 1 \right)}}{4 \times \left( \frac{V_p}{V_c} \right)^2} \quad (3-18)$$

With known Poisson's ratio ( $\nu$ ), Young's modulus (E), and constrained modulus (M); shear modulus (G) can be calculated as:

$$G = \frac{E}{2(1 + \nu)} \quad (3-19)$$

$$G = \frac{2M\nu - M}{2(\nu - 1)} \quad (3-20)$$

For our Free-Free RC testing, we used the same equipment used by Toros (2008) to measure very small-strain modulus of Florida base materials. A detailed back ground and mechanism explanation about Free-Free RC testing and equipment verification was given in Toros (2008) PhD. dissertation.

### **3.2.2 Equipment Setup:**

Modified Proctor compacted specimens without any confinement of casing or membrane are tested with this equipment. The same testing procedure, which was verified by Toros (2008) is followed. Our Free-Free RC testing system consists of a dynamic signal analyzer (DSA) or (oscilloscope), an instrumented impact hammer and an accelerometer (transducer). Specimens are oriented horizontally and suspended with flexible straps to achieve free-free boundary conditions (Figure 3-10). Excitation point with impact hammer is at the center of one end of the specimen, and location of accelerometer is at the center of other end of the specimen. Accelerometer is glued to the center of one end of the specimen.

The main difference between our testing procedure and Toros (2008) testing procedure is confinement with casing around specimen (Figure 3-11). Toros (2008) tested 6 inch diameter and 12 inch height specimens with plastic casing around them, where as we tested 4 inch diameter and 8 inch height naked specimens without any confining casing.

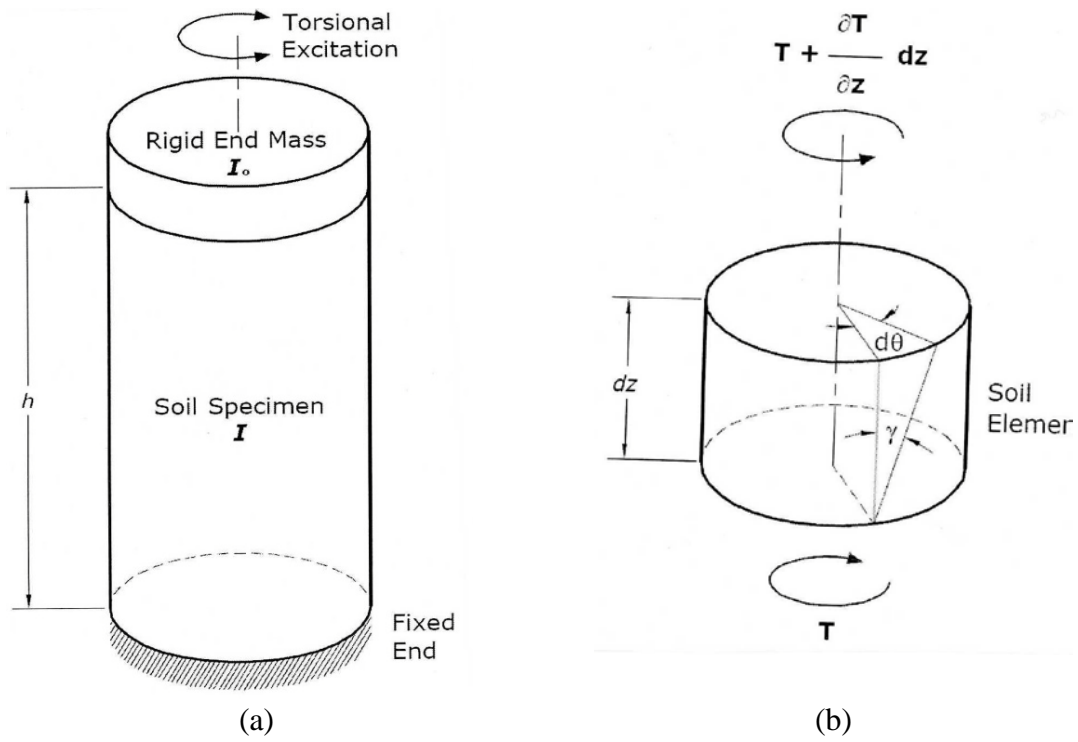


Figure 3-1. Fixed-Free RC testing specimen (a) Idealized testing specimen (b) Differential soil element

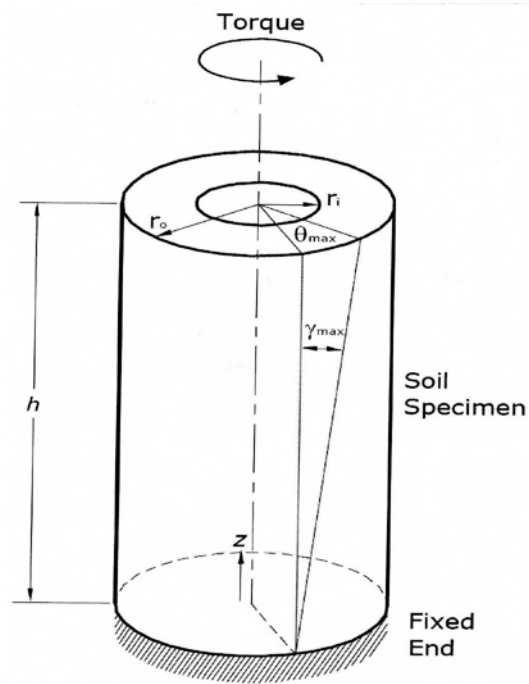


Figure 3-2. Shear Strain in soil specimen



Figure 3-3. Fixed-Free RC equipment used for our testing

(Photo courtesy of Ayithi (2011))

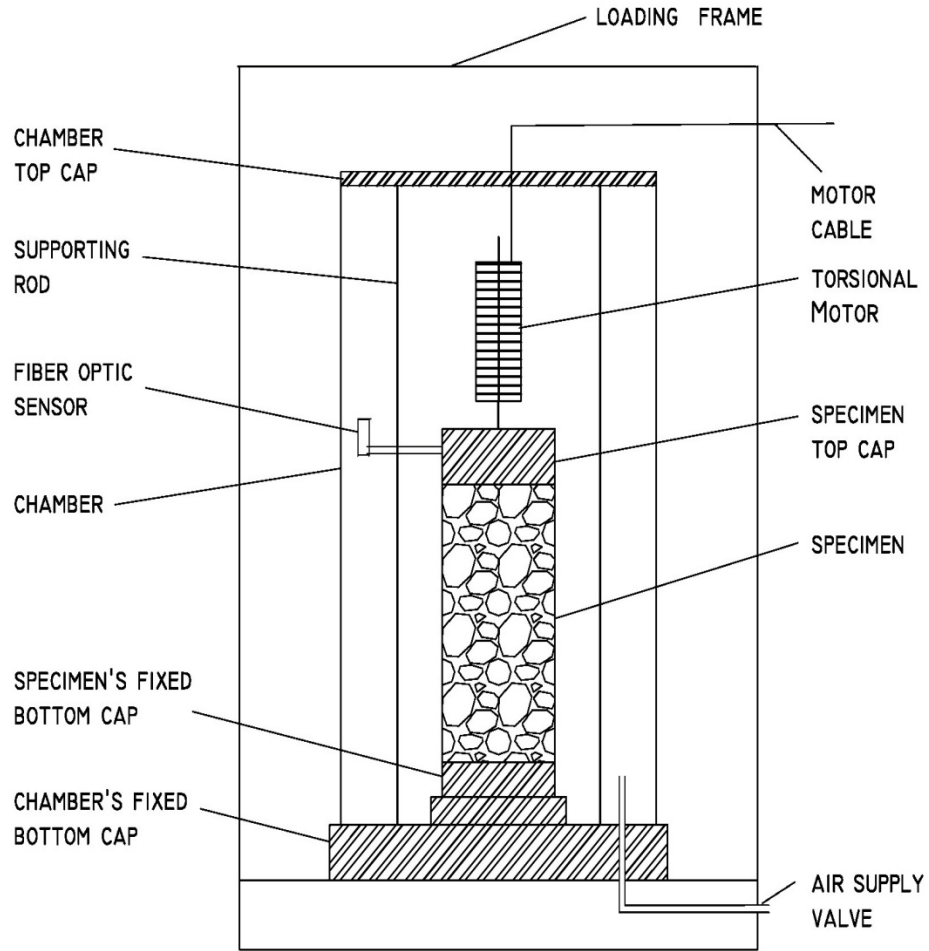


Figure 3-4. Sectional view of Fixed-Free RC testing equipment



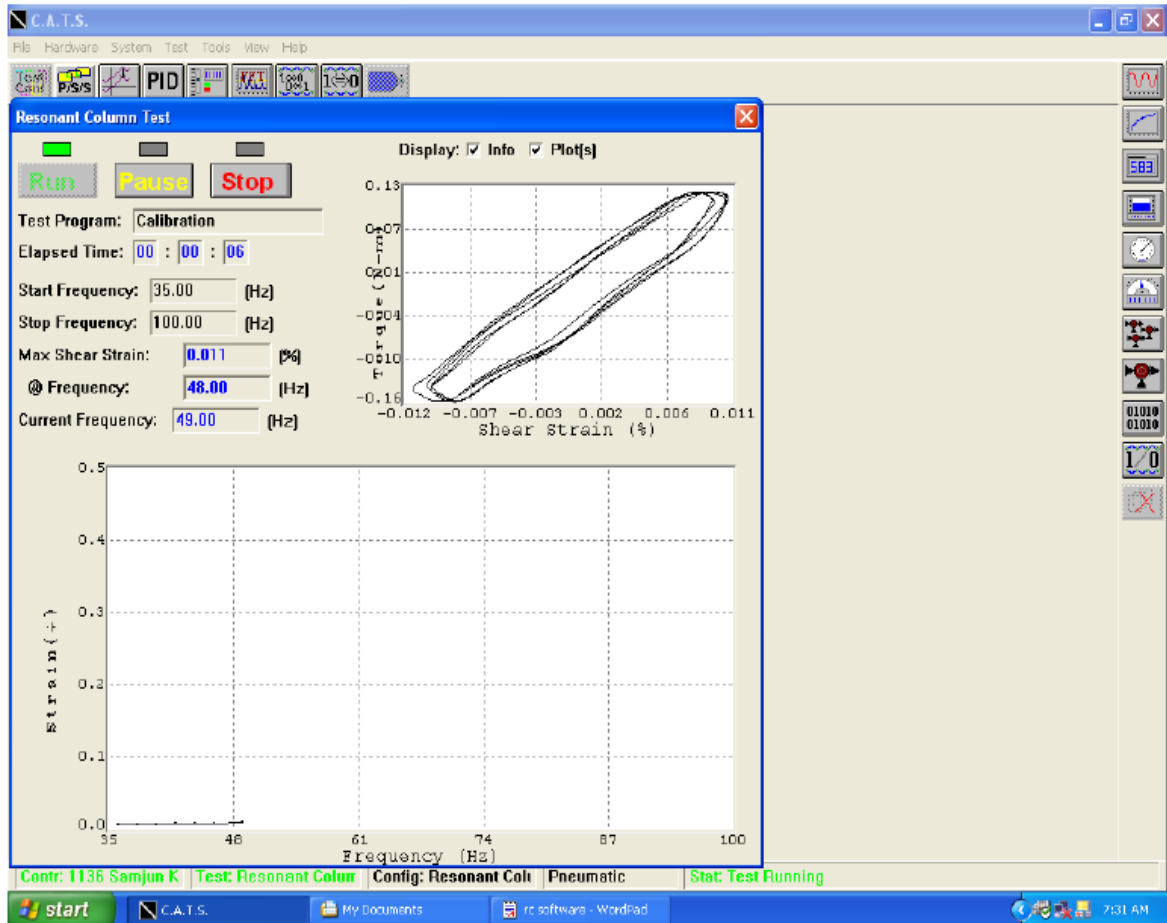


Figure 3-6. Real time test execution window, showing resonant frequency reaching loop  
 (Photo courtesy of Ayithi (2011))



Figure 3-7. Calibration specimen with added mass

(Photo courtesy of Ayithi (2011))

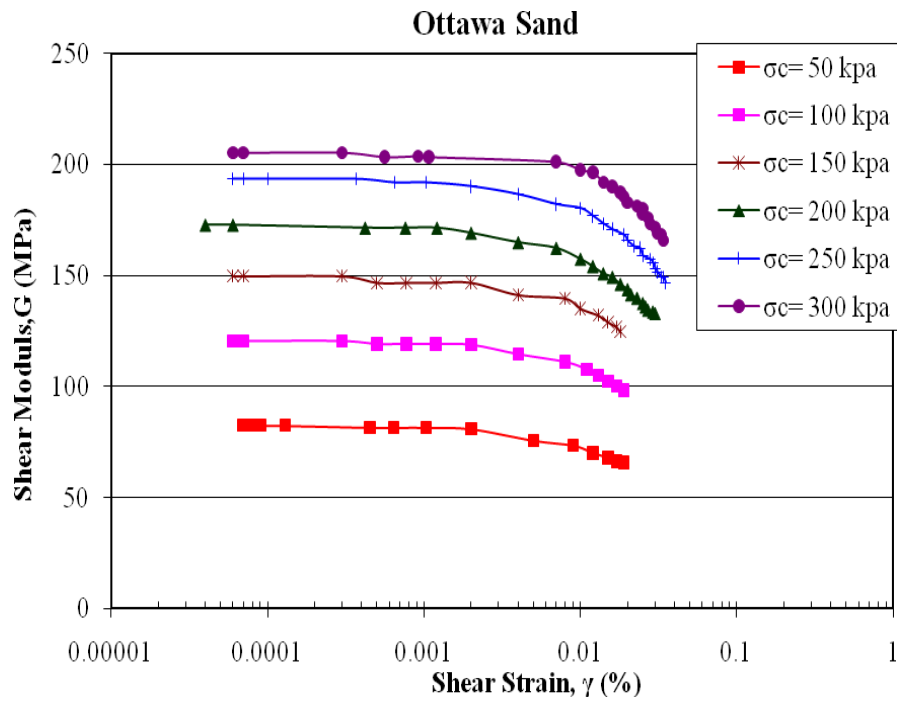


Figure 3-8. Shear modulus versus % shear strain curves at different confining pressures for Ottawa sand.

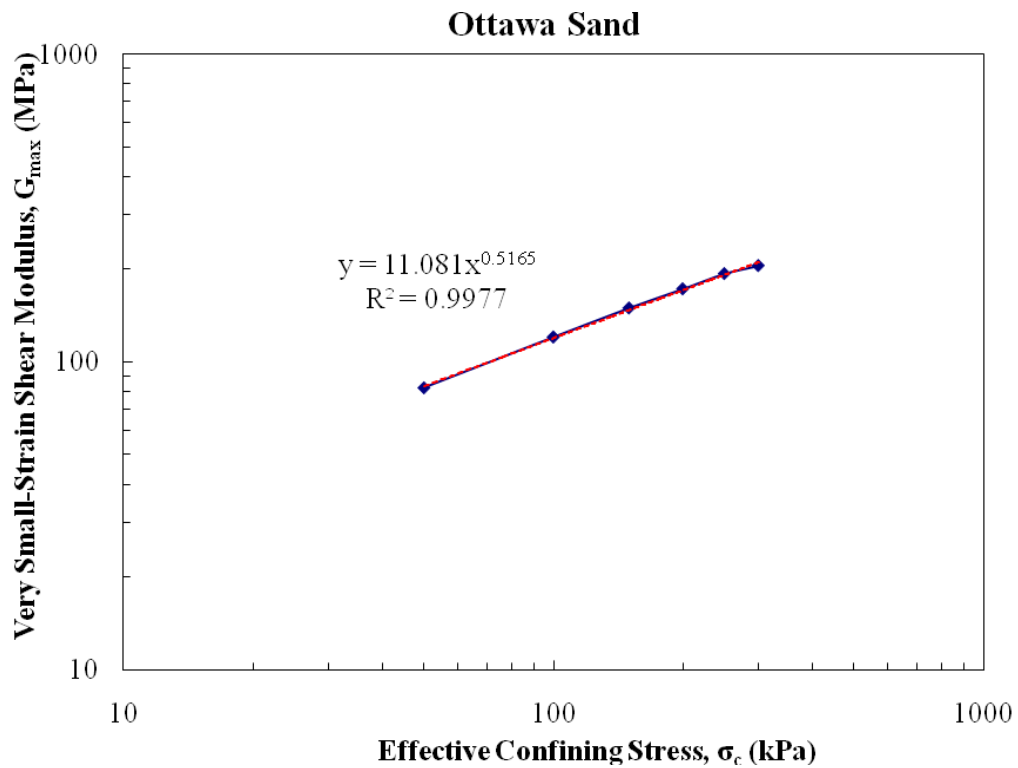
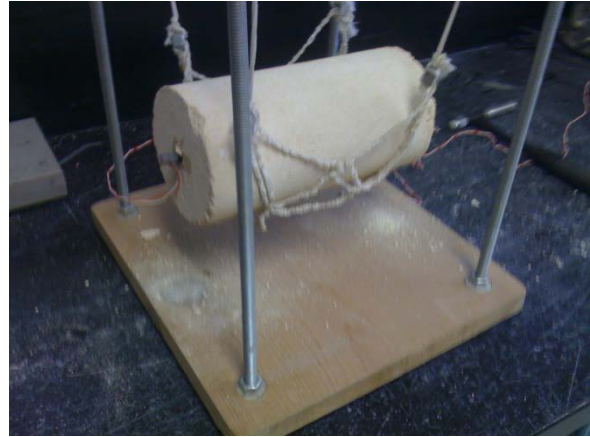


Figure 3-9.  $G_{max}$  versus  $\log \sigma_c$  relationship curve for Ottawa sand.



(a)

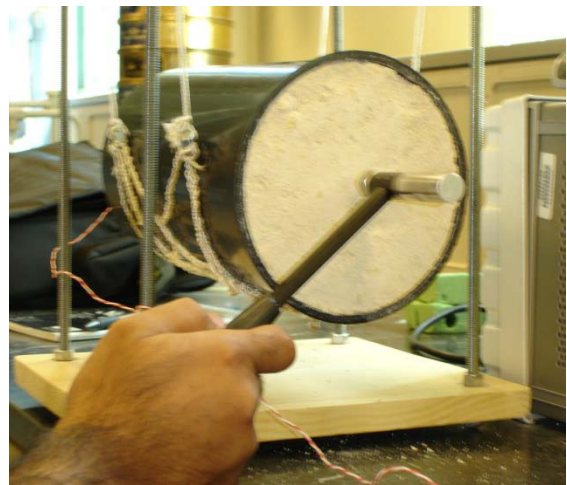


(b)

Figure 3-10. Free-Free Resonant Column test equipment setup a) Overall setup b) Specimen with transducer and instrumented impact hammer



(a)



(b)

Figure 3-11. Free-Free resonant column testing specimen a) Without confinement casing b) With confinement casing (tested by Toros (2008))

(Photo courtesy of Ayithi (2011))

## CHAPTER 4 MATERIALS AND SPECIMEN PREPARATION

In the State of Florida, limerock type aggregates are commonly used for base layer construction. For our testing, it is proposed to select one limerock material and one non-limerock material for our testing. Newberry limerock and Georgia graded aggregate base are used for our testing, representing one from each category. A detailed explanation about their source, particle size distribution, basic parameters and specimen preparation are given in this chapter.

### 4.1 Materials

#### 4.1.1 Sources

Newberry limerock and Georgia granite graded aggregate base are selected for our testing. Material sources for these two soils are given in Table 4-1.

Representative samples of these selected materials are collected by FDOT SMO (Florida Department of Transportation State Materials Office) staff, from mines mentioned in Table 4-1, following FDOT standard method, i.e. Florida Methods 1 (FM 1) T-002 that is similar to AASHTO T2.

#### 4.1.2 Characterization

These collected samples are transported in bags, to FDOT SMO laboratory for further characterization and lab testing. Before further testing, transported sample bags are placed in a thermostatically controlled drying oven at a temperature of 110°F until the samples are friable. After letting these oven dried samples to cool down, sieve analysis and basic parameter tests are conducted. Representative samples of these two materials are shown in Figure 4-1.

Sieve analysis is performed following the procedure AASHTO T27. Grain size distribution for particles larger than #200 size (i.e. 0.075 mm) is shown in Figure 4-2.

Specific gravity of fine and coarse aggregates are performed following the procedure FM 1 T-084 and T-085, which are similar to AASHTO T084 and T085 procedures, respectively. Atterberg limits are determined by following AASHTO T90 for plastic limit and plasticity index and AASHTO T89 for liquid limit. These basic material parameters are presented in Table 4-2.

## **4.2 Specimen Preparation and Installation**

Fixed-Free RC tests are conducted on both dry and wet (partially saturated) compacted cylindrical specimens and Free-Free RC tests are conducted on wet compacted specimens. 4 inch (10.16 cm) diameter and 8 inch (20.32 cm) height specimens are prepared following standard method for specimen preparation and detailed explanation is given in later sections.

Aggregate passing through  $\frac{3}{4}$  inch sieve only is used for specimen preparation. After oven drying of mine collected samples, aggregate that does not pass through  $\frac{3}{4}$  inch sieve is separated and sent through limerock crusher, so that all the aggregate is smaller than  $\frac{3}{4}$  inch. This crushed aggregate is mixed with uncrushed aggregate and the whole material is used for specimen preparation satisfying gradation requirements.

### **4.2.1. Dry Specimens**

#### **4.2.1.1 Dry specimen preparation**

Dry specimens are used in Fixed-Free RC testing only. Dry specimens are prepared at three different void ratios for each material as presented in Table 4-3.

Dry specimens are prepared following split mold and membrane method. Initially, a split mould with membrane on inner wall of mould is attached to specimen's bottom cap (pedestal) (Figure 4-3a). Dry aggregate is placed inside the split mold and compacted by dropping a loading hammer manually (Figure 4-3b). The amount of energy required (i.e. height of drop, no of layers and weight of hammer) to compact the dry aggregate to obtain targeted void ratio is determined by trial and error method. After completing compaction, to keep the specimen intact without

falling off after removal of split mould, vacuum is applied through bottom drainage line (Figure 4-3c). Our primary goal in dry compaction is to achieve targeted void ratio.

#### **4.2.1.2 Dry specimen installation**

For dry specimens, after completing compaction, top cap with vertical and horizontal serrations is placed firmly such that there is proper contact grip between soil and cap. Friction due to serrations on both top and bottom caps, provides a good grip between soil and cap. Due to this contact grip, entire soil column rotates as a single integral unit, when torsional load is applied. After attaching top cap and loading motor, confinement chamber is placed and required air confinement is applied through pressure control panel (Figure 4-3d). Once the dry compacted specimen stands stable by externally applied air confinement, vacuum application is disconnected and released off.

### **4.2.2 Wet (Partially Saturated) Specimens**

#### **4.2.2.1 Wet specimen preparation**

Wet specimens are compacted at optimum moisture content (OMC) using modified proctor compactor (Figure 4-4a). Before compaction, the soil-water mixture is soaked for at least 12 hours in a nylon sheet covered container (Figure 4-4b), for uniform distribution of water throughout the soil mixture. After soaking, the mixture is compacted in a standard size mold used for making 4 inch diameter and 8 inch height specimens (Figure 4-4c). Number of layers and number of blows required per each layer are estimated based on AASHTO D1557 (Standard test method for laboratory compaction characteristics of soils using modified effort). Specimens are compacted in total six layers and 36 blows per layer, which meets the required compaction effort of  $2700 \text{ kN}\cdot\text{m}/\text{m}^3$ , according to AASHTO D1557. After extruding from compaction mould, specimen is covered with a 0.012" thick rubber membrane and allowed to sit for 12-hours in an air-tight container at room temperature before testing.

#### **4.2.2.2 Wet specimen installation**

For wet OMC compacted specimens, specimen's top and bottom caps are glued to the specimen using bondo. Glue material is selected such that it should not influence the testing measurements (i.e. resonant frequency-  $\omega_n$ ) and material properties. Bottom cap of the specimen is attached firmly to the chamber's bottom plate, and top end of the specimen is left free to rotate. Torsional loading motor is attached to specimen's top cap with proper supporting system.

Table 4-1. List of materials used for testing and their sources

Material	Mine Number or Source	Type
Newberry limerock	26-002	Limerock
	Newberry Quarry	
Georgia granite	GA-178	Granite
Graded Aggregate Base (GAB)	Macon Quarry	

Table 4-2. Basic material parameters

Parameter	Georgia granite	Newberry limerock
Unified soil classification	GW-GM	GM
D <sub>50</sub> (mm) - mean grain size	5	3
D <sub>10</sub> (mm) - effective grain size	0.16	0.13
C <sub>u</sub> - the coefficient of uniformity	50	61.5
C <sub>c</sub> - the coefficient of curvature	1.76	0.15
G - Specific gravity	2.74	2.72
Maximum dry density (kN/m <sup>3</sup> ) ( $\gamma_{dry\ max}$ )	22.08	18.21
Optimum moisture content (OMC) (%)	5.5	13
Void ratio at OMC ( $e_{OMC}$ )	0.20	0.45
Plastic limit	NP	NP
Plasticity index	NP	NP
Liquid limit	NP	NP

where:  $C_u = D_{60} / D_{10}$ ,  $C_c = (D_{30})^2 / (D_{60} \times D_{10})$

Table 4-3. Selected void ratios for dry specimen testing

Material	Void Ratio (e)		
	1 ( $e_{OMC}$ )	2	3
Newberry limerock	0.45	0.50	0.55
Georgia granite	0.20	0.25	0.29



(a)



(b)

Figure 4-1. Representative samples a) Georgia granite b) Newberry limerock

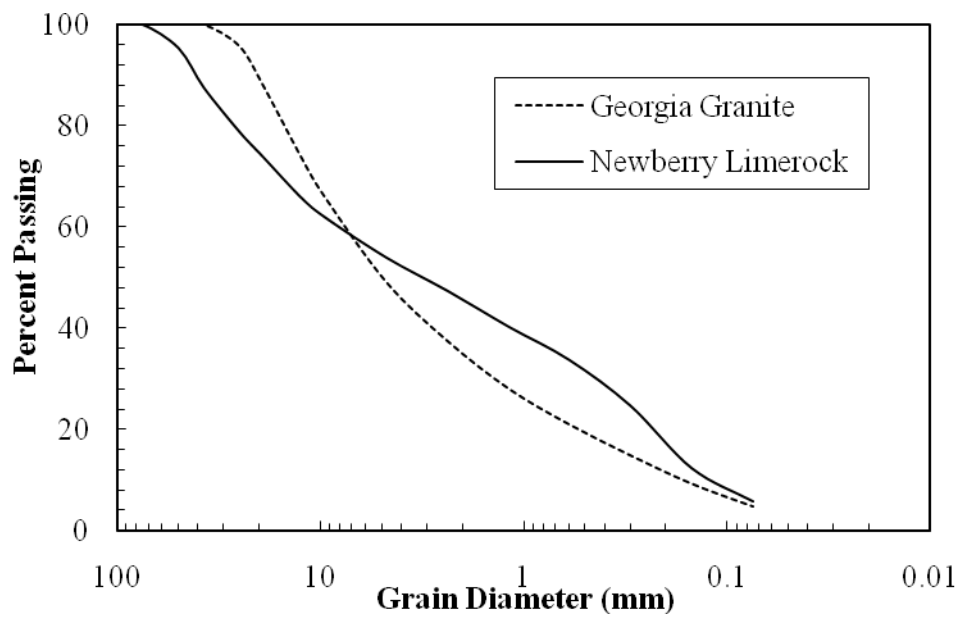


Figure 4-2. Grain size distribution



(a)



(b)



(c)



(d)

Figure 4-3. Dry specimen compaction and installation a) Split mould with membrane inside b) Split mould with dry compacted limerock c) After application of vacuum d) After installation of chamber and external confinement application.

(b)



(a)



(c)

Figure 4-4. Wet specimen compaction a ) Modified proctor compactor with 4 inch diameter and 8 inch height specimen mould b) Soaked aggregate trays with nylon cover sheet c) Compacted wet specimens of 4 inch diameter and 8 inch height

## CHAPTER 5 EXPERIMENTAL RESULTS AND ANALYSIS

The first objective of this research work is characterization of base soils modulus nonlinearity with respect to confinement stress, loading strain and moisture content, via laboratory testing. To achieve this objective, it is proposed to conduct Fixed-Free Resonant Column tests (Fixed-Free RC) and Free-Free Resonant column (Free-Free RC) tests on selected representative base soils. Testing mechanisms and their background are explained in detail in Chapter 3. Base soils selected for our testing, their basic properties characterization and specimen preparation methods are explained in Chapter 4.

Fixed-Free RC tests are conducted on both dry and unsaturated (wet) compacted specimens of Newberry limerock and Georgia granite to determine shear modulus ( $G$ ) under different confinement pressures and at strain levels as small as  $10^{-5}\%$  (very small level strains) and as high as  $10^{-1}\%$  (medium level strains). Free-Free RC tests are conducted on unsaturated (wet) compacted specimens of Newberry limerock and Georgia Granite to determine very small-strain modulus ( $E_{\max}$  or  $G_{\max}$ ) under no confinement. Specimen testing conditions such as water content, confinement pressure and strain magnitude are presented in followed sections. Experimental results are discussed and analyzed.

### **5.1 Fixed-Free Resonant Column Torsional Shear Testing**

#### **5.1.1 Dry Specimen Testing Results**

Dry compacted specimens of Newberry limerock and Georgia granite are tested at three different void ratios as reported in Table 4-3, to investigate the effect of void ratio. Specimen at each void ratio is subjected to four different confining pressures 50, 100, 150 and 200 kPa, to investigate confinement effect. Shear modulus ( $G$ ) versus % shear strain ( $\gamma$ ) testing results for

$e_{OMC}$  (i.e.  $e=0.45$  for Newberry limerock and  $e=0.20$  for Georgia granite) are shown in Figures 5-1 and 5-2. and plots corresponding to remaining two void ratios are presented in Appendix-A.

Based on literature (Seed et al. (1986), Menq (2003), Atkinson (2000)), for dry gravels, strains less than  $10^{-4}\%$  are referred as very small-level strains and corresponding shear modulus is at its maximum (i.e.  $G_{max}$ ). Thus by considering  $G$  value at  $\gamma=10^{-5}\%$  as  $G_{max}$ , normalized shear modulus ( $G/G_{max}$ ) versus % shear strain curves are developed and shown in Figures 5-3 and 5-4.

From Figures 5-1 and 5-2, it can be observed that At constant confining pressure, modulus decreases with increase in strain magnitude. At constant strain magnitude, modulus increases with increases in confinement and rate of increase is maximum at very small-strain (i.e.  $10^{-5}\%$ ). Modulus is maximum (i.e.  $G_{max}$ ) and elastic at strains lower than  $10^{-4}\%$  and starts decreasing thereafter with increase in strain. Modulus decreases linearly in the strain range of  $10^{-4}\%$  to  $10^{-3}\%$  and nonlinearly thereafter. Similar results for gravelly soils were reported by Menq (2003). Seed et al. (1986) and Rollins et al. (1998) also observed that in gravelly soils  $G$  starts decreasing from  $10^{-4}\%$  strain with increase in strain magnitude.

Based on Ottawa sand testing results (Figure 3-7a) and literature database, modulus of sands are maximum and elastic at strains smaller than  $10^{-3}\%$  and decrease thereafter, with increase in strain. By comparing results of gravelly soils with sands, it can be concluded that presence of gravel size aggregates increases nonlinearity in modulus reduction. This confirms with the findings of Seed et al. (1986) and Menq (2003) testing results on gravels. The difference in moduli at different confining pressures and for same strain magnitude, decreases with increase in strain. This indicates that confinement effect on modulus decreases with increase in strain magnitude. At strains higher than  $10^{-1}\%$ , modulus does not vary significantly with respect to either increase in strain or increase in confinement. This observation indicates that at larger

strains (i.e.  $10^{-1}\%$  and higher) pressure confinement and strain magnitude have no significant influence on moduli of gravelly soils.

For both soils, modulus reduction curves at constant confinement are flatter for 50 kPa and 100 kPa compared to 150 kPa and 200 kPa. This behavior implies that nonlinearity of modulus reduction increases with increases in confinement. Similar behavior in sands was reported by Pestana and Salvati (2006) for Monterey sand.

$G/G_{\max}$  normalized curves for any confining pressure (Figures 5-3 and 5-4) are falling on each other and behaving very similar. This indicates that rate of decrease in modulus with increase in strain does not depend on confining pressure. In Figure 5-5, normalized data points for both materials lie well within the maximum and minimum ranges of gravel soils, reported by Seed et al. (1986).

Normalized curves at different confining pressures are falling on each other and this behavior indicates that normalization of modulus nullifies the confinement effect on modulus. Lin et al. (2000) (Figure 2-5) and Yasuda and Matsumoto (1993) (Figure 2-3) reported same behavior for gravelly soils. But Rollins et al. (1998) reported that,  $G/G_{\max}$  versus  $\gamma$  curves are different for different confinements and move from low end of the data range towards high end with increase in confinement (Figure 2-12). However, they also pointed out that the deviation between various confinements curves are relatively small and use of same best-fit hyperbolic curve for any confining pressure would not likely cause significant error.

$G_{\max}$  values ( $G$  at  $10^{-5}\%$  strain) at different void ratios ( $e$ ) and different confining pressures are plotted on a log-log plot of modulus versus confining pressure and shown in Figure 5-6 and Figure 5-7. Empirical equations in the form of Equation 2-5 (shown below) are derived

for each material; by plotting trend line for whole set of  $G_{max}$  values at different void ratios as shown in Figure 5-8.

$$G_{max} = A_G F(e) (\sigma_c')^{n_G} \quad (2-5)$$

where  $F(e) = \frac{(2.17-e)^2}{(1+e)}$ ,  $A_G$  and  $n_G$  are material constants.

$G_{max}$  and  $\sigma_0$  are in kPa,

Derived empirical equations for each material are given below:

$$\text{For Newberry limerock, at any given void ratio (e), } G_{max} = (2575) F(e) (\sigma_c')^{0.702} \quad (5-1)$$

$$\text{For Georgia granite, at any given void ratio (e), } G_{max} = (816) F(e) (\sigma_c')^{0.6389} \quad (5-2)$$

Shear modulus of Newberry limerock is proportional to pressure confinement to the power of 0.702 and of Georgia granite is proportional to pressure confinement to the power of 0.6389. Values of  $n_G$  obtained from this testing complies well with the values given in literature, i.e. in the range of 0.5-0.85 for gravel type soils (Menq, (2003)). These equations can be used to calculate  $G_{max}$  of dry material at any confining pressure ( $\sigma_c'$ ) and void ratio (e).

### 5.1.2 Unsaturated (Wet) Specimen Testing Results

Primary goal of conducting Fixed-Free RC tests on unsaturated specimens is to characterize modulus nonlinearity at different water contents and different strain levels; and to evaluate suction effect, due to drying, on modulus. Based on previous research investigations conducted by Toros(2008), very small-strain modulus ( $G_{max}$ ) of base course soils increases with decrease in water content. He dried OMC compacted specimens in different environments and tested them at different water contents during the process of drying, starting from OMC to all the way close to zero water content. Cho and Santamarina (2001) reported that, specimen drying simulates actual drying in real filed conditions and makes the material stiffer compared to compacting the specimen at required water content. So, the modulus of material is higher in case

of dried specimen than in case of compacted specimen at targeted water content. Hence, to simulate actual field conditions, for our testing, it was decided to achieve different water contents by drying OMC compacted specimens.

For our testing program, 4 inch diameter and 8 inch height cylindrical specimens are compacted at OMC using modified proctor compactor. These OMC compacted specimens are allowed to dry in lab environment (i.e. at room temperature), by leaving them open in lab, without any membrane cover. Specimens dried to different water contents in this method are tested to determine modulus at different shear strain levels, as low as  $10^{-5}\%$  (very small-strain) and as high as  $10^{-1}\%$  (medium to large strains).

#### **5.1.2.1 Equipment limitations**

During our testing, a problem related to Fixed-Free RC equipment's inability to test a specimen dried to below certain water content is encountered. The basic mechanism of Fixed-Free RC testing is to determine the testing specimen's resonant frequency ( $\omega_n$ ) corresponding to applied torsional load, in order to calculate the shear wave velocity ( $V_s$ ) from which shear modulus ( $G$ ) can be estimated. Thus the resonant frequency of the testing specimen should be within the motor applicable frequency capacity, i.e. less than 300 Hz (also explained in 3.1.6). In other words, specimen's shear modulus value should be such that its resonant frequency is not more than 300 Hz. But, during our testing process, it is realized that modulus of specimen is increasing with decrease in water content. After reducing to certain water content, modulus is increasing such that its resonant frequency is going beyond 300 Hz, which is the maximum limit of torsional loading motor frequency. Hence, it is decided to conduct tests at water contents, for which the specimen's resonant frequency is less than 300 Hz. Based on this limitations, specimen tested water contents for both materials are given in Table 5-2.

### **5.1.2.2 Confinement effect on unsaturated specimens**

Similar to dry specimen testing, initially it is planned to tests unsaturated specimens under zero (i.e. no confinement), 50, 100, 150 and 200 kPa confinement pressures. But, when tests are run on unsaturated specimens under confinement, no increase in modulus is observed with increase in confinement. Possible reason for this phenomenon may be explained through unsaturated soil mechanics. In the science of soil mechanics, it is well known that modulus of soil increases with increase in confinement. It is also known in the science of unsaturated soil mechanics that under normal loading conditions, effective stress does not change with increase in total stress due to pore pressure effect in unsaturated soils and so the modulus. Based on these reasons, it is presumed that due to pore pressure effect inside the testing specimens, no increase in modulus is observed with increase in confinement. Thus to determine actual modulus of unsaturated specimen under confinement, it is necessary to measure pore pressure inside the specimen with proper pore pressure measuring equipment. But pore pressure measurement was not part of our initial testing plan, hence it is decided to conduct tests on unsaturated specimens with no confinement only. Based on these unconfined testing results, unsaturated material modulus under confinement can be calculated approximately by an indirect method, which is explained in later sections of this chapter.

### **5.1.2.3 Results and analysis**

Shear modulus versus strain plots of unsaturated specimens tested at different water contents, under no confinement are shown in Figure 5-9 for Newberry limerock and in Figure 5-10 for Georgia granite. Dry specimen testing curve corresponding to 50 kPa confining pressure is also included for comparison purpose. From these plots it can be observed that at constant strain magnitude, modulus increases with decrease in water content and is maximum (i.e.  $G_{\max}$ ) at very small-strain (i.e.  $10^{-5}\%$ ).  $G$  versus  $\gamma$  curves at different water contents, are behaving similar to

dry curves at different pressure confinements presented in Figure 5-1 and Figure 5-2 . Since the void ratio is same for both dry and wet specimens (i.e. @ $e_{OMC}$ ), increase in  $G$  with decrease in water content is probably due to increase in effective confinement with decrease in water content, which is probably due to increase in suction with decrease in water content. Though, we did not make any pore pressure measurements to prove the presence of suction, research investigations by Wu et al. (1984), Qian et al. (1993) and Cho and Santamarina (2001) reported that decrease in water content increases suction and thus additional confinement. This phenomenon is also well explained in unsaturated soil mechanics (Lu and Likos (2004)).

At different water contents, the difference in moduli at same strain magnitude decreases with increase in strain and similar phenomenon is also observed in dry soils at different confinements. This implies that suction confinement effect decreases with increase in strain.  $G$  decreases at faster rate with increase in  $\gamma$ , in low water content specimens compared to high water content specimens. This is probably due to failure of suction menisci at lower strains in low water content specimens and at higher strains in high water content specimens. Cho and Santamarina (2001), from their microscale particle menisci studies, reported that the strain at menisci failure decreases with decrease in water content and small menisci in relatively dry specimens may fail before the strain at peak strength of soil. Hence, at low water contents small suction menisci cause high small-strain modulus and modulus decreases at faster rate due to early menisci failure.

In dry condition, shear modulus is maximum (i.e  $G_{max}$ ) at  $10^{-4}\%$  strain and decrease to  $0.15G_{max}$  at  $10^{-1}\%$  strain. Whereas, in unsaturated condition, shear modulus is maximum at  $10^{-5}\%$  strain and decrease to  $0.075 G_{max}$  at  $10^{-1}\%$  strain. This implies that in unsaturated gravelly soils, presence of moisture increases nonlinearity in modulus reduction and modulus starts

decreasing from  $10^{-5}\%$  strain. This same behavior was observed by Menq (2003) in gravelly soils. Increase in modulus nonlinearity is probably due to water lubrication effect, which reduces inter particle frictional contact forces, allowing soil particle movement easier and irreversible, even at strains lower than  $10^{-4}\%$ . Similar to dry specimens, in wet specimens also, at strains near  $10^{-1}\%$  and higher, the difference in moduli at different water contents is very minimal. This implies that suction confinement effect on modulus becomes less significant at higher strains.

In case of Newberry limerock,  $G_{\max}$  at 13% (OMC) and 12% water content is lower than that of dry case at 50 kPa pressure confinement, which implies that additional confinement due to suction is less than 50 kPa at 13% and 12% water contents and higher than 50 kPa at water contents 11% and lower. Similarly, in case of Georgia Granite,  $G_{\max}$  at 5.5% (OMC) water content is almost equal to  $G_{\max}$  of dry soil at 50 kPa, which means at water contents lower than 5.5%, confinement due to suction is greater than 50 kPa. Additional confinement provided due to suction is calculated and corresponding results are reported in later sections.

Normalized curves of  $G/G_{\max}$  versus logarithmic % shear strain ( $\gamma$ ) for both dry and wet specimens together on the same plot, are shown in Figure 5-11 and Figure 5-12. From these plots, it can be observed that in the case of dry specimens, normalized curves for any confining pressure are falling on each other and behaving very similar. This indicates that rate of decrease in modulus with increase in strain does not depend on confining pressure. In the case of unsaturated specimens, normalized curves for any water content are falling on each other. This indicates that rate of decrease in modulus of unsaturated specimens, with increase in strain, does not depend on water content and its suction effect. Entire set of unsaturated specimens' normalized curves are falling below that of dry specimens' and this indicates that rate of decrease in modulus with increase in strain is higher in unsaturated soils compared to dry soils,

and hence the modulus nonlinearity is higher in unsaturated condition compared to dry condition. Based on microscale particle level studies of Cho and Santamarina (2001), higher modulus nonlinearity in unsaturated specimens is due to early failure of small menisci at very small level strains. Menq (2003) observed the same difference in case of dry and partially saturated gravelly soils behavior.

Shear modulus ( $G$ ) normalized with shear modulus at OMC ( $G_{OMC}$ ) versus water content plots for different strain levels are shown in Figures 5-13 and Figure 5-14. Curves of  $G/G_{OMC}$  versus water content, for different strain magnitudes are approximately falling on each other and behaving more or less similar. At any given strain magnitude, increase in  $G/G_{OMC}$  with decrease in water content is approximately same. In other words, additional confinement provided due to suction effect (various magnitudes at different water contents) is not changing, i.e. same at different strain levels. This behavior indicates that in unsaturated soils, for the range of strain magnitudes measured in this testing, at given water content, additional confinement due to suction effect remains same irrespective of strain magnitude. It appears that, unsaturated material under additional confinement due to suction, behaves similar to dry material under external constant confinement. Cho and Santamarina (2001) reported in their particle level studies that, in sands, menisci failure strains ( $\epsilon=0.01$  to 1) are higher than threshold strains for sands. Since our strain magnitudes are smaller than threshold strains, Cho and Santamarina's findings support our observations from the plots that suction effect remains same irrespective of increase in strain magnitude. Since it's an indirect conclusion, a further detailed particle study is required to analyze the strain level effect on menisci failure and its suction effect.

#### **5.1.2.4 Additional effective stress or additional confinement pressure provided due to suction, at $10^{-5}\%$ strain magnitude**

By comparing wet specimen testing results with that of dry specimen's, additional effective stress or confinement pressure provided due to suction can be evaluated. A detailed evaluation procedure is explained here.

From dry specimens testing results, Equations 5-1 and 5-2 are derived to calculate  $G_{\max}$  (i.e.  $G$  at  $\gamma = 10^{-5}\%$ ) of dry material at different confining pressures. At  $e_{\text{OMC}}$ ,  $G_{\max}$  for any chosen confining pressure can be calculated using equations 5-1 and 5-2.

By substituting unsaturated specimen's  $G_{\max}$  value obtained at given water content into these equations, confinement pressure required to be applied over a dry specimen to produce the equivalent modulus can be calculated. Since it is already known that all wet specimens are tested under no confinement, earlier calculated confinement pressure magnitude becomes the additional confinement pressure or effective stress being provide by suction in a wet specimen, at corresponding selected water content. Following this procedure, additional effective stress or confinement provide due to suction at different water contents or degree of saturation is determined and is shown in Figures 5-15 and Figure 5-16.

From Figure 5-15 and Figure 5-16, it can be observed that increase in additional confinement for same amount of decrease in water content is relatively very high in Georgia granite compared to Newberry limerock. This is due to low  $e_{\text{OMC}}$  and higher reduction in degree of saturation ( $S_r$ ) in Georgia granite. In soils with low void ratio, degree of saturation goes down faster compared to soils with high void ratio, for the same amount of reduction in water content. As the degree of saturation decreases faster, suction magnitude increases proportionally faster and hence increase in additional confinement at faster rate.

## 5.2 Free-Free Resonant Column Testing

Free-Free resonant column (Free-Free RC) tests are run on modified proctor compacted specimens of Newberry limerock and Georgia Granite, under no confinement to measure very small-strain Young's modulus ( $E_{\max}$ ). OMC compacted specimens are dried in laboratory environment and tested at different water contents during drying process, starting at OMC to all the way close to zero. These results are presented and discussed in followed sections.

Toros (2008) conducted same tests on relatively bigger specimens at different water contents similar to our drying process. He used a plastic cylindrical case around the specimens, which provides some confinement. Toros (2008) results are compared with our testing results.

### 5.2.1 Results and Discussion

Free-Free RC with no confinement test results for both Newberry lime rock and Georgia granite are shown in Figures 5-17 and 5-18 respectively. These results show that in both materials, very small-strain Young's modulus ( $E_{\max}$ ) increase with decrease in water content. Their trends are similar to results reported by Toros(2008). Toros (2008) concluded that, increase in modulus with decrease in water content is probably due to increase in additional confinement due to increase in suction and suction increase with decrease in water content. Cho and Santamarina (2001) also concluded the same for sands. Free-Free RC testing results are compared with Fixed-Free RC test results at very small-strain (i.e.  $10^{-5}\%$ ) and Free-Free RC results of Toros (2008), and presented in Figures 5-19 and 5-20.

From the results in Figures 5-19 and 5-20, it can be observed that Fixed-Free RC moduli values at  $10^{-5}\%$  strain are more or less equal to that of Free-Free RC results at corresponding water contents. This implies that strain magnitudes of Free-Free RC testing are nearly equal to  $10^{-5}\%$ . A close observation of these plots tells that Fixed-Free RC moduli value are slightly higher than Free-Free moduli values. This difference is probably due to the weight of motor and

top specimen cap attached to specimen top in Fixed-Free RC testing, which might provide some vertical confinement, hence resulting in little bit higher moduli values compared to Free-Free RC moduli values at no confinement.

At same water content, Toros (2008) Free-Free RC moduli values are higher than that of our Free-Free RC moduli value. The materials and method of compaction are same for both tests and the only difference is casing confinement. Our Free-Free RC tests are run on specimens with no casing and Toros(2008) Free-Free RC tests were run on specimens with plastic casing. Toros compacted specimens in plastic cylindrical moulds and tested specimens with the mould on. These plastic cylinders might be providing some confinement around the side surface of the specimen, which might have resulted in higher moduli values compared to that of specimens with no confinement.

### **5.2.2 A Method to Estimate Approximate Modulus at Given Conditions of Water Content, Confining Pressure and Strain Magnitude:**

$G_{\max}$  of dry material can be determined via Equations 5-1 and 5-2, which are derived based on dry material Fixed-Free RC testing results. By knowing  $G_{\max}$  at any water content under no confinement (either from Fixed-Free RC or Free-Free RC) and substituting this value in Equations 5-1 or 5-2, additional effective confinement stress provided due to suction can be calculated by following the procedure explained in Section 5.1.2.4.

By adding this additional confinement stress to the initially chosen confinement, where we need to estimate modulus, approximate  $G_{\max}$  value can be calculated, via Equations 5-1 and 5-2. From Figures 5-11 and 5-12, it is understood that  $G/G_{\max}$  versus strain ( $\gamma$ ) curves behave similar at any water content. Thus after calculating  $G_{\max}$  at given confinement and water content using

Equations 5-1 and 5-2, value of  $G/G_{\max}$  at required strain level can be determined through Figures 5-11 and 5-12, and finally approximate value of  $G$  can be calculated.

### 5.3 Laboratory Testing Results Closing Remarks

$G_{\max}$  of dry Newberry limerock and dry Georgia Granite at  $e_{\text{OMC}}$  and known confinement can be determined using Equations 5-1 and 5-2. Shear modulus of dry gravelly soils is maximum and elastic at strains lower than  $10^{-4}\%$  and starts decreasing linearly in the strain range of  $10^{-4}\%$  -  $10^{-3}\%$  and nonlinearly thereafter. Presence of gravel size aggregate makes modulus of gravelly soils more nonlinear compared to sands.

In unsaturated gravelly soils, capillary suction confinement increases with decrease in water content and has significant effect on  $G_{\max}$ . Shear modulus of unsaturated gravelly soils is maximum at  $10^{-5}\%$  strain and start decreasing thereafter with increase in strain. Presence of moisture increases modulus nonlinearity in unsaturated gravelly soils compared to dry gravelly soils.

In dry gravelly soils, rate of decrease in  $G$  with increase in strain is independent of confinement pressure magnitude. In unsaturated gravelly soils, rate of decrease in  $G$  with increase in strain is independent of water content and its suction confinement. In unsaturated gravelly soils, at constant water content, additional confinement due to does not change with increase in strain.

Strain magnitudes generated in Free-Free RC testing are approximately in the range of  $10^{-5}\%$  and corresponding moduli are nearly equal to very small-strain moduli obtained from Fixed-Free RC testing. Based on testing results, at  $10^{-5}\%$  strain magnitude, additional confinement provided due to suction can be as high as 900 kPa, which is equivalent to 39m of overburden

pressure confinement. Since confinement due to suction can influence soil modulus, it is necessary to consider suction effects in determination of base layer design modulus.

Table 5-1.  $n_G$  and  $A_G$  values for dry Newberry lime rock and Georgia granite.

Material	$n_G$	$A_G$
Newberry limerock	0.702	3166.00
Georgia granite	0.6389	750.70

Table 5-2a. List of unsaturated specimen tested water contents for Newberry Limerock

Material	void ratio at OMC ( $e_{OMC}$ )	Tested water contents (%)	Degree of saturation, $S_r$ (%)
Newberry limerock	0.45	13	78.6
		12	72.5
		11	66.5
		10	60.4

Table 5-2b. List of unsaturated specimen tested water contents for Georgia Granite

Material	void ratio at OMC ( $e_{OMC}$ )	Tested water contents (%)	Degree of saturation, $S_r$ (%)
Georgia Granite	0.2	5.5	75.3
		4.5	61.7
		3.5	48

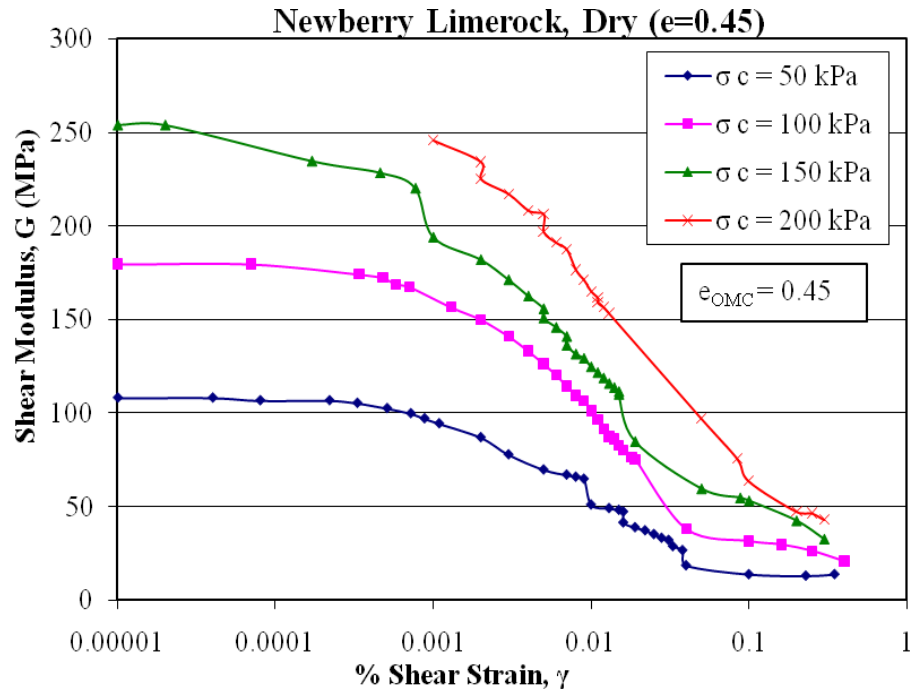


Figure 5-1. Shear Modulus (G) versus % Shear strain ( $\gamma$ ) curves for dry Newberry limerock at  $e_{OMC}$  (i.e.  $e = 0.45$ )

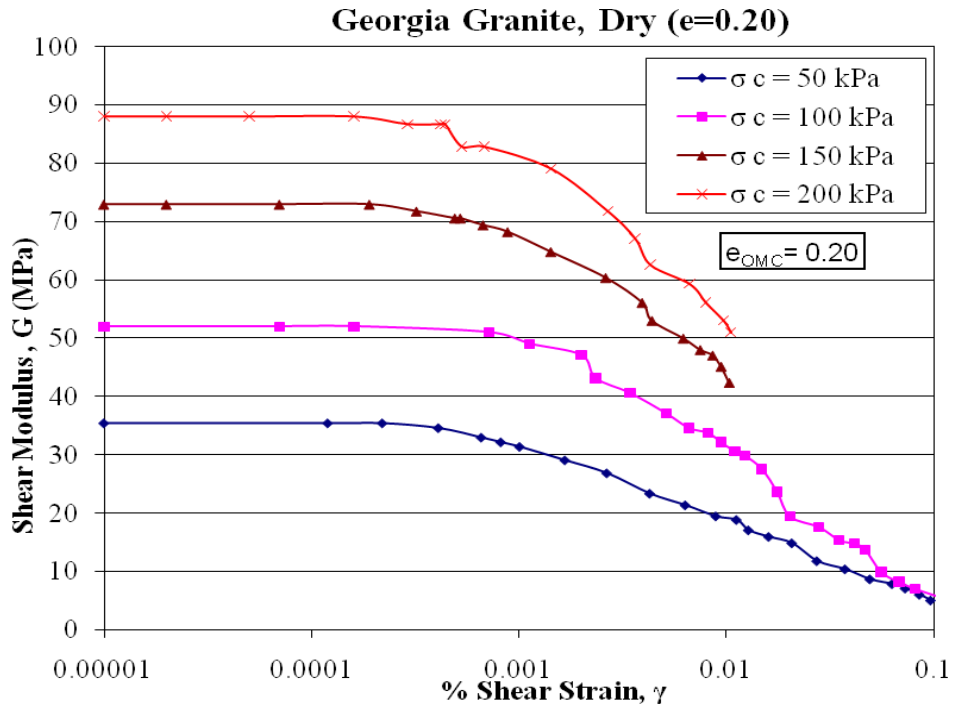


Figure 5-2. Shear Modulus (G) versus % Shear strain ( $\gamma$ ) curves for dry Georgia granite at  $e_{OMC}$  (i.e.  $e=0.20$ )

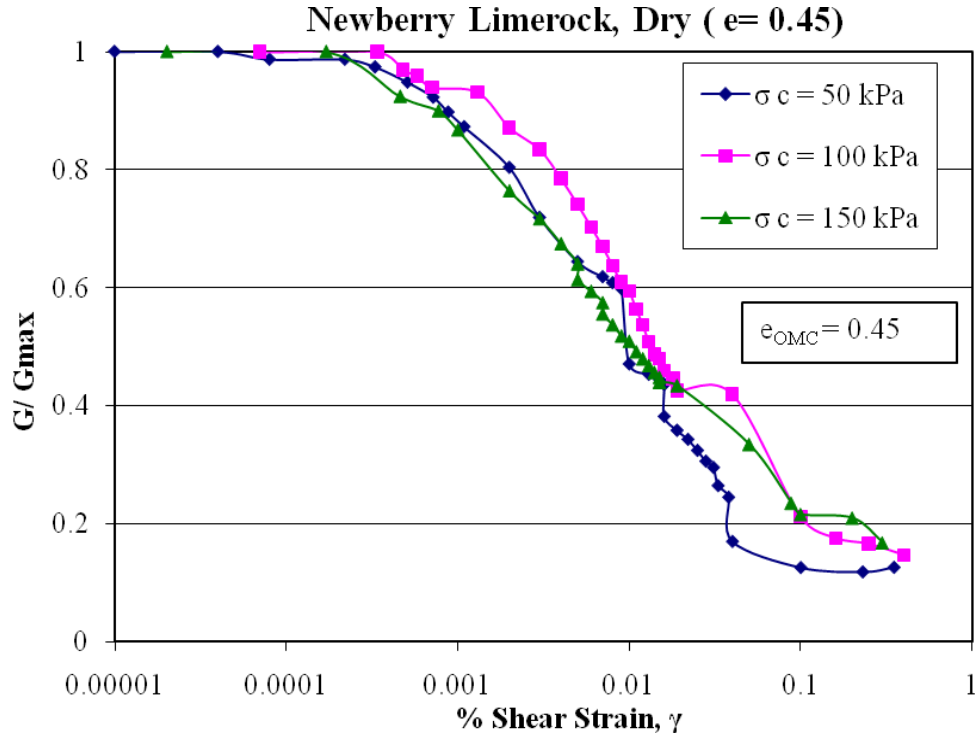


Figure 5-3.  $G/G_{max}$  versus % shear strain ( $\gamma$ ) curves at  $e = e_{OMC}$  for Newberry limerock

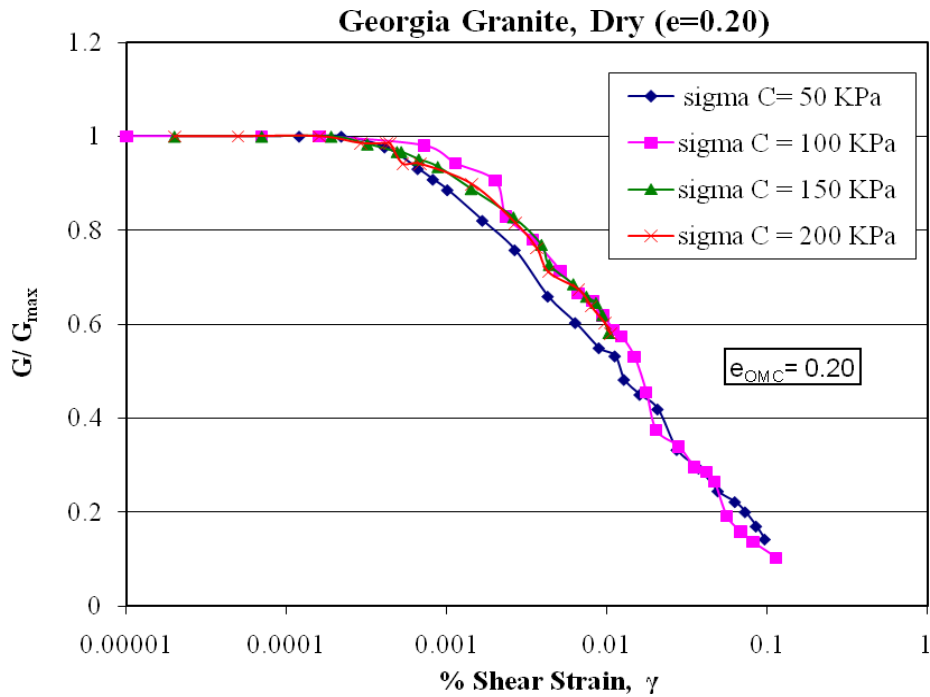


Figure 5-4.  $G/G_{max}$  versus % shear strain ( $\gamma$ ) curves at  $e = e_{OMC}$  for Georgia granite

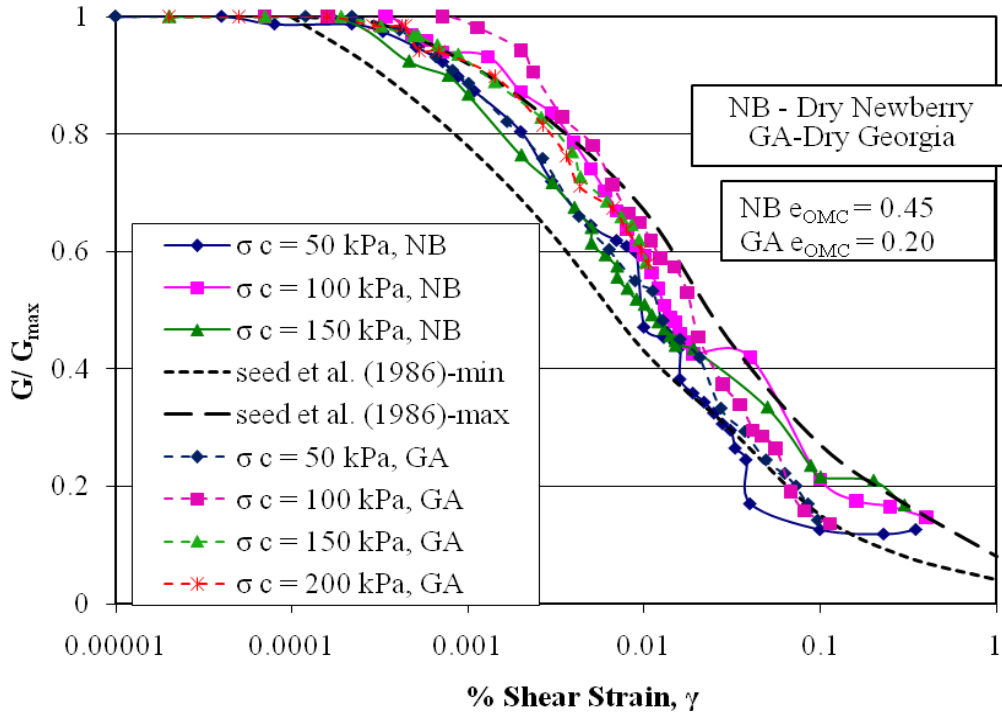


Figure 5-5. Comparison of  $G/G_{max}$  vs % shear strain ( $\gamma$ ) data of Newberry limerock and Georgia granite with Seed and Idriss (1986) maximum and minimum limits

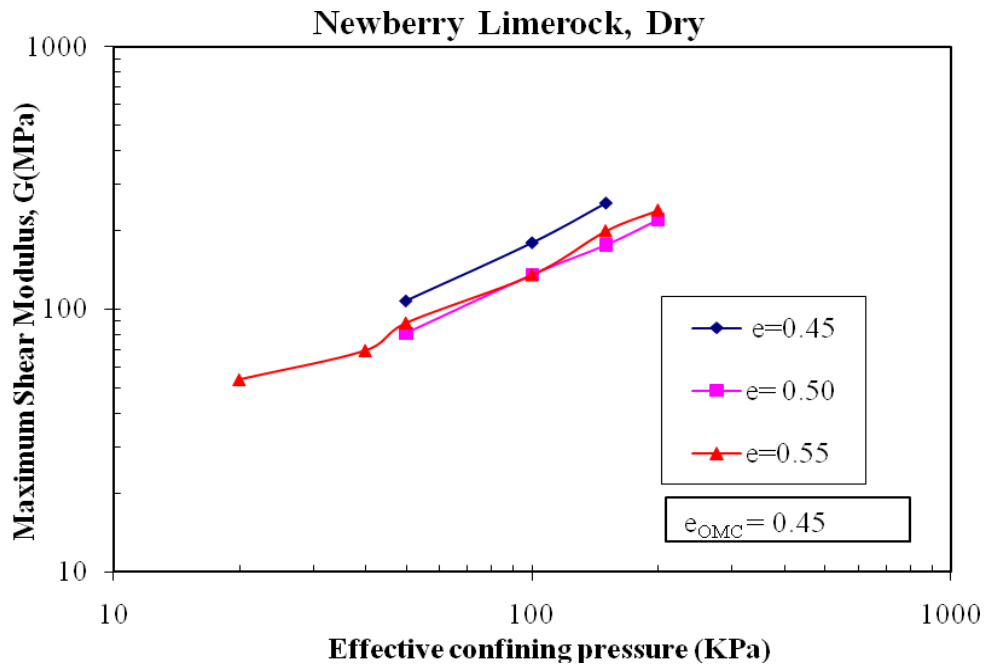


Figure 5-6.  $G_{max}$  versus confining pressure curve Newberry limerock at different void ratios

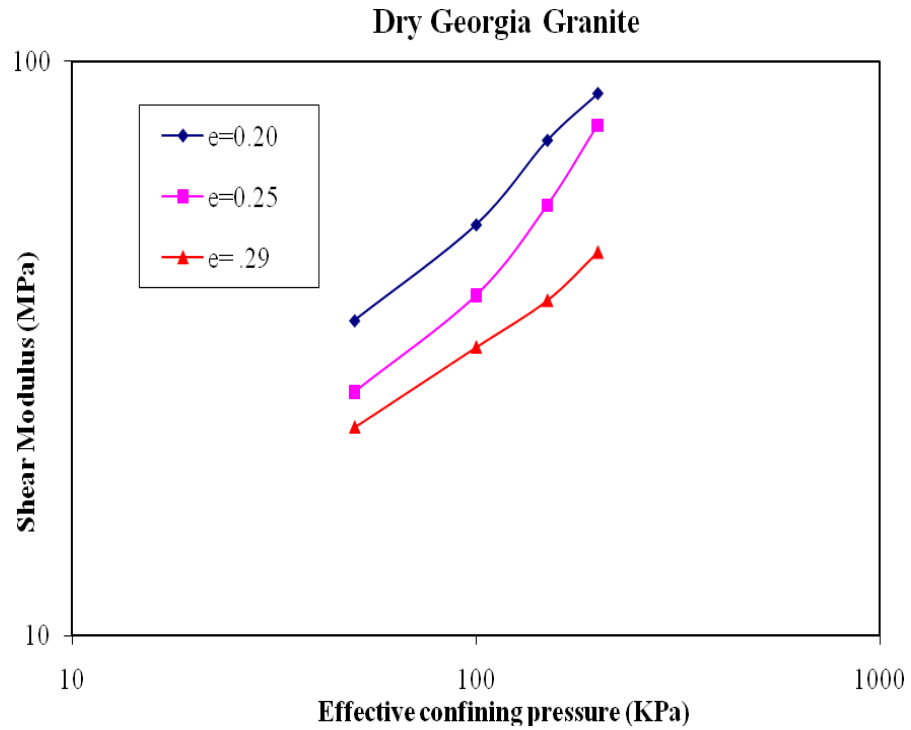


Figure 5-7.  $G_{max}$  versus confining pressure curve Georgia granite at different void ratios

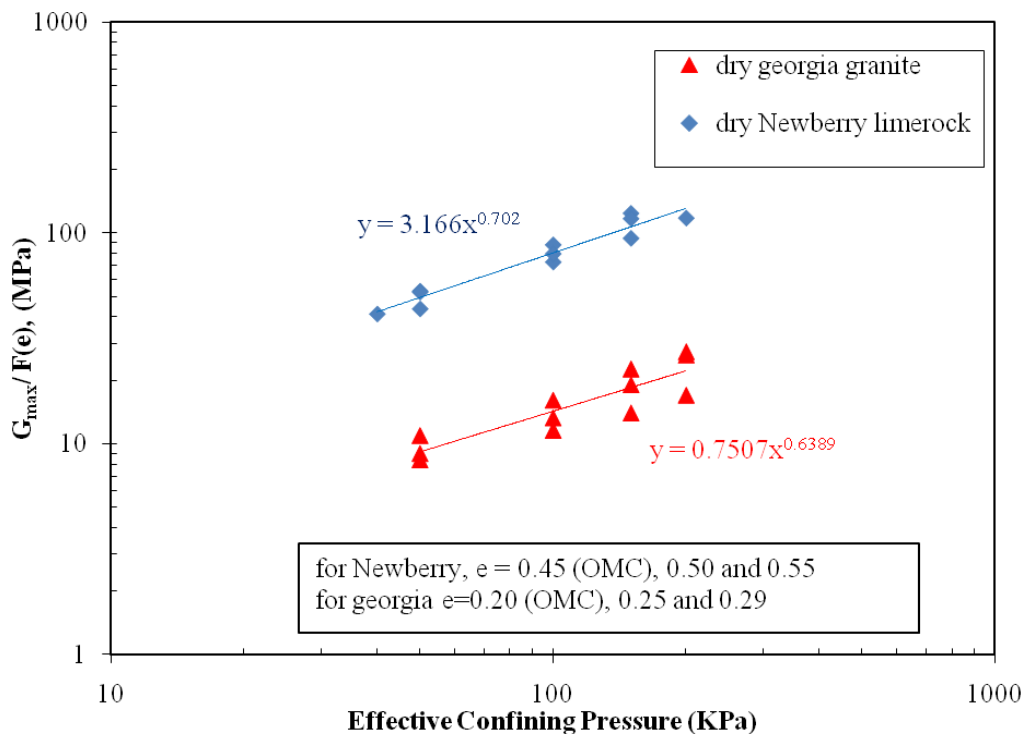


Figure 5-8.  $G_{max}$  empirical equations for Newberry limerock and Georgia granite

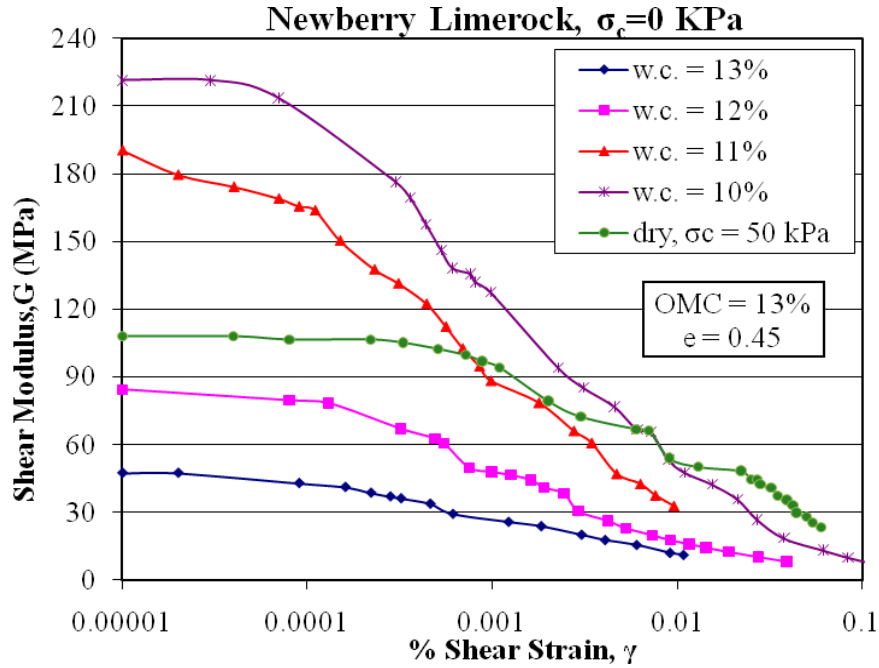


Figure 5-9. Shear moduli (G) versus % shear strain ( $\gamma$ ) curves for Newberry limerock at different water contents

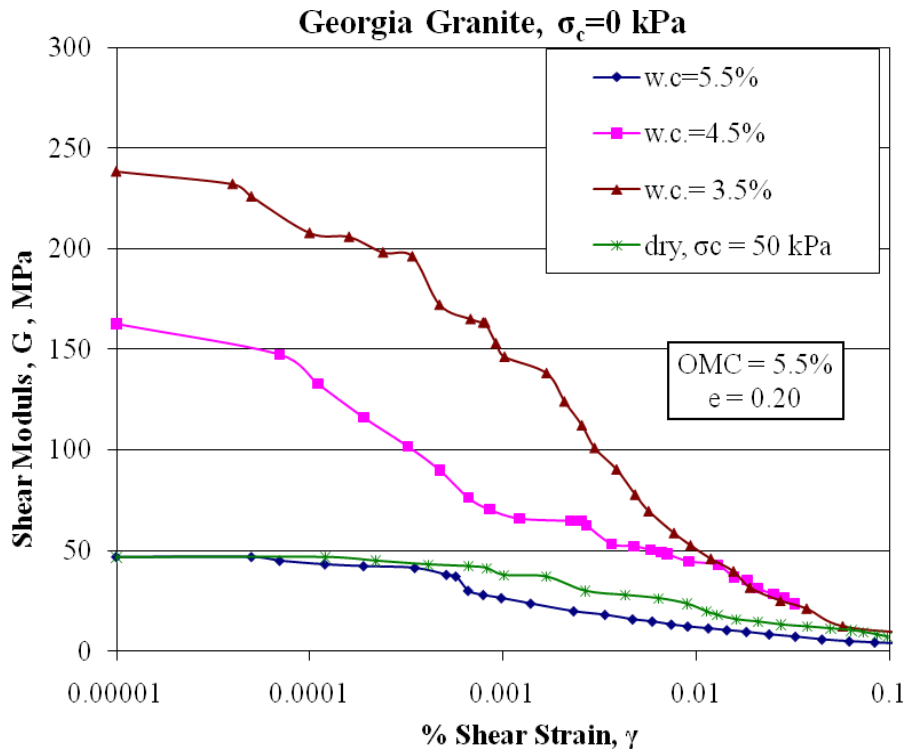


Figure 5-10. Shear modulus (G) versus %shear strain ( $\gamma$ ) curves for Georgia granite at different water contents

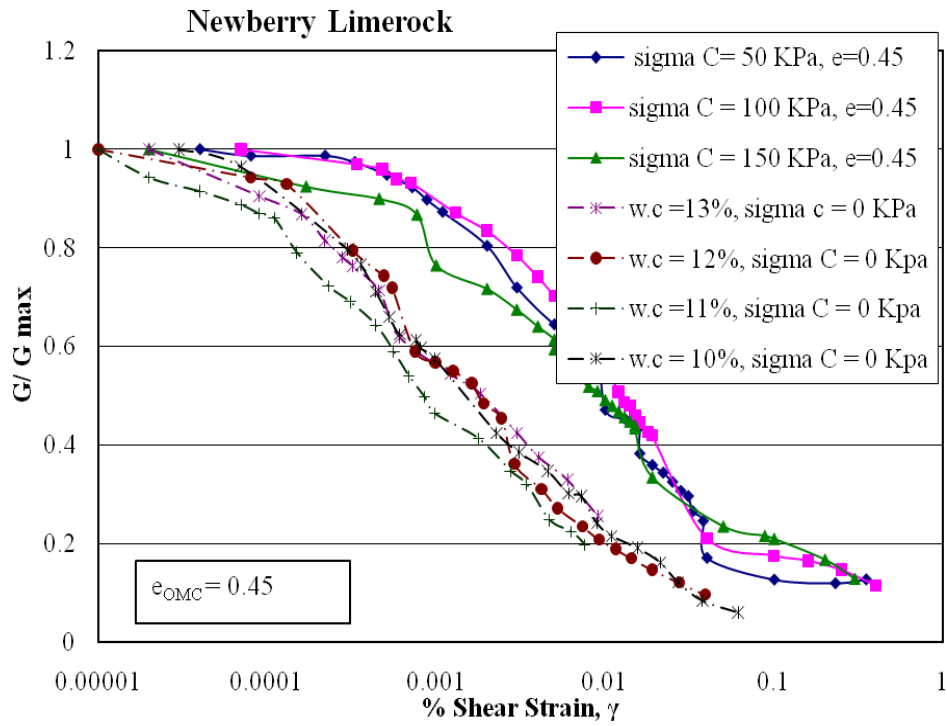


Figure 5-11.  $G/G_{max}$  versus shear strain curves for Newberry limerock for both dry & wet specimens

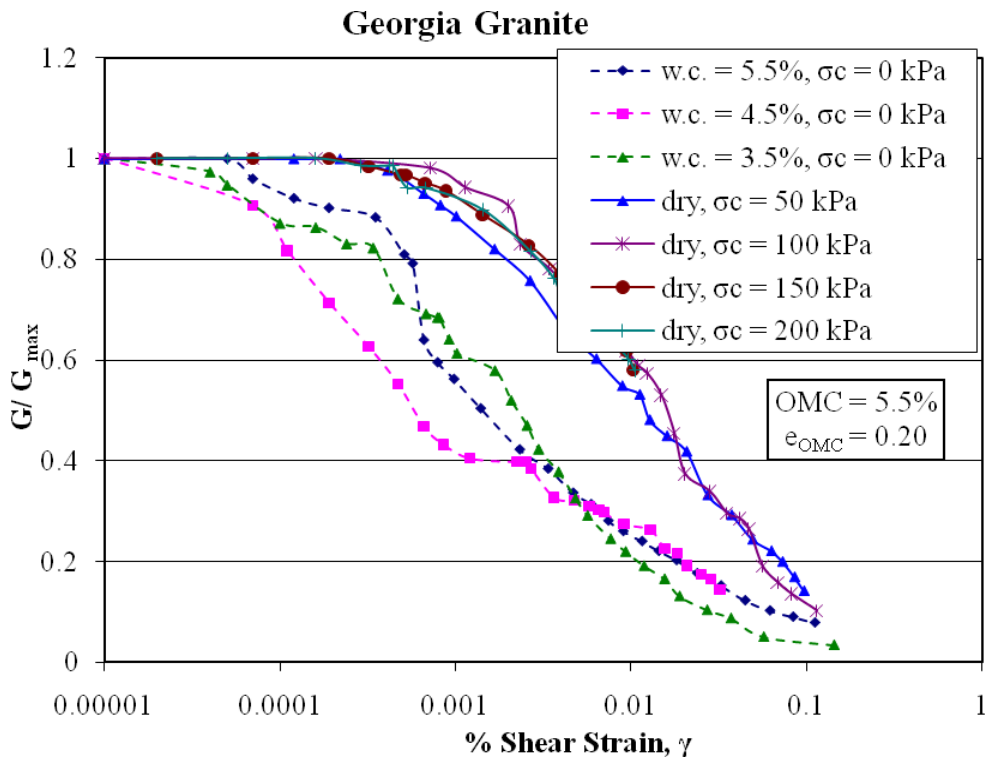


Figure 5-12.  $G/G_{max}$  versus % shear strain curves for Georgia granite, for both dry and wet specimens

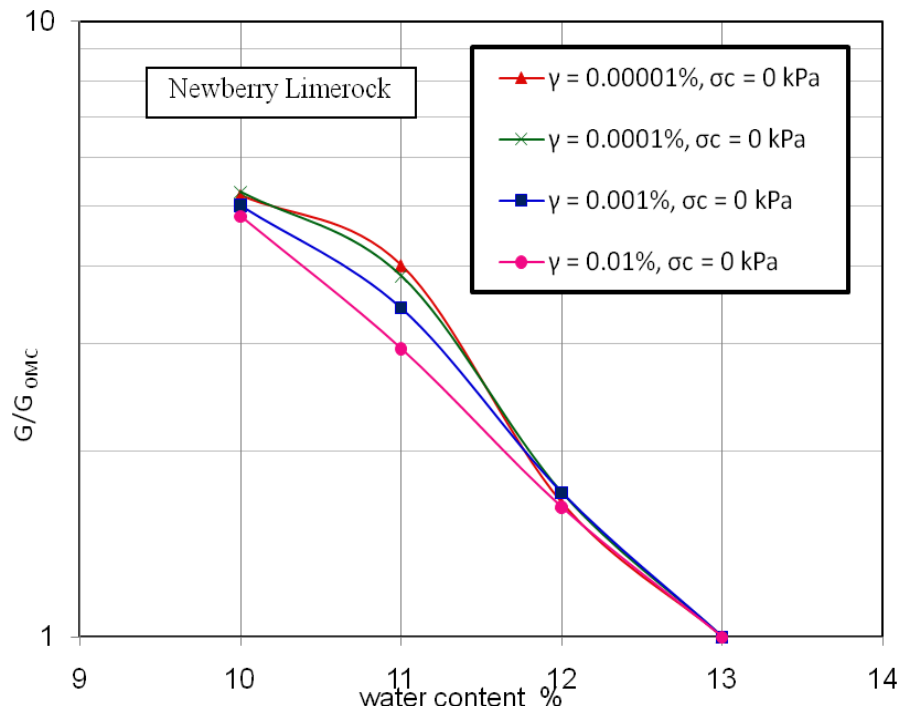


Figure 5-13.  $G/G_{OMC}$  versus water content (%) at different strain levels for Newberry limerock

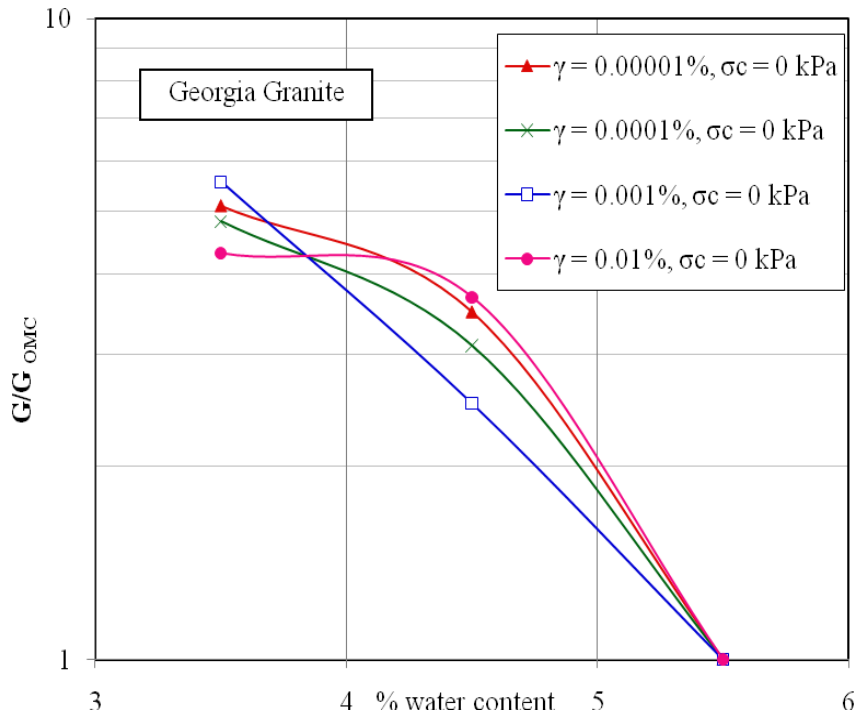


Figure 5-14.  $G/G_{OMC}$  versus water content (%) at different strain levels for Georgia granite

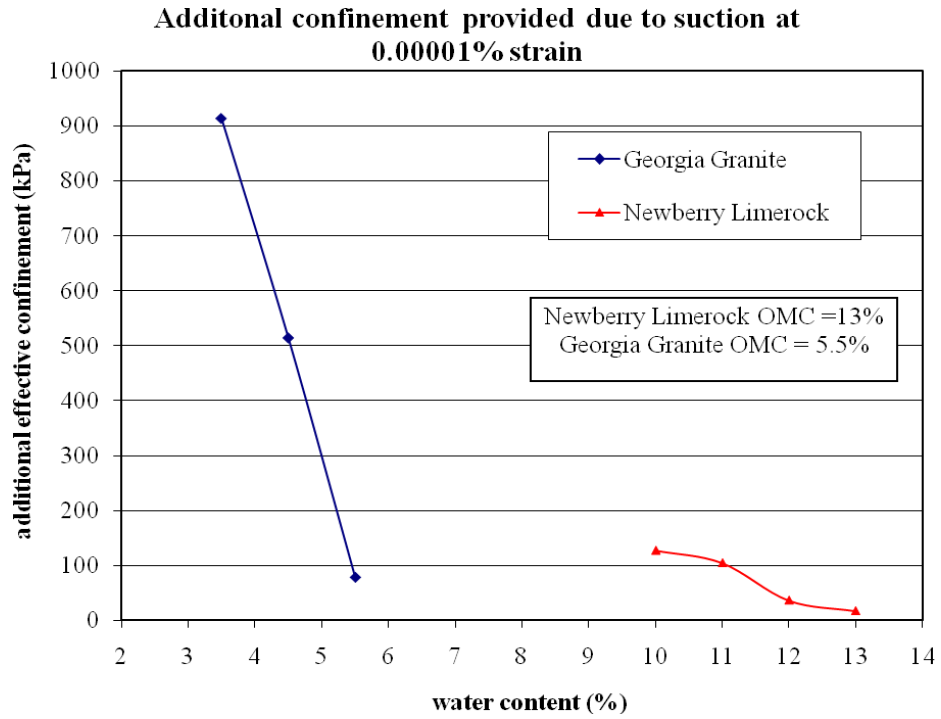


Figure 5-15. Additional confinement provided due to suction at  $10^{-5}\%$  strain magnitude, at different water contents

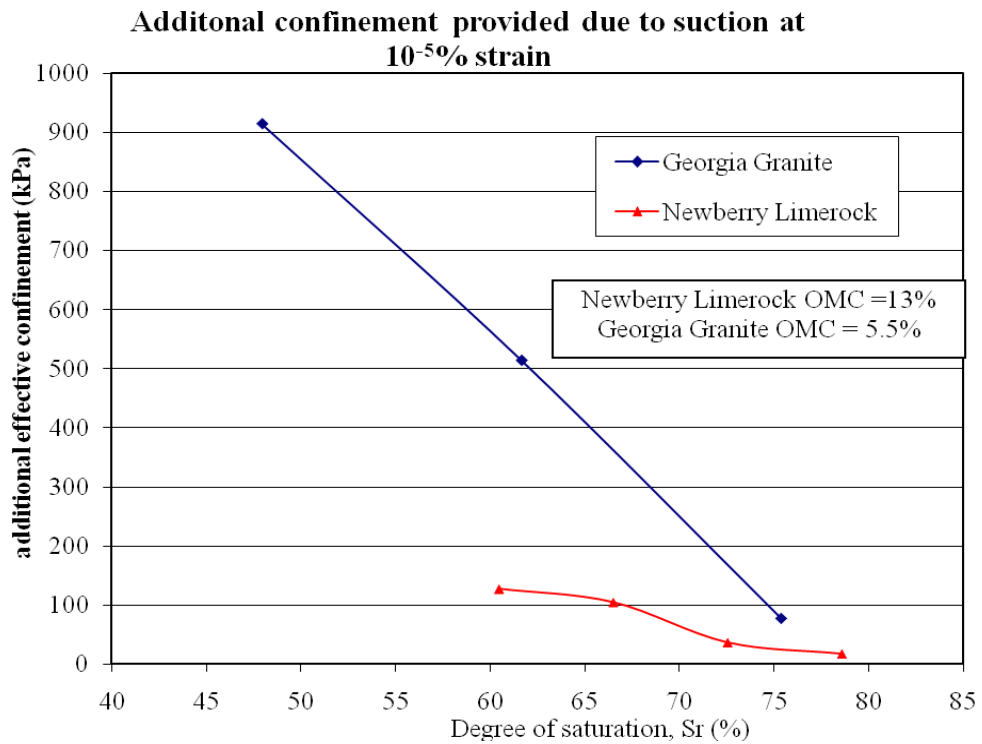


Figure 5-16. Additional confinement provided due to suction at  $10^{-5}\%$  strain magnitude at different degree of saturation

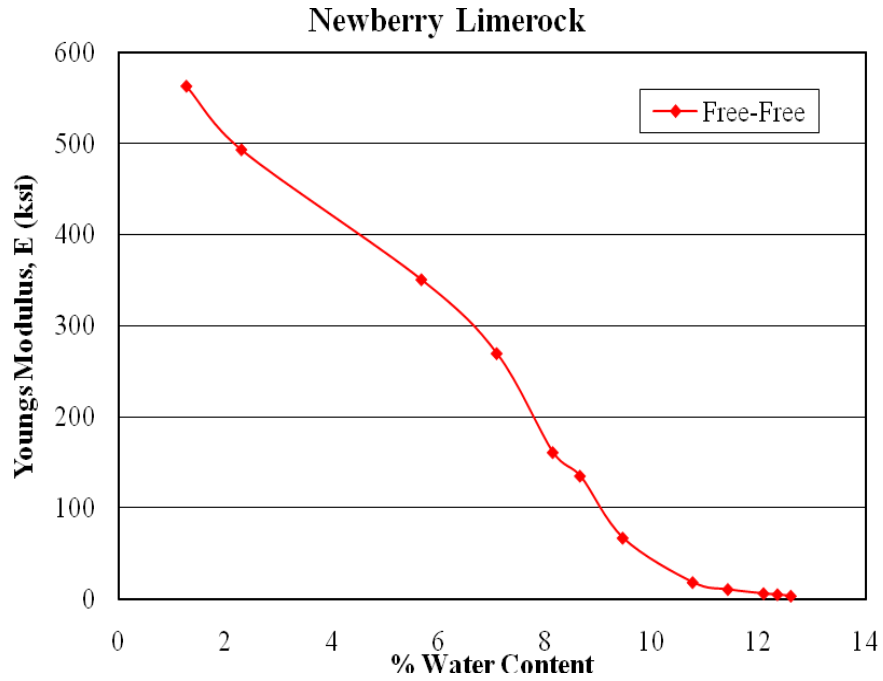


Figure 5-17. Young's Modulus versus % water content results obtained from Free-Free RC test on Newberry limerock

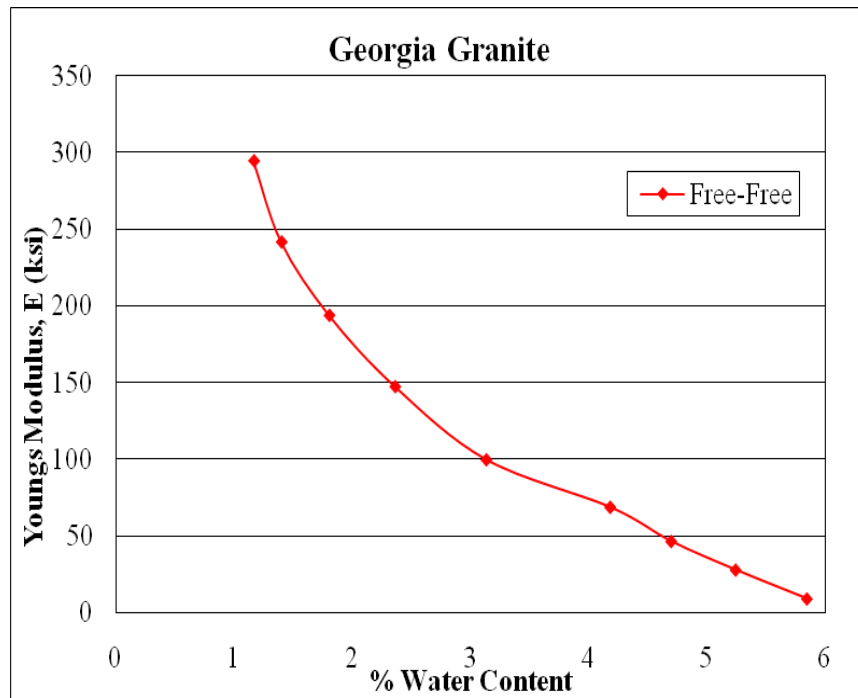


Figure 5-18. Young's Modulus versus % water content results obtained from Free-Free RC test on Georgia Granite

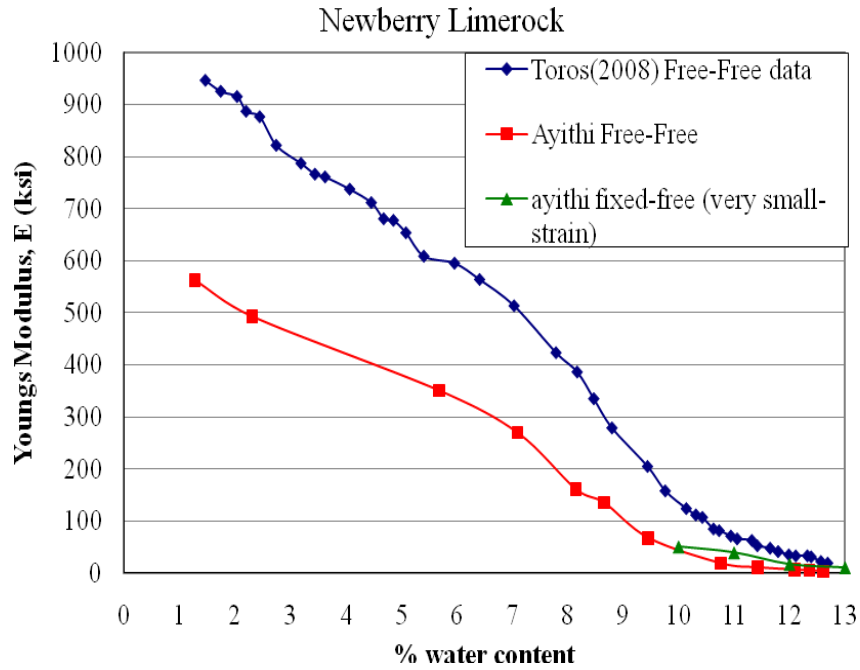


Figure 5-19. Comparison of Newberry limerock Free-Free RC test data with Fixed-Free RC very small-strain data and Toros (2008) data

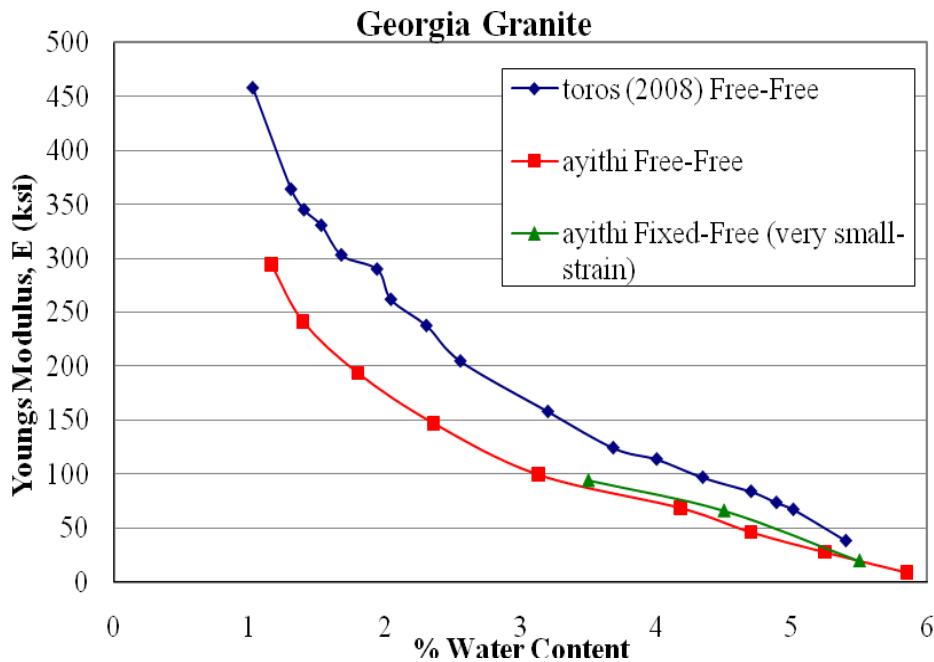


Figure 5-20. Comparison of Georgia granite Free-Free RC test data with Fixed-Free RC very small-strain data and Toros (2008) data

## CHAPTER 6 NONLINEAR FINITE ELEMENT MODELING OF BASE LAYER

One of the main objectives of this research study is to develop a nonlinear pavement response model utilizing laboratory testing results presented in Chapter 5, and incorporate base modulus nonlinearity with respect to effective stress confinement, loading strain and moisture content; and analyze under performance conditions. To perform a nonlinear analysis using stress and strain dependent nonlinear moduli for unbound base materials, it requires using a nonlinear finite element model that can compute pavement responses such as stress, strain and displacement; at any stress point of finite element pavement model.

PLAXIS-Hardening Soil small model (Plaxis-Hssmall), a nonlinear finite element model software is selected for our nonlinear analysis. A detailed discussion about its features, suitability for our analysis and analysis methodology are presented in this chapter.

### **6.1 PLAXIS: Hardening Soil-Small Model (Plaxis-Hssmall Model)**

PLAXIS is a special purpose two-dimensional finite element computer program used to perform deformation and stability analysis for various types of geotechnical applications. Real situations may be modeled either by a plain strain or an axisymmetric model.

Hssmall model is an elastoplastic type of hyperbolic model and incorporates strain dependent stiffness moduli, simulating the different reaction of soils to small strain (i.e. strains below  $10^{-3}\%$ ) and large strains (i.e. strains above  $10^{-1}\%$ ). Soil modulus behaves elastic at very small-strains (i.e. lower than  $10^{-4}\%$ ) and decreases nonlinearly with increase in strain amplitude. Figure 6-1 shows an example of typical s-shaped soil modulus reduction curve.

The most frequently used hyperbolic model to estimate nonlinear modulus reduction in soils (Figure 6-1), including both small-strains and large strains, is Hardin-Drnevich relationship and described as:

$$\frac{G}{G_{max}} = \frac{1}{1 + \left| \frac{\gamma}{\gamma_r} \right|} \quad (6-1)$$

where threshold strain is quantified as  $\gamma_r = \frac{\tau_{max}}{G_{max}}$  (6-2)

Hssmall model uses a more straight forward and less prone to error modified Hardin-Drnevich relationship proposed by Santos and Correia (2001), and is described as:

$$\frac{G}{G_{max}} = \frac{1}{1 + \alpha \left| \frac{\gamma}{\gamma_{0.7}} \right|} \quad (6-3)$$

where  $\alpha = 0.385$ ,  $\gamma_{0.7}$  is the shear strain at  $G = 0.7G_{max}$

Figure 6-2 shows fit of modified Hardin-Drnevich relationship (Equation 6-3) with Santos and Correia (2001) testing data.

Therefore, two parameters are needed to know to describe the modulus behavior at small strains, and they are:

- Initial or very small-strain modulus  $G_{max}$
- shear strain level at  $\gamma_{0.7}$  at which secant shear modulus  $G$  is reduced to 70% of  $G_{max}$

Some basic characteristics of Hssmall model are:

Stress dependent stiffness according to power law	Input parameter $m$
Plastic straining due to primary deviatoric loading	Input parameter $E_{50}^{ref}$
Plastic straining due to primary compression	Input parameter $E_{oed}^{ref}$
Elastic unloading/reloading	Input parameter $E_{ur}^{ref}, \nu_{ur}$
Failure according to the Mohr-Coulomb model	Input parameter $c, \phi$ and $\psi$
Nonlinear reduction of small-strain modulus	Input parameter $G_{max}, \gamma_{0.7}$

### 6.1.1 Parameters of Hssmall Model

Input parameters required for Hssmall model are presented in Table 6-1.

All stiffness related parameters (i.e.  $G_{max}^{ref}$ ,  $E_{50}^{ref}$ ,  $E_{oed}^{ref}$  and  $E_{ur}^{ref}$ ) are defined at a particular reference stress, at which they are determined in laboratory. Based on the stiffness value defined

at a particular reference stress, Plaxis-Hssmall model calculates stiffness values at any required stress for given conditions, using the following equations.

$$G_{max} = G_{max}^{ref} \left( \frac{c \cos \varphi - \sigma_1' \sin \varphi}{c \cos \varphi + p^{ref} \sin \varphi} \right)^m \quad (6-4)$$

$$E_{50} = E_{50}^{ref} \left( \frac{c \cos \varphi - \sigma_3' \sin \varphi}{c \cos \varphi + p^{ref} \sin \varphi} \right)^m \quad (6-5)$$

$$E_{ur} = E_{ur}^{ref} \left( \frac{c \cos \varphi - \sigma_3' \sin \varphi}{c \cos \varphi + p^{ref} \sin \varphi} \right)^m \quad (6-6)$$

$$E_{oed} = E_{oed}^{ref} \left( \frac{c \cos \varphi - \sigma_1' \sin \varphi}{c \cos \varphi + p^{ref} \sin \varphi} \right)^m \quad (6-7)$$

where  $\sigma_1'$  = vertical stress, at which test was conducted

$\sigma_3'$  = confining stress or minor principal stress at which test was conducted.

Based on parameter values for different soils found in literature (Benz (2006), Lehane et al. (2008)), it can be approximated that  $E_{ur} = E_{max}/3 = G_{max} 2(1+\nu)/3$ . PLAXIS-Hssmall model manual suggests to use  $E_{50} = E_{oed} = E_{ur}/3$ , by default.

### 6.1.2 Compatibility of Plaxis-Hssmall Model Modulus Reduction Model to Our Laboratory Determined Base Soils Modulus Reduction Behavior

In order to use Plaxis-Hssmall model to model Newberry limerock and Georgia granite, it is necessary to cross check the compatibility between Hssmall model's nonlinear modulus reduction model curve and lab testing results modulus reduction curves. For both materials,  $G/G_{max}$  versus  $\gamma/\gamma_{0.7}$  curves are developed following Santos and Correia (2001) modified hyperbolic curve Equation 6-3. These material curves are compared with theoretical and shown in Figure 6-3. From the curves in Figure 6-3, it can be concluded that Hssmall model hyperbolic model curve can be used to well represent the nonlinear small-strain modulus reduction behavior of Newberry limerock and Georgia granite.

## 6.2 Flexible Pavement Nonlinear Response Model

The primary basis of our finite element model for flexible pavement is adapted from MEPDG (2004), Appendix-RR (Finite Element Procedures for Flexible Pavement Analysis).

Some of the main features of MEPDG (2004) finite element model are:

- 1) Axisymmetric model
- 2) Static single wheel load with 150 mm radius circular cross sectional area and 550 kPa tire contact stress
- 3) Vertical side boundaries are 10 to 12 radii far from center of wheel load and horizontal bottom boundaries are 50 times of radii below from top of surface layer
- 4) Linear surface asphalt concrete (AC) layer and linear subgrade layer
- 5) Nonlinear base layer

These above mentioned MEPDG features are considered for our pavement model and their implementation is explained in detail in next followed sections.

### 6.2.1 Axisymmetric Model

Axisymmetric model with 15-node triangular elements is chosen for our pavement modeling and a typical pavement cross section and FE mesh formation is shown in Figures 6-4a and 6-4b. Size of the element, i.e. fineness of mesh is selected such that i) there is a smooth continuity of resulting stresses and strains between two adjacent elements and ii) time taken for processing is not too long. Since surface AC layer and subgrade layer are considered as elastic, fineness of mesh is critical for base layer only. Vertical side boundaries are at least 12 radii (i.e. > 1.8 m) from load center and bottom horizontal boundary is at least 50 radii (i.e. 7.5 m) below from the top of AC layer. It is also made sure that location of boundaries has no influence on load resulting deformations, by cross checking the deformations near boundaries are either zero or almost zero. Vertical side boundaries are fixed horizontally and allowed to move vertically; whereas horizontal boundaries are fixed both in horizontal and vertical directions.

## **6.2.2 Pavement Cross Sections**

Total six different pavement cross sections with different layer thicknesses are considered for nonlinear analysis, which are presented in Table 6-2 and also shown in Figure 6-5.

## **6.2.3 Loading Conditions**

Circular single wheel with 150 mm radius and 550 kPa of static contact stress is the only loading condition considered for our entire analysis.

## **6.2.4 Input Parameters for Surface and Subgrade Layers of Flexible Pavement**

Since our focus is on modulus nonlinearity of base layer, to single out its influence on performance of whole pavement, it is decided to model all remaining layers, i.e. AC surface and subgrade, as linearly elastic. Various parameters used for AC surface and subgrade layers are presented below.

Following the MEPDG Finite Element Analysis material property selection, both asphalt concrete (AC) surface layer and subgrade layer are considered elastic for our FE analysis. Three different elastic moduli for AC and four different elastic moduli for subgrade are chosen and presented in Table 6-3.

## **6.3 Initial Plaxis-HSsmall Pavement Model Runs and Recalibration**

Before conducting a full length pavement response analysis via a nonlinear response model, it is desirable to check the model's applicability and accuracy for analysis, by comparing some model analysis results against known in-situ measured pavement behavior results. From our literature survey, it is found that no in-situ measured actual pavement results, with proper nonlinear material data that can be utilized for our model analysis, are available in literature. Since there are no known results of pavement structures are available in literature, we looked for any other geotechnical structures in-situ measured known results that can be useful to serve our purpose of nonlinear response model applicability and accuracy check. It is found that in-situ

measured results are available from Perth sand footing field studies conducted by Lehane et al. (2008) and these results are selected for our model verification.

Lehane et al. (2008) conducted load tests on four different size footings built in Perth sand and made in-situ measurement of actual settlements for each footing. Comparison of settlements obtained from their actual in-situ measurements and settlement predictions from HSsmall model, for footing-1, is considered for our verification purpose.

### **6.3.1 Footing Model Analysis and Verification**

Footing-1 (of dimensions 1.5×1.5×1 m) nonlinear response model is developed via Plaxis-HSsmall model, similar to Lehane's finite element model as shown in Figure 6-6. Same regular material properties used by Lehane are used for our model and shown in Table 6-4. This footing model is subjected to loads similar to actual field test loads. Obtained settlement predictions are compared with actual measured settlements and shown in Figure 6-7a. This initial nonlinear analysis comparison revealed that the HSsmall model is soft and predictions are overestimated. Similar observations were reported by Lehane et al. (2008). This comparison exercise concludes that it is required to recalibrate our HSsmall response model such that its analysis results are equal to nearly equal or actual field results.

### **6.3.2 Model Recalibration**

From Section 6.1.1, it is understood that  $G_{\max}^{\text{ref}}$  and  $\gamma_{0.7}$  are the basic model input parameters and should be determined from lab testing. Other stiffness parameters, i.e.  $E_{50}^{\text{ref}}$ ,  $E_{\text{oed}}^{\text{ref}}$ ,  $E_{\text{ur}}^{\text{ref}}$  and  $m$  (power for stress-level dependency) are useful in analysis at larger strains. Plaxis recommends using default values for these stiffness parameters, which are based on and calculated from  $G_{\max}^{\text{ref}}$ ,  $\gamma_{0.7}$  and Poisson's ratio ( $\nu$ ).

One possible way to recalibrate our response model is to modify these input parameters such that actual footing settlements are equal or nearly equal to model predicted settlements.

Since  $G_{\max}^{\text{ref}}$ ,  $\gamma_{0.7}$  and  $m$  are determined from our lab testing and represent the true material behavior; it's not allowed to modify them. Hence, it is decided to modify other non-measured stiffness parameters, i.e.  $E_{50}^{\text{ref}}$ ,  $E_{\text{oad}}^{\text{ref}}$  and  $E_{\text{ur}}^{\text{ref}}$  to recalibrate the response model. These non-measured stiffness parameters are modified by trial and error method such that model predicted and actual in-situ settlements are matching.

After trial and error method, finally arrived calibrated parameters are shown in Table 6-5 comparing with regular parameters (i.e. non-calibrated). Comparison of settlement prediction after recalibration is shown in Figure 6-7b.

#### **6.4 Recalibrated Nonlinear Input Parameters of Base Soils for Plaxis**

Based on recalibration carried out in Section 6.3.2, input parameters for different materials used in our analysis are modified accordingly and reported in Table 6-7, 6-8 and 6-9. These recalibrated input parameters are obtained based on our experimental results presented in Chapter 5.

##### **6.4.1 Recalibrated Parameters of Newberry Limerock and Georgia Granite**

As explained in Chapters 3 and 4, compacted unsaturated specimens of Newberry limerock and Georgia granite are tested at different water contents under no confinement. Since the shear moduli values for different strain amplitudes are obtained at no confinement, reference stress ( $p_{\text{ref}}$ ) for model input is taken as 1 kPa. Value of  $m$ , which indicates stiffness dependence on stress, is obtained from dry material testing. From confinement stress versus shear moduli plots for dry materials (Figure 5-6), for Newberry limerock,  $m=0.702$  and for Georgia granite,  $m=0.6389$ .

Fixed-Free RC tests are run on Newberry limerock at 13, 12, 11 and 10 % water contents only.  $G_{\max}$  for water contents lower than 10% water content are obtained from Free-Free RC test results (Figure 5-15).

Final recalibrated input parameters for Newberry limerock at 13, 12, 11, 10, 8 and 5.5% w.c.; and for Georgia granite at 5.5, 4.5 and 3.5% w.c. are presented in Table 6-6 and Table 6-7 respectively.

#### **6.4.2 Input Parameters for Miami Limerock**

Miami limerock is another base layer material commonly used in the State of Florida. Toros (2008) research investigation on Miami limerock reported that “its modulus behavior is relatively different from other limerocks available in Florida and increases tremendously with drying, compared to other limerocks”. Therefore, in order to understand and compare its behavior with Newberry limerock, it is decided to perform nonlinear model analysis on Miami limerock also.

Since no experimental study is conducted on Miami limerock, it is decided to obtain approximate  $G_{max}$  versus % water content behavior curve from Free-Free RC testing results of Toros (2008). Since Toros (2008) test specimens have some confining due to casing on side surface area, approximate Free-Free test moduli values for Miami limerock with no casing confinement are calculated and presented in Figure 6-8. Based on this estimated approximate  $E_{max}$  versus water content curve for Miami limerock, HS-Small model recalibrated parameters are developed and reported in Table 6-8 for selected water contents.

#### **6.5 Demonstration of Response Model Nonlinear Behavior**

One of the main objectives of developing this response model and recalibrated material parameters is to incorporate both stress dependent and strain dependent modulus nonlinearity in base layer nonlinear analysis. Hence, it is necessary to demonstrate that i) Recalibrated parameters are capable of incorporating nonlinearity and ii) Developed pavement model (Figure 6-4a and Figure 6-4b) is capable of incorporating nonlinearity in base layer.

### **6.5.1 Demonstration of Input Parameters' Nonlinearity**

For nonlinear soils, deformations or strains increase nonlinearly with increase in load and our parameters also supposed to exhibit same behavior. For parameters' nonlinearity demonstration, the same footing used for model recalibration (Figure 6-6) is selected and subjected to different loads. 10% w.c Newberry limerock HSsmall parameters are assigned for soil under the footing. Settlement predictions obtained from this analysis are plotted in Figure 6-9. From Figure 6-9, it can be observed that footing settlements increase nonlinearly with load. Rate of increase in settlement with load is low at lower loads and high at higher loads, and demonstrates material nonlinearity.

### **6.5.2 Demonstration of Pavement Model's Nonlinearity**

Pavement model shown in Figure 6-4a is subjected to different wheel loads in the range of 350–800 kPa. Surface deflection profiles obtained from this analysis are plotted in Figure 6-10. From Figure 6-10, it can be observed that the deflection basin is varying nonlinearly with load, which demonstrates the nonlinearity of pavement model.

Table 6-1. Input parameters of Plaxis-HSsmall model

<b>Failure parameters</b>	
c	cohesion
$\varphi$	angle of internal friction
$\psi$	angle of dilatancy
<b>Basic parameters for nonlinear small-strain stiffness</b>	
$G_{\max}^{\text{ref}}$	The initial or very small-strain modulus at reference stress
$\gamma_{0.7}$	shear strain level at which shear modulus G is reduced to 70% of $G_{\max}$
<b>Basic parameters for soil stiffness</b>	
$E_{50}^{\text{ref}}$	Secant stiffness in standard drained triaxial test
$E_{\text{oed}}^{\text{ref}}$	Tangent stiffness for primary oedometer loading
$E_{\text{ur}}^{\text{ref}}$	Unloading /reloading stiffness (default $E_{\text{ur}}^{\text{ref}} = 3 E_{50}^{\text{ref}}$ )
m	Power for stress-level dependency
<b>Advanced parameters</b>	
$\nu_{\text{ur}}$	Poisson's ratio for unloading-reloading (default $\nu_{\text{ur}} = 0.2$ )
$p_{\text{ref}}$	reference stress for stiffness
$K_0^{\text{nc}}$	$K_0$ -value for normal consolidation (default $K_0^{\text{nc}} = 1 - \sin\varphi$ )
$R_f$	failure ratio $q_f/q_a$ (default $R_f = 0.9$ )
$\sigma_{\text{tension}}$	Tensile strength (default $\sigma_{\text{tension}} = 0$ stress units)
$c_{\text{increment}}$	As in Mohr-coulomb model (default $c_{\text{increment}} = 0$ )

Table 6-2. Different types of pavement structures considered for analysis

Structure Number	Asphalt Concrete Surface Thickness (mm)	Base Thickness (mm)
1	200	450
2	200	300
3	100	450
4	100	300
5	100	200
6	50	300

Table 6-3. Material input parameters for surface asphalt concrete and subgrade layers

	Elastic Modulus (MPa)	Poisson's ratio ( $\nu$ )	Unit weight ( $\text{kN/m}^3$ )
Asphalt Concrete	12500	0.39	23
	3000		
	1000		
Subgrade	125	0.32	18
	70		
	50		
	30		

Table 6-4. Input parameters used in HSsmall model for footing settlement predictions (Lehane et al. 2008)

Parameter	Unit	Value
$\gamma$	$\text{kN/m}^3$	18
$P_{\text{ref}}$	kPa	100
$E_{50}^{\text{ref}}$	MPa	20
$E_{\text{oed}}^{\text{ref}}$	MPa	20
$E_{\text{ur}}^{\text{ref}}$	MPa	45
$G_0^{\text{ref}}$	MPa	160
$m$		0.5
$c$	kPa	1
$\varphi$		$35^\circ$
$\psi$		0
$\nu_{\text{ur}}$		0.2
$\gamma_{0.7}$		2.50E-05

Table 6-5. Comparison of Actual and Modified calibration parameters

Stiffness Parameter	Suggested values	Modified values through Calibration
The initial or very small-strain modulus at reference stress	$G_{\max}$	$G_{\max}$
Secant stiffness in standard drained triaxial test ( $E_{50}$ )	$E_{ur}/3$	$E_{ur}/2$
Tangent stiffness for primary oedometer loading ( $E_{oed}^{ref}$ )	$E_{ur}/3 = E_{50}$	$E_{ur}/2$
Unloading /reloading stiffness (default $E_{ur}^{ref} = 3 E_{50}^{ref}$ )	$E_{ur}$	$0.85 E_{\max}^*$

Note: \*  $E_{\max} = 2(1+\nu)G_{\max}$

Table 6-6. Recalibrated HSsmall input parameters for Newberry limerock

Newberry limerock						
Water content (%)	13	12	11	10	8	5.5
$G_{\max}$ (Mpa)	47.38	84.48	190.3	221.39	449.61	906.536
$\gamma_{0.7}$	5.E-06	5.E-06	5.E-06	5.E-06	5.E-06	5.E-06
$P_{ref}$ (kPa)	1	1	1	1	1	1
$E_{\max}$ (MPa)	132.66	234.85	525.23	606.61	1227.44	2465.78
$E_{ur}$ (MPa)	112.76	199.63	446.44	515.62	1043.32	2095.91
$E_{oed}$ (MPa)	56.38	99.81	223.22	257.81	521.66	1047.96
$E_{50}$ (MPa)	56.38	99.81	223.22	257.81	521.66	1047.96
m	0.702	0.702	0.702	0.702	0.702	0.702
$\gamma$ (kN/m <sup>3</sup> )	21.42	20.45	20.2	20	19.64	18.95
$\nu$	0.4	0.39	0.38	0.37	0.365	0.36

Table 6-7. Recalibrated HSsmall input parameters for Georgia granite

Georgia granite			
Water content (%)	5.5	4.5	3.5
$G_{\max}$ (Mpa)	46.67	162.65	238.22
$\gamma_{0.7}$	5.E-06	5.E-06	5.E-06
$P_{\text{ref}}$ (kPa)	1	1	1
$E_{\max}$ (MPa)	133.48	455.42	657.49
$E_{\text{ur}}$ (MPa)	113.45	387.11	558.86
$E_{\text{oed}}$ (MPa)	56.73	193.55	279.43
$E_{50}$ (MPa)	56.73	193.55	279.43
m	0.6389	0.6389	0.6389
$\gamma$ (kN/m <sup>3</sup> )	21.42	20.45	20.2
$\nu$	0.43	0.4	0.38

Table 6-8. Recalibrated HSsmall input parameters for Miami limerock

Miami limerock			
Water content (%)	8	6	4
$G_{\max}$ (Mpa)	12.22	226.95	1286.8
$\gamma_{0.7}$	5.E-06	5.E-06	5.E-06
$P_{\text{ref}}$ (kPa)	1	1	1
$E_{\max}$ (MPa)	35.19	640.00	3500.10
$E_{\text{ur}}$ (MPa)	29.91	544.00	2975.08
$E_{\text{oed}}$ (MPa)	14.96	272.00	1487.54
$E_{50}$ (MPa)	14.96	272.00	1487.54
m	0.702	0.702	0.702
$\gamma$ (kN/m <sup>3</sup> )	21.42	20.45	20.2
$\nu$	0.44	0.41	0.36

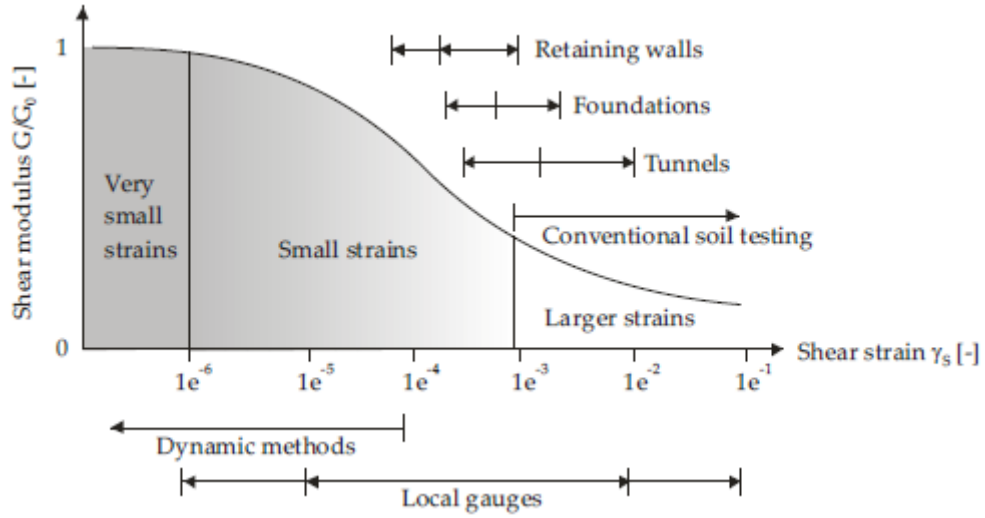


Figure 6-1. Characteristic modulus–strain behavior of soil with typical strain ranges for laboratory tests and structures. (Atkinson and Salfors, 1991)

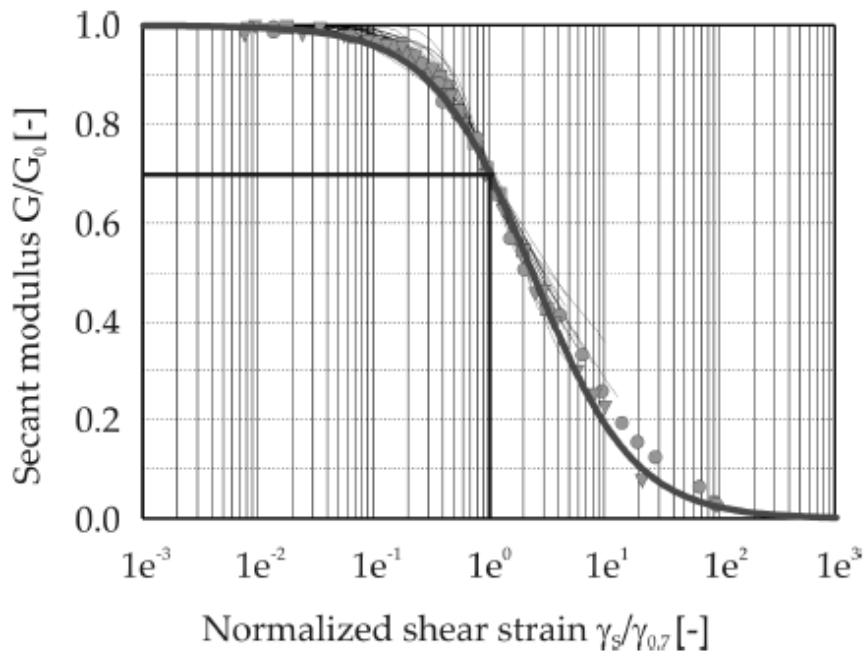


Figure 6-2. Results from modified Hardin-Drnevich relationship compared to test data by Santos and Correia (2001)

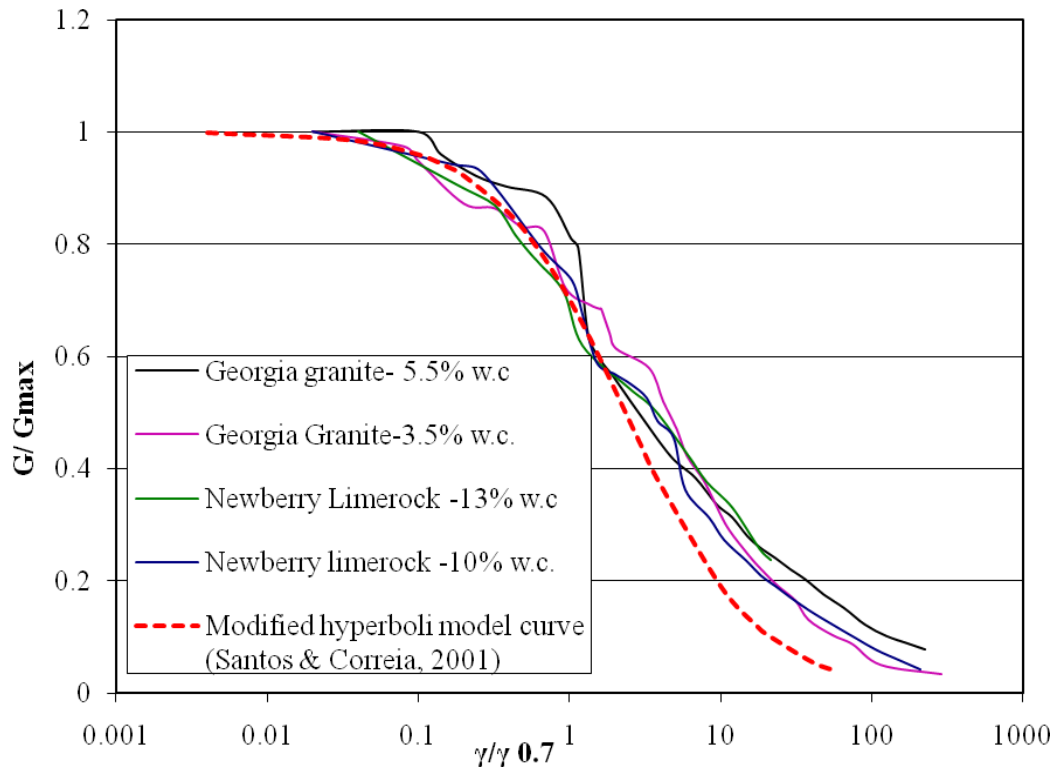


Figure 6-3. Comparison of Newberry limerock and Georgia granite actual testing data with HSsmall model's Santos and Correia (2001) modified hyperbolic curve

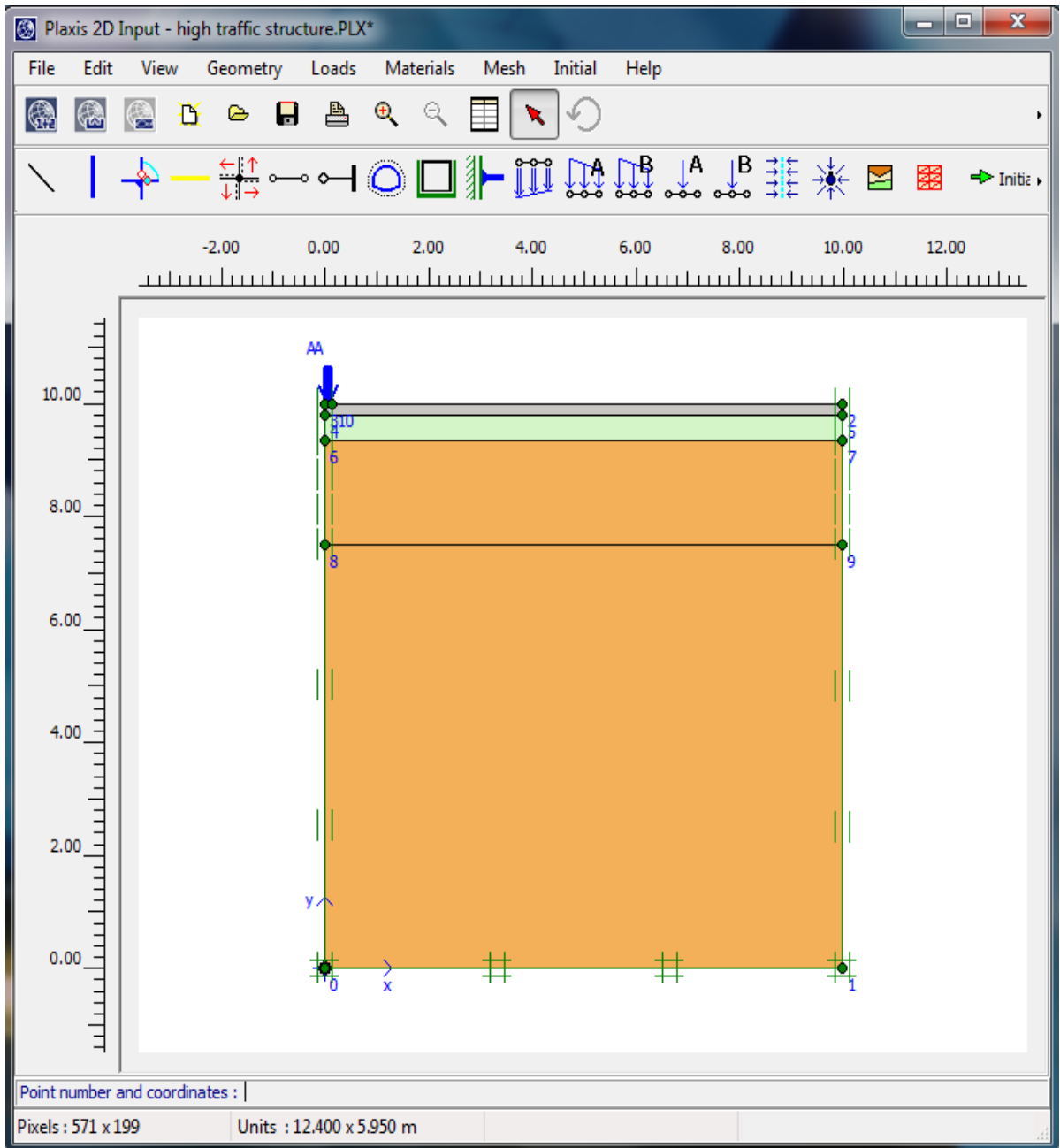


Figure 6-4. Typical Plaxis-HSsmall model cross section model used for nonlinear analysis.

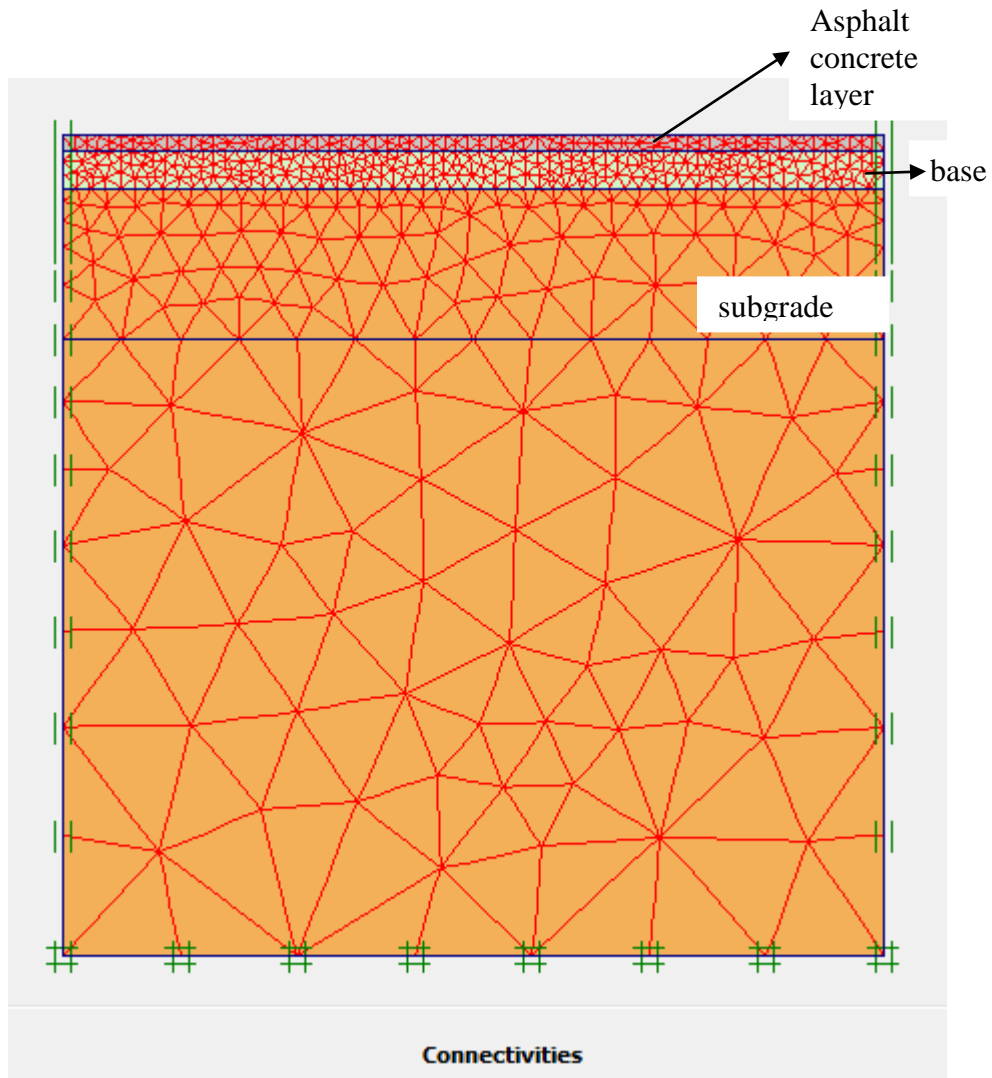
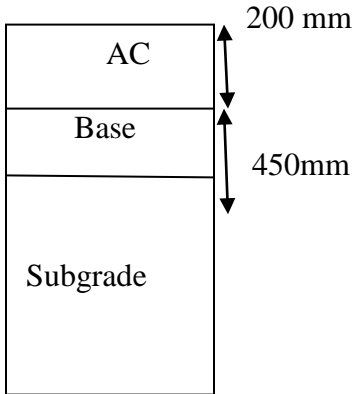
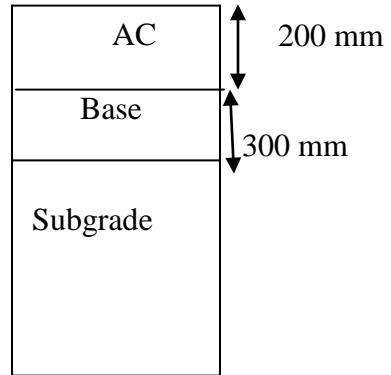


Figure 6-5. Typical HSsmall model finite element mesh of a pavement cross section

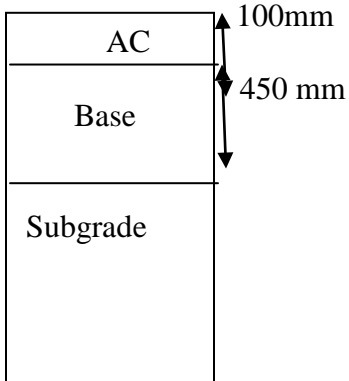
**Structure-1**



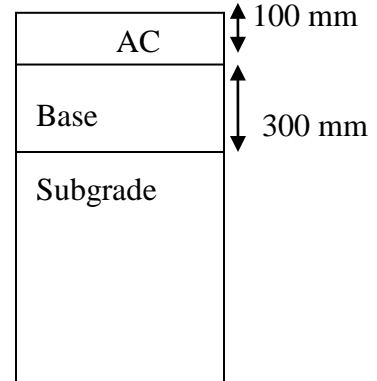
**Structure-2**



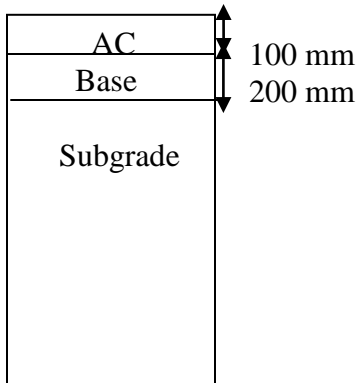
**Structure-3**



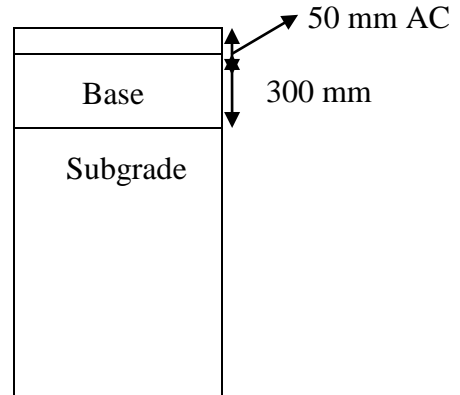
**Structure-4**



**Structure-5**



**Structure-6**



Note: AC – Asphalt Concrete

Figure 6-6. Cross sections considered for nonlinear base pavement analysis

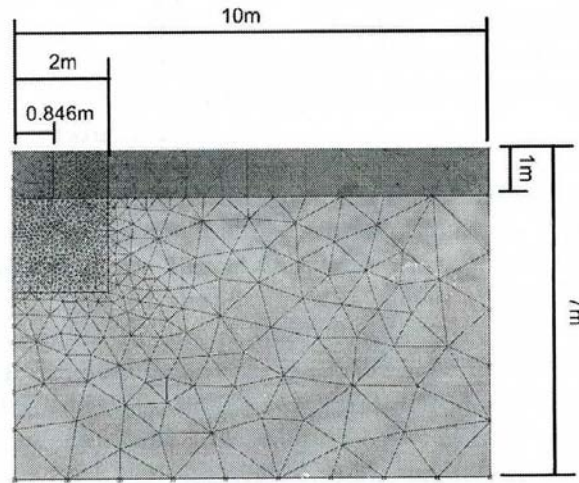


Figure 6-7. Finite element mesh used for model recalibration analysis (footing-1 by Lehane et al. (2008))

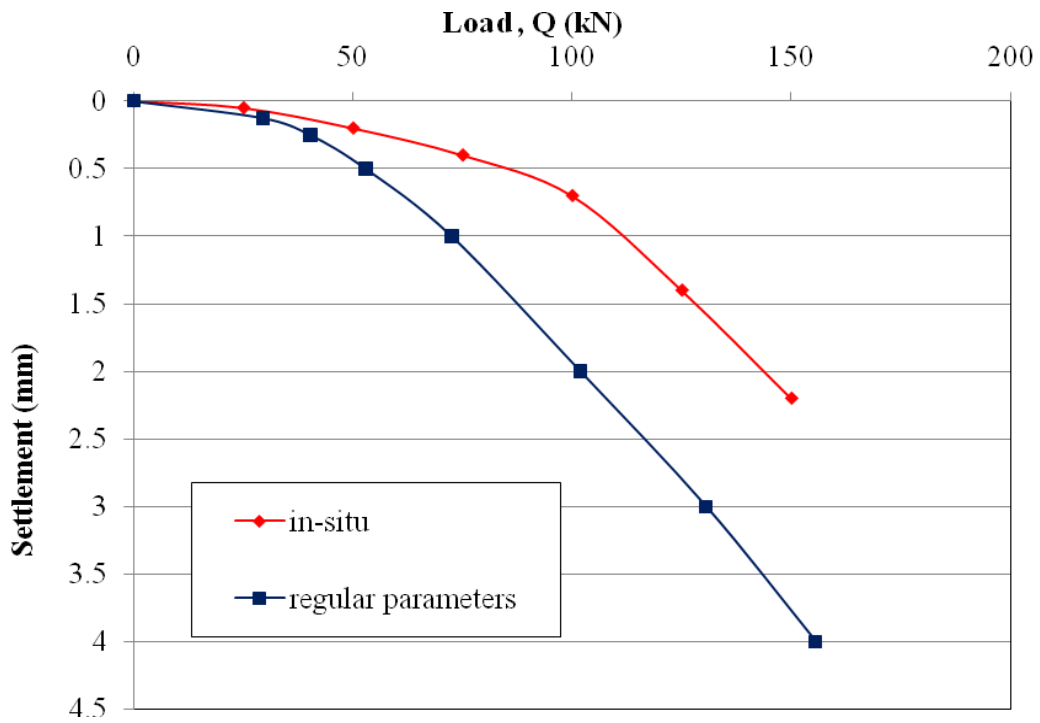


Figure 6-8. Comparison of actual settlements with settlements predicted using regular parameters via Plaxis-HSsmall footing model.

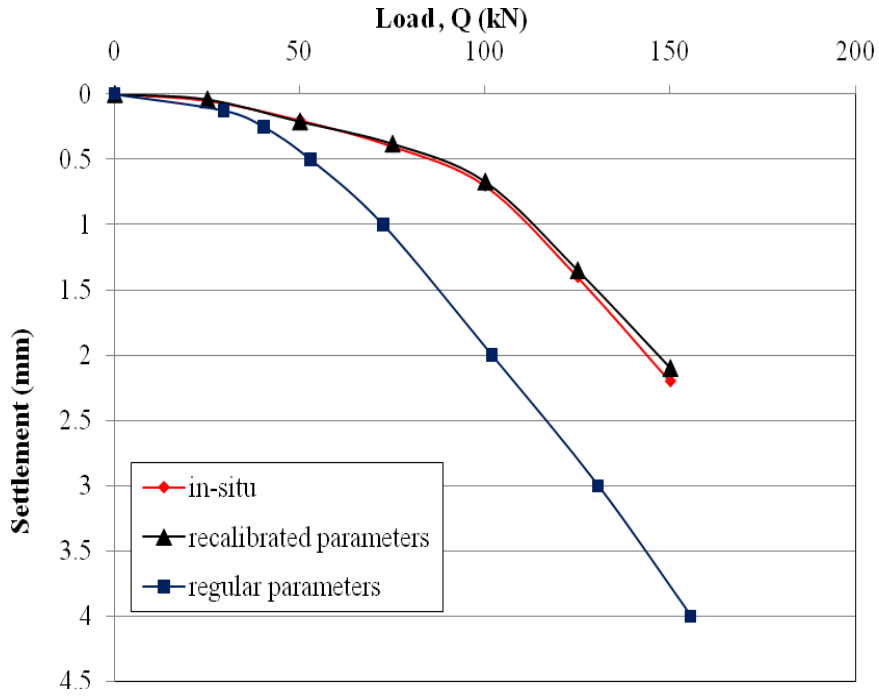


Figure 6-9. Comparison of actual settlements with settlements predicted using regular parameters and calibrated settlements via Plaxis-HSsmall footing model.

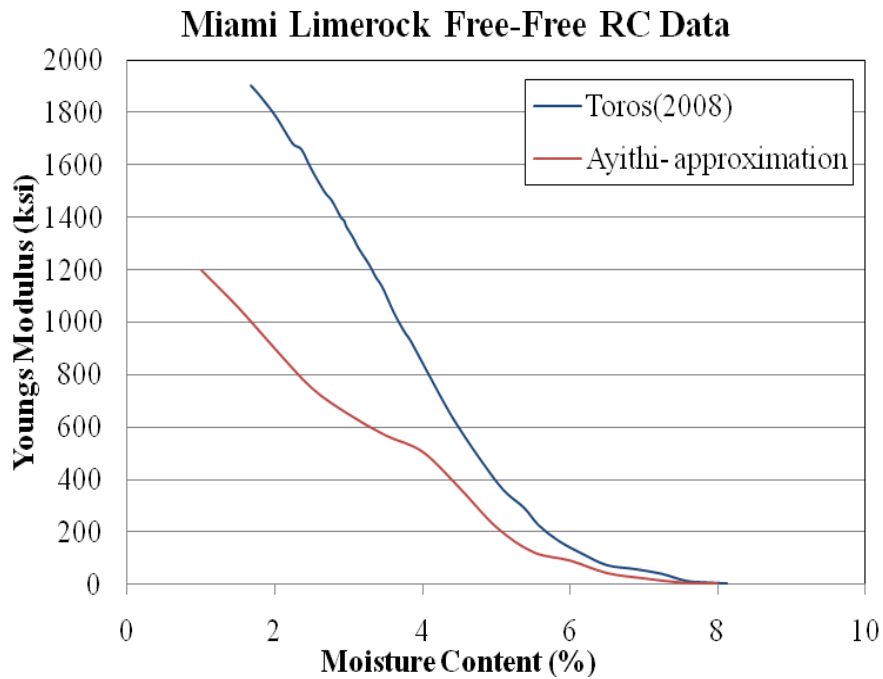


Figure 6-10. Approximate Miami limerock  $G_{max}$  versus water content plot.

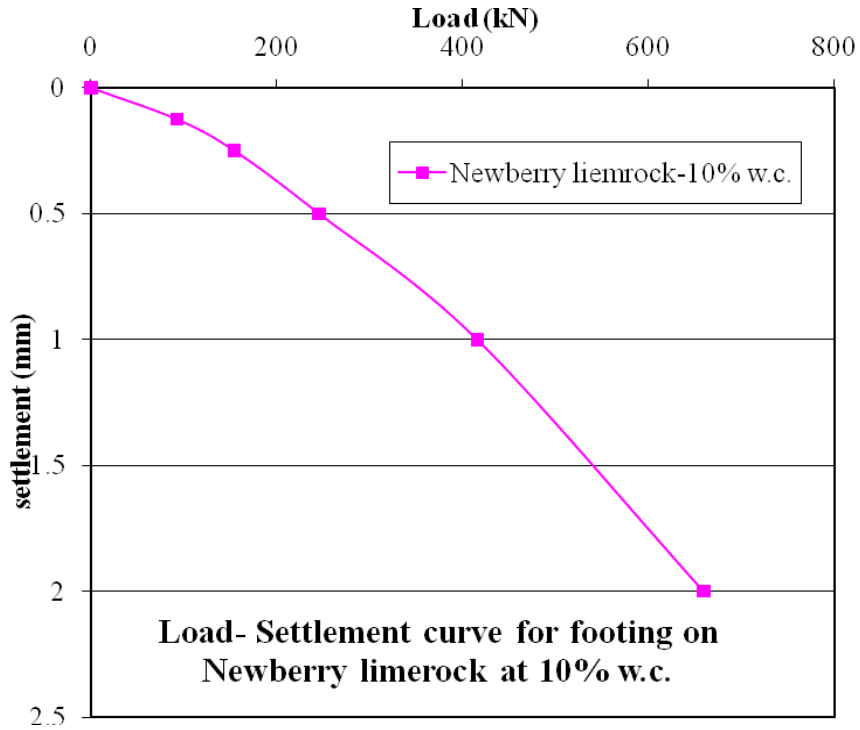


Figure 6-11. Load versus settlement curve to demonstrate material input parameters nonlinearity.

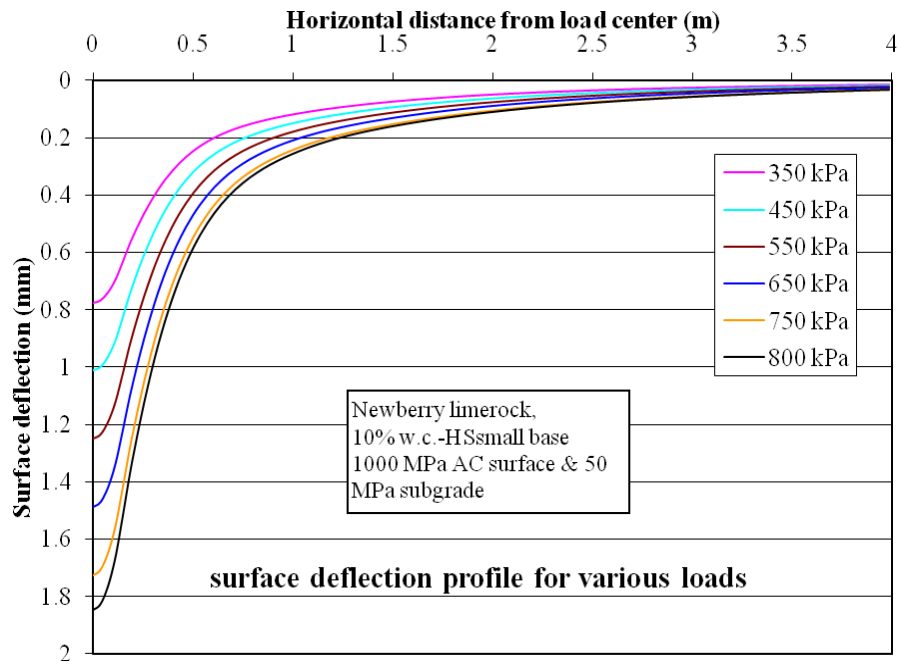


Figure 6-12. Pavement surface deflection basin for different load demonstrating pavement model nonlinearity.

## CHAPTER 7 BASE LAYER NONLINEAR MODELING ANALYSIS AND RESULTS

Characterization of modulus nonlinearity of base soils via lab testing program is discussed in Chapter 5. Using these laboratory test results, a workable nonlinear response model for pavement analysis is developed via PLAXIS. Nonlinear response model development procedure, model characteristics and calibration, pavement cross sections proposed for analysis, material parameters, and verification and demonstration of model's nonlinearity are presented in Chapter 6.

Now we have a functional operational nonlinear pavement response model ready for analysis. Next objective is using the responses obtained from response model nonlinear analysis of pavement; develop a methodology to calculate nonlinear equivalent single effective modulus for the whole base layer that can approximate known nonlinearities of base layer and can be used as MEPDG level-2 and level-3 parameter inputs for practical design applications. Pavement responses, obtained from nonlinear analysis, such as deformations, strains and stresses at various critical locations of pavement cross section can be considered for determining single effective base modulus that can approximately produce same pavement responses as in nonlinear analysis. Effective modulus determination methodology and its verification, influence of moisture content, subgrade modulus and overall structural cross section on single effective modulus, comparison of nonlinear and linear analyses responses, and effect of base nonlinearity on pavement performance are discussed in this chapter.

### **7.1 Nonlinear Equivalent Single Effective Base Modulus Determination**

#### **7.1.1 Methodology**

To derive the single effective linear modulus value for whole base layer, it is proposed to use pavement surface deflection basin as the single matching factor between nonlinear and linear

analysis. For nonlinear analysis, both AC surface and subgrade layers are considered linear and base layer is considered nonlinear. In other words, the moduli of surface and subgrade layer are linear (elastic) and the modulus of base layer is nonlinear. Using the maximum surface deflection value obtained from nonlinear analysis as the matching factor, an equivalent elastic modulus value for whole base layer is determined by trial and error method. Surface deflection profile obtained from single effective modulus base case should match well with nonlinear base case surface deflection profile. During this process, elastic moduli of AC surface layer and subgrade are kept same as in corresponding nonlinear case.

Once the equivalent single effective elastic modulus value for base layer is determined, pavement responses obtained at critical locations (Figure 7-1) for both linear and nonlinear cases can be compared for further comparison analysis.

### **7.1.2 An Example of Surface Deflection Basin Matching Between Nonlinear Modulus Base Case and Single Effective Elastic Modulus Base Case**

Nonlinear analysis via Plaxis-HSsmall nonlinear pavement response model (developed in Chapter 6) is performed on Structure-1 (refer to Figure 6-5) with 10% w.c. base. AC surface layer and subgrade layer are considered elastic with 1000 MPa and 50 MPa moduli, respectively. From nonlinear analysis, maximum surface deflection of 0.582 mm is obtained under a wheel load of 550 kPa. Keeping the elastic moduli of surface and subgrade layers same as in nonlinear base modulus case, equivalent single effective modulus for base layer that can produce the same maximum surface deflection of 0.582 mm is determined by trial and error method. Obtained surface deflection basins for both nonlinear modulus base and single effective elastic modulus base cases are plotted in Figure 7-2 for comparison purpose. From this figure, it can be observed that surface deflection basin obtained from single effective base modulus case matches very well with the surface deflection basin of nonlinear base modulus case.

### **7.1.3 Demonstration of Nonlinear Reduction of Single Effective Modulus with Increase in Load**

In the science of nonlinear material mechanics, it is well known that modulus of particulate material decreases nonlinearly with increase in strain. For particulate materials like soil, permanent strain or deformation increases nonlinearly with increase in load, and modulus decreases nonlinearly with increase in strain. One of the main objectives of our research work is to incorporate this modulus nonlinearity in pavement base layer design and analysis. Hence it is interesting to verify that equivalent single effective modulus of base layer, determined from nonlinear analysis surface deflection, reflects this nonlinearity. In other words, single effective modulus of base layer expected to decrease nonlinearly with increase in load.

A demonstration exercise is performed on structure-1 and structure-4, with Newberry limerock base at 13% and 10% moisture contents and Georgia granite base at 5.5% and 3.5% moisture contents. Moduli of AC surface layer and subgrade layer are kept as 1000 MPa and 50 MPa, respectively. After conducting nonlinear analysis at different loads via our Plaxis-HSsmall nonlinear response model, single effective base modulus for each load is determined following the single effective modulus determination methodology explained in section 7.1.1.

Results of these analyses are presented in Figures 7-3 and 7-4. From these plots it can be primarily demonstrated that single effective modulus of base material decreases with increase in load, in a nonlinear manner. It can also be observed that for both Newberry limerock and Georgia granite, modulus nonlinearity increases with decrease in water content. The rate of reduction in modulus with increase in load is higher in base layers with lower moisture contents than in higher moisture content. This tells us that as the water content starts decreasing, material starts behaving more nonlinear.

## **7.2 Single Effective Moduli Data for Base Layer**

### **7.2.1 Nonlinear Equivalent Single Effective Design Moduli Values for Base Layer**

Nonlinear analyses are run via Plaxis-HSsmall nonlinear response model, on six different pavement structures presented in Figure 6-5. Nonlinear material parameters presented in Tables 6-6, 6-7 and 6-8 for Newberry limerock, Georgia granite and Miami limerock at different water contents are assigned to base layer. AC surface layer is considered elastic with 1000 MPa modulus. Different subgrade elastic moduli presented in Table 6-3 are assigned to subgrade layer, to analyze the effect of subgrade elastic modulus on resulting base layer single effective modulus. Methodology explained in section 7.1.1 is followed to determine single effective design modulus for base layer.

Single effective moduli values determined for different structures are presented in Tables 7-1 to 7-3. Table 7-1 presents effective moduli values obtained for Newberry limerock base, and so Table 7-2 and Table 7-3 for Georgia granite and Miami limerock, respectively.

Following the procedure explained in section 5.2.2 and using Equations 5-1 and 5-2, maximum Young's modulus ( $E_{max}$ ) of base soil is calculated at in-situ overburden stress or confinement at middle depth of base layer. Single effective moduli values along with corresponding  $E_{max}$  and ratio of effective modulus to maximum Young's modulus (i.e.  $E/E_{max}$ ) are presented in Appendix B. This database would be primarily helpful in prior approximate estimation of effective moduli, from known  $E_{max}$ . It can be primarily observed that  $E/E_{max}$  decreases with decrease in water content, which indicates that modulus nonlinearity increases with decrease in water content.

#### **7.2.1.1 Influence of moisture content on base layer single effective design modulus**

For structures 1 to 6, at constant subgrade modulus, variation of single effective modulus with decrease in base material water content is shown in Figures 7-5, 7-6 and 7-7, for Newberry

limerock, Georgia granite and Miami limerock, respectively. From these column plots it can be observed that for same subgrade modulus, effective base modulus increases significantly with decrease in water content. Our laboratory test data showed that nonlinear small-strain modulus of base material increase significantly with decrease in water content. Decrease in water content increases additional confinement caused by suction, which in turn increases small-strain modulus. This increase in small-strain modulus is being reflected on equivalent single effective modulus and hence single effective modulus increases with decrease in water content.

Among all three different base materials, Miami limerock base has the highest single effective moduli values. From lab testing results, it is observed that increase in small-strain modulus due to suction also is highest for Miami limerock, among all three base materials. This indicates that highest increase in small-strain modulus due to suction, compared to other two materials, is reflected in equivalent single effective modulus. This also confirms the importance of small-strain modulus nonlinearity in determining single effective modulus for linear design methods.

#### **7.2.1.2 Influence of subgrade modulus on single effective base design modulus**

From the column plots in Figures 7-5, 7-6 and 7-7, it can be observed that for any given structure and base water content, single effective base modulus increases with increase in subgrade modulus. In our case, highest effective modulus for any base water content corresponding to a given structure occurs at 125 MPa. This indicates that single effective design modulus of base layer at any given water content depends on modulus of subgrade, which supports base layer. This behavior can be explained by basics of pavement mechanics. It is well known that pavement permanent deformation is mainly dependent on subgrade modulus and deformation decreases with increase in subgrade modulus. As the subgrade modulus increases, magnitude of deviatoric stresses acting on base layer decreases. Since soil modulus is nonlinearly

stress dependent and increases with decrease in deviatoric stress, base layer effective modulus increases with increase in subgrade modulus. Therefore, as the subgrade modulus increases, single effective base modulus increases at faster rate with decrease in moisture content.

### **7.2.1.3 Influence of structure type on single effective base design modulus**

For same base moisture content, variation of base single effective design modulus for different structures with different subgrade moduli is shown in Figures 7-8, 7-9 and 7-10 for Newberry limerock, Georgia granite and Miami limerock, respectively.

From these column plots, it can be observed that at any given moisture content and subgrade modulus combination, base layer single effective modulus value is dependent on structure type. In other words, single effective modulus is dependent on structure layers' thicknesses. As the thicknesses of different layers in pavement structure varies, the magnitude of wheel load deviatoric stresses being transferred from top layers to bottom layers also varies. Usually, as the thickness of a layer increases, deviatoric stresses being transferred to the layer beneath it decreases and corresponding modulus increases. Thus, since soil modulus is nonlinear with respect to stress, as the magnitude of deviatoric stress varies; its effective modulus also varies.

### **7.2.1.4 Comparison of single effective design moduli for different materials**

Single effective design moduli values obtained at 8% w.c. for Newberry limerock, 3.5% w.c. for Georgia granite and 4% for Miami limerock are compared with their respective optimum moisture contents (OMC), for structure-1 and structure-4 in Figure 7-11a and Figure 7-11b, respectively. Effective moduli values obtained with both 50 MPa and 125 MPa subgrade moduli are shown in these column plots. These column plots can provide an idea about “how fast and by how much magnitude, the effective modulus of each material increases due to drying, compared to other two materials?” From these comparison column plots, it can be primarily observed that

among all three materials Miami limerock behaves very different and its effective modulus increases at faster rate very significantly as the material dries out. At OMC, effective modulus of Miami limerock is much lower than that of Newberry limerock and Georgia granite. But as the material dries out, its modulus increases at a very faster rate compared to other two materials and reaches maximum among all three materials.

For structure-1 and structure-4 with 50 MPa and 125 MPa subgrade modulus, normalized single effective base modulus obtained at different base water contents, for all the three materials are compared in Figure 7-12a for structure-1 and Figure 7-12b for structure-4. Effective modulus ( $E$ ) at different water contents normalized with effective modulus at optimum moisture content ( $E_{opt}$ ) is shown on Y-axis and reduction in degree of saturation due to drying is shown on X-axis.

From these plots also, it can be observed that approximately for the same amount of decrease in degree of saturation, moduli of Newberry limerock and Georgia granite are increasing more or less at same rate with respect to  $E_{opt}$ , where as Miami limerock is increasing very significantly and behaving much different. Toros (2008), from his Free-Free RC test data, also observed very significant increase in  $E_{max}$  of Miami limerock as the material dries out, compared to Newberry limerock and Georgia granite.

For a decrease of 45% in degree of saturation, effective moduli of Newberry limerock and Georgia granite are increasing by around 3-3.5 times for both structure-1 and structure-4, where as effective modulus of Miami limerock is increasing by around 17 times for structure-1 and around 45 times for structure-4. These observations indicate that increase in design modulus with material drying is material specific. Since modulus tests are generally conducted at OMC, it is very important to be aware of this behavior, or else a pavement designer can get misled very easily.

### 7.2.1.5 Comparison of equivalent single effective design moduli with mepdg moisture effect model design moduli

MEPDG(2004) recommends below given generalized regression model to incorporate moisture effect (suction effect) on resilient modulus ( $M_R$ ).

$$\log \frac{M_R}{M_{Ropt}} = a + \frac{b - a}{1 + EXP(\beta + k_s \cdot (S - S_{opt}))} \quad (7-1)$$

For coarse grained soils:

$a=-0.3123$ ,  $b=0.3$ ,  $\beta=-0.0401$  and  $k_s=6.8157$ .

It would be interesting to see “if MEPDG moisture effect model can accurately estimate design modulus of our base soils or not?” In other words, can MEPDG moisture model determine design modulus at different moisture contents accurately for our base soils? For this purpose, single effective moduli values derived for our base soils (Tables 7-1, 7-2 and 7-3) are compared with MEPDG model derived moduli values.

Effective moduli values for selected structures with 50 MPa and 125 MPa subgrade moduli and at different base moisture contents are compared with MEPDG moisture model calculated moduli values, and shown in Figures 7-13, 7-14 and 7-15 for Newberry limerock, Georgia granite and Miami limerock, respectively. Effective modulus ( $E$ ) or resilient modulus ( $M_R$ ) normalized with modulus at optimum moisture content ( $E_{opt}$  or  $M_{R opt}$ ) is on Y-axis, and decrease in degree of saturation at different water contents is on X-axis. Legend indicates the structure number and its subgrade modulus.

From these figures, it can be observed that for MEPDG model, as the moisture content decreases, modulus can increase maximum up to two times of modulus at optimum moisture content. Whereas, effective base moduli values derived for our materials does not meet this criteria and in the case of Miami limerock it can increase up to 45 times.  $E/E_{opt}$  values for our

materials are determined only up to 40% decrease in degree of saturation and can increase further with further decrease in degree of saturation.

In general, for structures with low subgrade modulus (50 MPa for our plots), effective moduli are falling slightly near MEPDG moisture model values. As the subgrade modulus increases,  $E/E_{opt}$  values are moving away from moisture model curve and increases up to 3.5 times for Newberry limerock, 2.5 times for Georgia granite and 47 times for Miami limerock. From these observations, it can be concluded that MEPDG moisture effect model cannot incorporate moisture/suction effect accurately for Florida base materials.

### **7.3 Evaluation of Applicability of Single Effective Modulus in place of Nonlinear Modulus**

Design methodology to determine equivalent single effective design modulus for base layer is developed by considering surface deflection basin as the only matching factor. It is also shown via an example in section 7.1.2 that surface deflection basins generated from nonlinear base analysis and corresponding equivalent linear base analysis are matching well.

Now, as a next step, it is interesting to compare pavement responses generated from nonlinear and equivalent linear analyses models to assess the applicability of single effective modulus for base layer in lieu of nonlinear modulus. For this purpose, various pavement responses obtained from nonlinear and corresponding equivalent linear analysis are compared, at various critical locations (Figure 7-1).

#### **7.3.1 Comparison of Nonlinear and Equivalent Linear Analysis Responses**

Below given responses obtained from nonlinear analysis and corresponding equivalent linear analysis, at different locations of pavement structure (as shown in Figure 7-1) are compared.

- 1) Surface deflection
- 2) Horizontal stress ( $\sigma_{xx}$ , tensile stress) at top of AC layer

- 3) Horizontal strain ( $\epsilon_{xx}$ , tensile strain) at top of AC layer
- 4) Horizontal stress ( $\sigma_{xx}$ , tensile stress) at bottom of AC layer
- 5) Horizontal strain ( $\epsilon_{xx}$ , tensile strain) at bottom of AC layer
- 6) Vertical stress ( $\sigma_{yy}$ , compressive stress) at top of base layer
- 7) Vertical strain ( $\epsilon_{yy}$ , compressive strain) at top of base layer
- 8) Vertical stress ( $\sigma_{yy}$ , compressive stress) at bottom of base layer
- 9) Vertical strain ( $\epsilon_{yy}$ , compressive strain) at bottom of base layer
- 10) Vertical stress ( $\sigma_{yy}$ , compressive stress) at top of subgrade layer
- 11) Vertical strain ( $\epsilon_{yy}$ , compressive strain) at top of subgrade layer

The basis of selecting above responses for comparison is related to basics of pavement mechanics. In general, surface cracking and rutting are two most important distresses that occur in pavement structures. Surface cracking is primarily dependent on horizontal strain ( $\epsilon_{xx}$ , tensile strain) at bottom of AC layer and rutting is dependent on vertical strain ( $\epsilon_{yy}$ , compressive strain) at top of subgrade layer. Comparison of these two responses for nonlinear and linear analysis can illustrate “whether adopting single effective modulus in place of nonlinear modulus would influence the rutting and cracking performance of pavement?” Next, surface deflection is the basic matching factor between nonlinear and equivalent linear analysis. Remaining stress and strain responses at different locations can provide basic information about “how are the stresses and strains at different layer intersections varying and matching up, for nonlinear and equivalent linear analyses?”, and “does considering equivalent single effective modulus in place of nonlinear modulus would influence these responses?”

Pavement responses obtained from nonlinear and equivalent linear analysis of few selected pavement structures with 1000 MPa AC surface and 50 MPa subgrade modulus, and different base materials with different water contents, are compared. List of structures analyzed for responses comparison is given in Table 7-4. For all the cases given in Table 7-4, nonlinear and equivalent linear response curves comparison plots for all above mentioned pavement responses are presented in Appendix C. Magnitude of horizontal strain ( $\epsilon_{xx}$ , tensile strain) at bottom of AC

layer, obtained from nonlinear and equivalent linear analysis of structure-1 and structure-4, with different base water contents are compared in Figure 7-16a for Newberry limerock and Figure 7-16b for Georgia granite. Same set of comparison plots are developed for vertical strain ( $\epsilon_{yy}$ , compressive strain) at top of subgrade layer and shown in Figure 7-17a for Newberry limerock and Figure 7-17b for Georgia granite.

From Surface deflection comparison plots (Figures C-1 to C-8 for Newberry limerock and Figures C-89 to C-92 for Georgia granite, from Appendix C); it can be observed that the surface deflection profiles for nonlinear and equivalent linear analyses are matching well. Hence, considering single effective modulus in place of nonlinear modulus does not affect the real surface deflections. From the remaining response plots shown in Appendix C, except for vertical strain ( $\epsilon_{yy}$ ) at the top of subgrade plots (Figures C-81 to C-88 and C-129 to C-132), no significant differences in curves of nonlinear and corresponding linear analyses are observed and hence, single effective modulus is acceptable with respect to those responses as well.

From the comparison plots of horizontal tensile strain ( $\epsilon_{xx}$ ) at bottom of AC layer (Figure 7-16a to 7-16b), for both structure-1 and structure-4 with different base water contents, it can be observed that horizontal strain ( $\epsilon_{xx}$ ) at bottom of AC layer for nonlinear base modulus case is equal or nearly equal to equivalent linear case with single effective base modulus. In the science of pavement mechanics, it is well known that pavement surface cracking is generally dependent on horizontal tensile strain ( $\epsilon_{xx}$ ) at bottom of AC surface layer. Hence, this implies that considering equivalent single effective modulus for design of base layer thickness may not significantly affect the overall cracking performance of pavement.

Comparison plots of vertical strain ( $\epsilon_{yy}$ ) at the top of subgrade for nonlinear and equivalent linear cases are compared in Figures 7-17a to 7-17b for structure-1 and structure-4, with different

base water contents. In the case of structure-1, for both materials at different water contents,  $\epsilon_{yy}$  at top of subgrade (Figures C-81 to C-84 and Figure 7-17a) for nonlinear analysis is equal or nearly equal to that of corresponding equivalent linear analysis. As the water content decreases,  $\epsilon_{yy}$  of nonlinear case becomes very slightly higher than that of equivalent linear case, but not of significant magnitude. Whereas, in the case of structure-4, in general,  $\epsilon_{yy}$  at top of subgrade (Figures C-85 to C-88 and Figure 7-17b) for nonlinear analysis is higher than corresponding equivalent linear analysis, and this difference increases with decrease in water content. This indicates that the base material is behaving more and more nonlinear with decreases in water content. Since structure-4 is thinner than structure-1, this indicates that material nonlinearity increases as the structure thickness and base layer water content decreases, together.

According to pavement mechanics,  $\epsilon_{yy}$  at top of subgrade is critical for pavement's rutting performance. So, as the base material nonlinearity increases with decrease in structure thickness and base layer water content together, use of equivalent single effective design modulus may over estimate pavement's rutting performance. Hence, a new rutting performance criterion may be required to use single effective design modulus in place of nonlinear modulus, "when, both the structure thickness and base material water content decreases together".

In overall, for thick structures like structure-1, at different base water contents, no significant differences are observed in various pavement responses including  $\epsilon_{yy}$  at top of subgrade, obtained from nonlinear and equivalent linear analysis. Hence, equivalent single effective modulus for base layer, which is derived based on maximum surface deflection, can be adopted for practical design purposes for thick structures similar to structure-1. Whereas, for thin structures like structure-4, with the decrease of base layer thickness and water content together, it appears that modulus nonlinearity of base soil becomes more significant and affects pavement's

rutting performance and hence, equivalent linear method may overestimate rutting performance. Hence, in order to use equivalent effective modulus for base layer design calculations of thin structures, it may be required to develop a new rutting performance criterion.

### 7.3.2 Analysis of Nonlinear and Linear Responses in the Perspective of Rutting Performance Criteria

Based on observations made in last section, it is understood that “using equivalent single effective modulus in place of nonlinear modulus may affect the rutting performance of pavement”. Thus, it would be interesting to investigate the differences in pavement rutting performance, when a base layer is designed by i) nonlinear method considering modulus nonlinearity and ii) equivalent linear design method consider single effective modulus. Vertical strain ( $\epsilon_{yy}$ ) at top of subgrade layer is considered for this rutting performance comparison investigation.

It is well acknowledged in literature that pavement permanent deformation or settlement is primarily dependent on subgrade modulus (Huang (1993)). Several empirical equations have been developed for permanent deformation criteria. These equations are helpful in predicting allowable number of load repetitions related to vertical strain  $\epsilon_{yy}$  at top of subgrade. Asphalt Institute’s (AI) empirical equation for permanent deformation failure criterion is frequently used for pavement rutting performance analysis. AI’s equation assumes elastic behavior for all layers. Asphalt Institute’s empirical equation for rutting failure criteria is:

$$N_d = f_4(\epsilon_c)^{-f_5} \quad (7-2)$$

Where  $N_d$  - allowable number of load repetitions to limit permanent deformation

$\epsilon_c$  - compressive strain on the top of subgrade (i.e.  $\epsilon_{yy}$ —for our case)

$$f_4 = 1.365 \times 10^{-9}$$

$$f_5 = 4.477$$

It should be noted that Equation 7-2 was developed based on “elastic criteria”, i.e. all the layers are assumed to be elastic. Analyzing the vertical strain ( $\epsilon_{yy}$ ) at top of subgrade, obtained for both nonlinear and linear cases, to determine  $N_d$  using Equation 7-2, would help to identify the importance of considering base modulus nonlinearity in performance analysis. For structure-1 and structure-4 with selected base layer moisture contents,  $N_d$  is calculated from  $\epsilon_{yy}$  at top of subgrade layer and corresponding analyzed data is presented in Tables 7-5 and 7-6.

From the analysis data presented in Table 7-5 for structure-1, it can be observed that the ratio of  $N_{d\text{linear}}/N_{d\text{nonlinear}}$  is close to one, which means allowable number of load repetitions is nearly same. This implies that adopting equivalent single effective modulus for base layer thickness design in place of nonlinear modulus, may not significantly affect the overall rutting performance of structure-1. So, elastic criteria based empirical equation can be used for rutting performance analysis of thick structures, similar to structure-1.

From the data presented in Table 7-6 for structure-4, it can be observed that the ratio of  $N_{d\text{linear}}/N_{d\text{nonlinear}}$  is varying between 1.5 to 3 times, which means considering equivalent single effective modulus in place of nonlinear modulus for base layer may overestimate allowable number of load repetitions as many as three times. This implies that considering equivalent single effective modulus for base layer thickness design for structure-4, may overestimate the overall rutting performance of the pavement by as many as three times. It also implies that elastic design method may overestimate the actual rutting performance of the pavement structure-4. Hence, it may not be appropriate to use elastic criterion based empirical equations for rutting performance analysis of thin structures, similar to structure-4.

In the case of structure-4 with Georgia granite base (Table 7-6), a little difference of 0.03% in  $\epsilon_{yy}$  at top of subgrade, between linear and nonlinear case, is overestimating the rutting

performance by three times. We know that the above estimated difference (i.e. over estimation) in rutting performance is due to considering equivalent single effective modulus in place of nonlinear modulus, just for base layer only. This implies that considering nonlinearity in other soil layers of a pavement structure may influence pavement performance more significantly due to cumulative nonlinearity effect, compared to considering nonlinearity only in base layer.

Since pavement subgrade layers are generally built with soils and hence its nonlinearity also may affect the  $\epsilon_{yy}$  at top of subgrade and so rutting performance. Thus an investigation into subgrade nonlinearity may provide more information about importance of considering nonlinearity in soil layers and its influence on rutting performance.

Table 7-1. Equivalent elastic moduli values obtained for different pavement structures, with different subgrade moduli for Newberry limerock base

Subgrade Modulus (Mpa)	Structure	Moisture Content (%)					
		13	12	11	10	8	5.5
30	1	65	79	112	118	142	171
	2	58	70	92	94	118	139
	3	54	67	90	101	108	130
	4	49	60	69	70	76	78
50	1	79	102	140	153	196	230
	2	74	92	120	125	155	178
	3	66	89	112	124	148	168
	4	62	80	108	112	123	132
	5	73	---	100	---	---	102
	6	76	---	90	---	---	107
70	1	90	117	170	175	230	267
	2	85	109	143	149	184	207
	3	73	100	135	142	195	205
	4	71	96	129	135	139	144
125	1	108	157	227	241	310	387
	2	107	147	210	220	278	308
	3	93	141	214	220	281	311
	4	84	127	196	206	228	240
	5	105	---	189	---	---	209
	6	103	---	180	---	---	187

Table 7-2. Effective equivalent elastic moduli values obtained for different pavement structures, with different subgrade moduli for Georgia granite base

Subgrade Modulus (Mpa)	Structure	Moisture Content (%)		
		5.5	4.5	3.5
30	1	63	104	117
	2	56	94	104
	3	54	88	100
	4	46	74	75
50	1	76	135	152
	2	70	112	124
	3	66	115	119
	4	60	100	106
70	1	86	155	178
	2	82	135	150
	3	73	133	162
	4	67	123	137
125	1	112	210	243
	2	105	195	220
	3	90	207	220
	4	84	184	220

Table 7-3. Effective equivalent elastic moduli values obtained for different pavement structures and with different subgrade moduli for Miami limerock base

Subgrade Modulus (Mpa)	Structure	Moisture Content (%)		
		8	6	4
50	1	30	168	337
	4	6	54	159
125	1	31	260	545
	4	7	122	320

Table 7-4. List of structures analyzed for pavement's various responses comparison

Base Material	Type of Structure	Water Contents (%)
Newberry limerock	1 and 4	13
		10
		8
		5.5
Georgia granite	1 and 4	5.5
		3.5

Table 7-5. Asphalt Institute's rutting criteria analysis for structure-1 (200mm AC surface, 450 mm base)

Top of subgrade					
base layer water content	Analysis method	% $\epsilon_{yy}$	$\sigma_{yy}$ (kN/m <sup>2</sup> )	N <sub>D</sub> (AI empirical equation)	N <sub>d</sub> linear/N <sub>d</sub> nonlinear
Newberry Limerock					
10.0%	nonlinear	0.0415	31.60	1888562	1.25
	linear	0.0395	32.41	2363985	
13.0%	nonlinear	0.0458	32.08	1219731	1.19
	linear	0.0440	35.70	1446650	
Georgia Granite					
3.5%	nonlinear	0.0405	31.05	2099273	1.12
	linear	0.0395	33.57	2346634	
5.5%	nonlinear	0.0442	32.99	1422634	1.01
	linear	0.0441	36.49	1434653	

AC layer modulus = 1000 MPa  
Subgarde Modulus = 50 MPa

Table 7-6. Asphalt Institute's rutting criteria analysis for structure-4 (100 mm AC surface, 300 mm base)

base layer water content	Analysis method	% $\epsilon_{yy}$	$\sigma_{yy}$ (kN/m <sup>2</sup> )	$N_D$ (AI empirical equation)	$N_d$ linear/nonlinear	$N_d$
Newberry Limerock						
10.0%	nonlinear	0.10303	58.809	32218	2.18	
	linear	0.08653	50.073	70378		
13.0%	nonlinear	0.1349	73.247	9640	1.50	
	linear	0.1232	69.16	14470		
Georgia Granite						
3.5%	nonlinear	0.131926	66.955	10652	3.13	
	linear	0.102238	58.406	33350		
5.5%	nonlinear	0.141	68.023	7908	2.19	
	linear	0.11838	64.193	17301		

AC layer modulus = 1000 MPa

Subgrade Modulus = 50 MPa

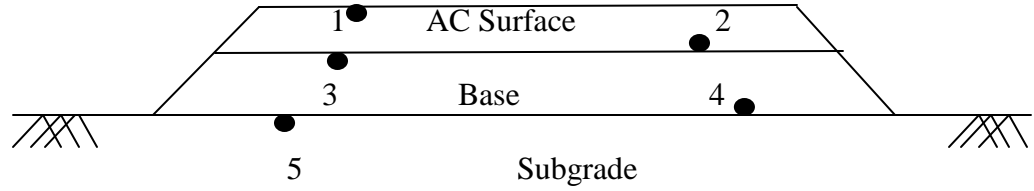


Figure 7-1. Critical locations for pavement response analysis

- 1 – Top of AC surface layer
- 2 – Bottom of AC surface layer
- 3 – Top of Base layer
- 4 – Bottom of Base layer
- 5 – Top of Subgrade layer

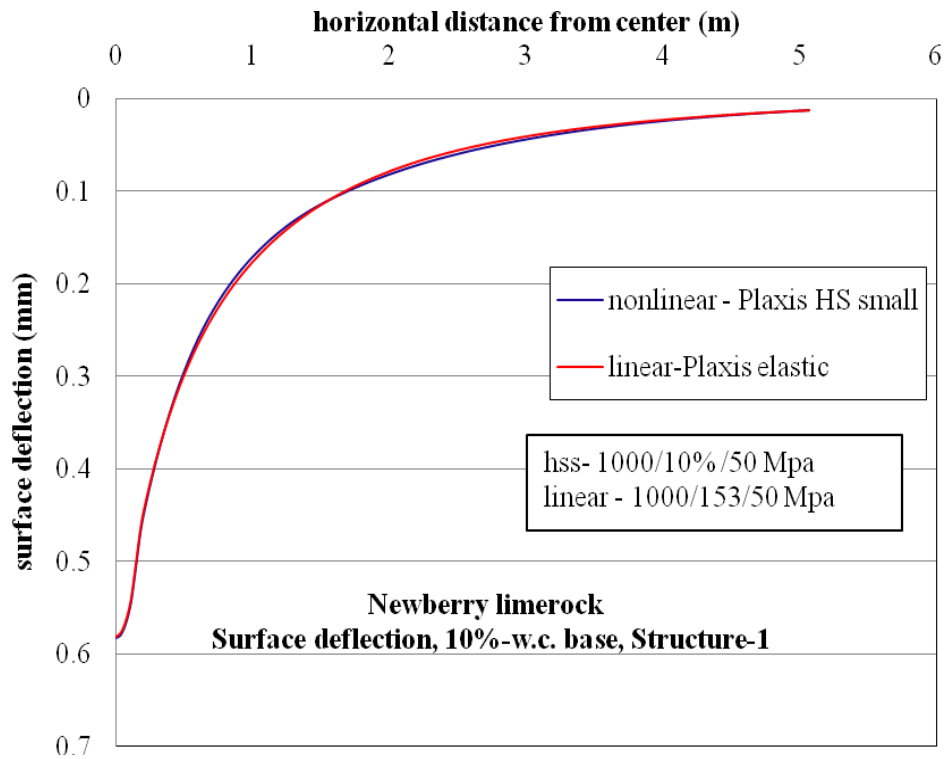


Figure 7-2. Surface deflection basin comparison for nonlinear and linear cases, for structure-1 with 10% w.c. base layer.

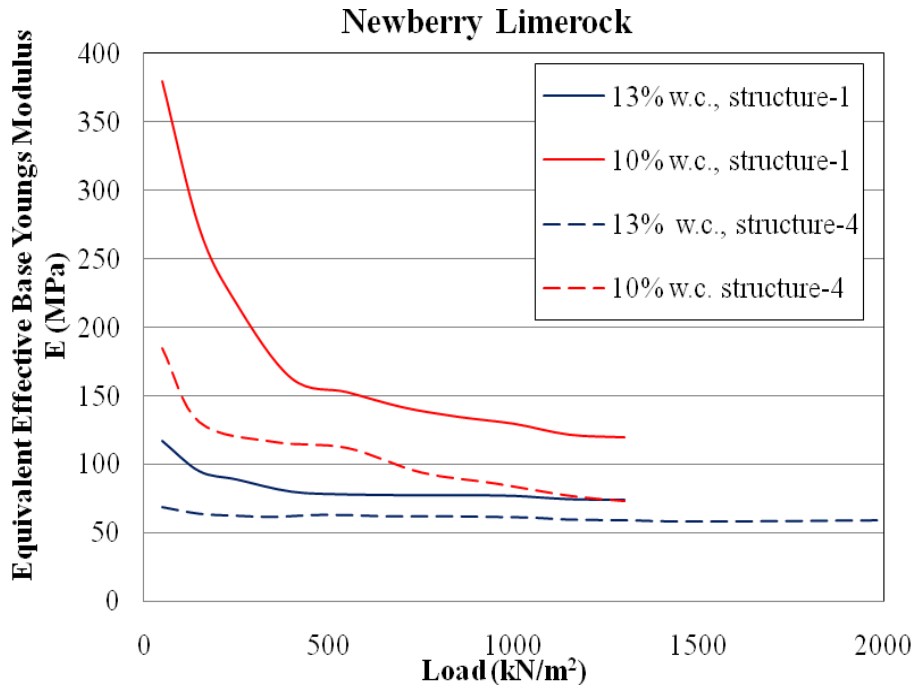


Figure 7-3. Nonlinear variation of single effective modulus with increase in load, for Newberry limerock base at 13% and 10% moisture contents.

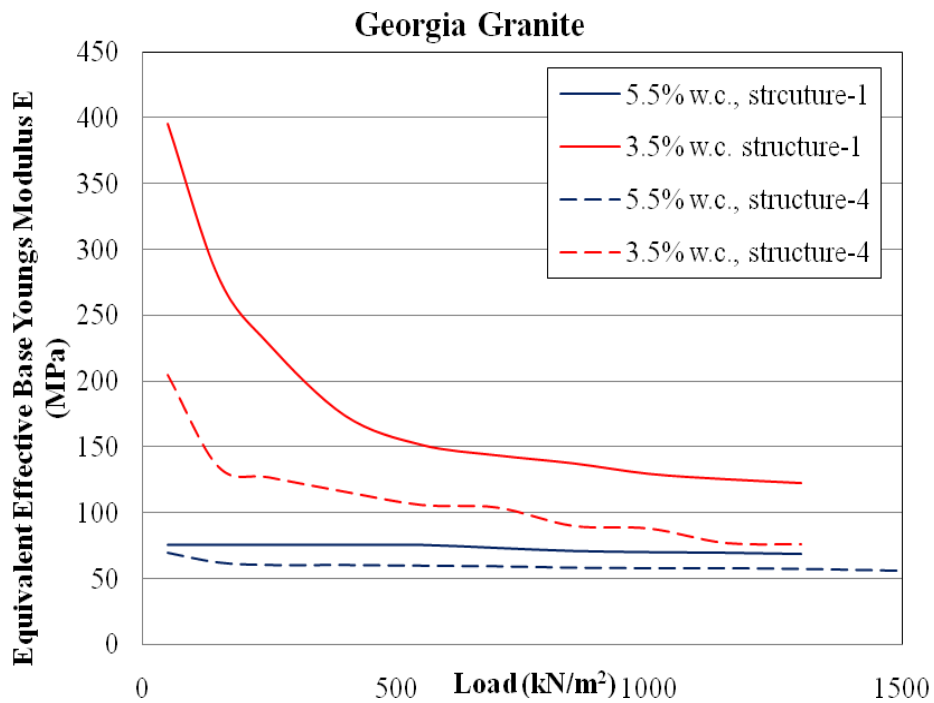


Figure 7-4. Nonlinear variation of effective modulus with increase in load, for Georgia granite base at 5.5% and 3.5% moisture contents.

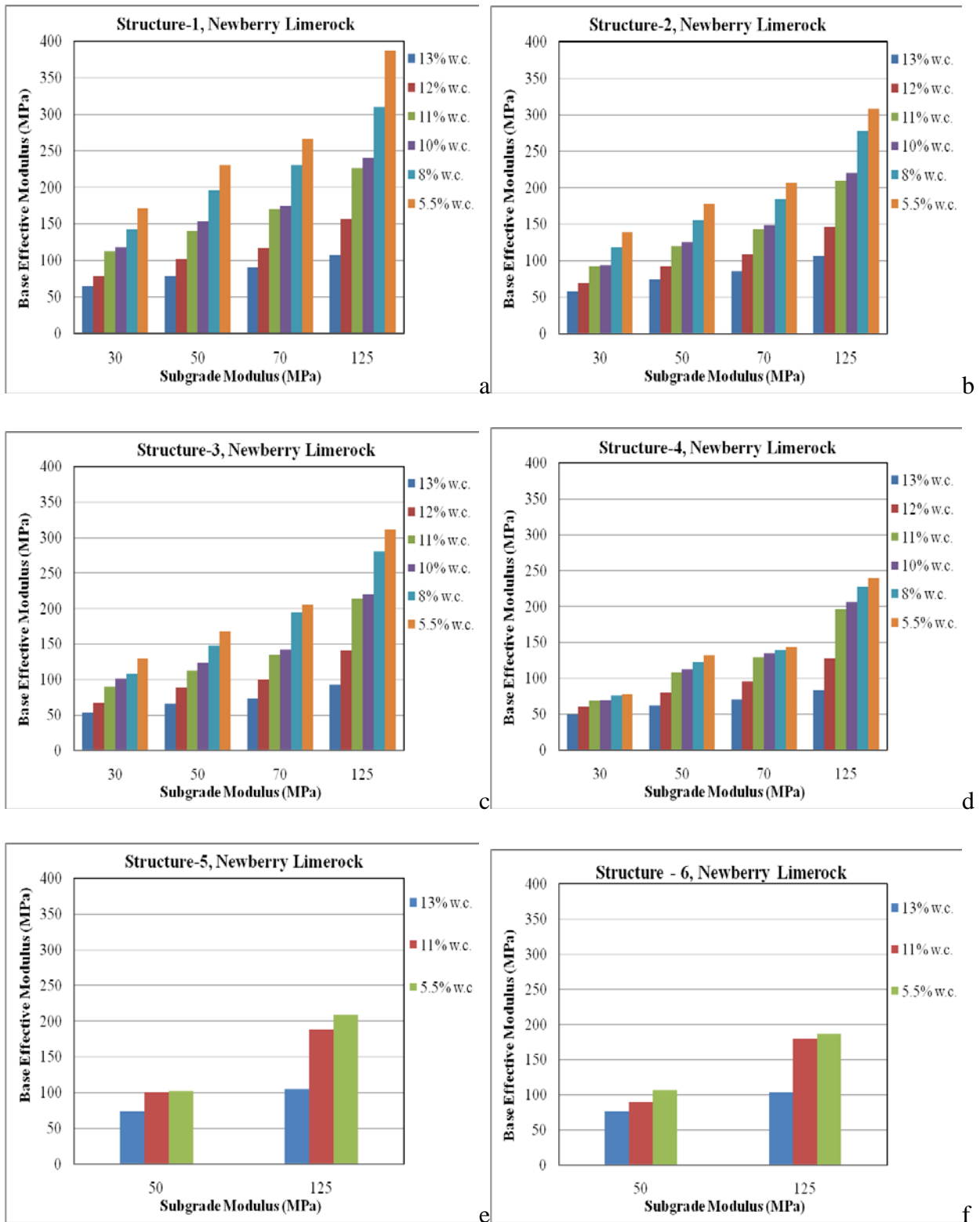


Figure 7-5. Newberry liemrock effective base modulus versus subgrade elastic modulus relationship with decrease in moisture content, for different structures a) Structure-1 b) Structure-2 c) Strcutrue-3 d) Strcutrue-4 e) Strcutrue-5 f) Strcutrue-6.

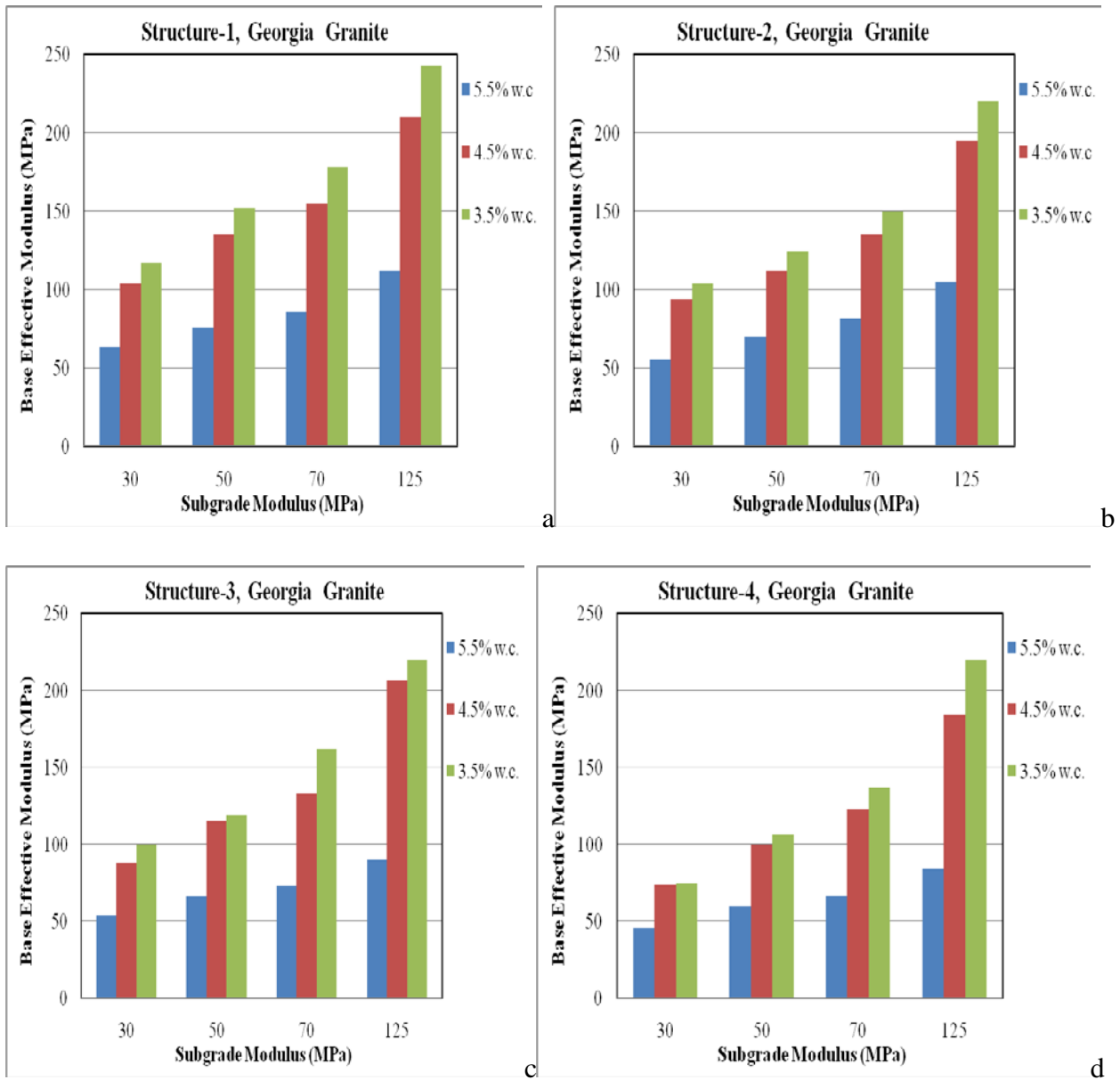
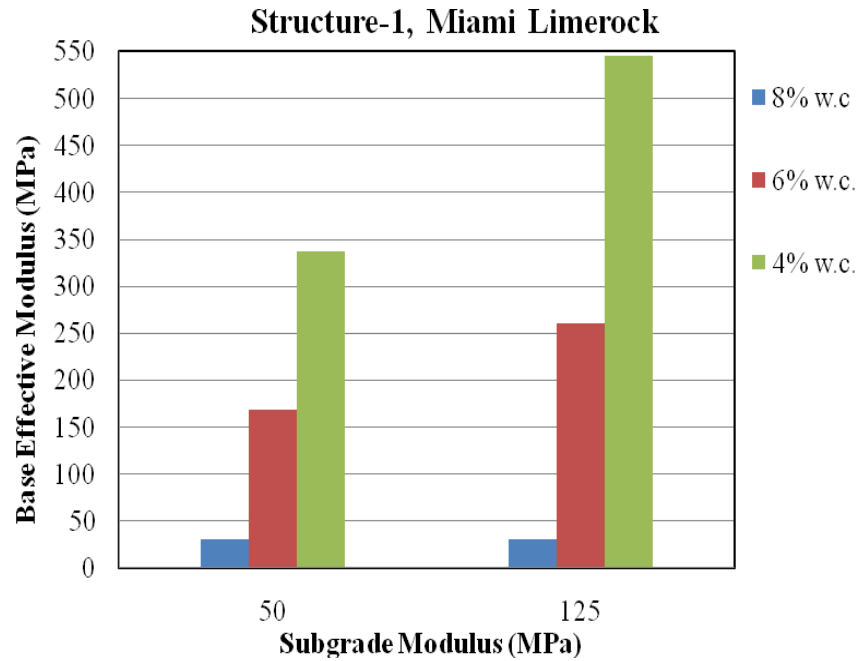
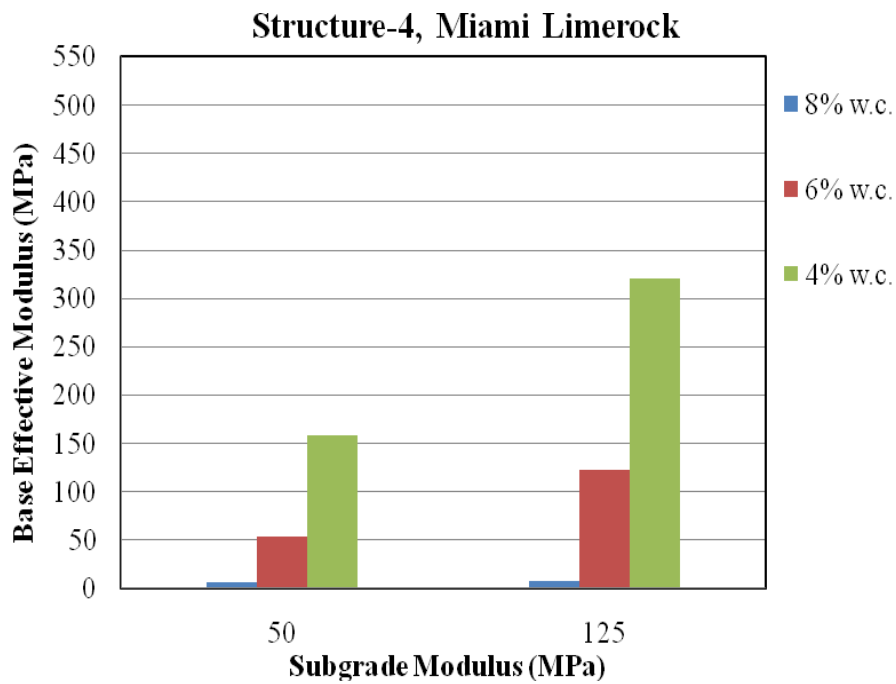


Figure 7-6. Georgia granite effective base modulus versus subgrade elastic modulus relationship with decrease in moisture content, for different structures a) Structure-1 b) Structure-2 c) Structure-3 d) Structure-4.



a



b

Figure 7-7. Miami limerock effective base modulus versus subgrade elastic modulus relationship with decrease in moisture content, for different structures a) Structure-1 b) Structure-4.

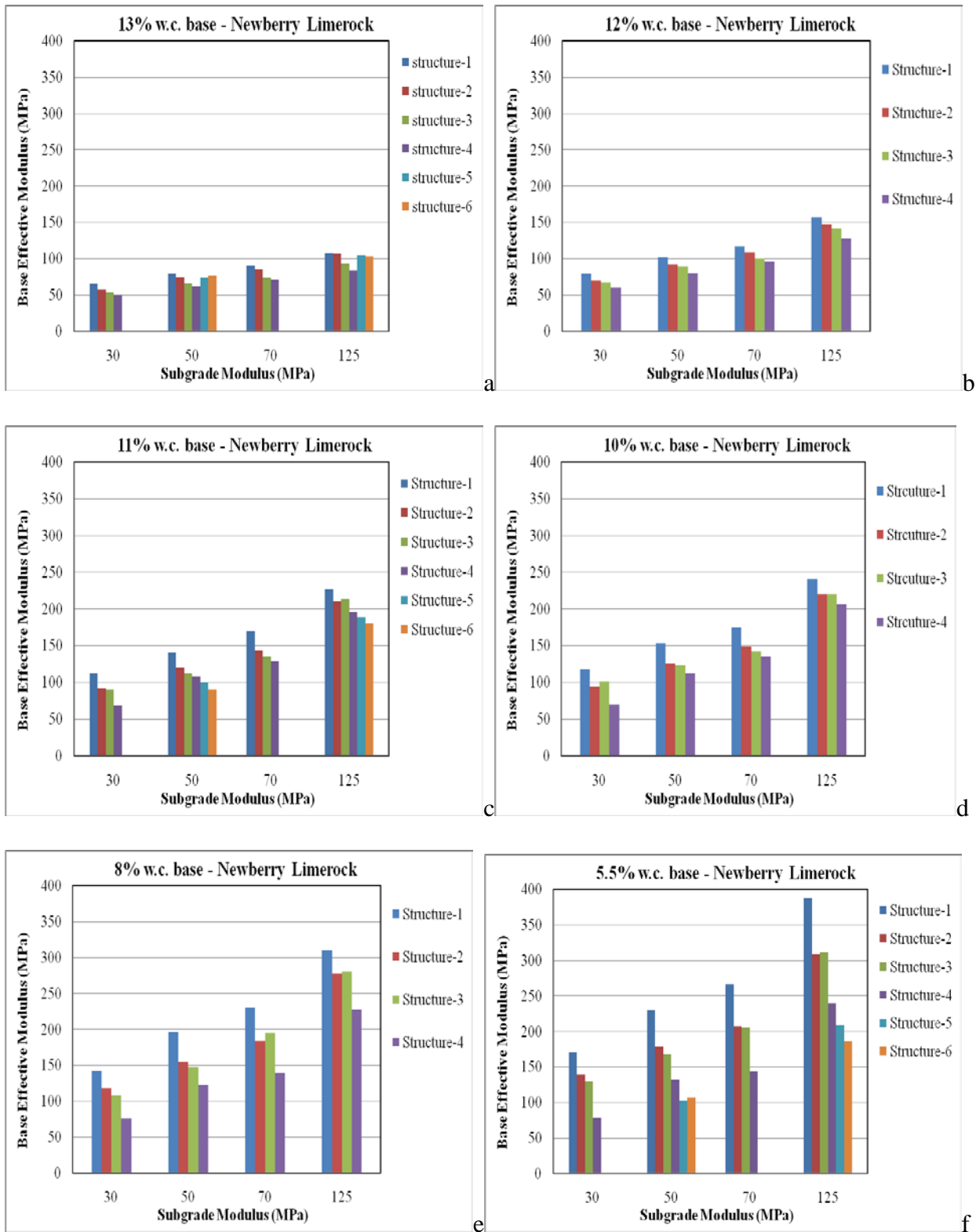
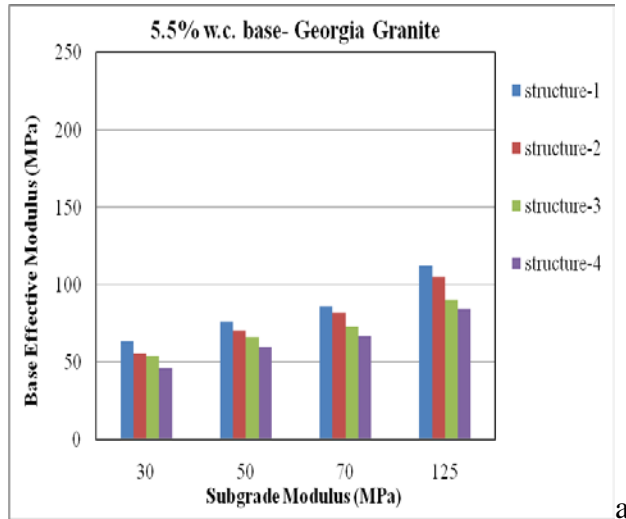
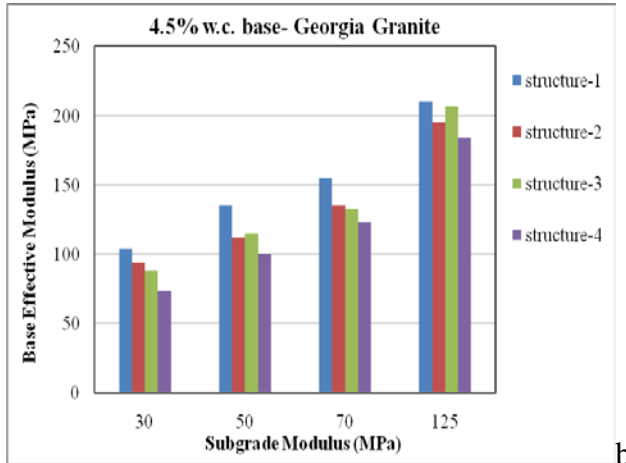


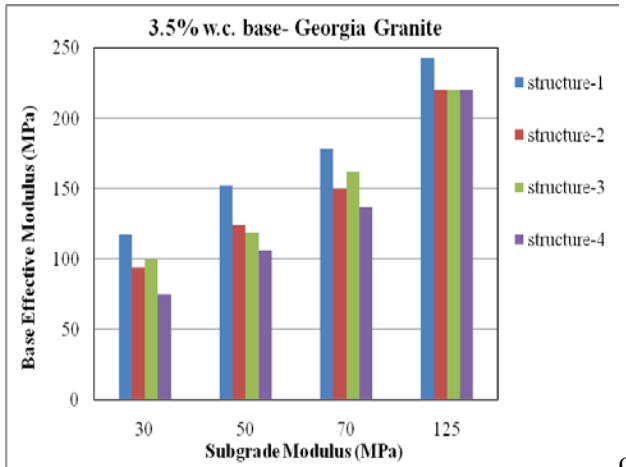
Figure 7-8. Newberry limerock effective base modulus versus subgrade elastic modulus relationship for different structures, at constant moisture content a) 13% w.c. b) 12% w.c. c) 11% w.c. d) 10% w.c. e) 8% w.c. f) 5.5% w.c.



a



b



c

Figure 7-9. Georgia granite effective base modulus versus subgrade elastic modulus relationship for different structures, at constant moisture content a) 5.5% w.c. b) 4.5% w.c. c) 3.5% w.c.

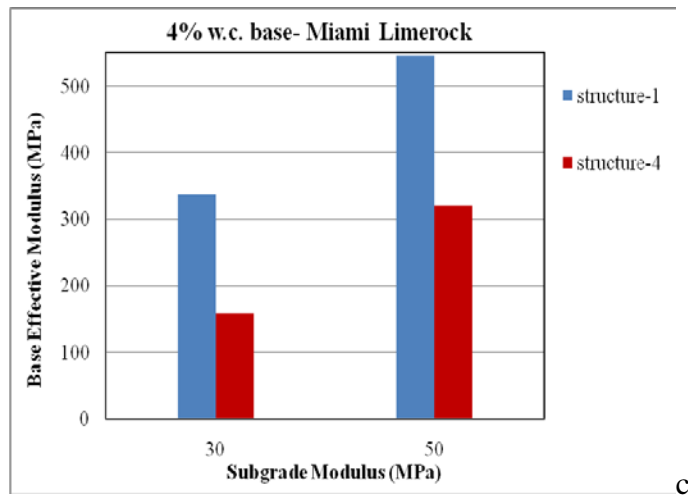
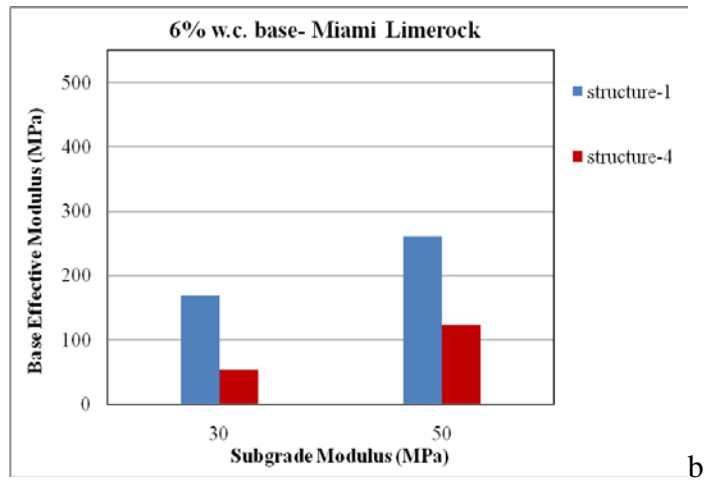
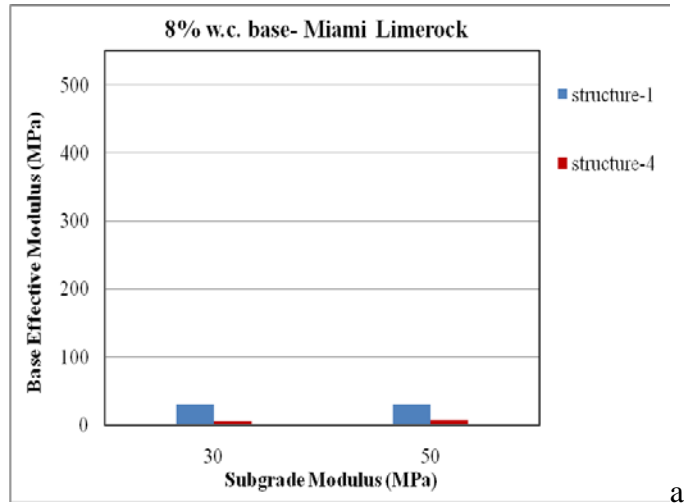


Figure 7-10. Miami limerock effective base modulus versus subgrade elastic modulus relationship for different structures, at constant moisture content a) 8% w.c. b) 6% w.c. c) 4% w.c.

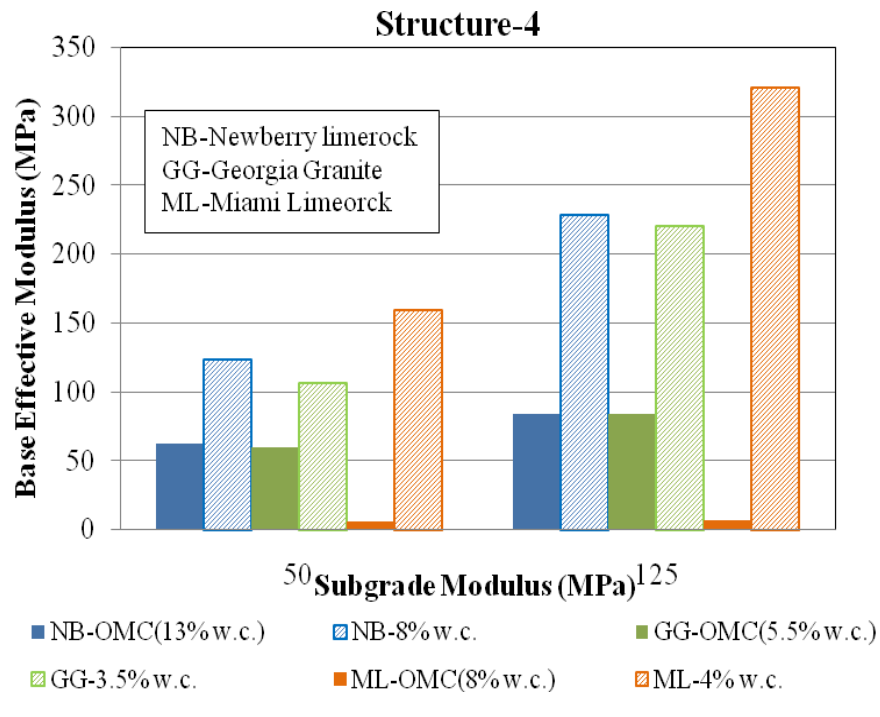
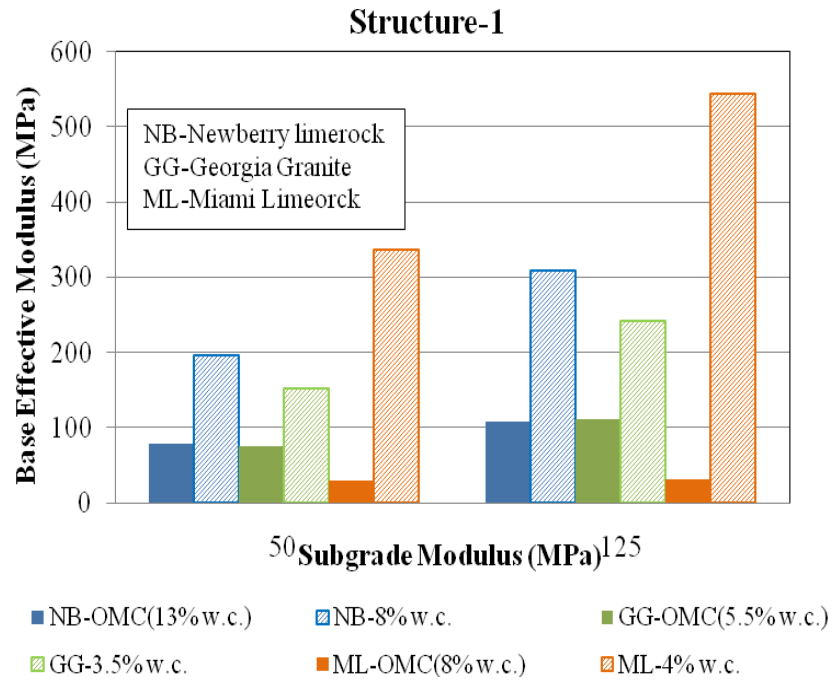


Figure 7-11. Comparison of effective moduli of all three materials at different base water contents and with subgrade modulus of 50 MPa and 125 MPa, obtained for a) Structure-1 b) Structure-4

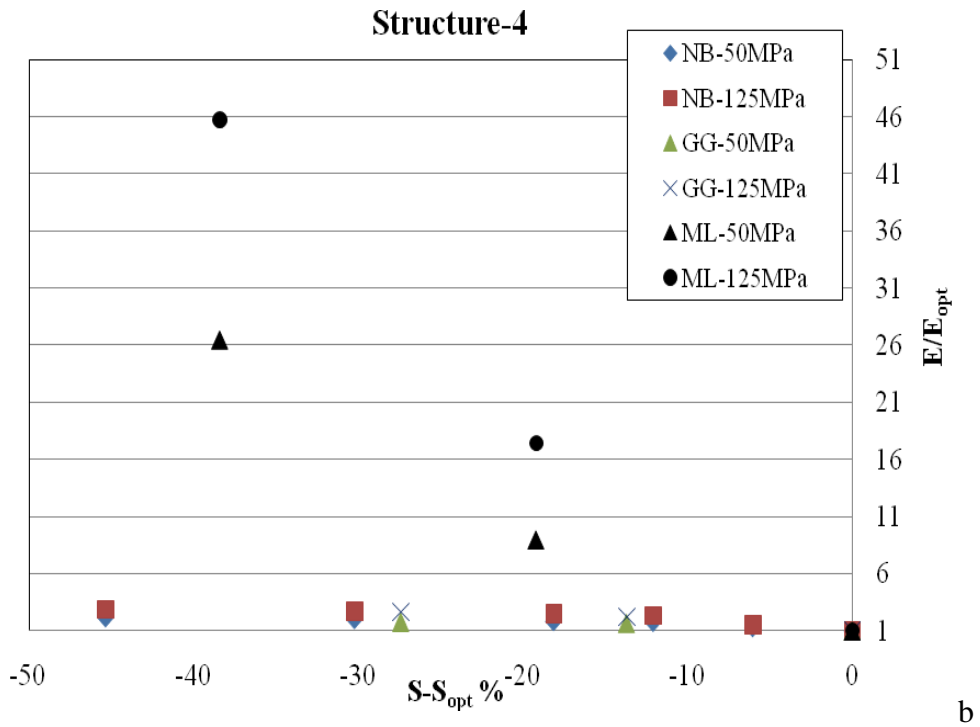
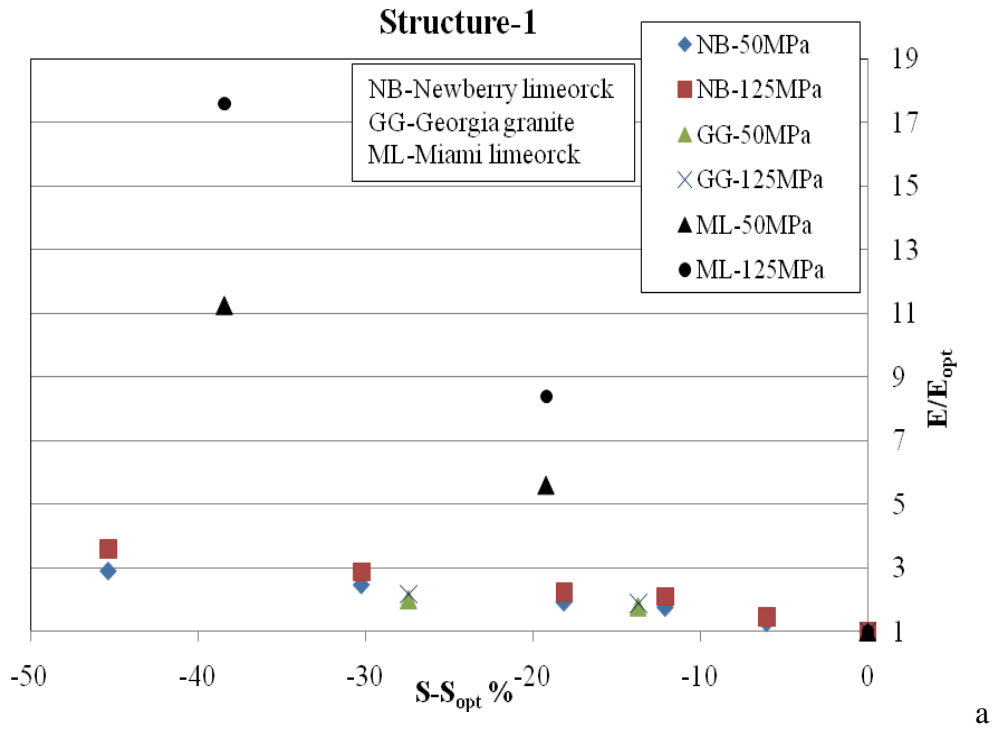


Figure 7-12. Comparison of normalized effective moduli of all three materials obtained with subgrade modulus of 50 MPa and 125 MPa, a) Structure-1, b) Structure-4

### Newberry Limerock

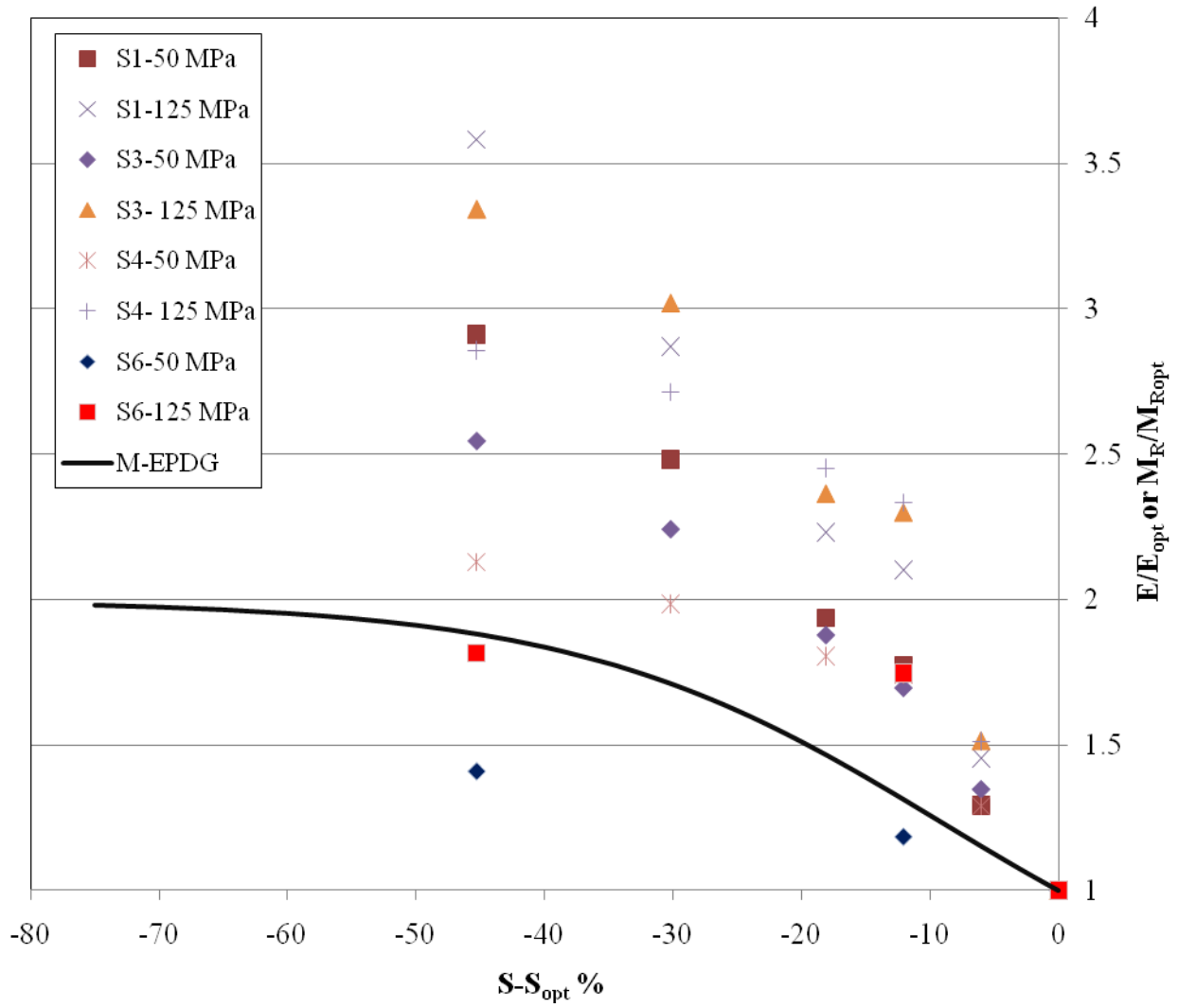


Figure 7-13. Comparison of Newberry limerock effective base moduli values with MEPDG moisture model

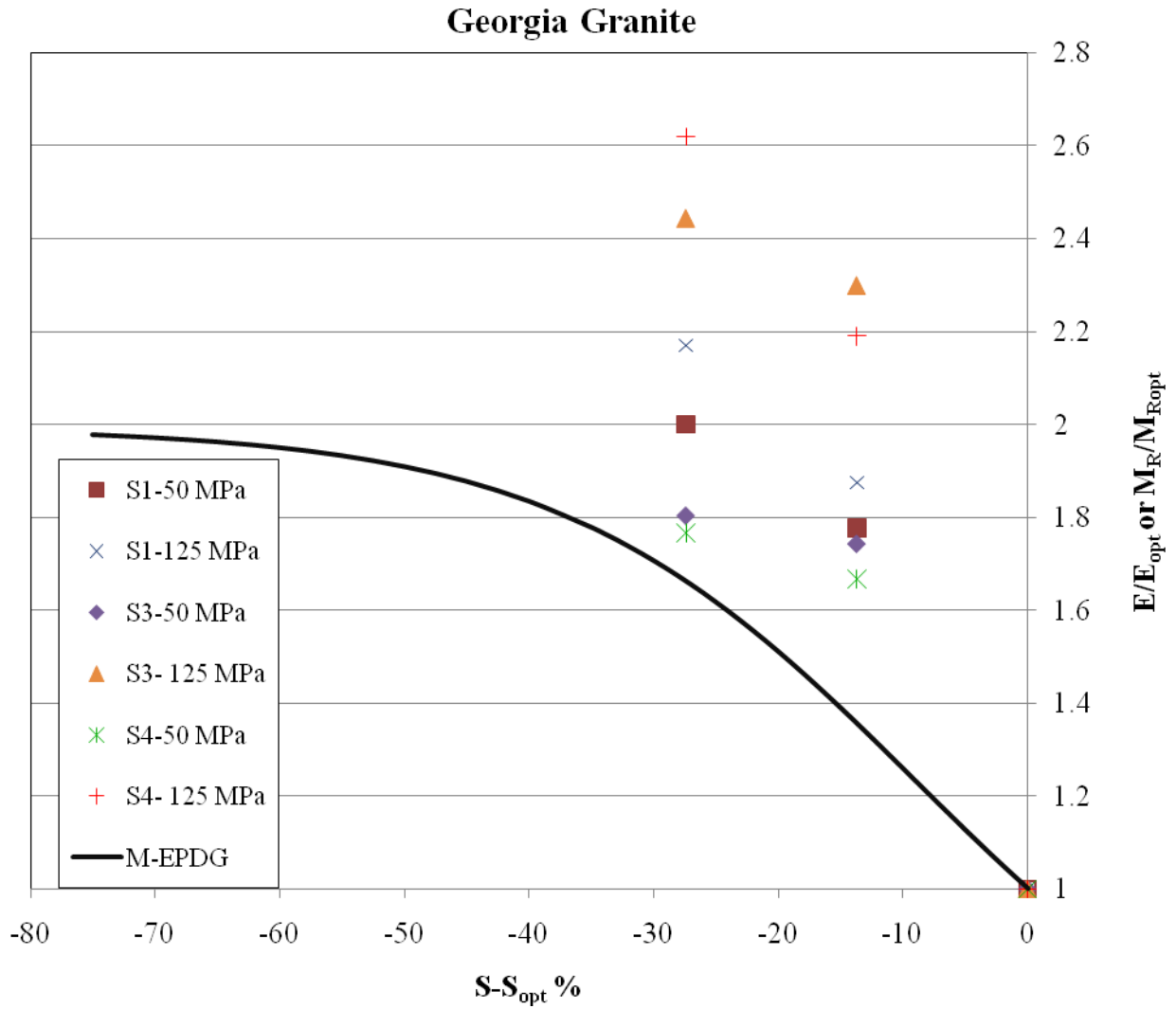


Figure 7-14. Comparison of Georgia granite effective base moduli values with MEPDG modulus moisture model

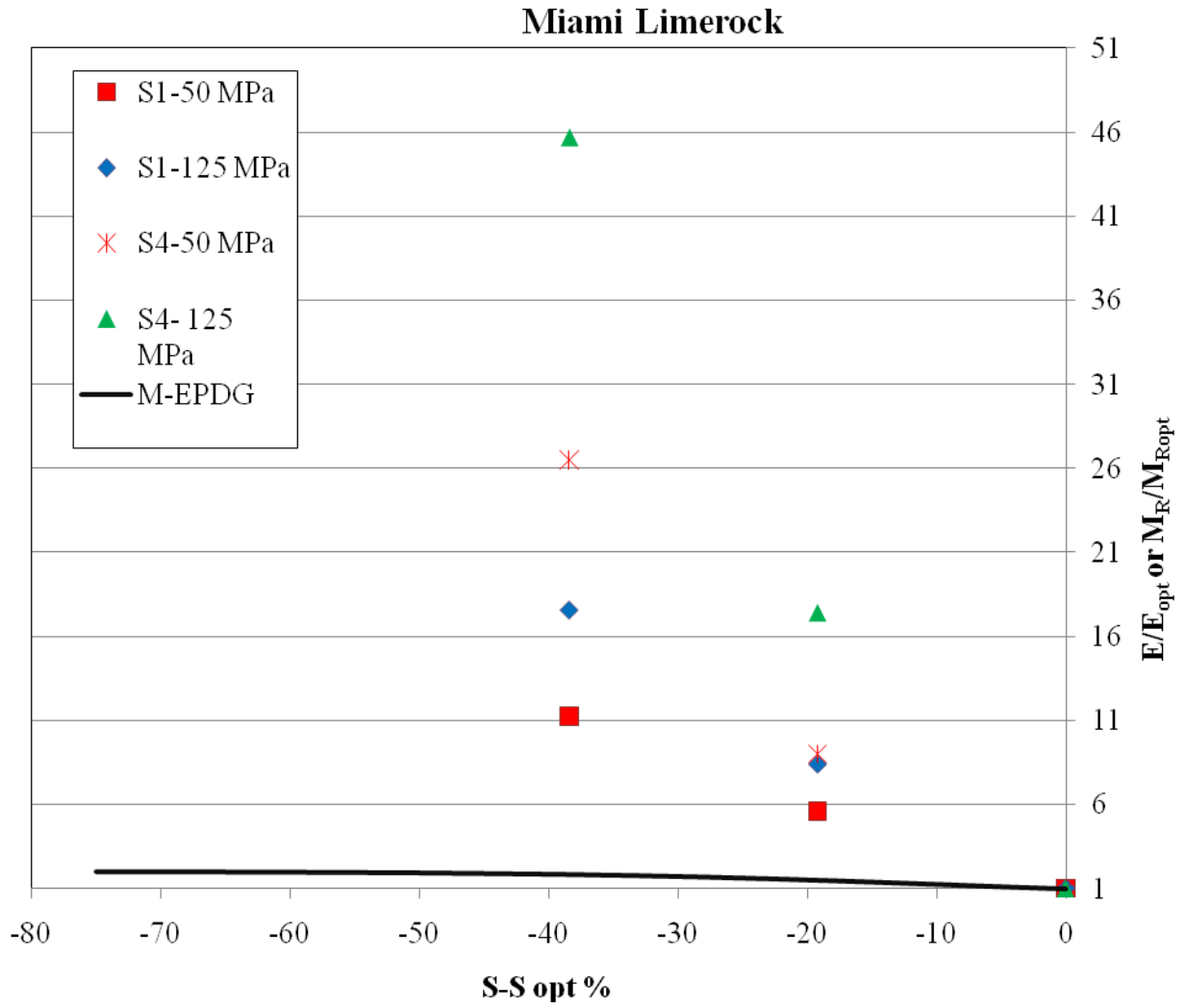
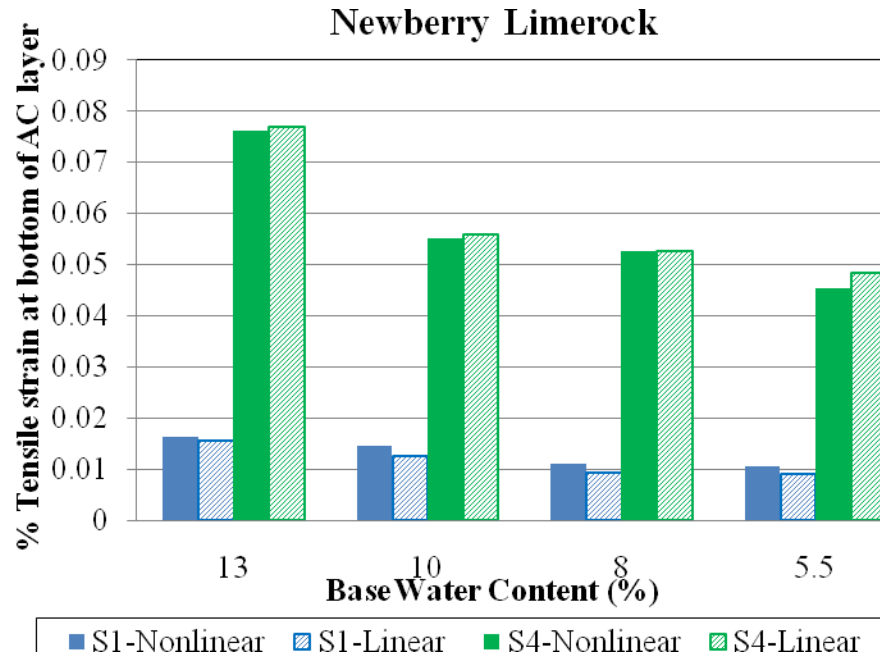


Figure 7-15. Comparison of Miami limerock effective base moduli values with MEPDG moisture model



a

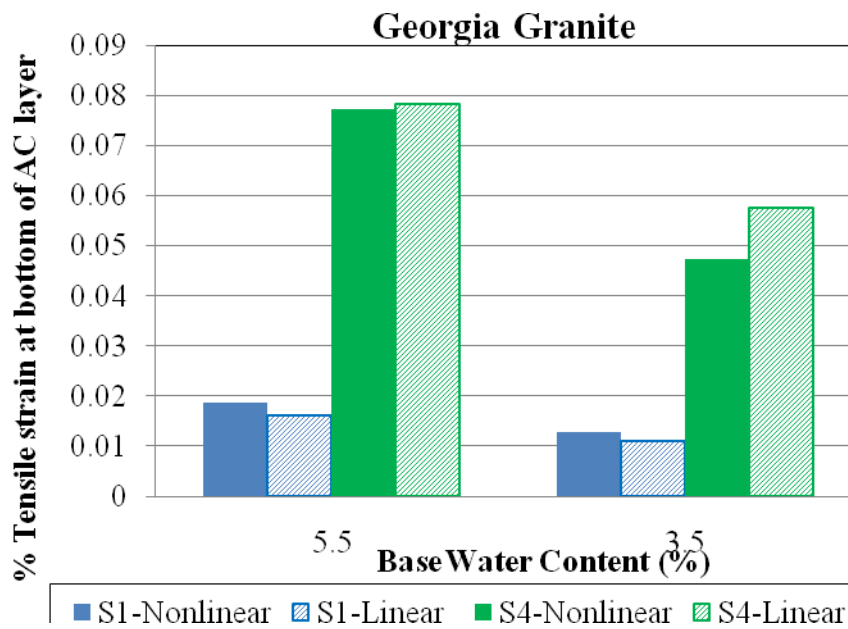
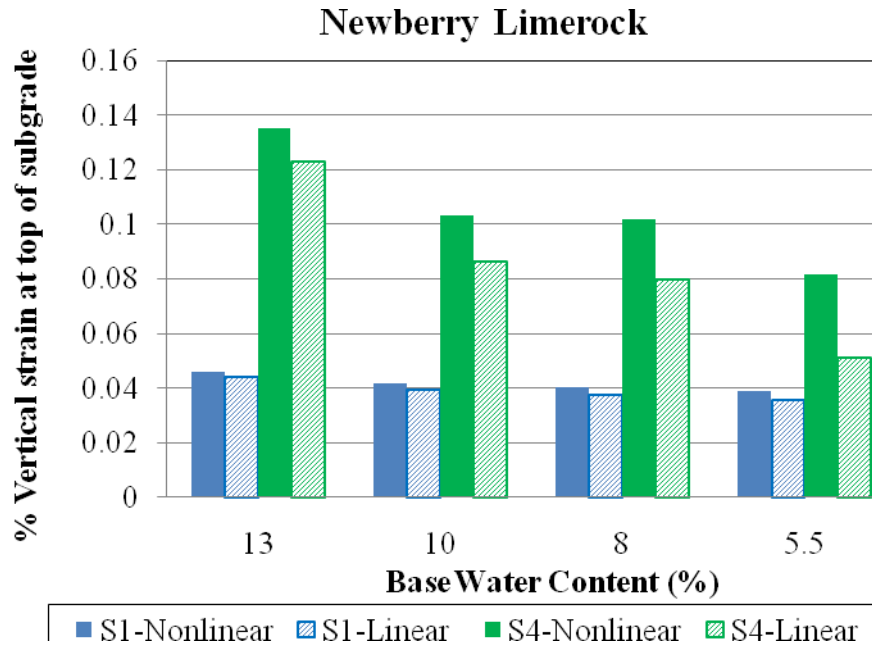
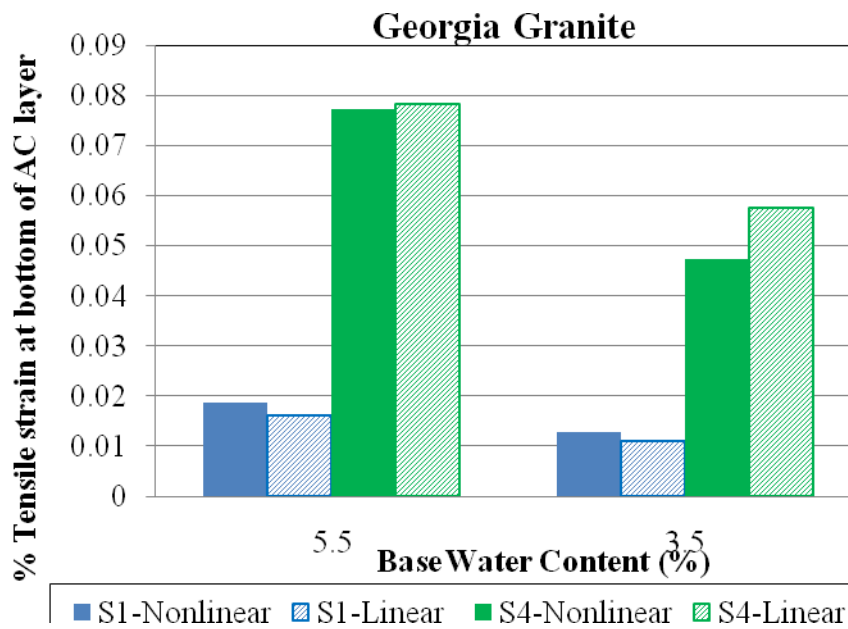


Figure 7-16. Comparison of horizontal tensile strain at bottom of AC layer ( $\% \epsilon_{xx}$ ) obtained for structure-1 and structure-4 with different base water contents of a) Newberry limerock b) Georgia granite



a



b

Figure 7-17. Comparison of vertical compressive strain at top of subgrade layer ( $\% \epsilon_{yy}$ ) obtained for structure-1 and structure-4 with different base water contents of a) Newberry limerock b) Georgia granite

## CHAPTER 8 SUBGRADE LAYER NONLINEAR MODELING ANALYSIS AND RESULTS

Primary focus of this research work is regarding modulus nonlinearity of base layer and determining single effective modulus of base layer for level-2 and level-3 design parameter inputs. A methodology to determine nonlinear equivalent single effective design modulus for base layer that can approximate the nonlinearities of base soil is developed in Chapter 7. Single effective moduli values for all three materials at different water contents, and for different structures with different subgrade moduli are derived following this methodology. By comparing nonlinear analysis with equivalent linear analysis, it is observed that nonlinear analysis which is more accurate than equivalent linear analysis results in more strain at top of subgrade layer than that of equivalent linear analysis with single effective base modulus. Since rutting is primarily based on vertical strain at top of subgrade, it indicates that equivalent linear design method for base layer overestimates pavement rutting performance compared to nonlinear design method.

It is concluded from Chapter 7 that by keeping both AC surface and subgrade layers elastic, and incorporating nonlinearity just in base layer; results in more vertical strain at top of subgrade layer, compared to equivalent linear design method which is commonly practiced. Since subgrade soils are also nonlinear in real field conditions, it is expected that incorporating modulus nonlinearity in subgrade layer also may result in further more vertical strain at top of subgrade, which can influence the rutting performance more significantly. Hence, out of our professional interest, it is proposed to conduct a nonlinear analysis by incorporating nonlinearity in both base and subgrade layers. This investigation will help us in obtaining some basic idea about the effect of subgrade nonlinearity on pavement rutting and cracking performances. Also, the inadequacies of elastic based design methods and performance criteria can be addressed.

## **8.1 Nonlinear Equivalent Single Effective Modulus Determination for Base and Subgrade Layers**

### **8.1.1 Methodology**

Main objective of this task is to investigate the influence of accounting nonlinearity in both and subgrade layers on pavement performance, by comparing nonlinear and equivalent linear analyses results. In other words, compare and evaluate pavement responses obtained from modeling analysis of following two cases:

- i) Linear AC, nonlinear base, nonlinear subgrade
- ii) Linear AC, equivalent elastic base and equivalent elastic subgrade.

Similar to nonlinear base analysis in Chapter 7, to derive equivalent single effective moduli values for both nonlinear base and nonlinear subgrade, it is proposed to use pavement surface deflection basin as the single matching factor. Since both base and subgrade layers are considered nonlinear, deriving equivalent single effective modulus for both layers by trial and error method based on surface deflection is not feasible. Hence, it is proposed to use Falling Weight Deflectometer (FWD) analysis procedure that can back calculate equivalent elastic modulus for multiple layers using surface deflection basin and layers thicknesses as inputs.

Falling Weight Deflectometer (FWD) method is a well known pavement in-situ testing and analysis method to back calculate equivalent moduli values for different layers of an existing pavement, based on deflection zone created by falling weight. It is mainly used to assess the working condition of an existing pavement. By analyzing the surface deflection profile obtained from nonlinear response model analysis (i.e. nonlinear analysis via Plaxis-HS small model for nonlinear base and nonlinear subgrade) via FWD analysis technique, equivalent elastic modulus for surface, base and subgrade layers can be determined. Once the equivalent single effective modulus value for each layer is determined, pavement responses can be obtained from equivalent

linear analysis. Then the pavement responses obtained from nonlinear and equivalent linear analyses can be compared for further evaluation.

### **8.1.2 Material Parameters and Structural Inputs**

For this analysis, both base and subgrade layers are considered nonlinear, where as AC surface layer is considered elastic. For this brief investigation, only selected pavement structures with selected base moisture contents and with one nonlinear subgrade modulus are analyzed.

Two types of structures, i.e. structure-1 and structure-4 (refer Figure 6-5) are considered for this analysis. Material moduli used for different layers are presented in Table 8-1. For subgrade layer, only Ottawa sand is considered as nonlinear material. Based on Ottawa sand lab testing results presented in Figure 3-7, recalibrated HSsmall model input parameters for Ottawa sand are developed and presented in Table 8-2. It should be noted that 1000 MPa is the only elastic modulus selected for AC surface layer and Ottawa sand is the only nonlinear material selected for subgrade. Nonlinear and equivalent linear analyses are performed following the procedure explained in 8.1.1.

### **8.1.3 An Example of Surface Deflection Basin Matching Between Nonlinear Base and Subgrade Case and Equivalent Linear Base and Subgrade Case**

Nonlinear analysis via Plaxis-HSsmall response model (developed in Chapter 6) is performed on Structure-1 (refer to Figure 6-5) with 10% w.c. base and Ottawa sand subgrade. AC surface layer is considered elastic with 1000 MPa modulus. From Plaxis-HSsmall nonlinear analysis, maximum surface deflection of 0.62 mm is obtained under wheel load of 550 kPa. Keeping the moduli of surface layer same, equivalent single effective modulus for base and subgrade layers that can produce the same surface deflection basin is determined via FWD analysis as explained in Section 8.1.1. Obtained surface deflection basins for both nonlinear case and equivalent linear case are compared in Figure 8-2. From this figure, it can be observed that

surface deflection basin obtained from equivalent effective elastic base and subgrade moduli case matches very well with the deflection basin obtained from nonlinear base and nonlinear subgrade moduli case.

## **8.2 Comparison of Nonlinear and Equivalent Linear Analysis Results**

### **8.2.1 Nonlinear Equivalent Single Effective Design Moduli Values for Base and Subgrade**

FWD back calculated single effective moduli values obtained for structure-1 and structure-4 with different water contents of Newberry limerock base and Ottawa sand subgrade are presented in Table 8-3 for structure-1 and in Table 8-4 for structure-4. Similar results with different water contents of Georgia granite base and Ottawa sand subgrade are presented in Table 8-5 for structure-1 and in Table 8-6 for structure-4.

From the data presented in Tables 8-3 to 8-6; it can be primarily observed that for both structures equivalent single effective moduli values for base layer increases with material drying. For structure-1, FWD back calculated effective modulus of base layer is greater than subgrade modulus. Whereas for structure-4, FWD back calculated effective modulus of base layer is lower than that of subgrade layer. This behavior is probably due to decrease in thickness of structure-4 compared to structure-1, which might be causing greater deviatoric stress act on base layer of structure-4. Due to decrease in structure thickness and greater deviatoric stresses, modulus nonlinearity increases and hence, greater strain magnitude and eventually lower equivalent single effective modulus.

When we compare the back calculated base effective moduli results with that of in Chapter 7, equivalent effective modulus of base layer for any water content is smaller than the corresponding equivalent elastic modulus obtained with elastic subgrade of 50 MPa (refer to Table 7.1 to 7.3). This decrease in base equivalent effective modulus might be due to the

additional effect of subgrade nonlinearity along with base nonlinearity, which eventually causes greater strain in base and lower equivalent effective moduli.

In the case of structure-1, back calculated effective moduli for subgrade layer is in the range of 55-60 MPa, where as for structure-4 it is 42-44 MPa. This decrease in subgrade effective modulus in structure-4 clearly indicates increase in subgrade nonlinearity due to decrease in structure thickness. Thus as the structure thickness decreases, material modulus nonlinearity increases.

Back calculated equivalent elastic modulus for AC layer is in the range of 800 MPa for thick structure and in the range of 1050 MPa for thin structure, where as the actual modulus value used for AC layer in nonlinear analysis is 1000 MPa. FWD analysis back calculates elastic moduli based on surface deflection zone input. This variation in AC layer back calculated modulus from actual value (i.e. 1000 MPa) may also have little bit influence on back calculated equivalent effective moduli value of base and subgrade layer.

### **8.2.2 Comparison of Nonlinear and Equivalent Linear Analyses Pavement Responses**

Various pavement responses (as given Section 7.3.1) obtained at different locations of pavement structure (as shown in Figure 7-1) from nonlinear analysis and corresponding equivalent linear analysis are compared for further analysis.

Pavement responses obtained from nonlinear and equivalent linear analyses of few selected pavement structures with 1000 MPa AC surface, different nonlinear base materials at different water contents and Ottawa sand nonlinear subgrade are compared. List of structures analyzed for responses comparison is given in Table 8-7. For all the cases given in Table 8-7, nonlinear and equivalent linear response curves comparison plots for all pavement responses mentioned in section 7.3.1 are presented in Appendix D.

Magnitude of horizontal strain ( $\epsilon_{xx}$ , tensile strain) at bottom of AC layer, obtained from nonlinear and equivalent linear analysis of structure-1 with different base water contents are compared in Figure 8-3a for Newberry limerock and Figure 8-3b for Georgia granite. Same set of comparison plots are developed for vertical strain ( $\epsilon_{yy}$ , compressive strain) at top of subgrade layer and shown in Figure 8-4a for Newberry limerock and Figure 8-4b for Georgia granite.

From Surface deflection comparison plots (Figures D-1 to D-3 for Newberry limerock and Figures D-34 to D-35 for Georgia granite, from Appendix D); it can be observed that the surface deflection profiles for nonlinear and equivalent linear analyses are matching well. Hence, considering back calculated effective moduli for base and subgrade layers in place of nonlinear moduli does not affect the actual surface deflections.

From the comparison column plots of horizontal tensile strain ( $\epsilon_{xx}$ ) at bottom of AC layer (Figure 8-3a and 8-3b), for structure-1 with different base water contents and Ottawa sand subgrade modulus, it can be observed that horizontal strain ( $\epsilon_{xx}$ ) at bottom of AC layer for nonlinear moduli case is equal or nearly equal to equivalent linear case with back calculated single effective moduli. This indicates that considering back calculated effective modulus for both base and subgrade layers in place of nonlinear moduli for pavement design may not significantly affect the overall cracking performance of pavement structure. Hence, subgrade nonlinearity may not influence the cracking performance of a pavement structure.

From the comparison plots of vertical strain ( $\epsilon_{yy}$ ) at top of subgrade (Figure 8-4a to 8-4b), for both Newberry limerock and Georgia granite, it can be observed that  $\epsilon_{yy}$  at top of subgrade for nonlinear analysis is almost two times greater than corresponding equivalent linear analysis. This indicates that the subgrade nonlinearity may influence pavement's rutting performance very significantly. Since the vertical strain ( $\epsilon_{yy}$ ) at top of subgrade calculated by nonlinear analysis is

greater than equivalent linear analysis, currently practiced elastic design methods might be overestimating rutting performance. Thus, a new rutting performance criterion may be required to design pavement structures using single effective design modulus in place of nonlinear modulus, for both base and subgrade layers. Since subgrade nonlinearity can significantly influence rutting performance, it may be necessary to consider subgrade nonlinearity in pavement design procedures and nonlinear response models.

### **8.2.3 Analysis of Nonlinear and Linear responses in the Perspective of Cracking and Rutting Performance Criteria**

Main purpose of this exercise is to investigate the effect of base and subgrade nonlinearity on cracking and rutting performance of a pavement structure.  $\epsilon_{xx}$  and  $\sigma_{xx}$  data at bottom of AC layer and  $\epsilon_{yy}$  and  $\sigma_{yy}$  data at top of subgrade layer for structure-1 with Newberry limerock and Georgia granite as base layers for selected water contents are given in Table 8-8.  $N_d$  for rutting failure is calculated based on Asphalt Institute rutting criterion (Equation 7-2).

From the analysis data presented in Table 8-8 for structure-1, it can be observed that  $\epsilon_{xx}$  at bottom of AC layer for nonlinear case is almost equal to that of linear case. It implies that subgrade nonlinearity may not affect the cracking performance of structure-1 and consideration of equivalent elastic modulus for both base and subgrade layers is acceptable in the aspect of cracking performance criterion.

$\epsilon_{yy}$  at top of subgrade layer for nonlinear case is almost two times that of linear case. It implies that subgrade nonlinearity may affect the rutting performance of pavement structure, significantly.

Asphalt Institute's empirical equation for rutting failure criteria is:

$$N_d = f_4(\epsilon_c)^{-f_3} \quad (7-2)$$

Where  $N_d$  - allowable number of load repetitions to limit permanent deformation

$\epsilon_c$  - compressive strain on the top of subgrade (i.e.  $\epsilon_{yy}$ —for our case)

$$f_4 = 1.365 \times 10^{-9}$$

$$f_5 = 4.477$$

Allowable number of load repetitions ( $N_d$ ) is calculated from  $\epsilon_{yy}$  using Equation (7-2) and are presented in Table 8-8. The value of  $N_d$  linear/  $N_d$  nonlinear for high water contents goes up to 15.7. This indicates that, by considering elastic modulus for subgrade layer in design procedures, rutting performance of pavement is being over estimated by almost 15 times to actual value. It also implies that elastic design methods overestimate the actual rutting performance of structure. It may not be appropriate to use elastic criterion based empirical equations for rutting performance analysis of pavement structures.

Based on nonlinear base analysis results obtained for structure-4 from Chapter 7, it is understood that as the structure thickness decreases modulus nonlinearity influence on pavement performance increases. Since modulus nonlinearity increases with decrease in structure thickness, it is expected that considering nonlinear base and subgrade for structure-4 would influence rutting performance more than that of structure-1.

Therefore, it may be necessary to consider subgrade nonlinearity in design and analysis of pavement structures and further research investigation is required for complete understanding of its influence on pavement performance.

Table 8-1. Different material properties used for nonlinear base and nonlinear subgrade analysis

Pavement Layer	Material	Modulus (MPa)
Surface	AC	1000
Base	Newberry limerock	13, 12, 11 & 10% w.c.
	Georgia granite	5.5, 4.5 & 3.5% w.c.
Subgrade	Ottawa sand	HS Small parameters are given in Table 8-2.

Table 8-2. HS Small model nonlinear material inputs for Ottawa sand subgrade layer

Parameter	Value
$G_{max}$ (Mpa)	120
$\gamma_{0.7}$	5.E-04
$P_{ref}$ (kPa)	100
$E_{max}$ (MPa)	316.80
$E_{ur}$ (MPa)	269.28
$E_{oed}$ (MPa)	134.64
$E_{50}$ (MPa)	134.64
$m$	0.5
$\gamma$ (kN/m <sup>3</sup> )	18.11
$\nu$	0.32

Table 8-3. Equivalent elastic moduli values obtained for structure-1 with Newberry limerock base and Ottawa sand subgrade

Layer	Nonlinear Plaxis-HSsmall model Analysis (MPa)	Linear FWD Analysis Modulus (MPa)
AC Surface Layer	1000	862
Base	13% w.c.	67.75
Subgrade	Ottawa sand	54.95
AC Surface Layer	1000	858.12
Base	12% w.c.	86.60
Subgrade	Ottawa sand	55.64
AC Surface Layer	1000	795.10
Base	11% w.c.	124.24
Subgrade	Ottawa sand	53.92
AC Surface Layer	1000	780.686
Base	10% w.c.	125.69
Subgrade	Ottawa sand	58.67

Table 8-4. Equivalent elastic moduli values obtained for structure-4 with Newberry limerock base and Ottawa sand subgrade

Layer	Nonlinear Plaxis-HSsmall model Analysis (Mpa)	Linear FWD Analysis (Mpa)
AC Surface Layer	1000	1073.79
Base	13% w.c.	24.82
Subgrade	Ottawa sand	44.61
AC Surface Layer	1000	1099.37
Base	12% w.c.	31.44
Subgrade	Ottawa sand	43.85
AC Surface Layer	1000	1012.98
Base	11% w.c.	42.06
Subgrade	Ottawa sand	43.85
AC Surface Layer	1000	1019.66
Base	10% w.c.	42.33
Subgrade	Ottawa sand	44.26

Table 8-5. Equivalent elastic moduli values obtained for structure-1 with Georgia granite base and Ottawa sand subgrade

Layer	Nonlinear Plaxis-HSsmall Analysis (Mpa)	Linear FWD Analysis (Mpa)
AC Surface Layer	1000 (elastic)	851.77
Base	5.5% w.c.	61.36
Subgrade	Ottawa sand	55.80
AC Surface Layer	1000 (elastic)	823.99
Base	4.5% w.c.	114.04
Subgrade	Ottawa sand	58.67
AC Surface Layer	1000 (elastic)	820.82
Base	3.5% w.c.	124.00
Subgrade	Ottawa sand	56.67

Table 8-6. Equivalent elastic moduli values obtained for structure-4 with Georgia Granite base and Ottawa sand subgrade

Layer	Nonlinear Plaxis-HSsmall Analysis (MPa)	Linear FWD Analysis (MPa)
AC Surface Layer	1000 (elastic)	1058
Base	5.5% w.c.	24.54
Subgrade	Ottawa sand	44.5
AC Surface Layer	1000 (elastic)	1005.32
Base	4.5% w.c.	40.47
Subgrade	Ottawa sand	44.68
AC Surface Layer	1000 (elastic)	944.44
Base	3.5% w.c.	46.19
Subgrade	Ottawa sand	45.02

Table 8-7. List of structures analyzed for pavement's various responses comparison

Base Material	Type of Structure	Water Contents
Newberry limerock	1	13
		10
	4	10
Georgia granite	1	5.5
		3.5

Table 8-8. Asphalt Institute's rutting criteria analysis for structure-1 with nonlinear base and nonlinear subgrade

base layer water content	Design method	% $\epsilon_{XX}$ (-)	$\sigma_{XX}$ (kN/m <sup>2</sup> ) (-)	% $\epsilon_{YY}$	$\sigma_{YY}$ (kN/m <sup>2</sup> )	N <sub>D</sub> (AI emperical equation)	N <sub>D</sub> linear / N <sub>D</sub> nonlinear
Newberry Limerock							
10.0%	nonlinear	0.0127	217.12	0.0724	22.51	155959	14.34
	linear	0.0121	137.40	0.0400	36.14	2236444	
13.0%	nonlinear	0.0179	304.57	0.0803	24.30	98558	15.52
	linear	0.0179	251.68	0.0435	37.74	1529735	
Georgia granite							
3.5%	nonlinear	0.0126	214.05	0.0711	23.42	169236	12.59
	linear	0.0121	147.80	0.0404	36.65	2129920	
5.5%	nonlinear	0.0191	325.58	0.0814	26.47	92731	15.71
	linear	0.0192	267.20	0.0440	39.23	1456394	
AC surface = 1000 MPa Ottawa sand subgrade							

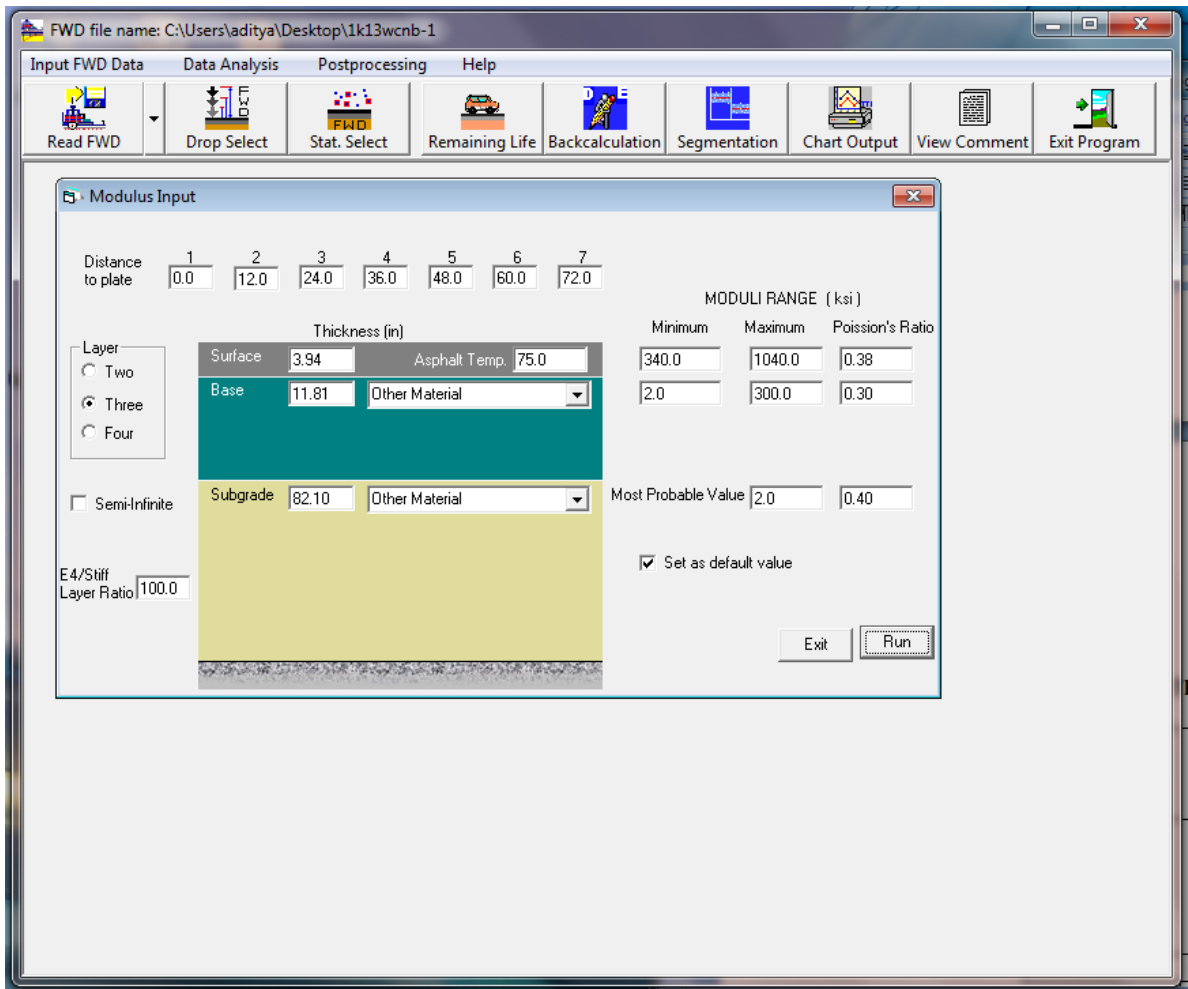


Figure 8-1. FWD analysis of structure-4

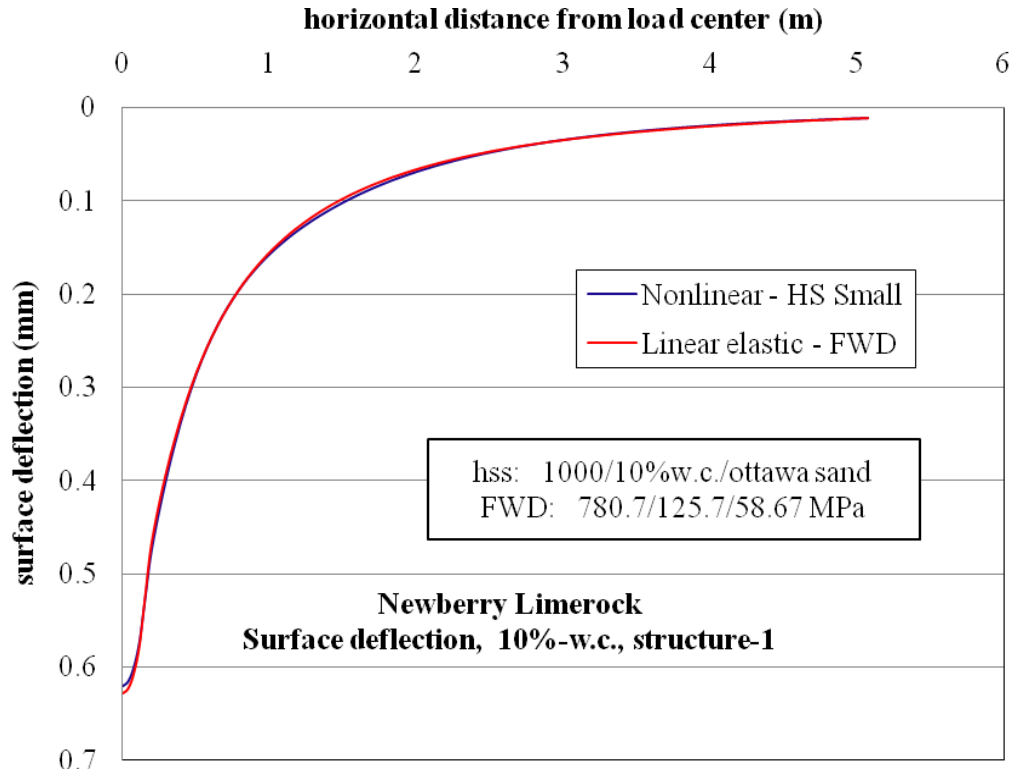
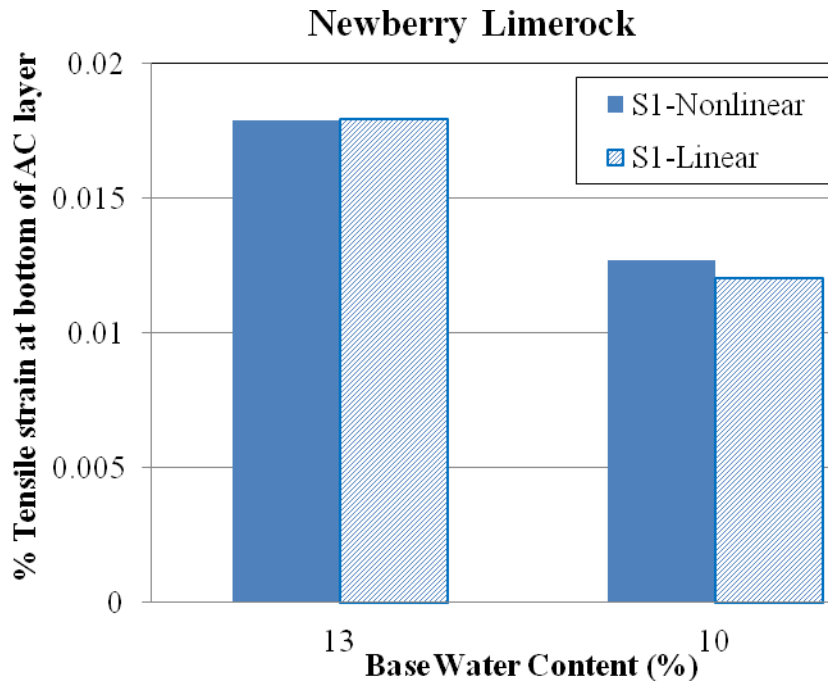
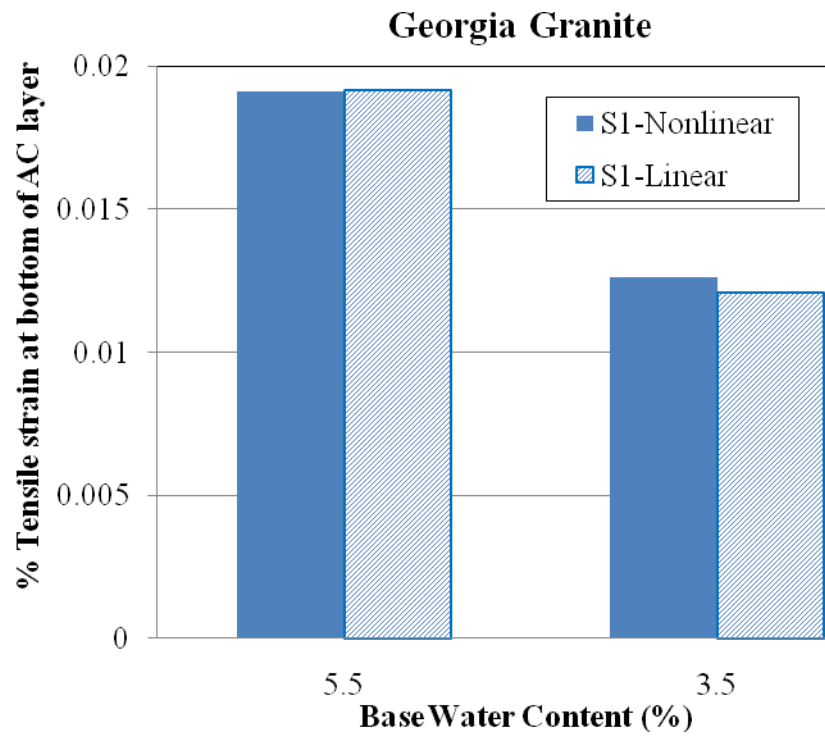


Figure 8-2. Comparison of nonlinear and linear surface deflections for structure-1 with 10% w.c. base and Ottawa sand subgrade.

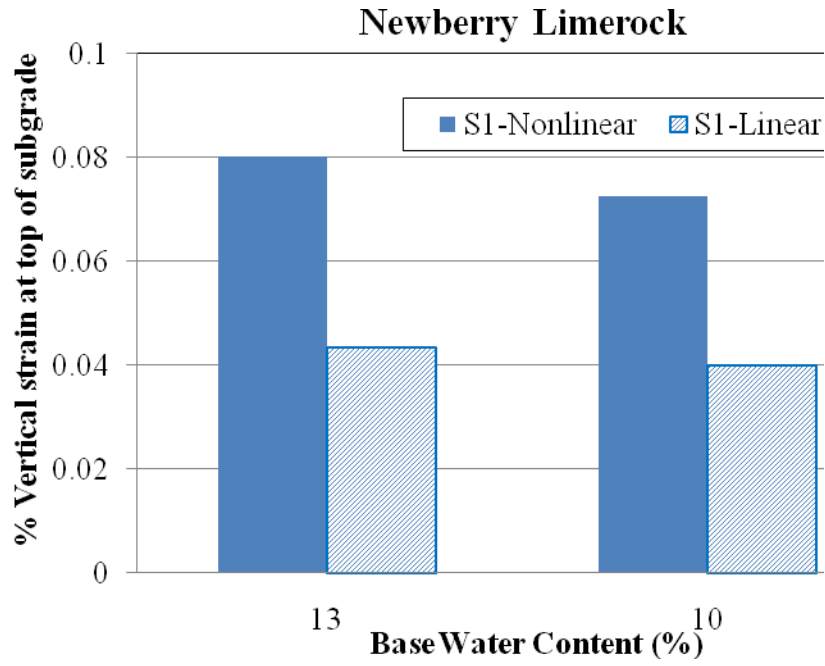


a

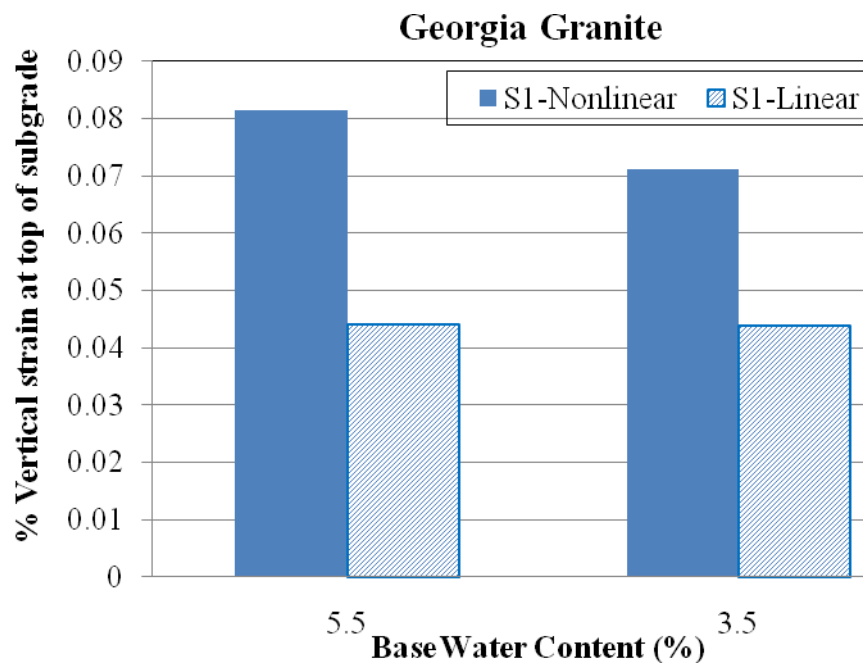


b

Figure 8-3. Comparison of horizontal tensile strain at bottom of AC layer ( $\% \epsilon_{xx}$ ) obtained for structure-1 with Ottawa sand subgrade and different base water contents of a) Newberry limerock b) Georgia granite



a



b

Figure 8-4. Comparison of vertical compressive strain at top of subgrade layer ( $\% \epsilon_{yy}$ ) obtained for structure-1 with Ottawa sand subgrade and different base water contents of a) Newberry limerock b) Georgia granite

## CHAPTER 9 CLOSURE

### 9.1 Summary of Findings

Main goal of this research investigation is to develop a design methodology to determine single effective modulus of base layer that can approximate known material modulus nonlinearities and can be used as MEPDG level-2 or level-3 material parameter input. In order to achieve this goal, it is proposed to conduct a lab testing program on base soils and develop a nonlinear response model using the lab testing results, which can assist in developing effective modulus determination methodology. First, a laboratory testing program is conducted on two base layer soils used in the State of Florida, to characterize their modulus nonlinearity with respect to stress, strains including small level strains and moisture content. Fixed-Free resonant column (Fixed-Free RC) tests that can measure shear modulus in the strain range of  $10^{-5}\%$  -  $10^{-1}\%$  while varying pressure confinement and moisture content, are conducted on modified proctor compacted cylindrical specimens of Newberry limerock and Georgia granite. Second, utilizing these laboratory tested parameters and results, a nonlinear finite element pavement response model that can account for the above mentioned modulus nonlinearities is developed via Plaxis-HSsmall model. Various types of pavement structures with nonlinear base and elastic AC surface and subgrade layers; are analyzed for single wheel loading via nonlinear response model. Based on pavement responses obtained from this nonlinear analysis, a practical design methodology is developed to determine nonlinear equivalent single effective elastic design modulus for whole base layer that can approximately account for nonlinearity in base layer under pavement loading conditions and can be used for MEPDG level-2 and level-3 material parameter inputs. Influence of base layer nonlinearity on pavement cracking and rutting performance is evaluated. Out of professional interest, influence of both base and subgrade modulus nonlinearity on pavement

performance is also evaluated for few selected pavement structures. Credibility of lab testing results and nonlinear response model is verified.

### **9.1.1 Laboratory Testing on Unbound Aggregate Base Soils**

Limerock is commonly used for pavement base layer construction in the State of Florida. Newberry limerock and Georgia granite are selected for lab testing, representing one limerock category and one non-limerock category. Fixed-Free Resonant Column tests (Fixed-Free RC) and Free-Free Resonant Column (Free-Free RC) test methods are followed. Fixed-Free RC equipment is upgraded to measure strains as small as  $10^{-5}\%$  strain using fiber optic sensor for strain measurement. Credibility of this upgraded apparatus is evaluated and verified by conducting tests on Ottawa sand specimens and comparing sand test results with the Ottawa sand data available in literature. Fixed-Free RC test are run on modified proctor specimens of Newberry limerock and Georgia granite to investigate the influence of effective confinement stress, loading strain including small level strains and moisture content. Modulus in the strain range of  $10^{-5}\%$  to  $10^{-1}\%$  is measured to analyze small-strain modulus nonlinearity of these soils. Testing specimens are dried in lab environment and tested at different water contents in the process of drying. Additional effective confinement provided due to suction at different water contents is evaluated. Empirical equations to calculate maximum shear modulus ( $G_{\max}$ ) of dry soils are developed. An approximate methodology to calculate shear modulus at any given effective confinement, strain level and water content is proposed. Free-Free RC tests are run on compacted specimens to determine very small-strain modulus (i.e.  $G_{\max}$  at  $\leq 10^{-5}\%$  strain) at different water contents ranging from OMC to near dry condition.

From above mentioned testing program, following findings have been derived: 1) Based on tests on dry specimens, shear modulus of Newberry limerock is proportional to pressure confinement to the power of 0.702 and of Georgia granite is proportional to pressure confinement to the

power of 0.6389. 2) For dry materials, shear modulus is maximum and elastic at strains lower than  $10^{-4}\%$  and starts decreasing linearly in the strain range of  $10^{-4}\%$ - $10^{-3}\%$  and decrease nonlinearly thereafter. Presence of gravel size aggregate makes modulus of dry gravelly soils more nonlinear compared to dry sands. 3)  $G_{\max}$  of dry Newberry limerock and dry Georgia Granite at known void ratio( $e$ ) and confinement ( $\sigma_c$ ) can be determined using following empirical equations:

$$\text{For Newberry limerock, } G_{\max} = (2575) F(e) (\sigma_c)^{0.702}$$

$$\text{For Georgia granite, } G_{\max} = (816) F(e) (\sigma_c)^{0.6389}$$

$$\text{where } F(e) = \frac{(2.17-e)^2}{(1+e)}$$

4) In unsaturated condition, shear modulus is maximum at  $10^{-5}\%$  strain and start decreasing thereafter with increase in strain. 5) In dry condition, shear modulus is maximum (i.e  $G_{\max}$ ) at  $10^{-4}\%$  strain and decreases to  $0.15 G_{\max}$  at  $10^{-1}\%$  strain. Whereas, in unsaturated condition, shear modulus is maximum at  $10^{-5}\%$  strain and decrease to  $0.075 G_{\max}$  at  $10^{-1}\%$  strain. Compared to dry gravelly soils, moisture presence increases modulus nonlinearity in unsaturated gravelly soils. 6) In unsaturated soils, decrease in water content due to material drying provides capillary suction confinement. This suction confinement increases with decrease in water content and increase  $G_{\max}$  very significantly. 7) Additional confinement due to suction at different moisture contents is material specific and need to be evaluated separately for each material, for accurate modulus nonlinearity analysis. 8) In dry soils, rate of decrease in  $G$  (i.e.  $G/G_{\max}$ ) with increase in strain is independent of confinement pressure magnitude. In unsaturated soils, rate of decrease in  $G$  with increase in strain is independent of water content and its suction confinement. 9) In unsaturated condition, at constant water content, additional confinement magnitude due to suction effect does not change with increase in strain. 10) Strain magnitudes generated in Free-

Free RC testing are approximately in the range of  $10^{-5}\%$  and corresponding moduli are nearly equal to very small-strain moduli of Fixed-Free RC tests.

### **9.1.2 Development of Nonlinear Response Model and Base Layer Nonlinear Modeling and Analysis**

Utilizing above laboratory testing data as material nonlinear inputs, a nonlinear finite element response model that can account for modulus nonlinearity is developed via Plaxis-HSsmall model. This response model can incorporate modulus nonlinearity with respect to effective stress confinement, strain magnitude including small level strains and moisture content. From initial pavement modeling and analysis exercises via Plaxis-HSsmall, it is observed that the response model behaves too soft and as a result produces high deformations. Hence the response model is recalibrated using Lehane et al. (2008) footing analysis results. Input parameters of the HSsmall model are recalibrated such that Lehane's footing analysis via recalibrated model, predicts deformations matching with actual field measured footing settlements. This recalibrated nonlinear response model is followed for our further pavement base layer modeling and analysis. Based on laboratory testing data of Newberry limerock, Georgia granite and Miami limerock, calibrated material input parameters for nonlinear response model are developed. Required functional capabilities of the response model to incorporate modulus nonlinearity with respect to input parameters and loading are verified.

To single out the influence of base layer modulus nonlinearity on pavement responses and performance, AC surface layer and subgrade layer are considered elastic; and base layer is considered nonlinear. Considering the surface deflection basin as the single matching factor between nonlinear and linear analysis, a new design methodology to determine nonlinear equivalent single effective modulus that can approximate the nonlinearities for whole base layer is developed. Single effective moduli data base for different structures with different subgrade

moduli and at different base water contents is developed. Influence of moisture content, subgrade modulus and structure type (thickness) on equivalent single effective modulus is evaluated. Effective moduli values of all three materials are compared with each other. Effective moduli data is also compared with MEPDG moisture (suction) model determined moduli data to verify the suitability of MEPDG moisture model for our base materials. Nonlinear and equivalent linear analyses pavement responses obtained at critical locations are compared to evaluate the applicability of base layer single effective modulus in place of nonlinear modulus. Pavement responses are analyzed to evaluate the effect of nonlinear base modulus on pavement performance in the perspective of rutting and cracking, in comparison with single effective modulus responses.

Following findings have been derived from base layer nonlinear modeling and analysis 1) For same subgrade modulus, effective base modulus increases significantly with decrease in water content. Rate of increase in effective modulus with decrease in moisture content is material specific. 2) Our lab testing data showed that decrease in water content increases additional confinement caused by suction, which in turn increases small-strain modulus. This increase in small-strain modulus is being reflected on equivalent single effective modulus and hence single effective modulus increases with decrease in water content. 3) For any given structure and base water content, single effective base modulus increases with increase in subgrade modulus. Single effective design modulus of base layer at any given water content depends on modulus of subgrade which supports base layer. 4) At any given moisture content and subgrade modulus combination, base layer single effective modulus value is dependent on structure's layers thicknesses. As the thicknesses of different layers in pavement structure varies, the magnitude of wheel load deviatoric stresses being transferred from top layers to bottom layers also varies.

Since soil modulus is nonlinear with respect to stress, as the magnitude of deviatoric stress varies; its effective modulus also varies. 5) Among all three materials, Miami limerock behaves very different and its effective modulus increases at faster rate very significantly as the material dries out. At OMC, effective modulus of Miami limerock is much lower than that of Newberry limerock and Georgia granite. But as the material dries out, its modulus increases at a very faster rate compared to other two materials and reaches maximum among all three materials. Therefore increase in design modulus with material drying is material specific. Since modulus tests are generally conducted at OMC, it is very important to be aware of this behavior, or else a pavement designer can get misled very easily. 6) For MEPDG moisture model, with decrease in water content, modulus can increase maximum up to two times of modulus at optimum moisture content. But, effective base moduli values derived for our materials do not meet this criterion.  $E/E_{opt}$  values increase up to 3.5 times for Newberry limerock, 2.5 times for Georgia granite and 47 times for Miami limerock.  $E/E_{opt}$  values for our materials are determined only up to 40% decrease in degree of saturation and can increase further with further decrease in degree of saturation. MEPDG moisture effect model cannot incorporate moisture/suction effect accurately for Florida base materials. 7) Surface deflection profiles for nonlinear and equivalent linear analyses are matching well and hence considering single effective modulus in place of nonlinear modulus does not affect the actual surface deflections. 8) Horizontal strain ( $\epsilon_{xx}$ ) at bottom of AC layer for nonlinear base modulus case is equal or nearly equal to equivalent linear case with single effective base modulus. Hence it appears that considering equivalent single effective modulus for design of base layer thickness may not affect the overall cracking performance of pavement. 9) For thick structures, vertical strain ( $\epsilon_{yy}$ ) at the top of subgrade for nonlinear base modulus is equal or nearly equal to equivalent linear case. For thin structures, the

difference in vertical strain ( $\epsilon_{yy}$ ) at the top of subgrade between nonlinear base modulus and equivalent linear case increases as the base material water content decreases. Hence it appears that as the structure thickness and base layer water content decreases together, material nonlinearity increases. 10) In overall, for both thick and thin structures, considering equivalent single effective design modulus in lieu of nonlinear modulus for base layer does not affect pavement's cracking performance and elastic based cracking performance empirical equation can be used for cracking performance evaluation. 11) For thick structures, use of single effective modulus does not affect rutting performance. As the structure thickness and base moisture content decreases together, equivalent linear design based on single effective design modulus of base layer may over estimate pavement's rutting performance. As the structure thickness and base moisture content decrease together, modulus nonlinearity of base soil becomes more significant and elastic analysis based performance criteria may not be applicable. Development of new performance criterion compatible with nonlinearity may be required for accurate performance analysis.

### **9.1.3 Nonlinear Modeling and Analysis of Base and Subgrade Layers**

From nonlinear modeling and analysis of pavement base layer, it is observed that nonlinear equivalent linear design methods may over estimate rutting performance of a pavement. Since rutting performance is mainly dependent on subgrade vertical strain and subgrade soils are also nonlinear, it is expected that subgrade nonlinearity may also influence pavement rutting performance significantly. Hence out of professional interest, it is decided to conduct nonlinear modeling and analysis of base and subgrade layers together, for few selected structures and evaluate effect of subgrade nonlinearity on pavement performance.

For this nonlinear modeling, both base and subgrade soils are considered nonlinear and AC layer is considered elastic. Ottawa sand is chosen as the only subgrade material. Considering

surface deflection basin obtained from nonlinear analysis as matching factor, FWD back calculation method is followed to back calculate equivalent elastic moduli for all layers. Elastic moduli obtained from FWD analysis are used for equivalent linear analysis. Pavement responses obtained from nonlinear analysis and equivalent linear analysis are compared to evaluate the influence of nonlinear subgrade nonlinearity on pavement performance in the perspective of rutting and cracking.

Following findings have been derived from nonlinear modeling and analysis of base and subgrade layers: 1) FWD back calculated subgrade moduli values for nonlinear subgrade structures with different base water contents are in the range of 40-44 MPa. By comparing the back calculated equivalent effective base moduli values of these nonlinear subgrade structures with that of same structures with 50 MPa elastic subgrade modulus, it can be observed that effective modulus of base layer with nonlinear subgrade is significantly lower than effective modulus of base layer with 50 MPa elastic subgrade layer. This significant decrease in base equivalent effective modulus for nonlinear subgrade structures is might be due to the additional effect of subgrade nonlinearity along with base nonlinearity, which eventually causes greater strain and lower equivalent effective moduli. 2) Surface deflection profiles for nonlinear and equivalent linear analyses are matching well. Hence, considering FWD back calculated effective moduli for base and subgrade layers in place of nonlinear moduli does not affect the actual surface deflections. 3) Horizontal strain ( $\epsilon_{xx}$ ) at bottom of AC layer for nonlinear base and subgrade moduli case is equal or nearly equal to equivalent linear case with back calculated single effective moduli. This indicates that considering back calculated effective modulus for both base and subgrade layers in place of nonlinear modulus, for pavement design may not significantly affect the overall cracking performance of pavement structure. Hence subgrade

nonlinearity may not influence the cracking performance of a pavement structure. 4) Vertical strain ( $\epsilon_{yy}$ ) at top of subgrade from nonlinear analysis is almost two times greater than corresponding equivalent linear analysis. This indicates that the subgrade nonlinearity may influence pavement's rutting performance very significantly. Since the vertical strain ( $\epsilon_{yy}$ ) at top of subgrade calculated by nonlinear analysis is greater than equivalent linear analysis, it appears that currently practiced elastic design methods might be overestimating rutting performance. 5) From number of load repetitions ( $N_d$ ) calculations, it is found that equivalent elastic design method overestimates the rutting performance by approximately 17 times, compared to nonlinear analysis with nonlinear base and subgrade. Thus, a new rutting performance criterion may be required to design pavement structures using single effective design modulus in place of nonlinear modulus, for both base and subgrade layers. Since subgrade nonlinearity can significantly influence rutting performance, it may be necessary to consider subgrade nonlinearity in pavement design procedures and nonlinear response models.

## 9.2 Conclusions

Based on above findings, following conclusions are drawn. First, nonlinear small-strain modulus of unbound aggregate base soils increases significantly with decrease in water content. It appears that decrease in water content due to material drying creates suction effect, which provides significant additional effective confinement. Suction effect created additional effective confinement, can increase nonlinear modulus significantly up to strain levels as high as  $10^{-2}\%$ . Second, it appears that single effective modulus, calculated based on surface deflection obtained from nonlinear analysis, can approximate modulus nonlinearities of base layer and can be used for MEPDG level-2 and level-3 material parameter inputs. Single effective modulus of base layer can be influenced by decrease in moisture content and its suction effect, subgrade modulus and structure thickness. Suction effect on effective modulus is material specific and need to be

evaluated for each material separately. It appears that increase in small-strain modulus due to suction effect is being reflected on nonlinear equivalent single effective modulus at different moisture contents, and hence small-strain modulus nonlinearity should be considered for thickness design analysis. Third, based on comparison of pavement responses obtained from nonlinear and equivalent linear analysis, it appears that base layer nonlinearity does not affect cracking performance, but affects rutting performance as the structure thickness and moisture content decreases together. As the structure thickness and moisture content decreases together, use of base layer single effective modulus in design analysis may overestimate rutting performance and hence it may be required to develop a suitable rutting performance criterion that can fit for the nonlinear rutting analysis. Last, subgrade nonlinearity appears to influence rutting performance very significantly and use of elastic modulus for whole subgrade layer overestimates rutting performance.

### **9.3 Recommendations**

The following recommendations are suggested after reviewing all of the findings and conclusions previously discussed: 1) Base course soils small-strain modulus nonlinearity and moisture suction effect on it, need to be implemented in pavement design guidelines. 2) Nonlinear equivalent single effective base modulus determination methodology can be implemented in MEPDG for determining level-2 and level-3 material parameter inputs. 3) Suction effect on base material nonlinear modulus is material specific and need to be analyzed for each material separately. MEPDG moisture model for suction effect need to modified or improved for local base course soils. 4) Nonlinear based rutting performance criteria needs to be developed for accurate nonlinear base and subgrade dependent rutting performance evaluation. 5) Influence of subgrade nonlinearity is analyzed for few selected structures and one subgrade material only. This analysis could be extended to more types of structures and different subgrade

soils for complete understanding of subgrade nonlinearity influence on pavement performance.

6) Our research work is limited to axisymmetric modeling of pavement structure subjected to single wheel loading. It may be further extended to three-dimensional modeling of pavement structure, under multiple wheel and axle loads for accurate nonlinear modeling of soil element stress state and further performance analysis. 7) A fully fledged field testing program to measure in-situ pavement responses is needed to verify computer based nonlinear response model results and modify the model accordingly for future pavement research. Field testing data will provide more insight into accurate pavement stress state and further fine tuning of nonlinear modeling. 8) Our research work is based on lab tested parameters only. Further research work based on in-situ tested material parameters may provide more accurate pavement responses and performance evaluation.

APPENDIX A  
FIXED-FREE RESONANT COLUMN TESTING DATA FOR DIFFERENT BASE SOILS

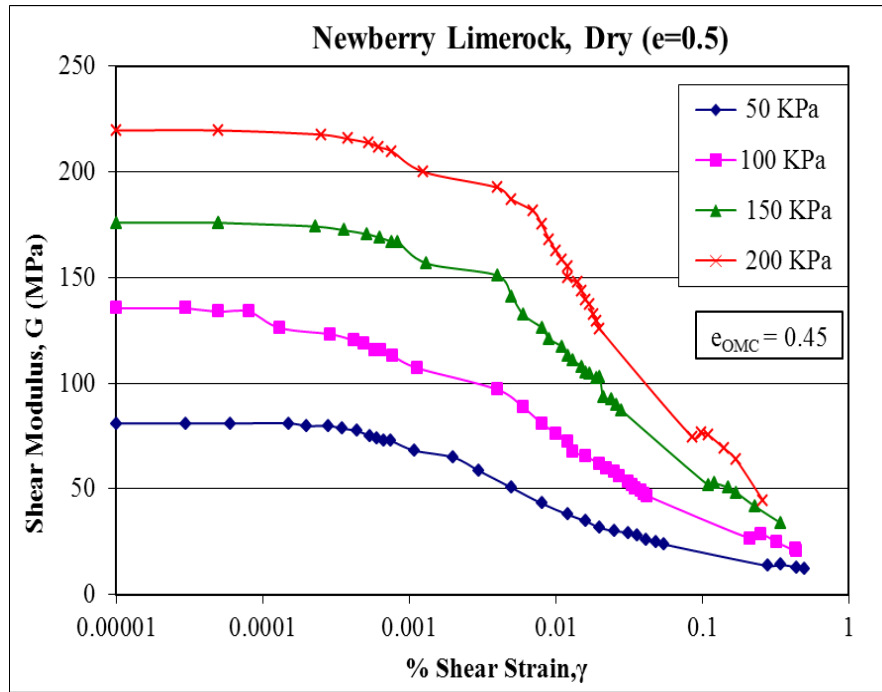


Figure A-1. Shear Modulus (G) versus % Shear strain ( $\gamma$ ) curves for dry Newberry limerock at  $e=0.5$

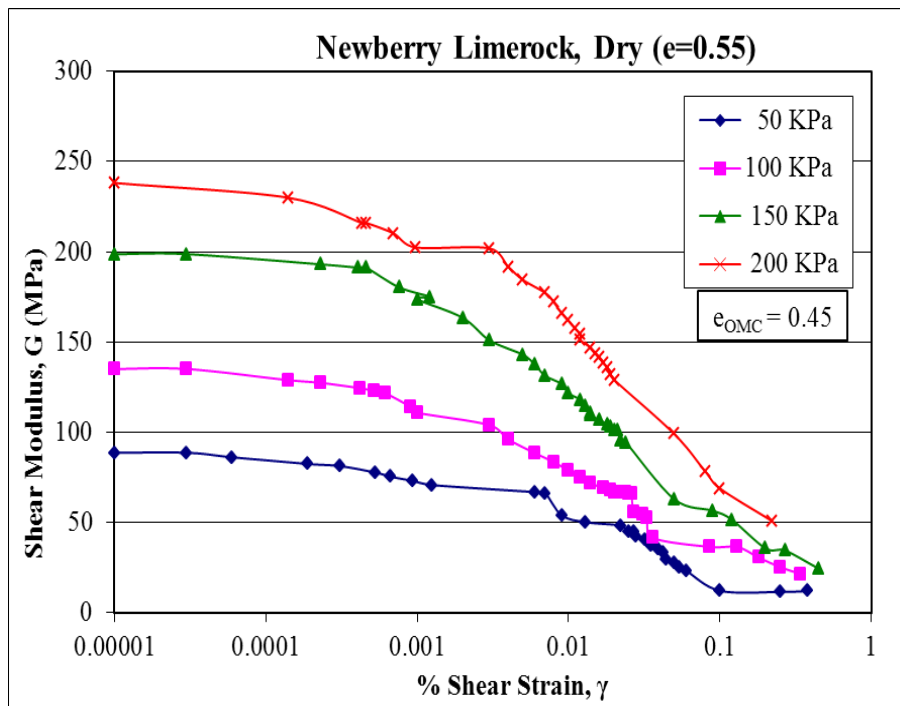


Figure A-2. Shear Modulus (G) versus % Shear strain ( $\gamma$ ) curves for dry Newberry limerock at  $e=0.55$

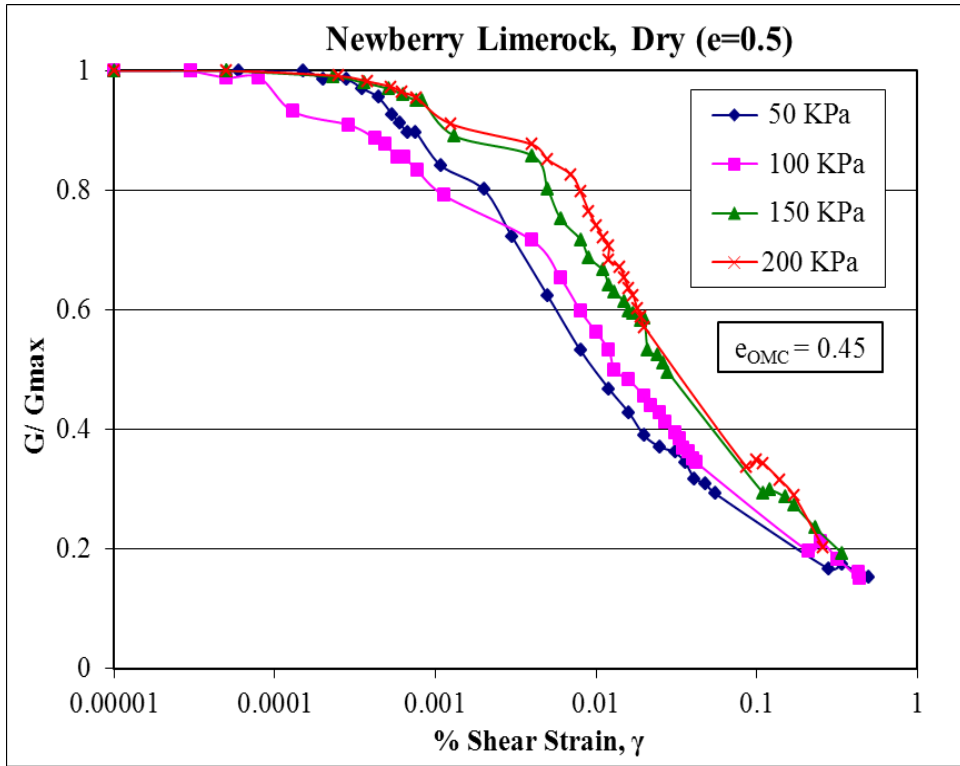


Figure A-3.  $G/G_{max}$  versus % shear strain( $\gamma$ ) curves at  $e=0.5$  for Newberry limerock

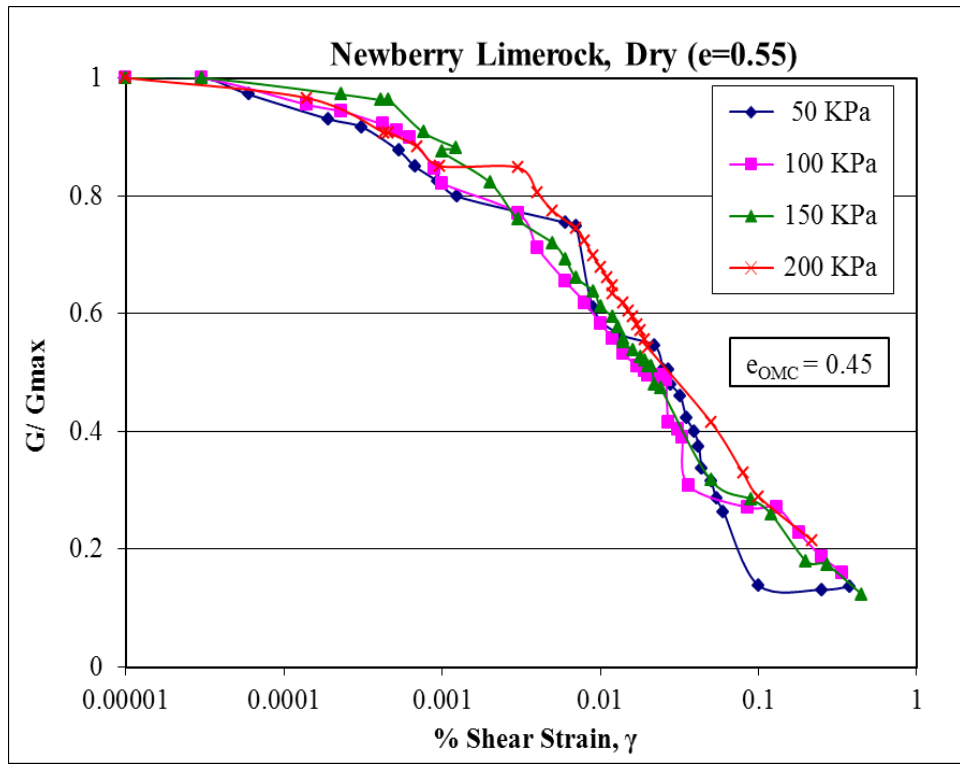


Figure A-4.  $G/G_{max}$  versus % shear strain ( $\gamma$ ) curves at  $e=0.55$  for Newberry limerock

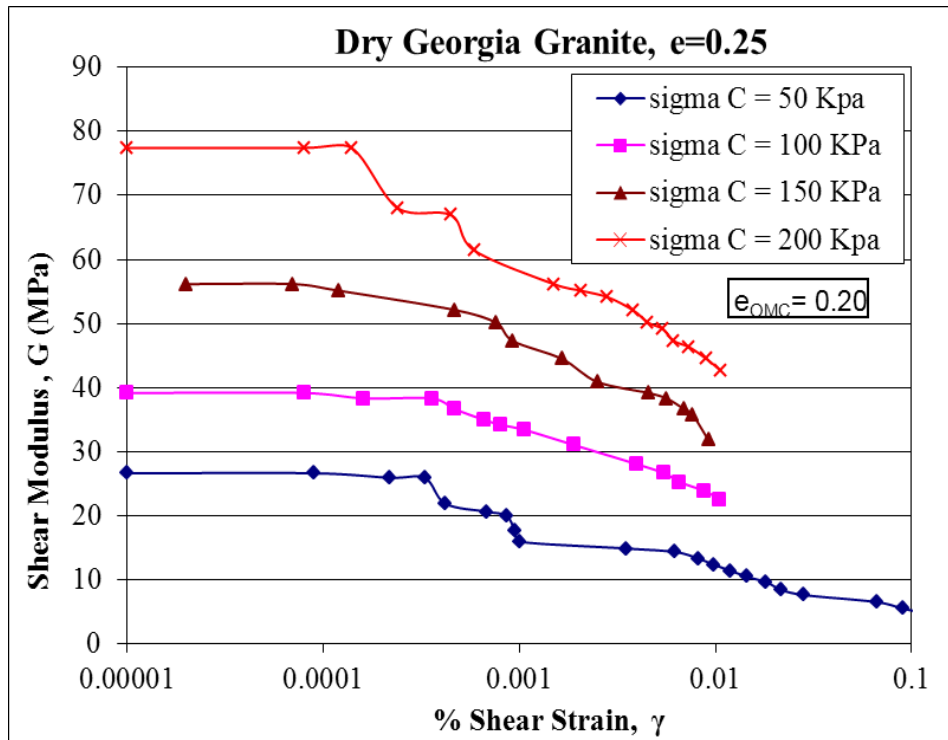


Figure A-5. Shear Modulus (G) versus % Shear strain ( $\gamma$ ) curves for dry Georgia granite at  $e=0.25$

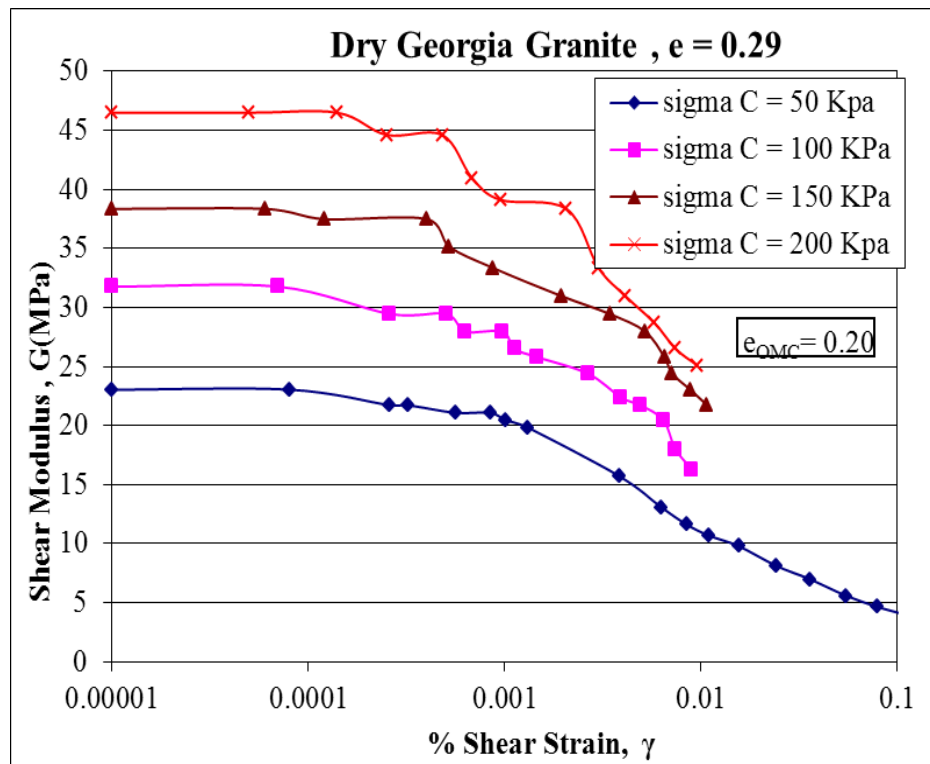


Figure A-6. Shear Modulus (G) versus % Shear strain ( $\gamma$ ) curves for dry Georgia granite at  $e=0.29$

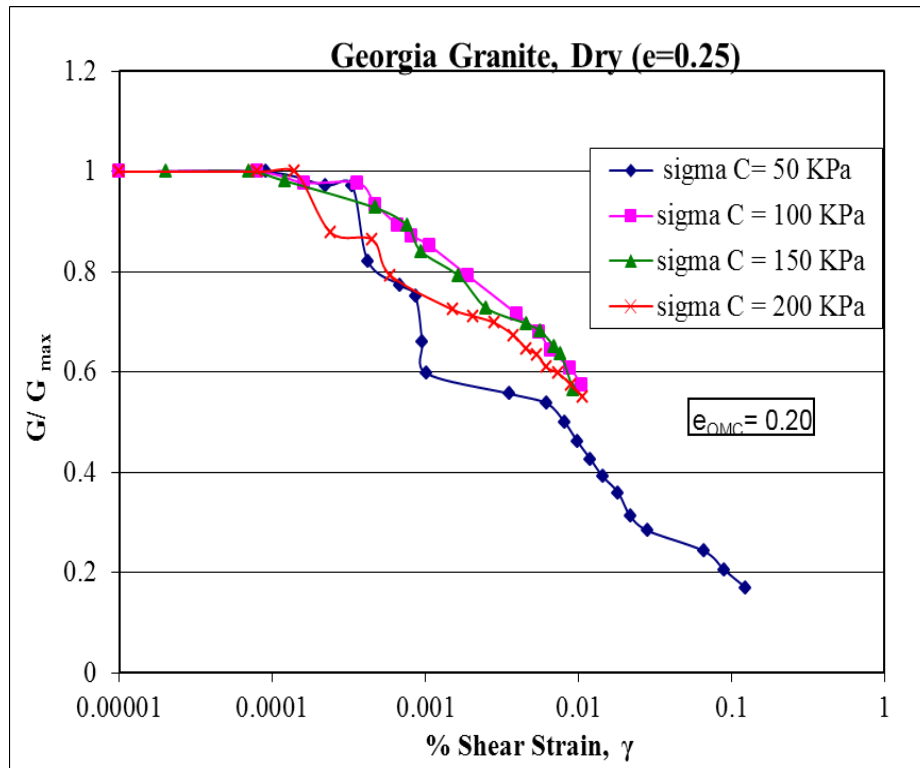


Figure A-7.  $G/G_{max}$  versus % shear strain( $\gamma$ ) curves at  $e=0.25$  for Georgia granite

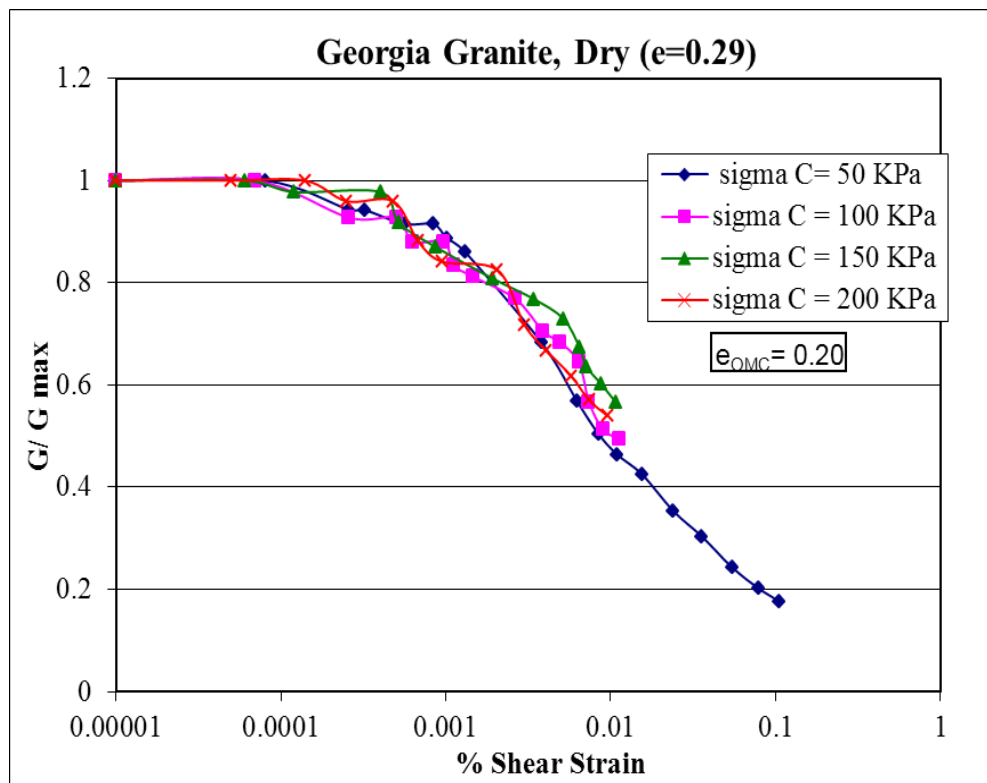


Figure A-8.  $G/G_{max}$  versus % shear strain( $\gamma$ ) curves at  $e=0.29$  for Georgia granite

APPENDIX B  
NONLINEAR EQUIVALENT LINEAR EFFECTIVE BASE MODULI DATA FOR  
DIFFERENT TYPES OF BASE SOILS

Table B-1. For structure-1, nonlinear equivalent linear effective moduli data for Newberry limerock base layer.

Base Layer Water Content	13%	12%	11%	10%	8%	5.5%
$E_{max}$ (Mpa)*	179.82	272.05	548.75	631.12	1249.55	2487.10
<b>Case 1: 50 Mpa subgrade</b>						
base E (Mpa)	79	102	140	153	196	230
$E/E_{max}$	0.44	0.37	0.26	0.24	0.16	0.09
<b>Case 2: 30 Mpa subgrade</b>						
base E (Mpa)	65	79	112	118	142	171
$E/E_{max}$	0.36	0.29	0.20	0.19	0.11	0.07
<b>Case 3: 70 Mpa subgrade</b>						
base E (Mpa)	90	117	170	175	230	267
$E/E_{max}$	0.50	0.43	0.31	0.28	0.18	0.11
<b>Case 4: 125 Mpa subgrade</b>						
base E (Mpa)	108	157	227	241	310	387
$E/E_{max}$	0.60	0.58	0.41	0.38	0.25	0.16

\*  $E_{max}$ - Maximum Young's modulus is calculated for in-situ overburden stress at middle height of base layer

Table B-2. For structure-2, nonlinear equivalent linear effective moduli data for Newberry limerock base layer.

Base Layer Water Content						
	13%	12%	11%	10%	8%	5.5%
$E_{\max}$ (Mpa)*	170.45	264.114	542.403	625.074	1245.22	2483.69
<b>Case 1: 50 Mpa subgrade</b>						
base E (Mpa)	74	92	120	125	155	178
$E/E_{\max}$	0.43	0.35	0.22	0.20	0.12	0.07
<b>Case 2: 30 Mpa subgrade</b>						
base E (Mpa)	58	70	92	94	118	139
$E/E_{\max}$	0.34	0.27	0.17	0.15	0.09	0.06
<b>Case 3: 70 Mpa subgrade</b>						
base E (Mpa)	85	109	143	149	184	207
$E/E_{\max}$	0.50	0.41	0.26	0.24	0.15	0.08
<b>Case 4: 125 Mpa subgrade</b>						
base E (Mpa)	107	147	210	220	278	308
$E/E_{\max}$	0.63	0.56	0.39	0.35	0.22	0.12

Table B-3. For structure-3, nonlinear equivalent linear effective moduli data for Newberry limerock base layer.

Base Layer Water Content						
	13%	12%	11%	10%	8%	5.5%
$E_{\max}$ (Mpa)*	166.819	260.58	539.487	622.215	1242.78	2481.57
<b>Case 1: 50 Mpa subgrade</b>						
base E (Mpa)	66	89	112	124	148	168
$E/E_{\max}$	0.40	0.34	0.21	0.20	0.12	0.07
<b>Case 2: 30 Mpa subgrade</b>						
base E (Mpa)	54	67	90	101	108	130
$E/E_{\max}$	0.32	0.26	0.17	0.16	0.09	0.05
<b>Case 3: 70 Mpa subgrade</b>						
base E (Mpa)	73	100	135	142	195	205
$E/E_{\max}$	0.44	0.38	0.25	0.23	0.16	0.08
<b>Case 4: 125 Mpa subgrade</b>						
base E (Mpa)	93	141	214	220	281	311
$E/E_{\max}$	0.56	0.54	0.40	0.35	0.23	0.13

Table B-4. For structure-4, nonlinear equivalent linear effective moduli data for Newberry limerock base layer.

Base Layer Water Content						
	13%	12%	11%	10%	8%	5.5%
$E_{\max}$ (Mpa)*	158.3	253.46	533.84	616.7	1238.44	2478.16
<b>Case 1: 50 Mpa subgrade</b>						
base E (Mpa)	62	80	108	112	123	132
$E/E_{\max}$	0.39	0.32	0.20	0.18	0.10	0.05
<b>Case 2: 30 Mpa subgrade</b>						
base E (Mpa)	49	60	69	70	76	78
$E/E_{\max}$	0.31	0.24	0.13	0.11	0.06	0.03
<b>Case 3: 70 Mpa subgrade</b>						
base E (Mpa)	71	96	129	135	139	144
$E/E_{\max}$	0.45	0.38	0.24	0.22	0.11	0.06
<b>Case 4: 125 Mpa subgrade</b>						
base E (Mpa)	84	127	196	206	228	240
$E/E_{\max}$	0.53	0.50	0.37	0.33	0.18	0.10

Table B-5. For structure-5, nonlinear equivalent linear effective moduli data for Newberry limerock base layer.

Base Layer Water Content			
	13%	11%	5.5%
$E_{\max}$ (Mpa)*	152.538	530.054	2457.67
<b>Case 1: 50 Mpa subgrade</b>			
base E (Mpa)	73	100	102
$E/E_{\max}$	0.48	0.19	0.04
<b>Case 2: 125 Mpa subgrade</b>			
base E (Mpa)	105	189	209
$E/E_{\max}$	0.69	0.36	0.09

Table B-6. For structure-6, nonlinear equivalent linear effective moduli data for Newberry  
limerock base layer.

Base Layer Water Content			
	13%	11%	5.5%
$E_{\max}$ (Mpa)*	152.112	529.529	2457.19
<b>Case 1: 50 Mpa subgrade</b>			
base E (Mpa)	76	90	107
$E/E_{\max}$	0.50	0.17	0.04
<b>Case 2: 125 Mpa subgrade</b>			
base E (Mpa)	103	180	187
$E/E_{\max}$	0.68	0.34	0.08

Table B-7. For structure-1, nonlinear equivalent linear effective moduli data for Georgia granite base layer.

Base Layer Water Content	5.5%	4.5%	3.5%
$E_{\max}$ (Mpa)	136.23	444.71	647.68
<b>Case 1: 50 Mpa subgrade</b>			
base E (Mpa)	76	135	152
$E/E_{\max}$	0.56	0.30	0.23
<b>Case 2: 30 Mpa subgrade</b>			
base E (Mpa)	63	104	117
$E/E_{\max}$	0.46	0.23	0.18
<b>Case 3: 70 Mpa subgrade</b>			
base E (Mpa)	86	155	178
$E/E_{\max}$	0.63	0.35	0.27
<b>Case 4: 125 Mpa subgrade</b>			
base E (Mpa)	112	210	243
$E/E_{\max}$	0.82	0.47	0.38

Table B-8. For structure-2, nonlinear equivalent linear effective moduli data for Georgia granite base layer.

Base Layer Water Content	5.5%	4.5%	3.5%
$E_{\max}$ (Mpa)	134.45	443.70	646.91
<b>Case 1: 50 Mpa subgrade</b>			
base E (Mpa)	70	112	124
$E/E_{\max}$	0.52	0.25	0.19
<b>Case 2: 30 Mpa subgrade</b>			
base E (Mpa)	56	94	104
$E/E_{\max}$	0.42	0.21	0.16
<b>Case 3: 70 Mpa subgrade</b>			
base E (Mpa)	82	135	150
$E/E_{\max}$	0.61	0.30	0.23
<b>Case 4: 125 Mpa subgrade</b>			
base E (Mpa)	105	195	220
$E/E_{\max}$	0.78	0.44	0.34

Table B-9. For structure-3, nonlinear equivalent linear effective moduli data for Georgia granite base layer.

Base Layer Water Content	5.5%	4.5%	3.5%
$E_{\max}$ (Mpa)	133.87	443.37	646.63
<b>Case 1: 50 Mpa subgrade</b>			
base E (Mpa)	66	115	119
$E/E_{\max}$	0.49	0.26	0.18
<b>Case 2: 30 Mpa subgrade</b>			
base E (Mpa)	54	88	100
$E/E_{\max}$	0.40	0.20	0.15
<b>Case 3: 70 Mpa subgrade</b>			
base E (Mpa)	73	133	162
$E/E_{\max}$	0.55	0.30	0.25
<b>Case 4: 125 Mpa subgrade</b>			
base E (Mpa)	90	207	220
$E/E_{\max}$	0.67	0.47	0.34

Table B-10. For structure-4, nonlinear equivalent linear effective moduli data for Georgia granite base layer.

Base Layer Water Content	5.5%	4.5%	3.5%
$E_{\max}$ (Mpa)	132.08	442.40	645.84
<b>Case 1: 50 Mpa subgrade</b>			
base E (Mpa)	60	100	106
$E/E_{\max}$	0.45	0.23	0.16
<b>Case 2: 30 Mpa subgrade</b>			
base E (Mpa)	46	74	75
$E/E_{\max}$	0.35	0.17	0.12
<b>Case 3: 70 Mpa subgrade</b>			
base E (Mpa)	67	123	137
$E/E_{\max}$	0.51	0.28	0.21
<b>Case 4: 125 Mpa subgrade</b>			
base E (Mpa)	84	184	220
$E/E_{\max}$	0.64	0.42	0.34

Table B-11. For structure-1, nonlinear equivalent linear effective moduli data for Miami limerock base layer.

Base Layer Water Content			
	8.0%	6.0%	4.0%
$E_{\max}$ (Mpa)	32.99	612.77	3474.36
<b>Case 1: 50 Mpa subgrade</b>			
base E (Mpa)	30	168	337
$E/E_{\max}$	0.91	0.27	0.10
<b>Case 2: 125 Mpa subgrade</b>			
base E (Mpa)	31	260	545
$E/E_{\max}$	0.94	0.42	0.16

Table B-12. For structure-4, nonlinear equivalent linear effective moduli data for Miami limerock base layer.

Base Layer Water Content			
	8.0%	6.0%	4.0%
$E_{\max}$ (Mpa)	32.99	612.77	3474.36
<b>Case 1: 50 Mpa subgrade</b>			
base E (Mpa)	6	54	159
$E/E_{\max}$	0.18	0.09	0.05
<b>Case 2: 125 Mpa subgrade</b>			
base E (Mpa)	7	122	320
$E/E_{\max}$	0.21	0.20	0.09

APPENDIX C  
COMPARISON OF NONLINEAR AND EQUIVALENT LINEAR RESPONSES OBTAINED  
FROM NONLINEAR BASE ANALYSIS

**C.1 Newberry Limerock**

**C.1.1 Surface Deflection Profiles**

**C.1.1.1 Structure-1**

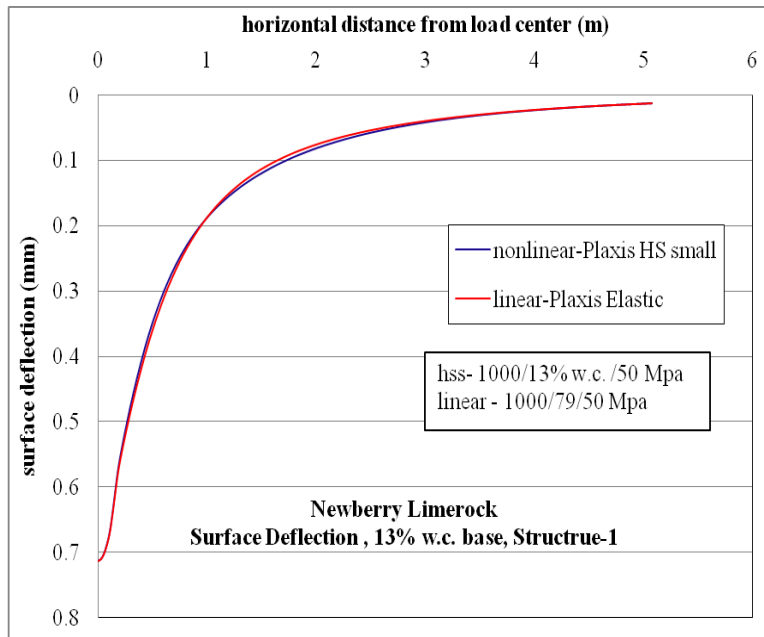


Figure C-1. Surface deflection comparison for nonlinear and linear cases, for structure-1 with 13% w.c. base layer.

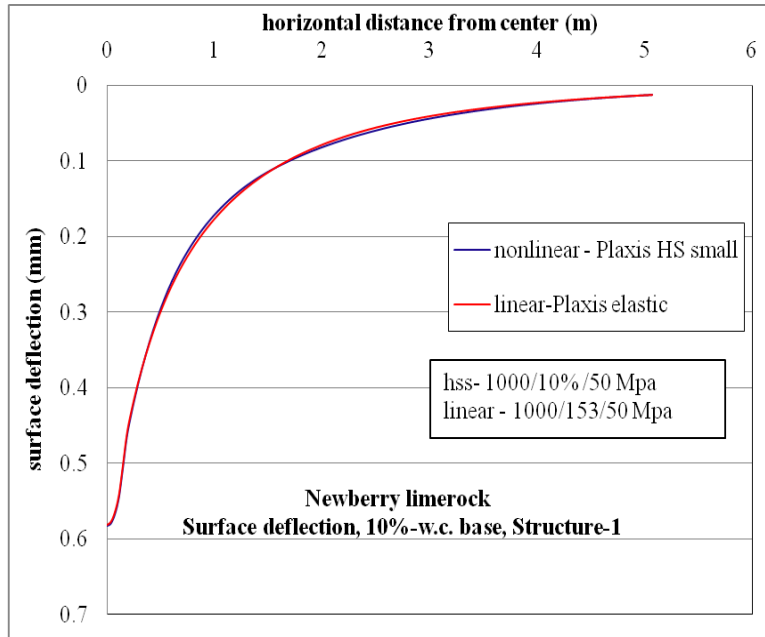


Figure C-2. Surface deflection comparison for nonlinear and linear cases, for structure-1 with 10% w.c. base layer.

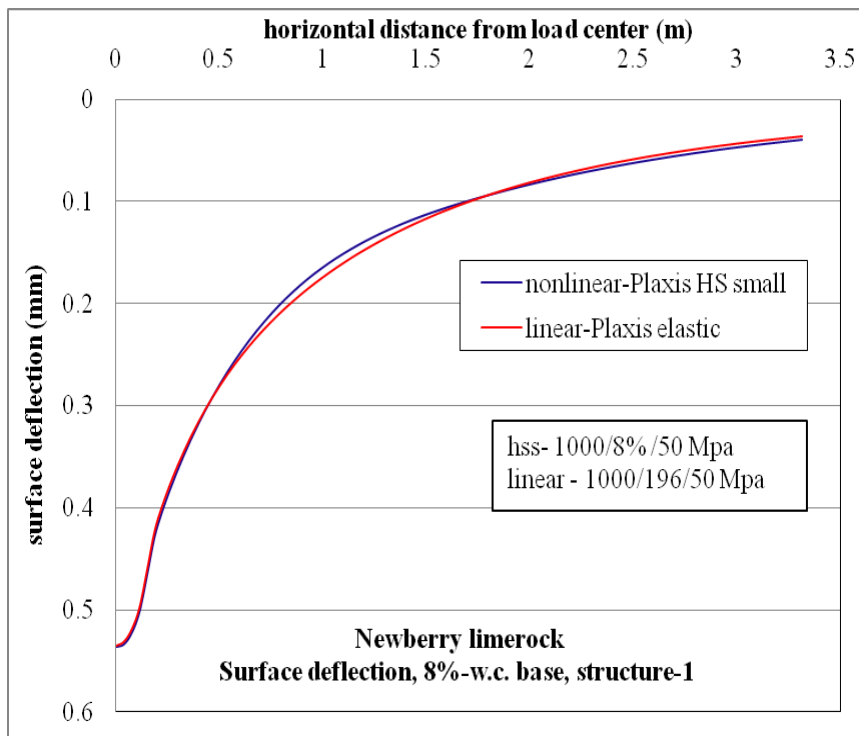


Figure C-3. Surface deflection comparison for nonlinear and linear cases, for structure-1 with 8% w.c. base layer.

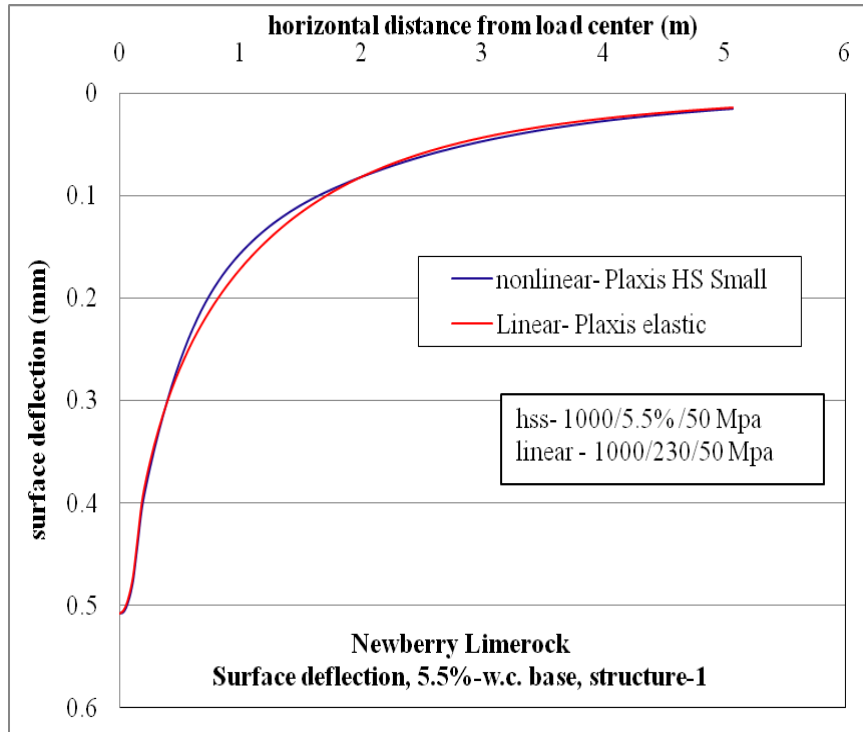


Figure C-4. Surface deflection comparison for nonlinear and linear cases, for structure-1 with 5.5% w.c. base layer

#### C.1.1.2 Structure-4

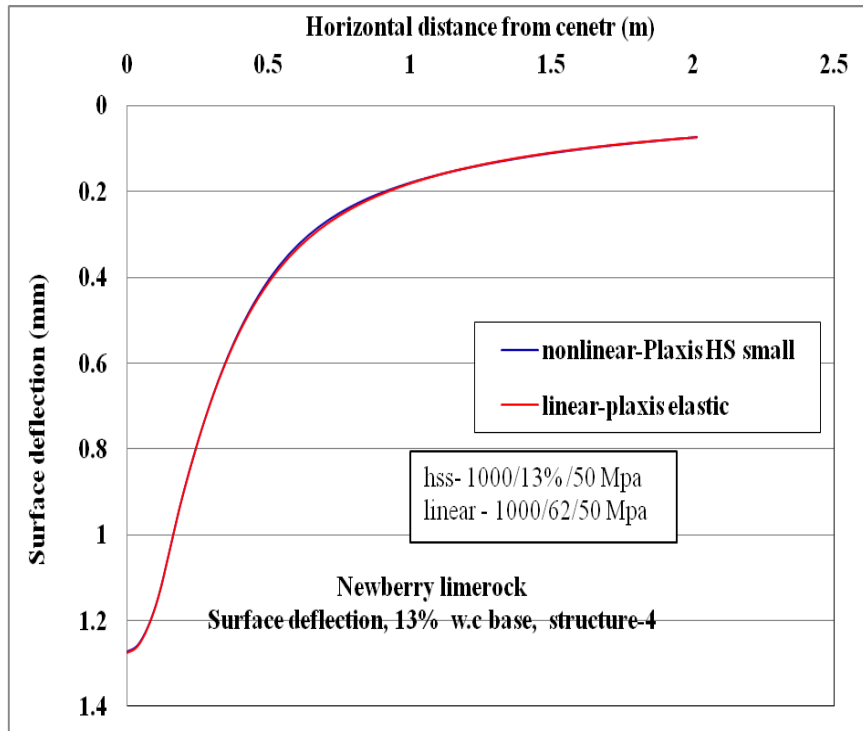


Figure C-5. Surface deflection comparison for nonlinear and linear cases, for structure-4 with 13% w.c. base layer.

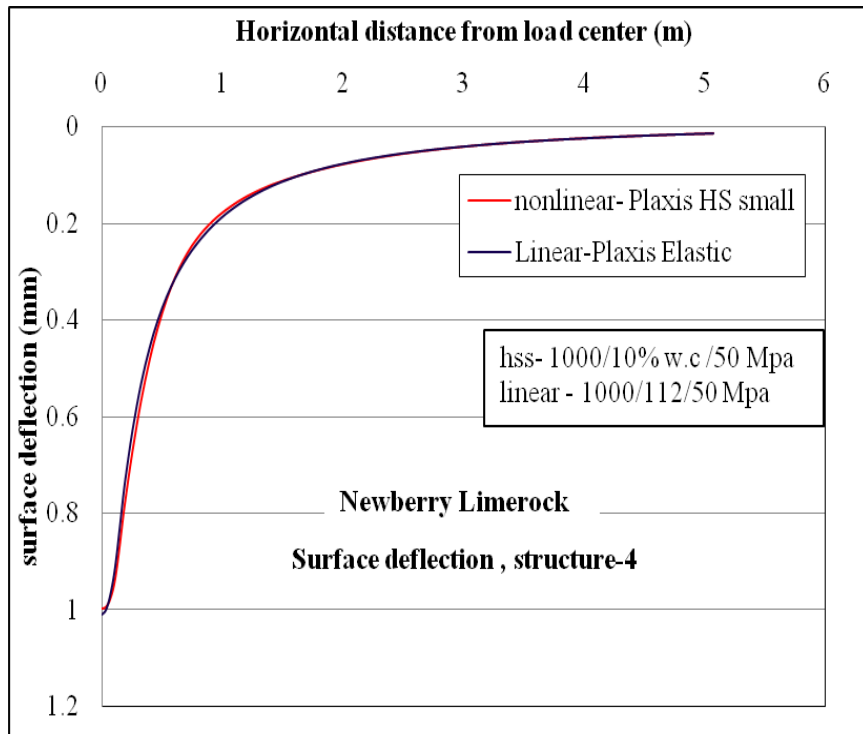


Figure C-6. Surface deflection comparison for nonlinear and linear cases, for structure-4 with 10% w.c. base layer.

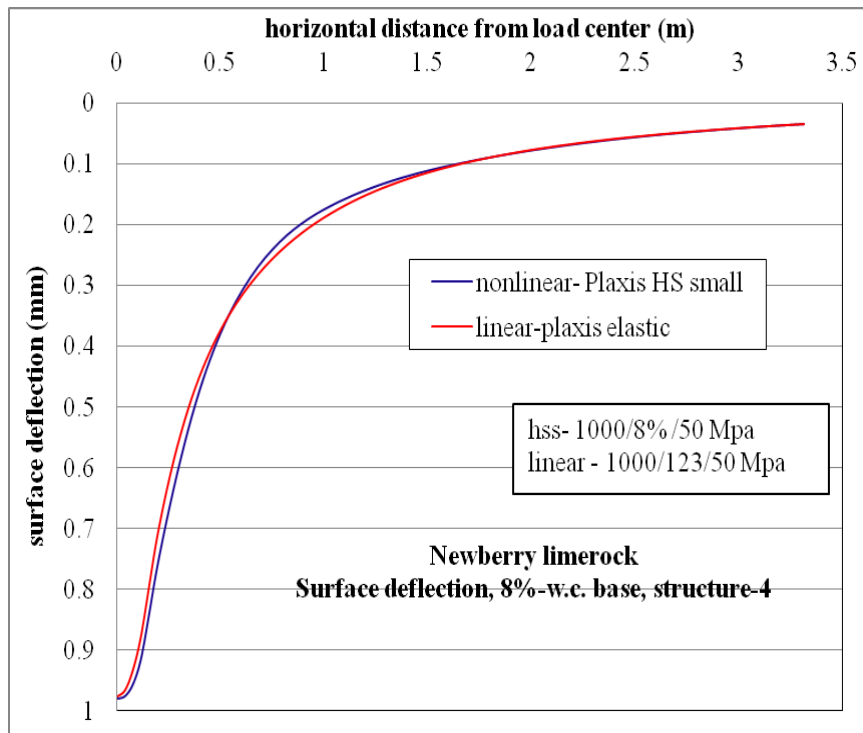


Figure C-7. Surface deflection comparison for nonlinear and linear cases, for structure-4 with 8% w.c. base layer.

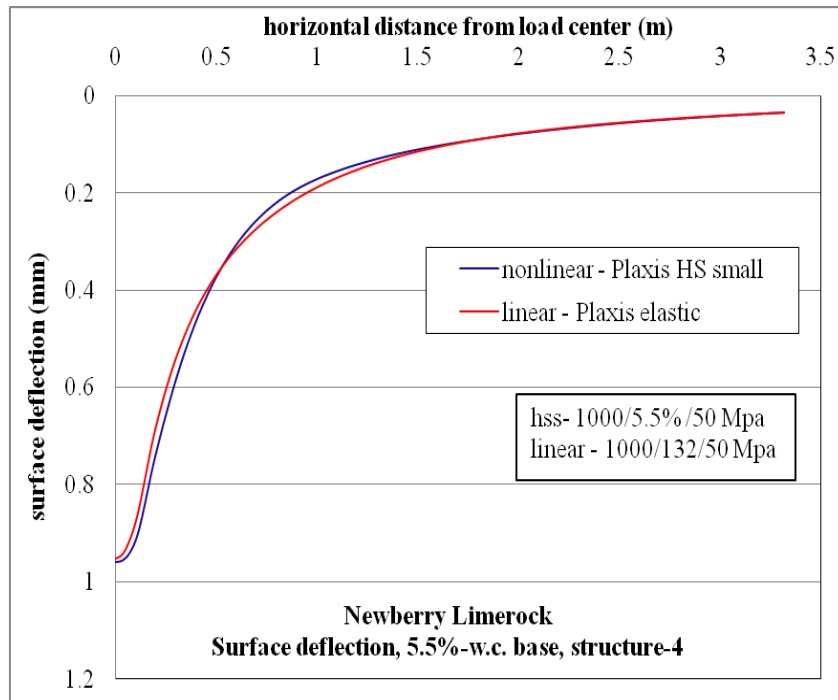


Figure C-8. Surface deflection comparison for nonlinear and linear cases, for structure-4 with 5.5% w.c. base layer.

## C.1.2 Horizontal Stress ( $\sigma_{xx}$ , Tensile Stress) at Top of AC Layer

### C.1.2.1 Structure-1

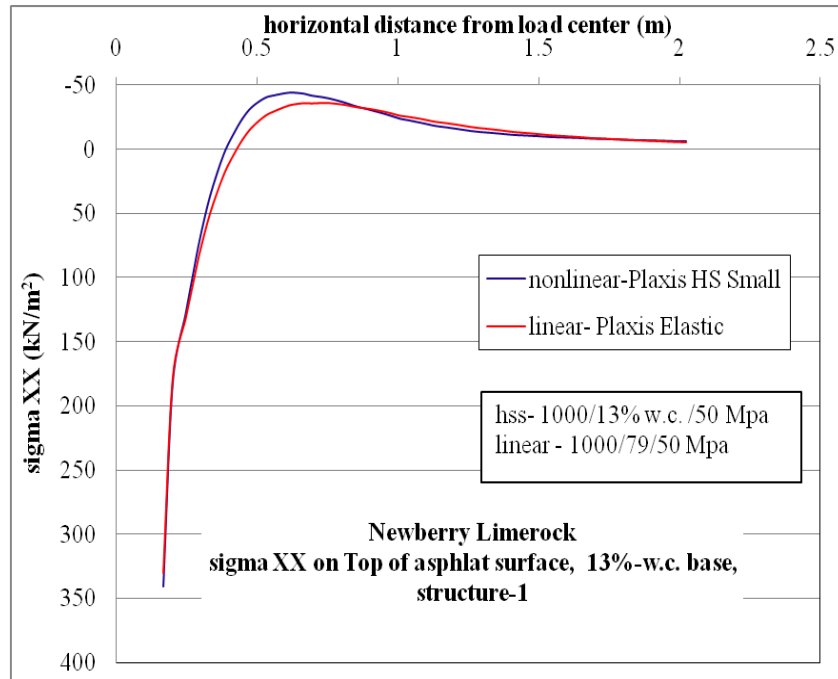


Figure C-9.  $\sigma_{xx}$  at top of AC layer comparison for nonlinear and linear cases, for structure-1 with 13% w.c. base layer.

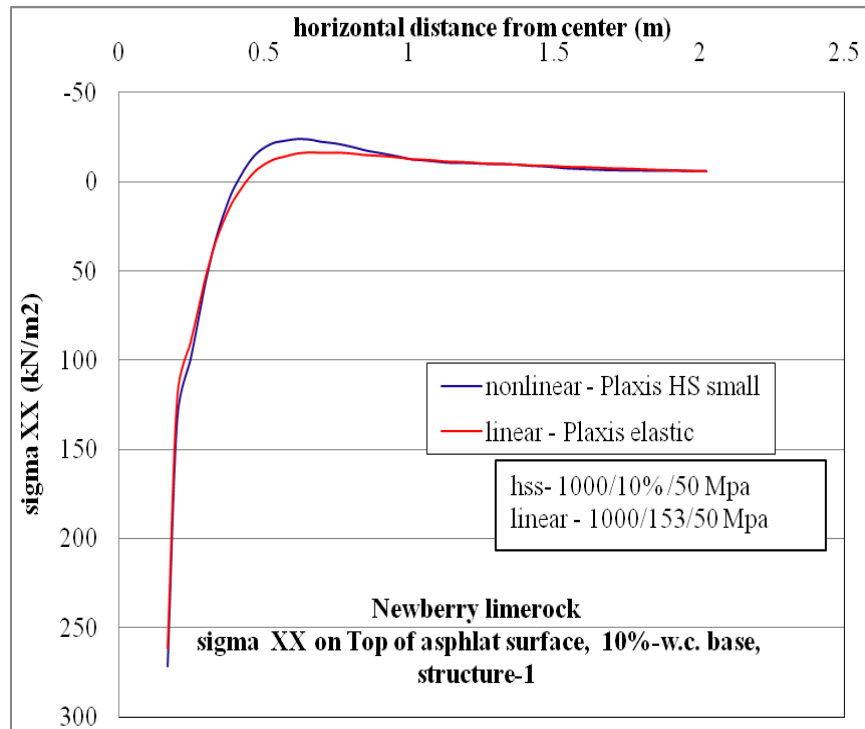


Figure C-10.  $\sigma_{xx}$  at top of AC layer comparison for nonlinear and linear cases, for structure-1 with 10% w.c. base layer.

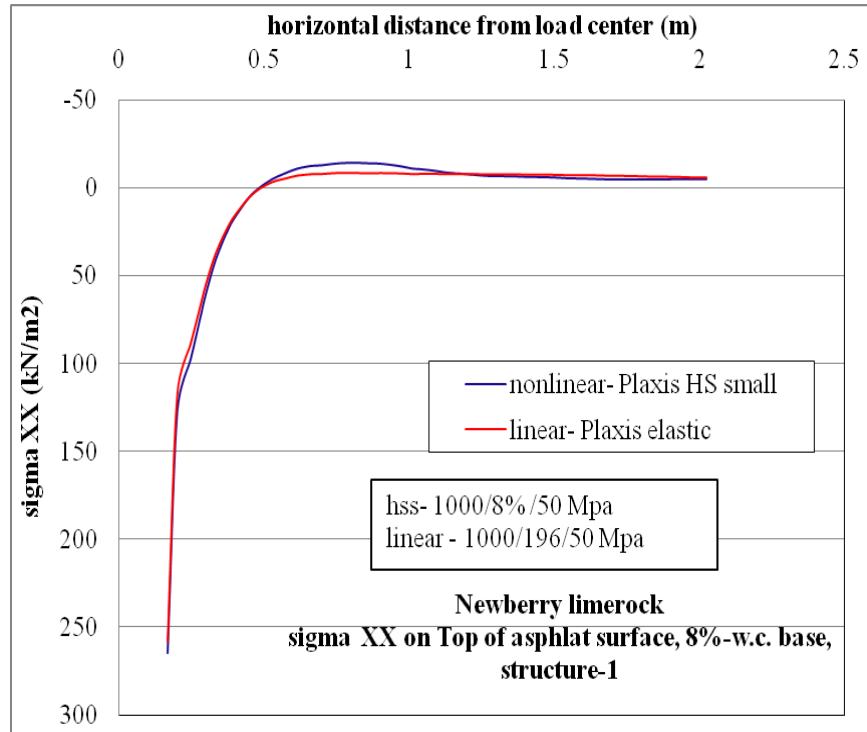


Figure C-11.  $\sigma_{xx}$  at top of AC layer comparison for nonlinear and linear cases, for structure-1 with 8% w.c. base layer.

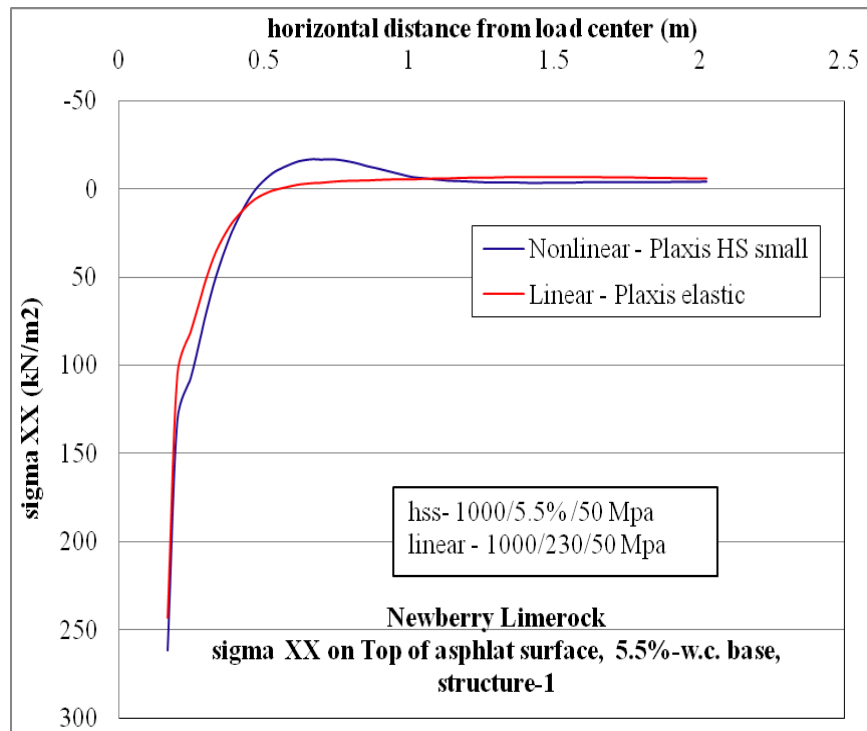


Figure C-12.  $\sigma_{xx}$  at top of AC layer comparison for nonlinear and linear cases, for structure-1 with 5.5% w.c. base layer.

### C.1.2.2 Structure-4

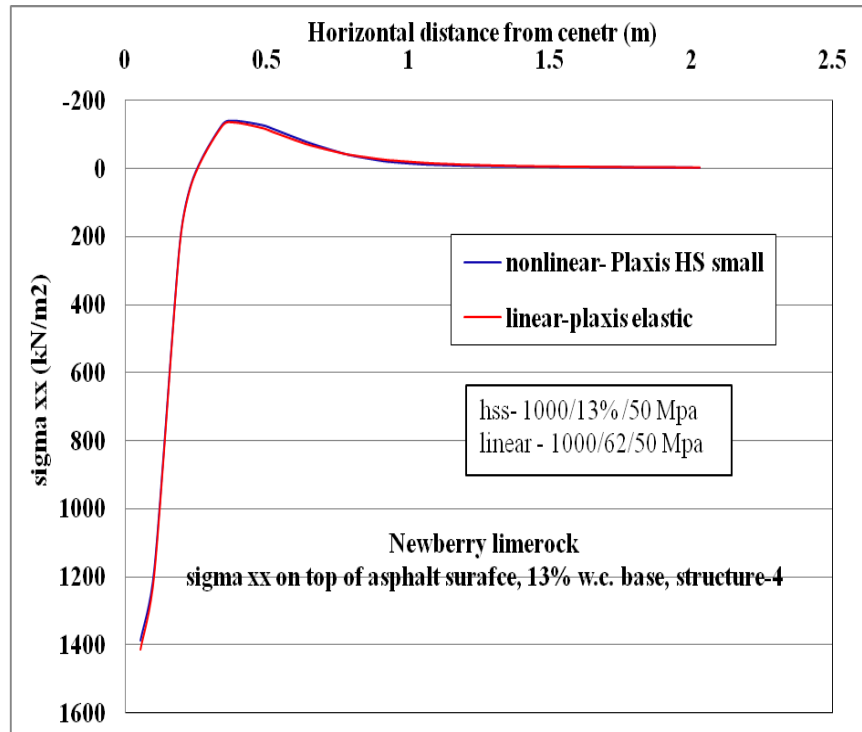


Figure C-13.  $\sigma_{xx}$  at top of AC layer comparison for nonlinear and linear cases, for structure-4 with 13% w.c. base layer.

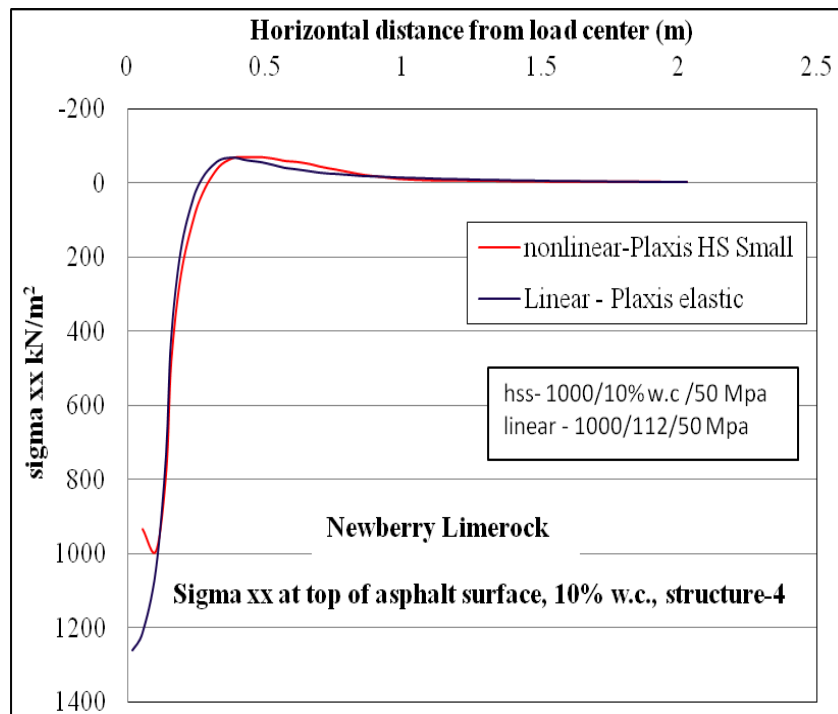


Figure C-14.  $\sigma_{xx}$  at top of AC layer comparison for nonlinear and linear cases, for structure-4 with 10% w.c. base layer.

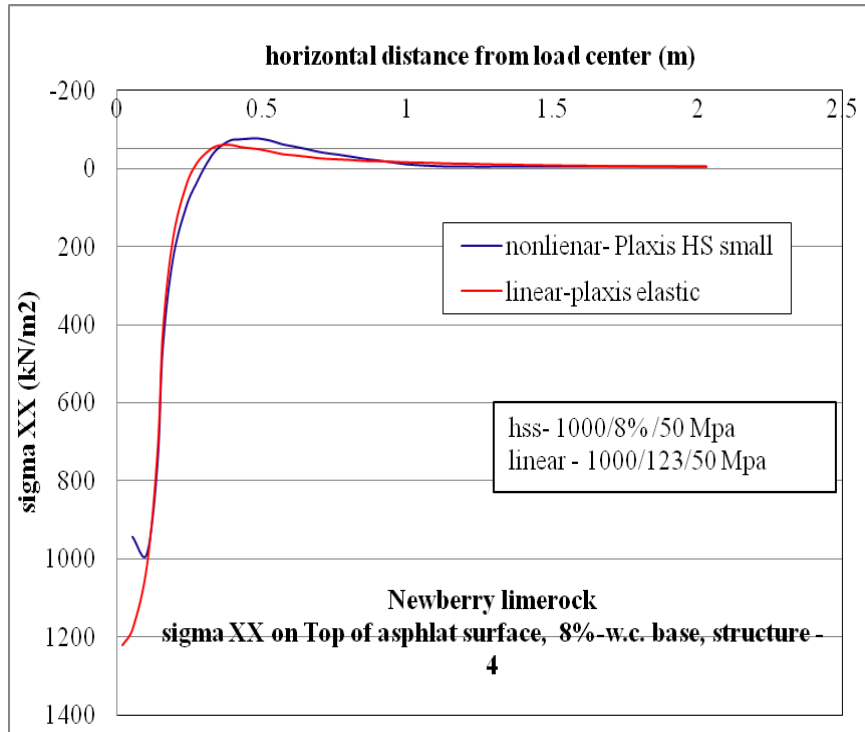


Figure C-15.  $\sigma_{xx}$  at top of AC layer comparison for nonlinear and linear cases, for structure-4 with 8% w.c. base layer.

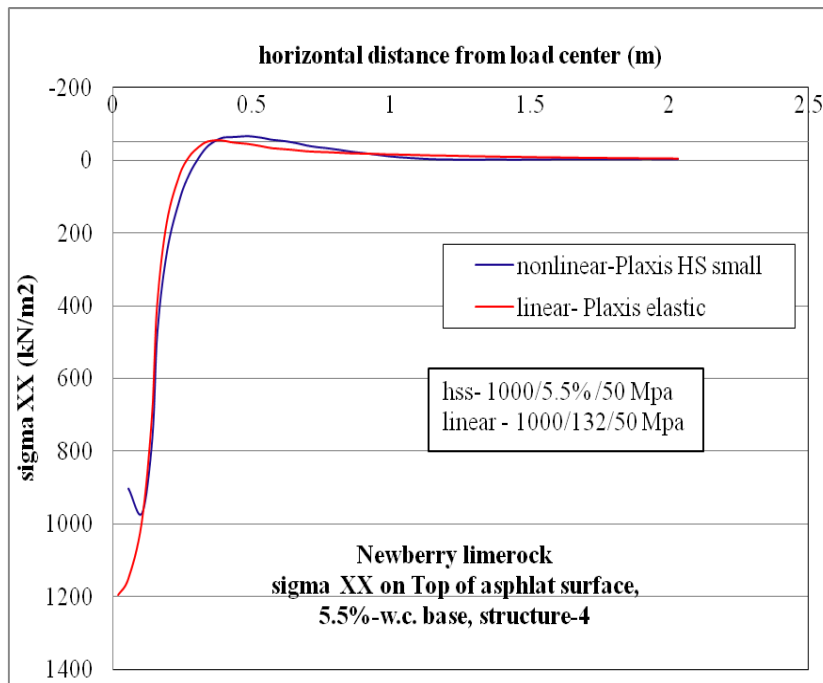


Figure C-16.  $\sigma_{xx}$  at top of AC layer comparison for nonlinear and linear cases, for structure-4 with 5.5% w.c. base layer.

### C.1.3 Horizontal Strain ( $\epsilon_{xx}$ , Tensile Strain) at Top of AC Layer

#### C.1.3.1 Structure-1

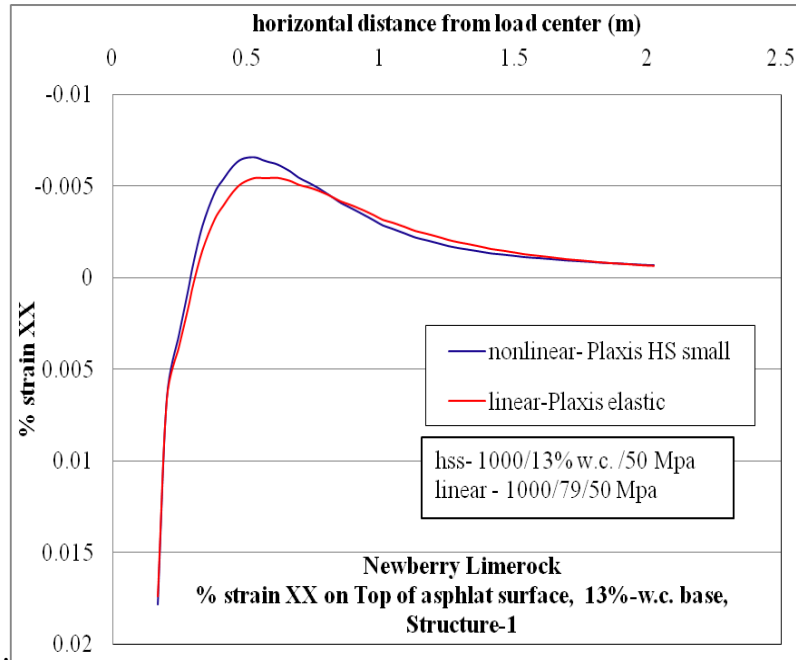


Figure C-17.  $\epsilon_{xx}$  at top of AC layer comparison for nonlinear and linear cases, for structure-1 with 13% w.c. base layer.

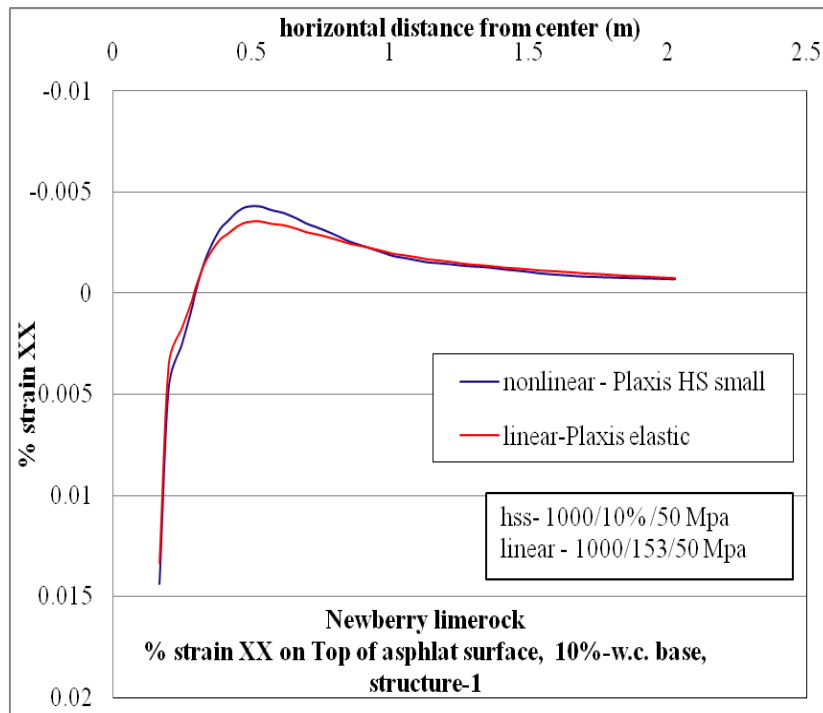


Figure C-18.  $\epsilon_{xx}$  at top of AC layer comparison for nonlinear and linear cases, for structure-1 with 10% w.c. base layer.

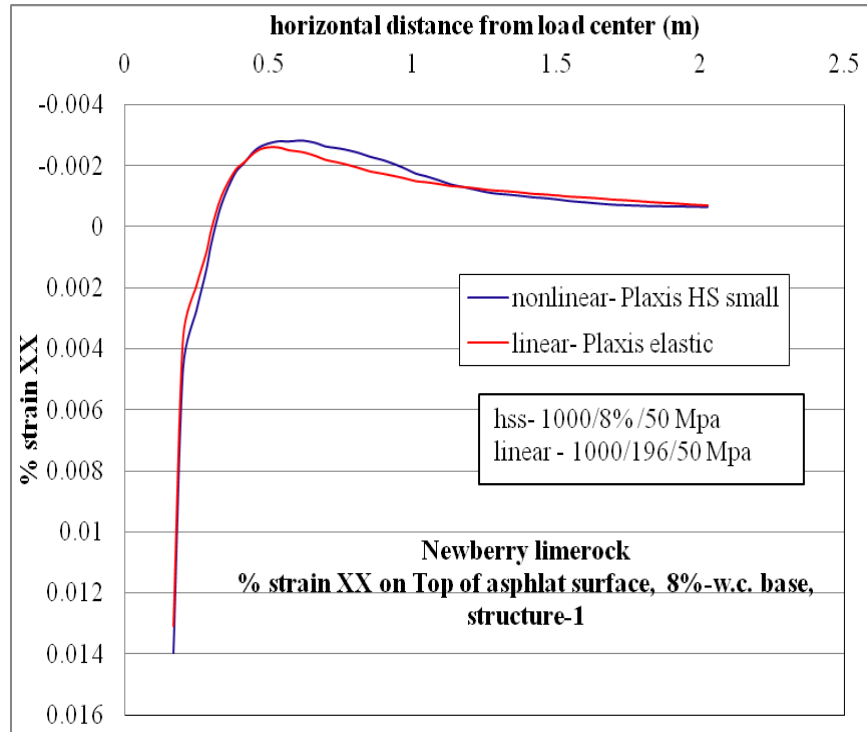


Figure C-19.  $\epsilon_{xx}$  at top of AC layer comparison for nonlinear and linear cases, for structure-1 with 8% w.c. base layer.

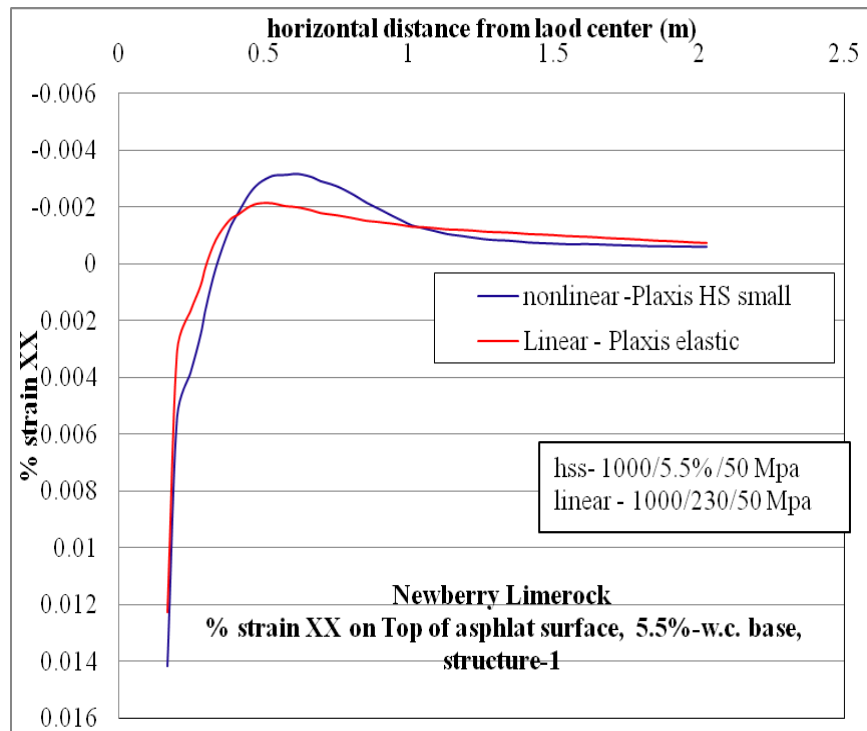


Figure C-20.  $\epsilon_{xx}$  at top of AC layer comparison for nonlinear and linear cases, for structure-1 with 5.5% w.c. base layer.

### C.1.3.2 Structure-4

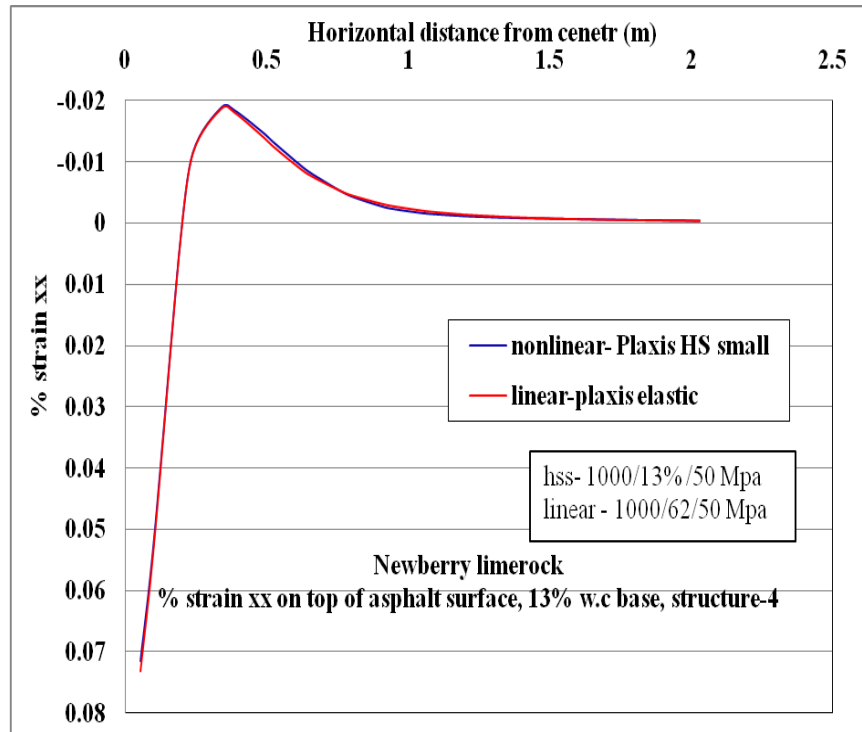


Figure C-21.  $\epsilon_{xx}$  at top of AC layer comparison for nonlinear and linear cases, for structure-4 with 13% w.c. base layer.

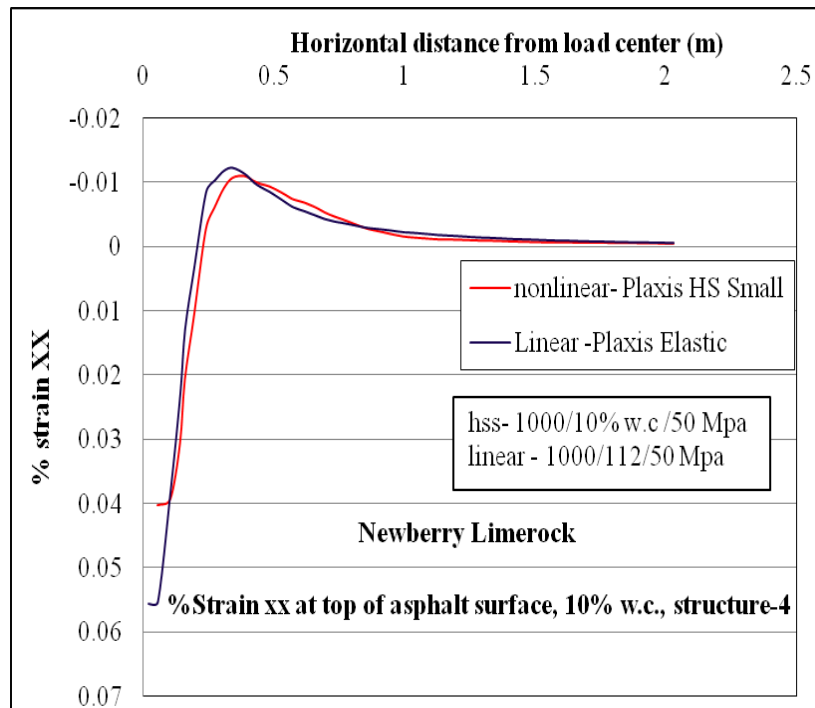


Figure C-22.  $\epsilon_{xx}$  at top of AC layer comparison for nonlinear and linear cases, for structure-4 with 10% w.c. base layer.

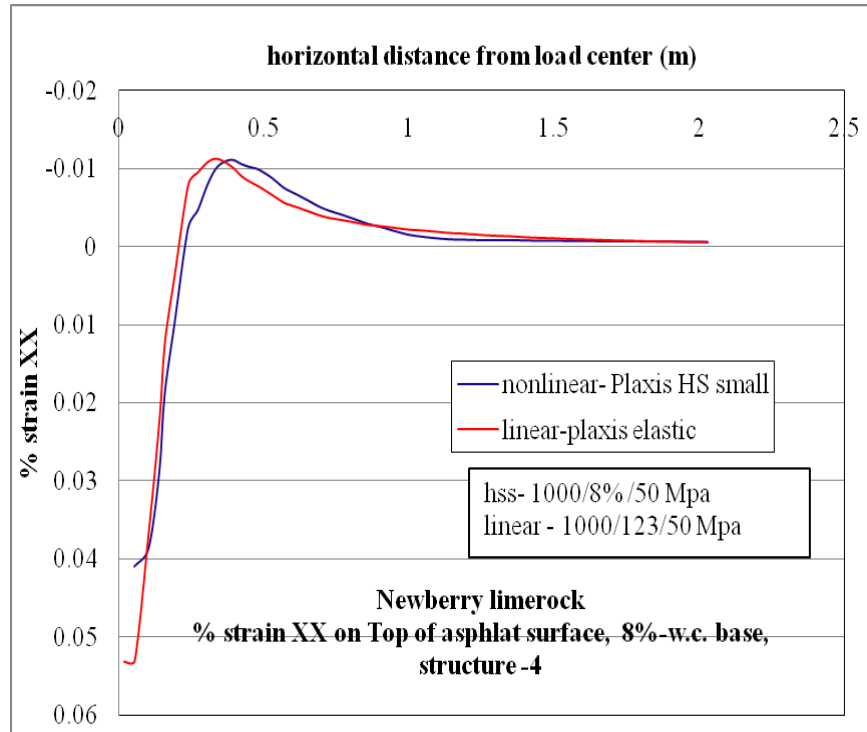


Figure C-23.  $\epsilon_{xx}$  at top of AC layer comparison for nonlinear and linear cases, for structure-4 with 8% w.c. base layer

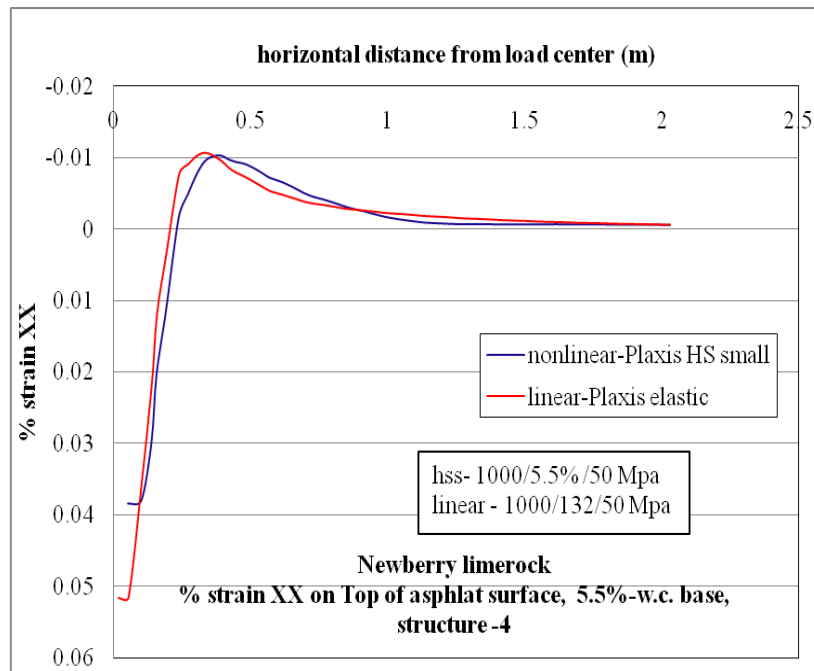


Figure C-24.  $\epsilon_{xx}$  at top of AC layer comparison for nonlinear and linear cases, for structure-4 with 5.5% w.c. base layer.

## C.1.4 Horizontal Stress ( $\sigma_{xx}$ , Tensile Stress) at Bottom of AC Layer

### C.1.4.1 Structure-1

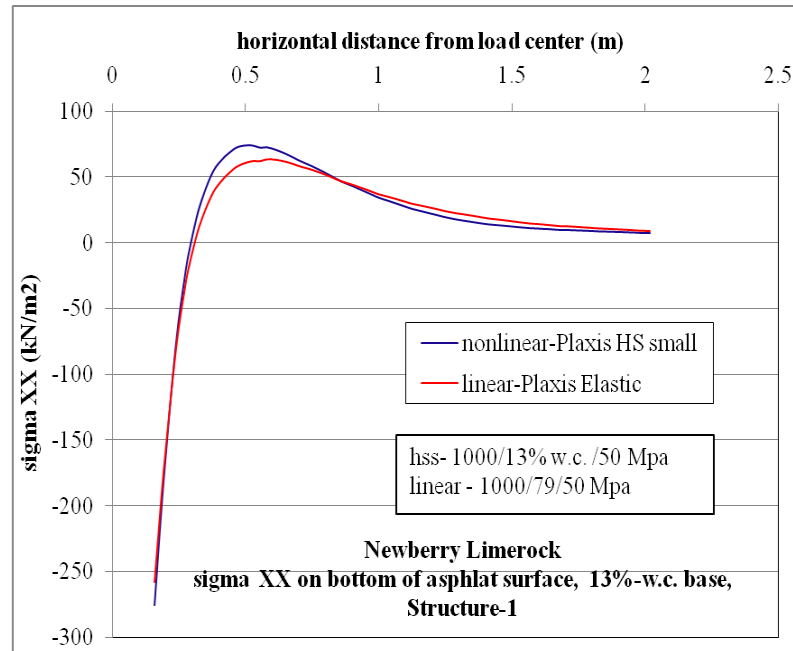


Figure C-25.  $\sigma_{xx}$  at bottom of AC layer comparison for nonlinear and linear cases, for structure-1 with 13% w.c. base layer.

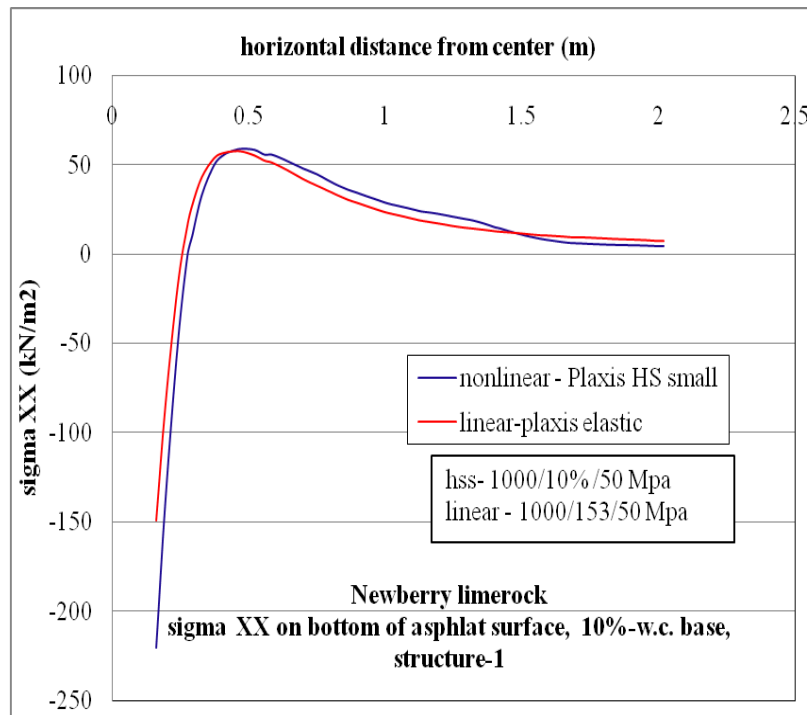


Figure C-26.  $\sigma_{xx}$  at bottom of AC layer comparison for nonlinear and linear cases, for structure-1 with 10% w.c. base layer.

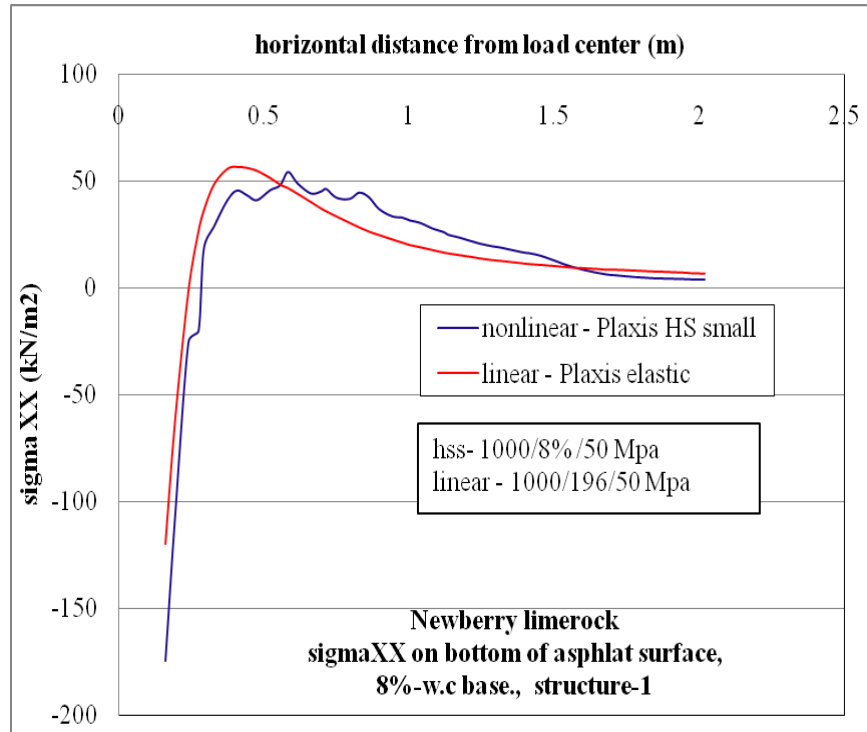


Figure C-27.  $\sigma_{xx}$  at bottom of AC layer comparison for nonlinear and linear cases, for structure-1 with 8% w.c. base layer.

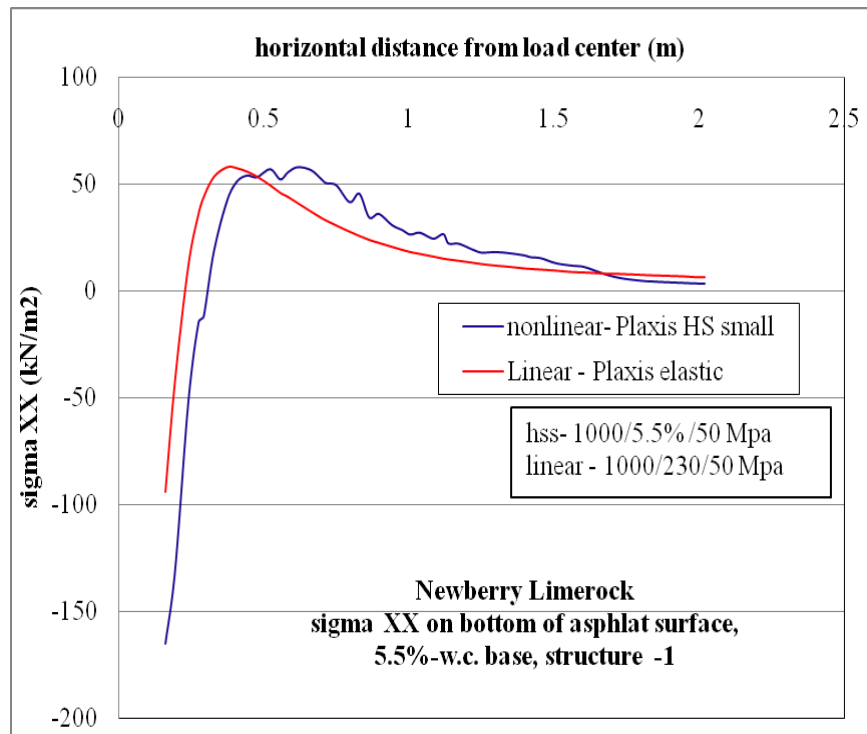


Figure C-28.  $\sigma_{xx}$  at bottom of AC layer comparison for nonlinear and linear cases, for structure-1 with 5.5% w.c. base layer.

### C.1.4.2 Structure-4

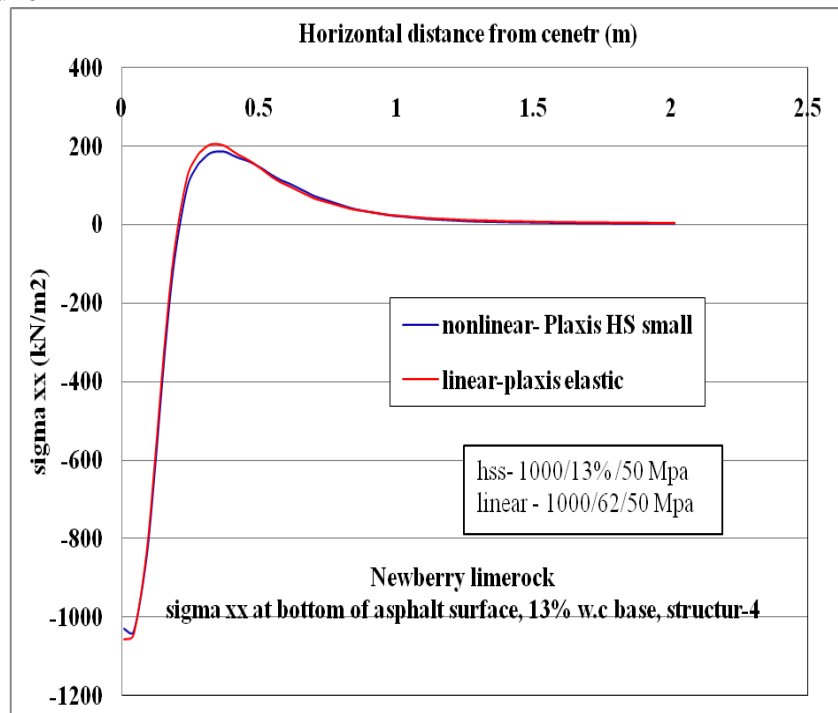


Figure C-29.  $\sigma_{xx}$  at bottom of AC layer comparison for nonlinear and linear cases, for structure-4 with 13% w.c. base layer.

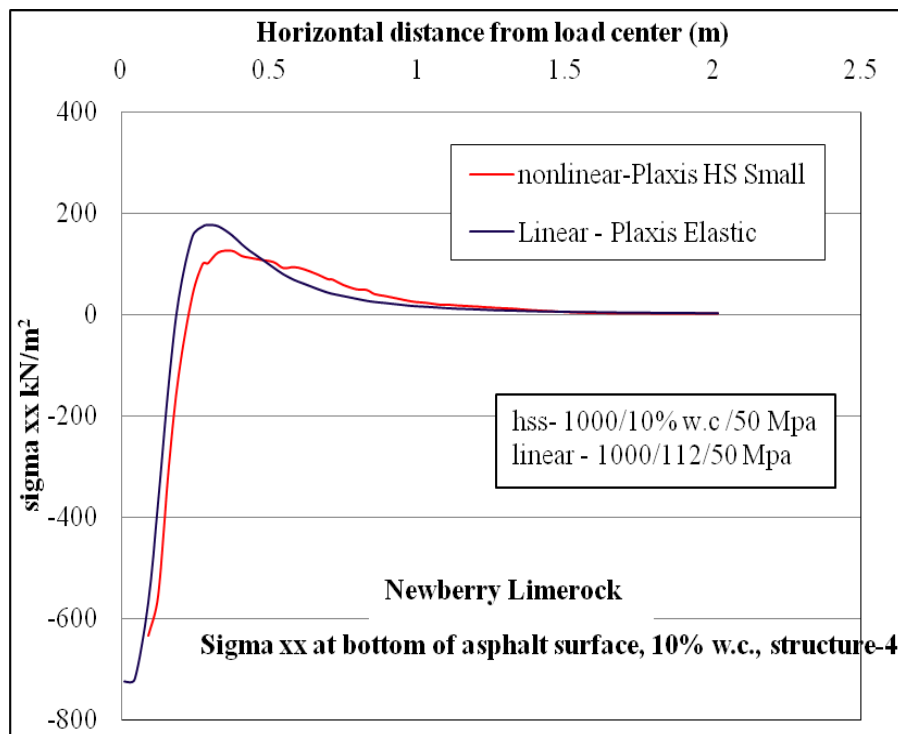


Figure C-30.  $\sigma_{xx}$  at bottom of AC layer comparison for nonlinear and linear cases, for structure-4 with 10% w.c. base layer.

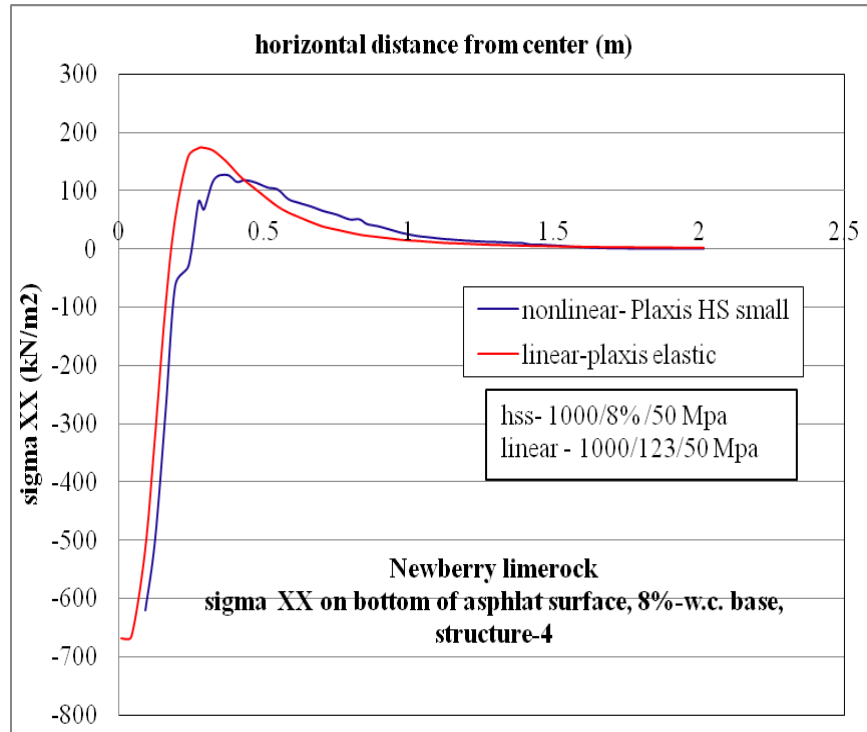


Figure C-31.  $\sigma_{xx}$  at bottom of AC layer comparison for nonlinear and linear cases, for structure-4 with 8% w.c. base layer.

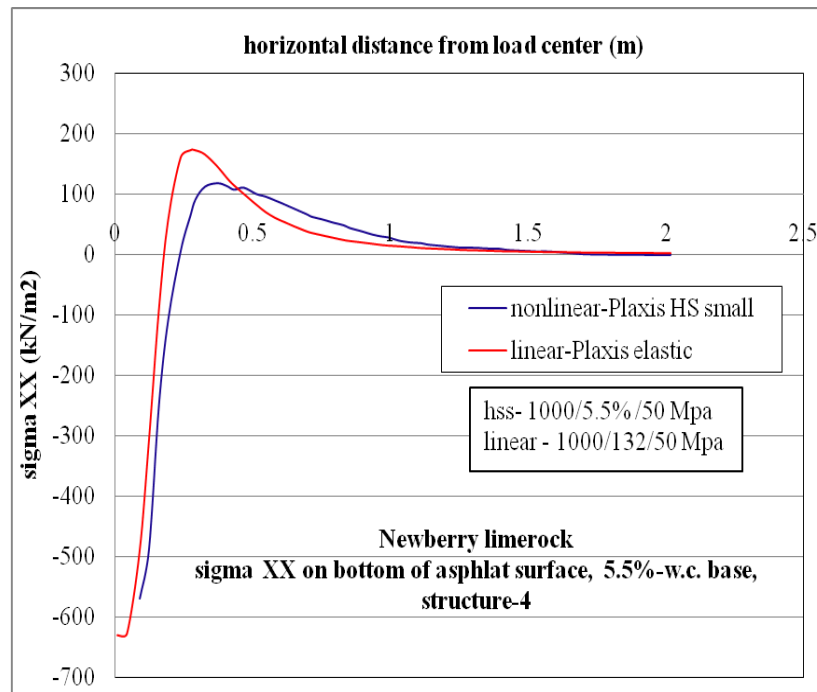


Figure C-32.  $\sigma_{xx}$  at bottom of AC layer comparison for nonlinear and linear cases, for structure-4 with 5.5% w.c. base layer.

### C.1.5 Horizontal Strain ( $\epsilon_{xx}$ , Tensile Strain) at Bottom of AC layer

#### C.1.5.1 Structure-1

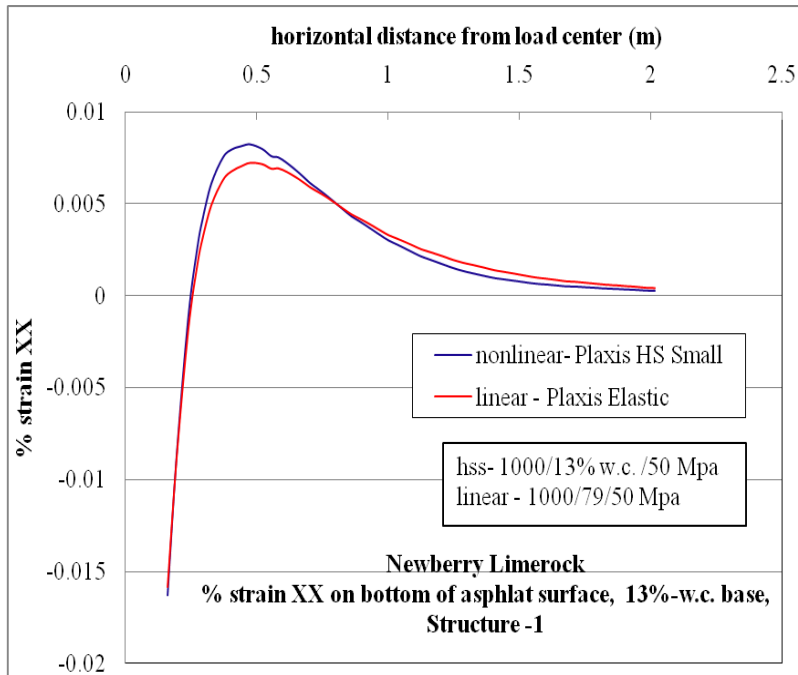


Figure C-33.  $\epsilon_{xx}$  at bottom of AC layer comparison for nonlinear and linear cases, for structure-1 with 13% w.c. base layer.

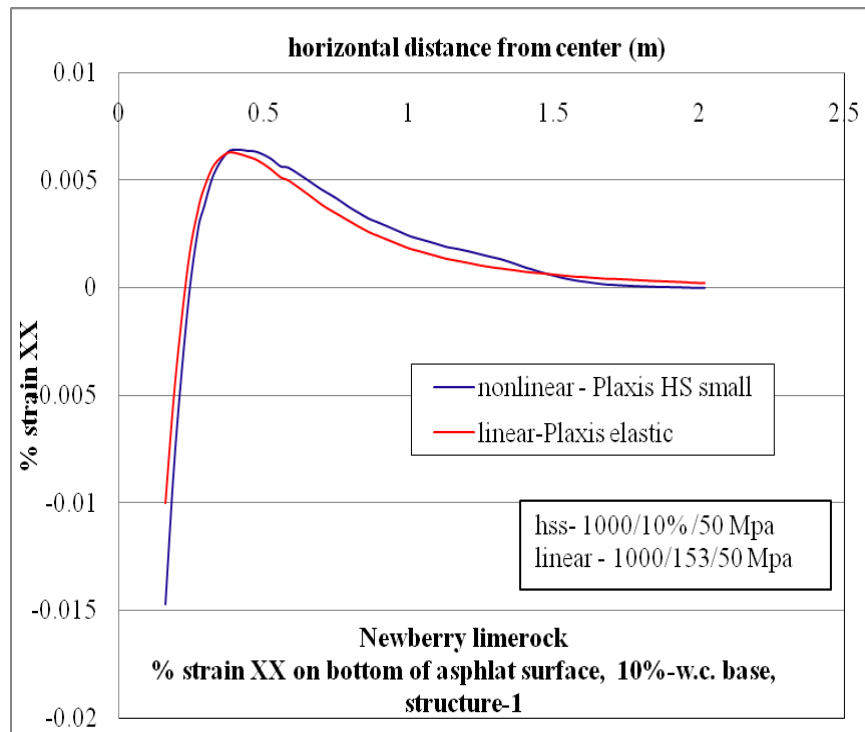


Figure C-34.  $\epsilon_{xx}$  at bottom of AC layer comparison for nonlinear and linear cases, for structure-1 with 10% w.c. base layer.

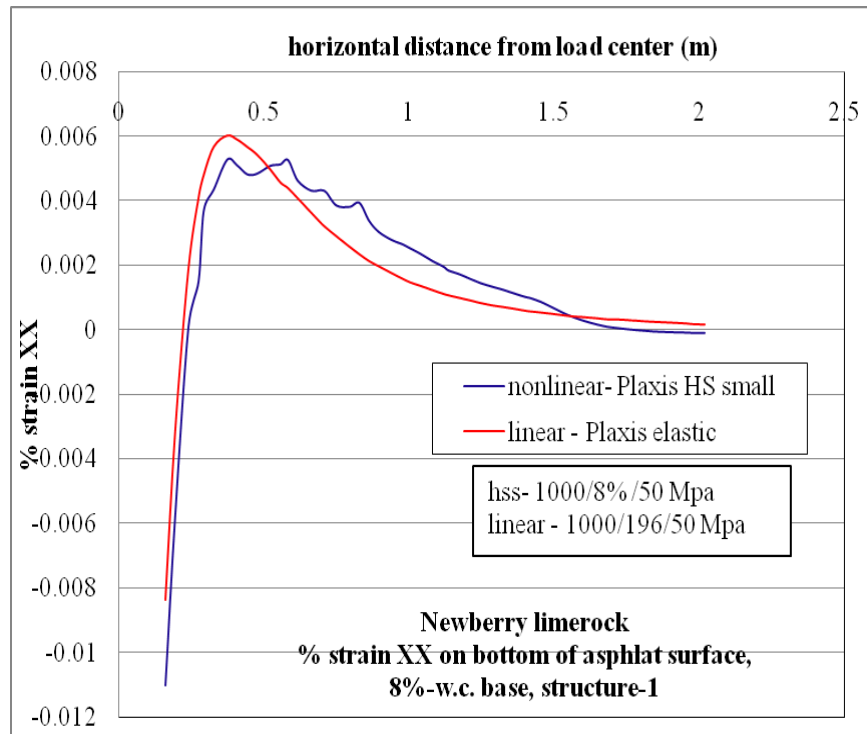


Figure C-35.  $\epsilon_{xx}$  at bottom of AC layer comparison for nonlinear and linear cases, for structure-1 with 8% w.c. base layer.

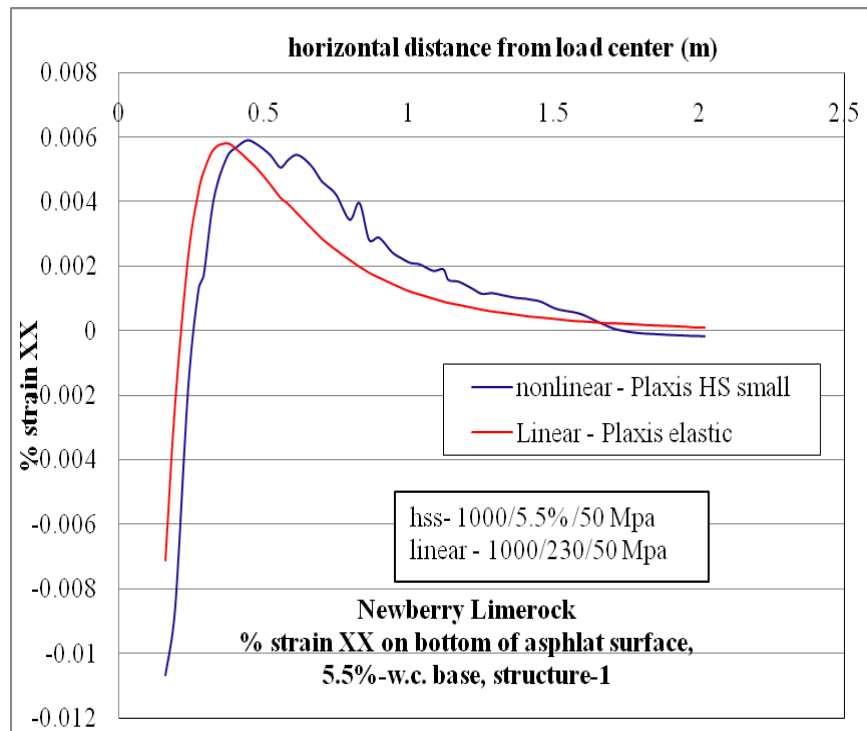


Figure C-36.  $\epsilon_{xx}$  at bottom of AC layer comparison for nonlinear and linear cases, for structure-1 with 5.5% w.c. base layer.

### C.1.5.2 Structure-4

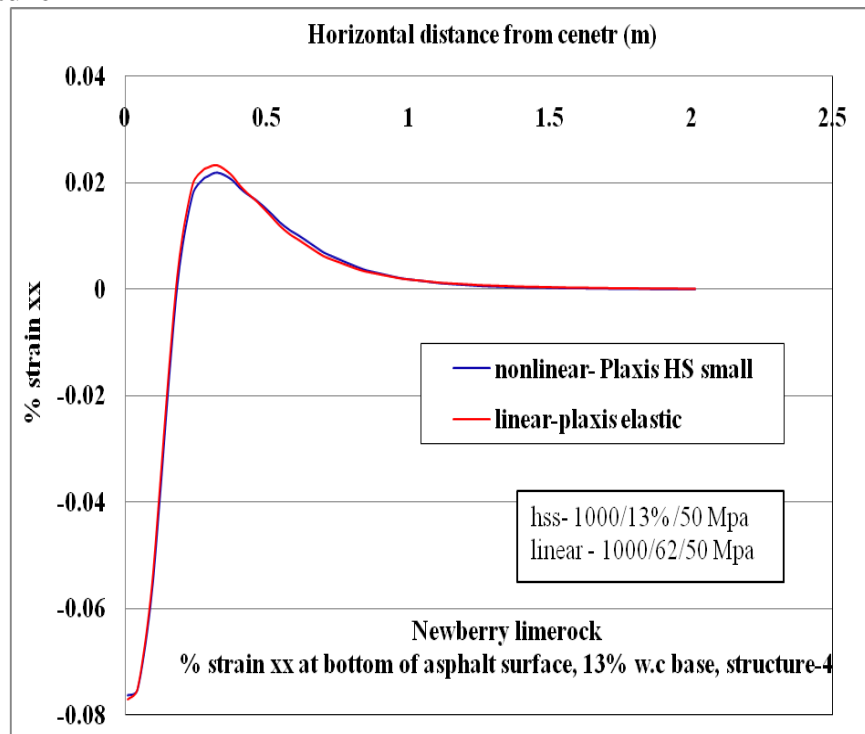


Figure C-37.  $\epsilon_{xx}$  at bottom of AC layer comparison for nonlinear and linear cases, for structure-4 with 13% w.c. base layer.

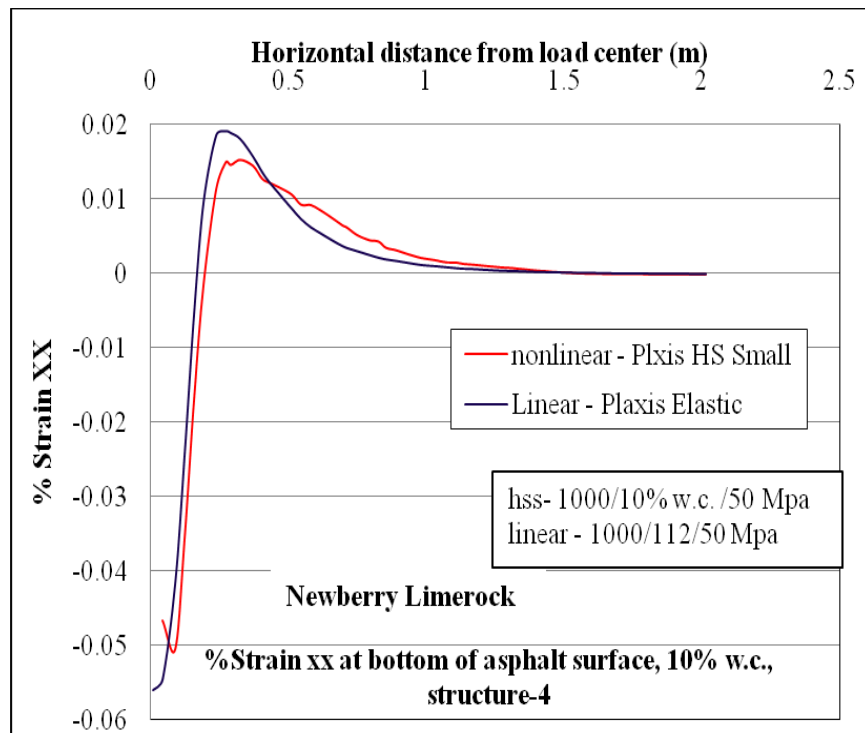


Figure C-38.  $\epsilon_{xx}$  at bottom of AC layer comparison for nonlinear and linear cases, for structure-4 with 10% w.c. base layer.

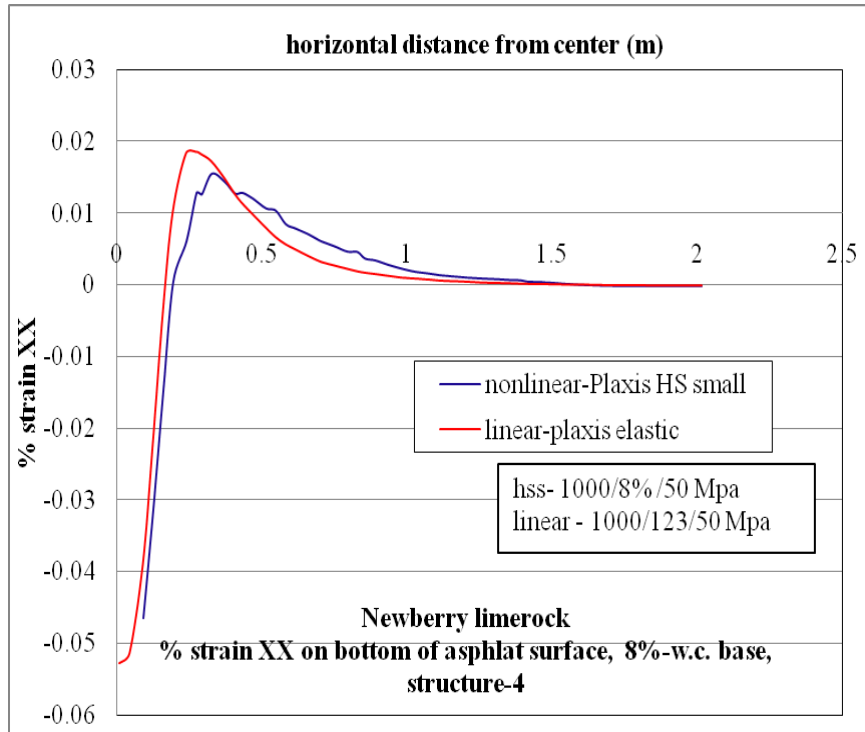


Figure C-39.  $\epsilon_{xx}$  at bottom of AC layer comparison for nonlinear and linear cases, for structure-4 with 8% w.c. base layer.

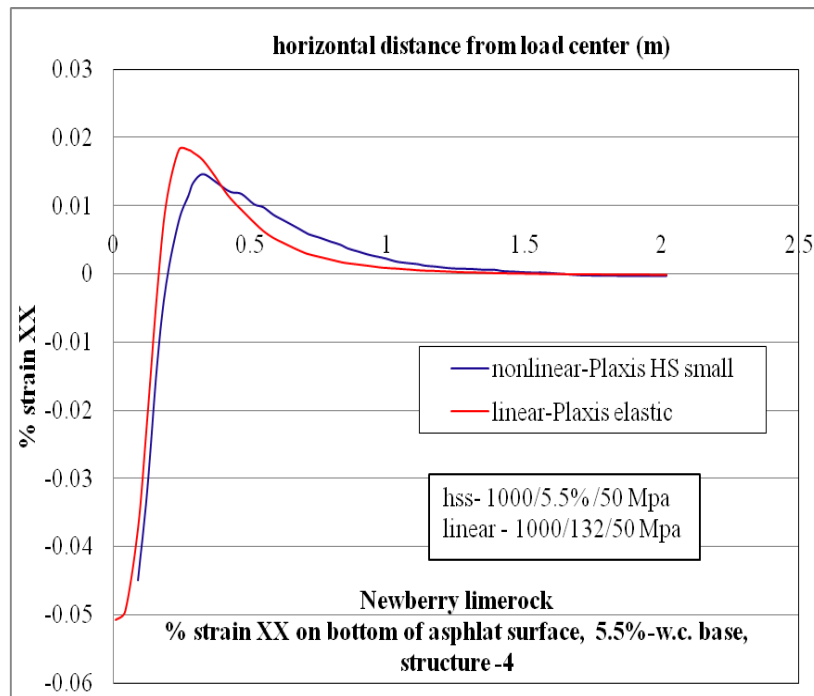


Figure C-40.  $\epsilon_{xx}$  at bottom of AC layer comparison for nonlinear and linear cases, for structure-4 with 5.5% w.c. base layer.

## C.1.6 Vertical stress ( $\sigma_{yy}$ , compressive stress) at top of base layer

### C.1.6.1 Structure-1

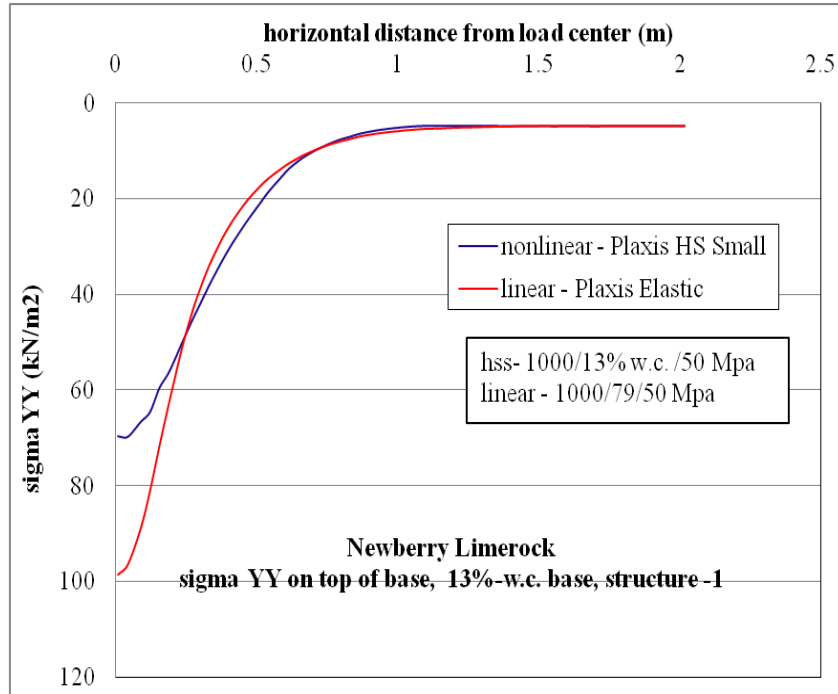


Figure C-41.  $\sigma_{yy}$  vertical stress at top of base layer comparison for nonlinear and linear cases, for structure-1 with 13% w.c. base layer.

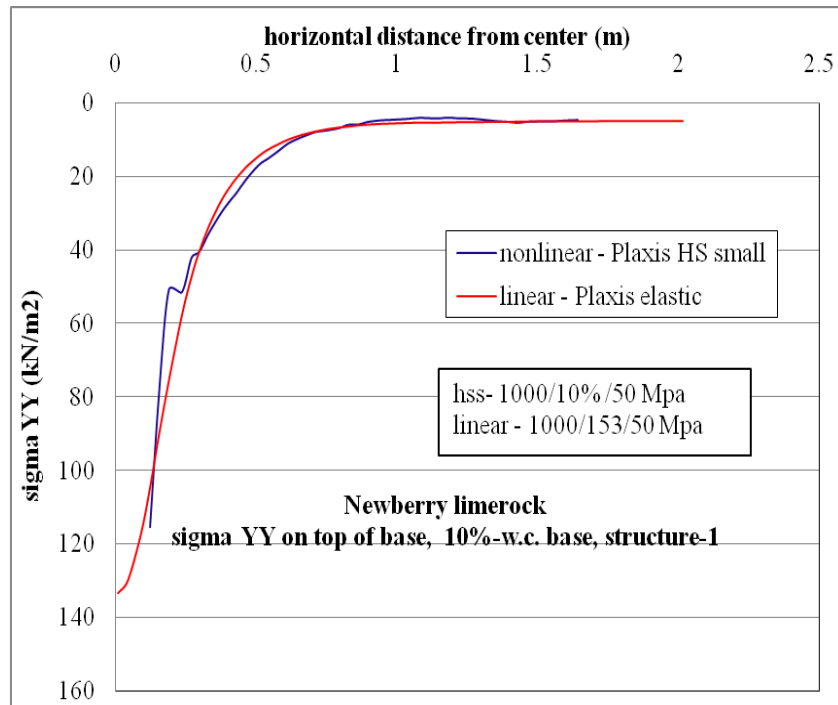


Figure C-42.  $\sigma_{yy}$  vertical stress at top of base layer comparison for nonlinear and linear cases, for structure-1 with 10% w.c. base layer.

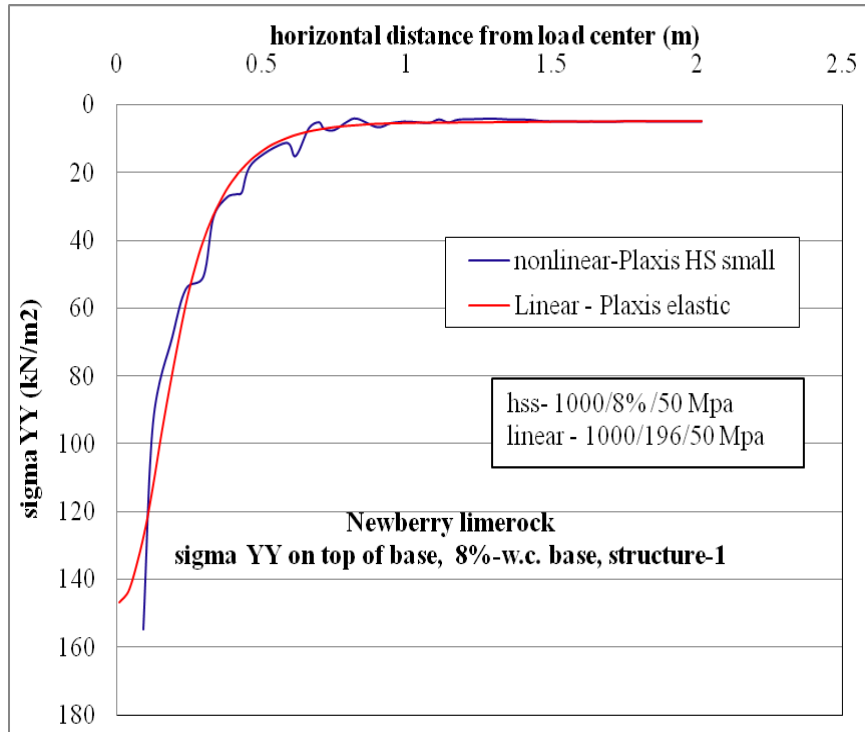


Figure C-43.  $\sigma_{yy}$  vertical stress at top of base layer comparison for nonlinear and linear cases, for structure-1 with 8% w.c. base layer

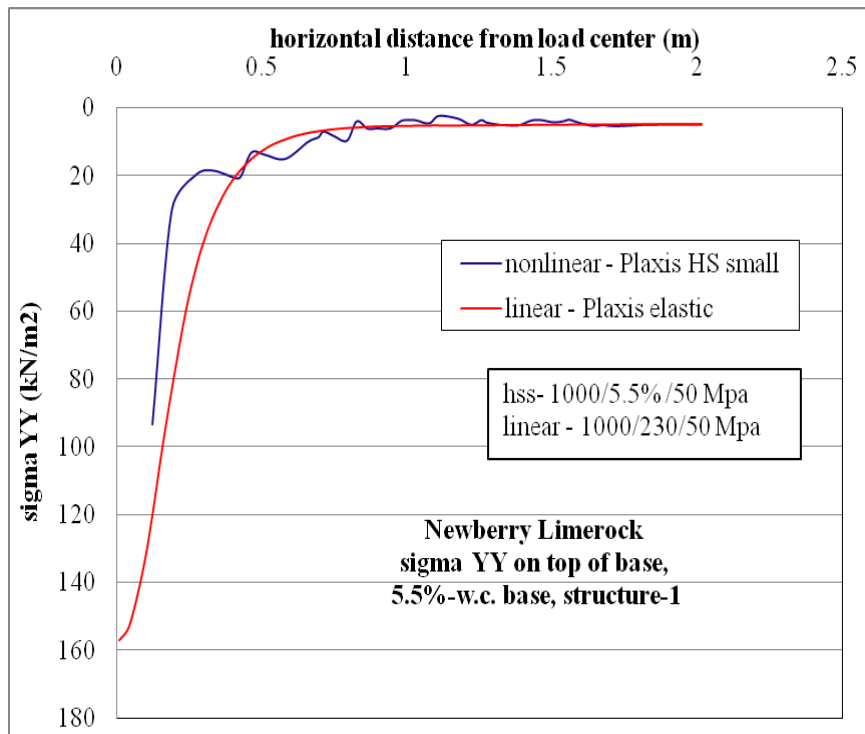


Figure C-44.  $\sigma_{yy}$  vertical stress at top of base layer comparison for nonlinear and linear cases, for structure-1 with 5.5% w.c. base layer.

### C.1.6.2 Structure-4

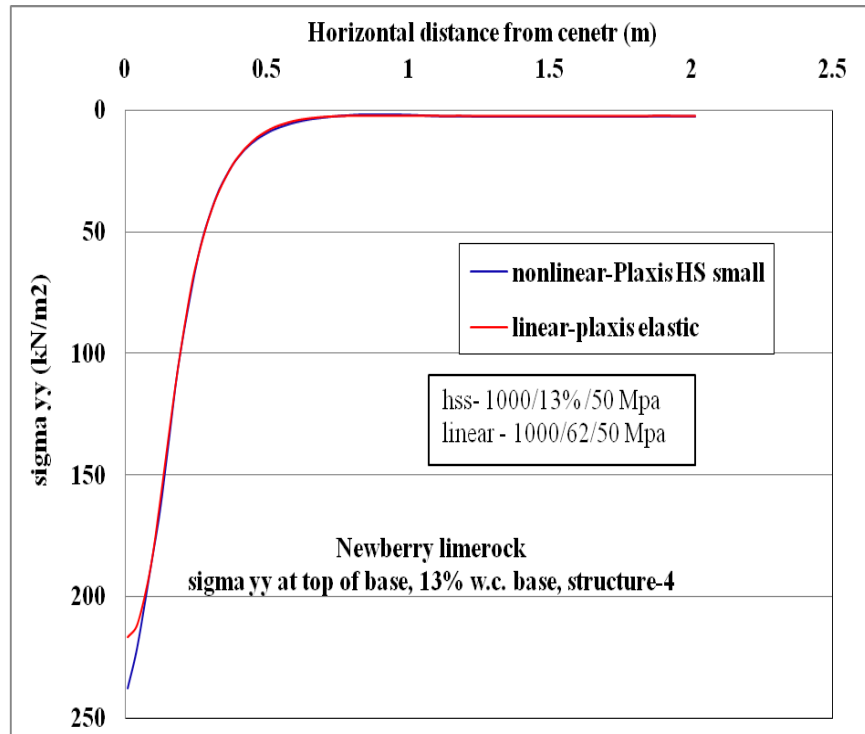


Figure C-45.  $\sigma_{yy}$  at top of base layer comparison for nonlinear and linear cases, for structure-4 with 13% w.c. base layer

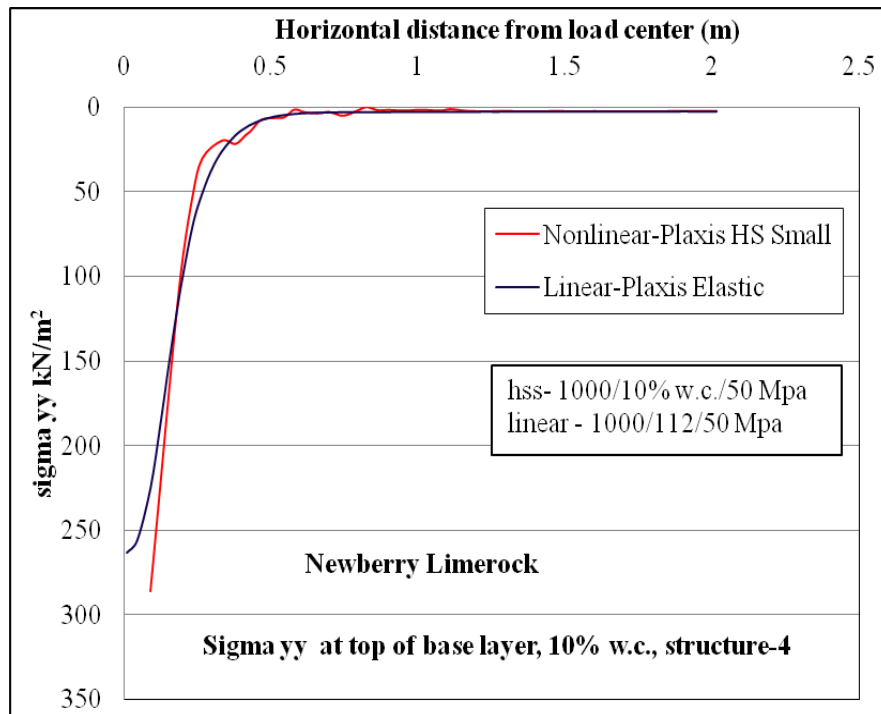


Figure C-46.  $\sigma_{yy}$  vertical stress at top of base layer comparison for nonlinear and linear cases, for structure-4 with 10% w.c. base layer.

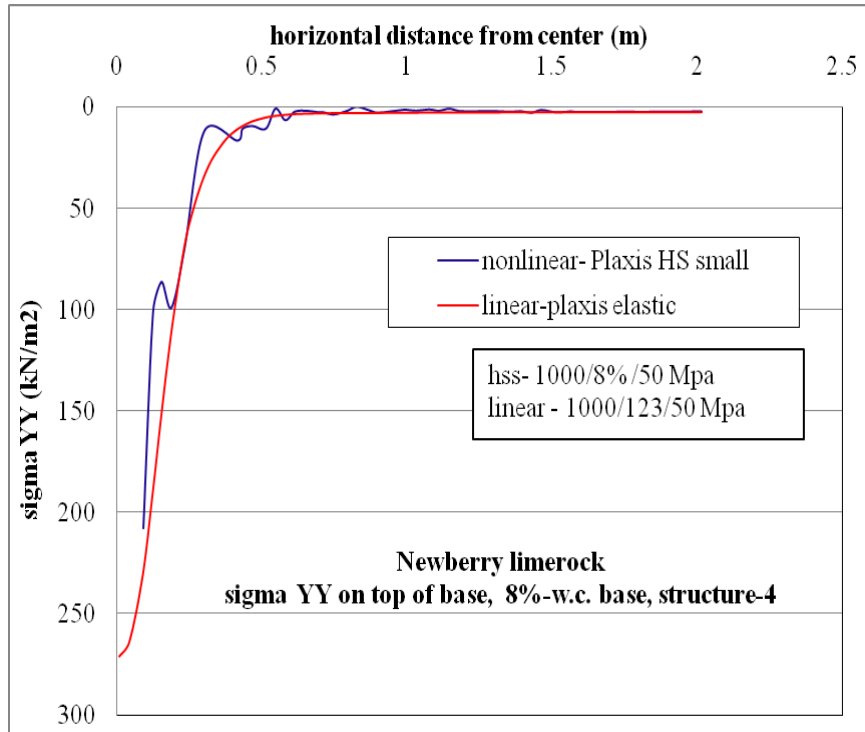


Figure C-47.  $\sigma_{yy}$  vertical stress at top of base layer comparison for nonlinear and linear cases, for structure-4 with 8% w.c. base layer.

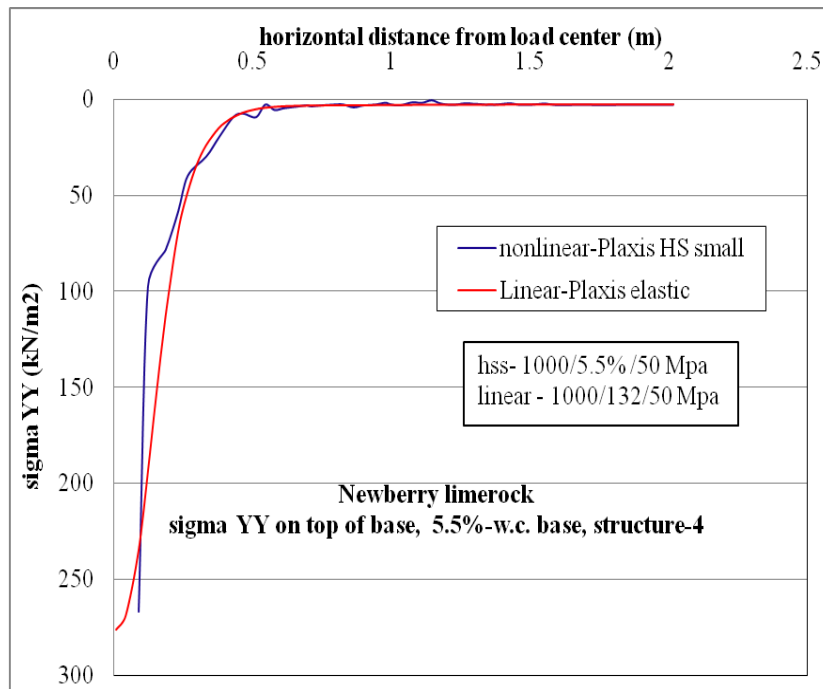


Figure C-48.  $\sigma_{yy}$  vertical stress at top of base layer comparison for nonlinear and linear cases, for structure-4 with 5.5% w.c. base layer.

## C.1.7 Vertical Strain ( $\epsilon_{yy}$ , Compressive Strain) at Top of Base Layer

### C.1.7.1 Structure-1

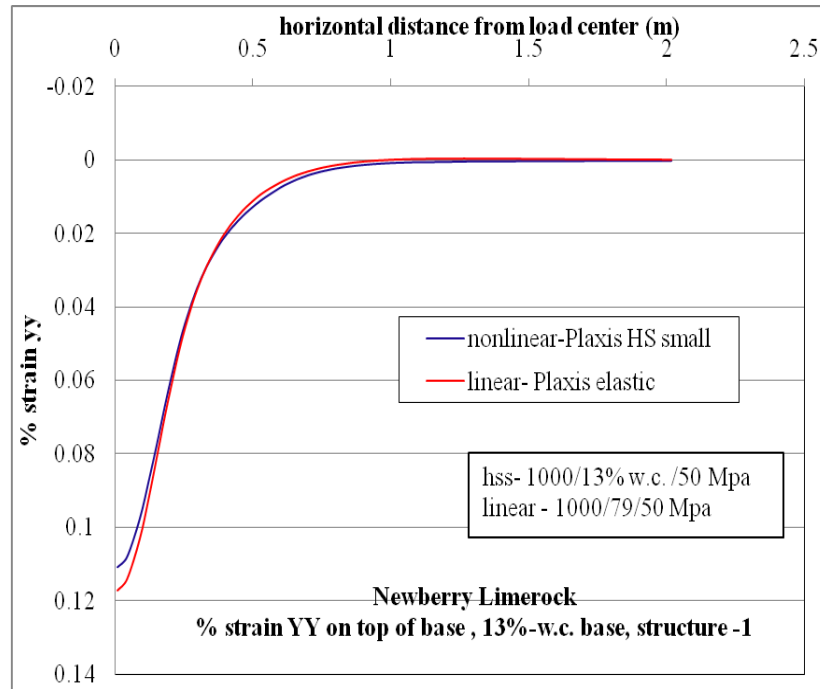


Figure C-49.  $\epsilon_{yy}$  at top of base layer comparison for nonlinear and linear cases, for structure-1 with 13% w.c. base layer.

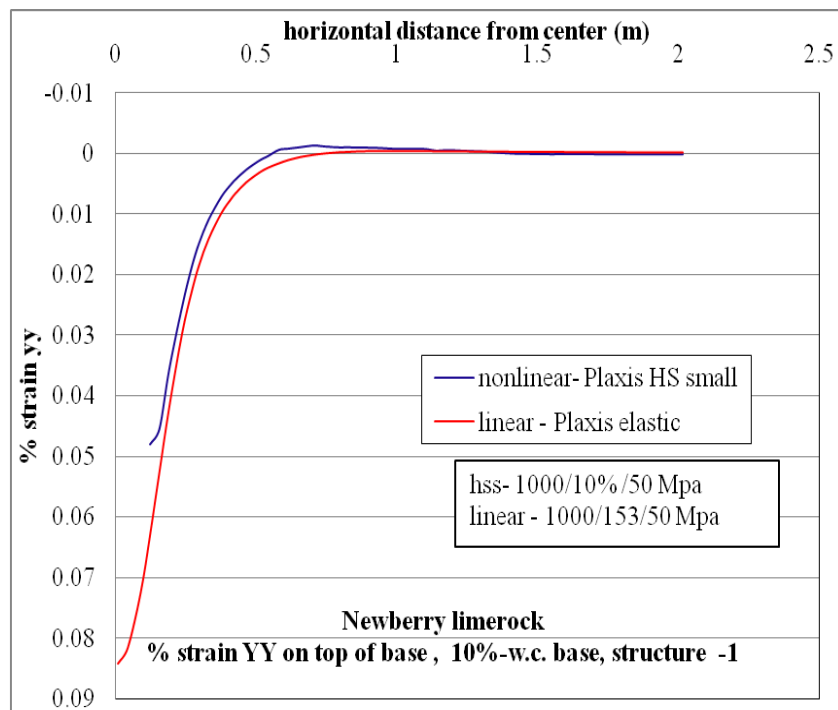


Figure C-50.  $\epsilon_{yy}$  at top of base layer comparison for nonlinear and linear cases, for structure-1 with 10% w.c. base layer.

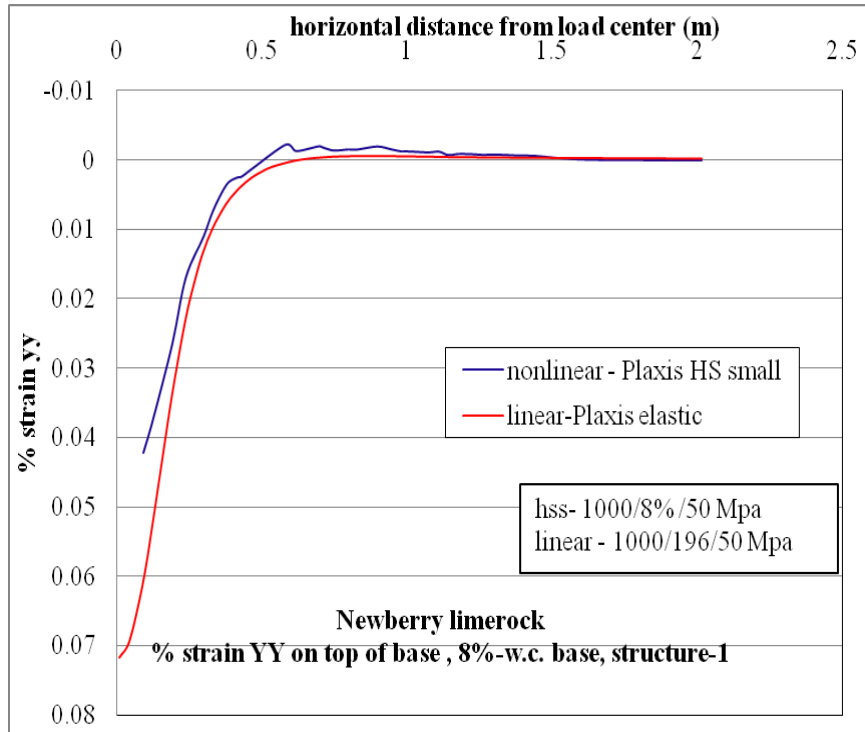


Figure C-51.  $\epsilon_{yy}$  at top of base layer comparison for nonlinear and linear cases, for structure-1 with 8% w.c. base layer.

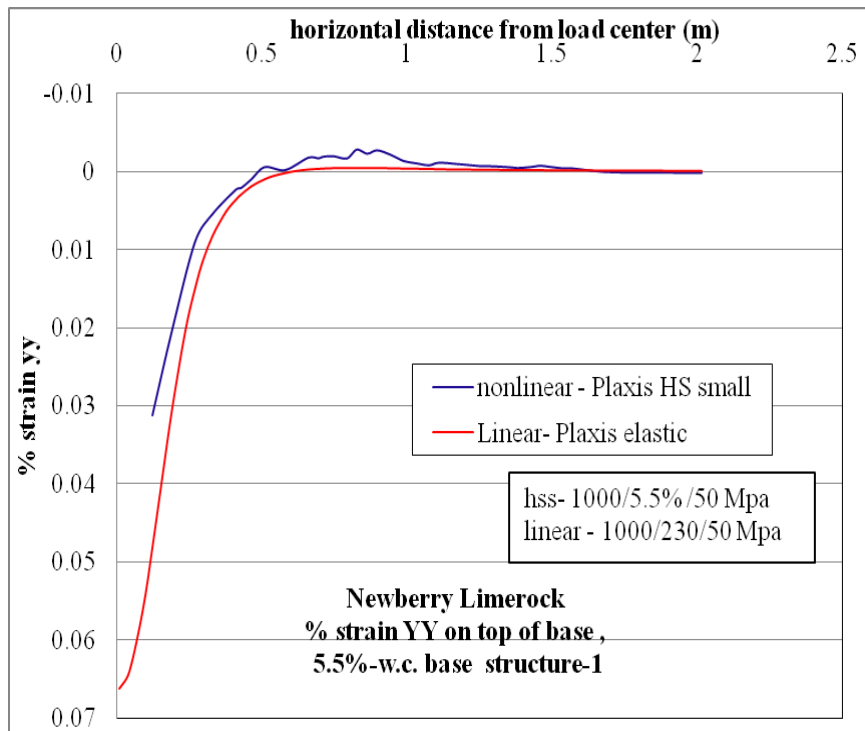


Figure C-52.  $\epsilon_{yy}$  at top of base layer comparison for nonlinear and linear cases, for structure-1 with 5.5% w.c. base layer.

### C.1.7.2 Structure-4

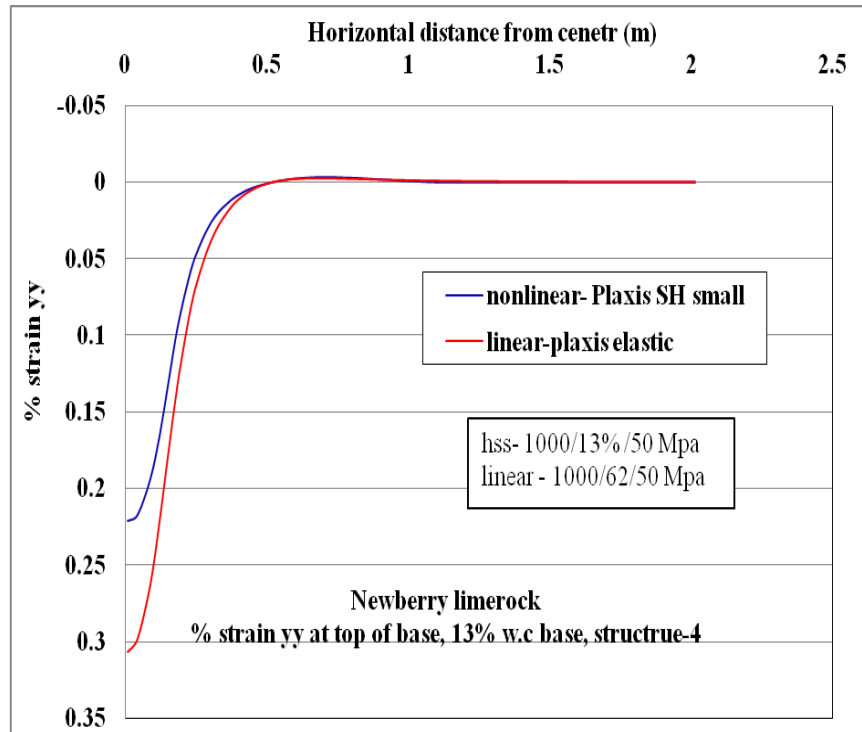


Figure C-53.  $\epsilon_{yy}$  at top of base layer comparison for nonlinear and linear cases, for structure-4 with 13% w.c. base layer.

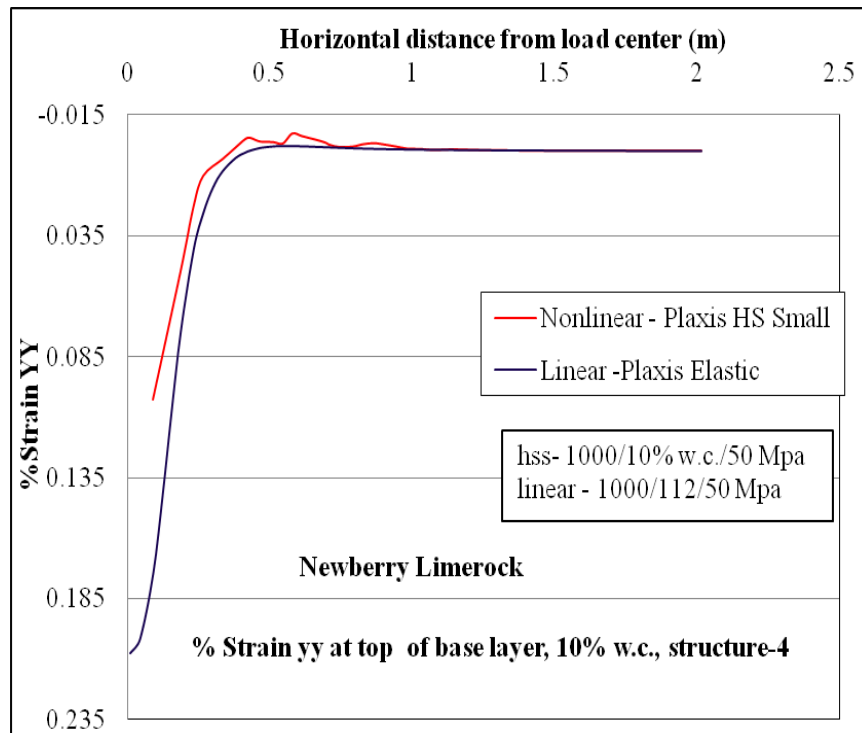


Figure C-54.  $\epsilon_{yy}$  at top of base layer comparison for nonlinear and linear cases, for structure-4 with 10% w.c. base layer.

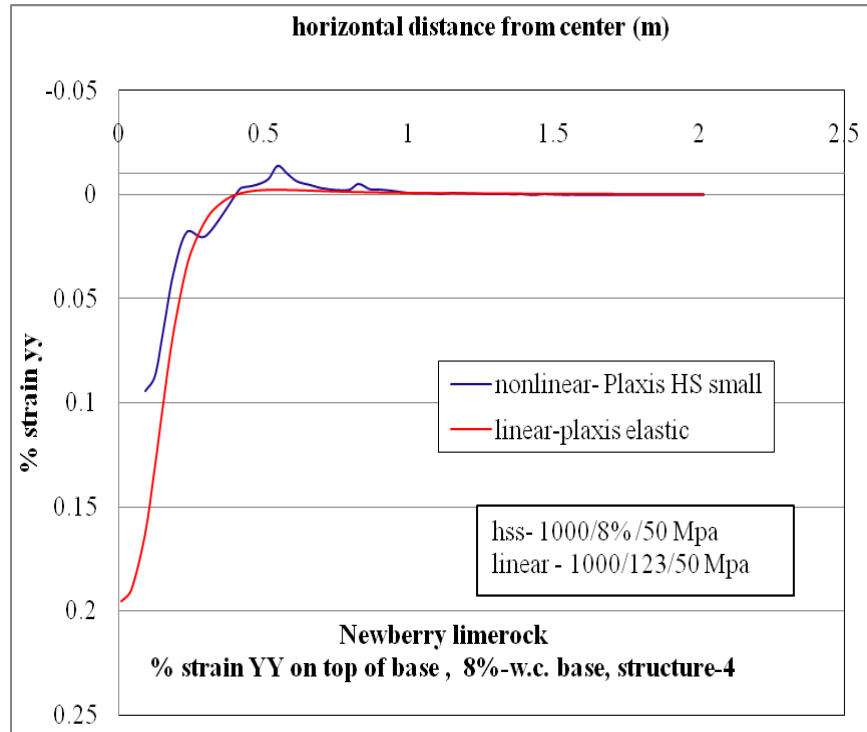


Figure C-55.  $\epsilon_{yy}$  at top of base layer comparison for nonlinear and linear cases, for structure-4 with 8% w.c. base layer.

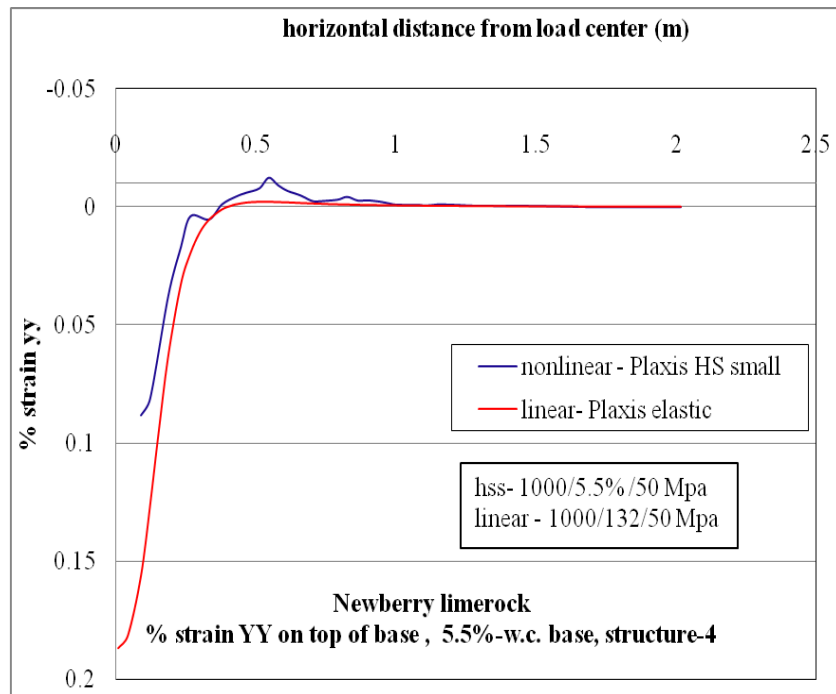


Figure C-56.  $\epsilon_{yy}$  at top of base layer comparison for nonlinear and linear cases, for structure-4 with 5.5% w.c. base layer.

## C.1.8 Vertical Stress ( $\sigma_{yy}$ , Compressive Stress) at Bottom of Base Layer

### C.1.8.1 Structure-1

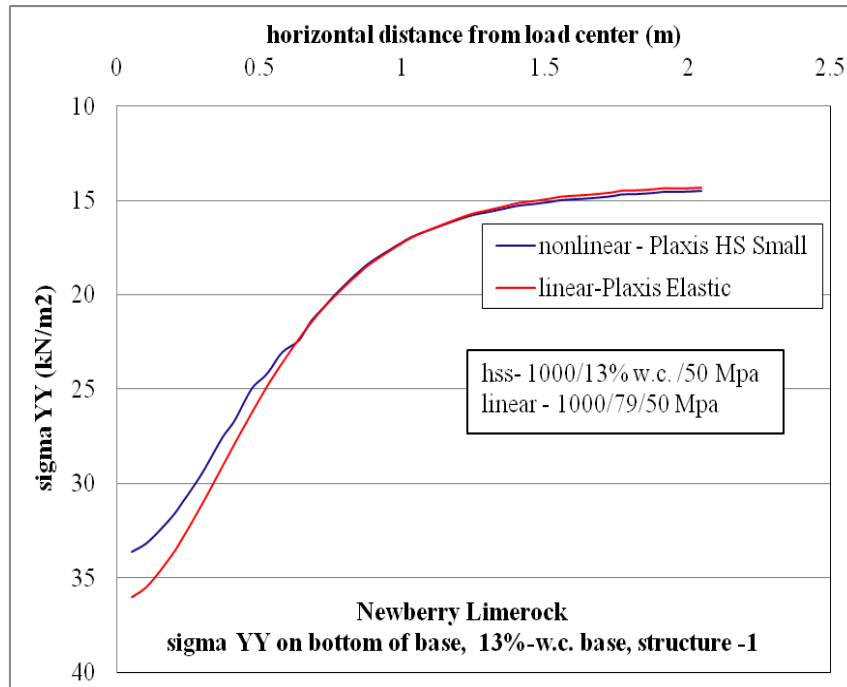


Figure C-57.  $\sigma_{yy}$  at bottom of base layer comparison for nonlinear and linear cases, for structure-1 with 13% w.c. base layer.

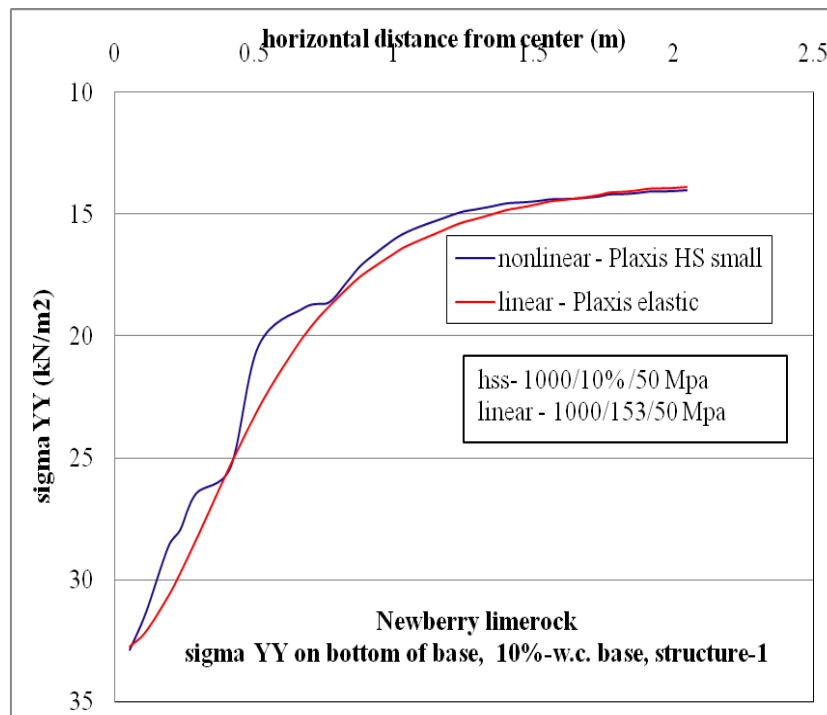


Figure C-58.  $\sigma_{yy}$  at bottom of base layer comparison for nonlinear and linear cases, for structure-1 with 10% w.c. base layer.

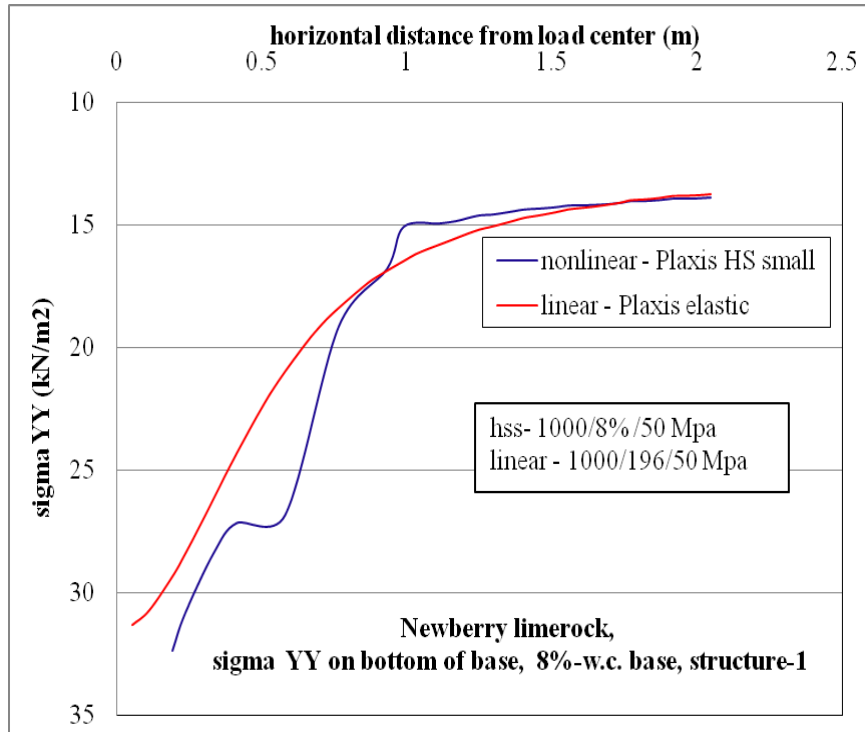


Figure C-59.  $\sigma_{yy}$  at bottom of base layer comparison for nonlinear and linear cases, for structure-1 with 8% w.c. base layer.

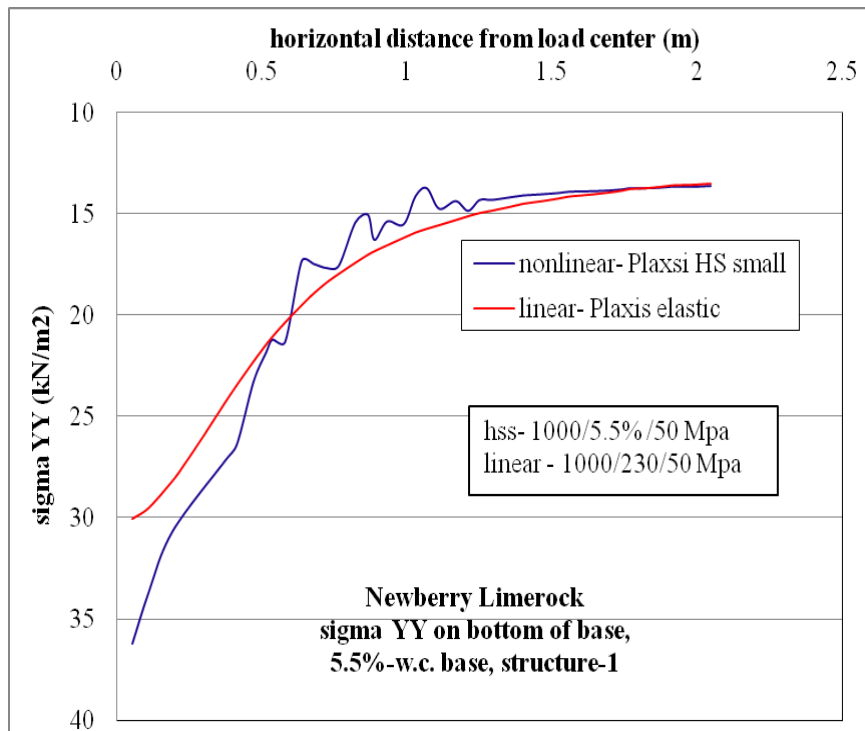


Figure C-60.  $\sigma_{yy}$  at bottom of base layer comparison for nonlinear and linear cases, for structure-1 with 5.5% w.c. base layer.

### C.1.8.2 Structure-4

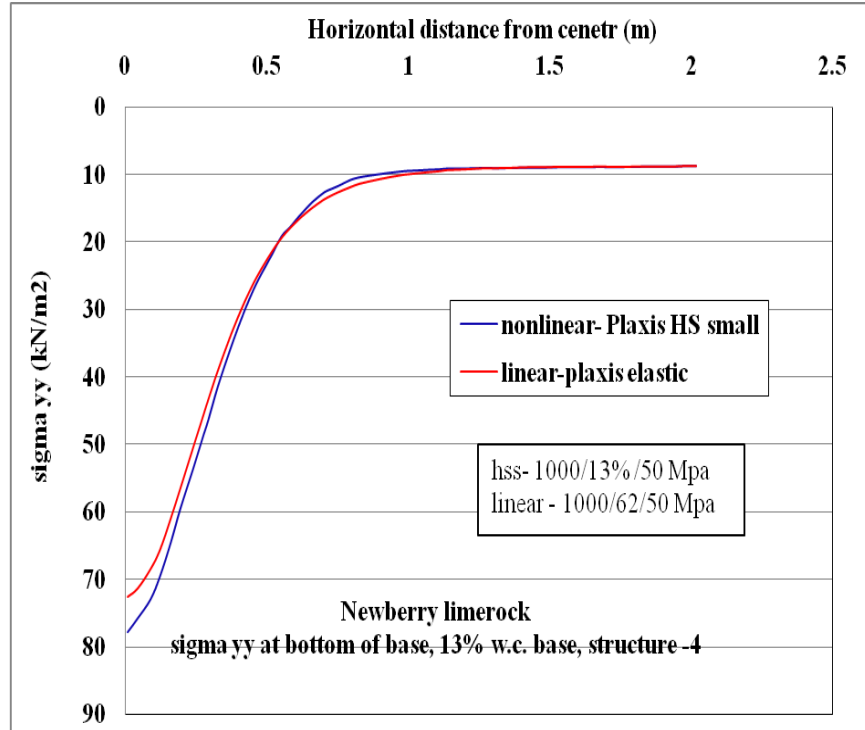


Figure C-61.  $\sigma_{yy}$  at bottom of base layer comparison for nonlinear and linear cases, for structure-4 with 13% w.c. base layer.

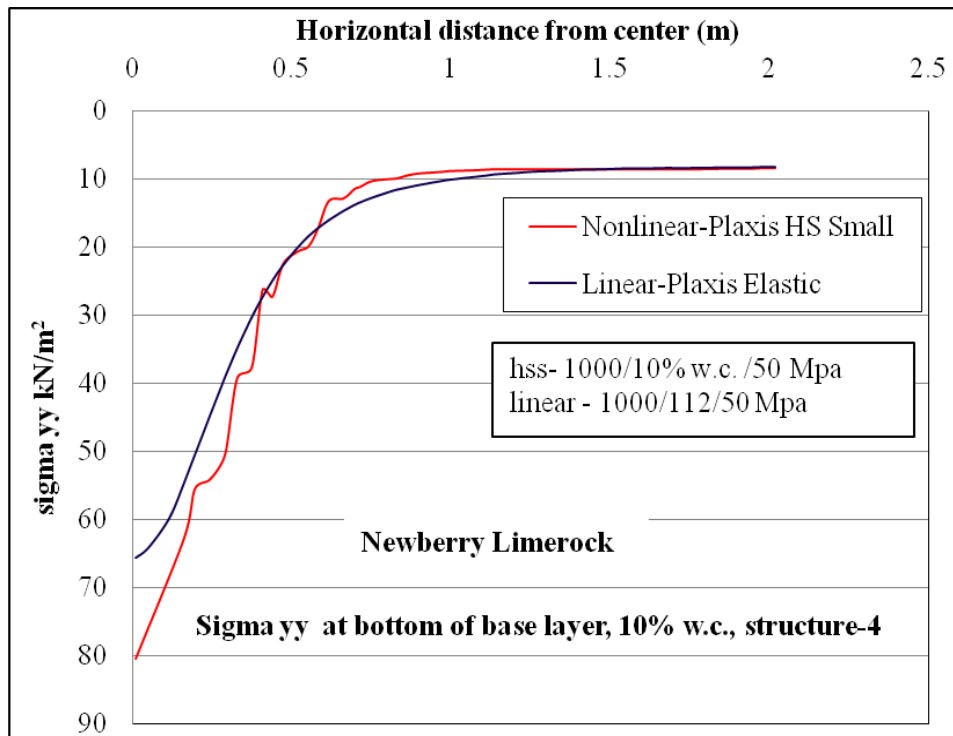


Figure C-62.  $\sigma_{yy}$  at bottom of base layer comparison for nonlinear and linear cases, for structure-4 with 10% w.c. base layer.

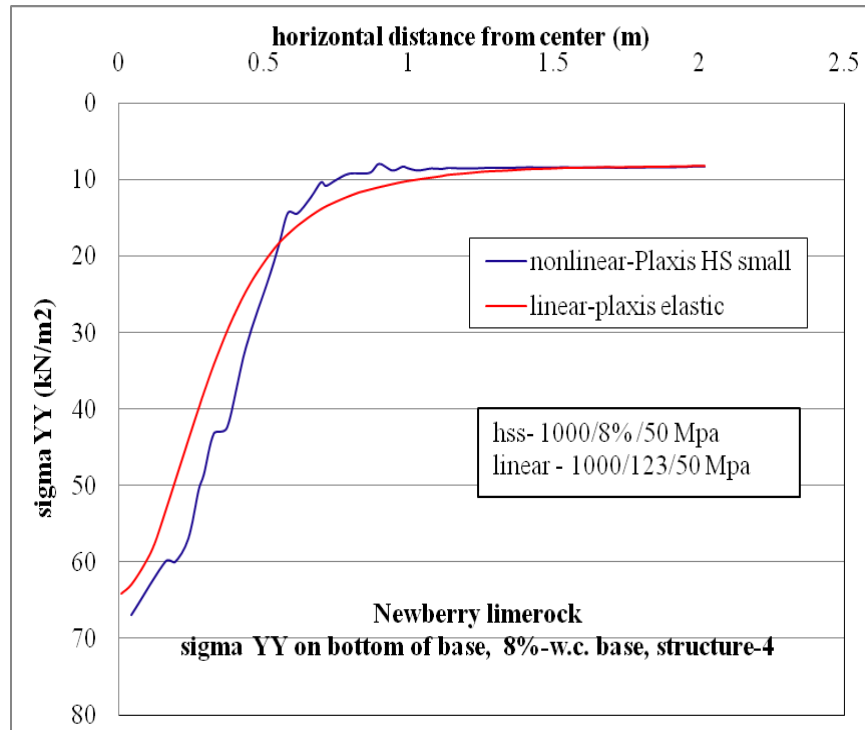


Figure C-63.  $\sigma_{yy}$  at bottom of base layer comparison for nonlinear and linear cases, for structure-4 with 8% w.c. base layer.

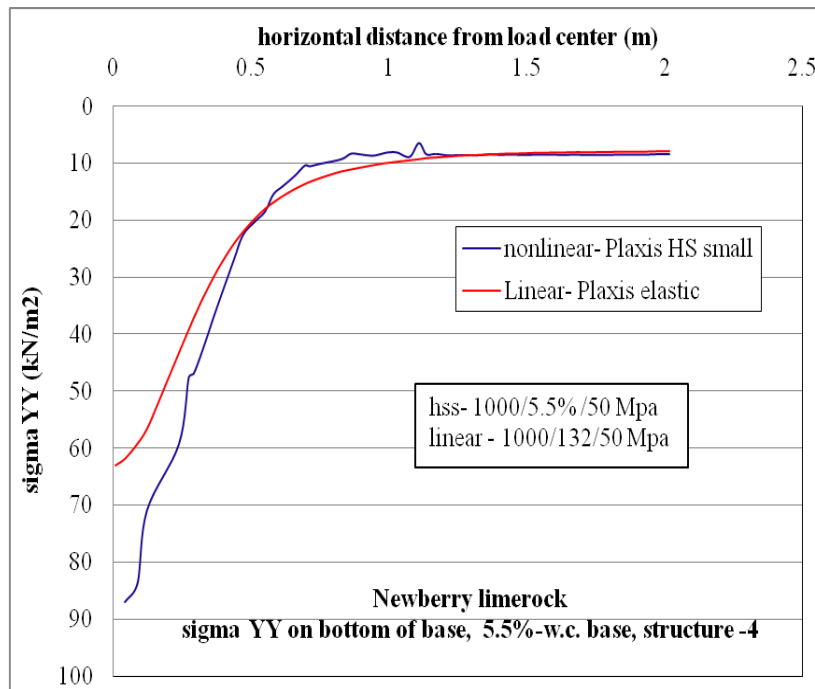


Figure C-64.  $\sigma_{yy}$  at bottom of base layer comparison for nonlinear and linear cases, for structure-4 with 5.5% w.c. base layer.

### C.1.9. Vertical Strain ( $\epsilon_{yy}$ , Compressive Strain) at Bottom of Base Layer

#### C.1.9.1 Structure-1

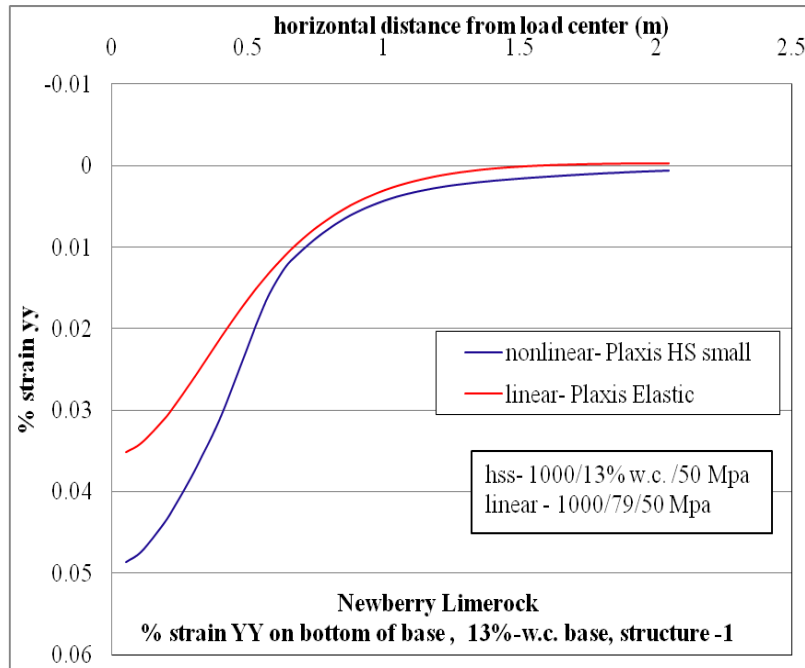


Figure C-65.  $\epsilon_{yy}$  at bottom of base layer comparison for nonlinear and linear cases, for structure-1 with 13% w.c. base layer.

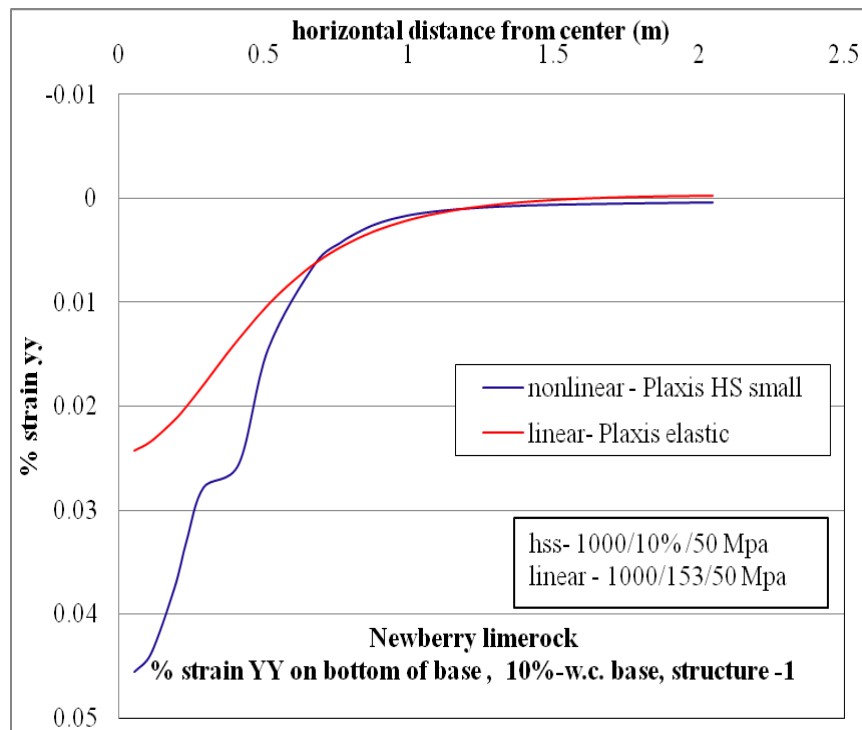


Figure C-66.  $\epsilon_{yy}$  at bottom of base layer comparison for nonlinear and linear cases, for structure-1 with 10% w.c. base layer

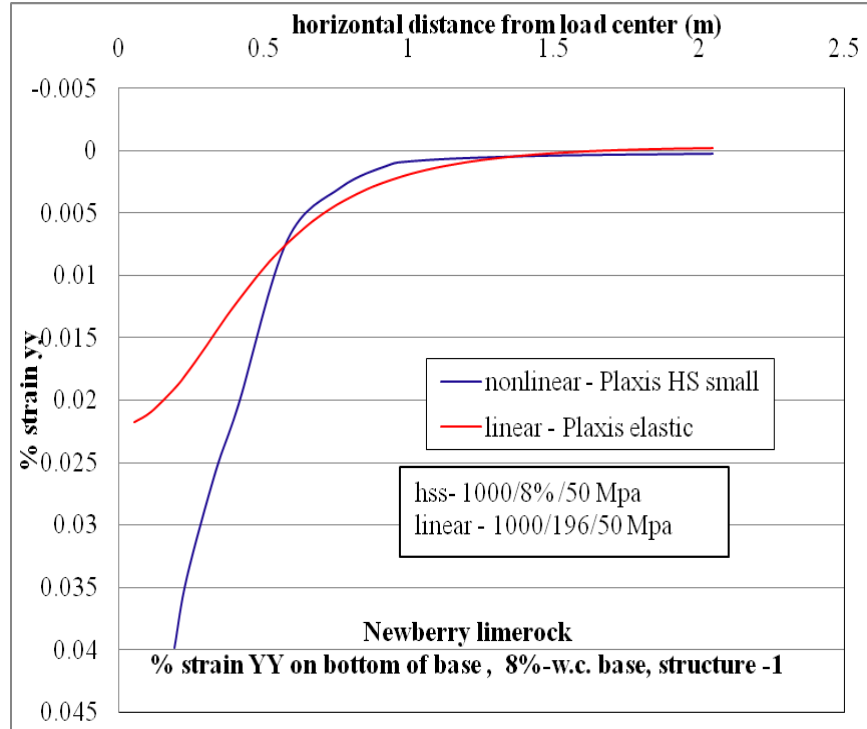


Figure C-67.  $\epsilon_{yy}$  at bottom of base layer comparison for nonlinear and linear cases, for structure-1 with 8% w.c. base layer.

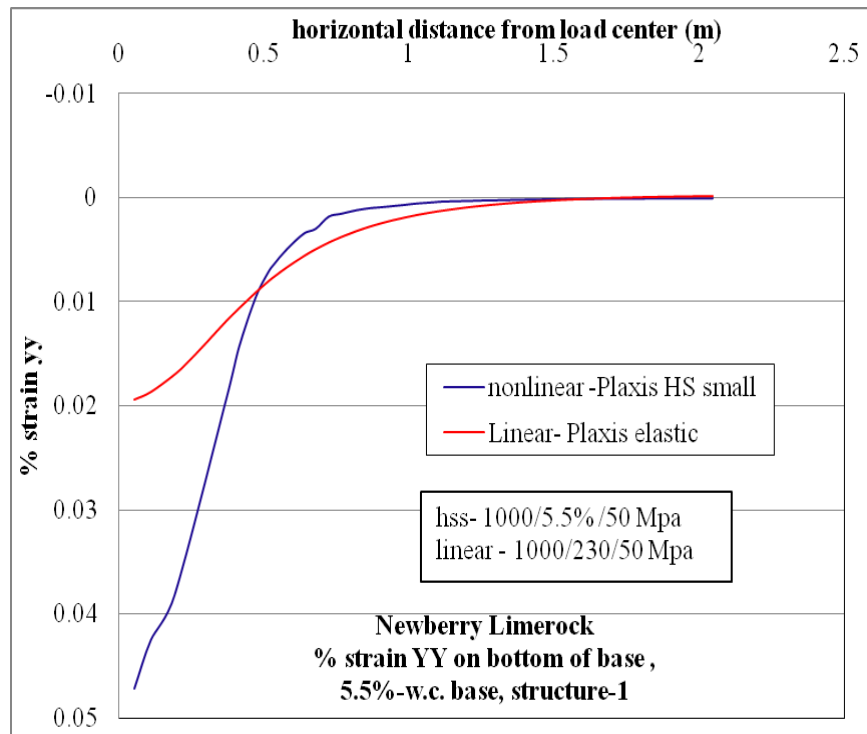


Figure C-68.  $\epsilon_{yy}$  at bottom of base layer comparison for nonlinear and linear cases, for structure-1 with 5.5% w.c. base layer.

**C.1.9.2 Structure-4**

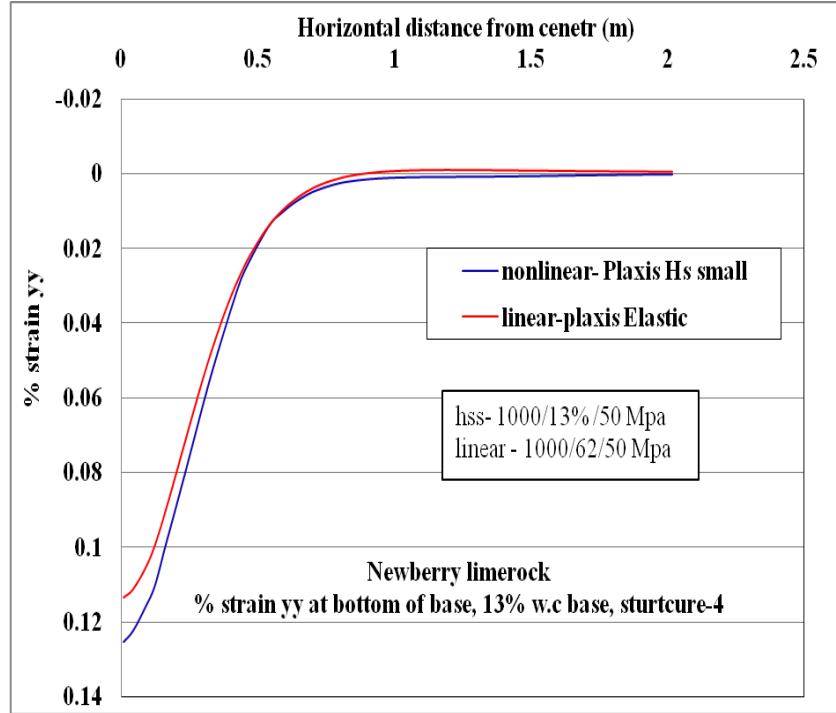


Figure C-69.  $\epsilon_{yy}$  at bottom of base layer comparison for nonlinear and linear cases, for structure-4 with 10% w.c. base layer.

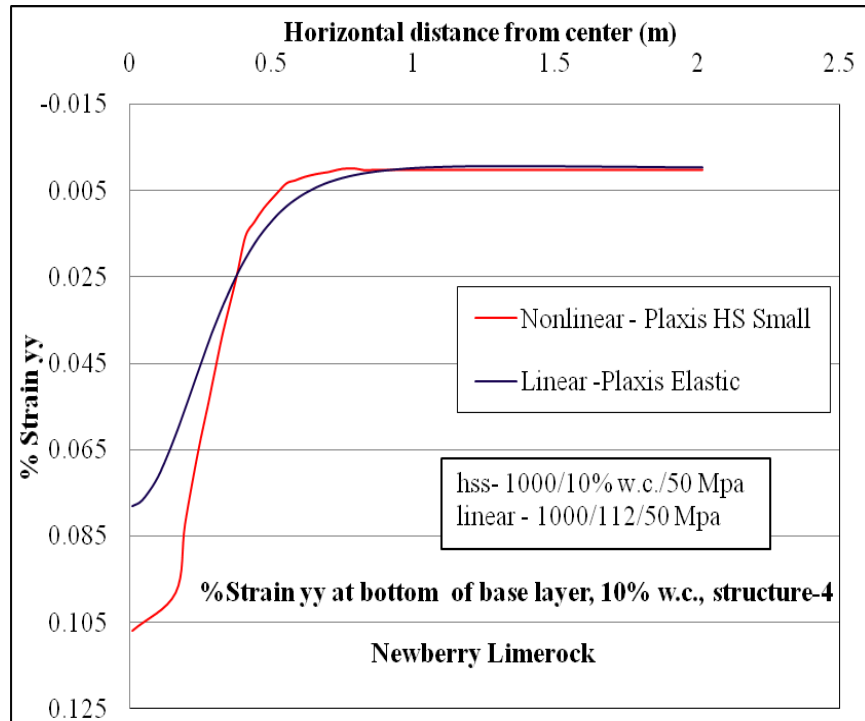


Figure C-70.  $\epsilon_{yy}$  at bottom of base layer comparison for nonlinear and linear cases, for structure-4 with 10% w.c. base layer.

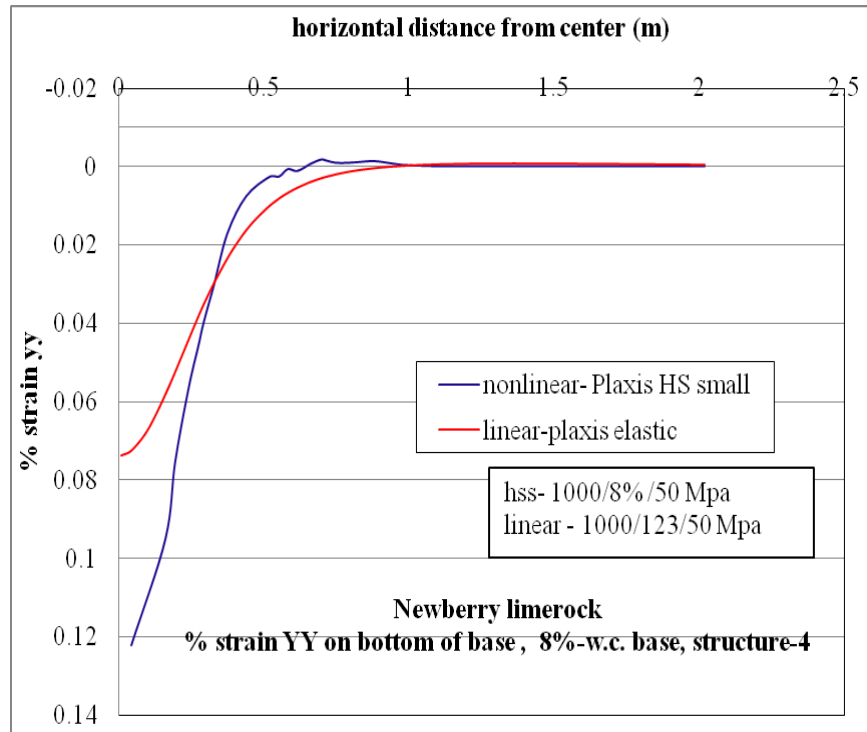


Figure C-71.  $\epsilon_{yy}$  at bottom of base layer comparison for nonlinear and linear cases, for structure-4 with 8% w.c. base layer.

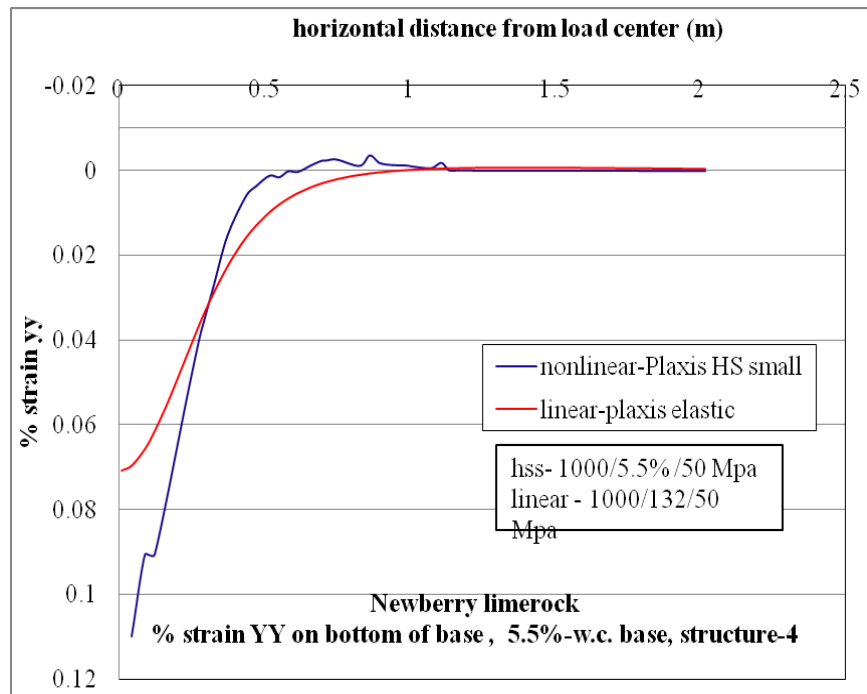


Figure C-72.  $\epsilon_{yy}$  at bottom of base layer comparison for nonlinear and linear cases, for structure-4 with 5.5% w.c. base layer

### C.1.10 Vertical Stress ( $\sigma_{yy}$ , Compressive Stress) at Top of Subgrade Layer

#### C.1.10.1 Structure-1

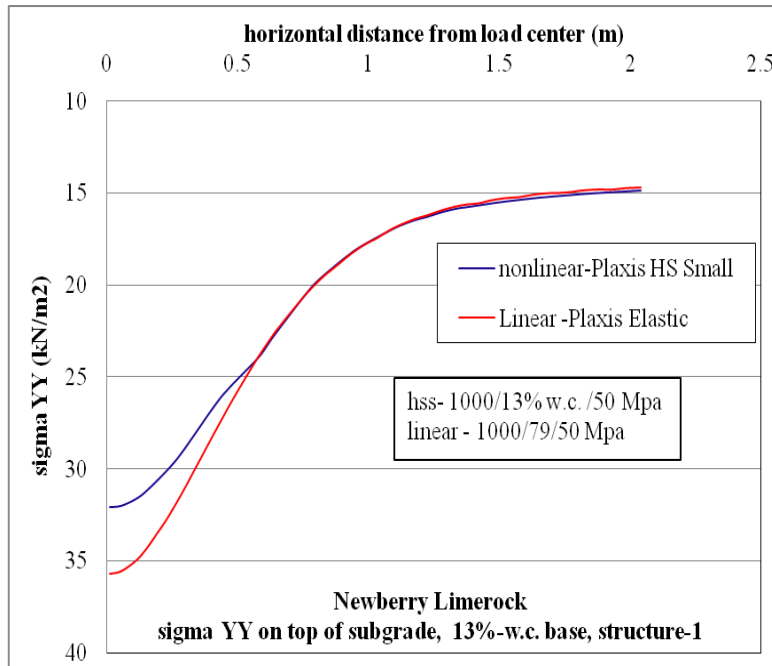


Figure C-73.  $\sigma_{yy}$  at top of subgrade comparison for nonlinear and linear cases, for structure-1 with 13% w.c. base layer.

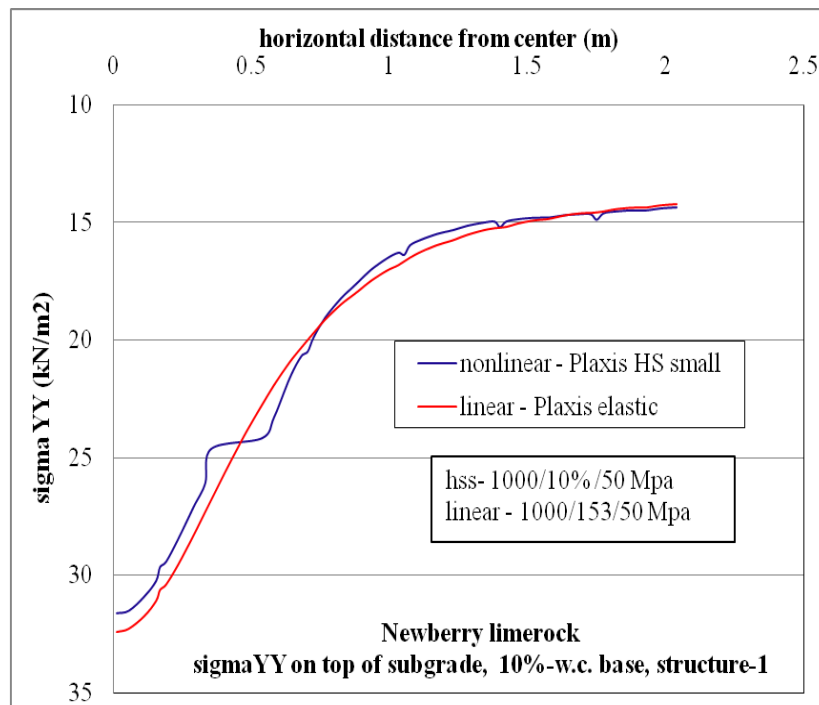


Figure C-74.  $\sigma_{yy}$  at top of subgrade comparison for nonlinear and linear cases, for structure-1 with 10% w.c. base layer

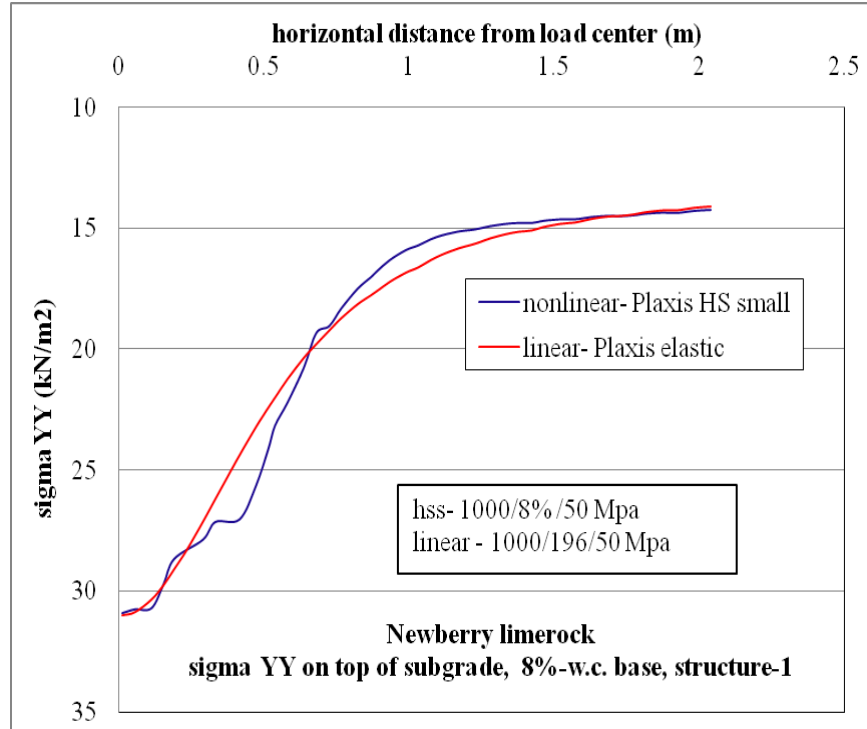


Figure C-75.  $\sigma_{yy}$  at top of subgrade comparison for nonlinear and linear cases, for structure-1 with 8% w.c. base layer.

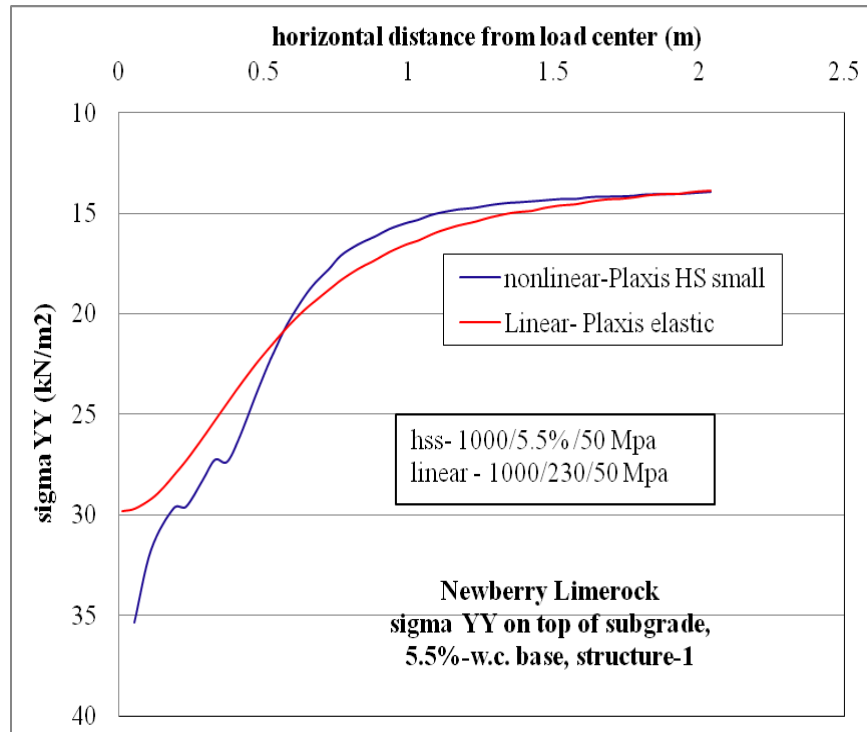


Figure C-76.  $\sigma_{yy}$  at top of subgrade comparison for nonlinear and linear cases, for structure-1 with 5.5% w.c. base layer.

**C.1.10.2 Structure-4**

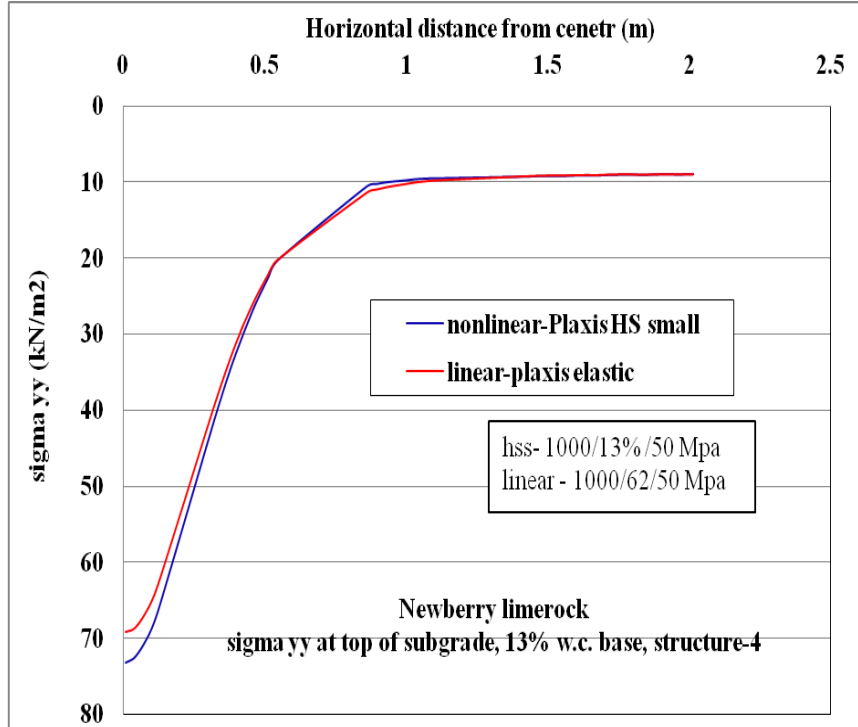


Figure C-77.  $\sigma_{yy}$  at top of subgrade comparison for nonlinear and linear cases, for structure-4 with 13% w.c. base layer.

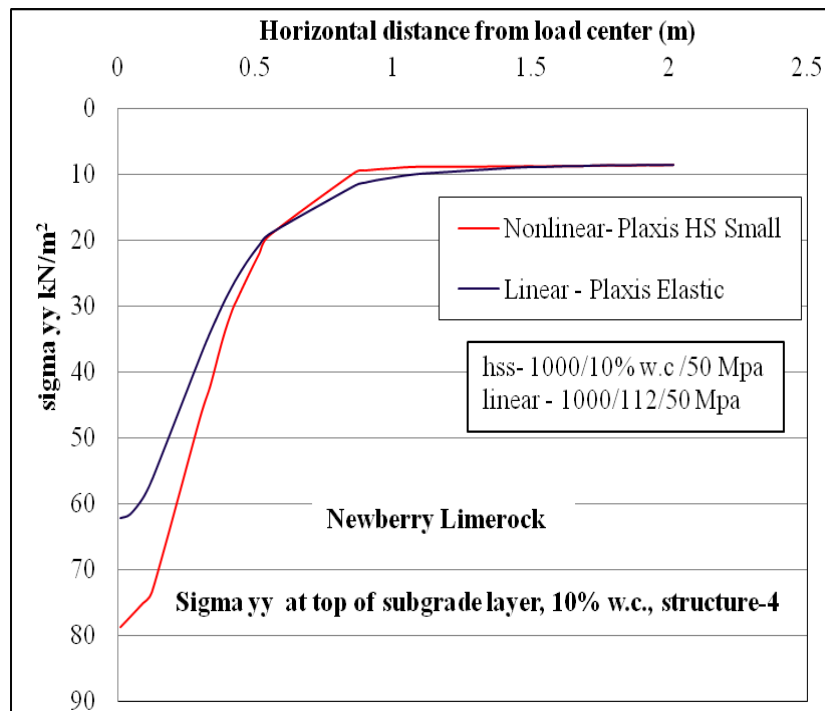


Figure C-78.  $\sigma_{yy}$  at top of subgrade comparison for nonlinear and linear cases, for structure-4 with 10% w.c. base layer.

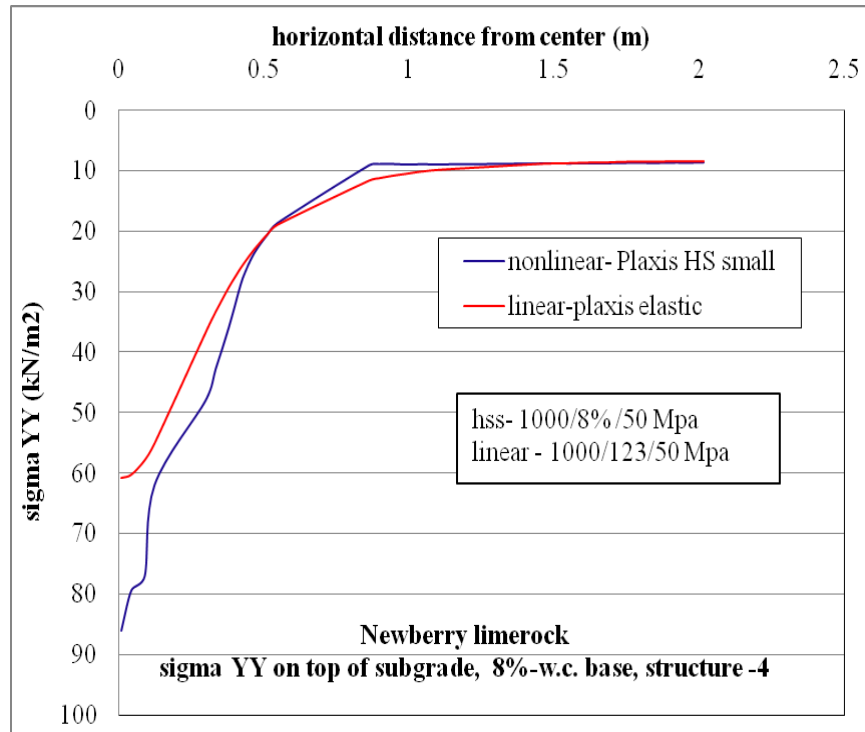


Figure C-79.  $\sigma_{yy}$  at top of subgrade comparison for nonlinear and linear cases, for structure-4 with 8% w.c. base layer.

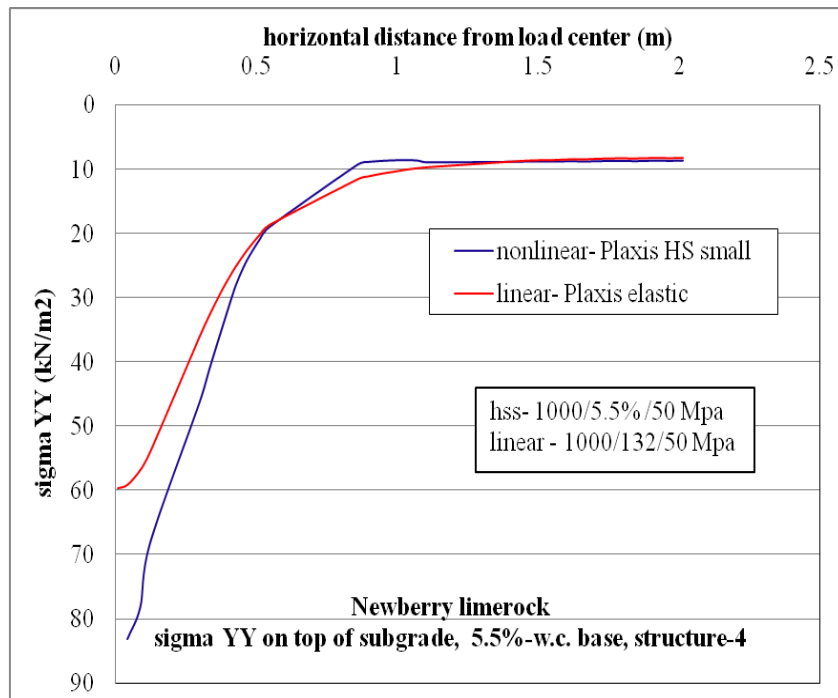


Figure C-80.  $\sigma_{yy}$  at top of subgrade comparison for nonlinear and linear cases, for structure-4 with 5.5% w.c. base layer.

### C.1.11 Vertical Strain ( $\epsilon_{yy}$ , Compressive Strain) at Top of Subgrade Layer

#### C.1.11.1 Structure-1

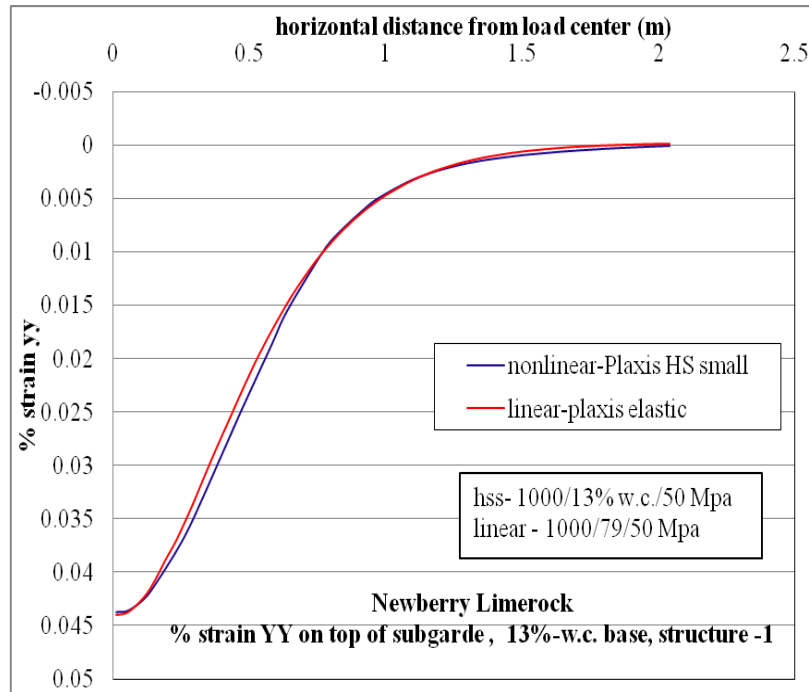


Figure C-81.  $\epsilon_{yy}$  at top of subgrade layer comparison for nonlinear and linear cases for structure-1 with 13% w.c. base layer.

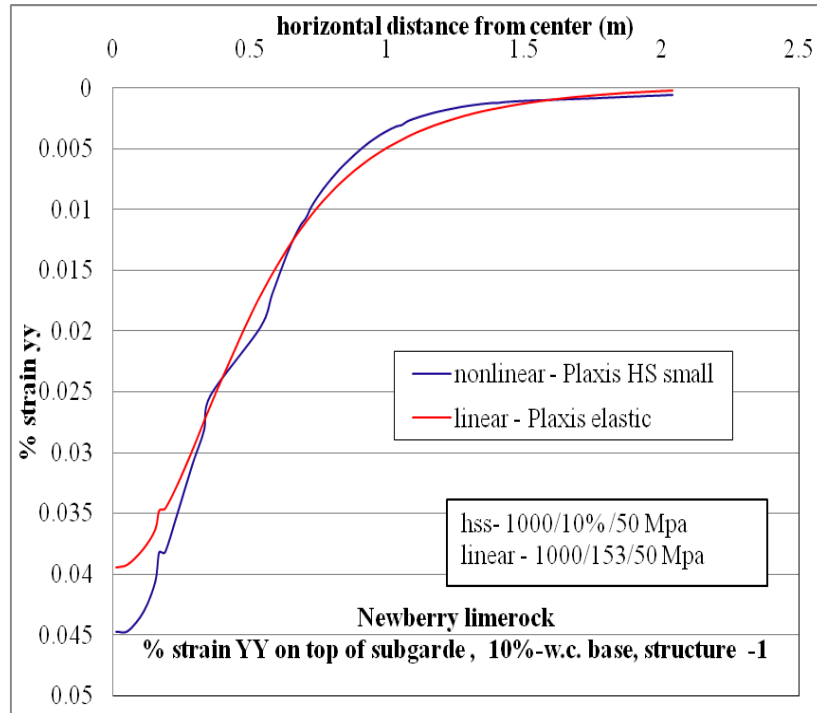


Figure C-82.  $\epsilon_{yy}$  at top of subgrade layer comparison for nonlinear and linear cases for structure-1 with 10% w.c. base layer.

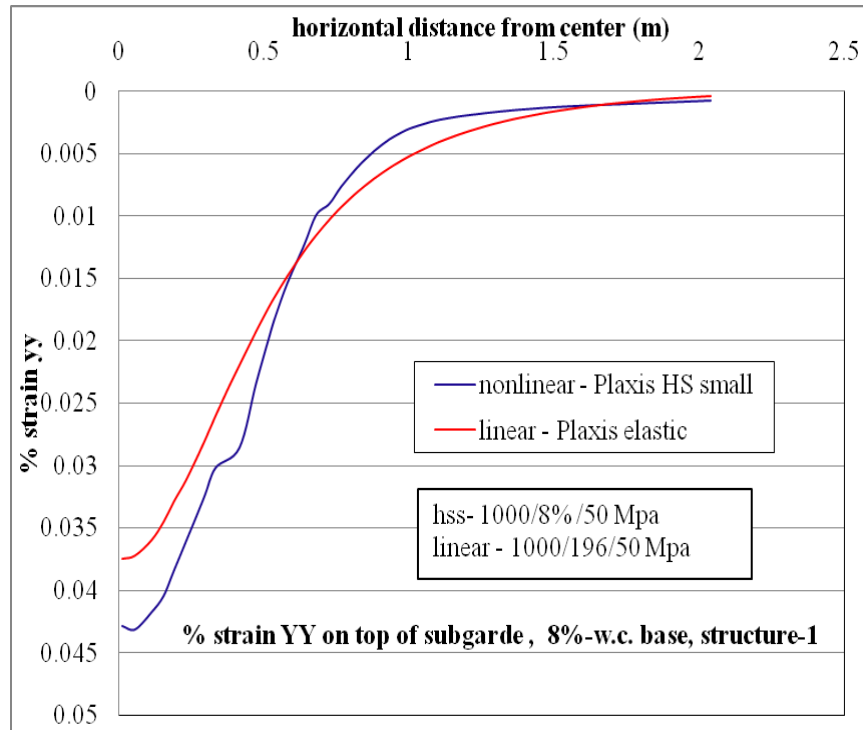


Figure C-83.  $\epsilon_{yy}$  at top of subgrade layer comparison for nonlinear and linear cases for structure-1 with 8% w.c. base layer.

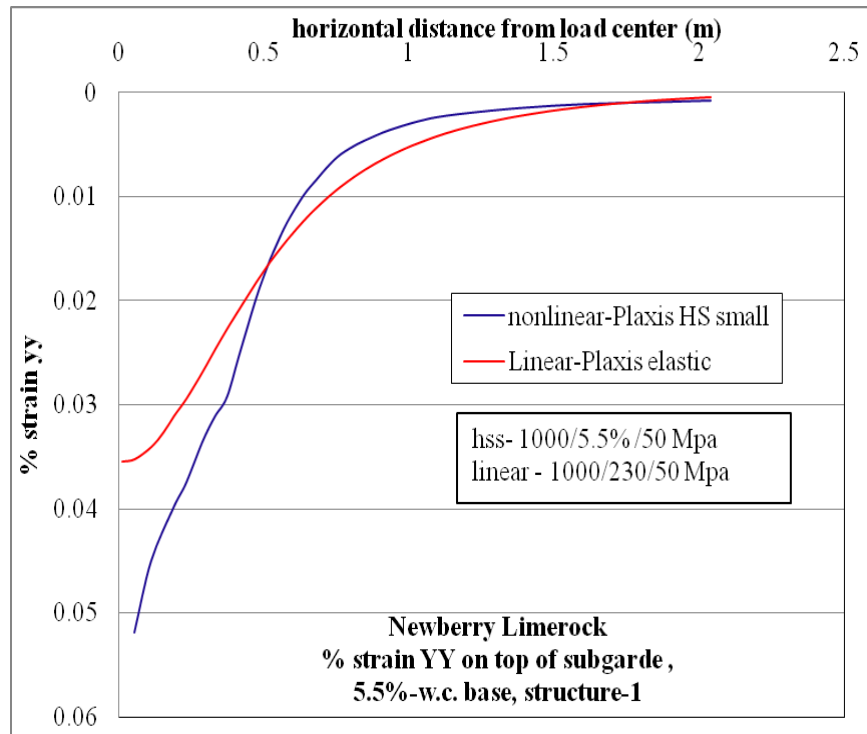


Figure C-84.  $\epsilon_{yy}$  at top of subgrade layer comparison for nonlinear and linear cases for structure-1 with 5.5% w.c. base layer.

#### C.1.11.2 Structure-4

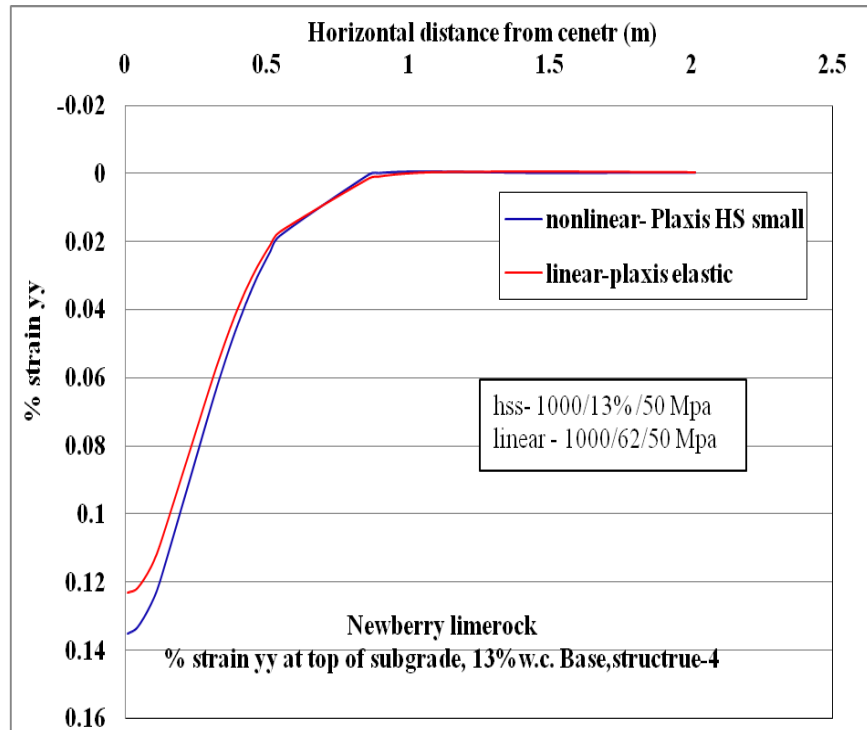


Figure C-85.  $\epsilon_{yy}$  at top of subgrade layer comparison for nonlinear and linear cases for structure-4 with 13% w.c. base layer.

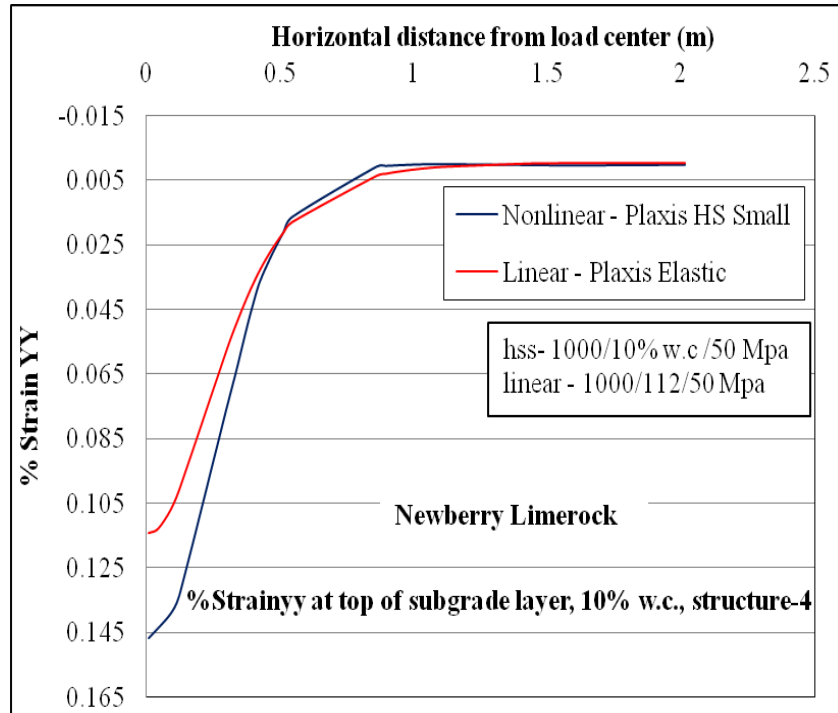


Figure C-86.  $\epsilon_{yy}$  at top of subgrade layer comparison for nonlinear and linear cases for structure-4 with 10% w.c. base layer.

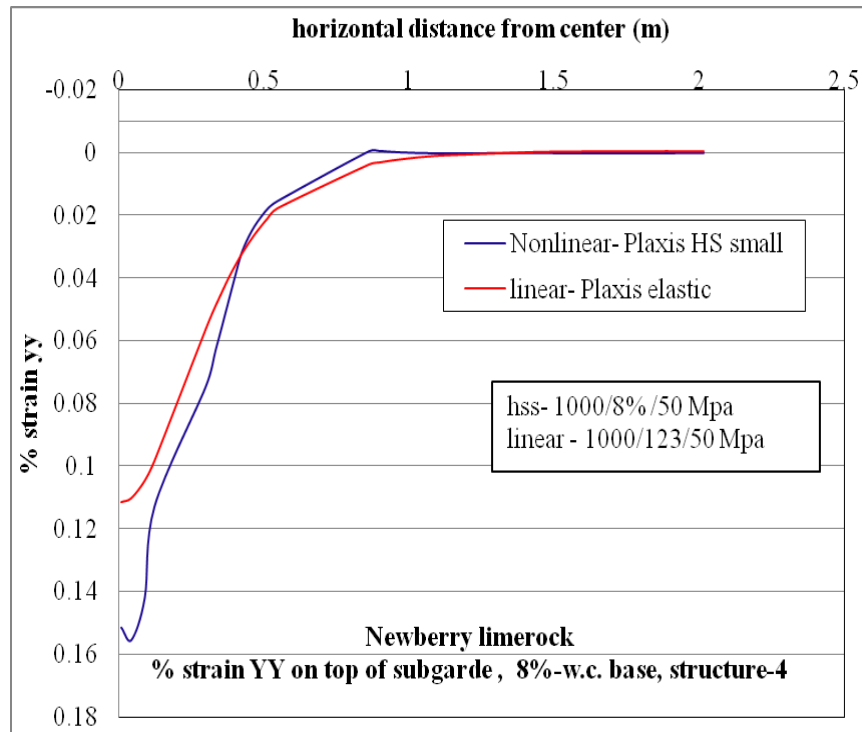


Figure C-87.  $\epsilon_{yy}$  at top of subgrade layer comparison for nonlinear and linear cases for structure-4 with 8% w.c. base layer.

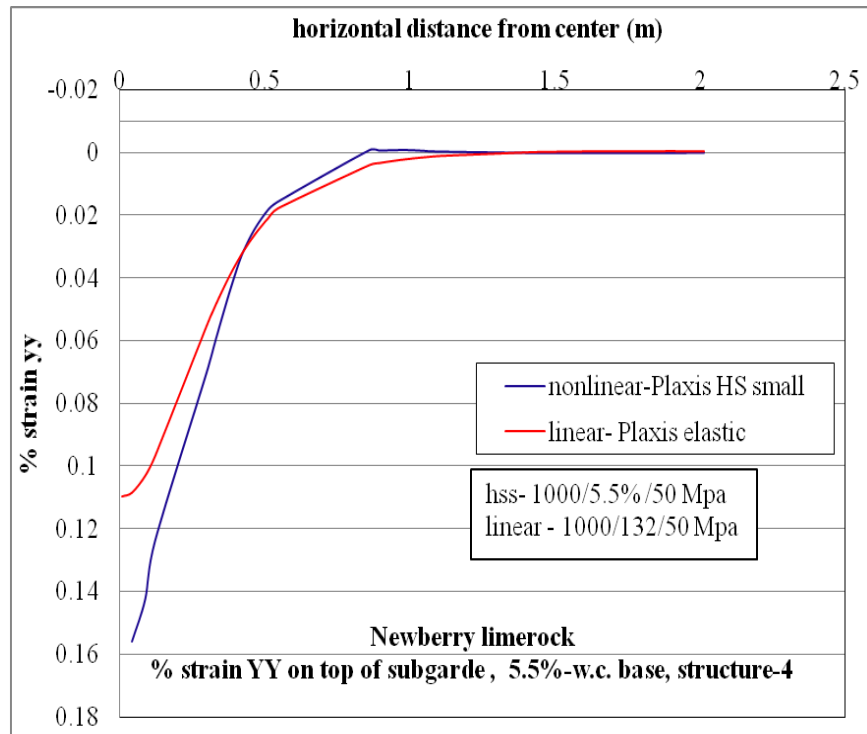


Figure C-88.  $\epsilon_{yy}$  at top of subgrade layer comparison for nonlinear and linear cases for structure-4 with 5.5% w.c. base layer.

## C.2 Georgia Granite

### C.2.1 Surface Deflection Profiles

#### C.2.1.1 Structure-1

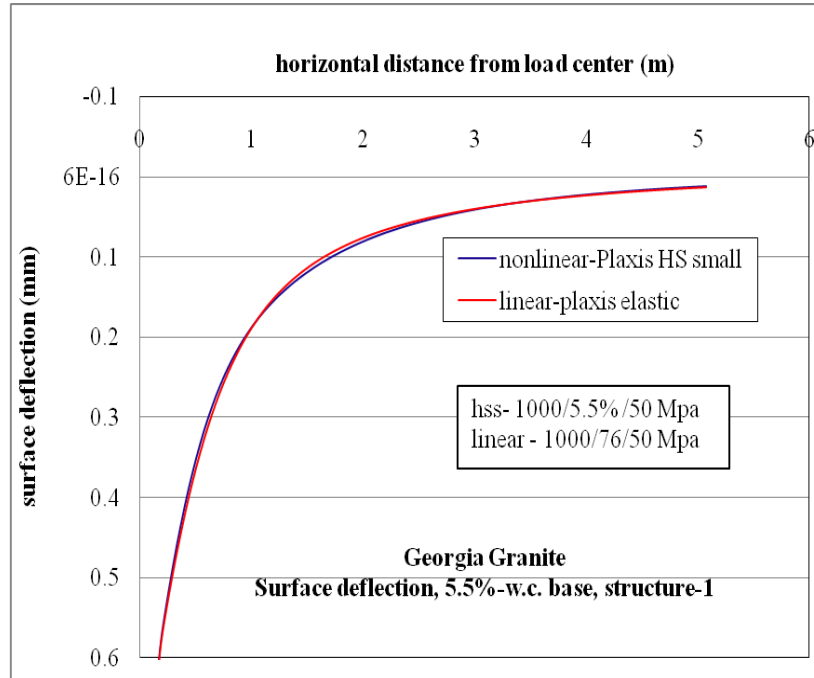


Figure C-89. Surface deflection comparison for nonlinear and linear cases, for structure-1 with 5.5% w.c. base layer.

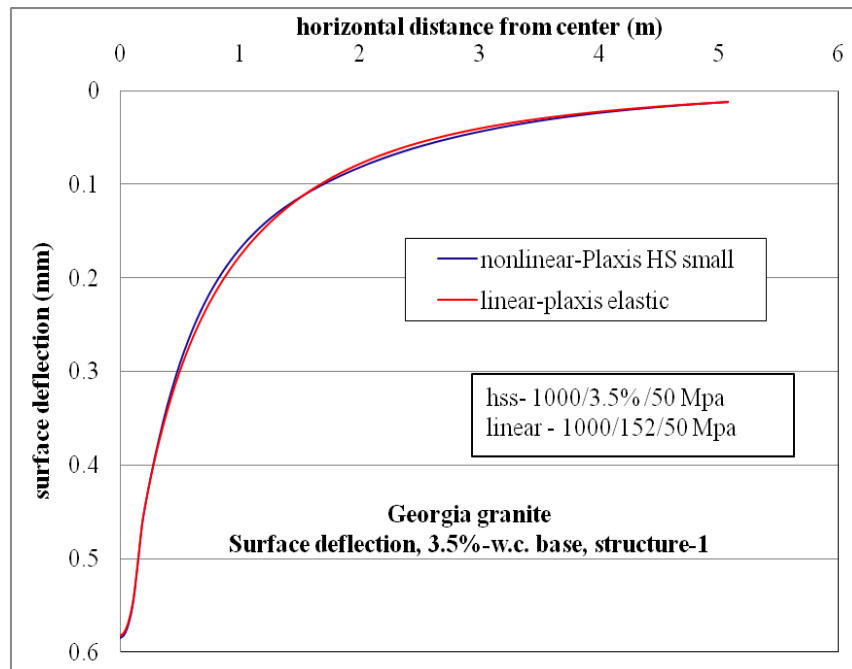


Figure C-90. Surface deflection comparison for nonlinear and linear cases, for structure-1 with 3.5% w.c. base layer.

### C.2.1.2 Structure-4

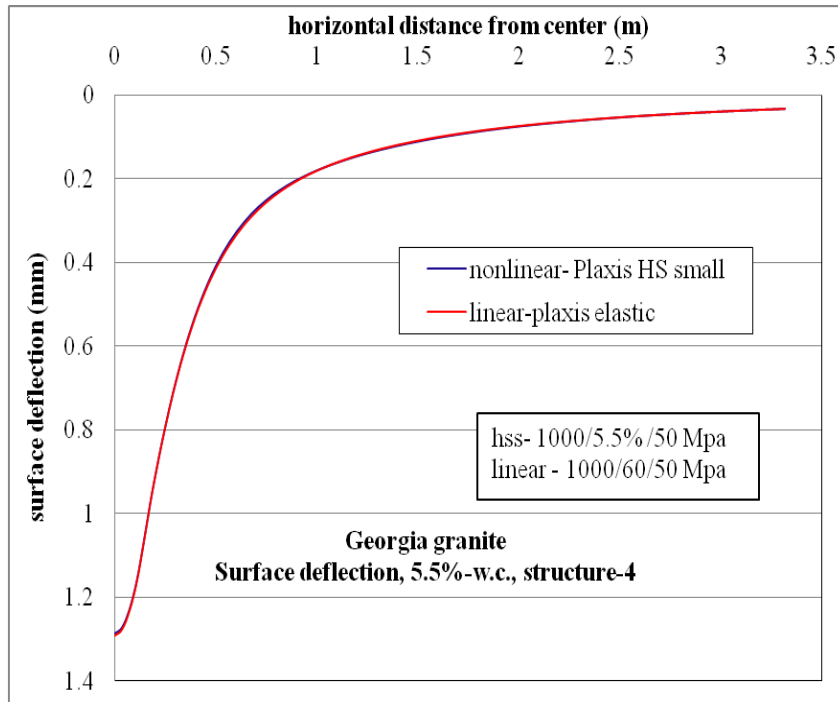


Figure C-91. Surface deflection comparison for nonlinear and linear cases, for structure-4 with 5.5% w.c. base layer.

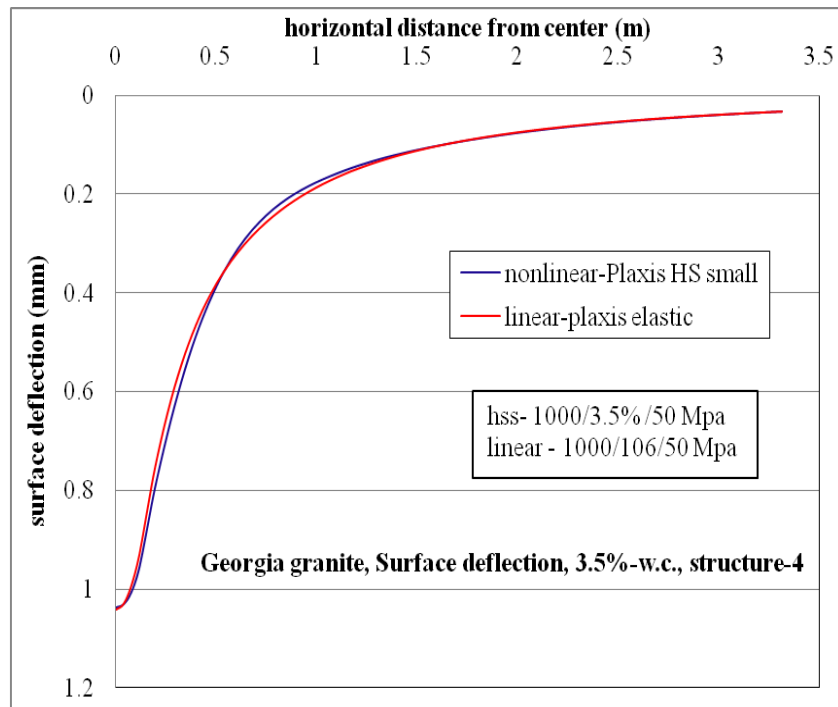


Figure C-92. Surface deflection comparison for nonlinear and linear cases, for structure-4 with 3.5% w.c. base layer.

## C.2.2 Horizontal Stress ( $\sigma_{xx}$ , Tensile Stress) at Top of AC Layer

### C.2.2.1 Structure-1

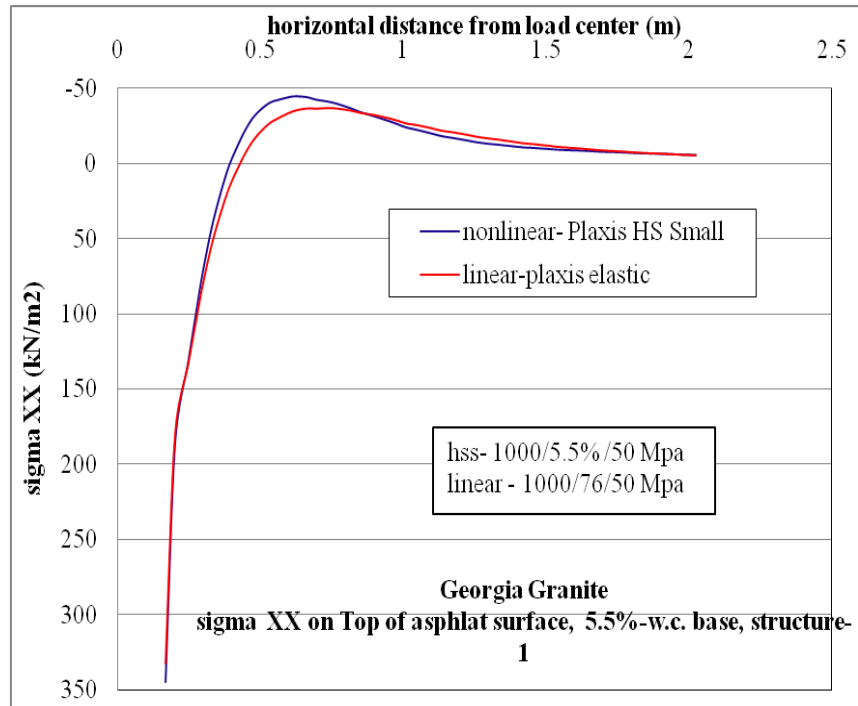


Figure C-93.  $\sigma_{xx}$  at top of AC layer comparison for nonlinear and linear cases, for structure-1 with 5.5% w.c. base layer.

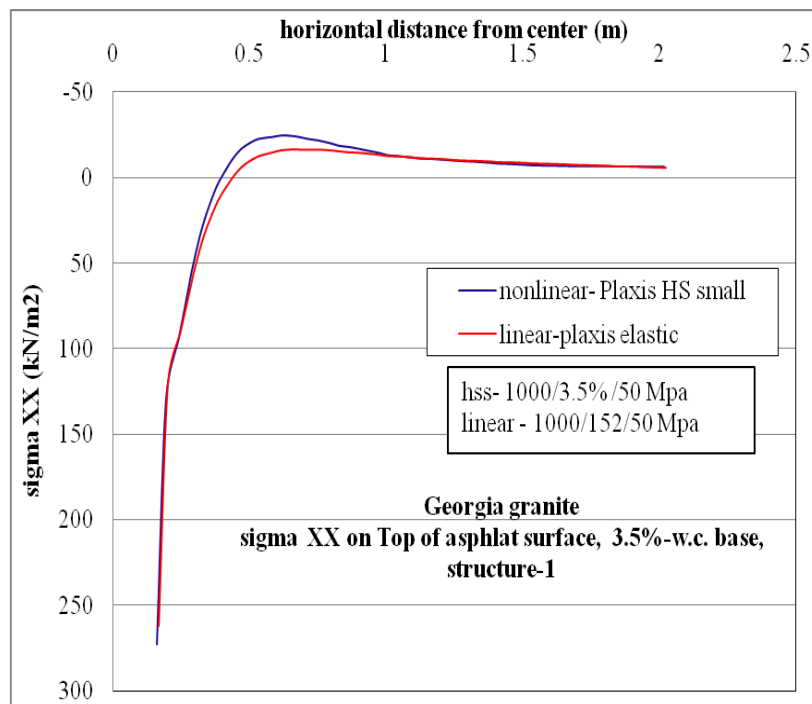


Figure C-94.  $\sigma_{xx}$  at top of AC layer comparison for nonlinear and linear cases, for structure-1 with 3.5% w.c. base layer

### C.2.2.2 Strcutrue-4

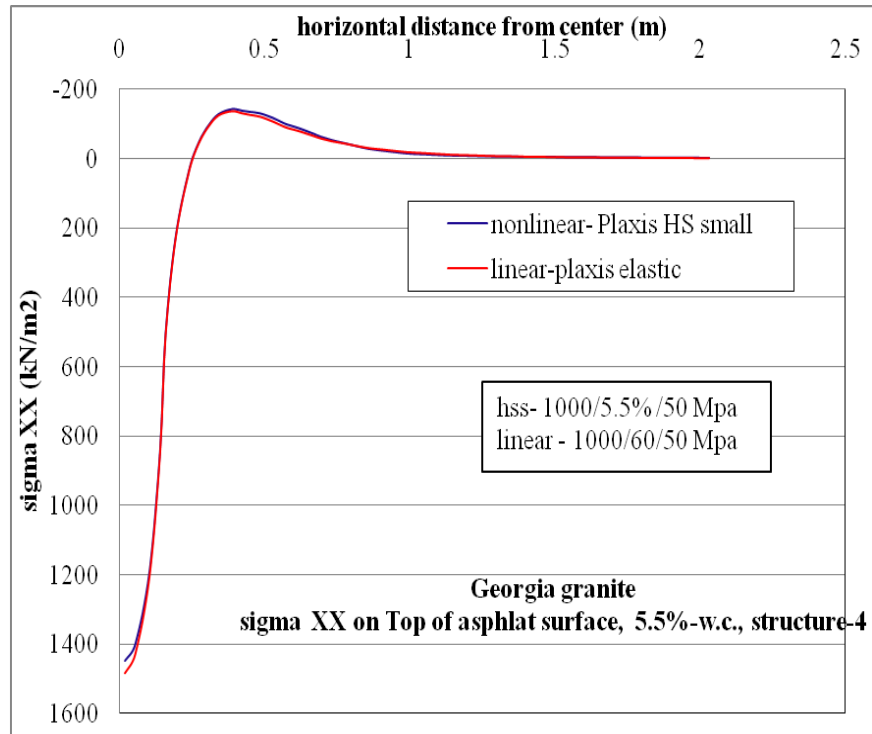


Figure C-95.  $\sigma_{xx}$  at top of AC layer comparison for nonlinear and linear cases, for structure-4 with 5.5% w.c. base layer.

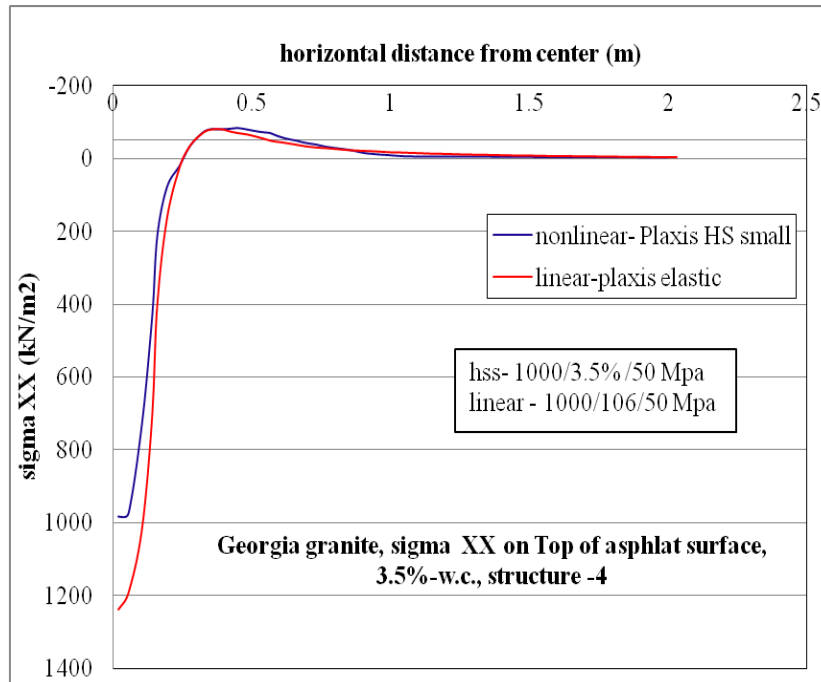


Figure C-96.  $\sigma_{xx}$  at top of AC layer comparison for nonlinear and linear cases, for structure-4 with 3.5% w.c. base layer.

### C.2.3 Horizontal Strain ( $\epsilon_{xx}$ , Tensile Strain) at Top of AC Layer

#### C.2.3.1 Structure-1

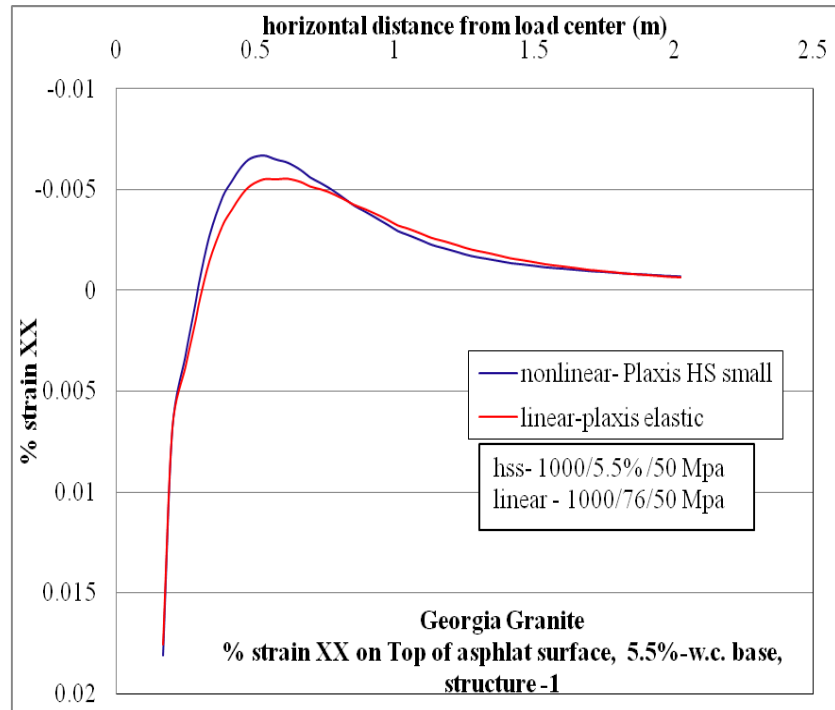


Figure C-97.  $\epsilon_{xx}$  at top of AC layer comparison for nonlinear and linear cases, for structure-1 with 5.5% w.c. base layer.

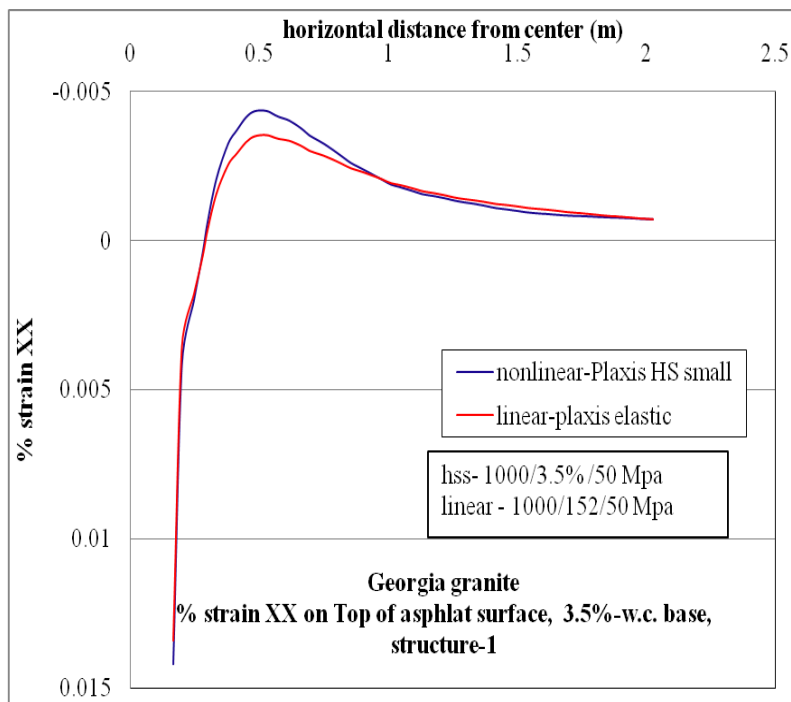


Figure C-98.  $\epsilon_{xx}$  at top of AC layer comparison for nonlinear and linear cases, for structure-1 with 3.5% w.c. base layer.

### C.2.3.2 Structure-4

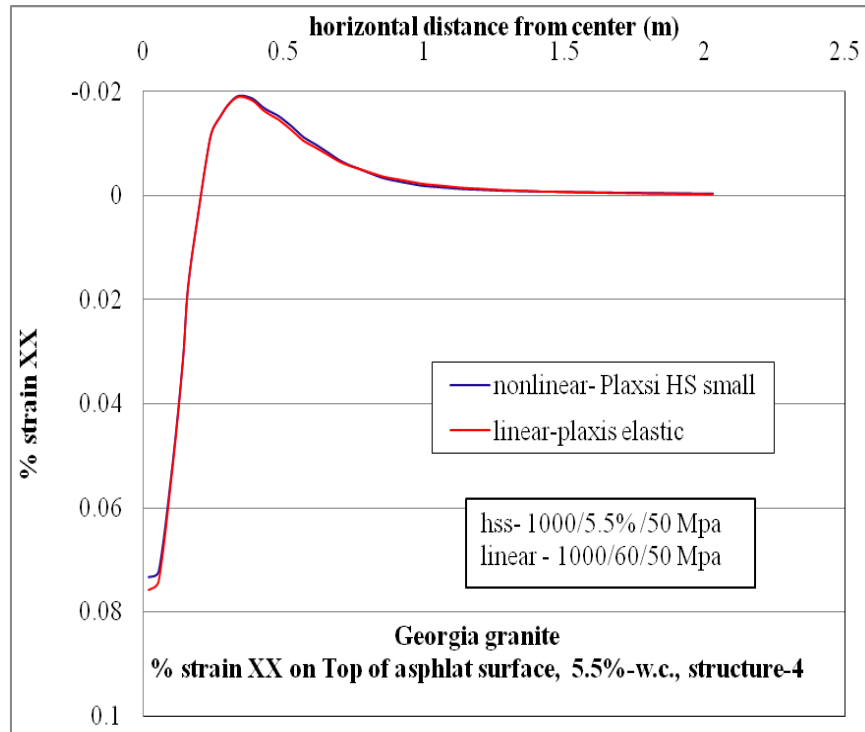


Figure C-99.  $\epsilon_{xx}$  at top of AC layer comparison for nonlinear and linear cases, for structure-4 with 5.5% w.c. base layer.

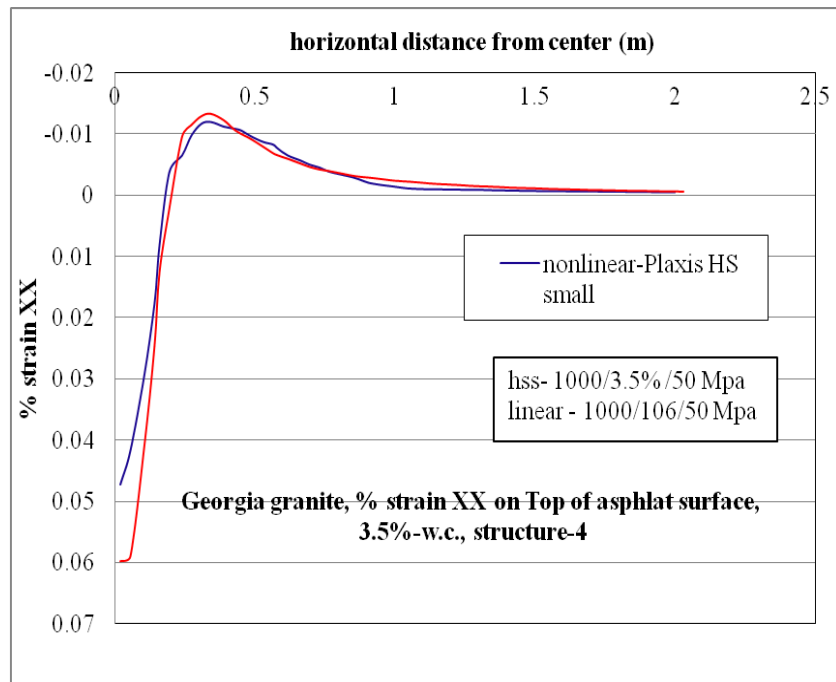


Figure C-100.  $\epsilon_{xx}$  at top of AC layer comparison for nonlinear and linear cases, for structure-4 with 3.5% w.c. base layer.

## C.2.4 Horizontal Stress ( $\sigma_{xx}$ , Tensile Stress) at Bottom of AC Layer

### C.2.4.1 Structure-1

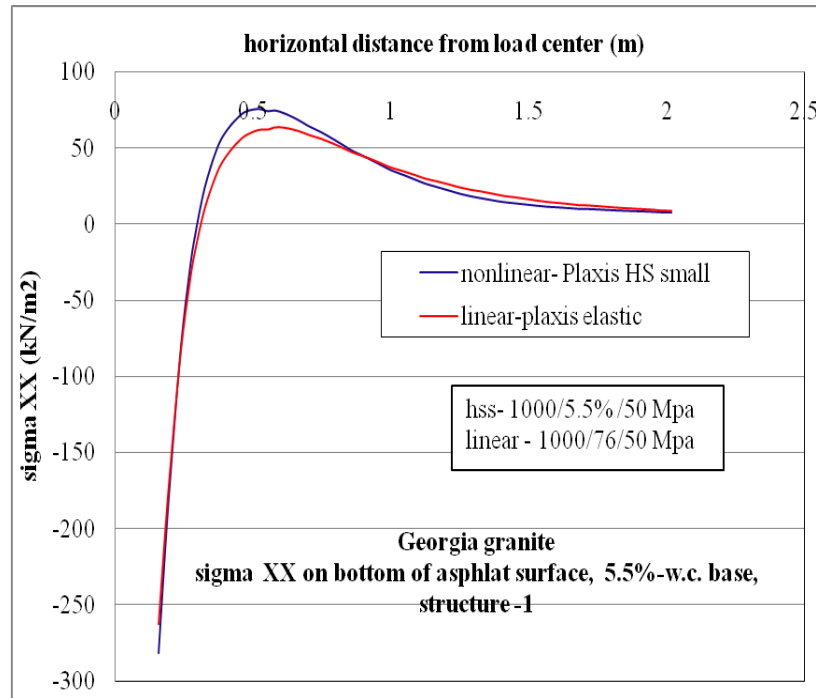


Figure C-101.  $\sigma_{xx}$  at bottom of AC layer comparison for nonlinear and linear cases, for structure-1 with 5.5% w.c. base layer.

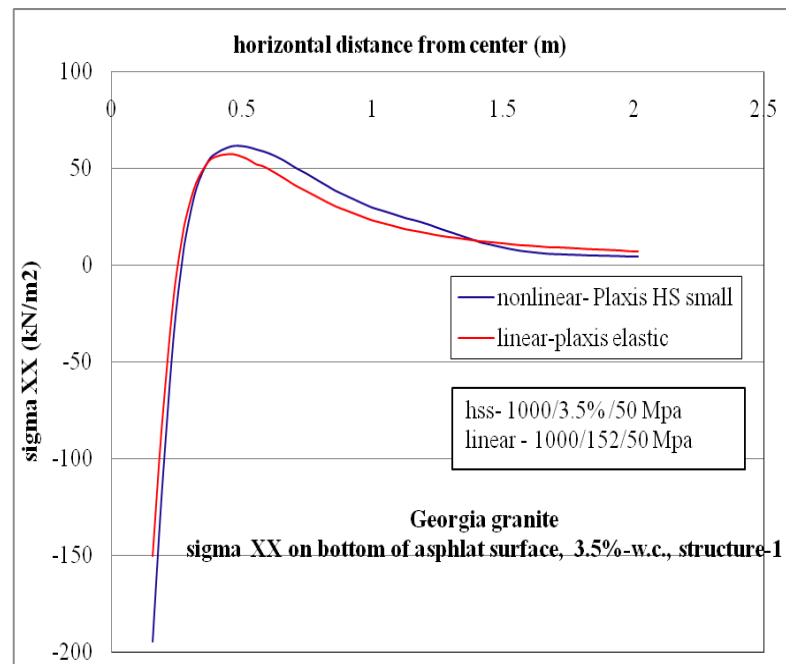


Figure C-102.  $\sigma_{xx}$  at bottom of AC layer comparison for nonlinear and linear cases, for structure-1 with 3.5% w.c. base layer.

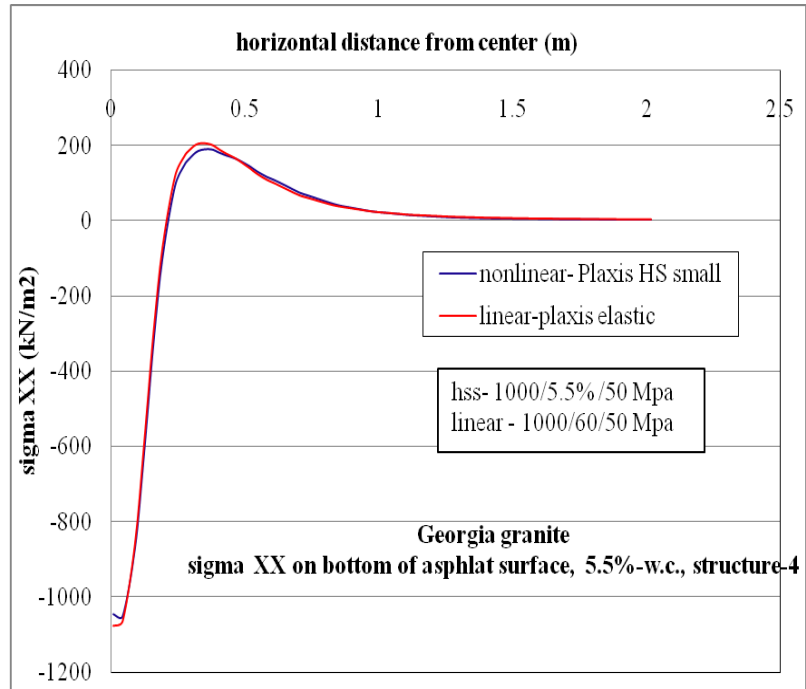


Figure C-103.  $\sigma_{xx}$  at bottom of AC layer comparison for nonlinear and linear cases, for structure-4 with 5.5% w.c. base layer

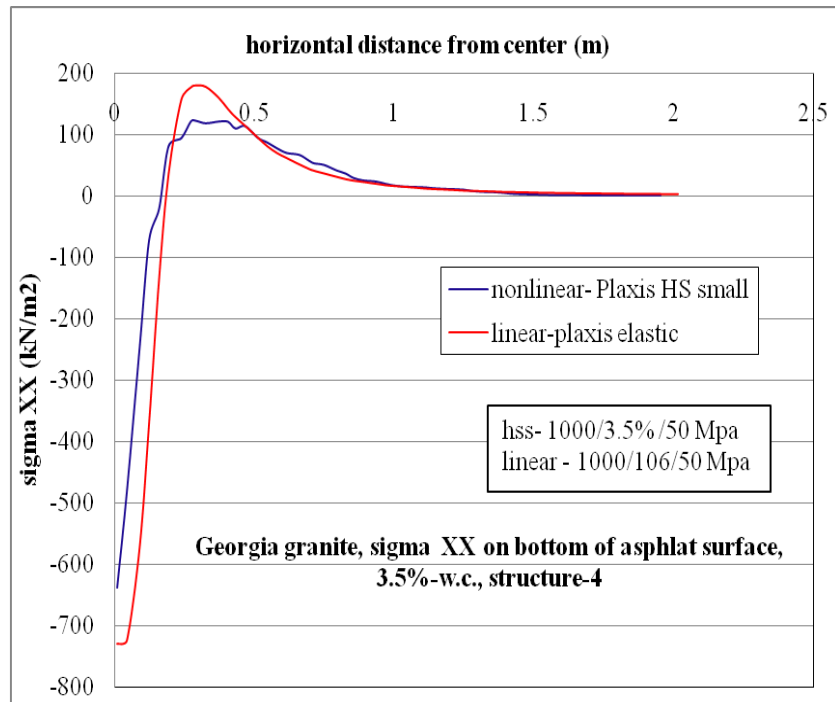


Figure C-104.  $\sigma_{xx}$  at bottom of AC layer comparison for nonlinear and linear cases, for structure-4 with 3.5% w.c. base layer.

## C.2.5. Horizontal Strain ( $\epsilon_{xx}$ , Tensile Strain) at Bottom of AC Layer

### C.2.5.1 Structure-1

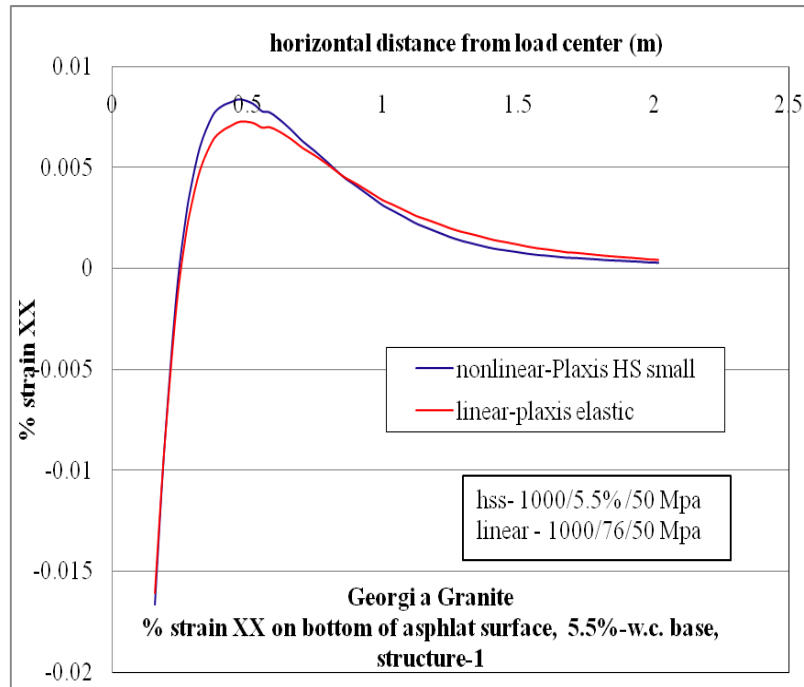


Figure C-105.  $\epsilon_{xx}$  at bottom of AC layer comparison for nonlinear and linear cases, for structure-1 with 5.5% w.c. base layer.

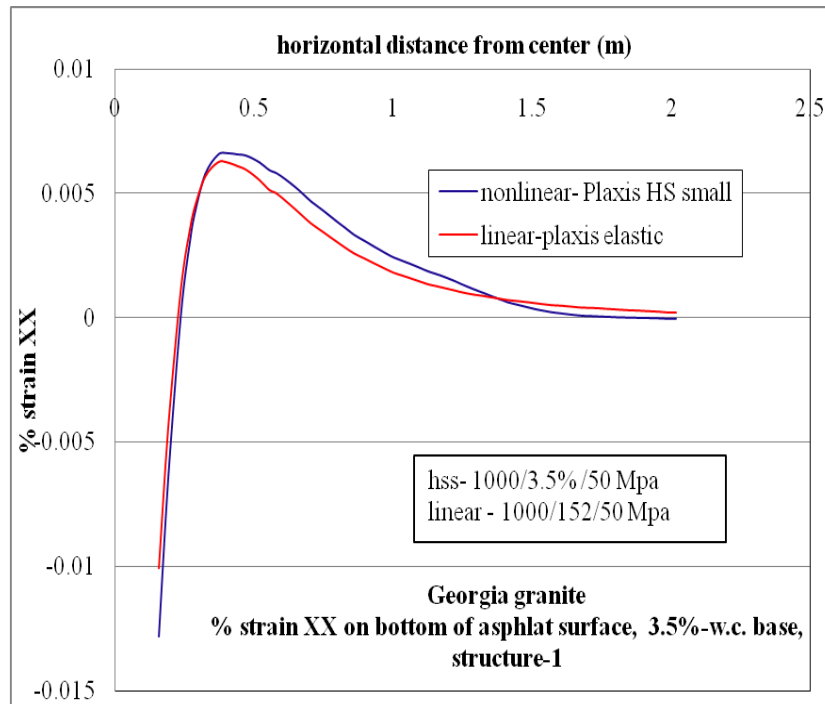


Figure C-106.  $\epsilon_{xx}$  at bottom of AC layer comparison for nonlinear and linear cases, for structure-1 with 3.5% w.c. base layer.

### C.2.5.2 Structure-4

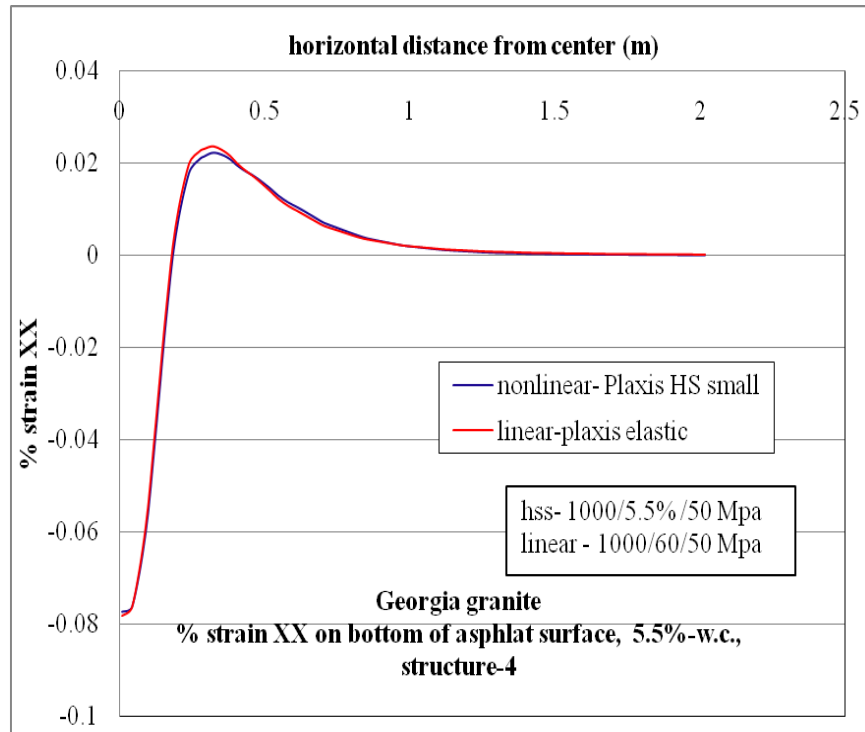


Figure C-107.  $\epsilon_{xx}$  at bottom of AC layer comparison for nonlinear and linear cases, for structure-4 with 5.5% w.c. base layer.

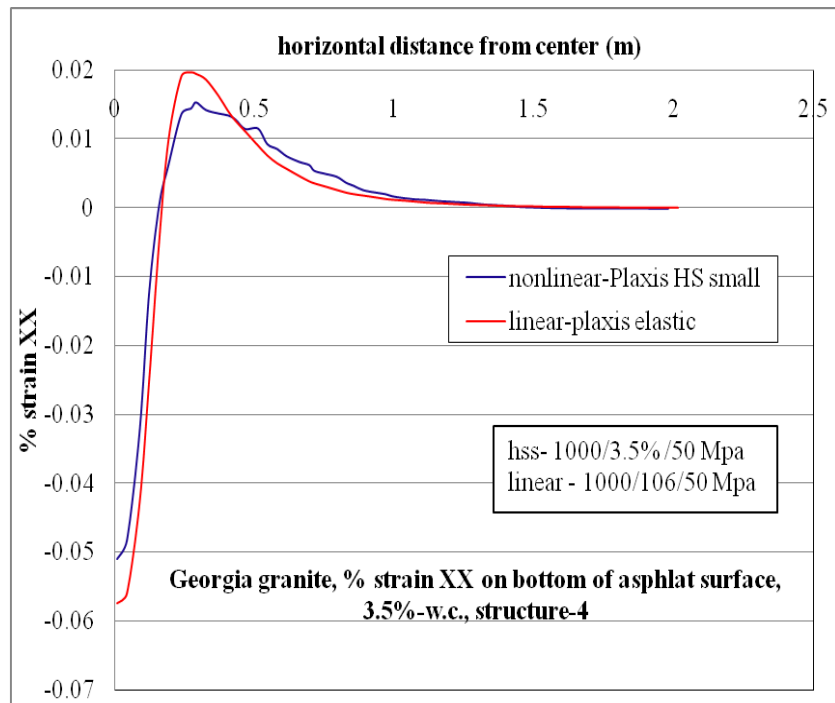


Figure C-108.  $\epsilon_{xx}$  at bottom of AC layer comparison for nonlinear and linear cases, for structure-4 with 3.5% w.c. base layer.

## C.2.6 Vertical Stress ( $\sigma_{yy}$ , Compressive Stress) at Top of Base Layer

### C.2.6.1 Structure-1

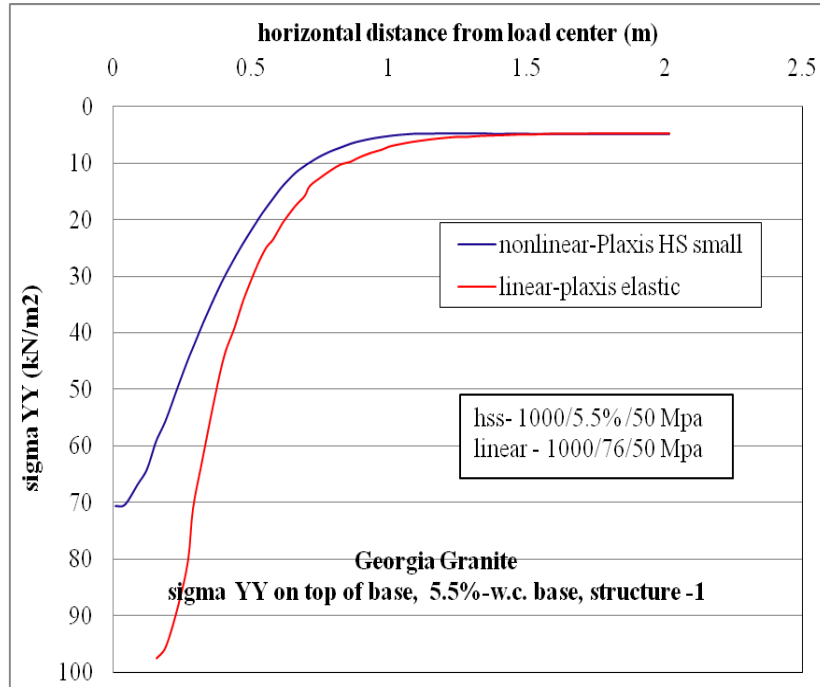


Figure C-109.  $\sigma_{yy}$  vertical stress at top of base layer comparison for nonlinear and linear cases, for structure-1 with 5.5% w.c. base layer.

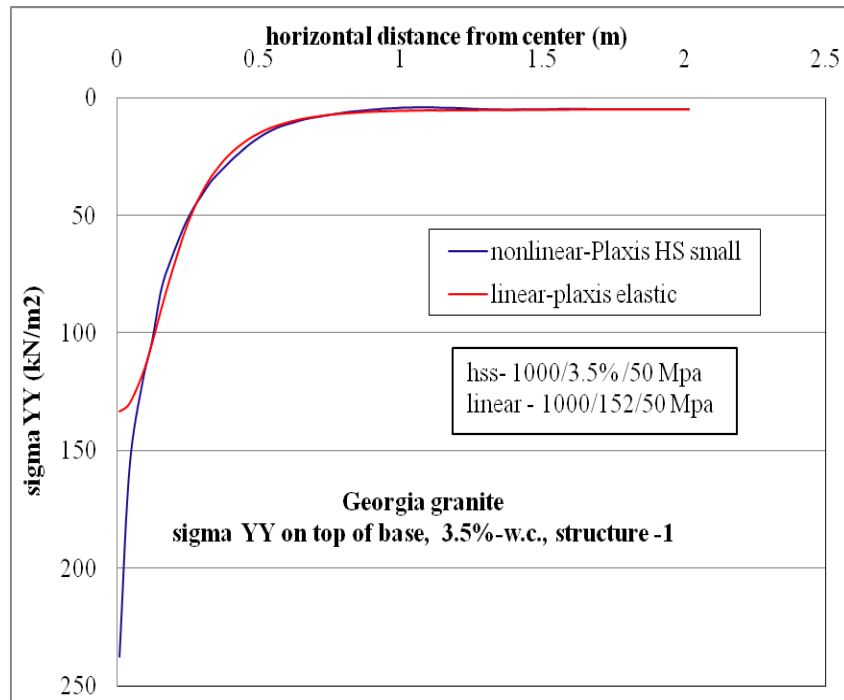


Figure C-110.  $\sigma_{yy}$  vertical stress at top of base layer comparison for nonlinear and linear cases, for structure-1 with 3.5% w.c. base layer.

### C.2.6.2 Structure-4

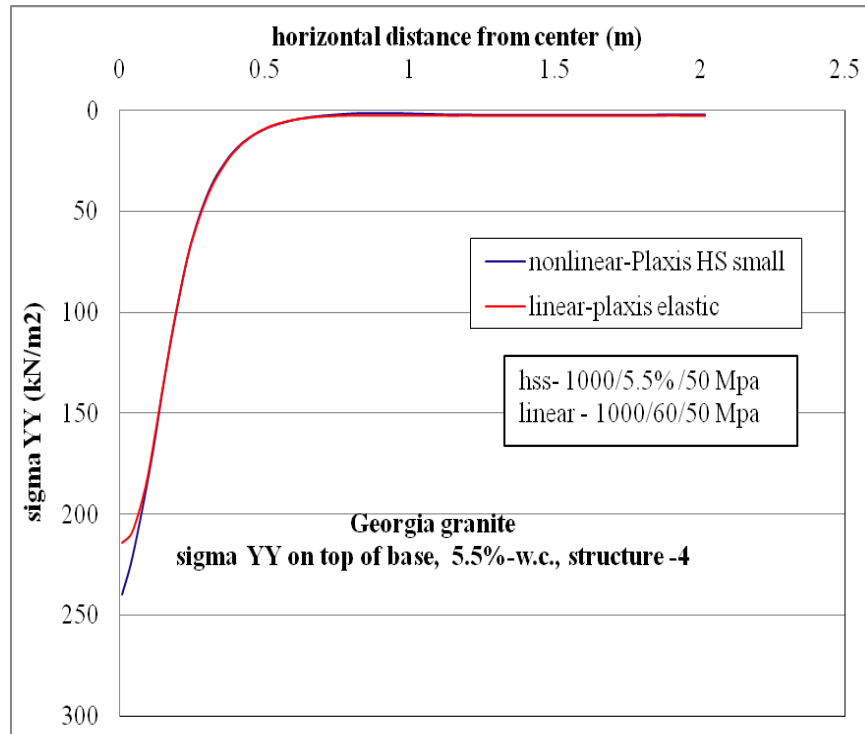


Figure C-111.  $\sigma_{yy}$  vertical stress at top of base layer comparison for nonlinear and linear cases, for structure-4 with 5.5% w.c. base layer.

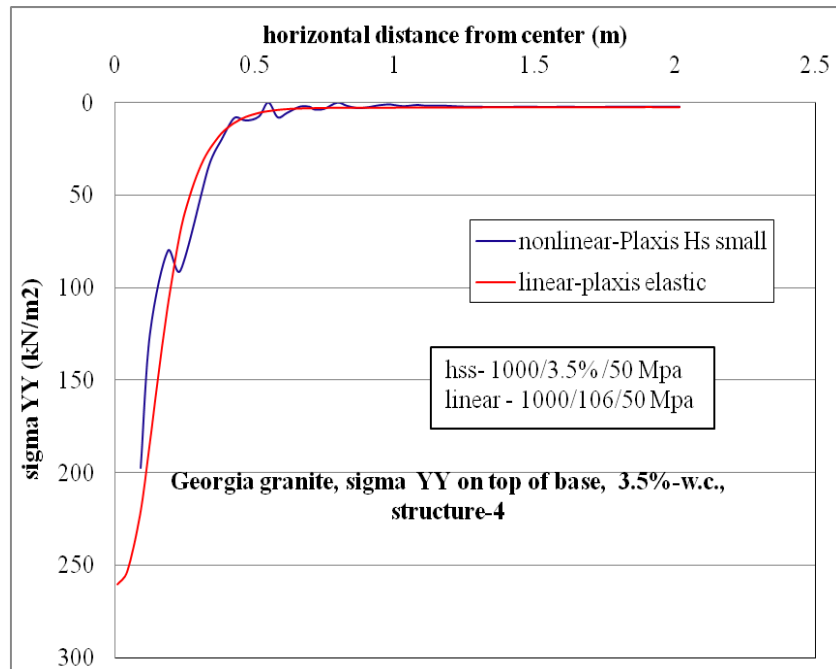


Figure C-112.  $\sigma_{yy}$  vertical stress at top of base layer comparison for nonlinear and linear cases, for structure-4 with 3.5% w.c. base layer.

## C.2.7 Vertical Strain ( $\epsilon_{yy}$ , Compressive Strain) at Top of Base Layer

### C.2.7.1 Structure-1

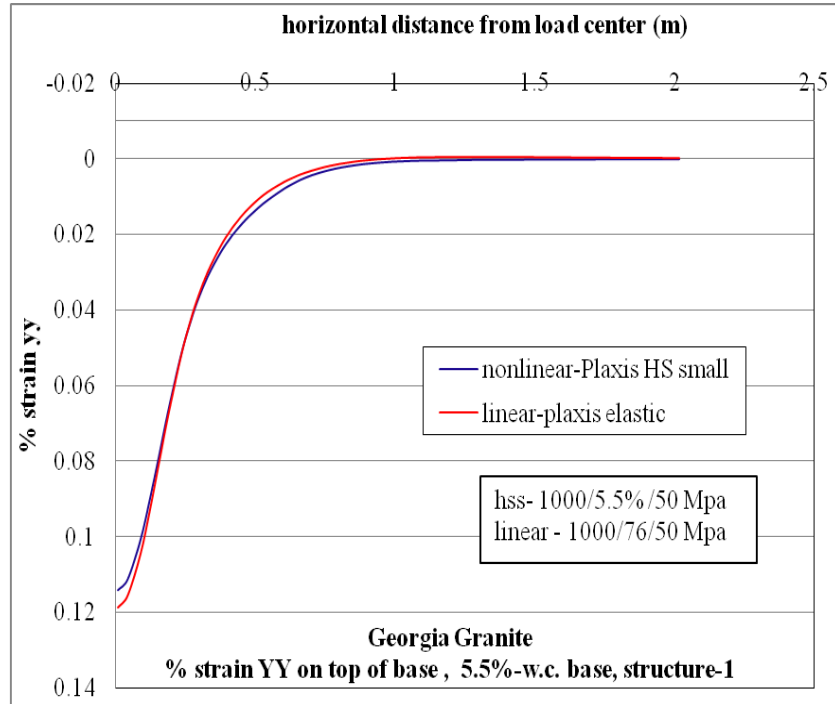


Figure C-113.  $\epsilon_{yy}$  at top of base layer comparison for nonlinear and linear cases, for structure-1 with 5.5% w.c. base layer.

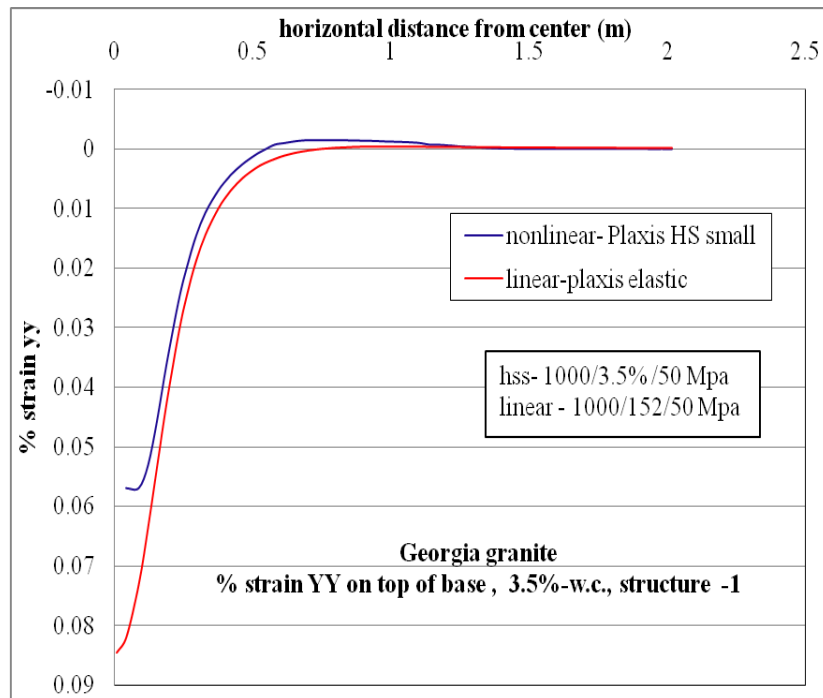


Figure C-114.  $\epsilon_{yy}$  at top of base layer comparison for nonlinear and linear cases, for structure-1 with 3.5% w.c. base layer.

### C.2.7.2 Structure-4

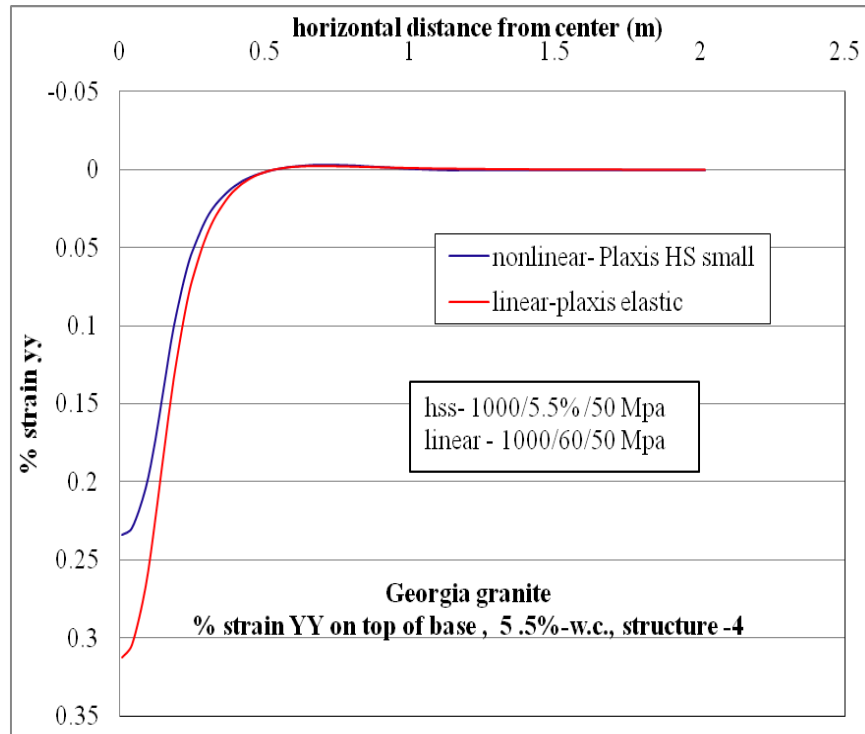


Figure C-115.  $\epsilon_{yy}$  at top of base layer comparison for nonlinear and linear cases, for structure-4 with 5.5% w.c. base layer.

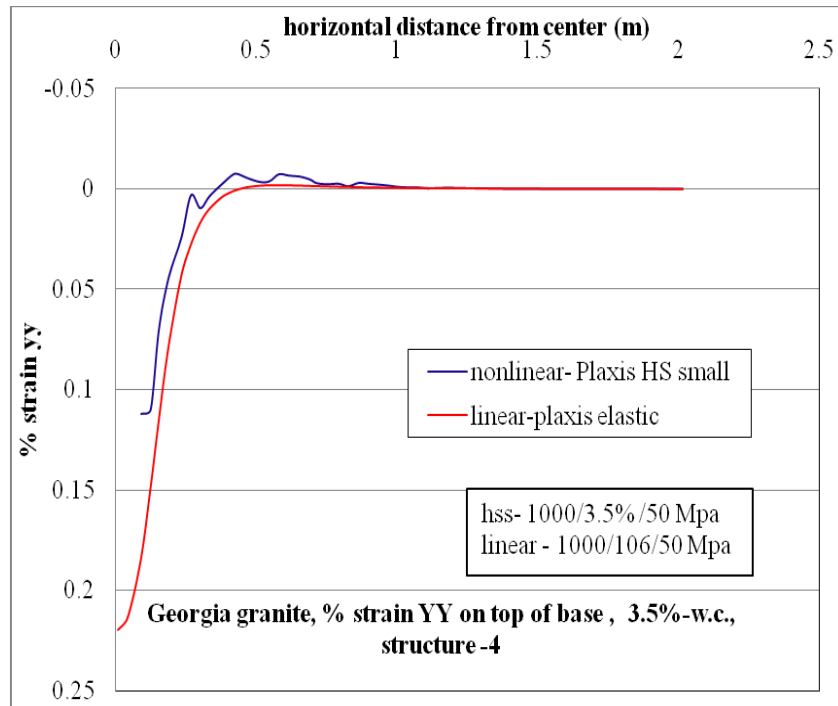


Figure C-116.  $\epsilon_{yy}$  at top of base layer comparison for nonlinear and linear cases, for structure-4 with 3.5% w.c. base layer.

## C.2.8 Vertical Stress ( $\sigma_{yy}$ , Compressive Stress) at Bottom of Base Layer

### C.2.8.1 Structure-1

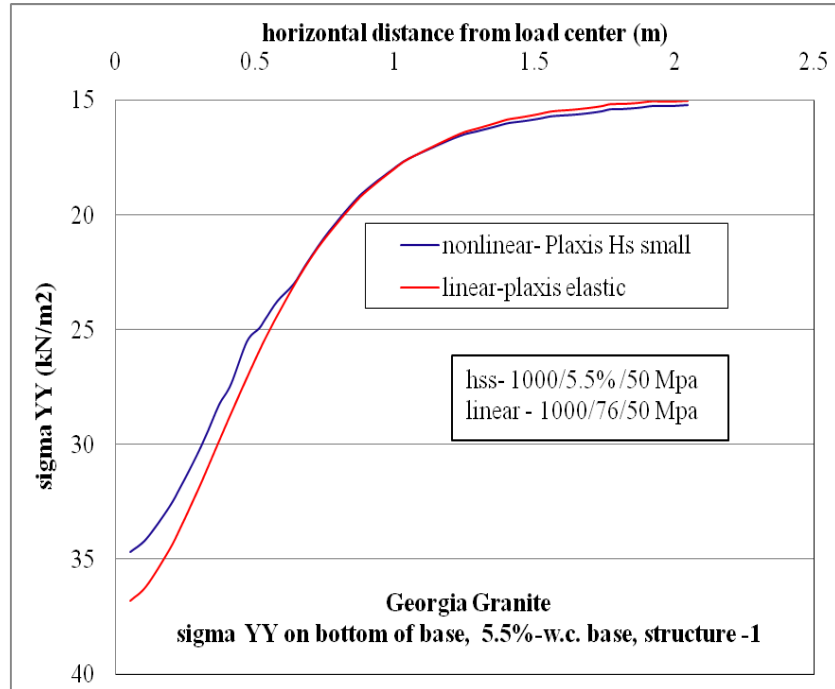


Figure C-117.  $\sigma_{yy}$  at bottom of base layer comparison for nonlinear and linear cases, for structure-1 with 5.5% w.c. base layer.

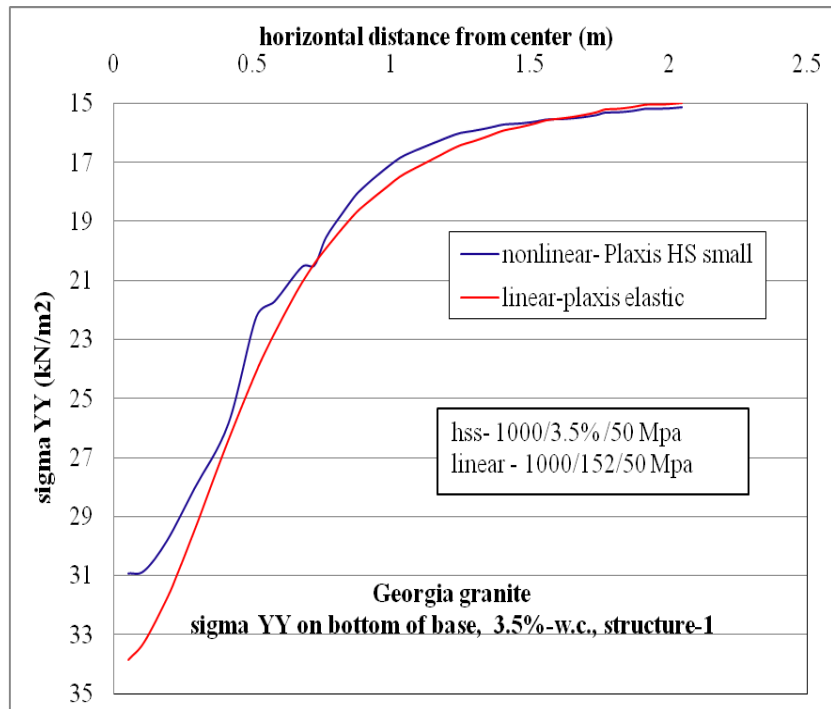


Figure C-118.  $\sigma_{yy}$  at bottom of base layer comparison for nonlinear and linear cases, for structure-1 with 3.5% w.c. base layer

### C.2.8.2 Structure-4

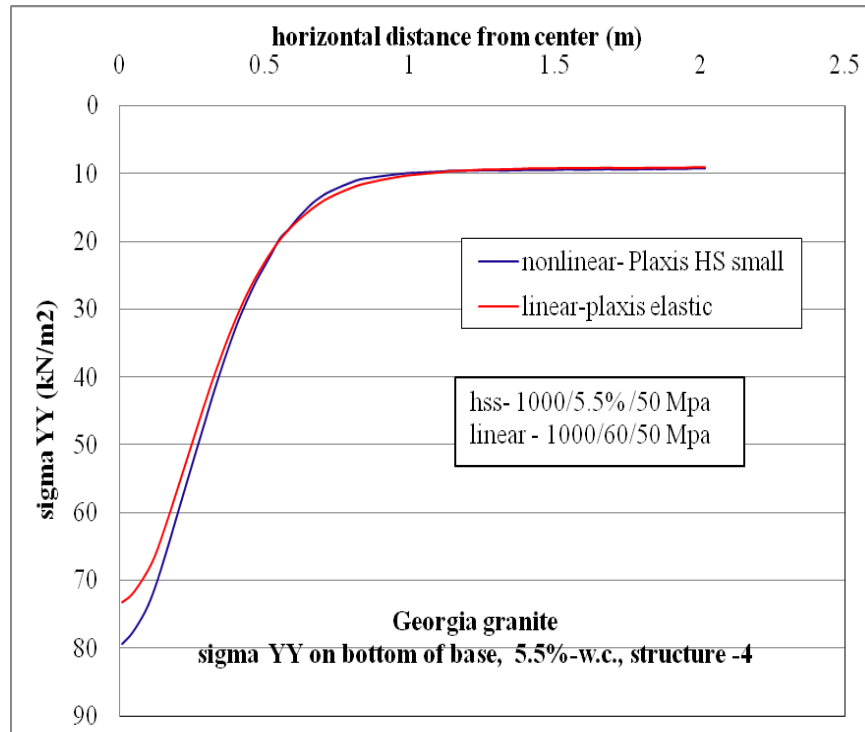


Figure C-119.  $\sigma_{yy}$  at bottom of base layer comparison for nonlinear and linear cases, for structure-4 with 5.5% w.c. base layer.

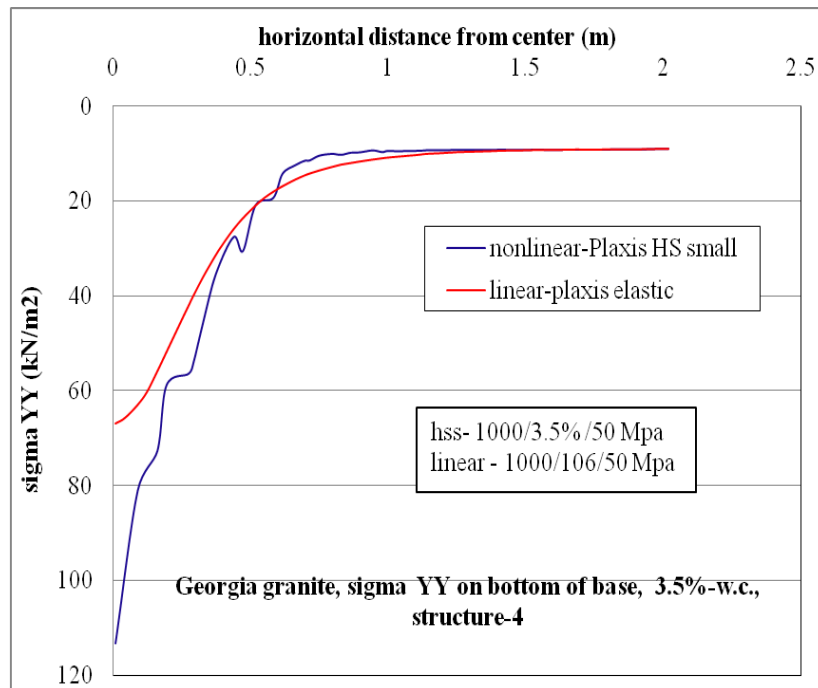


Figure C-120.  $\sigma_{yy}$  at bottom of base layer comparison for nonlinear and linear cases, for structure-4 with 3.5% w.c. base layer.

**C.2.9 Vertical strain ( $\epsilon_{yy}$ , Compressive Strain) at Bottom of Base Layer**  
**C.2.9.1 Structure-1**

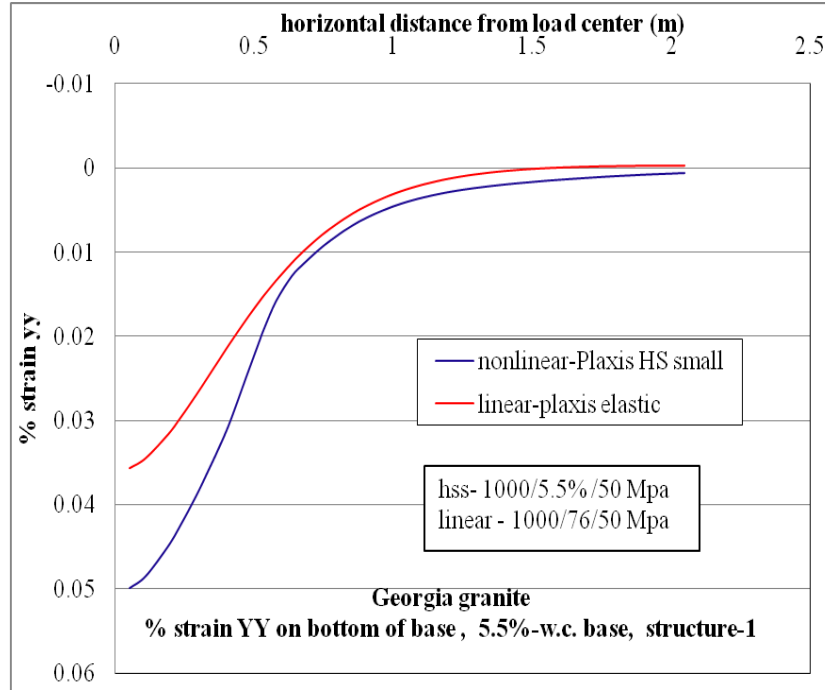


Figure C-121.  $\epsilon_{yy}$  at bottom of base layer comparison for nonlinear and linear cases, for structure-1 with 5.5% w.c. base layer.

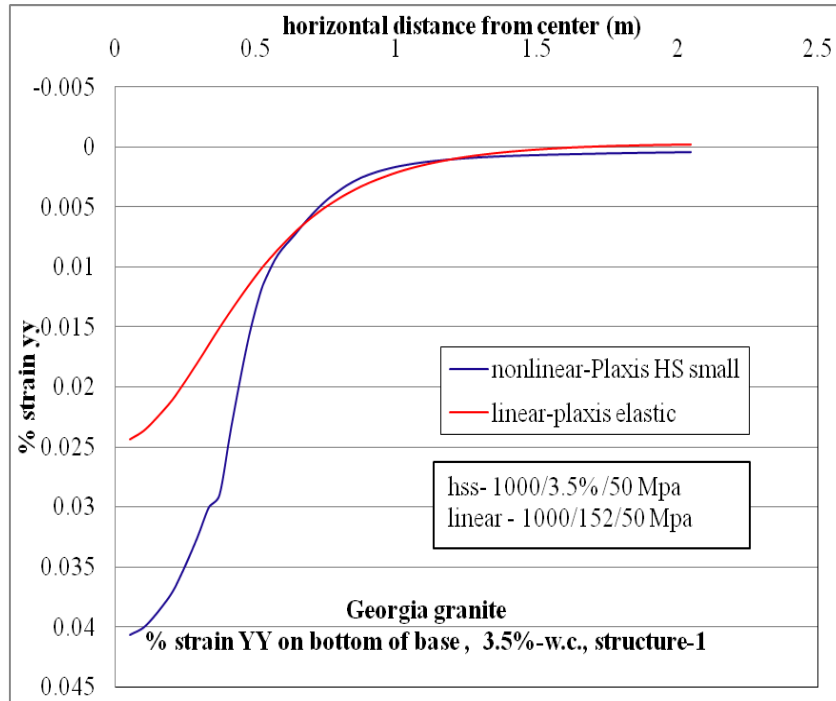


Figure C-122.  $\epsilon_{yy}$  at bottom of base layer comparison for nonlinear and linear cases, for structure-1 with 3.5% w.c. base layer.

### C.2.9.2 Structure-4

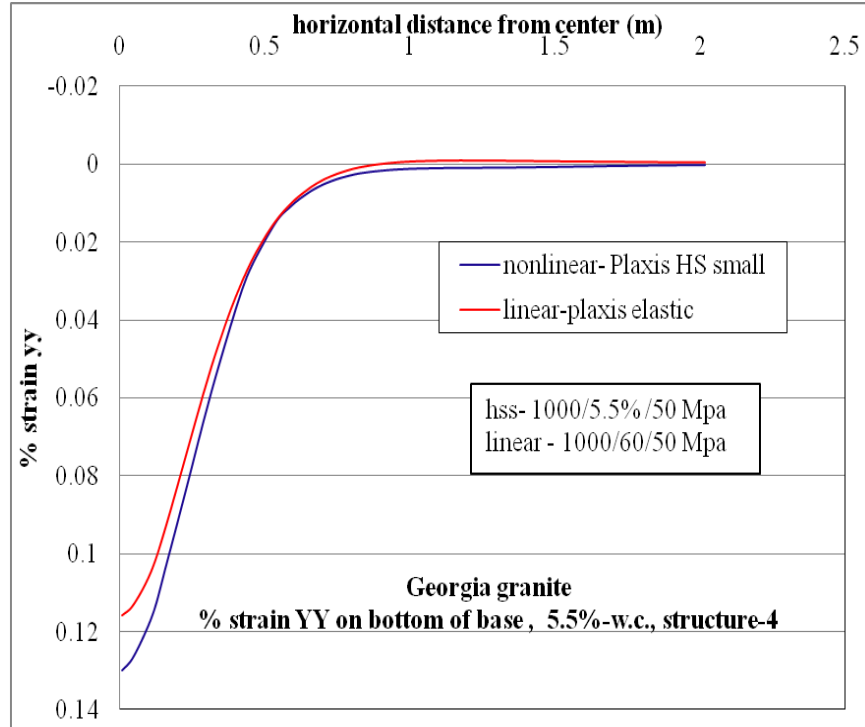


Figure C-123.  $\epsilon_{yy}$  at bottom of base layer comparison for nonlinear and linear cases, for structure-4 with 5.5% w.c. base layer.

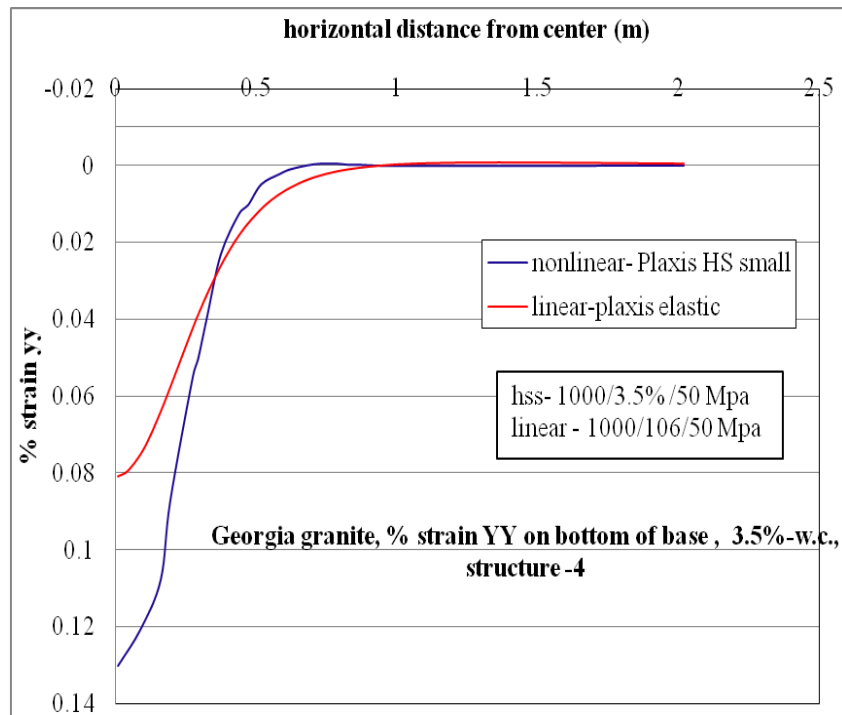


Figure C-124.  $\epsilon_{yy}$  at bottom of base layer comparison for nonlinear and linear cases, for structure-4 with 3.5% w.c. base layer.

## C.2.10 Vertical Stress ( $\sigma_{yy}$ , Compressive Stress) at Top of Subgrade Layer

### C.2.10.1 Structure-1

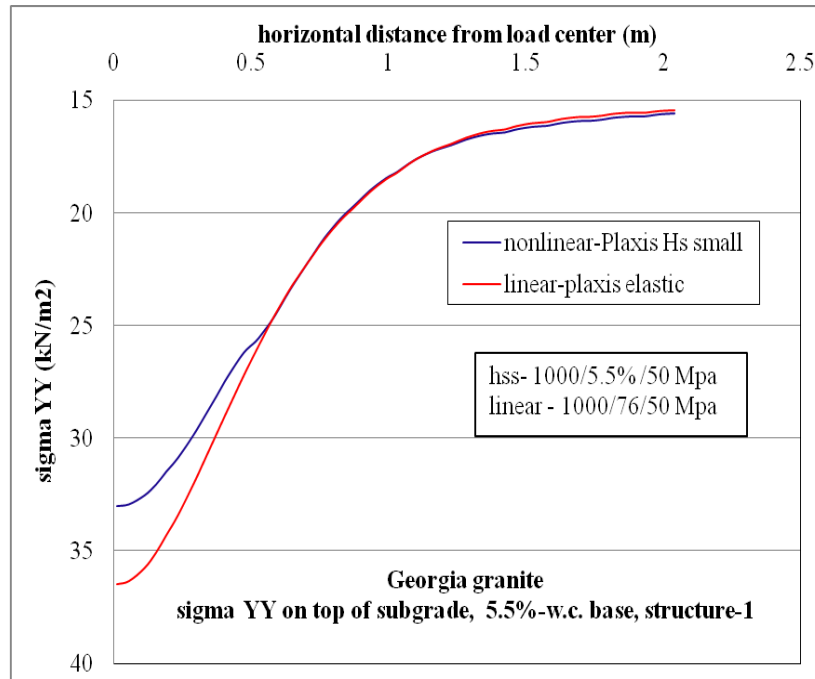


Figure C-125.  $\sigma_{yy}$  at top of subgrade comparison for nonlinear and linear cases, for structure-1 with 5.5% w.c. base layer.

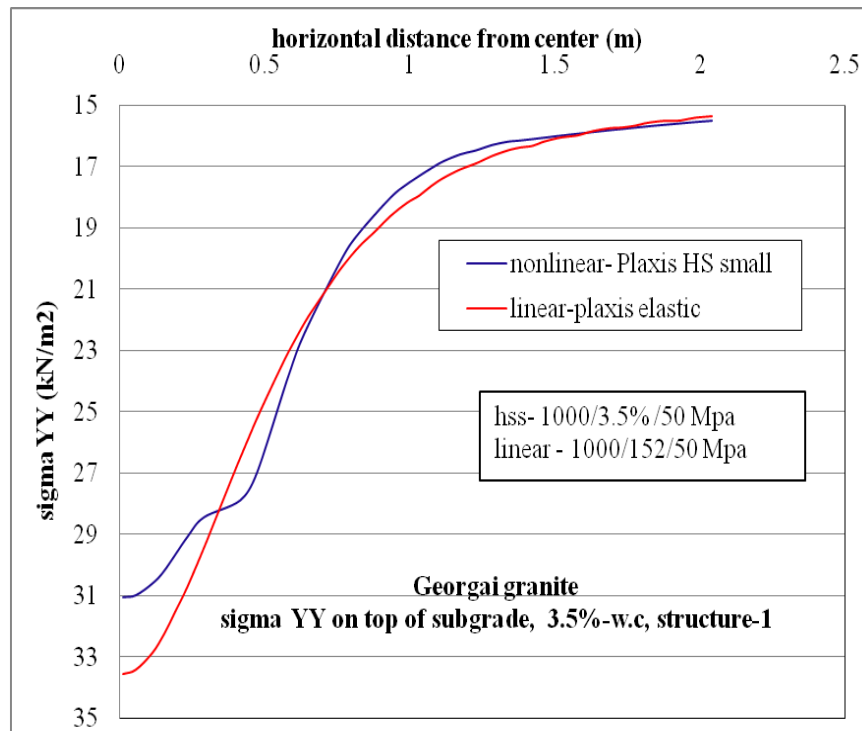


Figure C-126.  $\sigma_{yy}$  at top of subgrade layer comparison for nonlinear and linear cases for structure-1 with 3.5% w.c. base layer.

### C.2.10.2 Structure-4

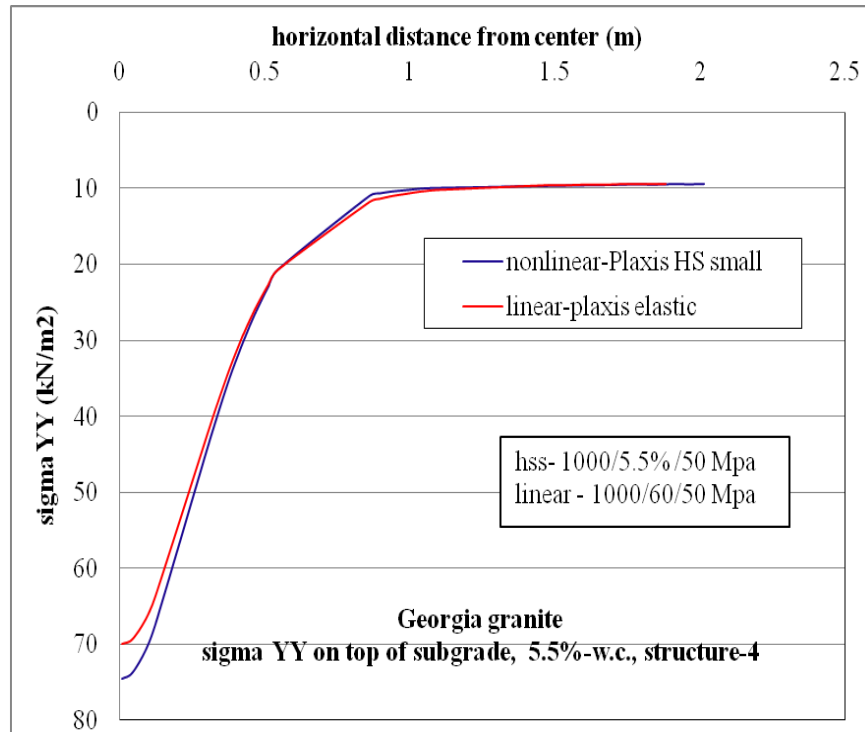


Figure C-127.  $\sigma_{yy}$  at top of subgrade layer comparison for nonlinear and linear cases, for structure-4 with 5.5% w.c. base layer.

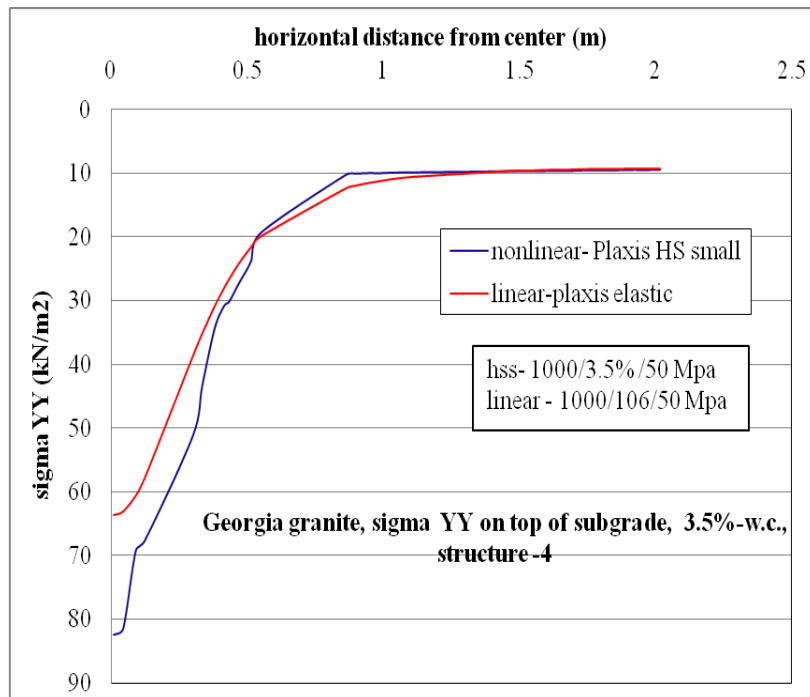


Figure C-128.  $\sigma_{yy}$  at top of subgrade layer comparison for nonlinear and linear cases for structure-4 with 3.5% w.c. base layer.

## C.2.11 Vertical Strain ( $\epsilon_{yy}$ , Compressive Strain) at Top of Subgrade Layer

### C.2.11.1 Structure-1

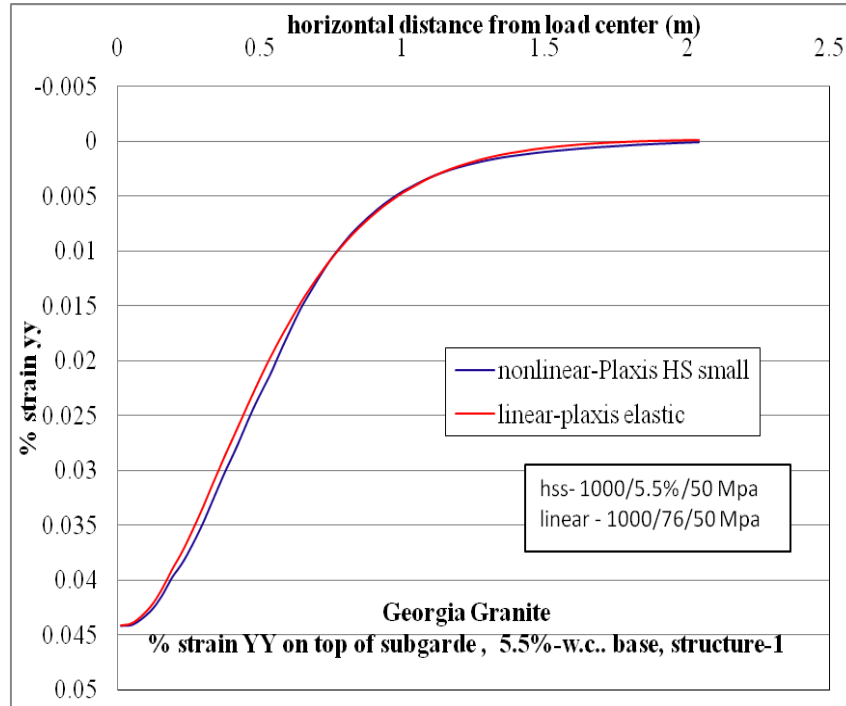


Figure C-129.  $\epsilon_{yy}$  at top of subgrade layer comparison for nonlinear and linear cases for structure-1 with 5.5% w.c. base layer.

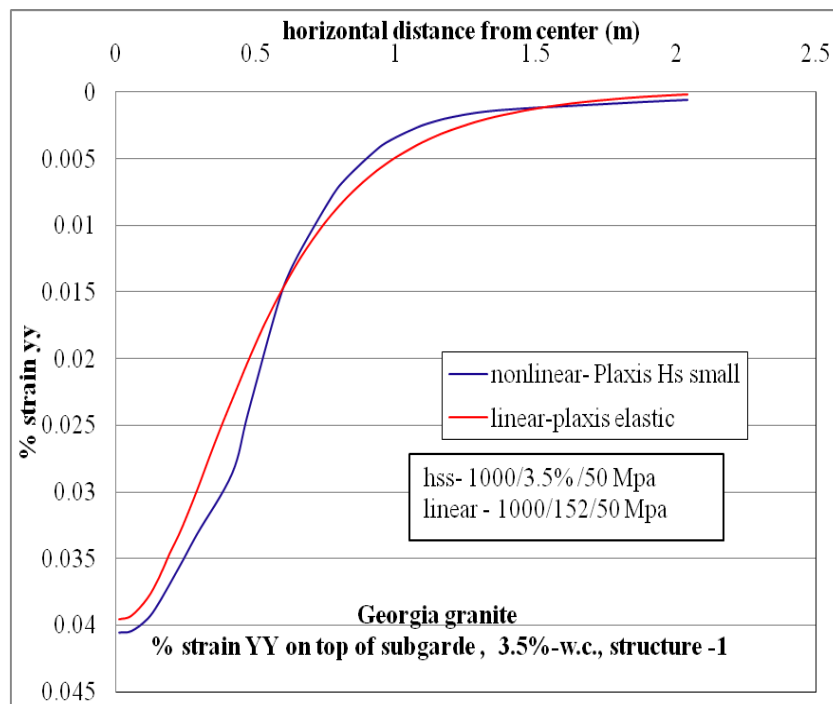


Figure C-130.  $\epsilon_{yy}$  at top of subgrade layer comparison for nonlinear and linear cases for structure-1 with 3.5% w.c. base layer.

### C.2.11.1 Structure-4

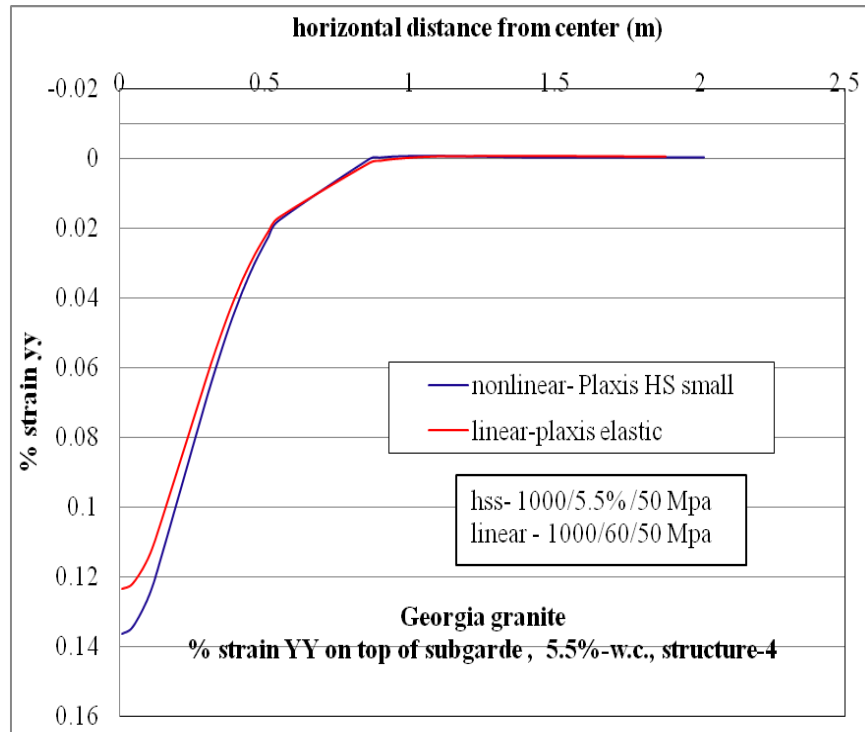


Figure C-131.  $\epsilon_{yy}$  at top of subgrade layer comparison for nonlinear and linear cases for structure-4 with 5.5% w.c. base layer.

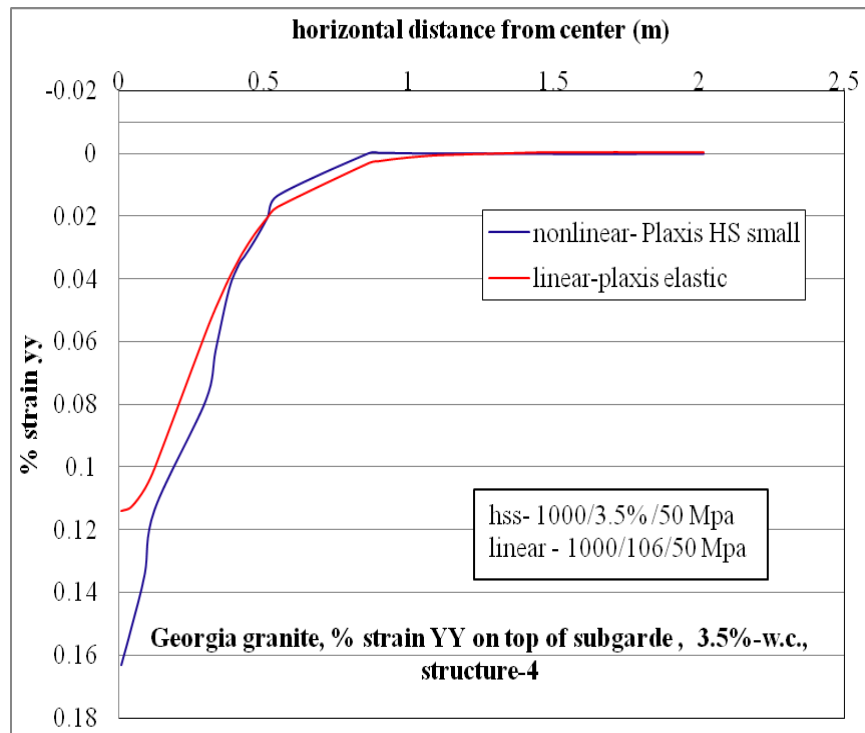


Figure C-132.  $\epsilon_{yy}$  at top of subgrade layer comparison for nonlinear and linear cases for structure-4 with 3.5% w.c. base layer.

APPENDIX D  
COMPARISON OF NONLINEAR AND EQUIVALENT LINEAR RESPONSES OBTAINED  
FOR NONLINEAR BASE AND NONLINEAR SUBGRADE ANALYSIS

**D.1 Newberry Limerock**

**D.1.1 Surface Deflection Profiles**

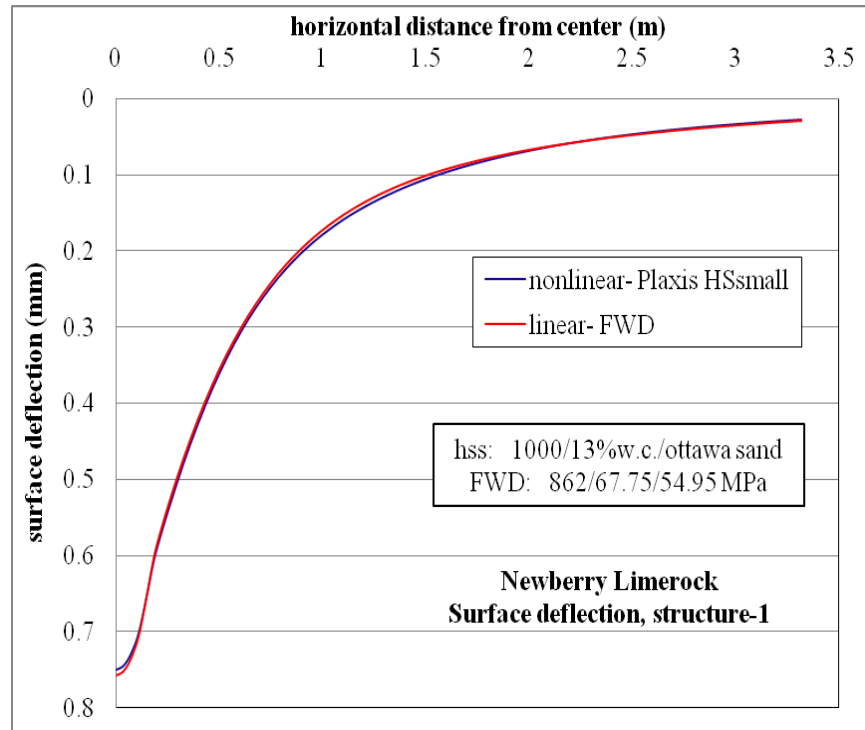


Figure D-1. Surface deflection comparison for nonlinear and linear cases, for structure-1 with 13% w.c. base layer and nonlinear Ottawa sand subgrade

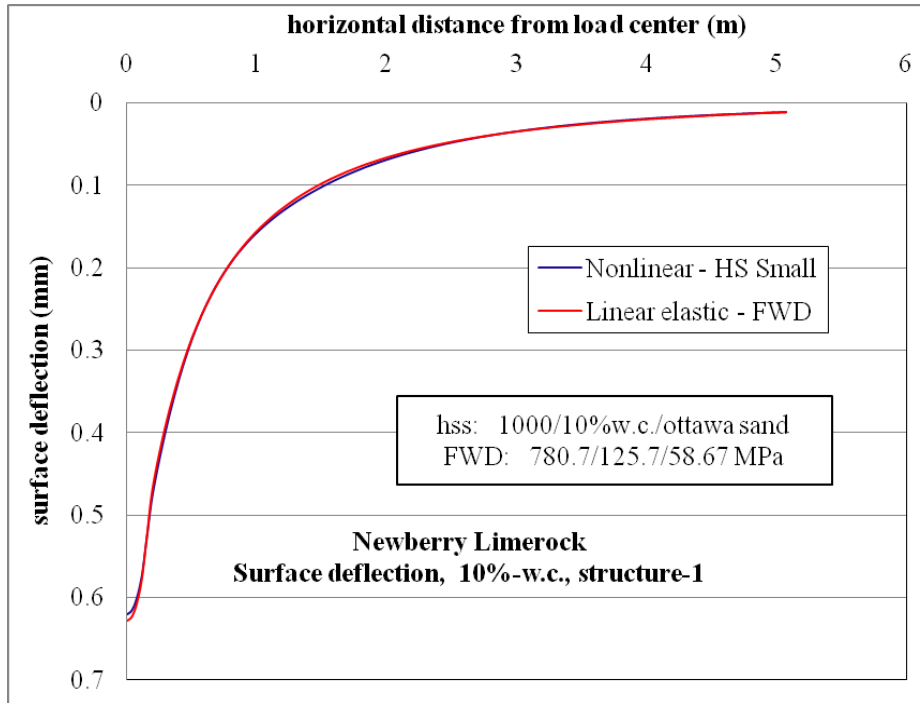


Figure D-2. Surface deflection comparison for nonlinear and linear cases, for structure-1 with 10% w.c. base layer and nonlinear Ottawa sand subgrade.

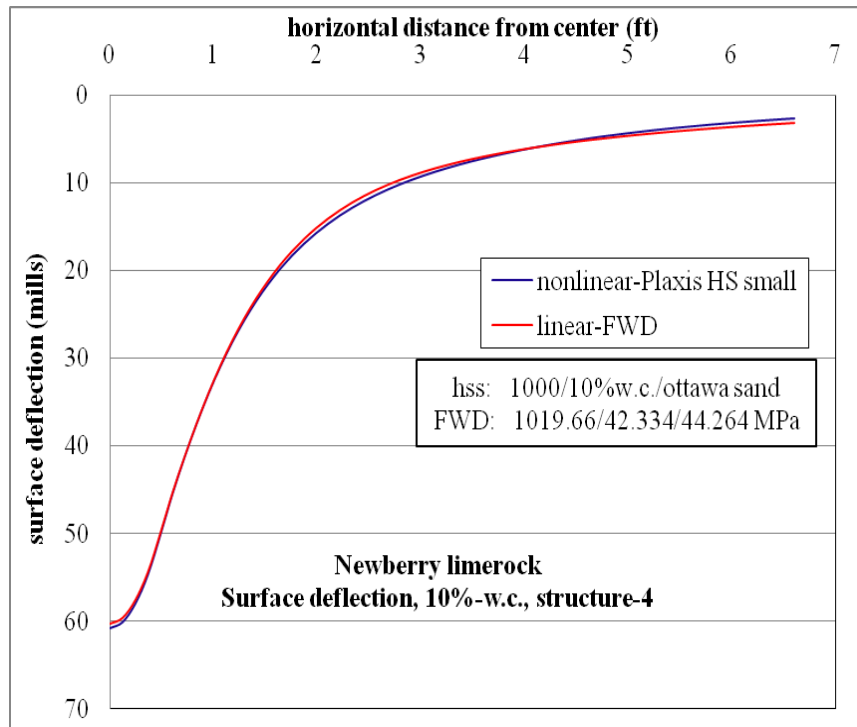


Figure D-3. Surface deflection comparison for nonlinear and linear cases, for structure-4 with 10% w.c. base layer and nonlinear Ottawa sand subgrade.

### D.1.2 Horizontal Stress ( $\sigma_{xx}$ , Tensile Stress) at Top of AC Layer

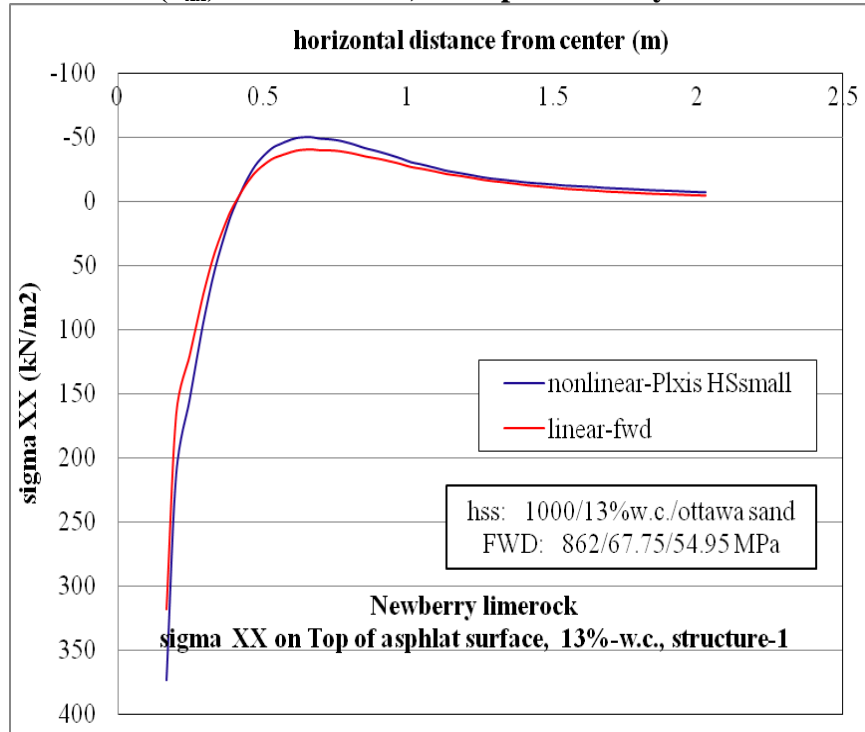


Figure D-4.  $\sigma_{xx}$  at top of AC layer comparison for nonlinear and linear cases, for structure-1 with 13% w.c. base layer and nonlinear Ottawa sand subgrade.

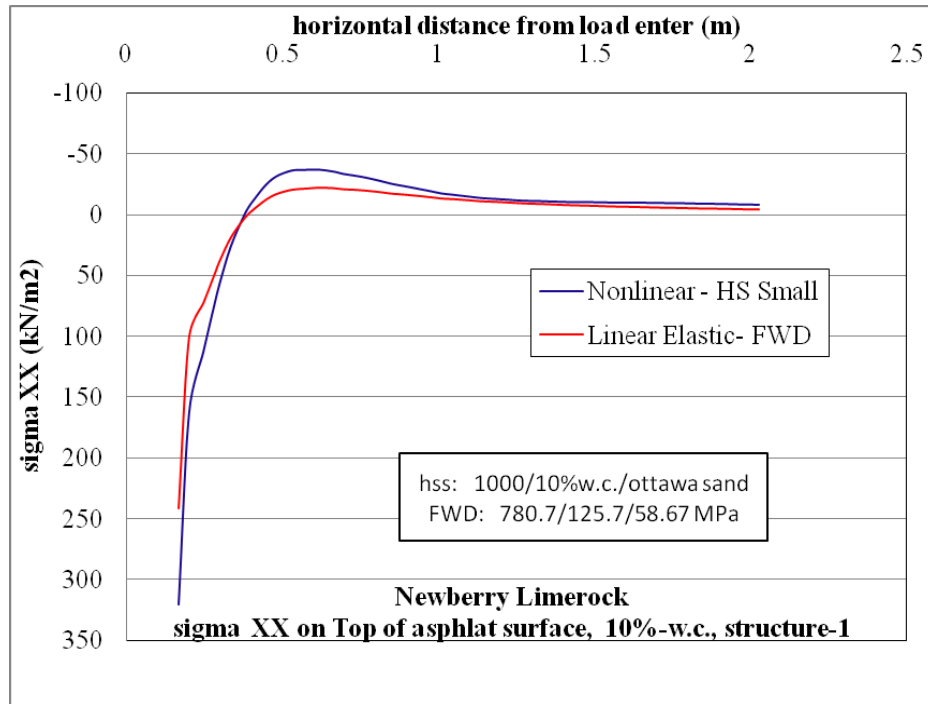


Figure D-5.  $\sigma_{xx}$  at top of AC layer comparison for nonlinear and linear cases, for structure-1 with 10% w.c. base layer and nonlinear Ottawa sand subgrade.

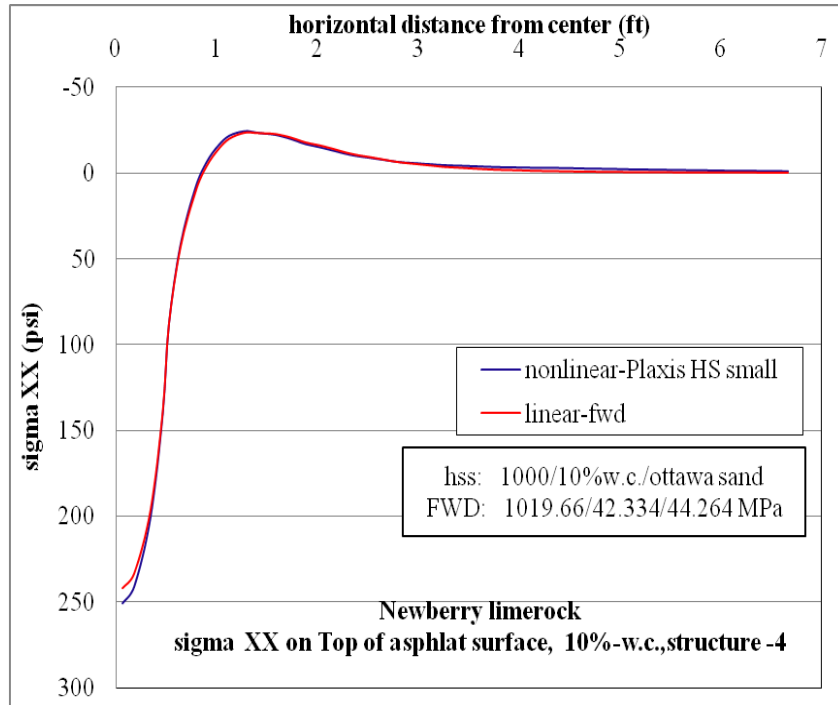


Figure D-6.  $\sigma_{xx}$  at top of AC layer comparison for nonlinear and linear cases, for structure-4 with 10% w.c. base layer and nonlinear Ottawa sand subgrade.

### D.1.3 Horizontal Strain ( $\epsilon_{xx}$ , Tensile Strain) at Top of AC Layer

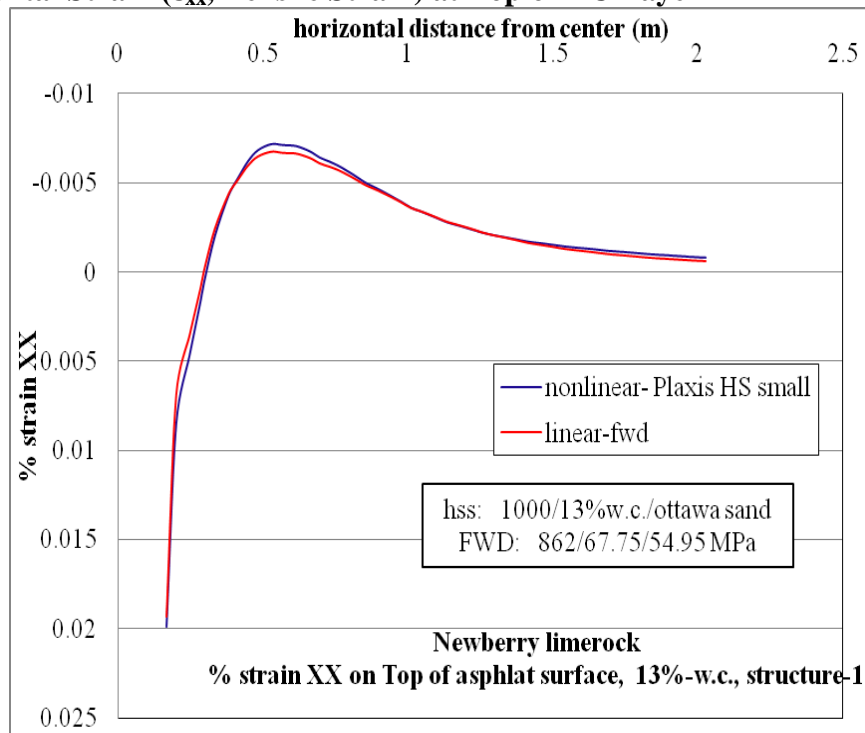


Figure D-7.  $\epsilon_{xx}$  at top of AC layer comparison for nonlinear and linear cases, for structure-1 with 13% w.c. base layer and nonlinear Ottawa sand subgrade.

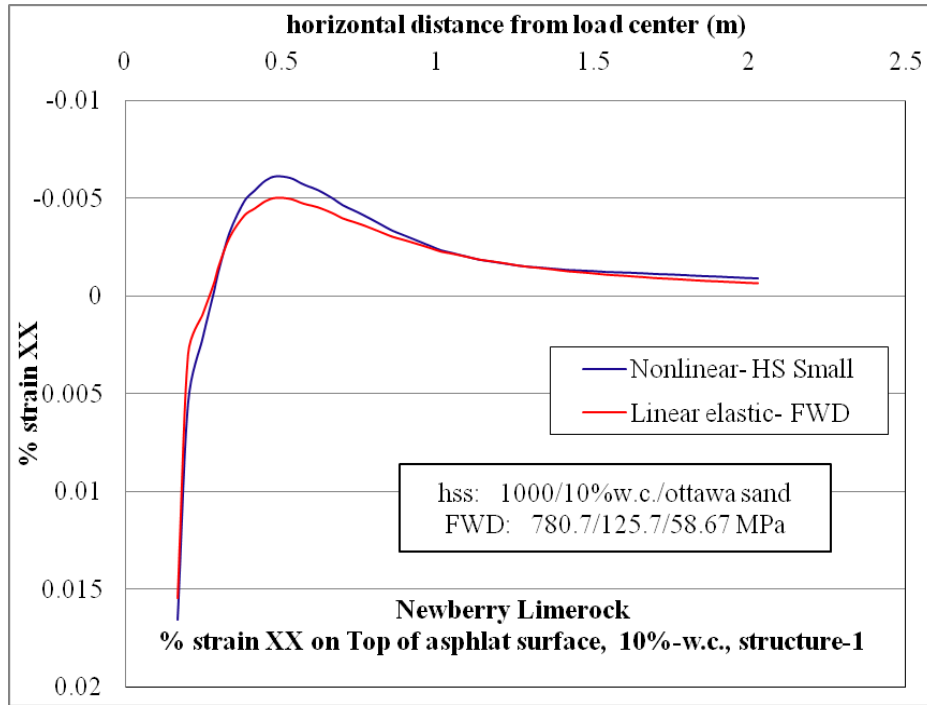


Figure D-8.  $\epsilon_{xx}$  at top of AC layer comparison for nonlinear and linear cases, for structure-1 with 10% w.c. base layer and nonlinear Ottawa sand subgrade.

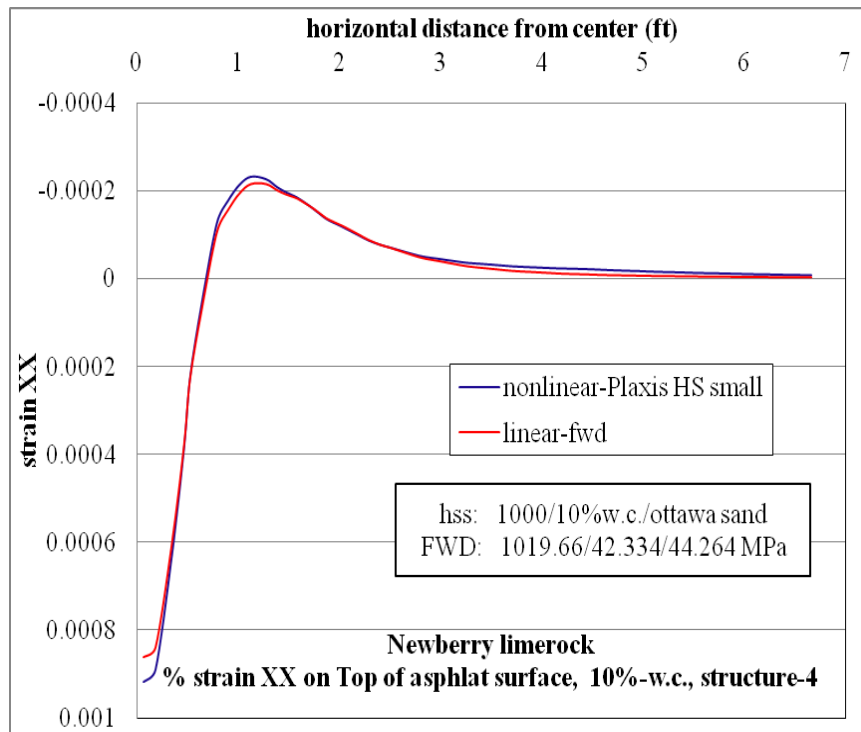


Figure D-9.  $\epsilon_{xx}$  at top of AC layer comparison for nonlinear and linear cases, for structure-4 with 10% w.c. base layer and nonlinear Ottawa sand subgrade.

### D.1.4 Horizontal Stress ( $\sigma_{xx}$ , Tensile Stress) at Bottom of AC Layer

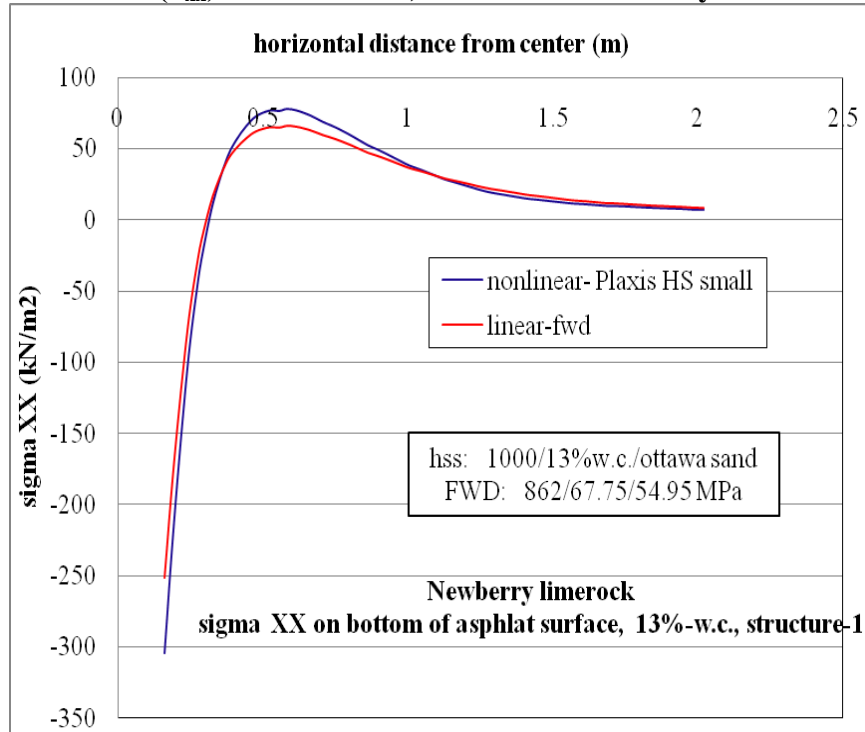


Figure D-10.  $\sigma_{xx}$  at bottom of AC layer comparison for nonlinear and linear cases, for structure-1 with 13% w.c. base layer and nonlinear Ottawa sand subgrade.

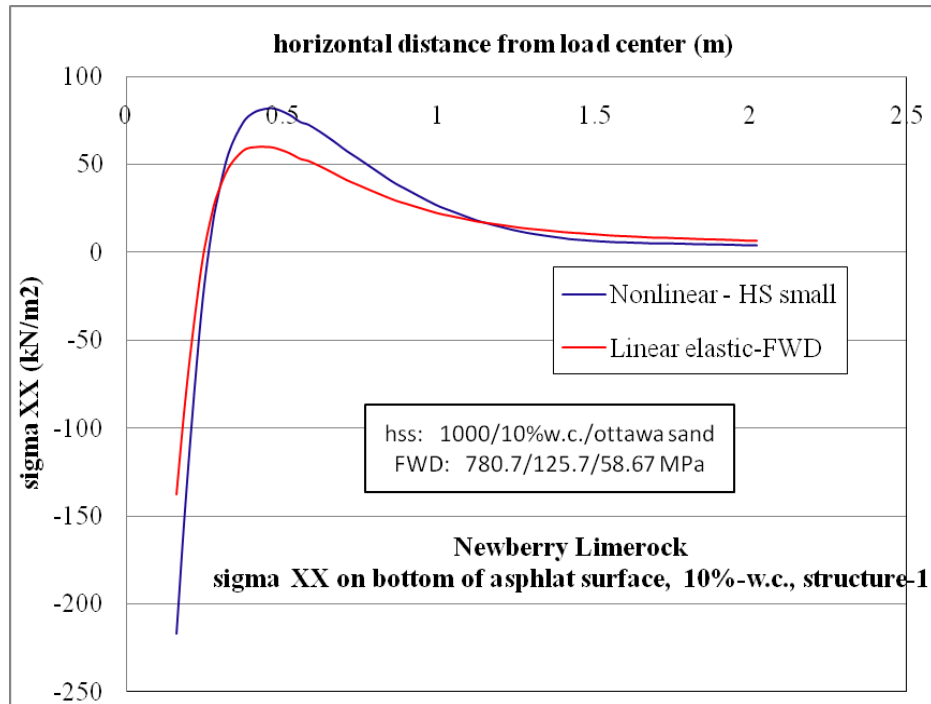


Figure D-11.  $\sigma_{xx}$  at bottom of AC layer comparison for nonlinear and linear cases, for structure-1 with 10% w.c. base layer and nonlinear Ottawa sand subgrade.

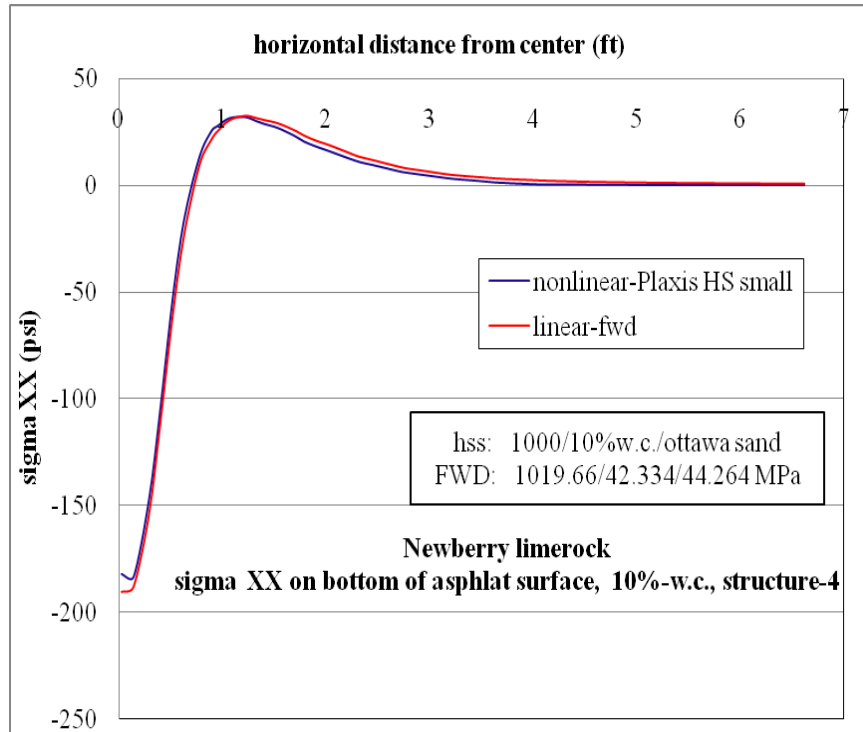


Figure D-12.  $\sigma_{xx}$  at bottom of AC layer comparison for nonlinear and linear cases, for structure-4 with 10% w.c. base layer and nonlinear Ottawa sand subgrade.

#### D.1.5 Horizontal Strain ( $\epsilon_{xx}$ , Tensile Strain) at Bottom of AC layer

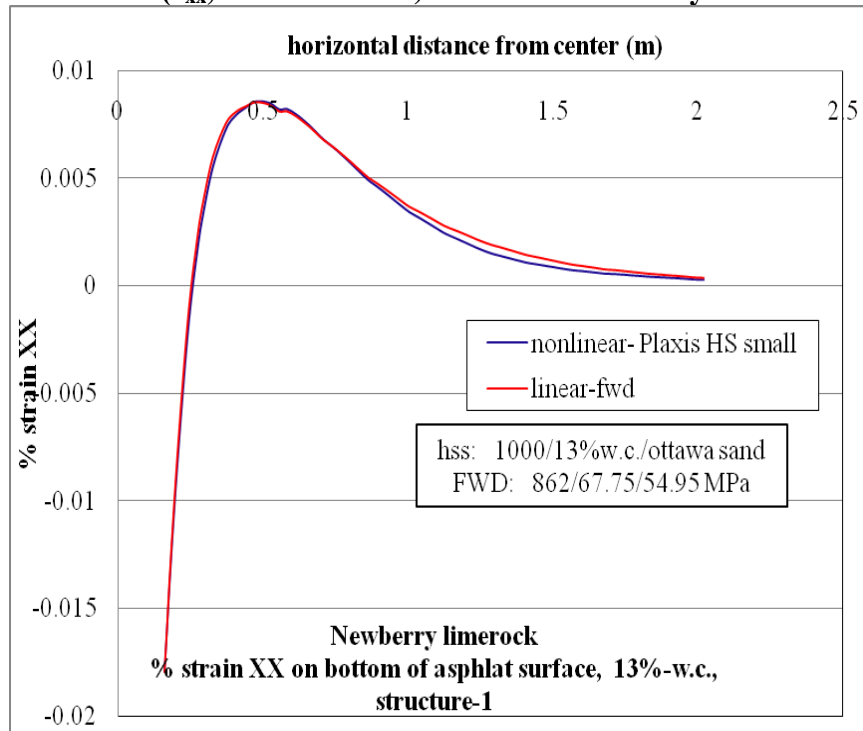


Figure D-13.  $\epsilon_{xx}$  at bottom of AC layer comparison for nonlinear and linear cases, for structure-1 with 13% w.c. base layer and nonlinear Ottawa sand subgrade.

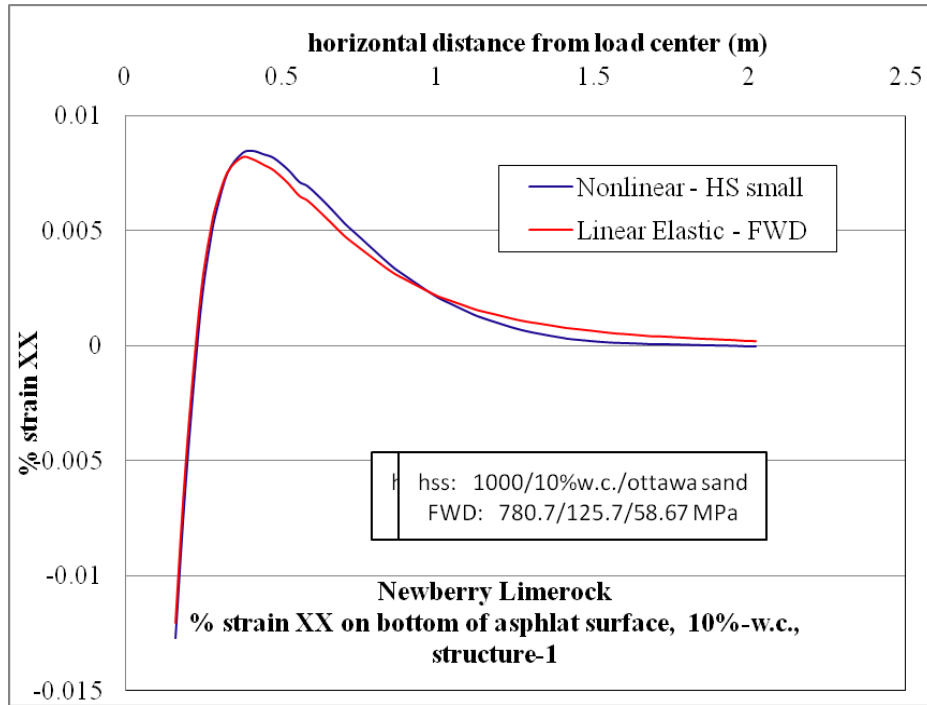


Figure D-14.  $\epsilon_{xx}$  at bottom of AC layer comparison for nonlinear and linear cases, for structure-1 with 10% w.c. base layer and nonlinear Ottawa sand subgrade.

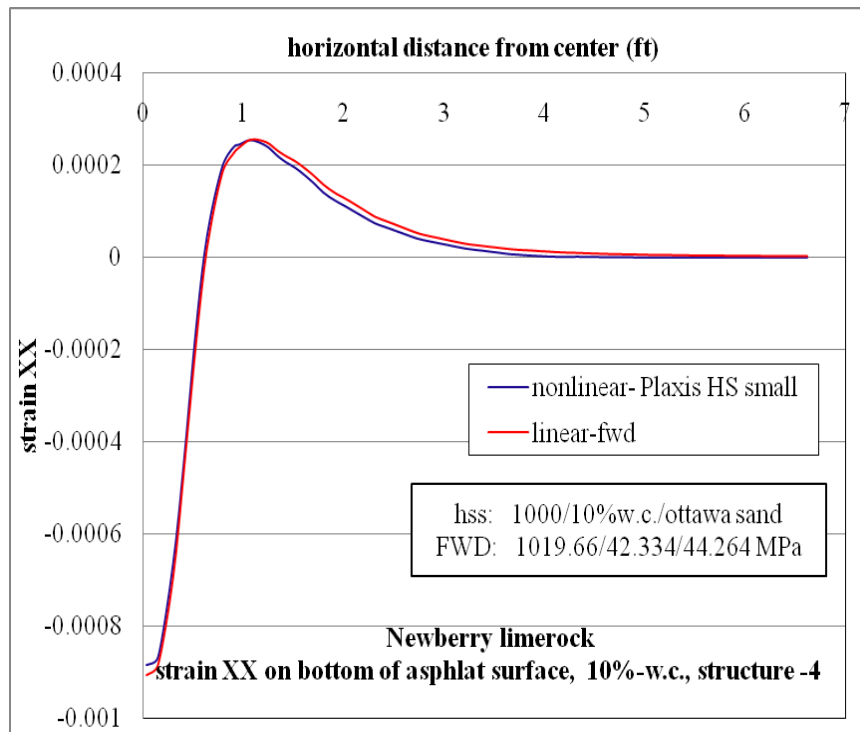


Figure D-15.  $\epsilon_{xx}$  at bottom of AC layer comparison for nonlinear and linear cases, for structure-4 with 10% w.c. base layer and nonlinear Ottawa sand subgrade.

**D.1.6 Vertical stress ( $\sigma_{yy}$ , compressive stress) at top of base layer**

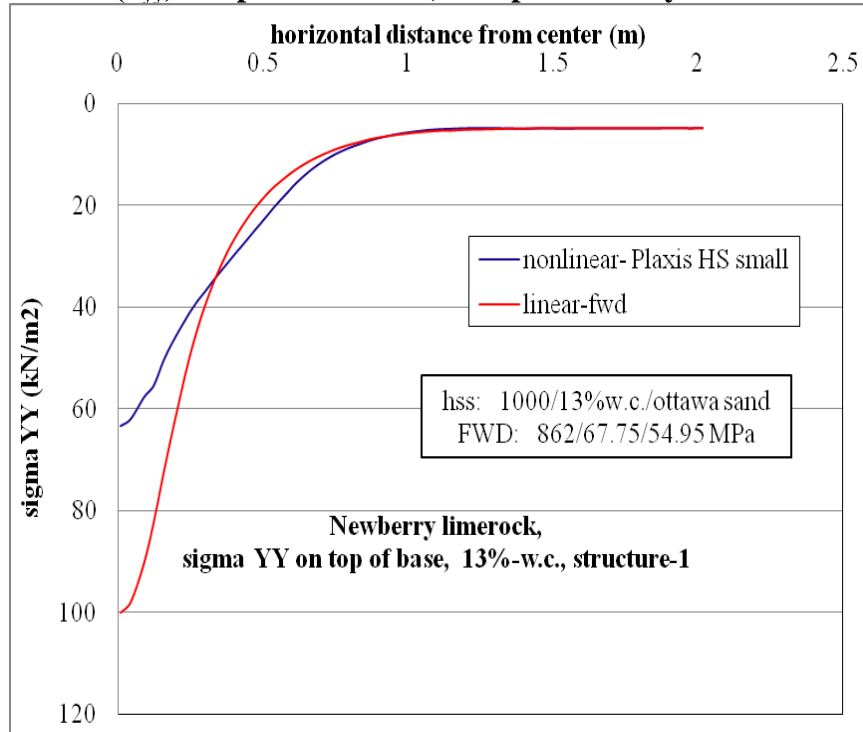


Figure D-16.  $\sigma_{yy}$  vertical stress at top of base layer comparison for nonlinear and linear cases, for structure-1 with 13% w.c. base layer and nonlinear Ottawa sand subgrade.

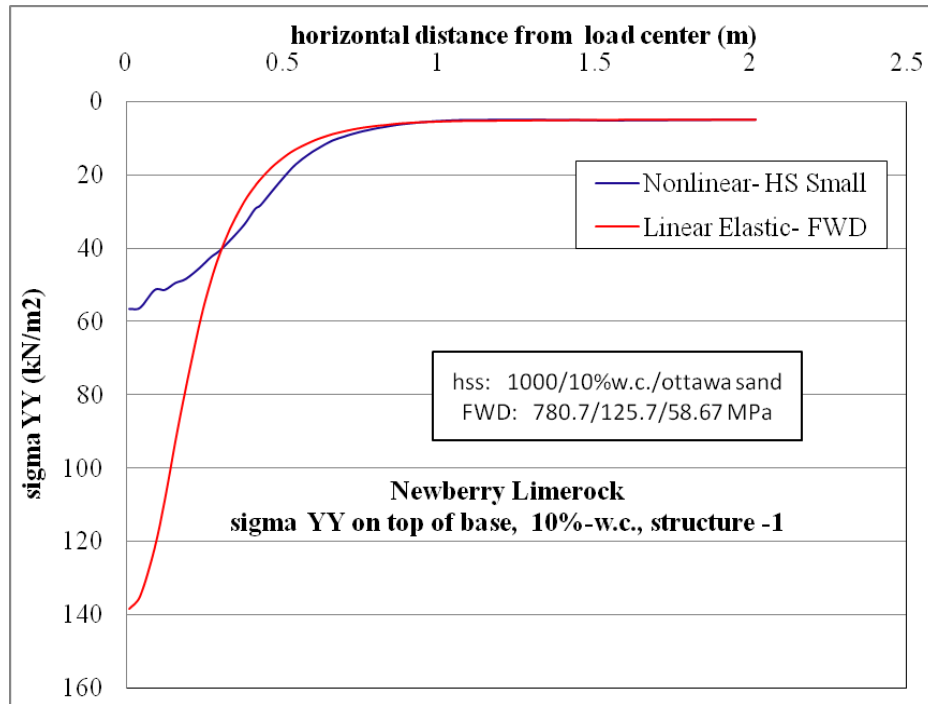


Figure D-17.  $\sigma_{yy}$  vertical stress at top of base layer comparison for nonlinear and linear cases, for structure-1 with 10% w.c. base layer and nonlinear Ottawa sand subgrade.

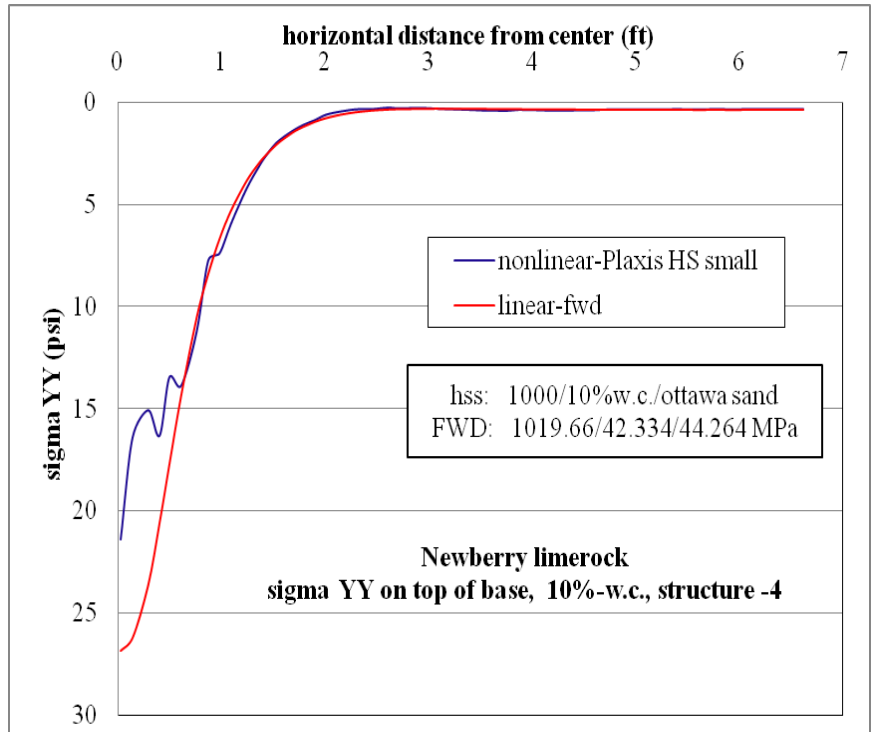


Figure D-18.  $\sigma_{yy}$  vertical stress at top of base layer comparison for nonlinear and linear cases, for structure-4 with 10% w.c. base layer and nonlinear Ottawa sand subgrade.

#### D.1.7 Vertical Strain ( $\epsilon_{yy}$ , Compressive Strain) at Top of Base Layer

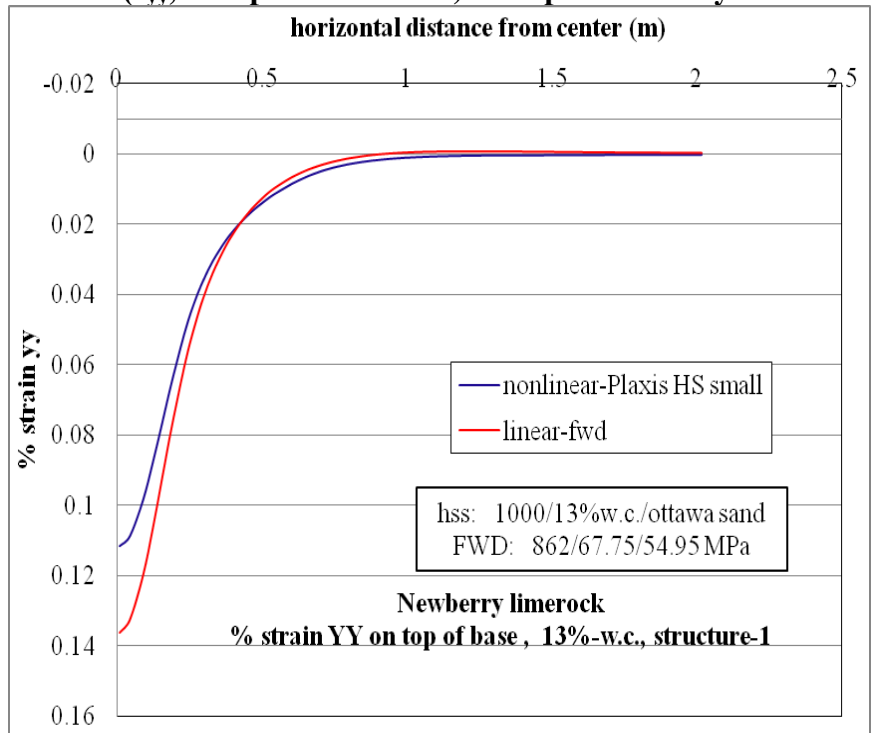


Figure D-19.  $\epsilon_{yy}$  at top of base layer comparison for nonlinear and linear cases, for structure-1 with 13% w.c. base layer and nonlinear Ottawa sand subgrade.

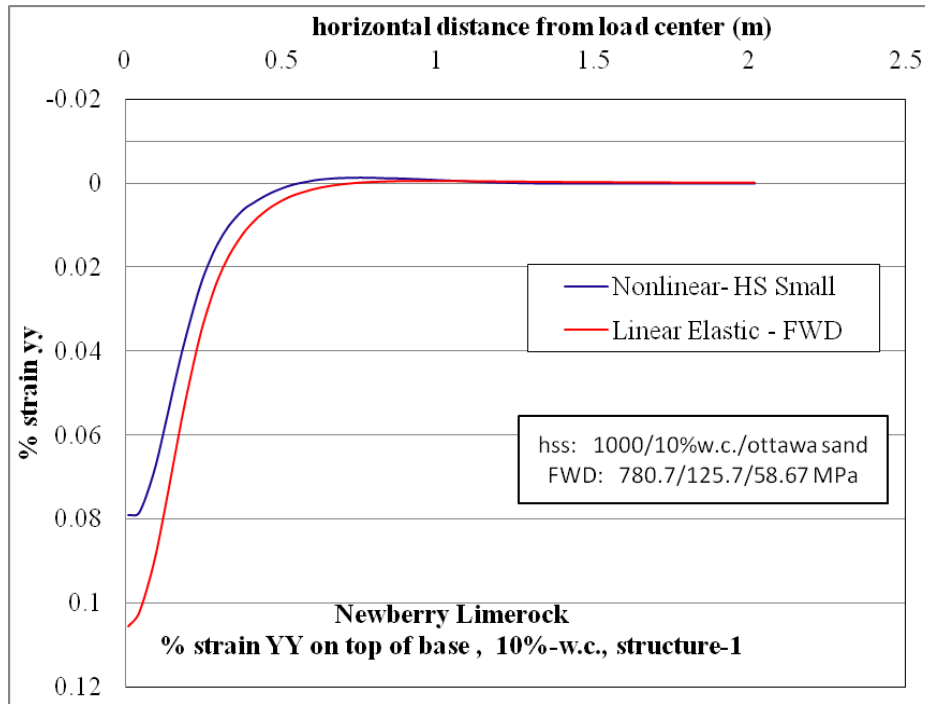


Figure D-20.  $\epsilon_{yy}$  at top of base layer comparison for nonlinear and linear cases, for structure-1 with 10% w.c. base layer and nonlinear Ottawa sand subgrade.

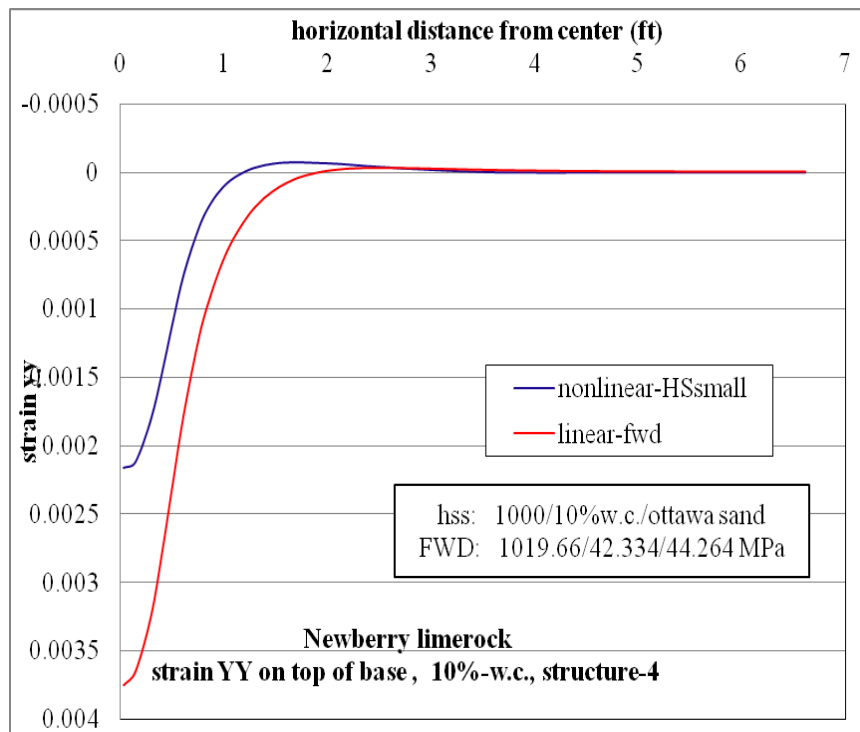


Figure D-21.  $\epsilon_{yy}$  at top of base layer comparison for nonlinear and linear cases, for structure-4 with 10% w.c. base layer and nonlinear Ottawa sand subgrade.

### D.1.8 Vertical Stress ( $\sigma_{yy}$ , Compressive Stress) at Bottom of Base Layer

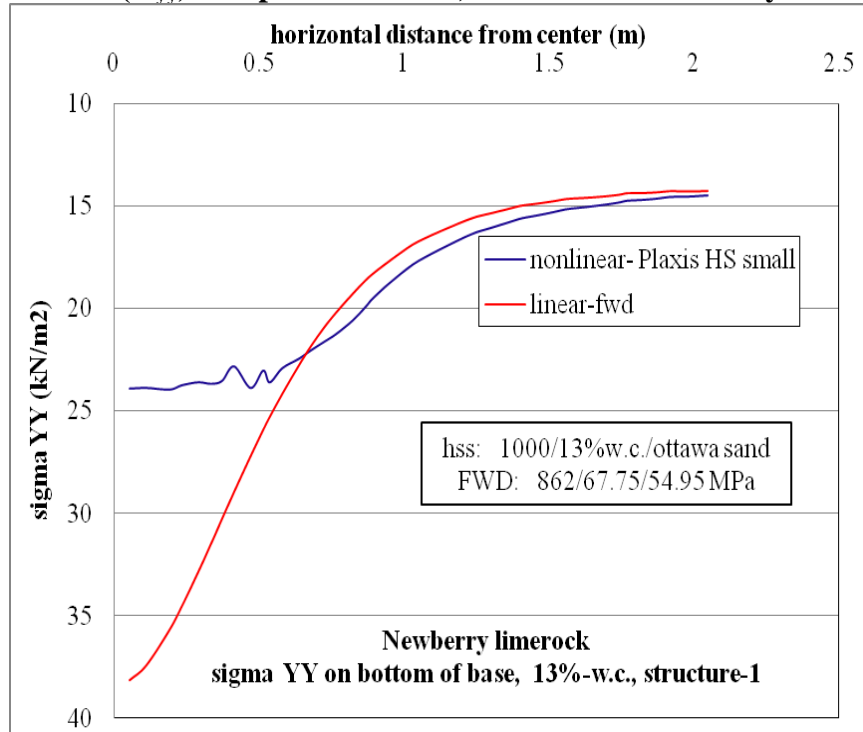


Figure D-22.  $\sigma_{yy}$  at bottom of base layer comparison for nonlinear and linear cases, for structure-1 with 13% w.c. base layer and nonlinear Ottawa sand subgrade.

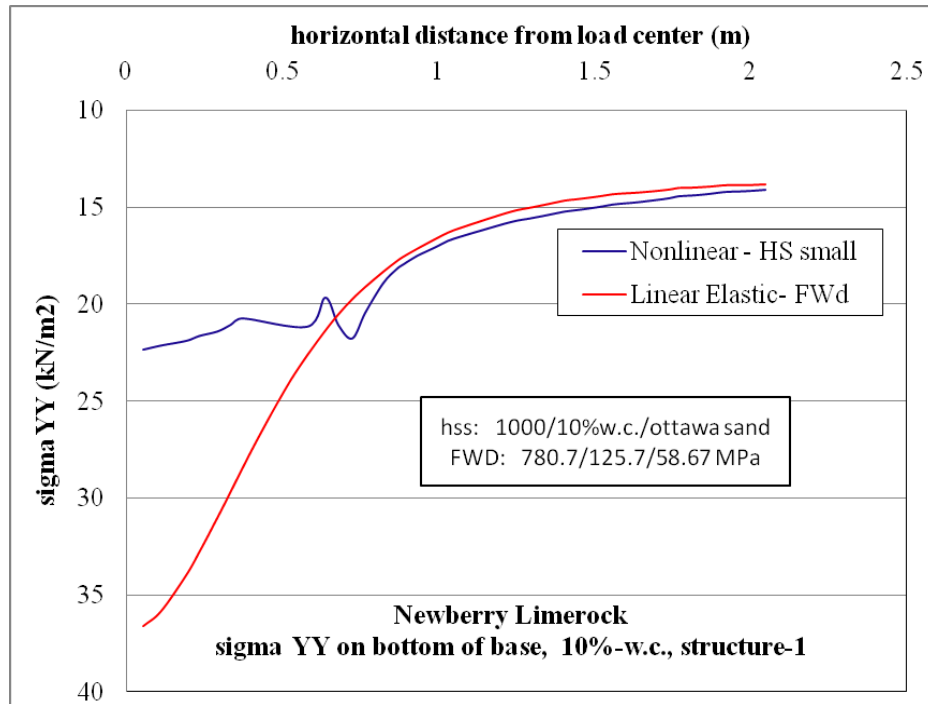


Figure D-23.  $\sigma_{yy}$  at bottom of base layer comparison for nonlinear and linear cases, for structure-1 with 10% w.c. base layer and nonlinear Ottawa sand subgrade.

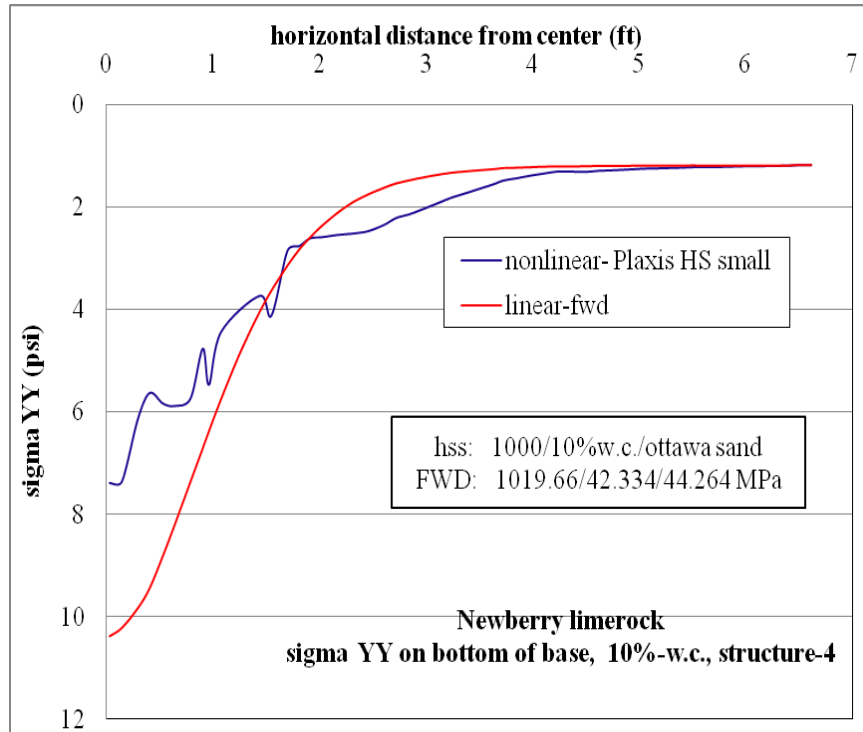


Figure D-24.  $\sigma_{yy}$  at bottom of base layer comparison for nonlinear and linear cases, for structure-4 with 10% w.c. base layer and nonlinear Ottawa sand subgrade.

**D.1.9. Vertical Strain ( $\epsilon_{yy}$ , Compressive Strain) at Bottom of Base Layer**

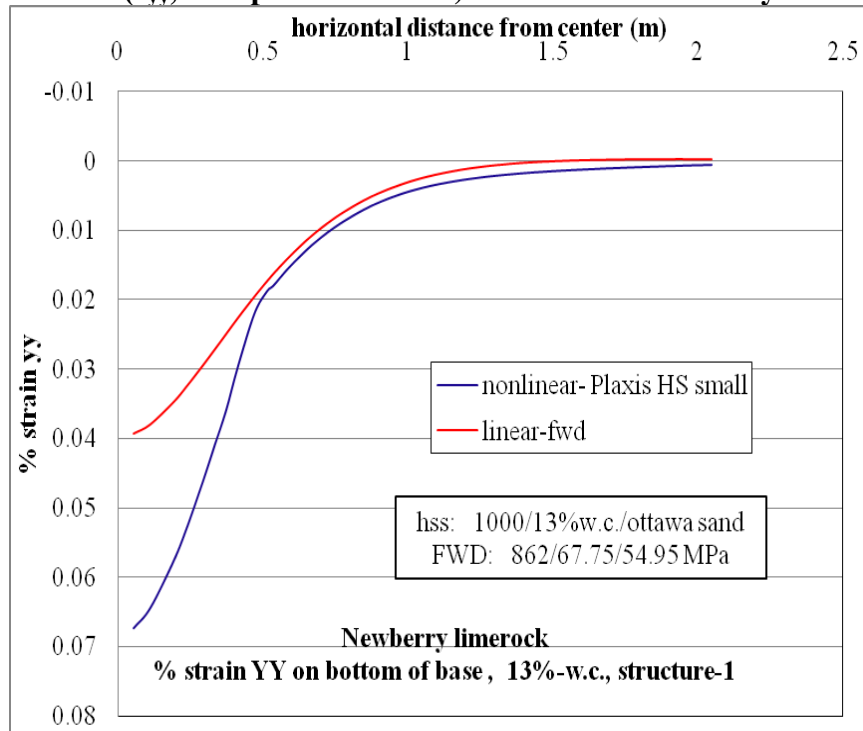


Figure D-25.  $\epsilon_{yy}$  at bottom of base layer comparison for nonlinear and linear cases, for structure-1 with 13% w.c. base layer and nonlinear Ottawa sand subgrade.

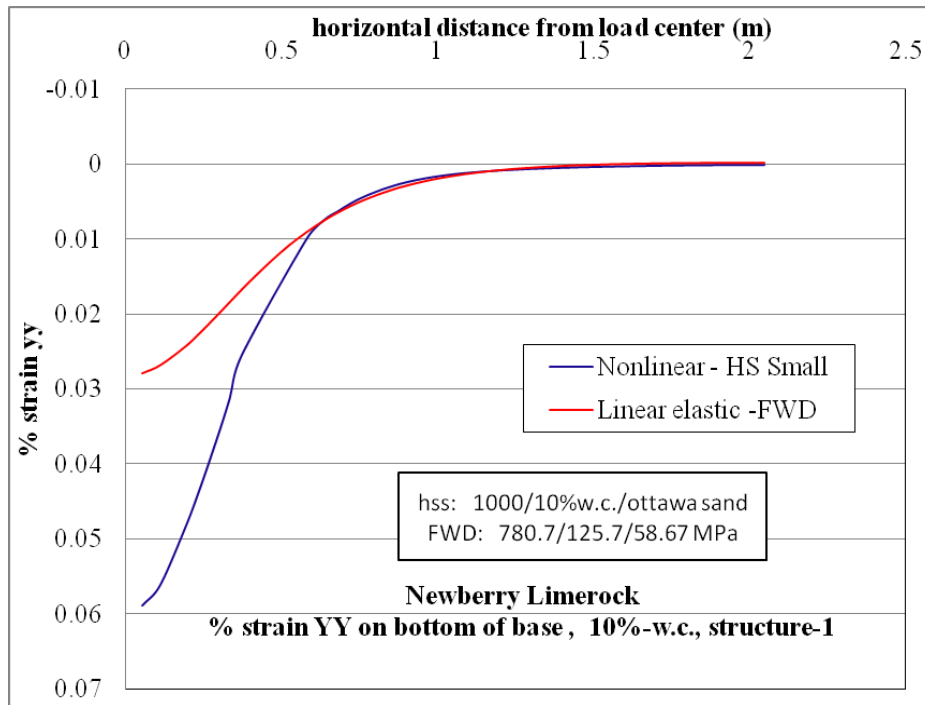


Figure D-26.  $\epsilon_{yy}$  at bottom of base layer comparison for nonlinear and linear cases, for structure-1 with 10% w.c. base layer and nonlinear Ottawa sand subgrade.

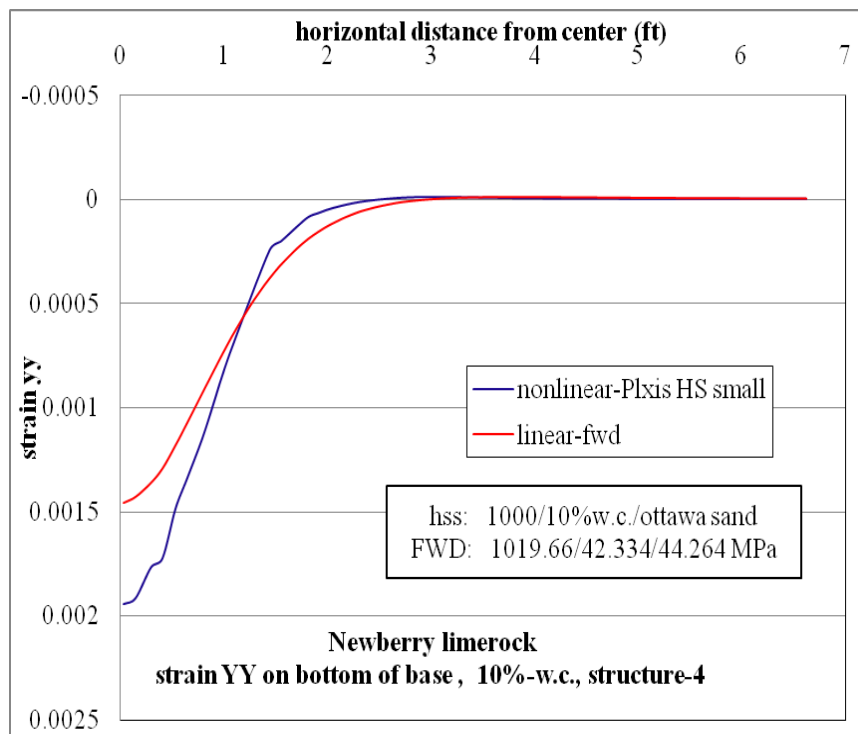


Figure D-27.  $\epsilon_{yy}$  at bottom of base layer comparison for nonlinear and linear cases, for structure-4 with 10% w.c. base layer and nonlinear Ottawa sand subgrade.

### D.1.10 Vertical Stress ( $\sigma_{yy}$ , Compressive Stress) at Top of Subgrade Layer

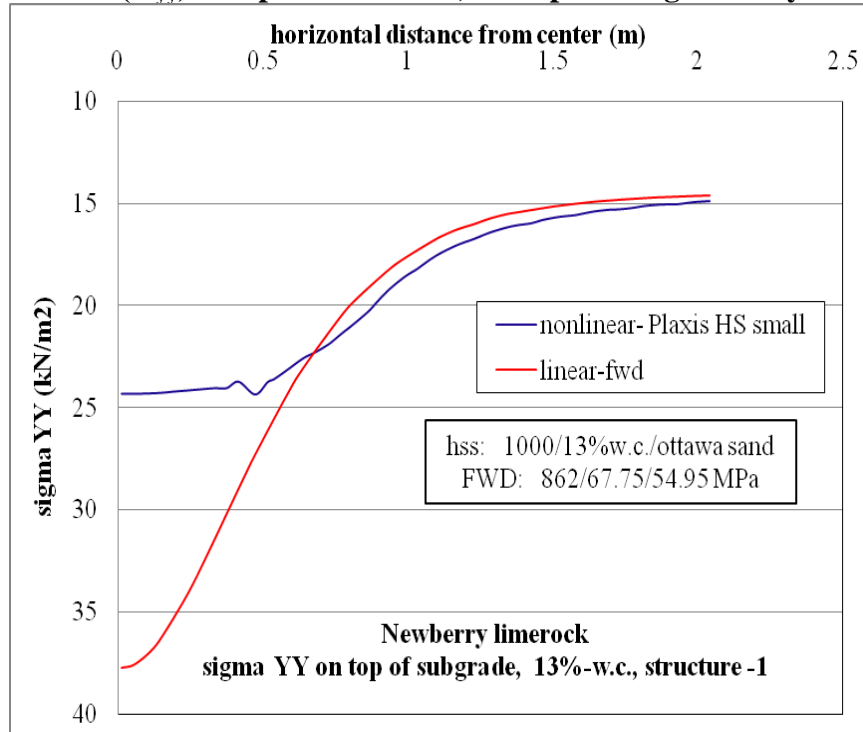


Figure D-28.  $\sigma_{yy}$  at top of subgrade comparison for nonlinear and linear cases, for structure-1 with 13% w.c. base layer and nonlinear Ottawa sand subgrade.

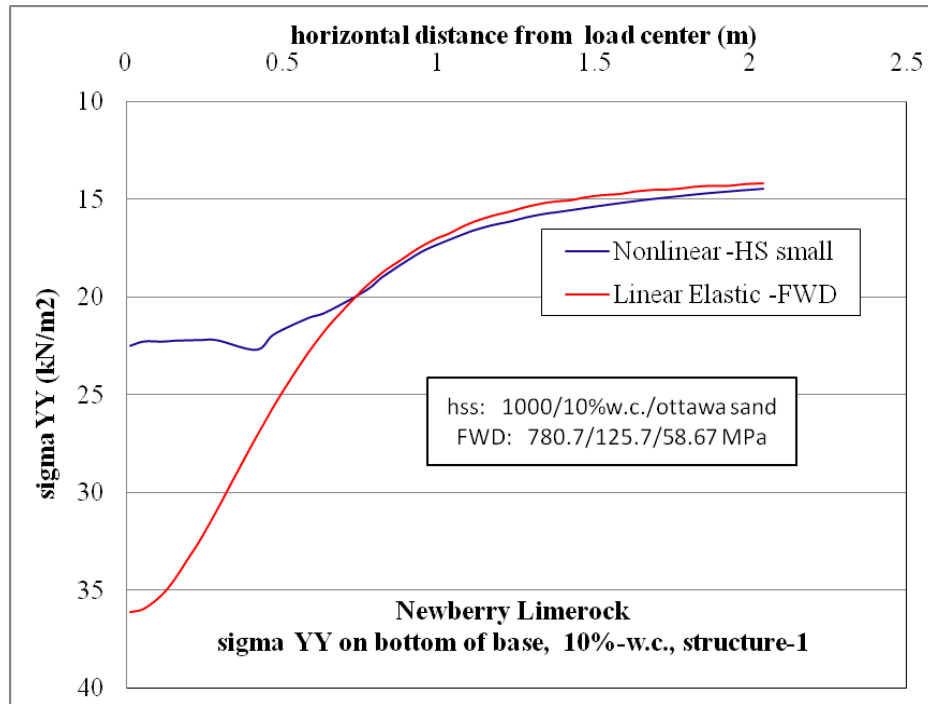


Figure D-29.  $\sigma_{yy}$  at top of subgrade comparison for nonlinear and linear cases, for structure-1 with 10% w.c. base layer and nonlinear Ottawa sand subgrade.

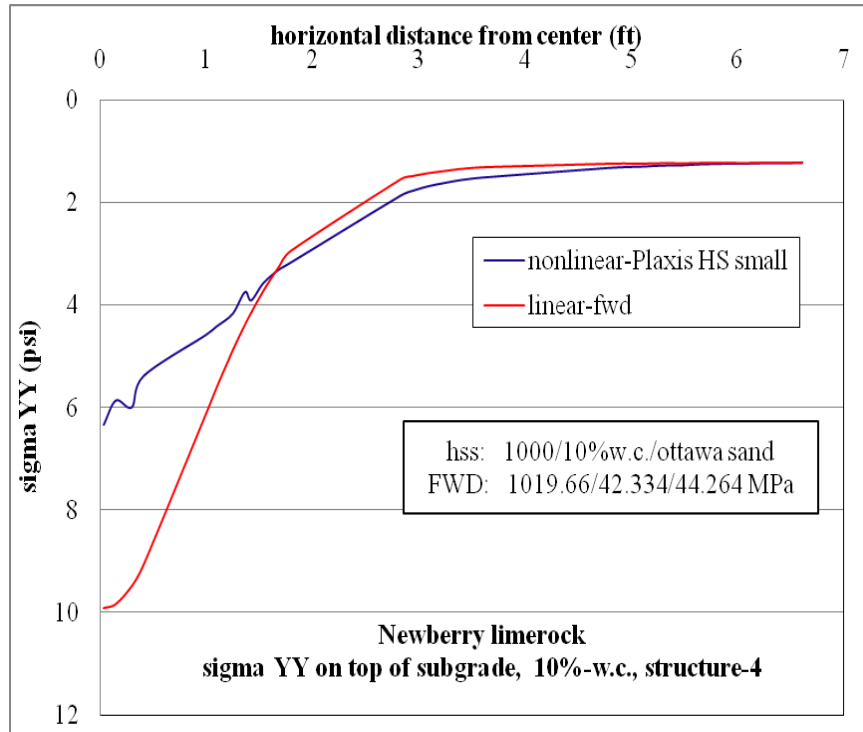


Figure D-30.  $\sigma_{yy}$  at top of subgrade comparison for nonlinear and linear cases, for structure-4 with 10% w.c. base layer and nonlinear Ottawa sand subgrade.

**D.1.11 Vertical Strain ( $\epsilon_{yy}$ , Compressive Strain) at Top of Subgrade Layer**

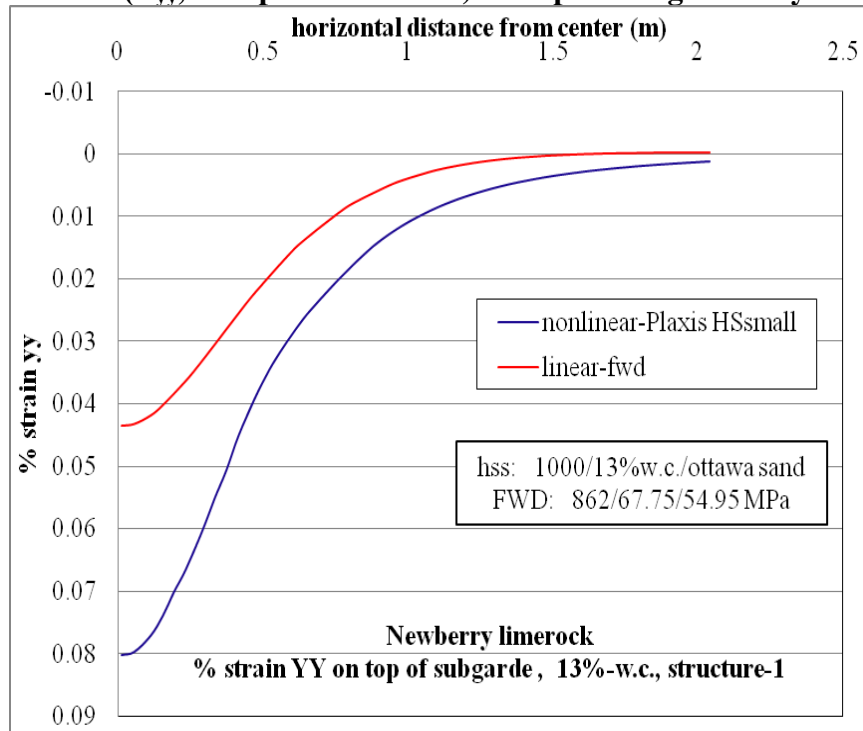


Figure D-31.  $\epsilon_{yy}$  at top of subgrade layer comparison for nonlinear and linear cases for structure-1 with 13% w.c. base layer and nonlinear Ottawa sand subgrade

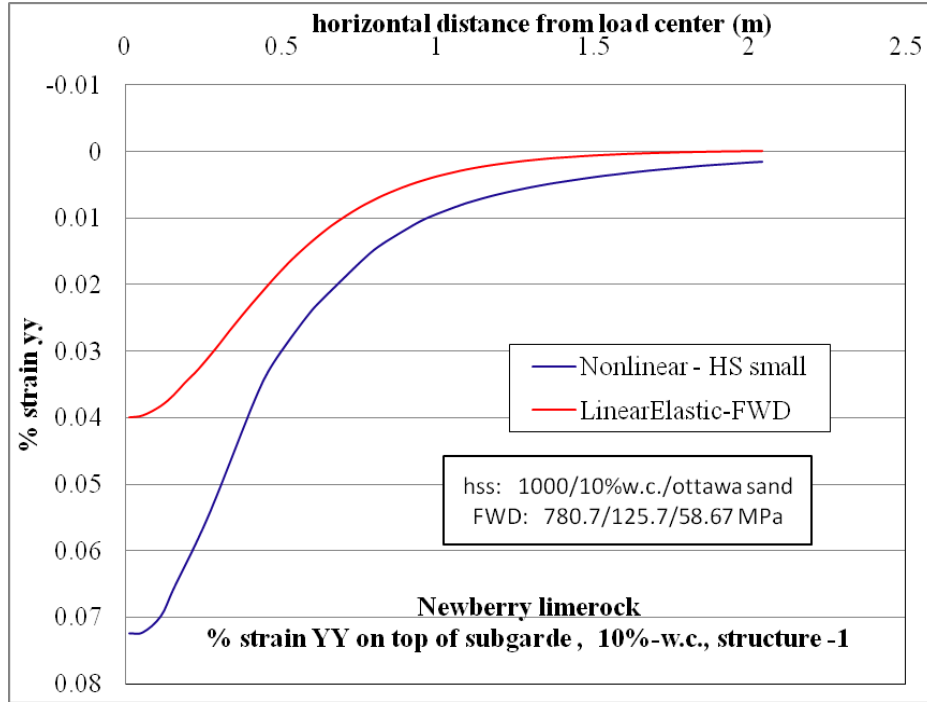


Figure D-32.  $\epsilon_{yy}$  at top of subgrade layer comparison for nonlinear and linear cases for structure-1 with 10% w.c. base layer and nonlinear Ottawa sand subgrade

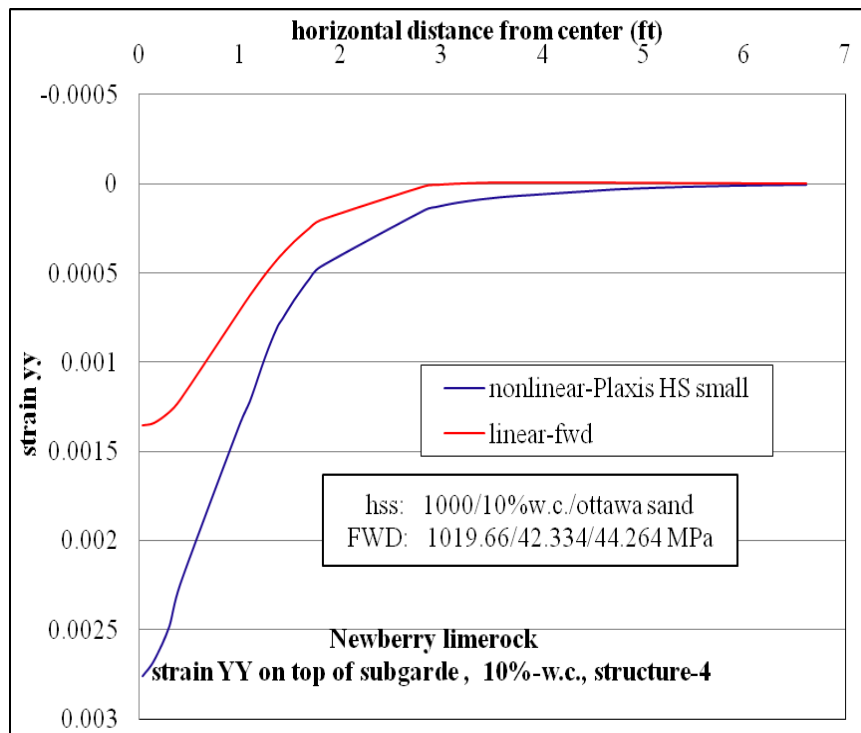


Figure D-33.  $\epsilon_{yy}$  at top of subgrade layer comparison for nonlinear and linear cases for structure-4 with 10% w.c. base layer and nonlinear Ottawa sand subgrade

## D.2 Georgia Granite

### D.2.1 Surface Deflection Profiles

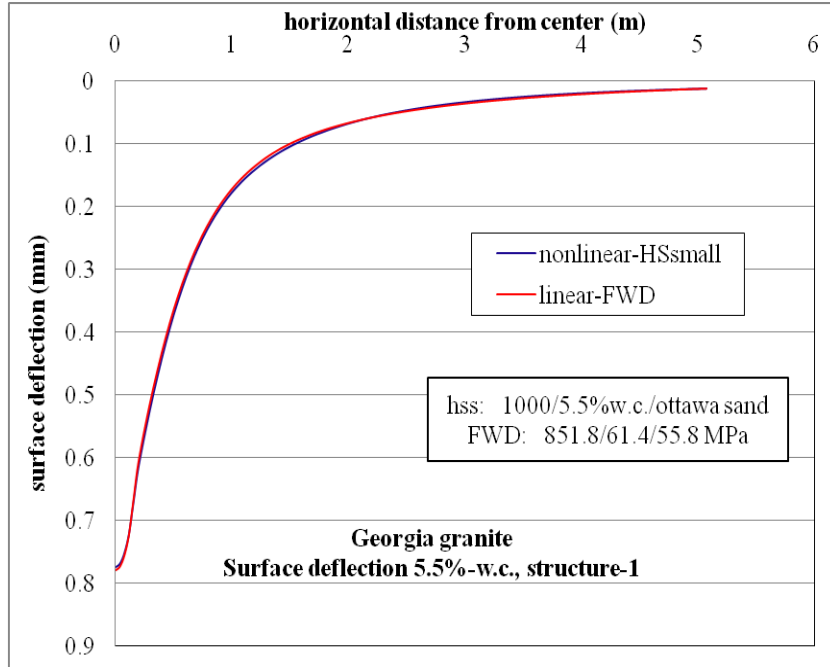


Figure D-34. Surface deflection comparison for nonlinear and linear cases, for structure-1 with 5.5% w.c. base layer and nonlinear Ottawa sand subgrade.

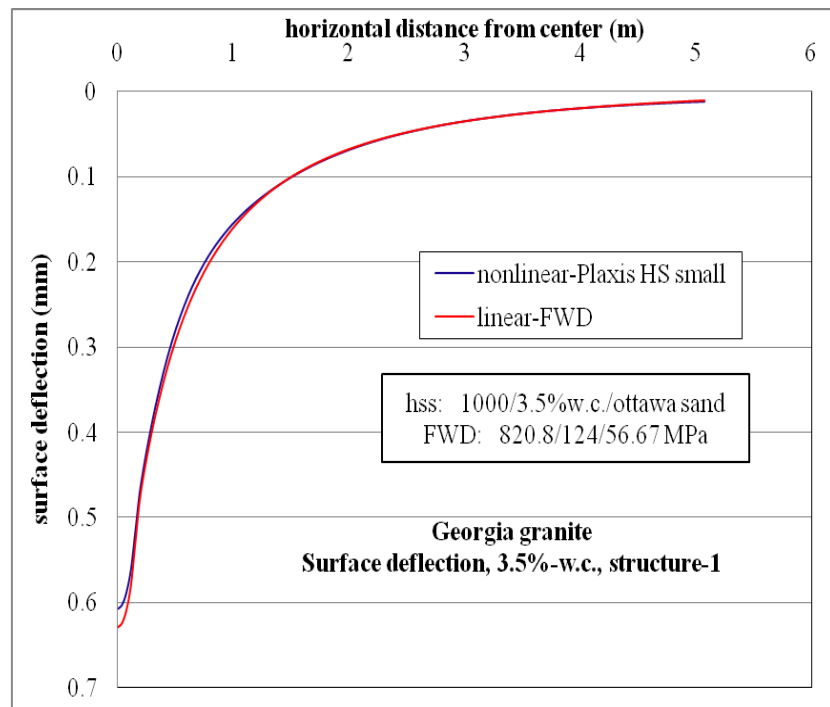


Figure D-35. Surface deflection comparison for nonlinear and linear cases, for structure-1 with 3.5% w.c. base layer and nonlinear Ottawa sand subgrade.

### D.2.2 Horizontal Stress ( $\sigma_{xx}$ , Tensile Stress) at Top of AC Layer

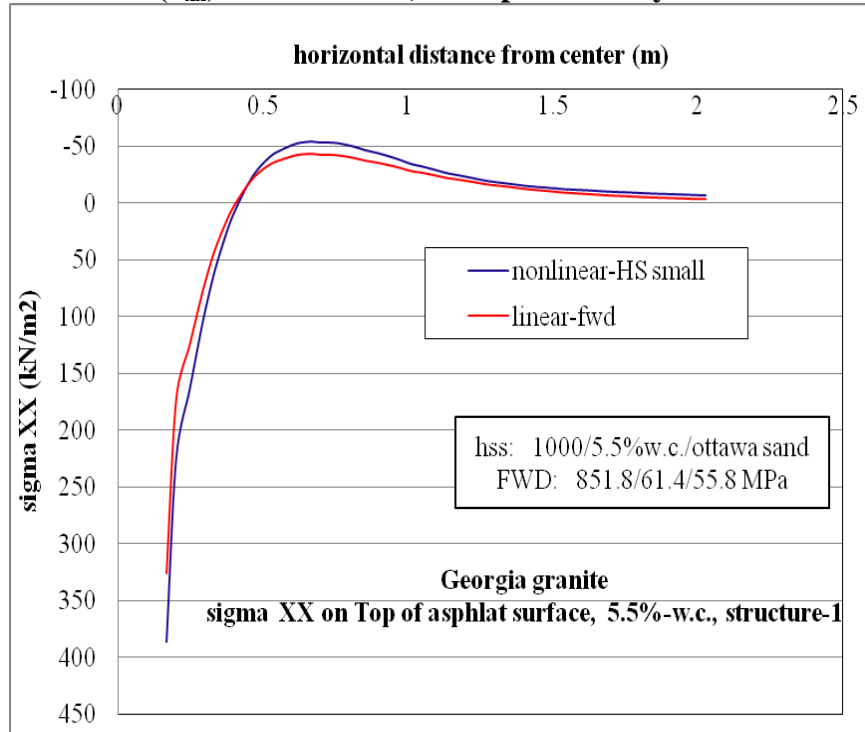


Figure D-36.  $\sigma_{xx}$  at top of AC layer comparison for nonlinear and linear cases, for structure-1 with 5.5% w.c. base layer and nonlinear Ottawa sand subgrade.

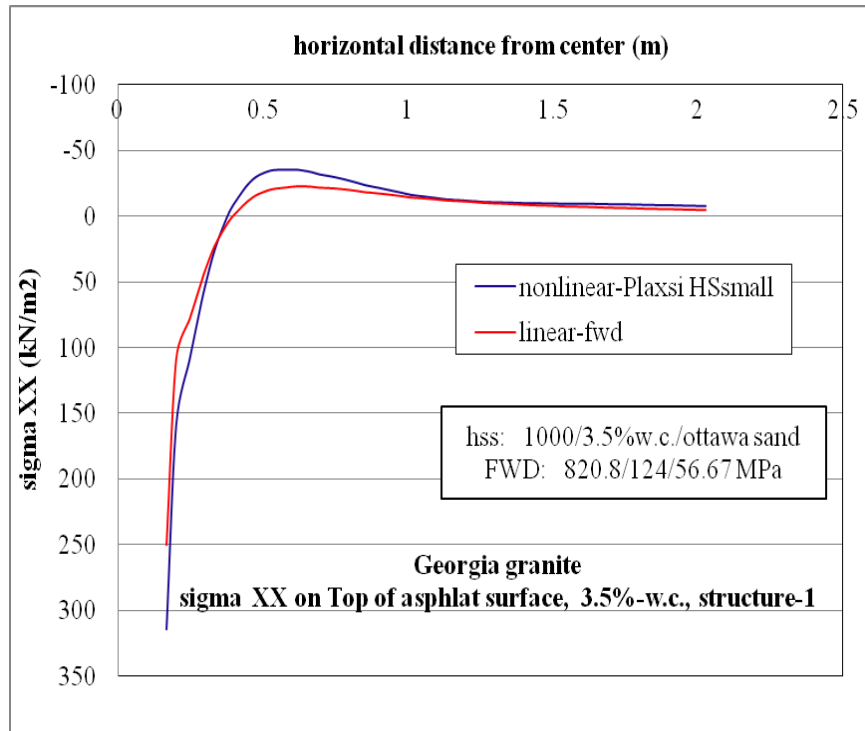


Figure D-37.  $\sigma_{xx}$  at top of AC layer comparison for nonlinear and linear cases, for structure-1 with 3.5% w.c. base layer and nonlinear Ottawa sand subgrade.

### D.2.3 Horizontal Strain ( $\epsilon_{xx}$ , Tensile Strain) at Top of AC Layer

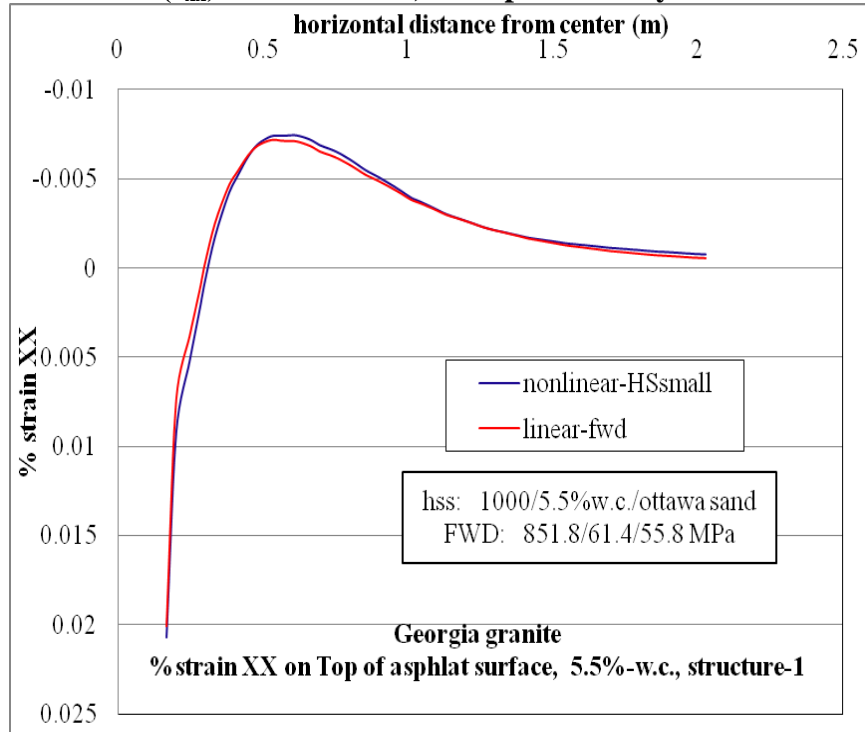


Figure D-38.  $\epsilon_{xx}$  at top of AC layer comparison for nonlinear and linear cases, for structure-1 with 5.5% w.c. base layer and nonlinear Ottawa sand subgrade.

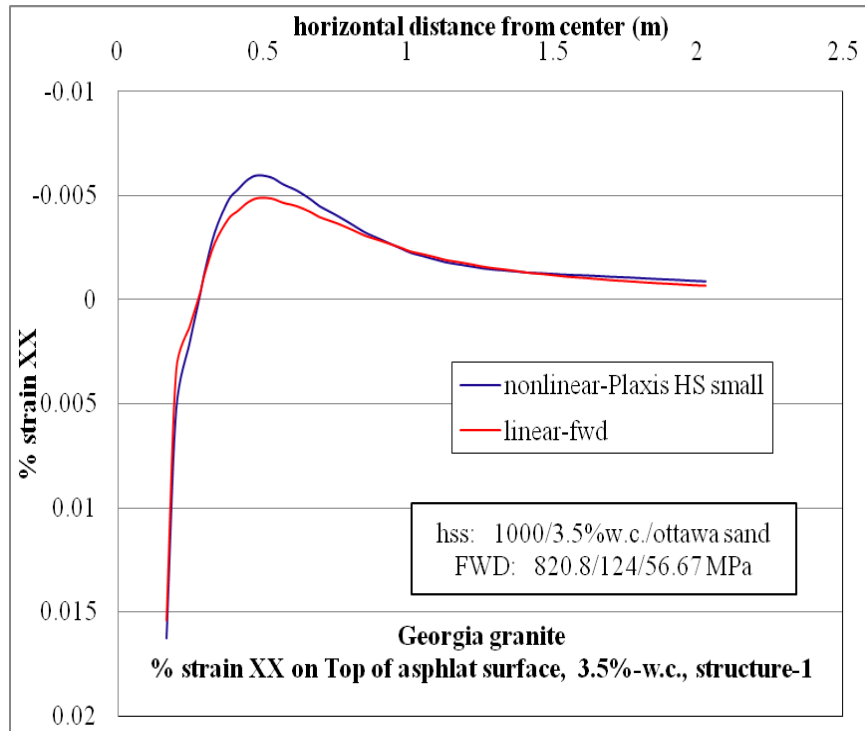


Figure D-39.  $\epsilon_{xx}$  at top of AC layer comparison for nonlinear and linear cases, for structure-1 with 3.5% w.c. base layer and nonlinear Ottawa sand subgrade.

### D.2.4 Horizontal Stress ( $\sigma_{xx}$ , Tensile Stress) at Bottom of AC Layer

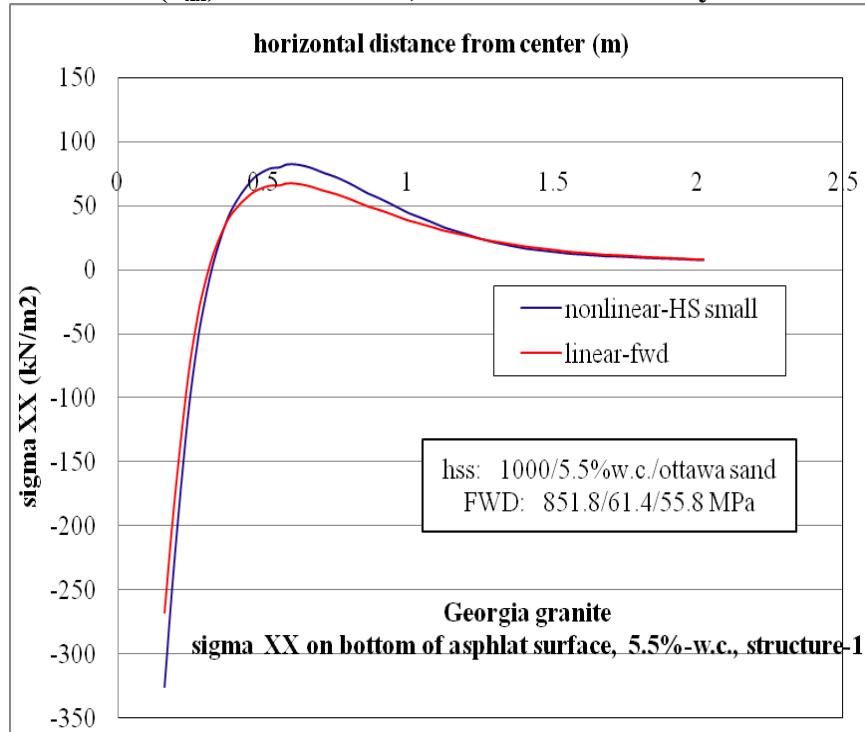


Figure D-40.  $\sigma_{xx}$  at bottom of AC layer comparison for nonlinear and linear cases, for structure-1 with 5.5% w.c. base layer and nonlinear Ottawa sand subgrade.

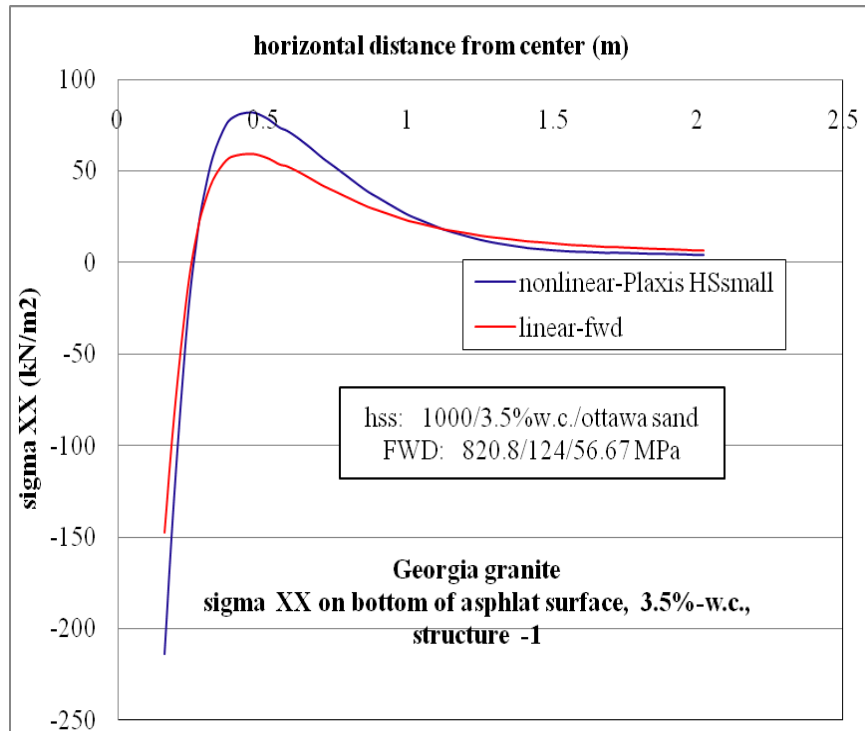


Figure D-41.  $\sigma_{xx}$  at bottom of AC layer comparison for nonlinear and linear cases, for structure-1 with 3.5% w.c. base layer and nonlinear Ottawa sand subgrade.

### D.2.5. Horizontal Strain ( $\epsilon_{xx}$ , Tensile Strain) at Bottom of AC Layer

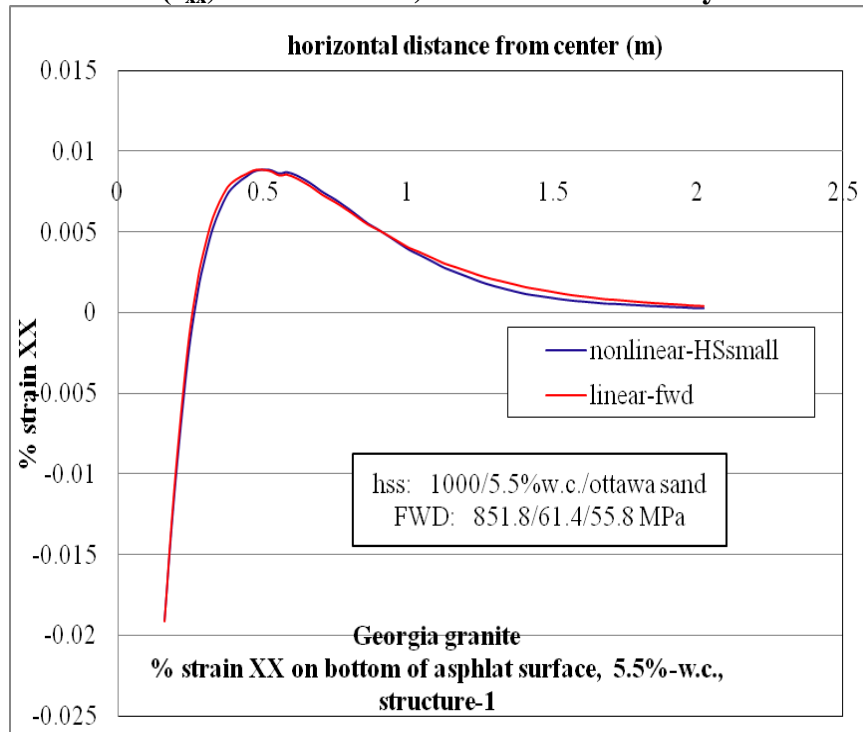


Figure D-42.  $\epsilon_{xx}$  at bottom of AC layer comparison for nonlinear and linear cases, for structure-1 with 5.5% w.c. base layer and nonlinear Ottawa sand subgrade.

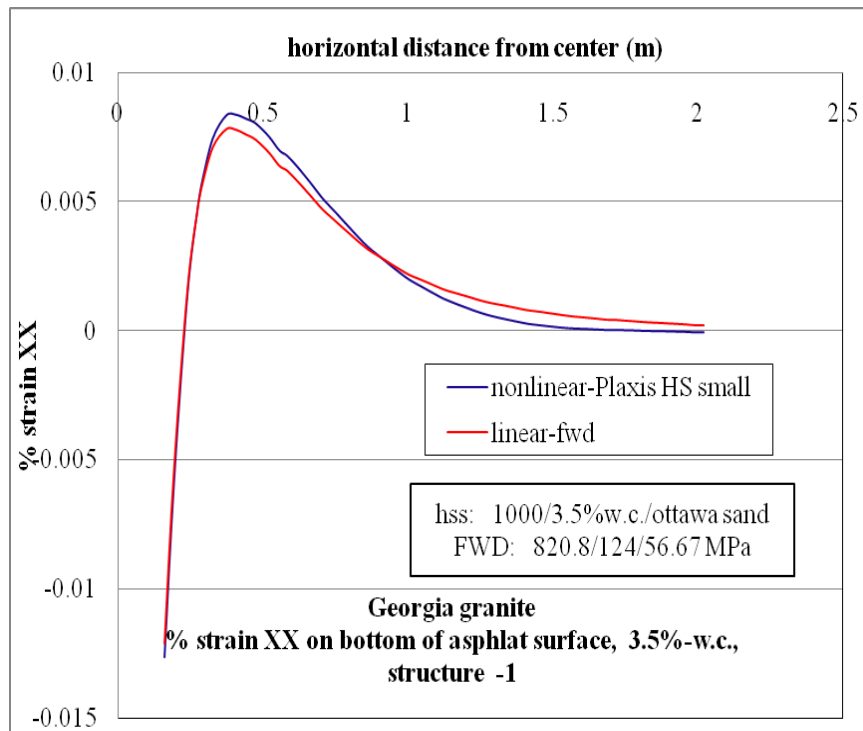


Figure D-43.  $\epsilon_{xx}$  at bottom of AC layer comparison for nonlinear and linear cases, for structure-1 with 3.5% w.c. base layer and nonlinear Ottawa sand subgrade.

### D.2.6 Vertical Stress ( $\sigma_{yy}$ , Compressive Stress) at Top of Base Layer

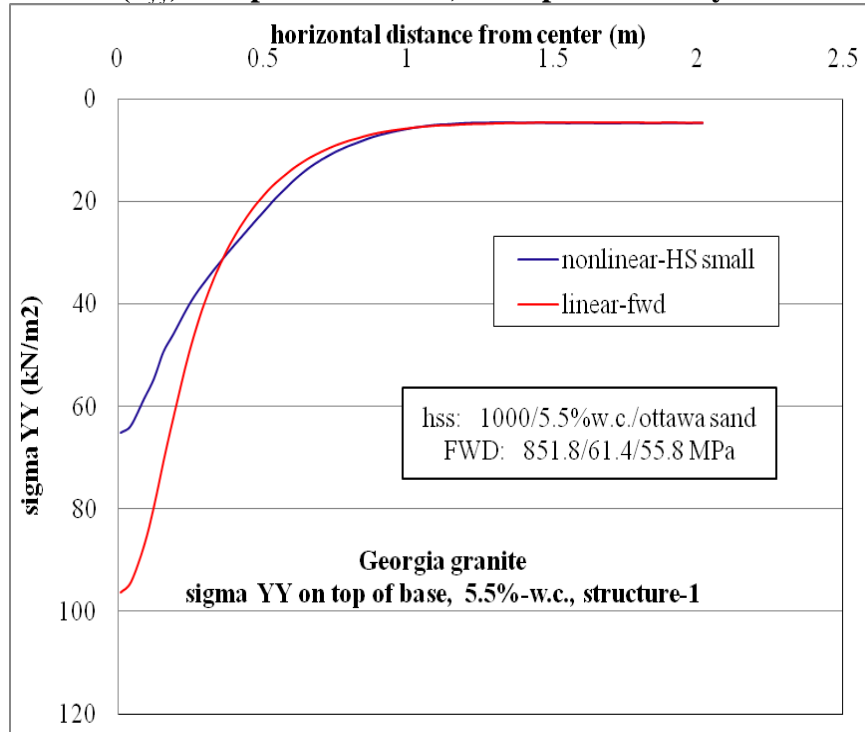


Figure D-44.  $\sigma_{yy}$  vertical stress at top of base layer comparison for nonlinear and linear cases, for structure-1 with 5.5% w.c. base layer and nonlinear Ottawa sand subgrade.

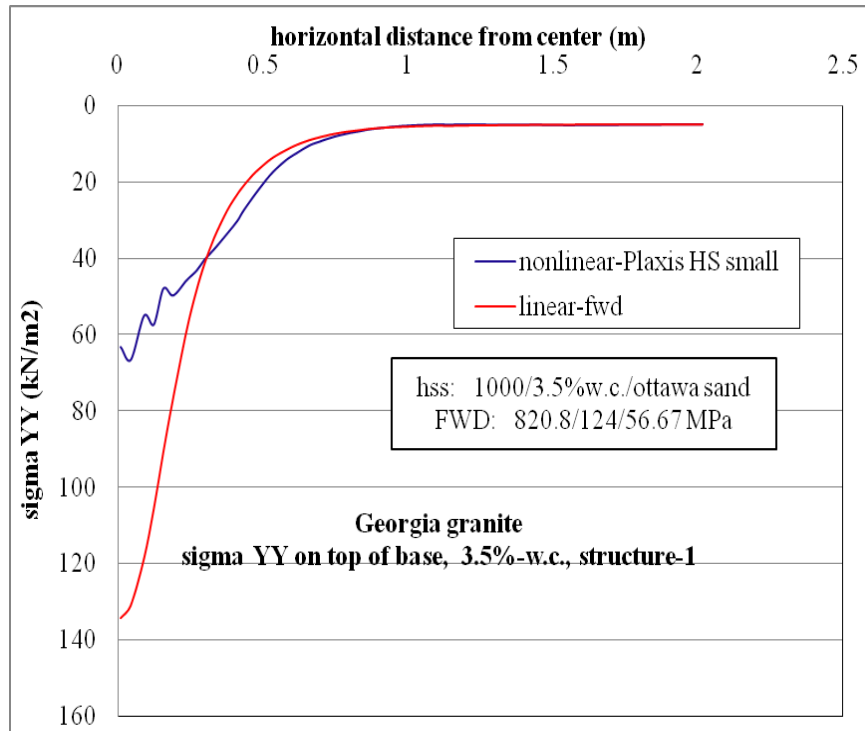


Figure D-45.  $\sigma_{yy}$  vertical stress at top of base layer comparison for nonlinear and linear cases, for structure-1 with 3.5% w.c. base layer and nonlinear Ottawa sand subgrade.

### D.2.7 Vertical Strain ( $\epsilon_{yy}$ , Compressive Strain) at Top of Base Layer

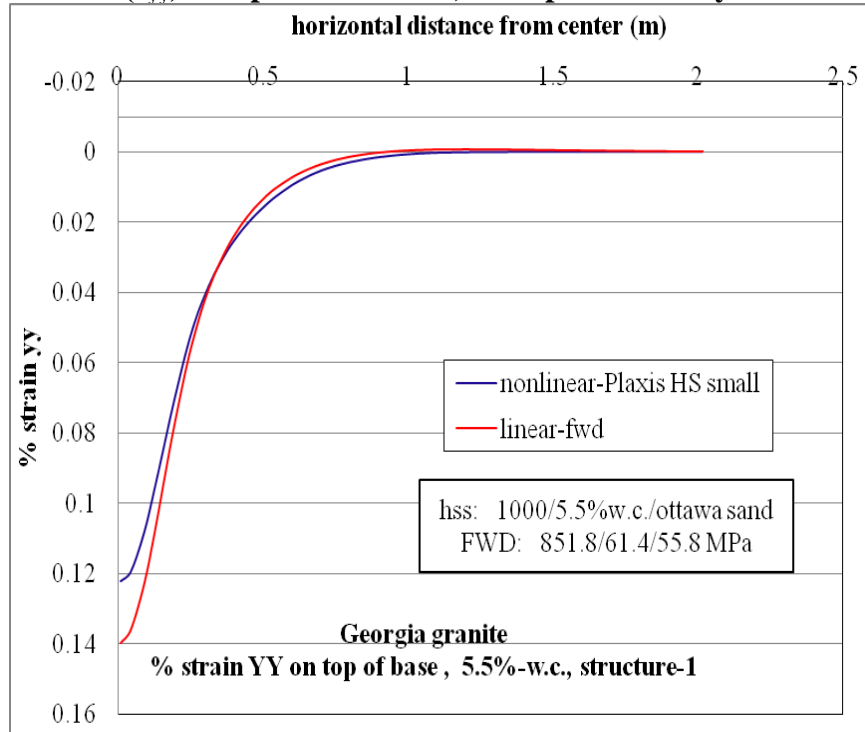


Figure D-46.  $\epsilon_{yy}$  at top of base layer comparison for nonlinear and linear cases, for structure-1 with 5.5% w.c. base layer and nonlinear Ottawa sand subgrade.

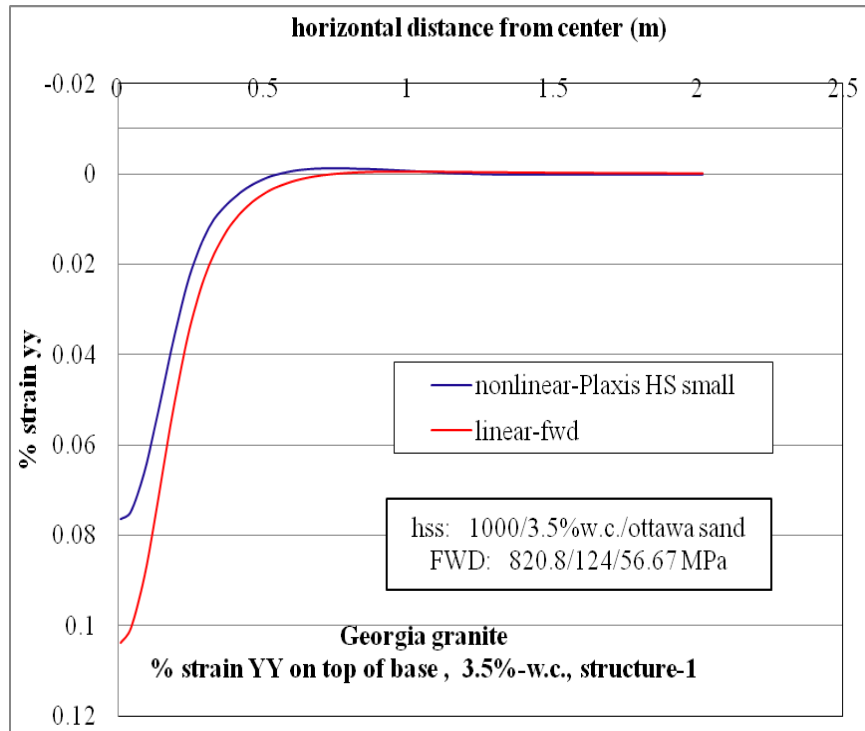


Figure D-47.  $\epsilon_{yy}$  at top of base layer comparison for nonlinear and linear cases, for structure-1 with 3.5% w.c. base layer and nonlinear Ottawa sand subgrade.

### D.2.8 Vertical Stress ( $\sigma_{yy}$ , Compressive Stress) at Bottom of Base Layer

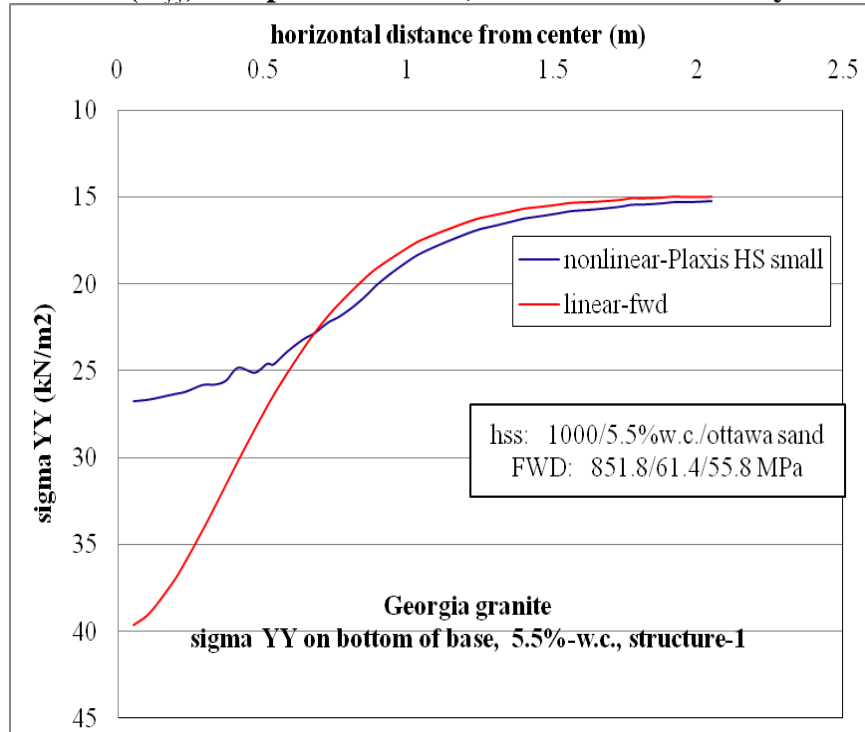


Figure D-48.  $\sigma_{yy}$  at bottom of base layer comparison for nonlinear and linear cases, for structure-1 with 5.5% w.c. base layer and nonlinear Ottawa sand subgrade.

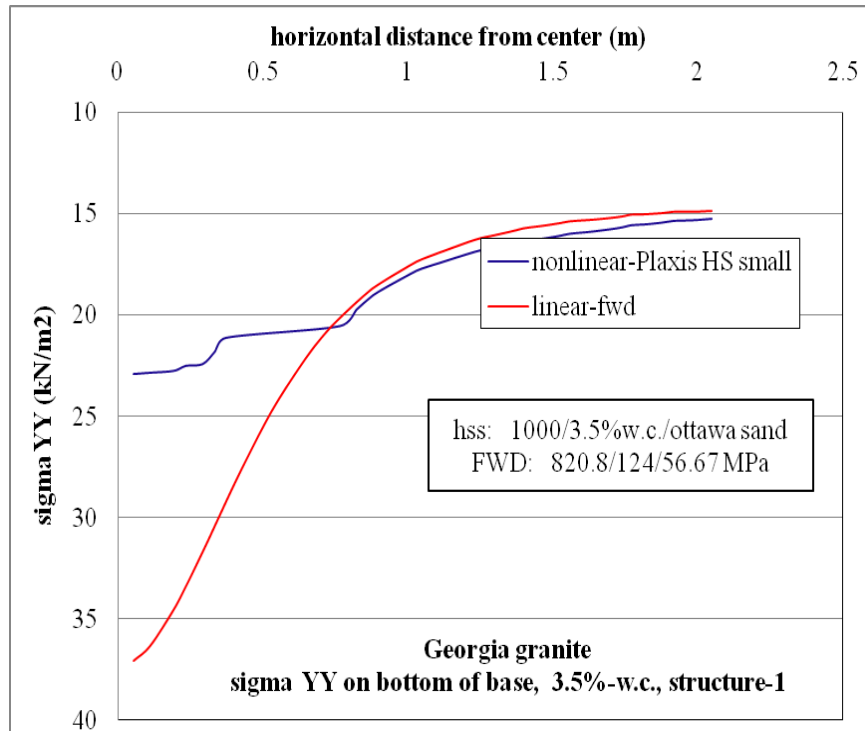


Figure D-49.  $\sigma_{yy}$  at bottom of base layer comparison for nonlinear and linear cases, for structure-1 with 3.5% w.c. base layer and nonlinear Ottawa sand subgrade.

### D.2.9 Vertical strain ( $\epsilon_{yy}$ , Compressive Strain) at Bottom of Base Layer

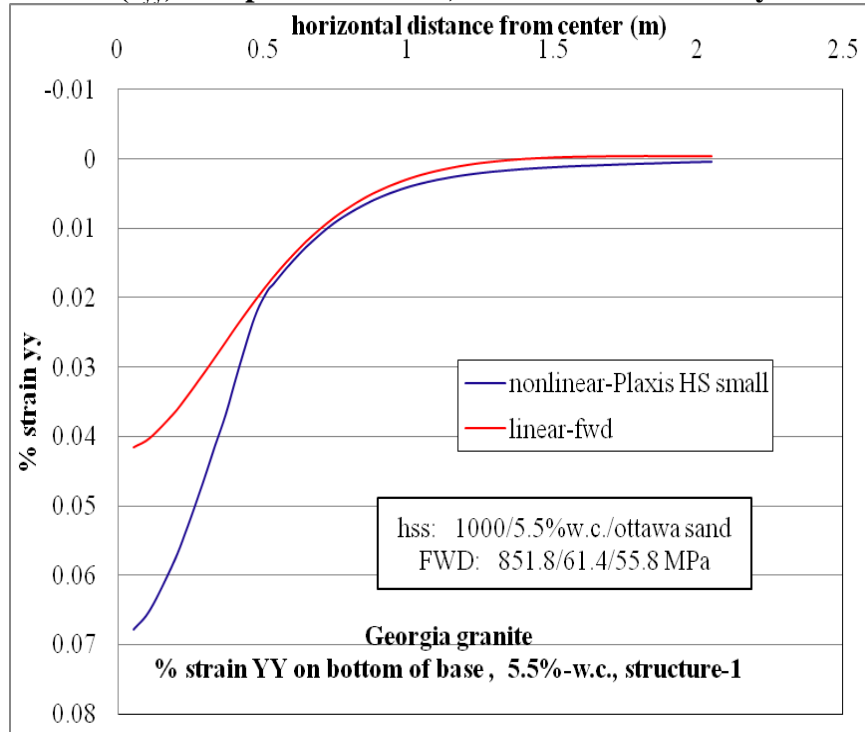


Figure D-50.  $\epsilon_{yy}$  at bottom of base layer comparison for nonlinear and linear cases, for structure-1 with 5.5% w.c. base layer and nonlinear Ottawa sand subgrade.

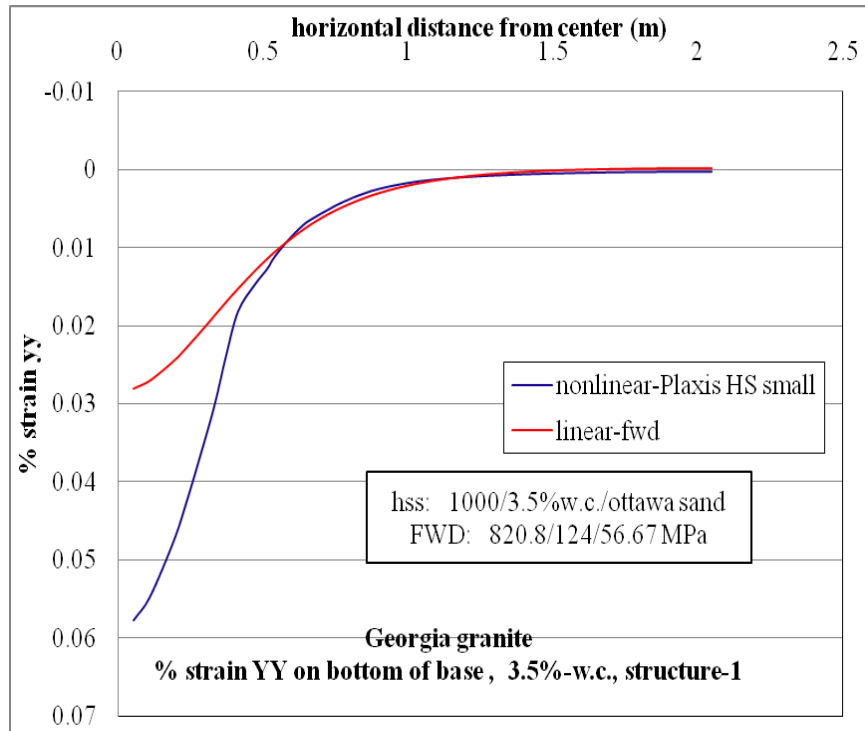


Figure D-51.  $\epsilon_{yy}$  at bottom of base layer comparison for nonlinear and linear cases, for structure-1 with 3.5% w.c. base layer and nonlinear Ottawa sand subgrade.

### D.2.10 Vertical Stress ( $\sigma_{yy}$ , Compressive Stress) at Top of Subgrade Layer

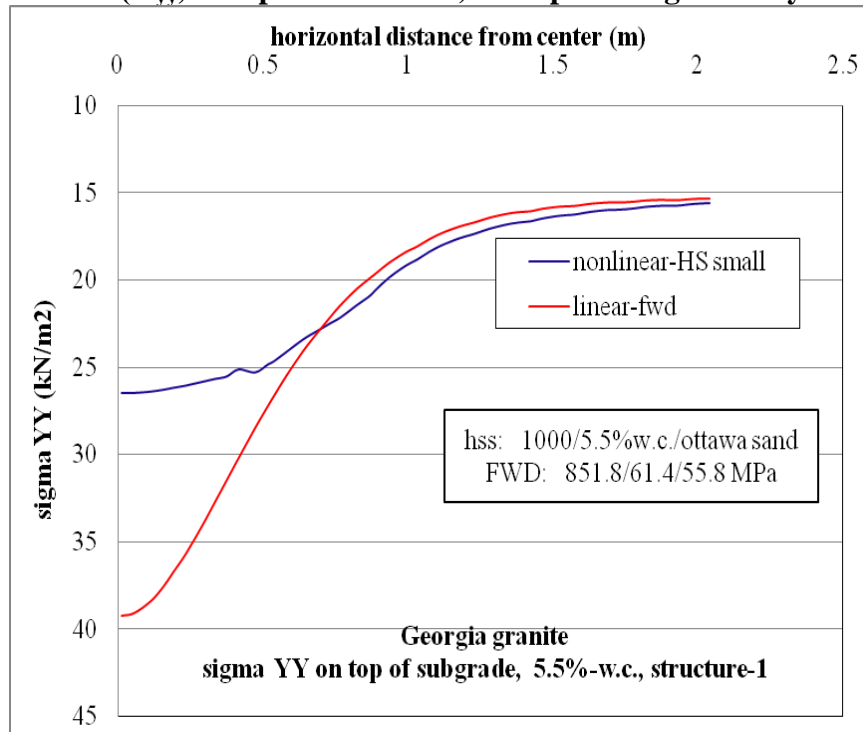


Figure D-52.  $\sigma_{yy}$  at top of subgrade comparison for nonlinear and linear cases, for structure-1 with 5.5% w.c. base layer and nonlinear Ottawa sand subgrade.

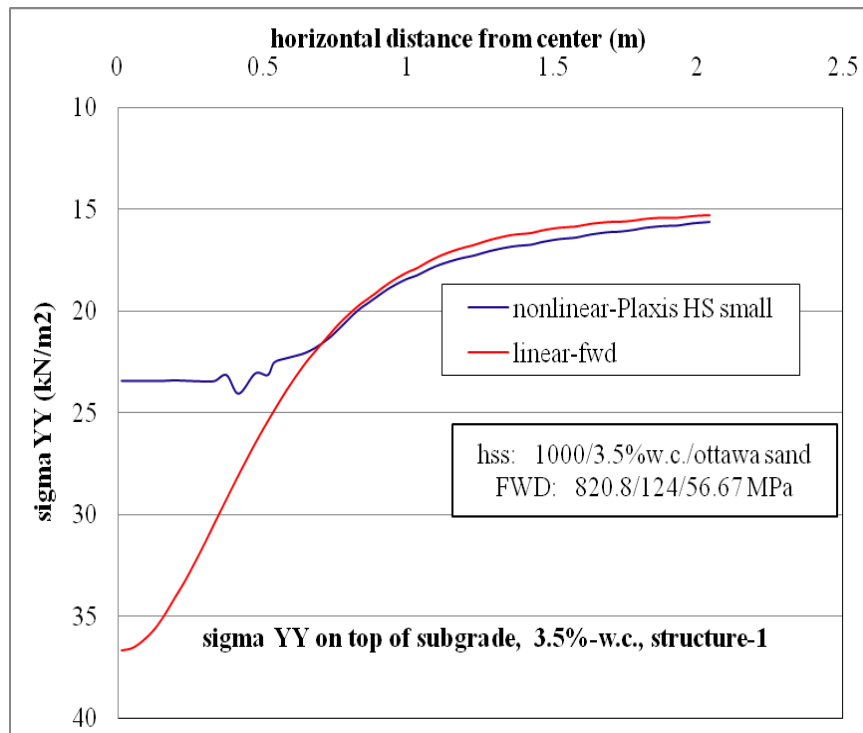


Figure D-53.  $\sigma_{yy}$  at top of subgrade comparison for nonlinear and linear cases, for structure-1 with 3.5% w.c. base layer and nonlinear Ottawa sand subgrade.

### D.2.11 Vertical Strain ( $\epsilon_{yy}$ , Compressive Strain) at Top of Subgrade Layer

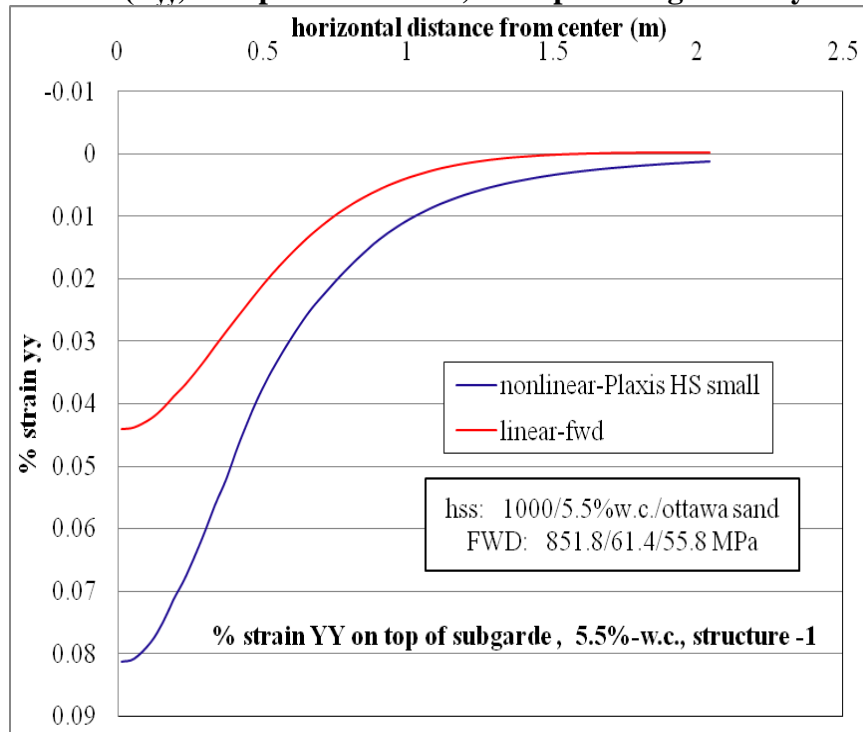


Figure D-54.  $\epsilon_{yy}$  at top of subgrade layer comparison for nonlinear and linear cases for structure-1 with 5.5% w.c. base layer and nonlinear Ottawa sand subgrade

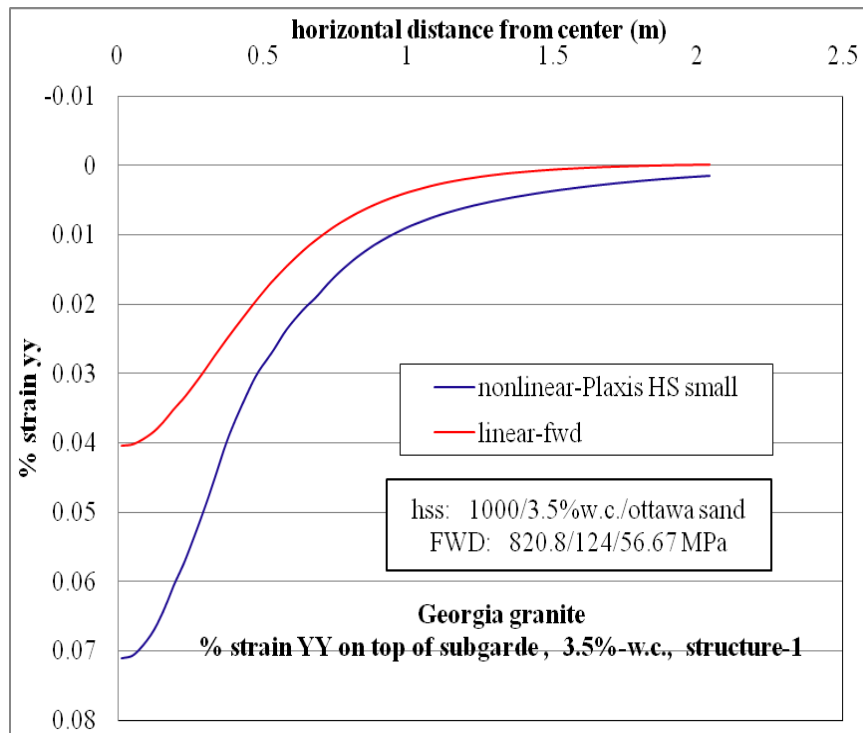


Figure D-55.  $\epsilon_{yy}$  at top of subgrade layer comparison for nonlinear and linear cases for structure-1 with 3.5% w.c. base layer and nonlinear Ottawa sand subgrade.

## LIST OF REFERENCES

- Atkinson, J.H. (2000). "Non-linear Soil Stiffness in Routine Design", *Geotechnique*, 50(5), 487-508.
- Atkinson, J.H., and Salfors, J. (1991). "Experimental Determination of Stress-Strain-Time Characteristics in Laboratory and In-situ Tests" Proceedings of Tenth European Conference on Soil Mechanics and Foundation Engineer, Rotterdam, Netherlands, 915-958.
- Cho, G.C., and Santamarina, J.C. (2001). "Unsaturated Particulate Materials – Particle Level Studies", *Journal of Geotechnical and Geoenvironmental Engineering*, 127(10), 84-96.
- Hardin, B.O., and Richart, F.E., Jr. (1963). "Elastic Waves in Granular Soils", *Journal of Soil Mechanics and Foundation Division*, 89(SM1), 33-65.
- Hardin, B.O., and Drnevich, V.P. (1972) "Shear Modulus and Damping in Soils: Measurement and Parameter Effects", *Journal of Soil Mechanics and Foundations Division*, 98(SM6), 603-624.
- Hardin, B.O., and Drnevich, V.P. (1972) "Shear Modulus and Damping in Soils: Design Equations and Curves", *Journal of Soil Mechanics and Foundations Division*, 98(SM7), 667-692.
- Hardin, B.O., and Kalinski, M.E., (2005). "Estimating Shear Modulus of Gravelly Soils", *Journal of Geotechnical and Geoenvironmental Engineering*, 131(7), 867-873.
- Hunag, W., Yang, S, Kung, J.H.S., and Lin, H. (2006). "Effect of Matric Suction on resilient Modulus of Compacted Subgrade Soils", *Transportation Research Board 85<sup>th</sup> Annual Meeting Compendium of Papers CD-ROM*. 21 pages
- Kokusho, T. (1987) "In-Situ Dynamic Soil Properties and Their Evaluations", *Proceedings of the 8<sup>th</sup> Asian Regional Conference on Soil Mechanics and Foundation Engineering*, Kyoto, vol. 2, 215-240.
- Lehane, B.M., Doherty, J.P., and Schneider, J.A. (2008). "Settlement Prediction for Footings on Sand", *Proceedings of the fourth international symposium on deformation Characteristics of Geomaterials*, Atlanta,(133-150).
- Lin, S., Lin, P.S., Luo, H., and Juang, C.H. (2000). "Shear Modulus and Damping Ratio Characteristics of Gravelly Deposits", *Canadian Geotechnical Journal*, 37, 638-651.
- Kim, M.K., Tutumluer, E., and Kwon, J. (2009). "Nonlinear Pavement Foundation Modeling for Three-Dimensional Finite-Element Analysis of Flexible Pavements", *International Journal of Geomechanics*, 9(5), 195-208.

- Picornell, M., and Nazarian, S. (1998). "Effect of Soil Suction on the Low-Strain Shear Modulus of Soils", *Proceedings of 2nd International Conference on Unsaturated Soils: UNSAT'98*, Beijing, China, 102-107.
- Pestana, J.M., and Salvati, L.A. (2006). "Small-Strain Behavior of Granular Soils.1:Model for Cemented and Uncemented Sands and Gravels", *Journal of Geotechnical and Geoenvironmental Engineering*, 132 (8), 1071-1081.
- Qian, X., Gray, D.H., and Richard, W. (1993). "Voids and Granulometry: Effects on Shear Modulus of Unsaturated Sands", *Journal of Geotechnical Engineering*, 119 (2), 295-314.
- Rollins, K.M., Evans, M.D., Dielhl, N.B., and Daily, W.D. (1998). "Shear Modulus and Damping Relationships for Gravels", *Journal of Geotechnical and Geoenvironmental Engineering*, 124(5), 396-405.
- Roque, R., Romero, P., and Hiltunen, D.R. (1992) "The Use of Linear Elastic Analysis to Predict the Nonlinear Response of Pavements", *Proceedings of 7<sup>th</sup> International Conference on Asphalt Pavements*, Nottingham University, U.K., 295-310.
- Santos, J.A., and Correia, A.G. (2001) "Reference Threshold Shear Strain for Soil. Its application to Obtain an Unique Strain-Dependent Shear Modulus Curve for Soil". *Proceedings of the 15<sup>th</sup> International Conference on Soil Mechanics and Geotechnical Engineering*, Istanbul, Vol 1, 267-270.
- Seed, H.B., Wong, R.T., Idriss, I.M., and Tokimatsu, K. (1986), "Moduli and Damping Factors for Dynamic Analyses of Cohesionless Soils", *Journal of Geotechnical Engineering* , 112(12), 1016-1032.
- Singh, A., Roberson, R., Ranaivoson, A., Siekmeir, J., and Gupta, S. (2006), "Water Retention Characteristics of Aggregates and Granular Materials", *Proceedings of the Fourth International Conference on Unsaturated Soils*, Carefree, AZ, 1326-1337.
- Wu, S., Gray, D.H., and Richart, F.E., Jr. (1984), "Capillarity Effects on Dynamic Modulus of Sands and Silts", *Journal of Geotechnical Engineering*, 110 (9), 1188-1203.
- Yasuda, N., Matsumoto, N. (1993), "Dynamic Deformation Characteristics of Sands and Rockfill Materials", *Canadian Geotechnical Journal*, 30, 745-757.
- Yasuda, N., Ohat, N., and Nakamura, A. (1996), "Dynamic Deformation Characteristics of Undisturbed Riverbed Gravels", *Canadian Geotechnical Journal*,, 33, 237-249.

## BIOGRAPHICAL SKETCH

Aditya Ayithi was born in 1978 in Vinukonda, India; and remained in Vinukonda until he graduated from Loyola High School in 1993. He enrolled in Pragathi residential college for Intermediate college education and graduated in 1995. He enrolled in Jawaharlal Nehru Technological University, Anantapur; in 1996 and with a Bachelor of Technology in civil engineering in summer 2000. After working in civil engineering private industry for one year, he enrolled in Indian Institute of Technology, Delhi for graduate studies in 2001 fall and graduated with Master of Technology in Soil Mechanics and Foundation engineering in fall, 2002. Before pursuing his Doctoral education, he worked for more than two and half years in civil engineering in various positions, such as research management scientist at Department of Science and Technology, Government of India, for two years and project engineer at RADISE International Inc., FL; for 7 months. He enrolled at the University of Florida in Gainesville, FL in August, 2005 where he worked as a graduate research assistant under Dr. Dennis R.Hiltunen. He completed his Master of Science in May, 2008 and Doctor of Philosophy in August, 2011.